Phone : +90 (312) 201 10 00
Fax : +90 (312) 287 91 88
Adress : MTA 06520 - Ankara - TURKEY
www.mta.gov.tr

BULLETIN OF THE MINERAL RESEARCH AND EXPLORATION

Foreign Edition | 2019 | 159 | ISSN : 0026-4563 E-ISSN : 2651-3048

CONTENTS

BULLETIN OF THE MINERAL RESEARCH AND EXPLORATION

Foreign Edition	2019	159	ISSN : 0026-4563 E-ISSN : 2651-3048

CONTENTS

CONTACT
Redaksiyon Kurulu Başkanlığı
Maden Tetkik ve Arama Genel Müdürlüğü
Genel Müdürlük Binası (A Block)
Üniversiteler Mah. Dumlupınar Bulvarı No: 139
06800 Çankaya/ANKARA/TURKEY
e-mail: redaksiyon@mta.gov.tr

Bull. Min. Res. Exp. is indexed and abstracted in TR Dizin, Emerging Source Citation Index (ESCI), Clarative Analytics Master List, Georef, Geological Abstracts, Mineralogic Abstracts, DOAJ and Scopus database. The Bulletin of the Mineral Research and Exploration is published in three issues in a year. Each bulletin is printed in Turkish and English languages as two separate issues. The English and Turkish issues of the "Bulletin of the Mineral Research and Exploration" can be obtained from "BDT Department" free of charge, either directly or ordered by adding postage fee from the correspondence address.
E-Mail: bdt@mta.gov.tr
The section of "notes to the authors", format, copyright and other information can be obtained from www.mta.gov.tr as PDF files.

Printed Date: 19/08/2019
Printing House: Kuban Matbaacılık - İvedik Organize Sanayi Matbaacılar Sitesi 1514. Sokak No: 20 Phone: 0312 395 2070 Fax: 0312 395 3723 www.kubanmatbaa.com

PERIODICAL

ISSN: 0026-4563

E-ISSN: 2651-3048

Bulletin of the Mineral Research and Exploration

http://bulletin.mta.gov.tr

The control of sea-level changes on sedimentation in the Mut Basin: Late Serravallian-Early Tortonian incised valley-fill

Ayhan ILGAR[a*], Tolga ESİRTGEN[b], Aynur HAKYEMEZ[c], Gönül CULHA[d], Serap DEMİRKAYA[e] and Banu TÜRKMEN BOZKURT[f]

[a]*General Directorate of Mineral Research and Exploration, Department of Geology Research. 06800, Ankara, Turkey. orcid.org/0000-0002-5185-9697*
[b]*General Directorate of Mineral Research and Exploration, Department of Geology Research. 06800, Ankara, Turkey. orcid.org/0000-0001-5199-0225*
[c]*General Directorate of Mineral Research and Exploration, Department of Geology Research. 06800, Ankara, Turkey. orcid.org/0000-0003-2470-1496*
[d]*General Directorate of Mineral Research and Exploration, Department of Geology Research. 06800, Ankara, Turkey. orcid.org/0000-0002-5362-4859*
[e]*General Directorate of Mineral Research and Exploration, Department of Geology Research. 06800, Ankara, Turkey. orcid.org/0000-0001-5711-6854*
[f]*General Directorate of Mineral Research and Exploration, Department of Geology Research. 06800, Ankara, Turkey. orcid.org/0000-0003-3347-0335*

Research Article

Keywords:
Fluvial, Lagoon, Shoal-water delta, Forced regression, Planktonic foraminifera.

ABSTRACT

Early–middle Miocene reefal limestones are overlain disconformably by late Serravallian–early Tortonian incised valley-fill deposits of Dağpazarı formation in the Mut Basin. Dağpazarı formation is composed of mudstone, siltstone, sandstone and conglomerates. Facies associations of the formation are: fluvial, lagoon, shoal-water delta, shoreface, beach and barrier island deposits. Loxoconcha tumida Brady and *Loxoconcha* sp. in the gray mudstones indicate the freshwater influence and decrease in salinity. *Hemicyprideis* sp. documents brackish water conditions. The shoreface sandstones alternating with the lagoonal mudstones, and oyster-rich beach deposits in different levels of the sequence indicate episodes of marine connections. The age of the Dağpazarı formation is provided by the planktonic foraminifera from the marine mudstones and marls below and above the formation, and corresponds to the MMi8–MMi10 biostratigraphic interval, which spans the late Serravallian–early Tortonian. Late Serravallian eustatic sea-level fall caused to the quick shallowing of the Mut Basin and subaerial exposure of the reefal limestones at the basin margin. Thus, the incised valley, formed upon the reefal limestones of the Mut formation. This incised valley reflects a regional forced regression and unconformity. The Dağpazarı formation was deposited within this incised valley following an early Tortonian relative sea-level rise.

Received Date: 14.04.2018
Accepted Date: 20.06.2018

1. Introduction

The Mut Basin in the Central Taurides consists of Oligo-Miocene terrestrial and marine deposits. In the basin, lacustrine carbonates and fluvial sediments have been deposited during the Oligocene-early Miocene time. Although the marine sequence of late Burdigalian-Tortonian age in the Mut Basin is mainly composed of reefal and platform carbonates, an unconformity reflecting a late Serravallian forced

Citation Info: Ilgar, A., Esirtgen, T., Hakyemez, A., Culha, G., Demirkaya, S., Türkmen Bozkurt, B. 2019. The control of sea-level changes on sedimentation in the Mut Basin: Late Serravallian-Early Tortonian incised valley-fill. Bulletin of Mineral Reserach and Exploration, 159, 1-27. *http://dx.doi.org/10.19111/bulletinofmre.501543*

* *Corresponding author: Ayhan ILGAR, ayhan.ilgar@mta.gov.tr*

regression can easily be defined because the Miocene sedimentary sequence of the Mut Basin contains well preserved sedimentary records of the relative sea level changes.

Mudstones, sandstones and conglomerates outcropping in vicinity of the Dağpazarı village in north of Mut, located on reefal limestones of the Mut formation (Figure 1) were studied and mapped as the Köselerli formation by Gedik et al. (1979). However, these rocks, which reflect terrestrial and transitional environments, were defined as the Sertavul formation by Demir (1997) as they differ from the Köselerli formation in terms of lithology, depositional environment and age. Sertavul formation reflects back-reef lagoon environment and

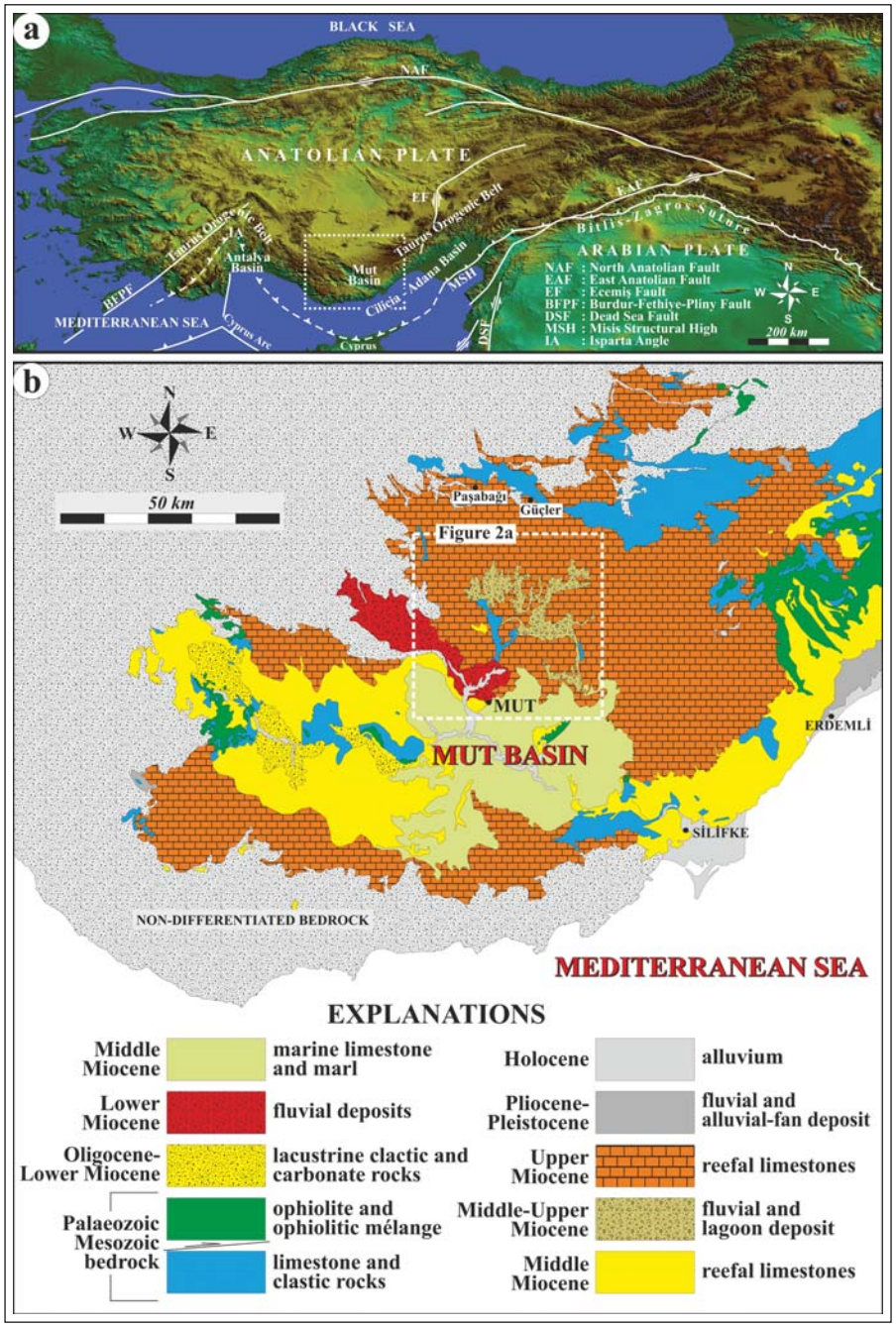

Figure 1- Location map of the study area, (a) location of the Mut Basin and main tectonic lines are seen on the topographical image of Anatolia (SRTM in 90 m resolution, from Jarvis et al., 2008), (b) simplified geological map of the Mut Basin (from Şenel, 2002 and Ulu, 2002).

occasionally fluvial deposits, coastal sands, coals and limestones (Demir, 1997). The same rock assemblage was defined by Atabey et al. (2000) as the Dağpazarı formation and interpreted as products of the back-reef lagoon and alluvial fan environments. According to Atabey et al. (2000), the Dağpazarı formation is a transitional unit with Mut and Köselerli formations, and was deposited during a regressive phase. Bassant et al. (2005) document the early-middle Miocene sea level changes in the Mut Basin, but they did not present data on regional exhumation related to these changes. Although Cipporalli et al. (2013) did not traced sea level changes in the basin, they argued that there should be effects of sea level changes in the stratigraphic sequence.

The Dağpazarı formation, which is the subject of this study consists of clastic terrestrial and transitional facies, and disconformably overlies the reefal limestones of the Mut formation. This erosional surface forms a negative paleotopographic depositional environment within the Mut formation. The boundary between the Mut and Dağpazarı formations also reflects abrupt facies changes in the stratigraphic sequence, and a basinward erosional shift of the late Serravallian shoreline and the forced regression. Occurrence of proximal facies over distal facies across an erosional surface constitutes the most important defining criteria for incised valleys (Zaitlin et al., 1994; Hampson et al., 1997). The Dağpazarı formation shows the deposition in an incised valley according to its stratigraphic and facies characteristics. This incised valley and valley fill represents the most important records of relative sea level change occurred in the Mut Basin during the late Serravallian-early Tortonian.

Incised valley fills are important deposits in stratigraphic sequences, because these valley fills are depositional complex and represent both the formation of the valley and the deposition of sediments in the formed valley (Boyd et al., 2006). The formation of these deposits is controlled by the interaction between sea level changes, tectonism, climate, sediment discharge into the basin and paleogeomorphology (Posamentier and Vail, 1988). Therefore, the identification of these deposits in stratigraphic sequences is of great importance for interpretation of stratigraphic relationships, paleogeographic reconstruction and understandings of depositional evolution (Archer and Feldman, 1995; Boyd et al., 2006).

The aim of this study is to explain the geological history of the late Serravallian-early Tortonian sea level changes in the Mut Basin and to discuss the relative roles of processes such as eustatic, local tectonic and the amount of sediment transportation that control these changes. For this purpose, the sedimentary facies analysis of an incised valley fill sandwiched between Miocene marine carbonates analyzed and dated with paleontological data.

2. Terminology

The sedimentological terms used in this study were described according to Harms et al. (1975, 1982) and Collinson and Thompson (1982). For the identification of planktonic foraminifer species, Kennett and Srinivasan (1983), Iaccarino (1985) and Bolli and Saunders (1985) were used. In biozone definitions, Sprovieri et al. (2002) and Iaccarino et al. (2007)'s "Mediterranean Planktonic Foraminiferal Biostratigraphy" was taken as the basis and biostratigraphic age was evaluated according to ATNTS2004 (Lourens et al., 2004) scale (Lourens et al., 2004).

The term "regression" denotes seaward displacement of shoreline and this leads to an increase in land areas (Posamentier and Vail, 1988; Posamentier et al., 1992). Regression reflects the interplay between the relative sea-level change and the supply of sediment to the shoreline. This interaction causes normal or forced regression (Posamentier et al., 1992; Posamentier and Morris, 2000). Normal regression refers to the shoreline displacement towards the sea due to high sediment supply during a relative sea-level stillstand or slow rise. The forced regression means the basinward shoreline displacement due to relative sea-level fall. The amount of sediment supply to the shoreline during the forced regression is not significant. The forced regression occurs due to eustatic sea level fall or a tectonic uplift.

An incised valley is a bigger, longer topographic depression than a single river channel excavated by fluvial erosion. Abrupt facies changes occur basinward along the bottom of these valleys (Zaitlin et al., 1994). Incised valleys are filled with sediments transported from rivers and seas (Dalrymple et al., 1992; 1994) and include deposits accumulated under the control of tidal, wave and fluvial processes.

The terminology of sequence stratigraphy was used as suggested by Catuneanu (2006). A relatively

conformable succession of genetically related strata bounded by unconformities are called as sequence (Mitchum, 1977). Each sequence is composed of system tracts and parasequences. A conformable succession of genetically related strata bounded by transgression surfaces form parasequences

In this study, three different system tracts were defined as; the "forced-regressive systems tract", "lowstand systems tract" and "transgressive systems tract". System tracts were defined according to the vertical stacking pattern of the sedimentary facies associations and the direction of displacement of the palaeoshoreline (Helland-Hansen and Martinsen 1996). The "forced-regressive systems tract" occurs during a relative sea level fall. The "lowstand systems tract" is a normal regressive coastal progradation deposited during a relative sea level fall and then remains stable. The units deposited during the rise of the relative sea level constitute the "transgressive systems tract".

3. Regional Geological Setting

The Taurides located in the eastern Mediterranean part of the Alpine-Himalayan mountain belt and the southern part of Turkey are studied by dividing them into three sections as; the West, East and the Central Taurides (Figure 1a). The Western Taurides extend from the Isparta Angle to the west towards the Hellenides. The Central Taurides are between the Isparta Angle and Ecemiş Fault. The Eastern Taurides extend from the Ecemiş Fault to the east into the Zagros Mountains. The orogeny forming Taurides continued until the end of Eocene in the Central Taurides (Şengör, 1987; Clark and Robertson, 2002). However, the compressional tectonics, indicating the latest movement of nappes, has continued until middle Oligocene (Kelling et al., 1987; Andrew and Robertson, 2002). In the Eastern Taurides, the orogenic deformation has continued until the late Miocene and the Misis Structural Uplift has been formed due to the folds and thrusts (Michard et al., 1984; Aktaş and Robertson, 1990; Dilek and Moores, 1990; Yılmaz, 1993; Yılmaz et al., 1993; Robertson, 2000; Sunal and Tüysüz, 2002). At the transition of the Western and Central Taurides, the Lycian Nappes collided with the Isparta Bend (Collins and Robertson, 1998, 2000; Poisson et al., 2003; Sagular and Görmüş, 2006). The Miocene thus saw the last stages of localised compressional deformation, while the Taurides in general had already become subject to post-orogenic isostatic uplift and crustal extension with the development of orogen-collapse basins (Seyitoglu and Scott, 1991, 1996; Jaffey and Robertson, 2005; Karabıyıkoğlu et al., 2005; Bartol et al., 2011; Koç et al., 2012; Cosentino et al., 2012). This orogen-collapse basins occurred in the form of grabens. The continental crust, which has excessively thickened during the Eocene period, caused the formation of the basin under the effect of gravity due to the disappearance of compression (Gautier et al., 1999; Dilek and Whitney, 2000). According to Le Pichon and Angelier (1981) and Gautier and Brun (1994), the extensional tectonic regime was formed by the back-arc spread as a southern retreat process of the northerly subducting Hellenic plate.

4. Dynamic Stratigraphy of the Mut Basin

The Mut Basin (Figure 1), located in Central Taurides, forms one of the molasse basins between the mountains during Neogene period. It is thought that Mut Basin was formed due to the orogenic collapse behind the extensional back-arc of the Cyprus arc in the south (Kempler and Ben-Avraham, 1987; Robertson, 2000; Kelling et al., 2001; Ünlügenç et al., 2001). The basin has then continued to develop under the influence of an extensional regime.

The bedrocks of the basin are Aladağ and Bozkır nappes emplaced in the late Eocene period (Özgül, 1976; Andrew and Robertson, 2002). The nappes are composed of Jurassic-Cretaceous limestones and Late Cretaceous ophiolitic melange (Figure 1b). These units are locally overlain by Eocene shallow marine limestones. Heavily eroded allochthonous bedrocks are overlain by the Oligocene lacustrine carbonates, which are called the Fakırca formation in the study area (Figure 2). These lacustrine units, which have limited lateral extent, form the initial productions of intramountain basins. Fakırca formation consists of thin to medium, planar to undulated bedded, planar parallel stratified and wave-rippled limestone and marl alternation. Pine needles, leaf fossils and *Planorbis* type gastropod fossils commonly observed in limestones and marls indicate the fresh water environment. Coal seams are observed at the bottom of the early-middle Oligocene Fakırca formation sequence (Tanar, 1989; Tanar and Gökçen, 1990).

Following the compressional tectonism that occurred towards the end of the middle Oligocene due to the latest movement of nappes the extensional

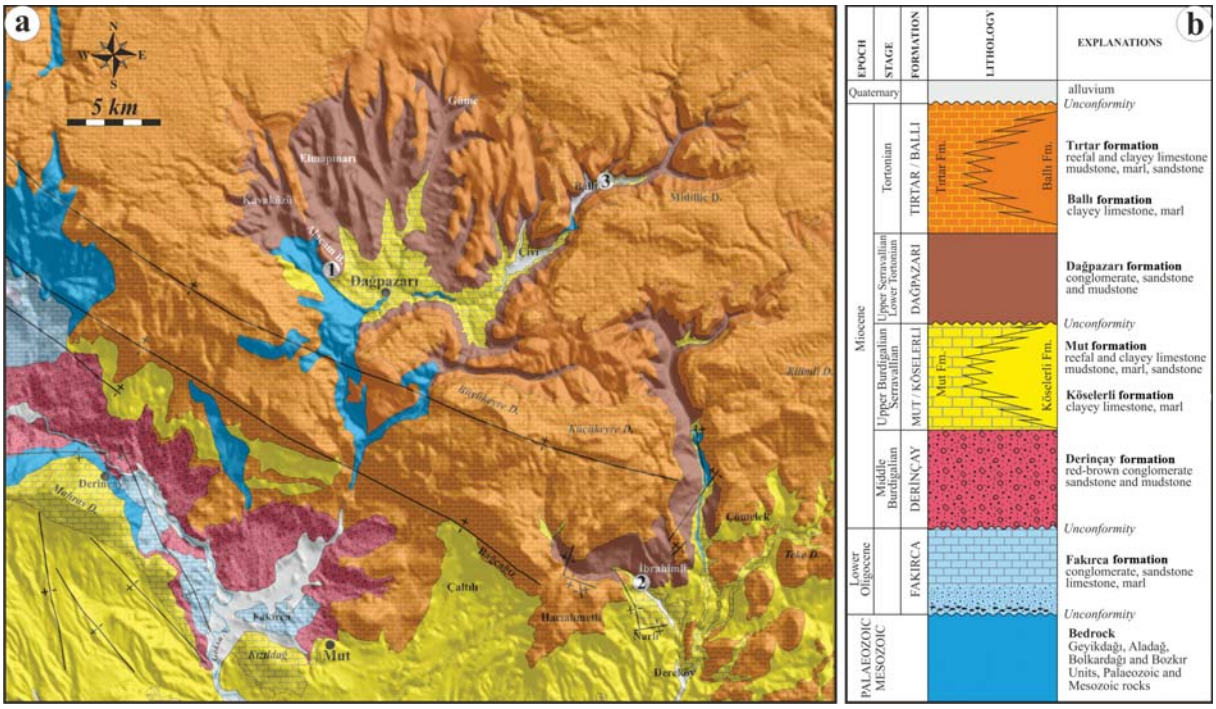

Figure 2- (a) Detailed geological map of the study area in the Mut Basin and the distribution of the Dağpazarı formation. Numbers 1-3 on the map indicate the section localities. 1. Alaçamburnu section, 2. İbrahimli section and 3. Ballı section, (b) Generalized stratigraphical section of the Mut Basin.

tectonic regime in the region has been dominant and the structural development of the basin was established. Due to continuous sedimentation in post Oligocene in the Mut Basin, the fluvial sediments of the Derinçay formation were unconformably deposited on the Fakırca formation in the early-middle Burdigalian period (Ünay et al., 2001) (Figure 2; Ilgar et al., 2016). Derinçay formation consisting of red conglomerate, sandstone and mudstone reflects the channel lag, sigmoidal point bar and flood plain deposits of a meandering river system. The marine transgression, which occurred in the late Burdigalian led to the drowning of Antalya, Mut and Adana basins and the development of the first marine deposition during the Neogene period in these basins. Thus, the reefal limestones, platform carbonates and the marl to thin bedded limestone forming the sediments of the Köselerli formation were deposited in the late Burdigalian–Serravallian (Figure 2). The shallow marine carbonate deposits of the Mut formation (Figure 3a), which forms onlapping structure due to the marine transgression on bedrocks towards the north (Figure 3a), pass into offshore deposits of the Köselerli formation towards south in the basinward direction (Figure 3b).

The relative sea level fall in the late Serravallian period led to the shoaling of the basin, migration of the reefal limestones of the Mut formation on to the Köselerli formation in basinward direction and to crop out on the basin margin. The sedimentary facies belonging to the Dağpazarı formation, which is the subject of this study, were deposited in an incised valley generated during this forced regression (Figure 2). The early Tortonian transgression caused the re-flooding of the northern parts of the Mut Basin and the deposition of the reefal limestones of the Tırtar formation on basin margins and the marl to thin bedded limestones of the Ballı formation inside the basin (Figure 3c). In the late Tortonian, the marine sedimentation in the Mut Basin terminated with the isostatic uplift of the Taurides and the basin began to expose (Cosentino et al., 2012; Ilgar et al., 2013*a, b*).

5. Dağpazarı Formation and its Sedimentary Facies

The Dağpazarı formation mainly composed of mudstone, sandstone and conglomerate outcropping in the north of Mut Basin is located between the reefal limestones and carbonate platform deposits of the Mut and Tırtar formations and observed in the form of incised valley fill deposits in the reefal limestones of the Mut formation (Figure 3c). The Dağpazarı formation, which is defined within belt in the north-

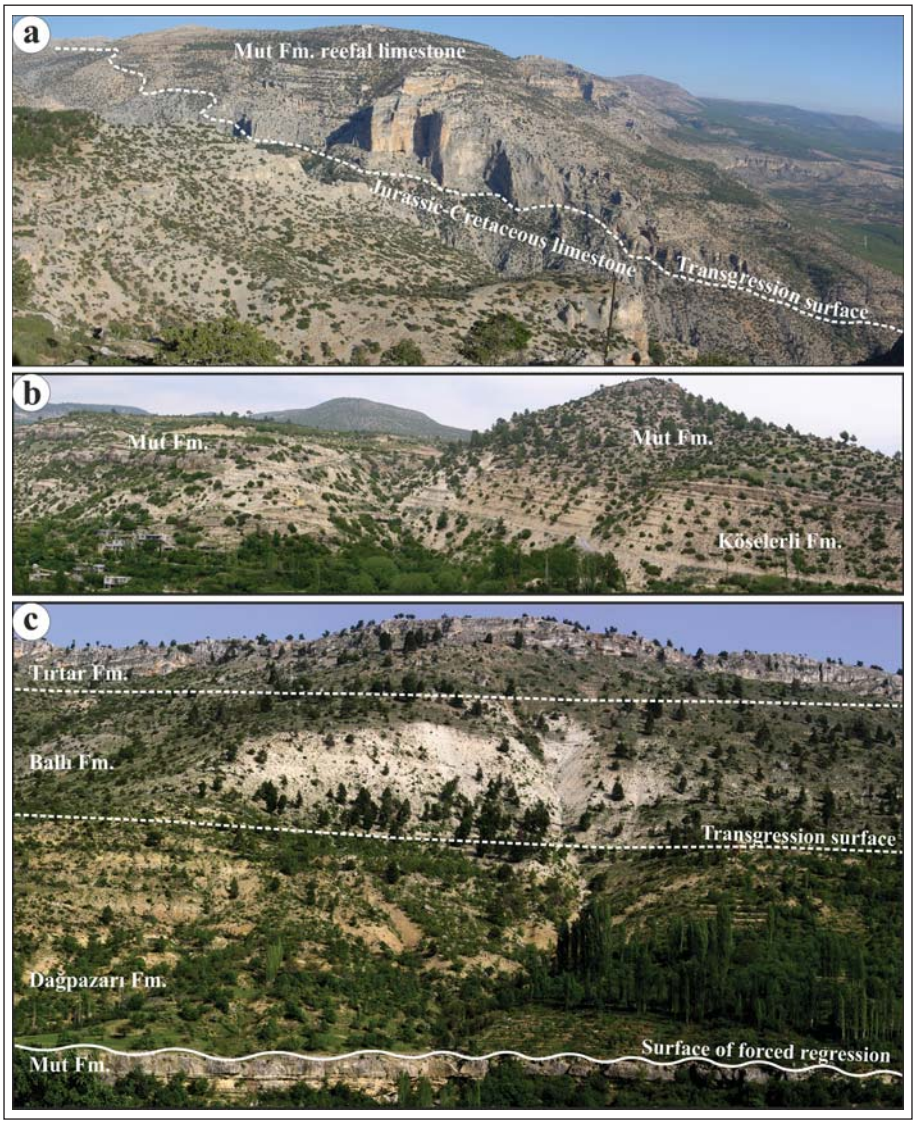

Figure 3- (a) Reefal limestone beds of the Mut formation onlapping on the basement rocks consisting of Jurassic-Cretaceous limestones, (b) Gradational transition of the Mut formation into marl-fine bedded limestones of the Köselerli formation in the basinward direction. (c) The stratigraphical relations of the Mut, Dağpazarı, Ballı and Tırtar formations around Dağpazarı Village in the north of Mut. The fluvial deposits of the Dağpazarı formation unconformably overlie the Mut formation.

south direction, consists of several branches to the north of the basin. The valley fill is approximately 35 km long, 0,5-2 km wide and 130 m thick.

The Dağpazarı formation unconformably overlies the reefal limestones of the Mut formation or shoreface sandstones and shell-rich fossilliferous pebbly beach deposits which is occasionally observed at the topmost layer of the formation. It is transgressively overlain by the reefal limestone, shoreface sandstone and pebbly beach sands of the Tırtar formation and marl to thin bedded limestones of the Ballı formation (Figure 3c).

At the Alaçamburnu locality, 2,5 km to the northwest of the Dağpazarı village is the type section of the formation (Figures 2a and 4a). The surround of Çivi and Ballı villages (Figure 2a) and the north of the Büyükeyre Mountain (Figure 3c) in the study area allow to observe the contacts with underlying Mut formation and the overlying Ballı and Tırtar formations.

The Dağpazarı formation is mainly composed of dark gray mudstone, light brown-brick red mudstone and siltstone, very fine to fine grained sandstone and medium to coarse grained sandstone and granule to fine

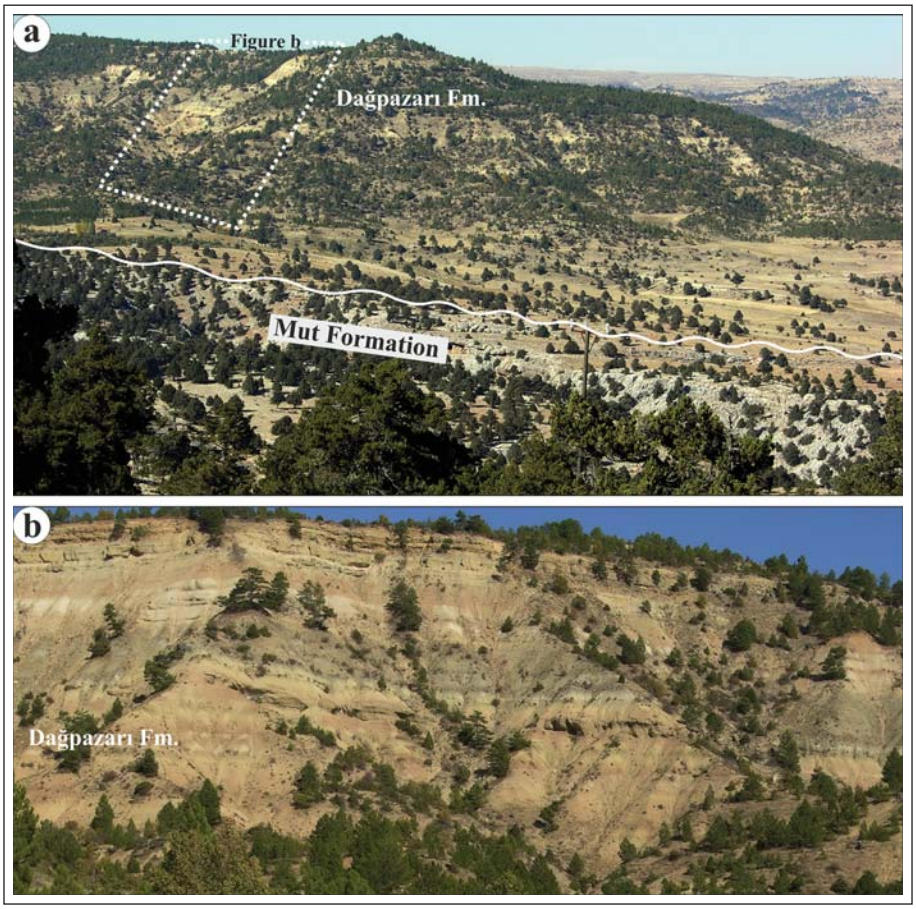

Figure 4- (a) The Alaçamburnu type section where the facies defined in the Dağpazarı formation are best observed. (b) Close-up view of the Alaçamburnu section. The fluvial, shoal water delta, lagoon, shoreface and beach facies associations were defined in this section.

pebble size conglomerate (Figures 4b and 5). In this formation, total of 6 facies associations were defined as fluvial, shoal water delta, lagoon, shoreface, beach and barrier island (Figure 5). These facies associations, which are lateral and vertical transitional, have variable lateral extent and thicknesses and are repeated several times in the succession. Since each facies association reflects the depositional environment and conditions, it is described under the headings of the environments and described below in detail.

5.1. Fluvial Deposits

The fluvial deposits defined in the Dağpazarı formation are mainly composed of pale brown-brick red mudstone, siltstone, sandstone and gray-pale brown sandstone, pebbly sandstone and conglomerate. Gray sandstones and conglomerates consist of bedsets which have maximum thicknesses of 2,5 m and do not have lateral continuity. These bedsets are located on pale brown-brick red mudstones and siltstones with a sharp and erosional bottom contact (Figure 6a). The amount of erosional relief reaches up to 1 m. The upper surfaces of bedsets are planar or undulatory. Chutes are often observed at the bottom of these deposits. These gray sandstone and conglomerate bedsets show thinning and fining upward units (Figure 6a). These sandstones and conglomerates, which have the main sedimentary structures of planar inclined or sigmoidal beds, are interpreted as meandering river deposits (Figure 6a). Pale brown-brick red, thin bedded mudstones and siltstones alternating with meandering river deposits form floodplain deposits (Figure 6a and b). These facies grades each other within vertical succession and alternates. Sedimentological characteristics of the meandering river and flood plain deposits are mentioned below.

5.1.1. Meandering River Deposits

The meandering river deposits described in the Dağpazarı formation are composed of the channel lag

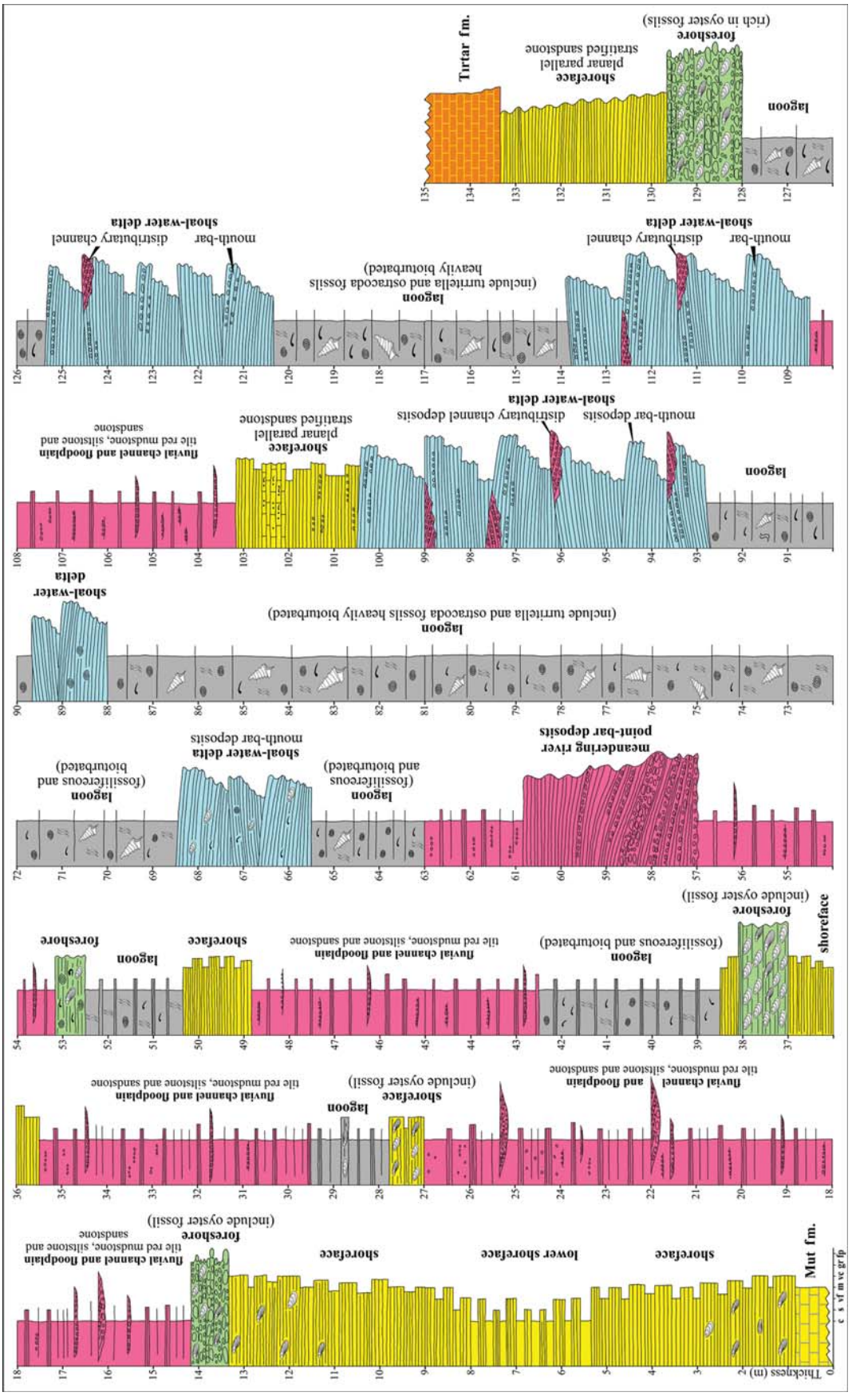

Figure 5- Sedimentological section of the Dağpazarı formation (section locality is seen in Figure 2a) and facies associations defined on this section.

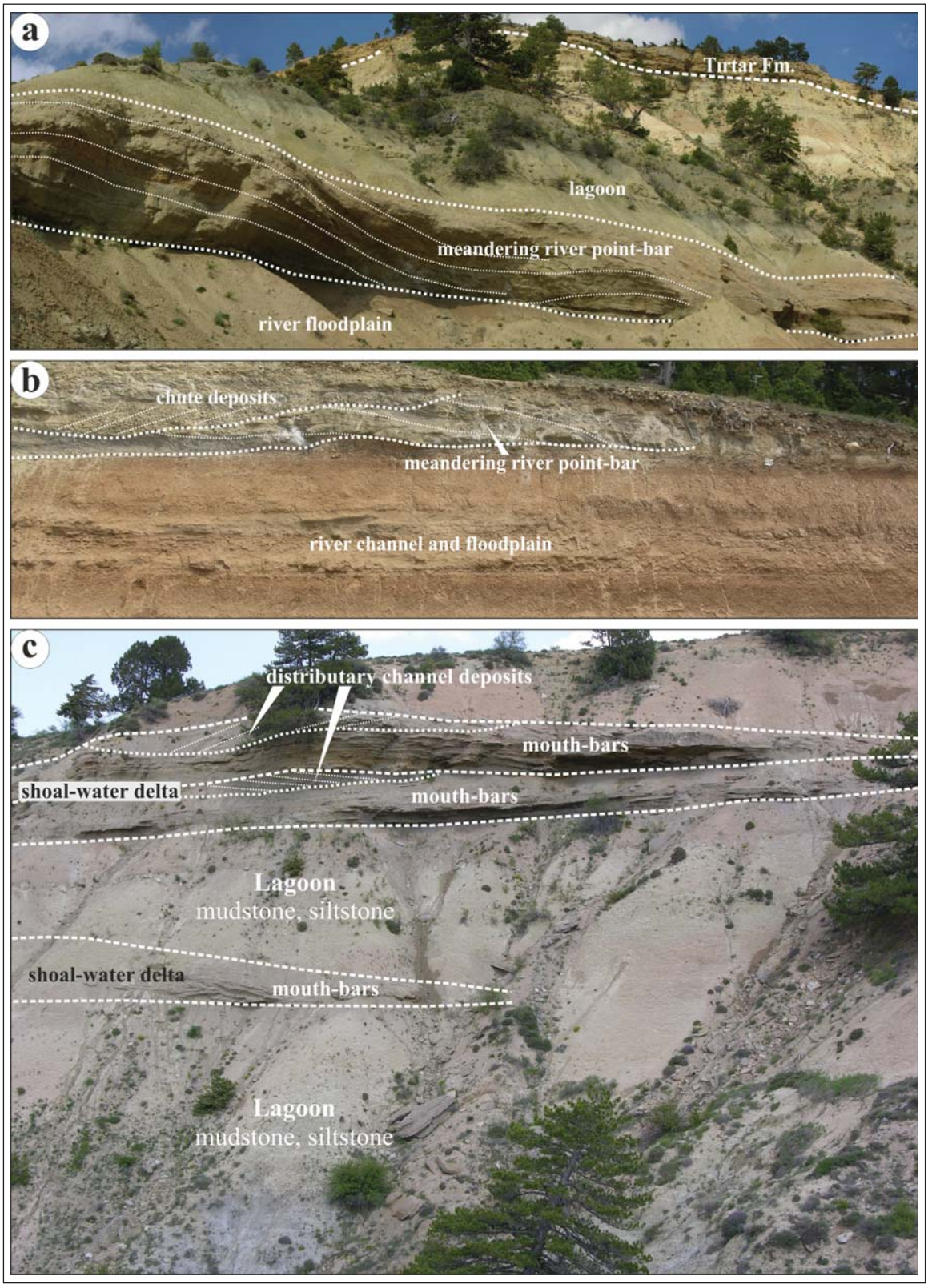

Figure 6- (a) Pale brown-brick red flood plain and meandering river point bar deposits composed of conglomerates and sandstones which are overlain by lagoon deposits. (b) River channel and flood plain deposits and meandering river point bar deposits, and overlying planar cross stratified chute deposits. (c) Shoal water delta deposits alternating with gray lagoonal mudstones. These deposits consists of distributary channel deposits and mouth bars.

deposits stored within the stream channel and point bar and chute sediments on them (Figure 6a, b).

The channel lag deposits (Miall, 1985; Nemec and Postma, 1993) are observed on the pale brown-brick red mudstones, siltstones, sandstones of the flood plain deposits or at the bottom of channels. These are isolated beds of pebble conglomerates, which have erosional bottom surface, and are laterally discontinuous. These small-medium pebble conglomerates have clast-supported, cobbly framework filled with medium to very coarse sand, granules. Point bar deposits are located above the channel floor lag deposits (Figures 5 and 6a, b).

Point bar deposits in cross sections are formed by sandstones, pebbly sandstones or conglomerates in planar inclined or sigmoidal geometry (Figure 6a, b). These deposits, which are formed by these planar dipping beds, has 1-2,5 m set heights and 10°-20° dip angles. The dip angles of sandstones with sigmoidal geometry decrease both in upward and downward slopes and tangentially pass to the channel lag (Figure 6a). These layers are planar parallel and planar cross stratified. The current ripples can also be seen in upward slopes of sandstones. The superimposed channel deposits in the sequence are separated from each other by erosional surfaces. These channel deposits also consist of planar inclined deposits at different dip amounts and directions.

At the uppermost part of horizontally inclined sandstones and conglomerates, channel deposits up to 50 cm at thick and 3 m in width take place (Figure 6b). These channels with erosional bottom surfaces were developed diagonally in the dip direction of horizontal dipping layers. Channel deposits consisting of small pebbly conglomerate and coarse grained sandstones are generally planar cross-stratified (Figure 6b).

Horizontally inclined bedded or sigmoidal point bar sediments defined in the meandering river deposits were interpreted as the meander-belt sediments that have been formed by lateral accretion due to the migration of river channels in lateral direction (Jackson, 1976; Nanson, 1980; Brierley, 1991). In upper levels of the point bar deposits planar to cross stratified and current rippled sandstones were formed due to bedload transportation. The channel lag deposits located below the point bar deposits and on the basal erosional surface are associated with laterally migrating channel bottom (Ghinassi et al., 2014). Small channellized deposits on top of point bars were interpreted as chute channel deposits. Chute deposits represent erosion and filling deposits formed during flood periods of the river (Mc Gowen and Gamer, 1970). The cross bedded sandstones deposited in chutes form chute bars deposited in the downstream side of bars (McGowen and Gamer, 1970; Ghinassi et al., 2014).

5.1.2. Flood Plain Deposits

Flood plain deposits associated with bar and chute deposits of the meandering rivers in stratigraphic succession consist of pale brown-brick red mudstone, gray siltstone and very fine to fine grained sandstones (Figures 5 and 6b). Massive mudstones form the dominant lithology of the succession. Very thin bedded siltstones and sandstones alternate with mudstones. These deposits are planar parallel stratified and are laterally widespread.

This facies association reflects sediments deposited on flood plains of meandering rivers (McGowen and Gamer, 1970). Planar parallel stratified sandstones and siltstones are the products of sedimentations that occurred at upper flow regime during floods (McGowen and Garner, 1970; Miall, 1985). The energy decrease in the non-channelized sheet-floods caused the deposition of mudstone from suspension (Collinson, 1996; Tooth, 1999).

5.2. Lagoon Deposits

Lagoon deposits alternating with fluvial, shoreface, beach and shoal water delta sediments in the succession mainly consist of yellowish-dark gray mudstone, siltstone and very fine to fine grained sandstones (Figure 5 and 6c). Massive mudstones are the dominant lithology of the succession. Mudstones alternate with very thin bedded siltstones and very fine grained sandstones. These deposits are rich in ostracod fossils and occasionally Ostrea fossils are observed. Because of dense bioturbation, the lamination or other sedimentary structures have not been generally preserved.

Ostracod species such as; *Loxoconcha tumida* Brady and *Loxoconcha* sp. in gray mudstones in the formation (Figure 7) indicate the fresh water entrances into the depositional environment, *Hemicyprideis* sp. on the other hand reflects brackish water conditions. The shoreface sandstones and oyster-rich beach deposits defined at different levels of the succession indicate the marine connections from time to time. The fossils of *Acanthocythereis hystrix* (Reuss),

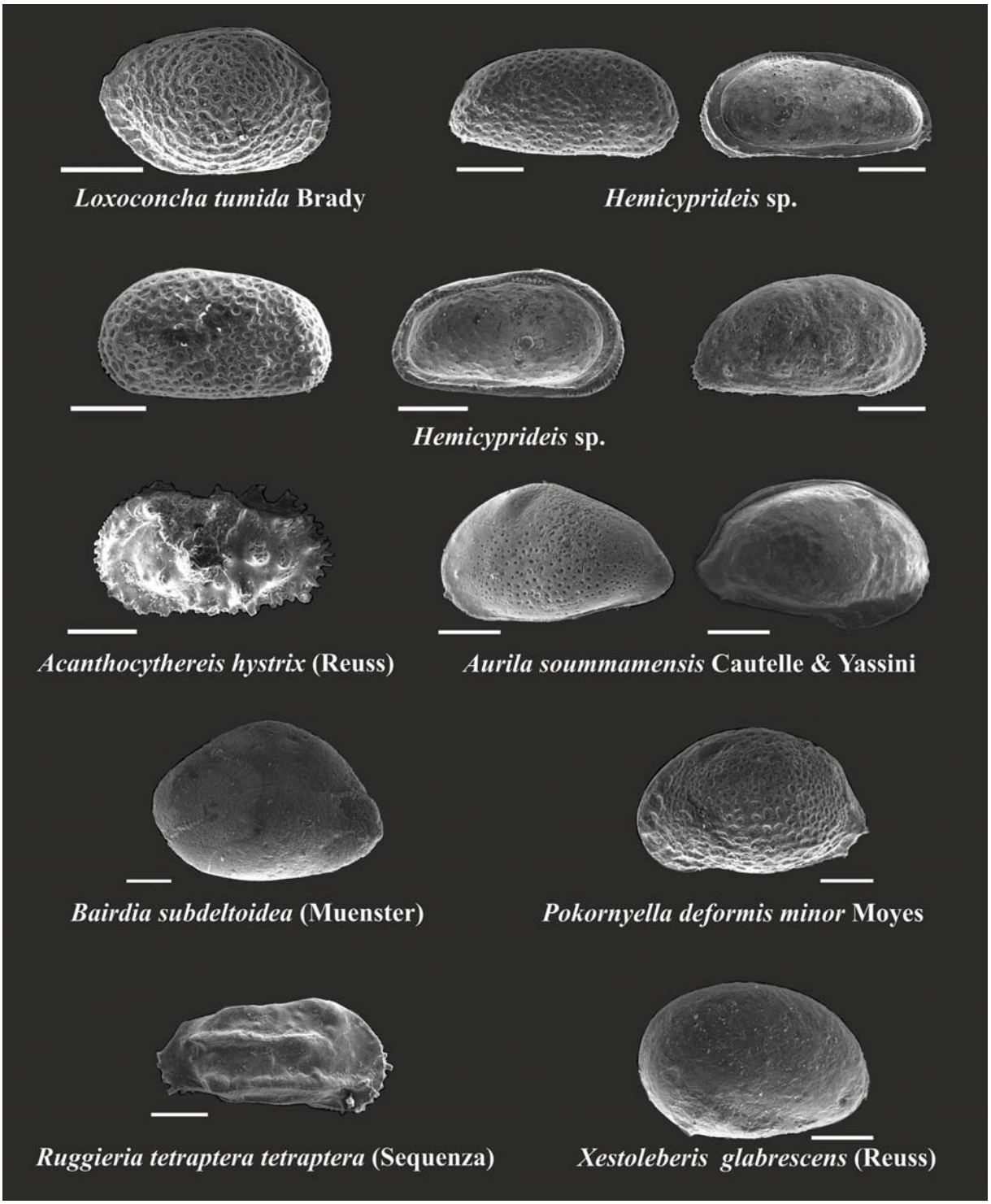

Figure 7- Ostracod species described in lagoonal mudstones of the Dağpazarı formation. Ostracod species such as *Loxoconcha tumida* Brady and *Loxoconcha* sp. reflect freshwater recharge into the depositional environment and the reduction in salinity, and *Hemicyprideis* sp. indicates the brackish water conditions. Fossils of *Acanthocythereis hystrix* (Reuss), *Aurila soummamensis* Cautella and Yassini, *Bairdia subdeltoidea* Müenster, *Paracypris polita* Sars, *Pokornyella deformis minor* (Moyes), *Ruggeria tetrateptera tetrateptera* (Sequenza), *Xestoleberis glabrescens* (Reuss) indicate that the depositional environment has sometimes marine connections. Bar scale 200 μm.

Aurila soummamensis Cautella and Yassini, *Bairdia subdeltoidea* Müenster, *Paracypris polita* Sars, *Pokornyella deformis minor* (Moyes), *Ruggeria tetrateptera tetrateptera* (Sequenza), *Xestoleberis glabrescens* (Reuss) also support that the depositional environment has sometimes connection with marine environment (Figure 7).

The lagoon deposits represent the sediments deposited in protected areas against the effects of wave and storm by limiting the open-marine connection due to the development of a barrier island.

5.3. Shoal Water Delta Deposits

The shoal water delta deposits are mainly composed of medium to very coarse grained sandstones (Figures 5 and 6c) with granule and fine pebbles. Deltaic deposits located on lagoonal mudstones with a sharp contact relationship form thickening and coarsening upward successions (Figures 5 and 6c). The shoal water delta deposits have 1,5-2 m thickness and 50-100 m lateral continuity. In these deposits, the beds becomes thinner and finer both downdip and laterally, and the delta passes into other deposits (Figure 6c). The sandstone beds are gently sloping (<10°) in both directions and display a lenticular package (Figure 6c). Each delta deposit is composed of distributary channel and mouth bars (Figures 5 and 6c). Similar delta deposits form delta package nearly in 5–8 meters thickness which developed on each other with lateral displacements (Figure 5). The displacement of shoal water deltas in lateral and vertical directions in delta packets is related with the stillstand or increasing relative water level. In case of stable water level, the deltas migrate laterally and when the water level increases the delta packets stacked upon one another. These delta packets are overlain by lagoonal mudstones or river flood plain deposits.

5.3.1. Mouth Bar Deposits

These mound-shaped mouth bar deposits are 1,5–2,5 m thick, typically thickening and coarsening upwards (Figure 5 and 6c). These sequences are composed of medium to very coarse grained sandstones, granules and very fine pebbly conglomerates. Among mouth bar successions, which are located in vertical or lateral directions, there are inclined erosional surfaces. Sandstones beds forming the mouth bar deposits have 5-25 cm thick. Sandstones are generally planar parallel stratified and rarely current and wave rippled cross stratified. Within sandstones, occasionally the granule-fine pebble layers parallel to stratification are observed. Conglomerates defined in mouth bar deposits have a thickness of 5-35 cm and consist of alternation of granule-fine pebbly conglomerate. Conglomerates, which have grain supported textures, are mostly planar parallel stratified. The grain sizes of sandstones and conglomerates forming the mouth bars decrease both laterally and towards basin, and the layer thickness becomes thinner and wedges out (Figure 6c). Thus, these rocks tend to form downlap structures on the beds below.

The sandstones forming the mouth bars were originated by stream frictional effluent (Wright, 1977). Thus, the planar parallel stratified sandstones and current ripples were formed. The wave ripples observed on sandstones are the products of wave activity developed after deposition. Similar mouth bar deposits developed in shoal water deltas were also defined by Ilgar and Nemec (2005), Leszczyński and Nemec (2014) and Ilgar (2015). Most of the mouth bar deposits are erosionally overlain by distributary channel deposits. In some of them, granule-fine pebbled, planar parallel stratified, well sorted beach deposits take place (Bluck, 1967, 1999). Beach deposits indicate that mouth bar and distributary channel deposits were reworked by wave activities (Ilgar, 2015).

5.3.2. Distributary Channel Deposits

Channel deposits, which are located in axial sections of the mouth bar bodies and have concave erosional bottom surfaces, form the distributary channel deposits of the shoal water deltas (Figure 5 and 6c). Distributary channel deposits consist of grain supported, medium sorted, semi rounded-rounded granule and fine pebble conglomerates. Distributary channel deposits, which are as solitary channel and form a fining upward sequence, have a thickness of 30-80 cm and maximum width of 5 m (Figure 6c). Medium to coarse pebble conglomeratic layers interpreted as the channel bottom lag deposits are observed at the erosional bottom surfaces of distributary channel deposits (Miall, 1985; Nemec ve Postma, 1993). Alternation of planar cross stratified granule-fine pebble conglomerate takes place on the channel bottom lag deposits. Planar cross stratified conglomerates are 25-60 cm high and reflect the transverse or mid channel bar deposits of the braided rivers (Miall, 1985).

5.4. Shoreface Deposits

Shoreface deposits consist of yellow-gray sandstones and very few amounts of siltstone and mudstones (Figures 5 and 8a). Well sorted, medium to coarse grained sandstones forming the shoreface facies are 15-50 cm thick and are laterally continuous. Sandstones, which have a sharp bottom contact, have horizontal lower boundary and planar to undulatory upper boundary. Planar parallel stratification or wave ripples in less amounts form main sedimentary structures of the sandstones (Figure 5 and 8a). Sandstones are rich in Ostrea (Figure 8b) and shells are observed in occasion (Figure 8c). The first shoreface deposits located over the Mut formation are quite rich in broken coral fragments. Some levels are formed by fully intricate, well developed coral fragments (Figure 8d).

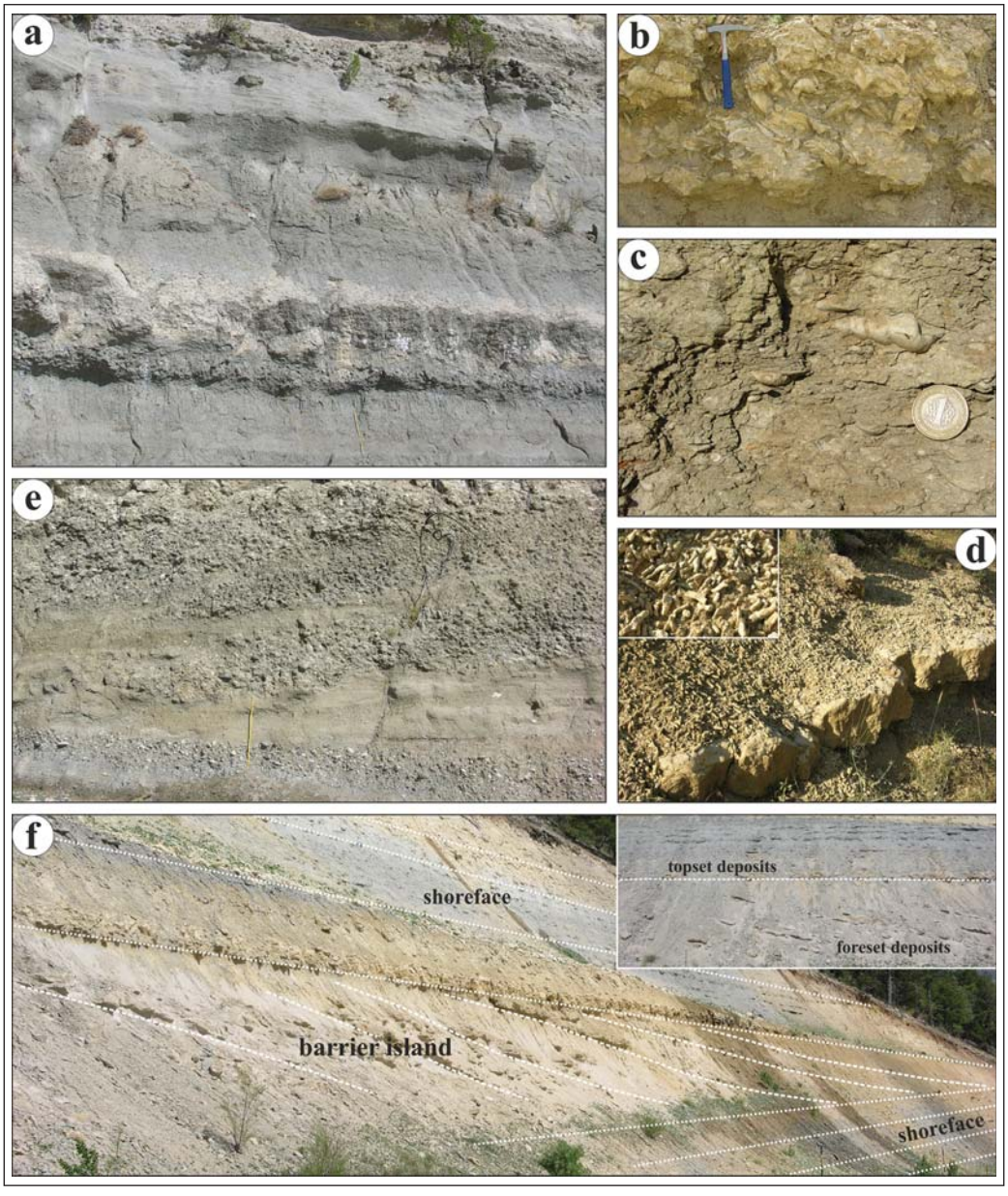

Figure 8- (a) Gray colored, planar parallel stratified shoreface sandstones defined in the Dağpazarı formation. (b) Sandstones are rich in ostrea fossils, (c) they also contain mollusc fossils in places. (d) Shoreface sandstones defined just on top of the Mut formation is quite rich in fragmented reef fossils. (e) Beach conglomerates which are laterally and vertically transitional with shoreface sandstones. (f) Barrier island deposits downlapping basinward defined between planar parallel stratified shoreface sandstones.

In intermediate levels of this shoreface deposit (Figure 5 between 5,5-8 m) very fine grained sandstone, siltstone and mudstone alternations take place. Thinly stratified (1-20 cm) sandstones and siltstones are laterally continuous. The upper boundaries of sandstones, which have a sharp and horizontal bottom contact on mudstones, are planar or undulatory. Well sorted sandstone and siltstone layers are normal graded, planar parallel stratified and wave rippled. Gray mudstones alternating with sandstones and siltstones are laterally continuous. Mudstones have massive appearance due to bioturbations. Shoreface sandstones are both laterally and vertically transitional with beach conglomerates.

Planar parallel stratified and wave rippled, medium to coarse grained, amalgamated sandstones indicate the deposition in the upper shoreface environment on the normal wave base (Walker and Plint, 1992; Ainsworth and Crowley, 1994). Mud sedimentation and preservation is difficult in this environment. The alternation of thin bedded sandstone, siltstone and mudstone defined in the shoreface succession indicate the sedimentation transported at certain time intervals such as the stormy periods in stable conditions. While the muds were deposited in normal conditions, the silt and other sand size grains were transported into the environment due to stormy conditions (Hunter and Clifton, 1982; Walker, 1984; Walker and Plint, 1992). This depositional environment indicates the lower shoreface environment at the normal wave base boundary or the offshore transition environment just below that environment (Ainsworth and Crowley, 1994).

5.5. Beach Deposits

Beach deposits, which are defined in the Dağpazarı formation and generally alternated with shoreface sandstones, consist of sandstones and conglomerates. These sandstones and conglomerates are rich in ostrea and these fossils are observed as mounds in occasion (Figure 5). Granular conglomerates and 5-20 cm thick, coarse to very coarse grained interbedded sandstones are planar to parallel stratified (Figure 8e).

Conglomerates are small-medium pebble sized, mostly well sorted, well rounded, spherical pebbles (Figure 8e). The intergranular voids in grain-supported conglomerates are filled with coarse sand or granule. The parallel or low angle stratifications are observed due to grain size difference in conglomerates. Sandstone and conglomerate beds are inclined basinward at a very low angle (Figure 8e). Conglomerates have gradational or sharp contact relationship with the sandstone. The bed boundaries with sharp contacts are mostly erosional (Figure 8e). There are observed coarsening upward sequences in places where the sandstones gradually pass into conglomerates.

The characteristics features of this facies association reflect the deposition that had occurred in the beach environment (Bluck, 1967, 1999; Clifton, 1973; Massari and Parea, 1988; Postma and Nemec, 1990). Well-sorted and well-rounded conglomerates and the stratifications developed due to grain size differences indicate that pebbles were washed and reworked by the waves and storms during the deposition (Clifton, 1973; Postma and Nemec, 1990). Coarsening upward sequences in beach deposits indicate prograding beaches (Maejima, 1983; Nemec and Steel, 1984).

5.6. Barrier Island Deposits

The barrier island deposits are located between the horizontally bedded shoreface sandstones and mainly consist of sandstones, granule and very fine pebble size conglomerates in few amounts. Foresets inclined towards the basin and the overlying topsets form the barrier island deposits (Figure 8f). Foreset deposits formed by inclined beds have 3-6 m thickness. Medium to coarse sandstones show thickness of 20-50 cm. Their lower boundary surfaces are planar whereas the upper contact is either planar or undulating. Sandstones are mostly planar parallel and in addition planar cross stratified in few amounts. Foreset deposits have the slope angle of 20-50° and the layers tangentially pass into shoreface deposits below. The boundaries of these sandstones with topset deposits are mostly erosional. Small scale erosional surfaces are also observed in foreset deposits.

Foreset deposits are overlain by nearly 1 m thick topset deposit and generally consist of coarse grained sandstones and granular conglomerates. Topset deposits are not laterally continuous in transverse sections and thin out into shoreface sandstones (Figure 8f). Sandstone and conglomerate layers have the thickness of 10-30 cm and planar parallel or planar cross stratified.

Deposits forming the barrier island pass landward into lagoonal mudstones and to shoreface sandstones in basinward direction (Figure 8f).

Barrier island, lagoon and estuaries are the characteristic depositional systems of transgressive shores (Swift et al., 1991). Sediments transported by waves and longshore currents form the barrier island ridges by being deposited in the form of sand bars parallel to the shore. The deposition occurs by the upward growing of beaches and shoreface bars due to the sea level rise (Swift, 1975). Erosional surfaces defined in foreset deposits reflect abrasions that occasionally developed due to storm events. The cross stratifications defined in topset deposits are mega ripples formed by strong longshore currents (Nielsen et al., 1988). Barrier islands are not stable in places and migrate landward as the sea level rises (Swift et al., 1991).

6. Biostratigraphic Dating

In order to determine the age of the Dağpazarı formation, total of 19 samples collected from the İbrahimli Stratigraphic Section at the lower boundary and from the Ballı Stratigraphical Section at the upper boundary of the formation are analyzed based on the planktonic foraminiferal biostratigraphy (Figure 2a). Planktonic foraminifera of the İbrahimli section are recorded in marine mudstones of the lower boundary of the Dağpazarı formation that can be conformably correlated in the basin. Planktonic foraminiferal assemblages are also determined in the marl samples from the lowermost part of the Ballı formation which overlies the Dağpazarı formation. Thus, the Dağpazarı formation is dated based on the age data obtained from the upper and lower boundaries of the formation.

The planktonic foraminiferal fauna in both sections are similar in terms of species diversity whereas they are different each other in the number of individual (abundance) and degree of preservation (fossilization). The İbrahimli section is characterized by abundant and well-preserved assemblages (Figure 9, 1-20). On the other hand, it is observed that the dominant fossil group is benthic foraminifers and planktonic foraminifera is low abundant and moderately preserved in the Ballı section (Figure 9, 21-25).

The planktonic foraminiferal fauna is represented by 25 species in the 11 marl samples from the İbrahimli section. *Paragloborotalia siakensis* (LeRoy), *Pg. partimlabiata* (Ruggieri and Sprovieri) and *Neogloboquadrina acostaensis* (Blow) are identified in all samples, whereas *Paragloborotalia mayeri* (Cushman and Ellisor) is recorded in a few samples (İBR 3, 4, 8) and *Globigerinoides subquadratus* Brönnimann is only in one sample (İBR 1) (Figure 9). While, *Globigerinoides trilobus* (Reuss), *Gs. quadrilobatus* (d'Orbigny), *Gs. sacculifer* (Brady), *Globigerina bulloides* d'Orbigny, *G. falconensis* Blow, *Orbulina universa* d'Orbigny, *O. suturalis* Brönnimann, *Globigerinella obesa* (Bolli), *D. baroemoenensis* (LeRoy) are represented by a large number of specimens, *G. praebulloides* Blow, *G. occlusa* Blow and Banner, *G. ciperoensis* Bolli, *Gs. bulloideus* Crescenti, *Dentoglobigerina altispira* (Cushman and Jarvis), *Globoturborotalita decoraperta* (Takayanagi and Saito), *Glt. woodi* (Jenkins), *Globigerinita glutinata* (Egger), *Tenuitellinata angustiumbilicata* (Bolli), *Globorotalia scitula* (Brady) and *Globigerinella siphonifera* (d'Orbigny) are observed in fewer specimens (Figure 9).

The presence of *Neogloboquadrina acostaensis* (Blow) and *Paragloborotalia siakensis* (LeRoy), which are the characteristic species of MMi8 - MMi9 zonal interval, shows that the İbrahimli section is late Serravallian - early Tortonian in age (Figure 10; Sprovieri et al., 2002; Lirer et al., 2002; Hilgen et al., 2005; Lirer et al., 2005 Iaccarino et al., 2007). The other marker planktonic foraminiferal species, *Pg. partimlabiata* (Ruggieri and Sprovieri), *Pg. mayeri* (Cushman and Ellisor) and *Globigerinoides subquadratus* Brönnimann also support this age interval (Figure 10; Hilgen et al., 2003; Aguilar et al., 2004; Hilgen et al., 2005).

The 8 mudstone samples of the Ballı section don't include *Paragloborotalia siakensis* (LeRoy) which is the biomarker of the MMi9 Zone and is present in all samples of the İbrahimli section. Two characteristic species of the Serravallian, *Pg. mayeri* (Cushman and Ellisor) and *Pg. partimlabiata* (Ruggieri and Sprovieri) are not also recorded in the samples. In addition, *Neogloboquadrina acostaensis* (Blow), one of the marker species of the late Serravallian MMi8 Zone and *Globigerinoides subquadratus* (Brönnimann) are found only in one each sample (BAL 6 and BAL 1), similar to those in the İbrahimli section (Figure 9). The Ballı section includes *Globigerinella pseudobesa* (Salvatorini) (BAL 1, 2, 7), *Globoturborotalita nepenthes* (Todd) (BAL 1) and *Neogloboquadrina atlantica atlantica* (Berggren) (BAL 1, 2, 3) (Figure 9) in contrast to the İbrahimli section in which these species are not determined. The other species identified in the assemblage are *Globigerinoides trilobus* (Reuss), *Gs. quadrilobatus* (d'Orbigny), *Gs.*

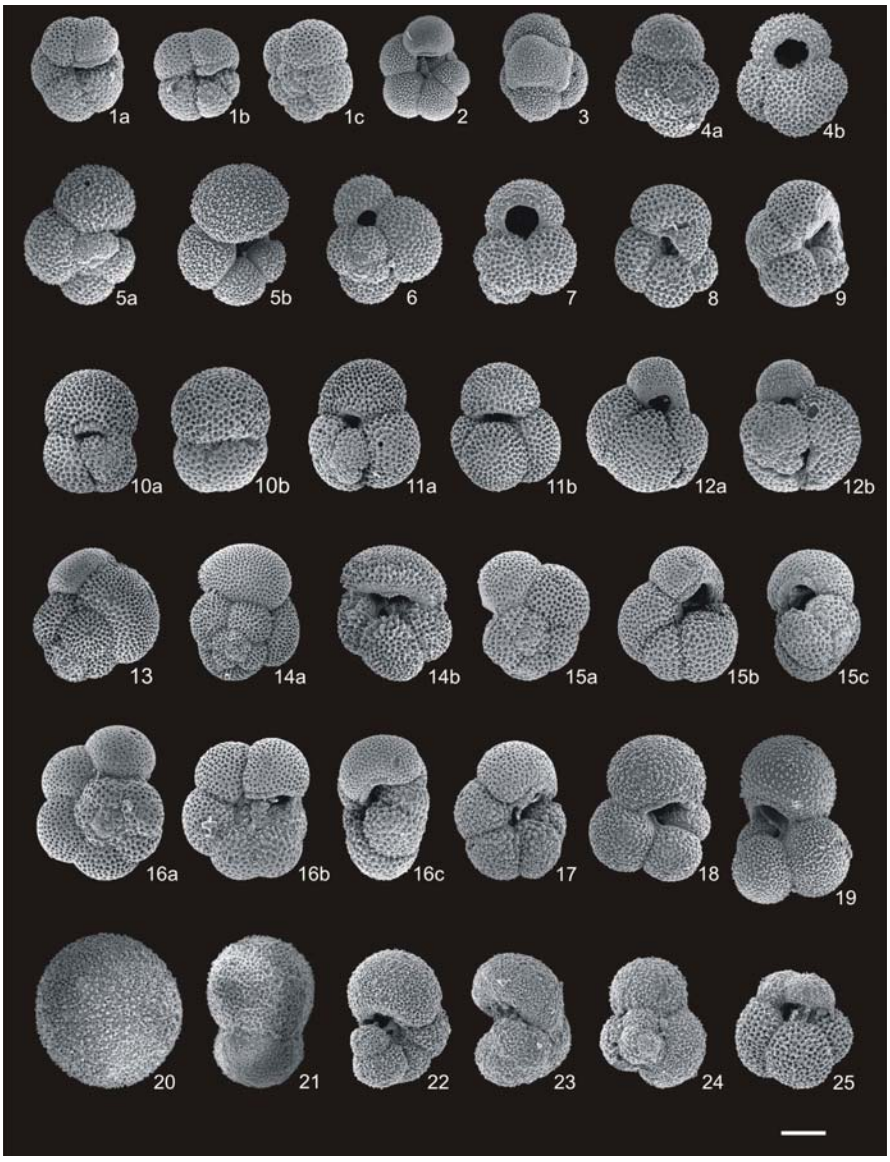

Figure 9- SEM views of the planktonic foraminifers described in the İbrahimli and Ballı sections (Scale: 1-9, 15-19, 24-25: 100 µm; 12b, 20, 21: 110 µm; 23: 120 µm; 10-12a, 13b-14: 125 µm). 1a-c. *Neogloboquadrina acostaensis* (Blow), (a) umbilical view, (b) umbilical view, (c) spiral view, İBR.4; 2. *Tenuitellinata angustiumbilicata* (Bolli), umbilical view, İBR.10; 3. *Globigerinita glutinata* (Egger) umbilical view, İBR.10; 4a, b. *Globoturborotalita woodi* (Jenkins), (a) spiral view, (b) umbilical view, İBR.4; 5a, b. *Globigerinella obesa* (Bolli), (a) spiral view, (b) umbilical view, İBR.10; 6. *Globigerinoides bulloideus* Crescenti, spiral view, İBR.5; 7. *Globigerinoides subquadratus* Brönnimann, umbilical view, İBR.1; 8. *Catapsydrax parvulus* Bolli, Loeblich and Tappan, umbilical view, İBR.10; 9. *Neogloboquadrina atlantica praeatlantica* Foresi, Iaccarino and Salvatorini, umbilical view, İBR.4; 10a, b. *Globigerinoides trilobus* (Reuss), (a) spiral view, (b) umbilical view, İBR.11; 11a, b. *Globigerinoides quadrilobatus* (d'Orbigny), (a) spiral view, (b) umbilical view, İBR.3; 12a, b. *Globigerinoides sacculifer* (Brady), (a) umbilical view, (b) spiral view, İBR.3; 13. *Dentoglobigerina altispira* (Cushman and Jarvis), spiral view, İBR.2; 14a, b. *Dentoglobigerina baroemoenensis* (LeRoy), (a) umbilical view, (b) spiral view, İBR.6; 15a-c. *Paragloborotalia partimlabiata* (Ruggieri and Sprovieri), (a) spiral view, (b) umbilical view, (c) side view, İBR.4; 16a-c. *Paragloborotalia siakensis* (LeRoy), (a) spiral view, (b) umbilical view, (c) side view, İBR.4; 17. *Paragloborotalia mayeri* (Cushman and Ellisor), umbilical view, İBR.4; 18. *Globigerina occlusa* Blow and Banner, umbilical view, İBR.10; 19. *Globigerina praebulloides* Blow, umbilical view, İBR.10; 20. *Orbulina universa* d'Orbigny, İBR.10; 21. *Orbulina bilobata* (d'Orbigny), BAL.6; 22. *Globigerinella siphonifera* (d'Orbigny), oblique view, BAL.2; 23. *Globigerinella pseudobesa* (Salvatorini), oblique view, BAL.1; 24. *Globigerinoides ruber* (d'Orbigny), spiral view, BAL.1; 25. *Neogloboquadrina atlantica atlantica* (Berggren), umbilical view, BAL.3.

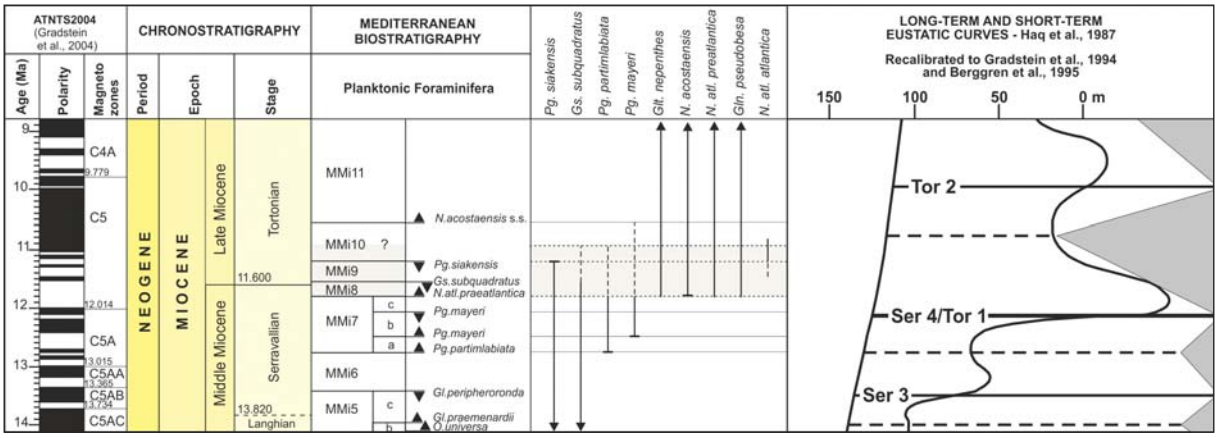

Figure 10- Mediterranean planktonic foraminifer stratigraphy and ATNTS2004 magnetic chronostratigraphy. The stratigraphical distribution of characteristic species described in samples of the Dağpazarı formation and eustatic sea level curves (Hardenbol et al., 1998).

sacculifer (Brady), *Orbulina universa* d'Orbigny, *O. suturalis* Brönnimann, *O. bilobata* (d'Orbigny), *Tenuitellinata angustiumbilicata* (Bolli), *Globigerina bulloides* d'Orbigny, *G.* cf. *ciperoensis* Bolli, *G.* cf. *praebulloides* Blow, *Globigerinella obesa* (Bolli), *Gln. siphonifera* (d'Orbigny), *Dentoglobigerina altispira* (Cushman and Jarvis), *Globorotalia scitula* (Brady), *Neogloboquadrina continuosa* (Blow), *Globoturborotalita decoraperta* (Takayanagi and Saito), *Neogloboquadrina atlantica praeatlantica* (Foresi, Iaccarino and Salvatorini) and *Globigerinita glutinata* (Egger) Thus, 23 planktonic framiniferal species are determined in the Ballı section.

The record of *Neogloboquadrina acostaensis* Blow, *N. atlantica praeatlantica* (Foresi, Iaccarino and Salvatorini), *Globigerinella pseudobesa* (Salvatorini) and *Globoturborotalita nepenthes* (Todd) which are firstly occurred in the MMi8 Zone indicates that the lowest age for the Ballı section is late Serravallian. On the other hand, the absence of *Paragloborotalia siakensis* (LeRoy), zonal marker of the MMi9 Zone, in any samples from the section, but the occurrence of *Neogloboquadrina atlantica atlantica* (Berggren) in some samples (BAL 1, 2, 3) reveals that the Ballı section can be correlated with the MMi10 Zone (Figure 10; Sprovieri et al., 2002; Lirer et al., 2002; Hilgen et al., 2005; Lirer et al., 2005; Iaccarino et al., 2007).

On the basis of the planktonic foraminiferal biostratigraphy, the valley fill deposits of the Dağpazarı formation correspond mainly to the MMi8 – MMi9 zonal interval (*Neogloboquadrina atlantica praeatlantica - Paragloborotalia siakensis* zones) and partly to the MMi10 Zone (*Globigerinoides obliquus* Zone) which span the 11,78-10,90 million years interval.

7. Sequence Stratigraphy and Paleogeographic Evolution

The marine transgression, which began in late Burdigalian in the Mut Basin, has continued until late Serravallian and the reefal and platform carbonates of the Mut formation in the basin have been deposited in this period. The late Serravallian basin boundary of the Mut Basin is represented by the reefal limestones of the Mut formation (Figure 1b) around Paşabağı and Güçler villages in the north. Shoreface, beach, fluvial, lagoon and shoal water delta deposits of the Dağpazarı formation disconformably overlie the reefal limestones which represent a highstand systems tract (Figures 11 and 12). These sediments, which were deposited in an incised valley in late Serravallian-early Tortonian time (Figure 12), are located 20 km to the south of the late Serravallian basin boundary of the Mut Basin in basin direction. The sedimentological characteristics of Mut and Dağpazarı formations reflect an abrupt facies change, an erosional displacement of the late Serravallian shoreline towards basin and, therefore, a forced regression in the stratigraphic sequence (Zaitlin et al., 1994; Hampson et al., 1997; Plint ve Nummedal, 2000). The forced regression and the incised valley indicate a relative sea level fall in the basin in late Serravallian. The decrease in relative sea level caused the partial exposure of the Mut Basin and the formation of valleys on the reefal limestones (Figure 12). Three different system tracts were defined as the "forced regressive systems tract", "lowstand systems tract" and "transgressive systems tract" which

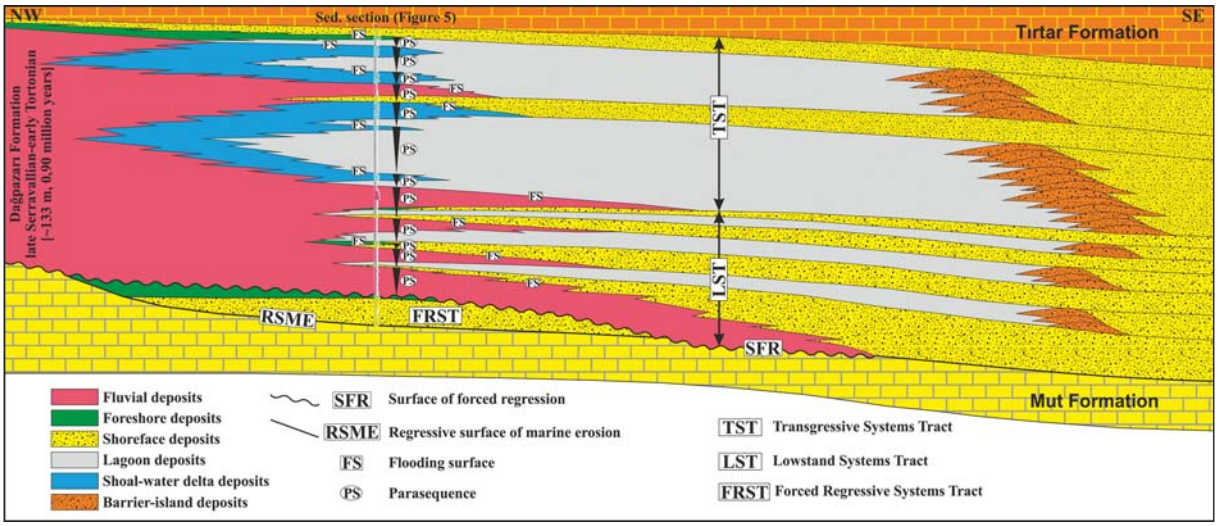

Figure 11- Sequence stratigraphy interpretation of the incised valley fill forming the Dağpazarı formation. This model was constructed based on the section shown in detail in figure 5.

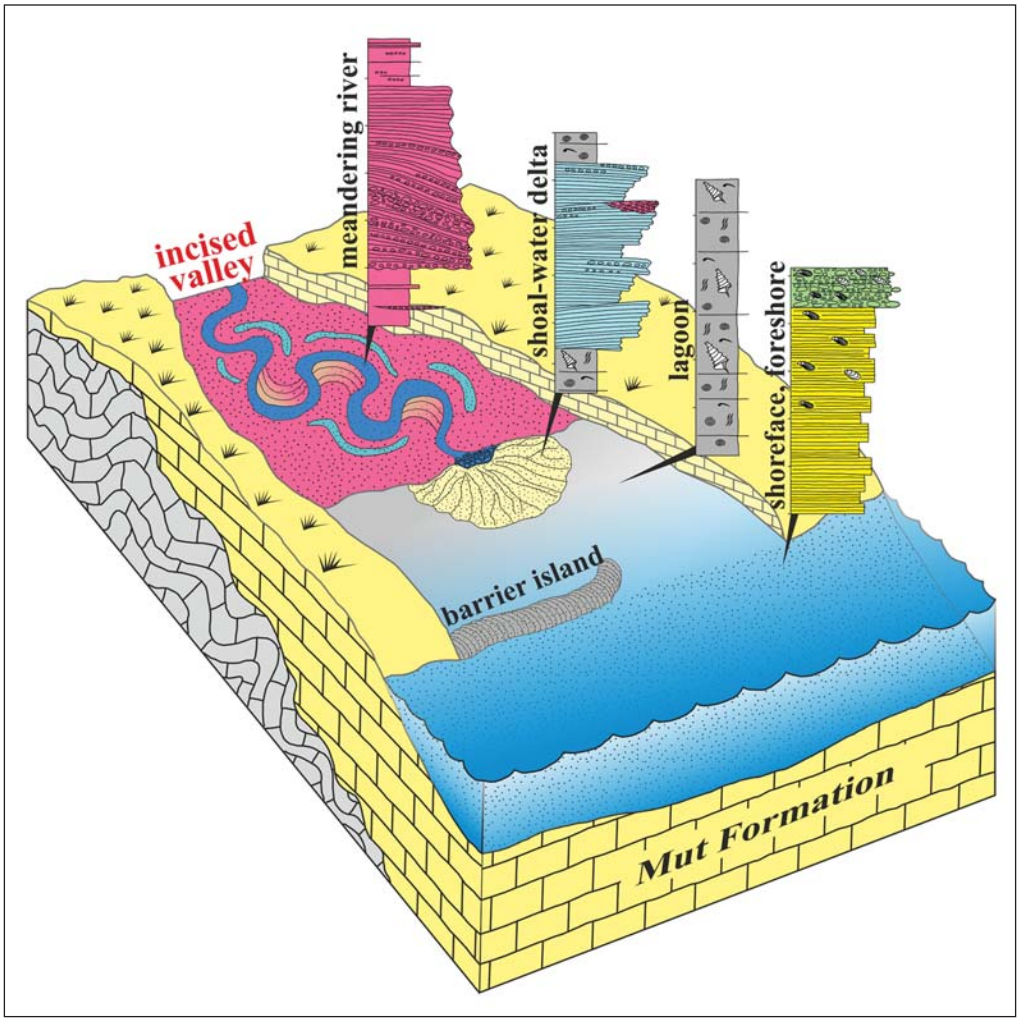

Figure 12- Schematical model of the incised valley where the facies associations forming the Dağpazarı formation deposited (not to scale).

formed during the relative sea level fall, lowstand and the increase of the sea level in the basin. System tracts reflect the paleogeographic changes through different types of deposition and boundary relationships.

7.1. Forced Regressive Systems Tract

While large erosional areas have been developed outside the basin due to the relative sea level decrease and the shoaling have occurred in the depositional area on the basin margin. Sediments derived from new erosional areas were transported into the basin and deposited on carbonate platforms with a sharp contact and formed shoreface and beach deposits. The presence of branched corals within shoreface sandstones in the form of fragmented components (figure 8d) indicates the exposure of reefal limestones and the transportation into the basin.

The sharp boundary between carbonate platforms and the overlying shoreface sandstones forms the "marine erosional surface of forced regression" (Plint, 1988) (Figure 11). The beginning of decrease in the relative sea level caused the lowering of the wave base in the shoreface environment and formation of marine erosional surface. Shoreface sandstones and beach pebbles were deposited on this surface.

In different sections of the basin, beach and shoreface deposits and the underlying platform carbonates were eroded by stream processes and fluvial sediments of the Dağpazarı formation were unconformably deposited (Figures 3c and 11). The deposition of fluvial facies indicates that the relative sea level fall continues. The unconformity surface is accepted as the sequence boundary (Mitchum, 1977) and units deposited on this boundary constitute the "lowstand systems tract" (Posamentier and Vail, 1988; Van Wagoner et al., 1988; Helland-Hansen and Gjelberg, 1994). The deposits, which were defined between the "highstand systems tract", "lowstand systems tract" and deposited during relative sea level fall were named as the "falling stage systems tract" by Nummedal et al. (1992) and the "forced regressive systems tract" by Hunt and Tucker (1992). The shoreface and beach deposits, which overlie the highstand carbonates of the Mut formation with a sharp contact and disconformably underlie the fluvial deposits, are interpreted as the "forced regressive systems tract" (Figure 11).

7.2. Lowstand Systems Tract

The fluvial sediments of the Dağpazarı formation were deposited on an unconformity surface restricting the upper surface of the forced regressive system tract and forming the sequence boundary in the Mut Basin (Figure 5 and 11). The fluvial deposits vertically alternate with shoreface and lagoon deposits in the lower parts of the Dağpazarı succession (Figures 5 and 11). This alternation indicates the relative sea level rise after the first fluvial deposition in the incised valley. Thus, parasequences restricted by marine flooding surfaces in the succession were formed. Each parasequence that begins with shoreface deposits passed upward into lagoon, beach and fluvial mud plains and reflects normal regressive shore progradations. Total of 5 parasequences with thickness varying between 2,5 and 14 m were defined in the lower part of the sequence. These parasequences form an aggradational deposition and were interpreted as the "lowstand systems tract" (Posamentier and Vail, 1988; Van Wagoner et al., 1988; Helland-Hansen and Gjelberg, 1994) (Figure 11). High sediment supply from the basin margin prevented the relative sea level rise to flood the incised valley. Thus, the development of a rapid transgression in the basin was prevented and the sediments of the lowstand systems tract were deposited although the relative sea level rise had begun.

7.3. Transgressive Systems Tract

The continuous rise in the relative sea level flooded the incised valley and caused the valley to turn into a bay. The fresh waters discharging into the bay by rivers and the barrier island development in the bay mouth diluted the normal water salinity and caused the formation of brackish water conditions in the lagoon. Mainly lagoonal mudstones and shoal water delta deposits and subordinate shoreface and fluvial sediments were deposited in this environment (Figures 5 and 11). The shoal water deltas developed on lagoonal mudstones reflect the normal regressive shore progradations and parasequences. In the upper section of succession (between 63-129 meters) seven parasequences were defined with thicknesses varying between 4-21 meters (Figure 11). The development of these parasequences within incised valley reflect the interaction between the marine transgression and sediment transportation into the basin. In periods when the sediment supply into the basin are high and the

relative sea level rise are low, the normal regressive deltaic shore progradations on basin margin occurred. The increase in the relative sea level rise and the decrease in the sediment supply caused an increase in the accommodation space and formation of lagoonal mudstones. These parasequences form backstepping bodies in which marine processes are dominant. The deposition which reflects the deepening in the basin and the retreat of the shoreline were interpreted as the "transgressive systems tract" (Figure 11).

Thick fluvial and delta deposits alternating with lagoon and shoreface deposits within the Dağpazarı incised valley were interpreted as an "overfilled incised valley" as a whole (Breda et al., 2009). The continuing transgression in the basin caused the drowning of the incised valley and flooding of very large areas of the Mut Basin. The retreat of the shoreline due to transgression allowed re-establishment of carbonate deposition, which has continued until late Tortonian.

8. Discussion

Incised valley fills are significant deposit types in stratigraphic successions as they present the formation and the deposition of the valley (Boyd et al., 2009). The formation of these sediments is controlled by the relative sea level changes, tectonism, climate, sediment supply into the basin and paleogeomorphology (Posamentier and Vail, 1988). Accordingly the definition of these sediments in stratigraphical successions has a great importance in interpreting the stratigraphical relationships, paleogeographical developments and evolutions of deposition (Archer and Feldman, 1995; Boyd et al., 2006).

The Mut Basin forms one of the molasse basins, which was opened due to post-orogenic collapse in Neogene (Kempler and Ben-Avraham, 1987; Robertson, 2000; Kelling et al., 2001). There is no any compressional tectonic deformation in Neogene in the basin, normal faults associated with post-orogenic tectonic extension in basin margin occur (Figure 13) (Ilgar et al., 2013; 2016). In addition, there is no any

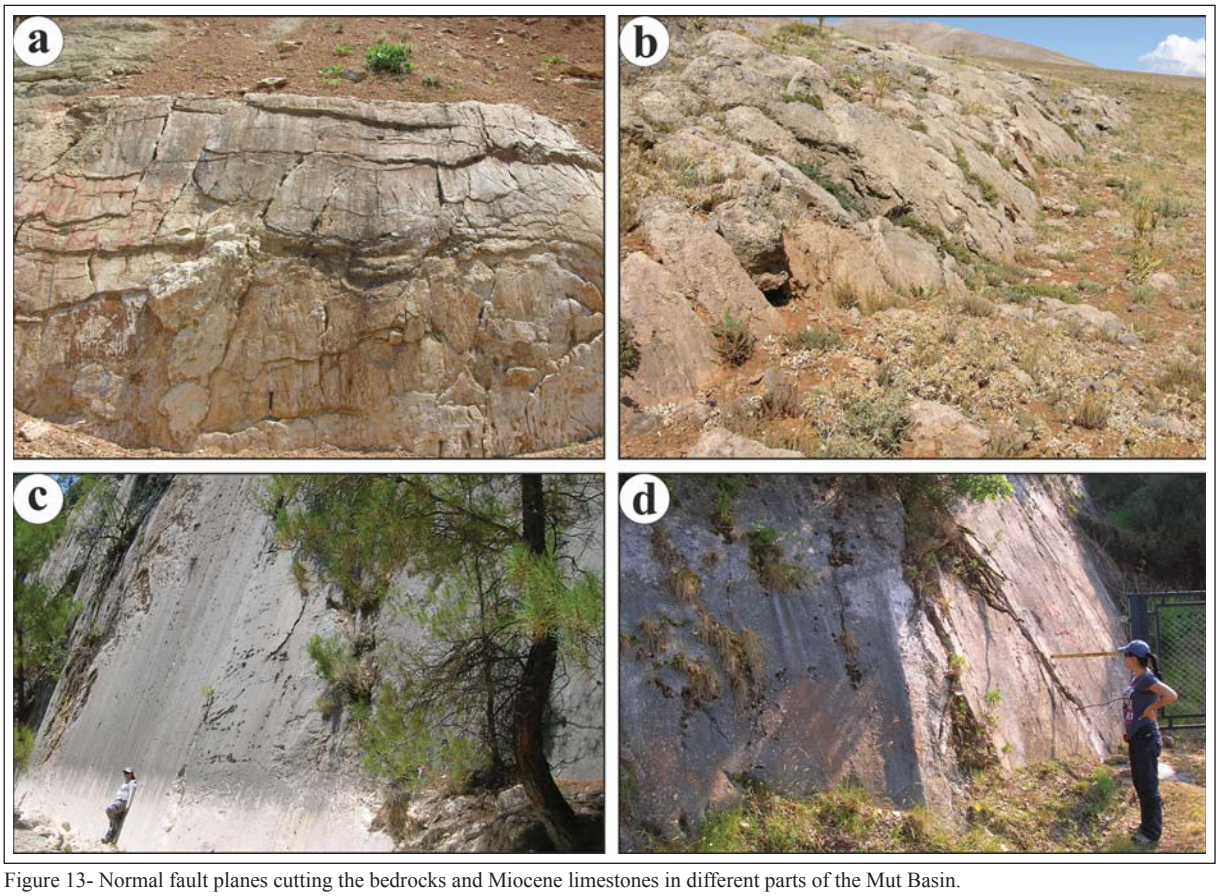

Figure 13- Normal fault planes cutting the bedrocks and Miocene limestones in different parts of the Mut Basin.

angular unconformity between the Mut formation and the overlying Dağpazarı formation. All these stratigraphical and structural characteristics of the Mut Basin show that the Miocene sedimentation in the basin has occurred in a post-orogenic quiet tectonic period. The isostatic rise of the Tauride began in late Tortonian and the Mut basin began to expose due to this rise which was seen in regional scale (Cosentino et al., 2012; Ilgar et al., 2013*a*). Local tectonic data of the Mut Basin and isostatic data of Tauride show that the exposure of the Mut Basin in late Serravallian and the formation of the incised valley did not develop depending on tectonism.

The planktonic foraminiferal biostratigraphy show that the youngest deposits below the forced regressional surface are located in the MMi7 biozone (12,77-11,78 million year interval) and the incised valley fill in MMi8 - MMi10 biozones (11,78-10,90 million years interval) (Ilgar et al., 2013*b*). The age of the forced regression surface, which causes the formation of the incised valley in the basin and can be correlated in regional scale, is conformable with the late Serravallian eustatic sea level fall (Ser4/Tor1; Figure 10). Therefore, the formation of the Dağpazarı incised valley can be associated with the late Serravallian eustatic sea level fall (eg. Rouchy and Saint Martin, 1992; Larsen, 2003; Roveri and Manzi, 2006; Ilgar et al., 2013*a, b*) which are also defined in Miocene basin around the Mediterranean.

During the migration of the shoreline, the sediments of the "forced regressive systems tract" can be either redeposited or completety eroded and shifted basinward. This situation depends on the amount of sediment supply and the drop velocity and amount in the relative sea level fall (Plint, 1988; Helland-Hansen and Gjelberg, 1994). The formation of the "forced regressive systems tract" during the relative sea level fall were interpreted in a such way that the sediment discharged into the Mut Basin was high. The fact that the exposure did not occur rapidly during the fall of the relative sea level probably indicates the contribute of subsidence in the basin. The deposition of thin-bedded sandstones and mudstones, which were interpreted as the lower shoreface facies during the deposition of coastal sandstones (Figure 5, 5.5-8 m), indicates the tectonic deepening of the basin.

Ser4/Tor1 eustatic sea level fall controls the exposure and the formation of the incised valley in the Mut Basin. In addition, it is also considered that the eustatic sea level rise (Figure 10) is one of the factors controlling the infilling of the incised valley. The beginning of the eustatic sea level rise has also caused the base level rise and terminated the erosion that caused the valley formation. Thus, thick fluvial deposits began to deposit within the incised valley.

In addition, the basin subsidence and the sediment supply into the basin also controlled the facies development in the incised valley. Eustatic sea level rise and the subsidence of the basin caused the deepening of the incised valley and the increase of the depositional area. The marine transgression in these periods flooded the incised valley and allowed the deposition of shoreface sandstones in the valley.

In times when relative sea level increased slowly, the formation of barrier-island and lagoonal basin conditions in protective areas behind barrier-island have developed. Thus, the mudstone deposition occurred in the lagoon during periods when it was protected from the effects of open sea processes such as waves and tides and was not intensely affected by fluvial processes. The shoal water deltas were formed within lagoon during high sediment supply periods. Most probably, the regional climatic fluctuations and changes in the amount of river sediment, have controlled the intensity of the stream activity.

The shoreface sandstones deposited on lagoon sediments indicate the times when the open sea connection was re-established through passing over barrier-islands due to the eustatic sea level rise and the subsidence in the basin.

The "lowstand systems tract" and "transgressive systems tract" forming the incised valley fill is consisted by 12 parasequences. These parasequences indicate small sea level rises occurred during the infilling of the incised valley. The facies analysis and sequence stratigraphy of the Dağpazarı formation in the Mut Basin, which is a subsidence area due to the post-orogenic tectonic extension, showed that the interaction between the eustatic sea level rise in small amounts, extensional tectonic regime and the variable sediment supply rate controlled the deposition.

9. Conclusion

The sedimentary facies analysis of the middle-late Miocene clastic sequence of the Mut Basin was carried out and then the sequence stratigraphic evolution was interpreted by detailed sedimentological study. The relative sea level changes that control the

development of sedimentary facies were dated by means of the planktonic foraminiferal biostratigraphy. Thus, the sedimentological and biostratigraphical data and the sequence stratigraphic interpretations were used in the basin and the middle and late Miocene sedimentological (paleogeographical) evolution of Mut basin and the processes controlling this development were discussed.

The reefal limestones and platform carbonates of the Mut formation were deposited during the late Burdigalian-late Serravallian in the Mut Basin. The shoreface, beach, fluvial, lagoon and shoal water delta deposits forming the Dağpazarı formation unconformably overlay the reefal limestones of the Mut formation and reflect a valley fill sequence deposited within incised valley. This sequence is located about 20 km to the south of the basin margin of the late Serravallian highstand reefal carbonates. The facies characteristics of the Mut and Dağpazarı formations reflect abrupt facies changes in the stratigraphic sequence, basinward erosional shift of the late Serravallian shoreline and the forced regression.

There is no any compressional tectonic deformation in Neogene Mut Basin which opened depending on post-orogenic tectonic extension. The Miocene sedimentation occurred relatively in a quiet tectonic period. The local tectonic data of the Mut Basin and the regional isostatic data of Tauride indicate that the late Serravallian exposure and incised valley formation in the basin did not develop due to tectonic.

The planktonic foraminiferal biostratigraphy shows that the incised valley fill was formed between the biozones of MMi8–MMi10 (11.78-10.90 million years interval) in the late Serravallian-early Tortonian. The age of the forced regression, which caused the formation of the incised valley in the basin, is conformable with the late Serravallian eustatic sea level fall (Ser4/Tor1). Therefore, the formation of the incised valley of Dağpazarı was associated with the late Serravallian eustatic sea level fall. It is thought that the post Ser4/Tor1 eustatic sea level rise in the Mut Basin is one of the factors controlling the valley filling. In addition, the basin subsidence in the extensional tectonic regime and varying sediment supply into the basin also controlled the facies development within incised valley.

Acknowledgements

This study was carried out within the project of "The Geology and Palaeogeographic Development of Neogene Rocks in Adana-Mut Basin" between 2009-2012 by the Department of Geological Researches of the General Directorate of Mineral Research and Exploration (MTA). The SEM photos of Ostracod fossils were taken in laboratories of the Mineral Analysis and Technology Department in MTA. The SEM photos for the planktonic foraminifers were taken in the Microscopy and Microanalysis Laboratory of the Department of Metallurgical and Materials Engineering at the Middle East Technical University (METU). We thank to referees who read and gave support for the development of this article. Massimiliano Ghinassi kindly improved the English version of the manuscript.

References

Aguilar, J-P., Berggren, W.A., Aubry, M-P., Kent, D.V., Clauzon, G., Benammi, M., Michaux, J. 2004. Mid-Neogene Mediterranean marine-continental correlations: an alternative interpretation. Palaeogeography, Palaeoclimatology, Palaeoecology 204, 165–186.

Ainsworth, R. B., Crowley, S. F. 1994. Wave-dominated nearshore sedimentation and 'forced' regression: post-abandonment facies, Great limestone cyclothem, Stainmore, UK. Journal of the Geological Society of London 151, 681–695.

Aktaş, G., Robertson, A.H.F. 1990. Tectonic evolution of the Tethys suture zone in SE Turkey: evidence from the petrology and geochemistry of Late Cretaceous and Middle Eocene extrusives. Malpas, J., Moores, E.M., Panayiotou, A., Xenophontos, C. (Ed.). Ophiolites – Oceanic Crustal Analogues. Proceedings of the International Symposium Troodos 1987, Cyprus Geological Survey, Nicosia, pp. 311−328.

Andrew, T., Robertson, A.H.F. 2002. The Beyşehir-Hoyran-Hadım nappes: genesis and emplacement of Mesozoic marginal and oceanic units of the northern Neotethys in southern Turkey. Journal of the Geological Society of London 159, 529−543.

Archer, A.W., Feldman, H.R. 1995. Incised valleys and estuarine facies of the Douglas Group (Virgilian)– Implications for similar Pennsylvanian sequences in the U.S. Mid-Continent. Hyne, N.J. (Ed.). Sequence Stratigraphy of the Mid-Continent. American Geological Society, Tulsa, pp. 119–140.

Atabey, E., Atabey, N., Hakyemez, A., İslamoğlu, Y., Sözeri, Ş., Özçelik, N. N., Saraç, G., Ünay, E., Babayiğit, S. 2000. Mut-Karaman arası Miyosen havzasının litostratigrafisi ve sedimantolojisi (Orta Toroslar). Maden Tetkik ve Arama Dergisi 122, 53–72.

Bartol, J., Govers, R., Wortel, R. 2011. The Central Anatolian Plateau: relative timing of uplift and magmatism. EGU2011 Geophysical Research Abstracts 13, 10326.

Bassant, P., van Buchem, F.S.P., Görür, N. 2005. The stratigraphic architecture and evolution of the Burdigalian carbonate–siliciclastic sedimentary systems of the Mut Basin, Turkey. Sedimentary Geology 173, 187–232.

Berggren, W.A., Kent, D.V., Swisher, C.C. III, Aubry, M.-P. 1995. A revised Cenozoic geochronology and chronostratigraphy. Berggren W.A., Kent D.V., Aubry M.-P., Hardenbol J. (Ed.). Geochronology, time scales and global stratigraphic correlation. Society of Economic Paleontologists and Mineralogists, Special Publication 54, 129–212.

Bluck, B.J. 1967. Sedimentation of beach gravels: examples from South Wales. Journal of Sedimentary Petrology 37, 128–156.

Bluck, B.J. 1999. Clast assemblages, bed-forms and structure in gravel beaches. Transactions of the Royal Society of Edinburgh Earth Sciences 89, 291– 332.

Bolli, H.M., Saunders, J.B. 1985. Oligocene to Holocene low latitude planktonic foraminifera. Bolli, H.M., Saunders, J.B., Perch-Nielsen, K. (Ed.). Plankton Stratigraphy. Cambridge University Press, Cambridge, pp. 155–262.

Boyd, R., Dalrymple, R.W., Zaitlin, B.A. 2006. Estuarine and incised-valley facies models. Posamentier, H.W., Walker, R.G. (Ed.). Facies Models Revisited. Society of Economic Paleontologists and Mineralogists Special Publication 84, 171–235.

Breda, A., Mellere, D., Massari, F., Asioli, A. 2009. Vertically stacked Gilbert-type deltas of Ventimiglia (NW Italy): The Pliocene record of an overfilled Messinian incised valley. Sedimentary Geology 219, 58−76.

Brierley, G.J. 1991. Bar sedimentology of the Squamish River, British Columbia: definition and application of morphostratigraphic units. Journal of Sedimentary Petrology 61, 211–225.

Catuneanu, O. 2006. Principles of Sequence Stratigraphy. Elsevier, Amsterdam, 375 p.

Cipollari, P., Halasova, E., Gürbüz, K., Cosentino, D. 2013. Middle-Upper Miocene paleogeography of southern Turkey: insights from stratigraphy and calcareous nannofossil biochronology of the Olukpınar and Başyayla sections (Mut-Ermenek Basin). Turkish Journal of Earth Sciences 22, 820–838.

Clark, M., Robertson, A.H.F. 2002. The role of the Early Tertiary Ulukışla Basin, southern Turkey, in suturing of the Mesozoic Tethys Ocean. Journal of the Geological Society of London 159, 673–690.

Clifton, H.E. 1973. Pebble segregation and bed lenticularity in wave-worked versus alluvial gravel. Sedimentology 20, 173–187.

Collins, A.S., Robertson, A.H.F. 1998. Processes of Late Cretaceous to Late Miocene episodic thrust-sheet translation in the Lycian Taurides, SW Turkey. Journal of the Geological Society of London 155, 759–772.

Collins, A.S., Robertson, A.H.F. 2000. Evolution of the Lycian allochthon, western Turkey, as a north-facing Late Palaeozoic to Mesozoic rift and passive margin. Geological Journal 34, 107–138.

Collinson, J.D. 1996. Alluvial sediments. Reading, H.G. (Ed.). Sedimentary Environments: Processes, Facies and Stratigraphy. Blackwell Science, Oxford, pp. 37–82.

Collinson, J.D., Thompson, D.B. 1982. Sedimentary Structures. Allen and Unwin, London, 207 p.

Cosentino, D., Schildgen, T.F., Cipollari, P., Faranda, C., Gliozzi, E., Hudáčková, N., Lucifora, S., Strecker, M.R. 2012. Late Miocene surface uplift of the southern margin of the Central Anatolian plateau, Central Taurides, Turkey. Bulletin of the Geological Society of America 124, 133–145.

Dalrymple, R.W., Zaitlin, B.A., Boyd, R. 1992. Estuarine facies models: conceptual basis and stratigraphic implications. Journal of Sedimentary Petrology 62, 1130–1146.

Dalrymple, R.W., Boyd, R., Zaitlin, B.A. 1994. Incised-valley systems: origin and sedimentary sequences. Society of Economic Paleontologists and Mineralogists Special Publication 51, 391 pp.

Demir, N. E. 1997. Mut doğu yöresi Miyosen yaştaki kayaçların stratigrafisi, Yük. Müh. Tezi, H.Ü. Fen Bilimleri Enstitüsü 93 s., Ankara.

Dilek, Y., Moores, E.M. 1990. Regional tectonics of the eastern Mediterranean ophiolites. Malpas, J., Moores, E.M., Panayiotou, A., Xenophontos, C. (Ed.). Ophiolites, oceanic crustal analogues: Proceedings of the symposium Trodos 1987: Geological Survey Department, Nicosia, Cyprus, p.295–309.

Dilek, Y., Whitney, D.L. 2000. Cenozoic crustal evolution in Central Anatolia: Extension, magmatism and landscape development. Panayides, I., Xenophontos, C., Malpas, J. (Ed.). Proceedings of the Third International Conference on the Geology of the Eastern Mediterranean: Geological Survey Department, Nicosia, Cyprus, p.183–192.

Gautier, P., Brun, J.P. 1994. Ductile crust exhumation and extensional detachments in the central Aegean (Cyclades and Evvia Islands). Geodinamica Acta 7, 57–85.

Gautier, P., Brun, J.P., Moriceau, R., Sokoutis, D., Martinod, J., Jolivet, L. 1999. Timing, kinematics and cause of the Aegean extention: A scenario based on a comparison with simple analogues experiments. Tectonophysics 315, 31–72.

Gedik, A., Birgili, Ş., Yılmaz, H., Yoldaş, R. 1979. Mut-Ermenek-Silifke yöresinin jeolojisi ve petrol olanakları. Türkiye Jeoloji Kurumu Bülteni 22, 7–26.

Ghinassi, M., Nemec, W., Aldinucci, M., Nehyba, S., Özaksoy, V., Fidolini, F. 2014. Plan-form evolution of ancient meandering rivers reconstructed from longitudinal outcrop sections. Sedimentology 61 (4), 952–977. doi:10. 1111/sed.12081.

Gradstein, F.M., Agterberg, F.P., Ogg, J.G., Hardenbol, J., van Veen, P., Thierry, J., Huang, Z. 1994. A Mesozoic time scale. Journal of Geophysical Research 99, B12, 24051–24074.

Hampson, G.J., Elliott, T., Davies, S.J. 1997. The application of sequence stratigraphy to Upper Carboniferous fluvio-deltaic strata of the onshore UK and Ireland: implications for the southern North Sea. Journal of the Geological Society of London 154, 719–733.

Haq, B.U., Hardenbol, J., Vail, P.R. 1987. The chronology of fluctuating sea level since the Triassic. Science 235, 1156–1167.

Hardenbol, J., Thierry, J., Farley, M.B., Jacquin, T., de Graciansky, P-C., Vail, P.R. 1998. Mesozoic and Cenozoic sequence chronostratigraphic chart. de Graciansky, P-C., Hardenbol, J., Jacquin, T., Vail, P.R. (Ed.). Mesozoic and Cenozoic sequence stratigraphy of European Basins. Society of Economic Paleontologists and Mineralogists Special Publication 60.

Harms, J.C., Southard, J.B., Spearing, D.R., Walker, R.G. 1975. Depositional Environments as interpreted from Primary Sedimentary Structures and Stratification Sequences. Society of Economic Paleontologists and Mineralogists, Short Course No. 2 Lecture Notes, 161 pp.

Harms, J.C., Southard, J.B., Walker, R.G. 1982. Structures and Sequences in Clastic Rocks. Society of Economic Paleontologists and Mineralogists, Short Course No. 9 Lecture Notes, 250 pp.

Helland-Hansen, W., Gjelberg, J.G. 1994. Conceptual basis and variability in sequence stratigraphy: a different perspective. Sedimentary Geology 92, 31–52.

Helland-Hansen, W., Martinsen, O.J. 1996. Shoreline trajectories and sequences: description of variable depositional-dip scenarios. Journal of Sedimentary Research 66, 670–688.

Hilgen, F.J., Abdul Aziz, H., Krijgsman, W., Raffi, I., Turco, E. 2003. Integrated stratigraphy and astronomical tuning of the Serravallian and lower Tortonian at Monte dei Corvi (Middle-Upper Miocene, northern Italy). Palaeogeography, Palaeoclimatology, Palaeoecology 199, 229–264

Hilgen, F.J., Abdul Aziz, H., Bice, D., Iaccarino, S., Krijgsman, W., Kuiper, K., Montanari, A., Raffi, I., Turco, E., Zachariasse, W-J. 2005. The global boundary stratotype section and point (GSSP) of the Tortonian stage (Upper Miocene) at Monte Dei Corvi. Episodes, 28, 6–17.

Hunt, D., Tucker, M.E. 1992. Stranded parasequences and the forced regressive wedge systems tract: deposition during base-level fall. Sedimentary Geology 81, 1–9.

Hunter, R. E., Clifton, H. E. 1982. Cyclic deposits and hummocky-cross-stratification of probable storm origin in Upper Cretaceous rocks of Cape Sebastian area, southwestern Oregon. Journal of Sedimentary Petrology 52, 127–143.

Iaccarıno, S.M. 1985. Mediterranean Miocene and Pliocene planktic foraminifera. Bolli, H.M., Saunders, J.B., Perch-Nielsen, K. (Ed.). Plankton Stratigraphy. Cambridge University Press, Cambridge, pp. 283–314.

Iaccarino, S.M., Premoli Silva, I., Biolzi, M., Foresi, L.M., Lirer, F., Turco, E., Petrizzo, M.R. 2007. Practical Manual of Neogene Planktonic Foraminifera. International School on Planktonic Foraminifera 6th Course, Università di Perugia Press, Perugia, 181 p.

Ilgar, A. 2015. Miocene sea-level changes in northernmost Anatolia: Sedimentary record of eustasy and tectonism at the peri-Pontide fringe of Eastern Paratethys. Sedimentary Geology 316, 62–79. DOI: 10.1016/j.sedgeo.2014.11.006.

Ilgar, A., Nemec, W. 2005. Early Miocene lacustrine deposits and sequence stratigraphy of the Ermenek Basin, Central Taurides, Turkey. Sedimentary Geology 173, 217–249.

Ilgar, A., Nemec, W., Hakyemez, A., Karakuş, E. 2013*a*. Messinian forced regressions in the Adana Basin: a near-coincidence of tectonic and eustatic forcing. Çiner, A., Strecker, M.R., Bertotti, G. (Ed.). Late Cenozoic Evolution of the Central Anatolia Plateau. Turkish Journal of Earth Sciences Special Publication 22, 864–889. DOI: 10.3906/yer-1208-3.

Ilgar, A., Nemec, W., Hakyemez, A., Esirtgen, T., Messina, C., Türkmen, B., Çiner, A. 2013*b*. The varied development and regional implications of late Serravalian erosional unconformity in the peri-Mediterranean basins of southern Turkey. RCMNS, 14th Congress of Regional Committee on Mediterranean Neogene Stratigraphy, İstanbul, Turkey, p. 21.

Ilgar, A., Esirtgen, T., Türkmen Bozkurt, B., Demirkaya, S., Hakyemez, A., Culha, G., Danacı, F., Aydın, A., Gürler, G., Baykal Dölen, M., Çınar Durgut, S.N., Beşter Bengü, B., Akpınar, S., Karakuş, E. 2016. Adana-Mut (İçel) Arasında Yüzeylenen Neojen Yaşlı Kayaçların Jeolojisi ve Paleocoğrafik Gelişimlerinin Kurulması. Maden Tetkik ve Arama Genel Müdürlüğü Jeoloji Etütleri Dairesi, Report No: 11915, Ankara (unpublished).

Jackson, R.G., II. 1976. Depositional model of point bars in the Lower Wabash River. Journal of Sedimentary Petrology 46, 579–594.

Jaffey, N., Robertson, A.H.F. 2005. Non-marine sedimentation associated with Oligocene–Recent exhumation and uplift of Central Taurus Mountains, S Turkey. Sedimentary Geology 173, 53–89.

Jarvis, A., Reuter, H.I., Nelson, A., Guevara, E. 2008. Hole-filled SRTM for the Globe, Version 4. CGIAR-CSI SRTM 90m Database http://srtm.csi.cgiar.org.

Karabıyıkoğlu, M., Tuzcu, S., Çiner, A., Deynoux, M., Örçen, S., Hakyemez, S. 2005. Facies and environmental setting of the Miocene coral reefs in the late-orogenic fill of the Antalya Basin, western Taurides, Turkey: implications for tectonic control and sea-level changes. Sedimentary Geology 173, 345–371.

Kelling, G., Gökçen, S., Floyd, P., Gökçen, N. 1987. Neogene tectonics and plate convergence in the eastern Mediterranean: new data from southern Turkey. Geology 15, 425–429.

Kelling, G., Egan, S. E., Gürbüz, K., Şafak, Ü., Ünlügenç, U.C. 2001. Oligo-Miocene basins of south-central Turkey: Synthesis and appraisal. Fourth International Turkish Geology Symposium, p.17.

Kempler, D., Ben-Abraham, Z. 1987. The tectonic evolution of the Cyprean Arc. Ann. Tecton. 1, 58–71.

Kennett, J.P., Srinivasan, M.S. 1983. Neogene Planktonic Foraminifera: A Phylogenetic Atlas. Hutchinson ve Ross, Stroudsburg, Pennsylvania, USA.

Koç, A., Kaymakçı, N., Van Hinsbergen, D.J.J., Kuiper K.F., Vissers, R.L.M. 2012. Tectono-sedimentary evolution and geochronology of the Middle Miocene Altınapa Basin, and implications for the Late Cenozoic uplift history of the Taurides, southern Turkey. Tectonophysics 532, |34–155.

Larsen, E. 2003. Stratigraphic Architecture of Littoral to Neritic Clastic Wedges: Sedimentology, Morphodynamics and Implications for Spatial Lithofacies Predictions. Dr. Sc. Dissertation, Bergen University, Bergen, 272 pp.

Le Pichon, X., Angelier, J. 1981. The Aegean sea. Philosophical Transactions of the Royal Society of London 300, 357–371.

Leszczyński, S., Nemec, W. 2014. Dynamic stratigraphy of peripheral composite unconformity in a foredeep basin. Sedimentology 62 (3), 645–680. doi: 10.1111/sed.12155.

Lirer, F., Caruso, A., Foresi, L.M., Sprovieri, M., Bonomo, S., Di Stefano, A., Di Stefano, E., Iaccarino, S.M., Salvatorini, G., Sprovieri, R., Mazzola, S. 2002. Astrochronological calibration of the upper Serravallian-lower Tortonian sedimentary sequence at Tremiti Islands (Adriatic Sea, Southern Italy). Iaccarino S.M. (Ed). Integrated Stratigraphy and Paleoceanography of the Mediterranean Middle Miocene. Riv. It. Paleont. Strat. 108, 241-256.

Lirer, F., Persico, D., Vigorito, M. 2005. Calcareous plankton biostratigraphy and age of the Middle Miocene deposits of Longano Formation (Eastern Matese Mountains, Southern Apennines). Rivista Italiana di Paleontologia e Stratigrafia, 111 (2), 91-108.

Lourens, L.J., Hilgen, F.J., Laskar, J., Shackleton, N.J., Wilson, D. 2004. The Neogene Period. Gradstein, F.M., Ogg, J.G., Smith, A.G. (Ed.). A Geologic Time Scale. Cambridge University Press, Cambridge, pp. 409–440.

Maejima, W. 1983. Prograding gravelly shoreline deposits in the Early Cretaceous Yuasa Formation, western Kii Peninsula, Southwest Japan. Journal of the Geological Society of Japan 89, 645–660.

Massari, F., Parea, G.C. 1988. Progradational gravel beach sequences in a moderate-to high-energy. Microtidal marine environment. Sedimentology 35, 881–913.

McGowen, J.H., Garner, L.E. 1970. Physiographic features and stratification types of coarse-grained point bars: modern and ancient examples. Sedimentology 14, 77–111.

Miall, A.D. 1985. Architectural-element analysis: a new method of facies analysis applied to fluvial deposits. Earth-Science Reviews 22, 261–308.

Michard, A., Whitechurch, H., Ricou, L.E., Montigny, R., Yazgan, E. 1984. Tauric subduction (Malatya-Elazığ provinces) and its bearing on tectonics of the Tethyan realm in Turkey. Dixon, J.E., Robertson, A.H.F. (Ed.). The Geological Evolution of the Eastern Mediterranean. Geological Society, London, Special Publications 17, 349–360.

Mitchum, R.M., Jr. 1977. Seismic stratigraphy and global changes of sea level, part 11: glossary of terms used in seismic stratigraphy. Payton, C.E. (Ed. Seismic Stratigraphy– Applications to Hydrocarbon Exploration. American Association of Petroleum Geologists Memoir 26, 205–212.

Nanson, G.C. 1980. Point bar and floodplain formation of the meandering Beatton River, northeastern British Columbia, Canada. Sedimentology 27, 3–29.

Nemec, W., Steel, R.J. 1984. Alluvial and coastal conglomerates: their significant features and some comments on gravelly mass-flow deposits. Koster, E.H., Steel, R.J., (Ed.). Sedimentology of Gravels and Conglomerates. Canadian Society of Petroleum Geologists, Memoir 10, 1–31.

Nemec, W., Postma, G. 1993. Quaternary alluvial fans in southwestern Crete: sedimentation processes and geomorphic evolution. Marzo, M., Puigdefabregas, C. (Ed.). Alluvial Sedimentation. International Association of Sedimentologists Special Publication 17, 235–276.

Nielsen, L.H., Johannessen, P.N., Surlyk, F. 1988. A Late Pleistocene coarse-grained spit-platform sequence in northern Jylland, Denmark. Sedimentology 35, 915–937.

Nummedal, D. 1992. The falling sea-level systems tract in ramp settings. Society of Economic Paleontologists and Mineralogists Theme Meeting, Fort Collins, Colorado (abstracts), p.50.

Özgül, N. 1976. Torosların bazı temel jeoloji özellikleri. Türkiye Jeoloji Kurumu Bülteni 19, 65–78.

Plint, A.G. 1988. Sharp-based shoreface sequences and 'offshore bars' in the Cardium Formation of Alberta: their relationship to relative changes in sea level. Wilgus, C.K., Hastings, B.S., Posamentier, H.W., Ross, C.A., Kendall, C.G.St.C., Van Wagoner, J.C. (Ed.). Sea-Level Changes: An Integrated Approach, SEPM Special Publication 42, 357–370.

Plint, A.G., Nummedal, D. 2000. The falling stage systems tract: recognition and importance in sequence stratigraphic analysis. Hunt, D., Gawthorpe, R.L. (Ed.). Sedimentary Responses to Forced Regression. Geological Society of London, Special Publication 172, 1–17.

Poisson, A., Yağmurlu, F., Bozcu, M., Şentürk, M. 2003. New insights on the tectonic setting and evolution around the apex of the Isparta Angle (SW Turkey). Geological Journal 38, 257−282.

Posamentier, H.W., Vail, P.R. 1988. Eustatic controls on clastic deposition: II. Sequence and systems tract models. Wilgus, C.K., Hastings, B.S., Posamentier, H.W., Ross, C.A., Kendall, C.G.St.C., Van Wagoner, J.C. (Ed.). Sea-Level Changes: An Integrated Approach, SEPM Special Publication 42, 125–154.

Posamentier, H.W., Morris, W.R. 2000. Aspects of the stratal architecture of forced regressive deposits. Hunt, D., Gawthorpe, R.L. (Ed.). Sedimentary Responses to Forced Regression. Geological Society of London, Special Publication 172, 19–46.

Posamentier, H.W., Allen, G.P., James, D.P., Tesson, M. 1992. Forced regressions in a sequence stratigraphic framework: concepts, examples, and exploration significance. Bulletin of the American Association of Petroleum Geologists 76, 1687–1709.

Postma, G., Nemec, W. 1990. Regressive and transgressive sequences in a raised Holocene gravelly beach, southwestern Crete. Sedimentology 37, 907–920.

Robertson, A.H.F. 2000. Mesozoic-Tertiary tectonic-sedimentary evolution of a south Tethyan oceanic basin and its margins in southern Turkey. Bozkurt, E., Winchester, J.A., Piper, J.D.A. (Ed.). Tectonics and Magmatism in Turkey and the Surrounding Area. Geological Society of London Special Publication 173, 97–138.

Rouchy, J.M., Saint Martin, J.P. 1992. Late Miocene events in the Mediterranean as recorded by carbonate-evaporitic relations. Geology 20, 629–632.

Roveri, M., Manzi, V. 2006. The Messinian salinity crisis: Looking for a new paradigm? Palaeogeography Palaeoclimatology Palaeoecology 238, 386–398,

Sağular, E.K., Görmüş, M. 2006. New stratigraphical results and significance of reworking based on nannofossil, foraminiferal and sedimentological records in the Lower Tertiary sequence from the northern Isparta Angle, Eastern Mediterranean. Journal of Asian Earth Sciences 27, 78−98.

Seyitoğlu, G., Scott, B.C. 1991. Late Cenozoic crustal extension and basin formation in west Turkey. Geological Magazine 128, 155–166.

Seyitoğlu, G., Scott, B.C. 1996. The cause of N-S extensional tectonics in western Turkey: tectonic escape vs back-arc spreading vs orogenic collapse. Journal of Geodynamics 22, 145–153.

Sprovieri, R., Bonomo, S., Caruso, A., Di Stefano, A., Di Stefano, E., Foresi, L.M., Iaccarino, S.M., Lirer, F., Mazzei, R., Salvatorini, G. 2002. An integrated calcareous plankton biostratigraphic scheme and biochronology for the Mediterranean Middle Miocene. Iaccarino S.M. (Ed). Integrated Stratigraphy and Paleoceanography of the Mediterranean Middle Miocene. Riv. It. Paleont. Strat., 108, 337–353.

Sunal, G., Tüysüz, O. 2002. Palaeostress analysis of Tertiary post-collisional structures in the Western Pontides, northern Turkey. Geological Magazine 139, 343–359.

Swift, D.J.P. 1975. Barrier island genesis: evidence from the Middle Atlantic Shelf, Eastern USA. Sedimentary Geology 14, 1–43.

Swift, D.J.P., Phillips, S., Thorne, J.A. 1991. Sedimentation on continental margins, IV: lithofacies and depositional systems. Swift, D.J.P., Oertel, G.F., Tillman, R.W., Thorne, J.A. (Ed.). Shelf Sand and Sandstone Bodies. IAS Special Publication 14, 89–152.

Şengör, A.M.C. 1987. Tectonics of the Tethysides: orogenic collage development in a collisional setting. Annual Review of Earth and Planetary Sciences 15, 213–244.

Şenel, M. 2002. 1:500.000 ölçekli Türkiye Jeoloji Haritası, Pafta No: 14 (Konya). Maden Tetkik ve Arama Genel Müdürlüğü, Ankara.

Tanar, Ü. 1989. Mut havzası Tersiyer istifinin stratigrafik ve mikropaleontolojik (Ostrakod ve Foraminifer) incelemesi; Ç.Ü. Fen Bilimleri Enst. Doktora Tez., 199 s, Adana.

Tanar, Ü., Gökçen, N. 1990. Mut-Ermenek Tersiyer istifinin stratigrafisi ve paleontolojisi. Maden Tetkik ve Arama Dergisi 110, 175–180.

Tooth, S. 1999. Downstream changes in floodplain character on the Northern Plains of arid Central Australia. Smith, N.D., Rogers, J. (Ed.). Fluvial Sedimentology VI, IAS Special Publication 28, 93–112.

Ulu, U. 2002. 1:500.000 ölçekli Türkiye Jeoloji Haritası, Pafta No: 15 (Adana). Maden Tetkik ve Arama Genel Müdürlüğü, Ankara.

Ünay, E., Atabey, E., Saraç, G. 2001. Small mammals and foraminifera from the Anatolian (Central Taurus) early Miocene. Annals of Carnegie Museum 70, 4, 247–256.

Ünlügenç, U.C., Demirkol, C., Kelling, G., Williams, G.D., Kop, A. 2001. Timing and causes of Tertiary deformation in the Çukurova Basin Complex, southern Turkey: new seismic-sequence stratigraphic interpretations. Abstracts 4th International Symposium on Geology of Turkey and Its Surroundings–Work in Progress. Çukurova University, Adana, p. 281.

Van Wagoner, J.C., Posamentier, H.W., Mitchum Jr., R.M., Vail, P.R., Sarg, J.F., Loutit, T.S., Hardenbol, J. 1988. An overview of the fundamentals of sequence stratigraphy and key definitions. Wilgus, C.K., Hastings, B.S., Posamentier, H.W., Ross, C.A., Kendall, C.G.St.C., Van Wagoner, J.C. (Ed.). Sea-Level Changes: An Integrated Approach, SEPM Special Publication 42, 39–45.

Walker, R.G. 1984. Shelf and shallow marine sands. Walker, R.G., James, N.P. (Ed.). Facies Models: Response to Sea Level Change. Geological Association of Canada, St. John's, pp. 141–170.

Walker, R.G., Plint, A.G. 1992. Wave- and storm-dominated shallow marine systems. Walker, R.G., James, N.P. (Ed.). Facies Models: Response to Sea Level Change. Geological Association of Canada, St. John's, pp. 219–238.

Wright, L.D. 1977. Sediment transport and deposition at river mouths: a synthesis. Geological Society of America Bulletin 88, 857–868.

Yılmaz, Y. 1993. New evidence and model on the evolution of the southeast Anatolian orogen. Geological Society of America Bulletin 105, 251–271.

Yılmaz, Y., Yiğitbaş, E., Genç, Ş.C. 1993. Ophiolitic and metamorphic assemblages of southeast Anatolia and their significance in the geological evolution of the orogenic belt. Tectonics 12, 1280–1297.

Zaitlin, B., Dalrymple, R.W., Boyd, R. 1994. The stratigraphic organization of incised-valley systems. Dalrymple, R.W., Boyd, R., Zaitlin, B. (Ed.) Incised-Valley Systems: Origin and Sedimentary Sequences. SEPM Special Publication 51, 45–60.

Bulletin of the Mineral Research and Exploration

http://bulletin.mta.gov.tr

Active tectonic and paleoseismologic characteristics of the Yenice-Gönen fault, NW Turkey, in light of the 18 March 1953 Yenice-Gönen Earthquake (Ms=7.2)

Akın KÜRÇER[a*], Selim ÖZALP[b], Ersin ÖZDEMİR[c], Çağıl UYGUN GÜLDOĞAN[d] and Tamer Y. DUMAN[e]

[a]*General Directorate of Mineral Research and Exploration, Directorate of Geological Studies Department, 06800, Çankaya, Ankara, Turkey orcid.org/ 0000-0001-8646-5113*

[b]*General Directorate of Mineral Research and Exploration, Directorate of Geological Studies Department, 06800, Çankaya, Ankara, Turkey. orcid.org/0000-0002-6755-4206*

[c]*General Directorate of Mineral Research and Exploration, Directorate of Geological Studies Department, 06800, Çankaya, Ankara, Turkey orcid.org/0000-0002-8987-8842*

[d]*General Directorate of Mineral Research and Exploration, Energy Raw Materials Survey and Exploration Department, 06800, Çankaya, Ankara, Turkey orcid.org/ 0000-0002-1039-6542*

[e]*Fugro Sial Geoscience Consulting and Engineering Limited Company, Ankara, Turkey orcid.org/ 0000-0003-3556-2217*

Research Article

Keywords:
1953 Yenice-Gönen earthquake, Yenice-Gönen fault, North Anatolian Fault System, Slip rate, Paleoseismology

ABSTRACT

The Yenice-Gönen Fault (YGF) is located in the central part of the Biga Peninsula between Gönen and Yenice and is a right-lateral strike-slip active fault with general trending N65°E. On 18 March 1953 there was an earthquake on the YGF that died 263 people (Ms=7.2) and a 70 km surface rupture developed during this earthquake. In this study measurements of slip distribution were performed on the surface rupture of the Yenice-Gönen Earthquake (YGE) and the annual slip rate on the YGF was calculated. Right-lateral displacements of between 1.70±0.1 and 3.20±0.2 metres were measured on the surface rupture of the YGE. The maximum displacements were in an area close to the central part of the YGF (between Çakır and Karaköy village) and these values decreased relatively in NE and SW directions, documenting that was the bilaterally surface rupture propogation during the YGE. In the last 300.000 years, a total offset of 800±50 metres was measured on Gönen River and annual slip rate of 2.65±0.15 mm was calculated along the YGF. Current GPS studies show right-lateral strike-slip faults in the South Marmara region have slip rates of 6-8 mm/year. This slip rate is assessed as being partitioned between the YGF, Sarıköy Fault and Çan-Biga Fault zones which represent extensions of the North Anatolian Fault system within the South Marmara region. Paleoseismology studies determined that in the last 6200 years 6 earthquakes resulting in surface ruptures have occurred on the YGF, including the 1953 earthquake. According to the ^{14}C and OSL dating results, the variable and irregular earthquake recurrence interval of YGF is ranging from 505 to 1793 years. In this study average earthquake recurrence interval of YGF was determined as 1180 years.

Received Date: 30.01.2018
Accepted Date: 14.05.2018

1. Introduction

As a result of progressive deformation developing linked to continental collision between the African, Arabian and Eurasian plates in the Eastern Mediterranean Region, four main neotectonic regions have developed separated by the North Anatolian Fault system (NAFS), East Anatolian Fault system (EAFS), Dead Sea Fault Zone (DSFZ) and the active subduction zone of the Aegean-Cyprus arc (McKenzie, 1972, 1978; Şengör, 1979, 1980; Jackson and McKenzie, 1984; Şengör et al., 1985; Taymaz et

Citation Info: Kürçer, A., Özalp, S., Özdemir, E., Uygun Güldoğan, Ç., Duman, T. Y. 2019. Active tectonic and paleoseismologic characteristics of the Yenice-Gönen Fault, NW Turkey, in light of the 18 March 1953 Yenice-Gönen Earthquake (Ms=7.2). Bulletin of Mineral Research and Exploration, 159, 29-62. *http://dx.doi.org/10.19111/bulletinofmre.500553*

** Corresponding author: Akın KÜRÇER, akin.kurcer@mta.gov.tr*

al., 1991; LePichon et al., 1995; Armijo et al., 1999; Bozkurt, 2001). Currently, NW Turkey, is deformed by the western extensions of the NAFS (Figure 1).

The North Anatolian Fault system (NAFS) is a right-lateral strike-slip active fault system with nearly 1500 km length characterised by large earthquakes produced in the last century (Figure 1; Barka and Kadinsky-Cade, 1988). One of the most active fault systems in the Eastern Mediterranean Region in terms of seismicity, the NAFS begins at the Karlıova triple junction and extends in a linear zone to nearly 100 km east of Adapazarı. The NAFS divides into a northern and southern branch in this region due to the effect of variable stress states and forms a large-scale horsetail structure (Barka and Gülen, 1988; Şengör and Barka, 1992) (Figure 1). From east of Adapazarı the northern branch of the NAFS extends within Lake Sapanca to the Sea of Marmara. Within the Sea of Marmara, the system is represented by the Adalar, Avcılar, Kumburgaz and Tekirdağ segments from east to west, respectively (Emre et al., 2013). The northern branch extends nearly W-E through the Sea of Marmara, before bending toward the SE near Şarköy to enter the Gulf of Saros and the North Aegean Sea (Figure 2).

The southern branch extending with nearly E-W trending in Dokurcun Valley and south of the Sea of Marmara, is represented by the Geyve, İznik-Mekece and Gemlik Faults in this area from east to west, respectively. Between the Bay of Gemlik and Kapıdağ Peninsula, along the south coast of the Sea of Marmara, the southern branch makes a restraining bend to the SW from Kapıdağ Peninsula to extend into the Biga Peninsula. The southern branch of the NAFS extends from the NE of the Biga Peninsula to the SW and is represented by the Edincik, Sinekçi, Çan-Biga fault zone, Sarıköy, Bekten, Yenice-Gönen, Evciler faults and Edremit fault zone (Figure 2).

Destructive earthquakes have occurred in the historical and instrumental periods on the western part of the NAFS (Tables 1 and 2) (Figure 2). The YGF, one of the most active fault segments of the NAFS in south of Marmara produced an Ms=7.2 magnitude earthquake on 18 March 1953 and this earthquake

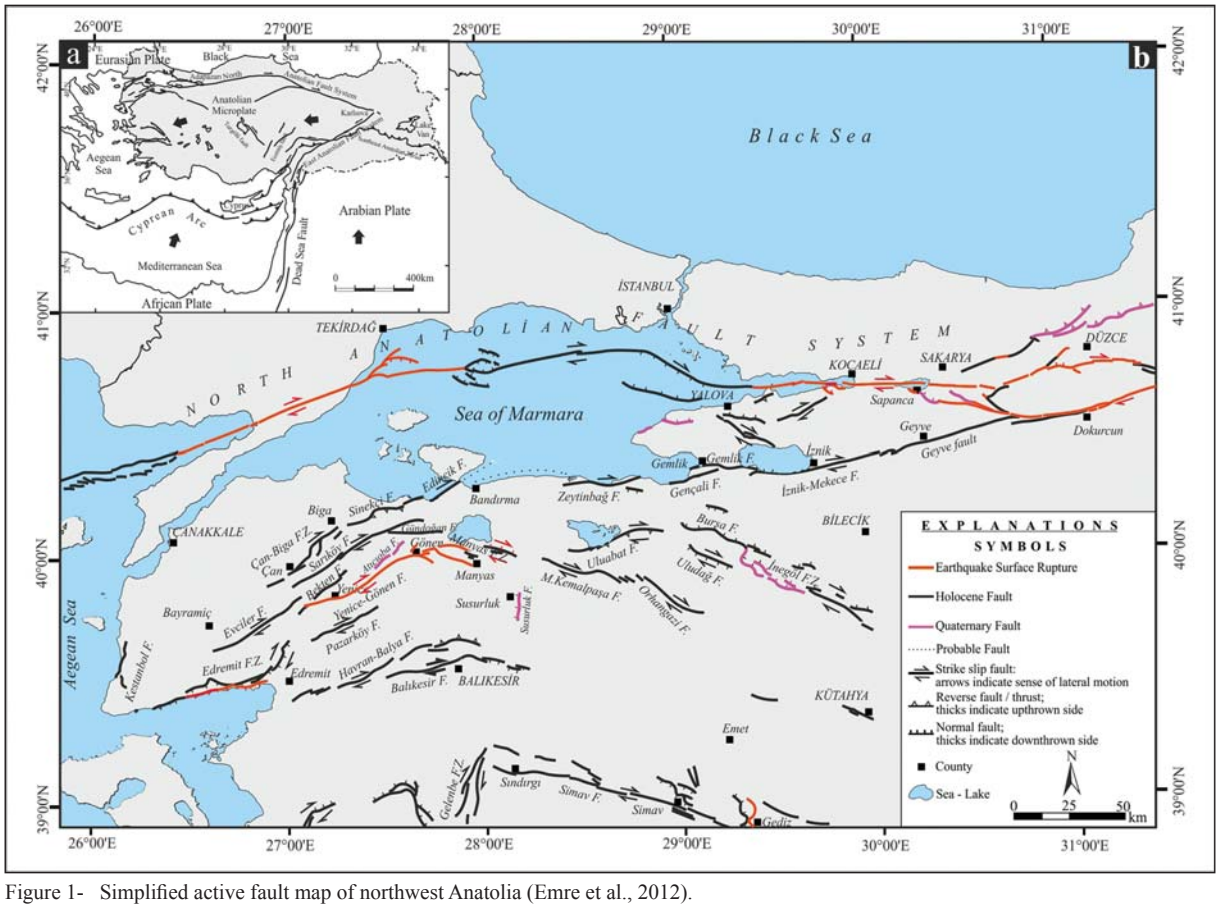

Figure 1- Simplified active fault map of northwest Anatolia (Emre et al., 2012).

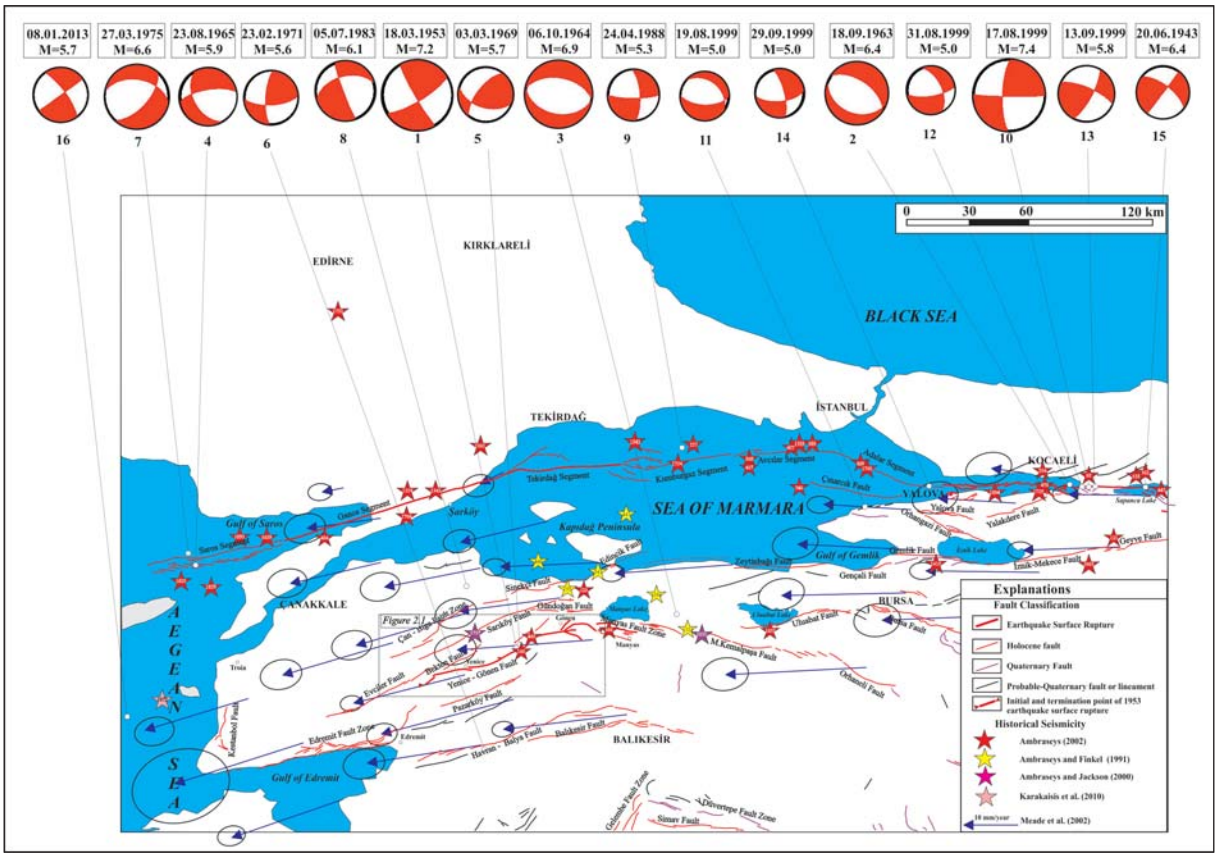

Figure 2- Active and capable active faults were drawn from Emre et al (2013) and in their references. GPS vectors taken from Meade et al. (2002). For historical and instrumental period earthquakes and focal mechanism solution references please see tables 1 and 2.

caused a surface rupture with nearly 70 km length between the east of Gönen and the southwest of Yenice (Kürçer, 2006; Kürçer et al., 2008) (Figure 2).

After the 18 March 1953 YGE the first macroseismic observations were made by Ketin and Roesly (1953), who recorded right lateral displacements varying from 4,3 m to 1,5 m along the surface rupture with total length of 50 km. Ketin and Roesly (1953) proposed the rupture progressed from E to W during the earthquake considering the P and S wave motion times. Another macroseismic study related to the YGE was completed by Pınar (1953). According to Pınar (1953), the YGE occurred on the southern branch of the NAFS and created a surface rupture with total 60 km length between the Sea of Marmara and the Gulf of Edremit. Focal mechanism solutions indicating the YGE was caused by a NE-SW striking right lateral strike-slip fault were made by McKenzie (1972). According to Herece (1990), the length of the surface rupture developing during the YGE was 50 km. The researcher stated the YGF experienced several faulting periods in the Quaternary based on fault scarps at different erosion levels observed during surface rupture mapping. Herece (1990) proposed that the total right lateral offset of the YGF was 2,8 km from the Late Pliocene to the present and annual slip rate was 1,4 mm. A study of active tectonism in central and northern Aegean by Taymaz et al. (1991) stated the thrust component was dominant during the 1969 Gönen earthquake (see figure 2) and indicated that the Biga Peninsula was rising due to this compression.

GPS studies in the Marmara region (Straub, 1996; Straub and Kahle, 1997; Reilinger et al., 1997; Meade et al., 2002; Kreemer et al., 2004; Reilinger et al., 2006) reveal the annual right lateral movement of the Anatolian block relative to Eurasia is 20-25 mm and this is mainly distributed along the NAFS. Straub (1996) proposed that the majority of this movement was on the northern branch of the NAFS with the remaining portion distributed along the southern branch. Meade et al. (2002) proposed annual slip rates from right-lateral strike-slip faults and normal faults which were extensions of the NAFS in the Marmara region based on GPS measurements. Accordingly, the

Table 1- Large historical earthquakes occurring in northwest Turkey.

Date	Degree of latitude (N)	Degree of longitude (E)	Magnitude (M)	Location	Reference
32	40,5	30,5	7,0	Nicaea (İznik)	Ambraseys (2002)
68	40,7	30,0	7,2	Nicaea (İznik)	Ambraseys (2002)
121	40,5	30,1	7,4	Nicomedia (İzmit)	Ambraseys (2002)
10.11.123	40,3	27,7	7,0	Cyzicus (Erdek)	Ambraseys (2002)
155				Hellespont and Bithynia	Ambraseys and Finkel (1991)
160	40,0	27,5	7,1	Hellespont (Ç. straits)	Ambraseys (2002)
03.05.180	40,6	30,6	7,3	Nicomedia (İzmit)	Ambraseys (2002)
268	40,7	29,9	7,3	Nicomedia (İzmit)	Ambraseys (2002)
24.08.358	40,7	30,2	7,4	İzmit	Ambraseys (2002)
02.12.362	40,7	30,2	6,8	İzmit	Ambraseys (2002)
11.10.368	40,5	30,5	6,8	Persis	Ambraseys (2002)
368	40,1	27,8	6,8	Germe	Ambraseys (2002)
01.04.407	40,9	28,7	6,8	Hebdomon (Bakırköy)	Ambraseys (2002)
25.09.437	40,8	28,5	6,8	İstanbul	Ambraseys (2002)
06.11.447	40,7	30,3	7,2	Nicomedia (İzmit)	Ambraseys (2002)
07.04.460				Cyzicus (Erdek)	Ambraseys and Finkel (1991)
25.09.478	40,7	29,8	7,3	Helenopolis	Ambraseys (2002)
484	40,5	26,6	7,2	Callipolis	Ambraseys (2002)
06.09.543				Cyzicus (Erdek)	Ambraseys and Finkel (1991)
16.08.554	40,7	29,8	6,9	Nicomedia (İzmit)	Ambraseys (2002)
14.12.557	40,9	28,3	6,9	Silivri	Ambraseys (2002)
26.10.740	40,7	28,7	7,1	Marmara	Ambraseys (2002)
23.05.860	40,8	28,5	6,8	Marmara	Ambraseys (2002)
09.01.869	40,8	29,0	7,0	CP	Ambraseys (2002)
02.09.967	40,7	31,5	7,2	Bolu	Ambraseys (2002)
25.10.989	40,8	28,7	7,2	Marmara	Ambraseys (2002)
23.09.1063	40,8	27,4	7,4	Panio	Ambraseys (2002)
1065	40,4	30,0	6,8	Nicaea (İznik)	Ambraseys (2002)
01.06.1296	40,5	30,5	7,0	Bithynia	Ambraseys (2002)
1323				İstanbul	Ambraseys and Finkel (1991)
18.10.1343	40,7	27,1	6,9	Ganos	Ambraseys (2002)
18.10.1343	40,9	28,0	7,0	Heraclea	Ambraseys (2002)
01.03.1354	40,7	27,0	7,4	Hexamili	Ambraseys (2002)
15.03.1419	40,4	29,3	7,2	Bursa	Ambraseys (2002)
10.09.1509	40,9	28,7	7,2	CP	Ambraseys (2002)
10.05.1556				Sea of Marmara	Ambraseys and Finkel (1991)
18.05.1625	40,3	26,0	7,1	Saros	Ambraseys (2002)
17.02.1659	40,5	26,4	7,2	Saros	Ambraseys (2002)
14.02.1672	39,7	25,8	7,0	Bozcaada	Karakaisis et al. (2010)
25.05.1719	40,7	29,8	7,4	İzmit	Ambraseys (2002)
06.03.1737	40,1	27,3	7,0	Aşağı İnova	Ambraseys and Jackson (2000)
29.07.1752	41,5	26,7	6,8	Edirne	Ambraseys (2002)
02.09.1754	40,8	29,2	6,8	İzmit	Ambraseys (2002)
22.05.1766	40,8	29,0	7,1	Marmara	Ambraseys (2002)
05.08.1766	40,6	27,0	7,4	Ganos	Ambraseys (2002)
19.04.1850	40,1	28,3	6,1	Between Lakes Manyas and Uluabat	Ambraseys and Jackson (2000)
28.02.1855	40,1	28,6	7,1	Bursa	Ambraseys (2002)
21.08.1859	40,3	26,1	6,8	Saros	Ambraseys (2002)
09.02.1893	40,5	26,2	6,9	Saros	Ambraseys (2002)

Table 2- Fault plane solutions for the instrumental period earthquakes listed in figure 2 (adapted from Şengör et al., 2004).

No	Date (day. month. year)	Time (hour: minute) GMT	Degree of latitude (N)	Degree of longitude (E)	Magnitude	Depth (km)	Strike (°)	Dip (°)	Rake (°)	Reference
1	20.06.1943	15:33	40,83	30,48	6,4	?	176	76	0	McKenzie (1972)
2	18.03.1953	19:06	40,01	27,49	7,2	10*	59	84	14	McKenzie (1972), Ayhan et al. (1981)
3	26.05.1957	06:33	40,58	31,00	7,0	?	87	78	179	McKenzie (1972)
4	26.05.1957	09:36	40,80	30,80	6,0	?	114	24	-166	Canıtez and Üçer (1967)
5	27.05.1957	11:01	40,70	31,00	5,5	?	293	74	157	Canıtez and Üçer (1967)
6	18.09.1963	16:58	40,71	29,09	6,4	15	304	56	-82	Taymaz et al. (1991)
7	06.10.1964	14:31	40,20	28,20	6,9	14	100	40	-90	Taymaz et al. (1991)
8	23.08.1965	14:08	40,39	26,12	5,9	33	261	70	-132	Kocaefe and Ataman (1976)
9	22.07.1967	16:56	40,67	30,69	7,1	12	275	88	-178	Taymaz et al. (1991)
10	30.07.1967	01:32	40,72	30,52	5,6	16	301	50	70	McKenzie (1972)
11	03.03.1969	00:59	40,08	27,50	5,7	4	219	65	45	McKenzie (1972)
12	23.02.1971	19:41	39,62	27,32	5,6	10	86	66	160	Papadopoulos et al. (1986)
13	27.03.1975	05:15	40,45	26,12	6,6	15	279	46	-43	Jackson and McKenzie (1984)
14	05.07.1983	23:02	40,33	27,21	6,1	15	254	49	-173	Harvard Univ. (1998)
15	24.04.1988	20:49	40,88	28,24	5,3	15	356	71	-11	Harvard Univ. (1998)
16	17.08.1999	00:01	40,70	29,99	7,4	9	91	87	164	GCMT Catalogue
17	17.08.1999	03:14	40,59	30,62	5,3	8	192	32	-82	Örgülü and Aktar (2001)
18	19.08.1999	15:17	40,65	29,09	5,0	4	92	60	-110	Örgülü and Aktar (2001)
19	31.08.1999	08:10	40,74	29,99	5,0	8.6	80	70	-143	Özalaybey et al. (2002)
20	13.09.1999	11:55	40,76	30,07	5,8	12	293	73	164	Örgülü and Aktar (2001)
21	29.09.1999	00:13	40,71	29,30	5,0	8	85	63	-161	Örgülü and Aktar (2001)
22	11.11.1999	14:41	40,78	30,29	5,5	20	307	66	179	Örgülü and Aktar (2001)
23	08.01.2013	14:16	39,65	25,50	5,7	8	54	89	-166	Kürçer et al. (2015)

right-lateral slip rate along the Uluabat and Manyas faults in the southern Marmara region was 3,6±2,0 mm with vertical offset rate of 8,0±3,4 mm; while along the YGF and Sarıköy İnova fault the annual right lateral offset was 6,8±2,3 mm and vertical slip rate was 0,8±3,4 mm. Another GPS study of active faults in the southern Marmara region by Kremmer et al. (2004) calculated the right-lateral strike-slip annual slip rate was 7 mm along the southern branch of the NAFS defined as the Bursa-Yenice-Gönen line. The approximately 7 mm/year right-lateral slip rate calculated by Meade et al. (2002) and Kremmer et al. (2004) for all faults belonging to the southern branch of the NAFS must be shared between different faults led by the Yenice Gönen and Sarıköy faults (Kürçer, 2008).

The first studies researching the paleoseismologic properties of the YGF were completed by Kürçer (2006) and Kürçer et al. (2008). Kürçer et al. (2008) dated three earthquakes on the YGF causing surface ruptures in the last 1400 years including the 1953 earthquake. The first of these earthquakes was in 620 AD and the second was in 1440 AD. Based on this age data, they proposed the average earthquake recurrence interval for the YGF was 660±160 years. Using the earthquake recurrence interval and a displacement amount of 4,2 metres, the researchers calculated the annual slip rate for the YGF as 6.3 mm and noted the compliance of this value with results obtained from GPS measurements. Dirik et al. (2008) in a study researching the neotectonic and paleoseismologic properties of the YGF reported the surface rupture length of the YGF was 60 km. The researchers measured 65 to 495 cm right lateral displacement during the YGE. Cumulative displacement amounts measured along the YGF varied from 6,8 to 38 m. Based on the cumulative offset values on the Seyvan,

Karasu and Gönen segments, Dirik et al. (2008) proposed at least five earthquakes had occurred. A study of the seismotectonics of the Biga Peninsula and south Sea of Marmara by Özden et al. (2008) revealed that the faults located in the north of the Biga Peninsula were currently transpressive while the faults located in the south were mainly transtensive in character. On the Revised Turkish Active Fault map, Emre et al. (2013) assessed the YGF as a 67 km long, active fault comprising 4 geometric segments. The researchers adapted the 5 km value recommended by Duru et al. (2012) in the Hallaçlar formation near Yenice as the total offset on the YGF. Based on GPS studies (Meade et al., 2002; Kremmer et al., 2004), Emre et al. (2013) proposed that the recommended 6-8 mm total annual slip rate proposed for all the NE-SW oriented faults in the Biga Peninsula was equally shared between the YGF, Sarıköy Fault and Biga-Çan fault zone. From this aspect, they proposed the annual slip rate on the YGF was 2-3 mm. A study researching historical earthquakes affecting ancient city of Troy by Kürçer et al. (2012) proposed that Troy III (2200-2050 BC) and Troy VI (1800-1275 BC) settlements were destroyed by earthquakes and that these earthquakes may be due to active faults in the area. According to izoseist maps of the 1912 Şarköy-Mürefte (Mw=7.2), 1953 Yenice-Gönen (Mw=7.2) and 1983 Biga (Mw=6.8) earthquakes occurring near Troy in the last century, the researchers stated these earthquakes affected the Troy region with VIII-X intensity (MSK). Based on this they noted that active faults in the Biga Peninsula may have affected the Troy region in the historical period. The researchers recommended that earthquake dates obtained from paleoseismological studies to be completed in the Biga Peninsula should be compared with the destruction times of Troy III and VI settlements.

In this study, comprehensive active fault and paleoseismology studies completed on the surface rupture of the 18 March 1953 Yenice-Gönen earthquake were used to research the active tectonic and paleoseismologic properties of the YGF and re-evaluate it within the regional tectonic framework.

2. Geology of Yenice-Gönen Fault and Surroundings

In the study area, there are outcrops of different age from the Palaeozoic to the present and types of rock units (Figure 3). Pre-Tertiary aged rocks in the Biga Peninsula and surroundings are composed of four tectonic belts with trending NE-SW (Duru et al., 2012). These are the İzmir-Ankara Zone / Bornova Flysch, Sakarya Zone, Çetmi Melange and Ezine Zone, from east to west, respectively.

The basement units near the YGF and surroundings located in the central part of the Biga Peninsula comprises the Kazdağ Metamorphics belonging to the Sakarya zone. In the study area the Kazdağ Metamorphics are represented by the Sütüven formation (Cs).

These units are overlain by the metamorphics of the Late Paleozoic age Kalabak Group with a tectonic contact. Comprising low-grade metamorphics, the Kalabak Group Metamorphics are represented by the Torasan formation (Pzt) comprising marble and phyllite and schists with metaserpentinite lenses at the base and the Sazak formation (Pzs) comprising metatuffs with marble intercalations at the top (Duru et al., 2012).

The Torasan metamorphics in the Kalabak Group are cut by the Çamlık Metagranodiorite (Pzç) consisted of metagranodiorite and granitic gneiss (Duru et al., 2012).

The Kalabak Group Metamorphics are tectonically overlain by Karakaya Complex (Okay and Göncüoğlu, 2004; Aysal et al., 2012*a*,*b*). The Karakaya Complex comprises Late Permian (?)-Triassic aged units with mainly tectonic contacts but occasional transitions. Within the Karakaya Complex, undifferentiated units of metaconglomerate, metasandstone, sandy limestone, tuff, metavolcanics and Devonian, Carboniferous and Permian-aged limestone blocks are defined as Karakaya Complex units (Trkk) (Duru et al., 2012). Additionally, the Karakaya Complex is represented by arkosic sandstone (Trka), Mehmetalan formation (Trkm) and Çal formation (Trkç) from bottom to top.

The Karakaya Complex units are unconformably overlain by the Lias-aged Bayırköy formation comprising continental and shallow marine conglomerates, sandstone, mudstone and limestone.

Toward the top of the Bayırköy formation, there is a transition to the Callovian-Hauterivian-aged Bilecik formation comprising platform-type limestones. Above the Bilecik formation, there is a conformable transition to the hemipelagic, micritic limestone and claystone alternations of the Hauterivian-Albian-aged

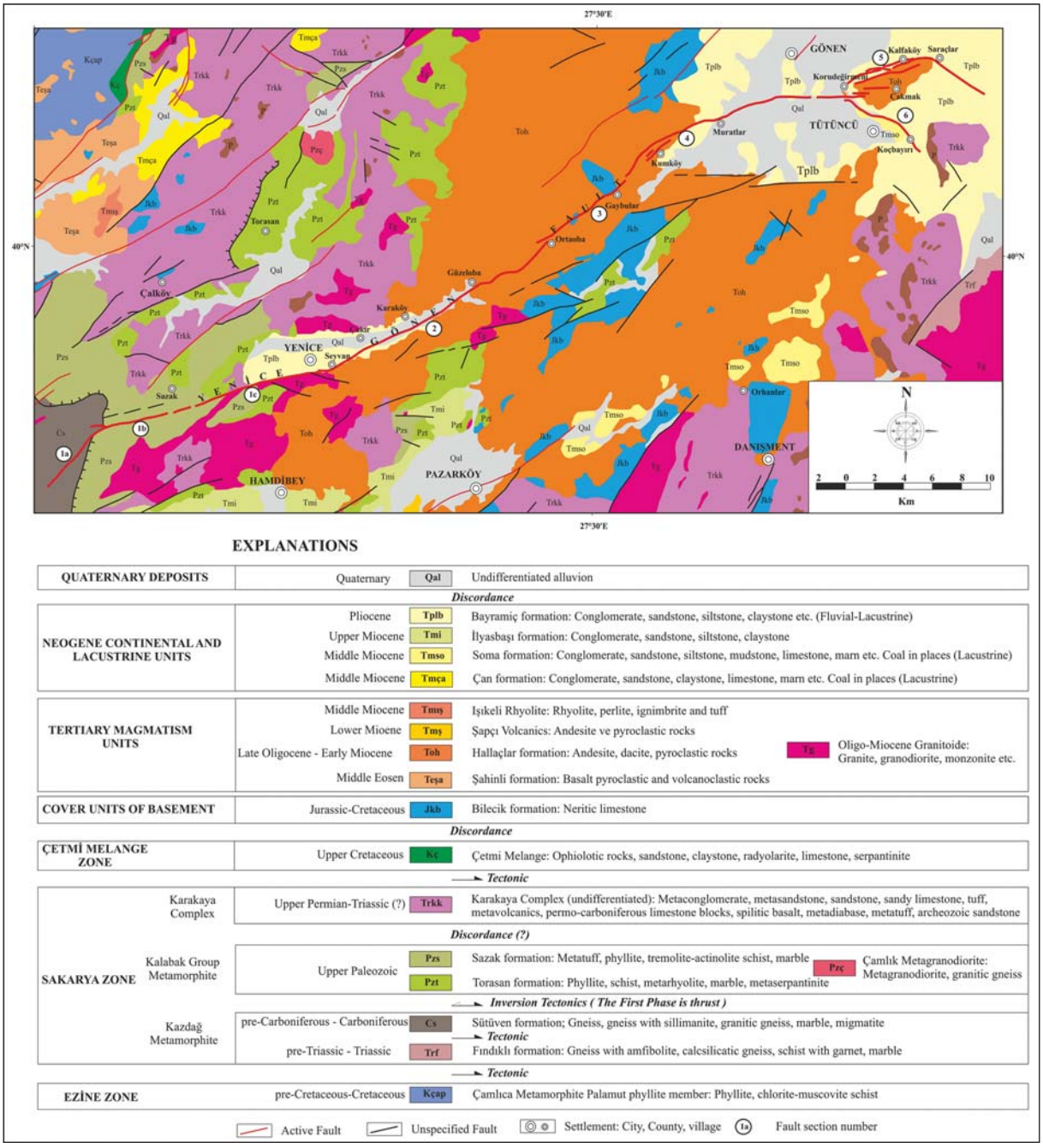

Figure 3- Geologic map of the central part of the Biga Peninsula (adapted from Duru et al., 2012).

Pınar formation (Duru et al., 2012). These cover units above basement units are only represented within the study area by the Bilecik formation with very limited outcrop area NE of Yenice.

The study area contains, volcanic units of Tertiary magmatism, volcanosedimentary sequences and granitoids (Altunkaynak et al., 2012; Aysal, 2015). Products of Tertiary magmatism outcrop in larger areas of the central part of the Biga Peninsula and are represented by the Middle Eocene Şahinli formation, Late Oligocene-Early Miocene Hallaçlar formation and the coeval Tertiary granitoids, Lower Miocene Şapçı Volcanics and Middle Miocene Işıkeli Rhyolite (Karacık et al., 2008; Aysal et al., 2012*b*). In the Biga Peninsula, mainly closed basins developed under control of active faults with terrestrial sediments and/or lacustrine carbonate rocks deposited in fluvial or

lake environments. These units comprise Middle Miocene sediments and coals of the Çan and Soma formations, Upper Miocene sediments of the İlyasbaşı formation and Pliocene sediments and occasional carbonates of the Bayramiç formation. Quaternary-Holocene modern sediments unconformably cover all these units.

3. Segment Structure of Yenice-Gönen Fault

The YGF is an active fault that has produced more than one earthquake resulting in surface rupture in the geologic past. In the literature, "earthquake segments" are defined as differentiable sections of an active fault producing earthquakes with two or more surface ruptures (dePolo et al., 1989, 1991). Therefore, the YGF is assessed as an earthquake segment with proven seismicity based on the 1953 earthquake and paleo-earthquakes identified in this study. Within fault segments, shorter sections separated from each other by step or bend structures are assessed as fault sections.

The YGF comprises 6 fault sections with lengths varying from 5,5 to 19 km separated by restraining or releasing bends or steps. These are named the Sazak, Çakır, Gaybular, Muratlar, Kalfaköy and Tütüncü fault sections from SW to NE (Figures 3 and 4).

The Sazak section has total length of 19 km and comprises three sub-sections separated by en-echelon offset-overlapping steps (Figure 3). The section in the SW has N45°E strike and 6 km length (1a on Figure 3). This section of the fault extending from Sakardağı to Sazak Stream is observed within the Sütüven formation (Cs) belonging to the Kazdağ Metamorphics. The second subsection of the Sazak section is 6,5 km long and begins in the west at Kale Hill and is observed to continue west of Sazak Valley with N75°E strike (1b on Figure 3). In this section the fault cuts a normal fault contact between the Sütüven formation (Cs) belonging to the Kazdağ Metamorphics and the Sazak formation (Pzs) belonging to the Kalabak Group, offsetting it to the right-laterally. The easternmost part of the Sazak section is 9,5 km long (1c on Figure 3). The fault in this section extends with N85°E strike between Sazak Valley and Yenice and forms the boundary between the Sazak formation (Pzs) and Quaternary-aged alluvial sediments in the Sazak Valley. From east of Sazak Valley to Yenice, it controls the contacts between the Sazak formation (Pzs) with the Torasan formation (Pzt) of the Kalabak Group, between Tertiary granitoids (Tg) and Karakaya Complex units (Trkk) and between Tertiary granitoids and Plio-Quaternary basin sediments of the Yenice Basin (Tplb) (Figure 3).

The Sazak section is separated from the Çakır section by a 200 m wide and 500 m long restraining step in the south of Yenice. The Çakır section has total length of 19 km between Yenice and Ortaoba (2 on Figure 3). With E-W strike between Yenice and Seyvan, the fault bends to the left SW of Seyvan Village to extend towards the east of Çakır with

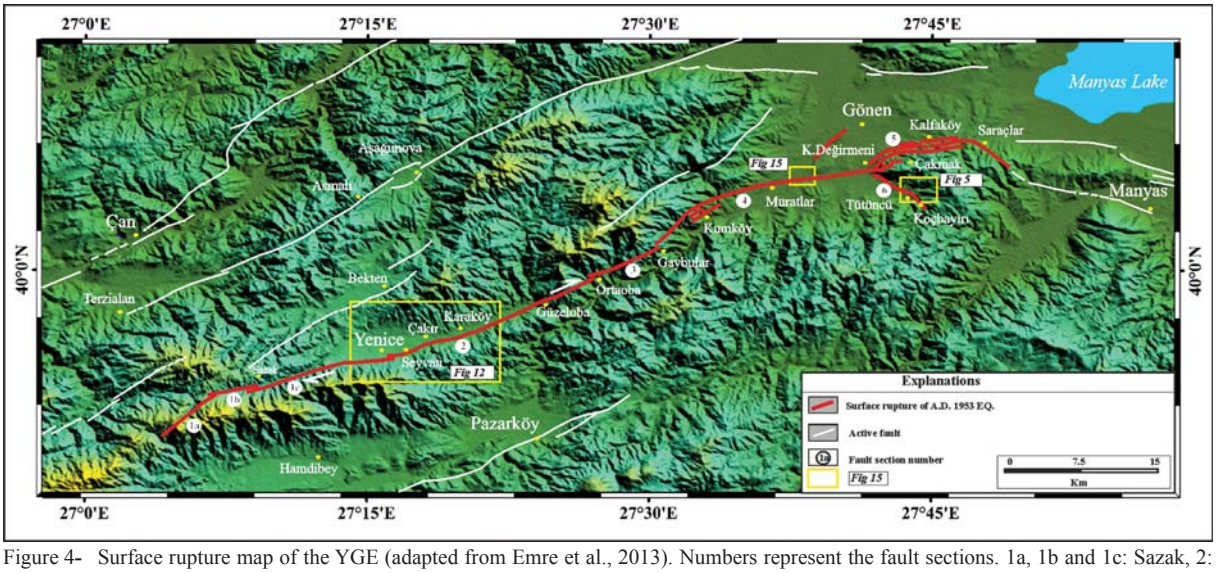

Figure 4- Surface rupture map of the YGE (adapted from Emre et al., 2013). Numbers represent the fault sections. 1a, 1b and 1c: Sazak, 2: Çakır, 3: Gaybular, 4: Muratlar, 5: Kalfaköy, 6: Tütüncü..

N67°E general trending. In this section the fault has reverse component the effect of restraining bending. East of Çakır the fault again bends toward the left and extends to the west of Güzeloba with N67°E strike. The remaining easternmost part of the Çakır section between Güzeloba and Ortaoba villages is characterised by bends to the right and left. The Çakır section cuts Tertiary granitoids and the Late Oligocene-Early Miocene Hallaçlar formation between Yenice and Seyvan. South of Seyvan, the fault controls the contact between the Hallaçlar formation and Yenice basin sediments and occasionally cuts Late Quaternary-Holocene alluvial sediments in this area. Between Çakır and Karaköy, the fault mainly cuts Yenice (Small Agonia) stream sediments entering the Hallaçlar formation east of Karaköy and is observed within these units until the east boundary of the fault section.

NW of Ortaoba, a 750 m long, 250 m wide left step separates the Çakır section from the Gaybular section with 10 km length (3 on Figure 3). Extending from southwest of Kumköy to Çatalçal hill with N55°E trending, the Gaybular section is mainly observed within the Hallaçlar formation, occasionally cutting neritic limestones belonging to the Jurassic-Cretaceous Bilecik formation.

The Gaybular section is separated from the Muratlar section by a 3 km long, 500 m wide restraining bend west of Kumköy (4 on Figure 3). The Muratlar section has total length of 16 km and extends with N65°E trending between Kumköy and Gönen Stream before bending toward the right from Gönen Stream to extend west of Çakmak Village with E-W trending. The Muratlar section brings the Hallaçlar formation side-by-side with Pliocene clastic sediments of the Bayramiç formation between Kumköy and Muratlar. East of Muratlar, the fault cuts alluvial sediments of Gönen Stream, before cutting sediments from the Bayramiç formation south of Korudeğirmeni and ending within the Hallaçlar formation.

Comprising the easternmost section of the main body of the YGF, the Kalfaköy section extends with general trend of N60°E from west of Korudeğirmeni to east of Saraçlar village (5 on Figure 3). With total length of 6 km, the section is represented by a 300 m wide deformation zone. The Kalfaköy section ends with a bend to the SE (Saraçlar bend) near Saraçlar village. This section is also to the section where the Yenice-Gönen Fault overlaps with the surface rupture of the 1964 Manyas earthquake. The majority of the Kalfaköy section controls the contact between the Hallaçlar formation and the Bayramiç formation.

The 5,5 km section of the YGF between Korudeğirmeni and Koçbayırı villages with N70°W trending is named the Tütüncü section (6 on Figure 3). The Tütüncü section is a splay fault of the YGF extending toward the SE. The fault gains a reverse component making a bend to the left north of Tütüncü (Figure 5). The majority of the Tütüncü section controls the contact between the Bayramiç formation and the Soma formation, occasionally cutting the Soma formation and alluvial fan sediments.

4. 18 March 1953 Yenice-Gönen Earthquake (Ms=7.2) Surface Rupture

On 18 March 1953 at 19:06 (GMT) in southern Marmara (Coordinates: 40.01 N – 27.49 E), an earthquake (Ms=7.2) occurred with 10 km focal depth (Ayhan et al., 1981). As a result of the earthquake, 263 people died, more than 8000 buildings were damaged, 211 schools, 176 official buildings and 27 mosques were destroyed (Barka et al., 2002). The earthquake was felt in Çanakkale, Edirne, İstanbul, Adapazarı, Bursa, Balıkesir, Dikili, Foça and Karaburun. According to focal mechanism solutions, the source of earthquake is a N59°E trending right-lateral strike-slip fault (Canıtez and Üçer, 1967; McKenzie, 1972). A total surface rupture length of 70 km was caused by the YGE (see figures 3 and 4). In this study, observations of the 1953 YGE surface rupture were made at a total of 28 points (Table 3).

The first point where the 1953 YGE surface rupture traces can be observed is Dede Çeşme near Taşlıburun Ridge southwest of Yenice (YGF-01 in Table 3). At this location the YGE offsets a stream by 1,70±10 cm right-laterally and 50±5 cm vertically.

South of Yenice a 200 m wide and 500 m bend toward the left divides the Sazak section from the Çakır section, with total length of 19 km between Yenice and Ortaoba. Following E-W strike between ancient Yenice and Seyvan, the surface rupture bends 15° to the left from southwest of Seyvan Village with N75°E strike east of Çakır. In this area, the fault has reverse component due to the effect of restraining bends. This characteristic is clearly observed in trenches ezcavated south of Seyvan. The 1953 surface rupture is characterised by linear fault scarps between ancient

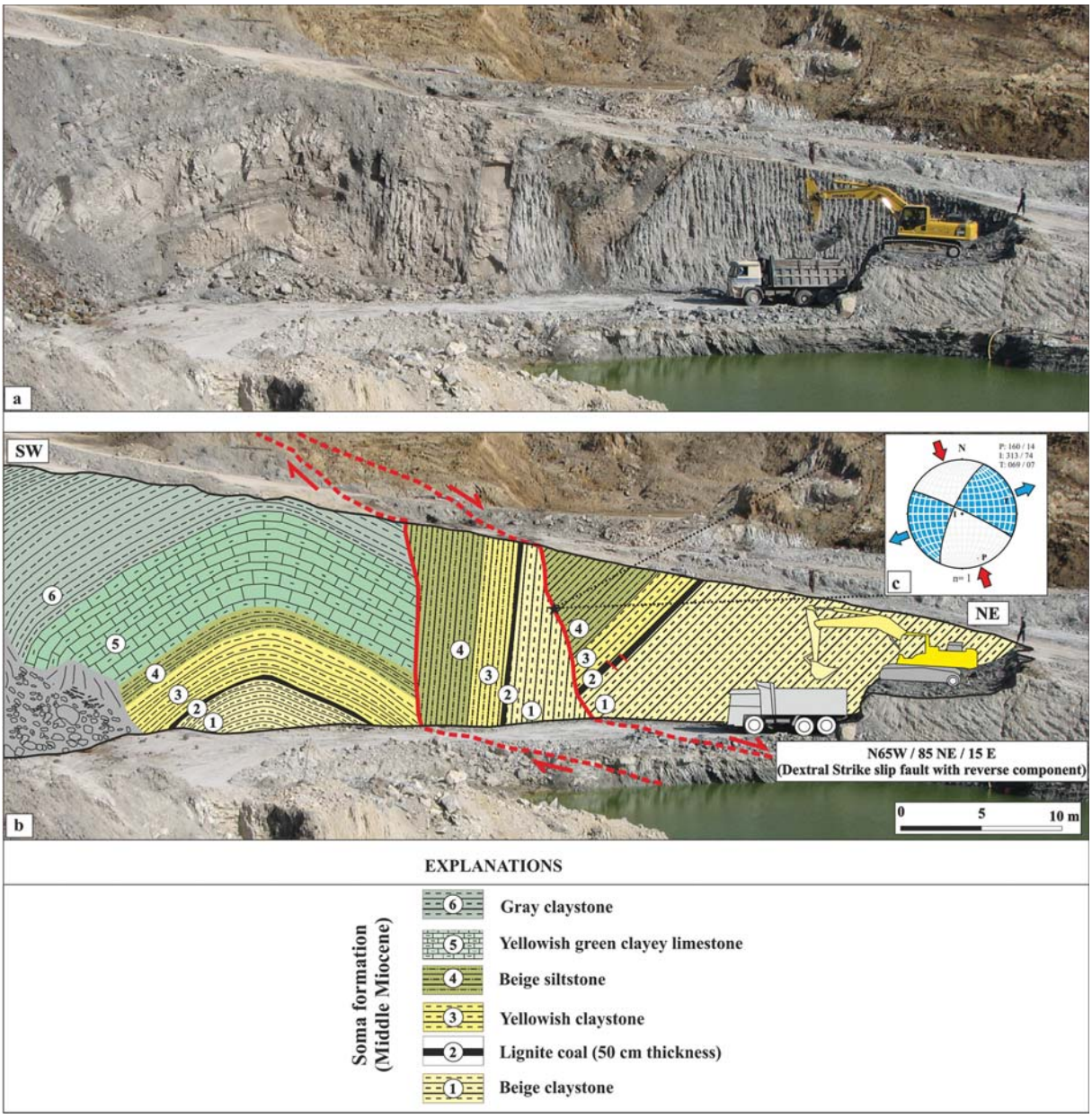

Figure 5- Structural properties of the Tütüncü fault section north of Tütüncü Village, a) Field photograph, b) Geological cross-section, c) Fault plane solution on Schmidt network hemisphere using Faultkin program (Almendinger et al., 2012).

Yenice and Seyvan (Figure 6). South of Seyvan, the fault forms the contact between the Late Oligocene-Early Miocene Hallaçlar formation and the Pliocene Bayramiç formation, cutting occasional alluvial fan sediments and slope debris. From east of Seyvan, the fault enters the Bayramiç formation and reaches south of Çakır by cutting the Yenice – Pazarköy road (Figure 7) N75°E (YGF-03 in Table 3).

The surface rupture of the 1953 earthquake extends with N70°E strike between Karaköy and Güzeloba. The easternmost part of the Çakır section between Güzeloba and Ortaoba villages is characterised by bends to the right and left. In this section the surface rupture is observed within the Late Oligocene-Early Miocene Hallaçlar formation. The surface rupture is observed as a crushed-brecciated fault zone in a stabilised road cut at the Kuştepe locale (YGF 17 in Table 3) located 1 km NE of Güzeloba village. According to information obtained from witnesses of the earthquake, there was a surface rupture southwest of Namazlık stream in Karasu (Karasuçam)

Table 3- Observation points of surface rupture of YGE (adapted from Kürçer, 2006).

Observation no	Sheet no	Coordinates (UTM)	Displacement amount (cm)	Explanation
YGF-01	İ 18 a2	35 0519481 E 44 18504 N	170±10 (right lateral) 50±5 (vertical)	Offset stream in Dede Çeşme locale west of Yenice
YGF-02	İ 18 b1	35 0525157 E 44 19713 N	2.86 (right lateral) 50±10 (vertical)	Linear fault scarps in trench area south of Seyvan
YGF-03	İ 18 b1	35 0527 125 E 44 21120 N	2.50 (right lateral)	Point where 1953 surface rupture cuts Yenice-Gönen road
YGF-04	İ 18 b1	35 0528759 E 44 21870 N	320±50 (right lateral)	South of Çakır, offset tree line west of the bridge
YGF-05	İ 18 b1	35 0528987 E 4421983 N	200±10 (right lateral)	South of Çakır, offset field boundary east of the bridge
YGF-06	İ 18 b1	35 0528786 E 4421884 N	190±30 (right lateral)	South of Çakır, offset field boundary west of the bridge
YGF-07	İ 18 b1	35 0528808 E 4421917 N	220±20 (right lateral)	South of Çakır, offset field boundary at west edge of the bridge
YGF-08	İ 18 b1	35 0529329 E 4421931 N	2200±200 (right lateral)	Cumulative stream offset SE of Çakır
YGF-09	İ 18 b1	35 0529655 E 4422068 N	2300±200 (right lateral)	Cumulative stream offset SE of Çakır
YGF-10	İ 18 b1	35 0528886 E 4421778 N	200±10 (right lateral)	Offset field boundary SE of Çakır
YGF-11	İ 18 b1	35 0529263 E 44 22035 N	320±20 (right lateral)	South of Çakır, offset field boundary east of the bridge
YGF-12	İ 18 b1	35 0529998 E 44 22325 N	300±30 (right lateral)	Offset field boundary SE of Çakır
YGF-13	İ 18 b1	35 0530015 E 44 22328 N	320±20 (right lateral)	Offset field boundary SE of Çakır
YGF-14	İ 18 b1	35 0530053 E 44 22358 N	310±20 (right lateral)	Offset field boundary SE of Çakır
YGF-15	İ 18 b2	35 0531779 E 4423208 N	1800±200 (right lateral)	Cumulative stream offset SE of Karaköy
YGF-16	İ 18 b2	35 0532046 E 44 23454 N	2100±200 (right lateral)	Cumulative stream offset SE of Karaköy
YGF-17	İ 18 b2	35 0536199 E 44 26017 N		Crush zone 1 km NE of Güzeloba
YGF-18	İ 18 b2	35 0538042 E 44 26787 N		N50°E-trending surface rupture 500 m SW of Karasukabaklar
YGF-19	İ 18 b2	35 0532046 E 44 23454 N		Reidel fracture in Karasubaklar Village
YGF-20	H 18 c3	35 0538883 E 44 28291 N		Earthquake surface rupture at Yolçatı locale 2 km north of Karasukabaklar
YGF-21	H 18 c3	35 0538883 E 44 28291 N		Earthquake surface rupture at Akpınar stream locale 4 km north of Ortaoba
YGF-22	H 19 d4	35 0542834 E 44 31164 N		Earthquake surface rupture and sag pond 2 km southwest of Gaybular
YGF-23	H 19 d4	35 0547376 E 44 34888 N	175±15 cm (right lateral)	Offset fence, pressure ridge and linear fault scarp north of Kumköy
YGF-24	H 19 d4	35 0550525 E 44 36293 N	150 cm (right lateral) 10 cm (vertical)	Offset old village road northeast of Muratlar
YGF-25	H 19 d4	35 0550731 E 44 36368 N		Point where surface rupture cuts Muratlar-Gönen road
YGF-26	H 19 d3-d4	35 0553674 E 4437384 N	800±50 m (right lateral)	Total offset of Gönen Stream
YGF-27	H 19 d3	35 0562103 E 44 39833 N		YGF cutting Hallaçlar formation southwest of Kalfaköy
YGF-28	H 19 d3	35 64139 E 44 40556 N	50 cm (vertical)	Surface rupture south of Gökçesu

Figure 6- Linear fault scarp (looking south) (YGF-02) south of Seyvan Village (Photograph taken from Kürçer, 2006).

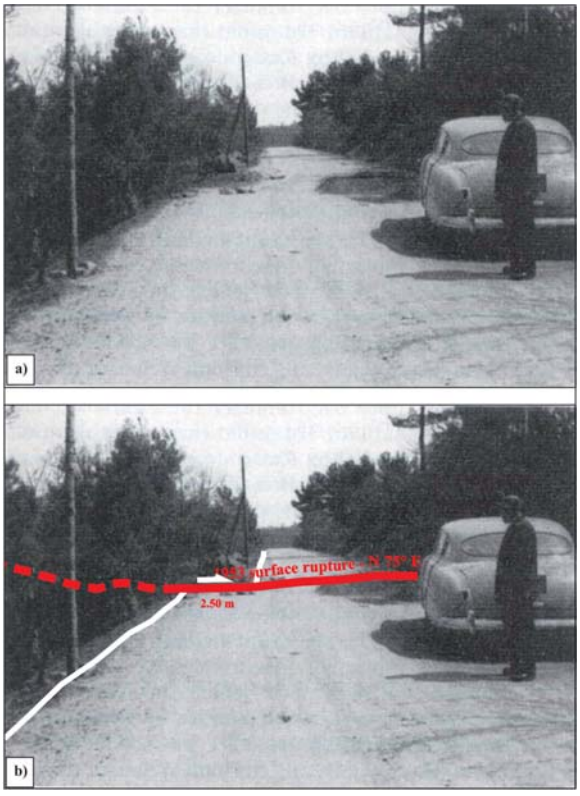

Figure 7- Offset due to the YGE surface rupture on the Yenice – Gönen road (photograph taken from Ketin and Roesly, 1953) (YGF-03) (View to the east).

Village and the north block fell down nearly 50 cm. The strike of the surface rupture between Karasu and Karasukabaklar village was N50°E. Within Karasukabaklar Village, a N70°W surface rupture developed during the 1953 earthquake. This rupture is interpreted as an R fracture developing within a right-lateral strike-slip system.

Northwest of Ortaoba, the Çakır section is separated from the 10 km Gaybular section by a 750 long and 250 m wide step to the left. With N55°E strike, the Gaybular section extends from southwest of Kumköy to Çatalçal Hill and is observed mainly within the Hallaçlar formation in this area, occasionally cutting neritic limestones of the Jurassic-Cretaceous Bilecik formation. The first point in the Gaybular section where the earthquake surface rupture is observed is at Yolçatı locale 2 km north of Karasukabaklar Village (YGF-20 in Table 3). At Yolçatı locale, a surface rupture with N58°E strike developed. The earthquake surface rupture is clearly observed in the northwest slope of Çaltepe 4 km north of Ortaoba. From north of Çaltepe until west of Gaybular, the surface rupture has N60°E strike with a small-scale sag pond occurring in the area northwest of Bozkıraç Hill (YGF-22 in Table 3). The surface rupture forms the contact between the

Jurassic-Cretaceous neritic limestones of the Bilecik formation and the Late Oligocene-Early Miocene Hallaçlar formation in the near southwest of Gaybular Village.

West of Kumköy, the Gaybular section is separated from the Muratlar section with total length of 16 km by a 3 km long and 500 m wide restraining bend. The Muratlar section extends with N65°E strike between Kumköy and Gönen Stream. North of Kumköy in the area of the earthen football pitch (YGF-23 in Table 3), the surface rupture is characterised by offset cultural structures, a small-scale pressure ridge and linear fault scarps.

Between Kumköy and Muratlar, the surface rupture follows the contact between the Hallaçlar formation and Bayramiç formation with N70°E strike and enters ancient alluvial sediments of Gönen River from the north of Muratlar. Ketin and Roesly (1953) reported an old village road east of Muratlar was offset by 1,5 m to the right with the south block falling nearly 10 cm during the YGE (Figure 8) (YGF-24 in Table 3). From here, the surface rupture cuts the Muratlar – Gönen asphalt road with N70°E strike (YGF-25 in Table 3), toward the NE it continues 2 km within alluvial sediments of Gönen River. Just west of Gönen River, Kalaylı Hill rises in the form of a pressure ridge appropriate to the geometry of the fault. The Muratlar section bends 20° to the right from Gönen River to extend toward Çakmak village with E-W strike. In this section, east of Gönen River, the fault cuts the Bayramiç formation and ancient alluvial sediments of the Gönen River in a limited area south of Pilevne and Tirnova neighbourhoods before returning to alluvial sediments until south of Korudeğirmeni. The Muratlar section of the surface rupture enters the Hallaçlar formation south of Korudeğirmeni and continues within this unit west of Çakmak Village where it ends.

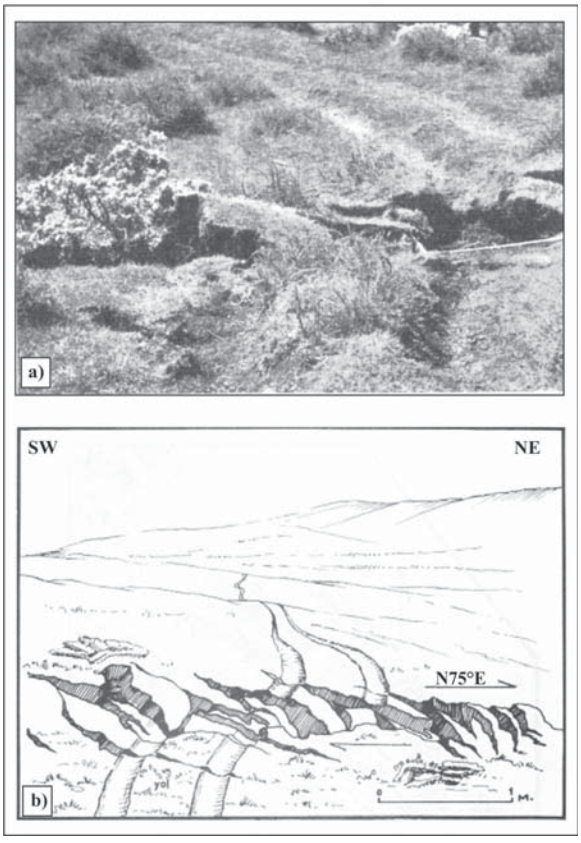

Figure 8- Offset of Muratlar village road during YGE a) Field photograph, b) Sketch (taken from Ketin and Roesly, 1953).

The Kalfaköy section forms the easternmost section of the main body of the YGF. This section extends with strike of N60°E between Korudeğirmeni in the west and Saraçlar in the east. With total length of 6 km, the Kalfaköy section is represented by a deformation zone nearly 300 m wide. The Kalfaköy section ends in a bend toward the SE near Saraçlar village. This section is also equivalent to the region where there is overlap with the surface rupture from the 1964 Manyas earthquake on the YGF (Emre et al., 2012; Kürçer et al., 2017). Most of the Kalfaköy section controls the contact between the Hallaçlar formation and the Bayramiç formation and is occasionally observed within the Bayramiç formation.

The data related to the surface rupture in the Kalfaköy section is limited, but some observations were made that can reveal the structural characteristics of the fault. For example, a nearly 3 m wide crushed and brecciated fault zone was observed southwest of Kalfaköy within the Hallaçlar formation (YGF-27 in Table 3) (Figure 9). From east of Kalfaköy, the fault controls the contact between the Hallaçlar formation and the Bayramiç formation and continues within the Bayramiç formation from south of Gökçesu to reach the Saraçlar bend. South of Gökçesu, the northern block of the earthquake surface rupture fell down nearly 50 cm (YGF-29 in Table 3) and is currently observed as a linear fault scarp (Figure 10). The Saraçlar region represents the easternmost section of the main section of the 1953 YGE surface rupture. In this region, the surface rupture bends toward the SE before continuing 1 km further and ending SE of Saraçlar village. This easternmost 1 km of the surface rupture also ruptured in the 1964 Manyas Earthquake.

Figure 9- YGF cutting Late Oligocene-Early Miocene Hallaçlar formation (Toh) southwest of Kalfaköy (view towards SSW).

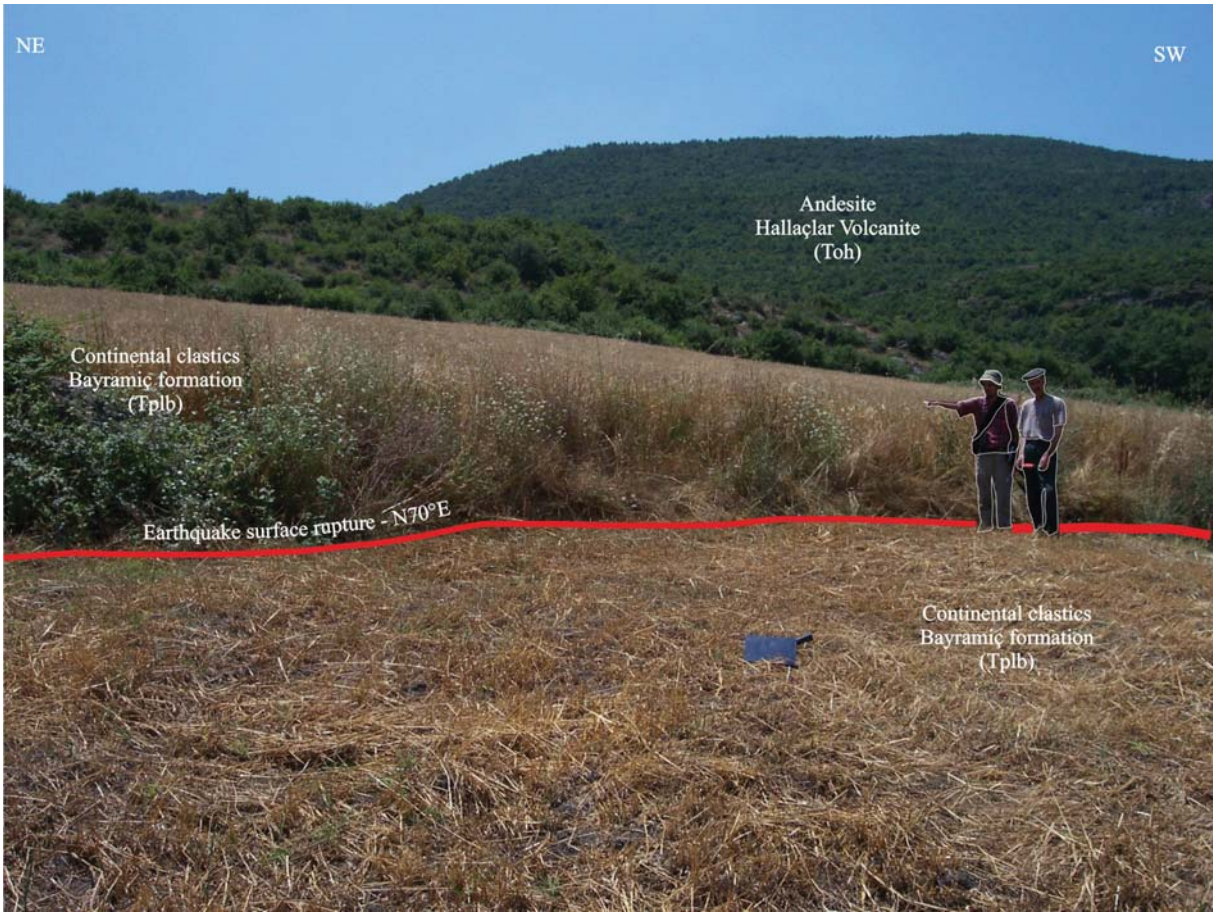

Figure 10- Earthquake surface rupture in the south of Gökçesu village (YGF-24) (Photograph taken from Kürçer, 2006) (view toward SSW).

The 5,5 km section of the YGF extending N70°W between Korudeğirmeni and Koçbayırı villages is named the Tütüncü section. The Tütüncü section is a splay fault separating from the YGF toward the SE (Figure 11). The fault bends toward the left north of Tütüncü and gains a reverse component. Most of the Tütüncü segment controls the contact between the Soma formation and the Bayramiç formation, occasionally cutting the Bayramiç formation and alluvial fan sediments.

5. Offset Measurements the Yenice-Gönen Fault

On the YGE surface rupture, right-lateral displacements varying from 1,70±0,1 m to 3,2±0,2 m were measured (Figure 12, 13 and table 4). Additionally, total displacements varying from 18±2 m and 24±2 m were measured in the Holocene drainage systems in the Çakır section (Figure 13 and 14). The Total station and tape meter were used for these measurement of displacements.

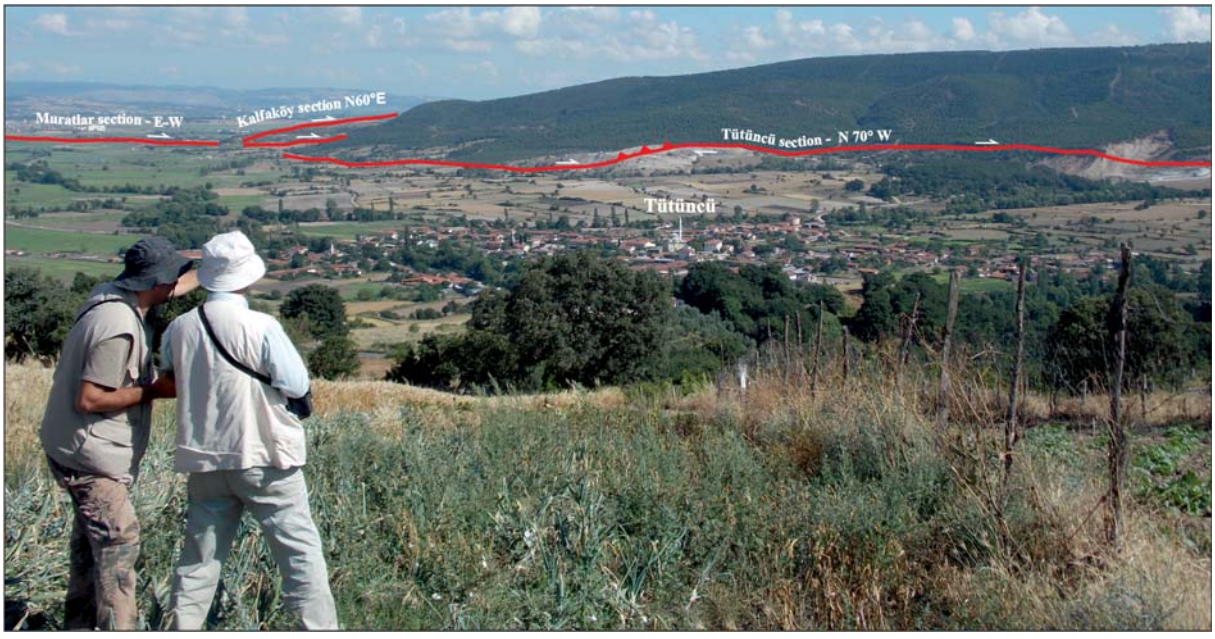

Figure 11- Panoramic view of Tütüncü section of YGF (view north from Tütüncü – Kavakoba road).

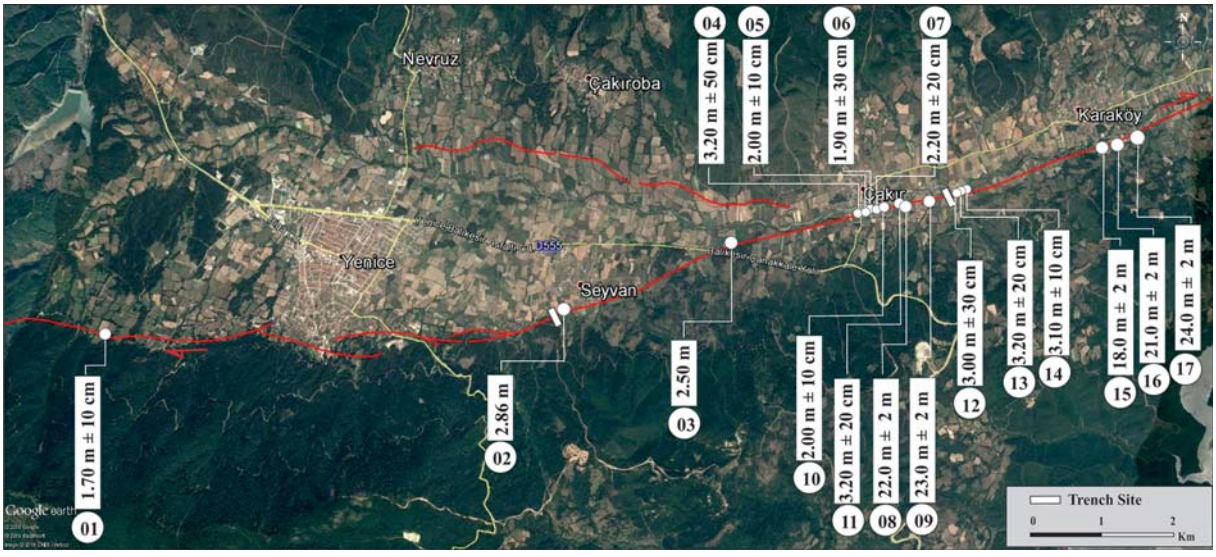

Figure 12- Displacement measurements along the Çakır fault section.

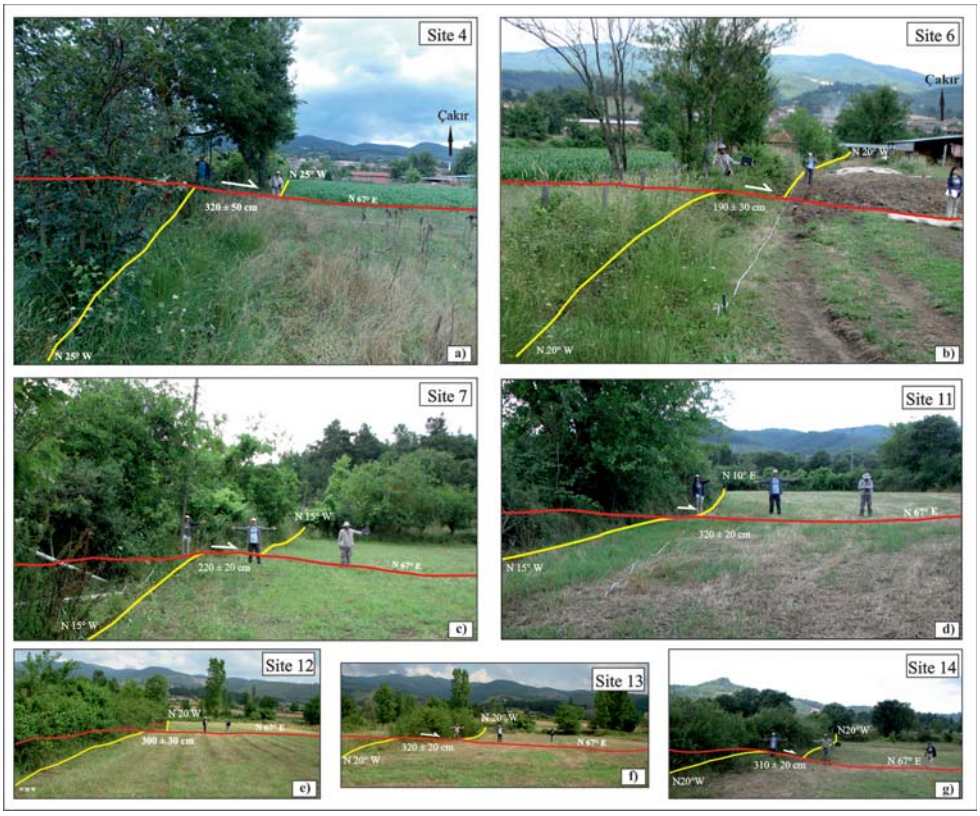

Figure 13- Displacements measured on the YGE surface rupture at some points described in figure 12 and table 4.

Table 4- Displacement measurements along the surface rupture of the YGE.

Station number	Location	Latitude (N)	Longitude (E)	Displacement (m)	Measurement quality	Offset properties and thoughts
01	SW of Yenice	4418504	35 0519481	1,70±10 cm 0,50±5 cm	B	Offset dry stream
02	SW of Seyvan	4419869	35 0525124	2,86	A	Offset dry stream
03	NE of Seyvan	4421120	35 0527125	2,50	A	Yenice – Pazarköy road
04	SSW of Çakır	4421870	35 0528759	3,20±50 cm	C	Field boundary
05	SSW of Çakır	4421884	35 0528786	200±10 cm	A	Field boundary
06	SSW of Çakır	4421884	35 0528801	1,90±30 cm	B	Field boundary
07	SSW of Çakır	4421917	35 0528808	2,20±20 cm	B	Field boundary
08	E of Çakır	4421936	35 0529326	22,00±2 m	B	Offset stream bed (total displacement)
09	E of Çakır	4422075	35 0529653	23,00±2 m	B	Offset stream bed (total displacement)
10	S of Çakır	4421983	35 0528987	2,00±10 cm	A	Field boundary
11	SSE of Çakır	4422035	35 0529263	3,20±20 cm	B	Field boundary
12	SE of Çakır	4422325	35 0529998	3,00±30 cm	A	Field boundary
13	SE of Çakır	4422328	35 0530015	3,20±20 cm	A	Field boundary
14	SE of Çakır	4422358	35 0530053	3,10±10 cm	A	Field boundary
15	SE of Karaköy	4423201	35 531769	18±2 m	B	Offset stream bed (total displacement)
16	SE of Karaköy	4423251	35 531955	21±2 m	B	Offset stream bed (total displacement)
17	SE of Karaköy	4423394	35 532242	24±2 m	B	Offset stream bed (total displacement)
18	N of Kumköy	4434888	35 0547376	1,75±15 cm	B	Field boundary
19	E of Muratlar	4436118	35 0550464	1,50	A	Village road
20	W of Gönen	4437400	35 553605	800±50 m	B	Gönen Stream

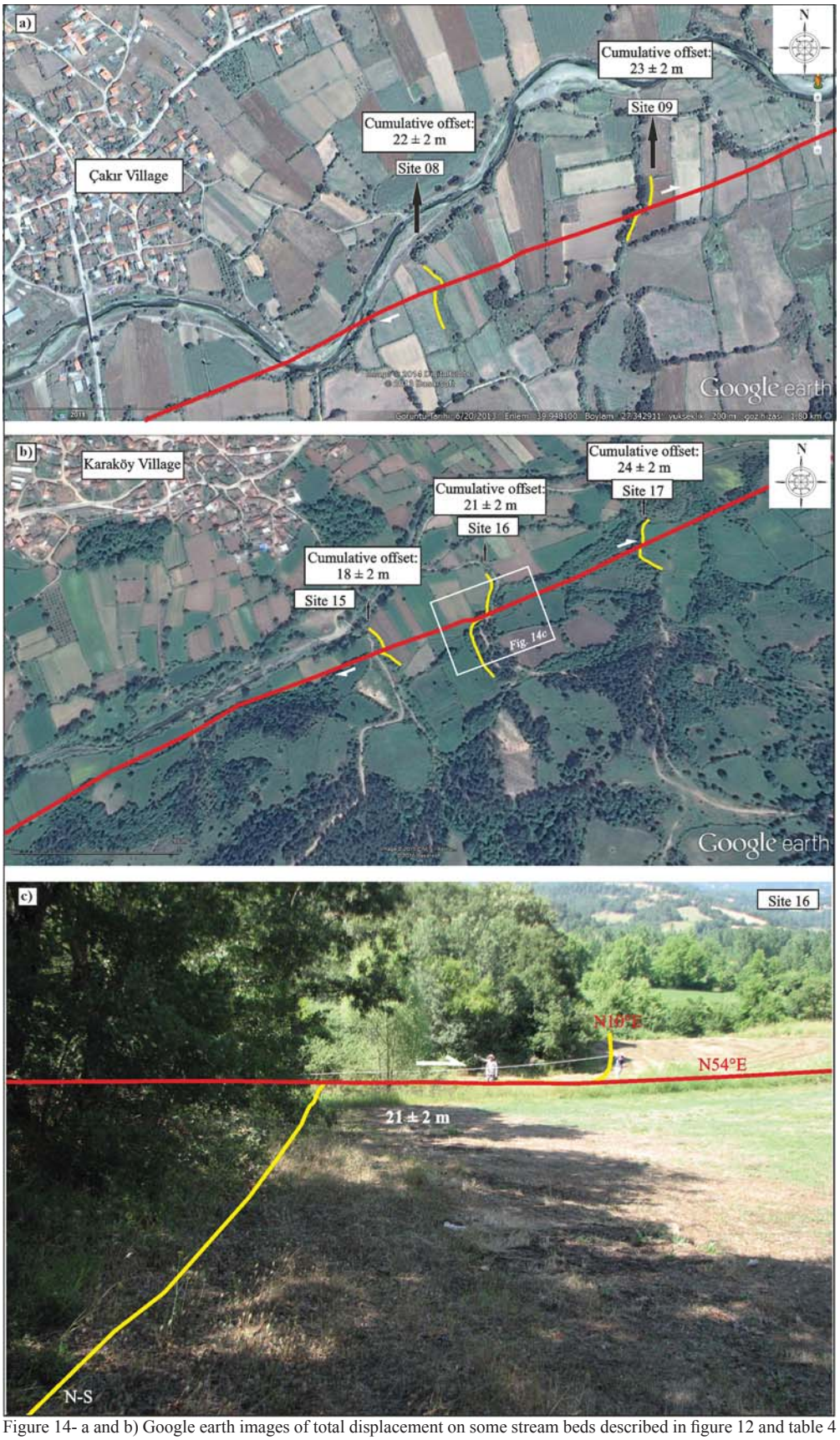

Figure 14- a and b) Google earth images of total displacement on some stream beds described in figure 12 and table 4 along the Çakır fault section, c) Field photograph of station 16.

6. Palaeoseismology Studies

On the Çakır Fault section of the Yenice-Gönen earthquake segment, palaeoseismic trench studies were completed in the Seyvan and Çakır trenches (see figure 12) selected as a result of air photograph analysis and detailed surface rupture mapping. The trench areas firstly had microtopographic maps produced using total station equipment (Figure 16 and 20). All trenches had 1 m^2 gridding applied, and the trench walls were logged with the photomosaic technique. Palaeoseismologic results are presented on sections from the Seyvan 2013-1 trench west wall, Seyvan 2013-2 trench west wall and Çakır 2013 trench west wall.

6.1. Seyvan 2013-1 and Seyvan 2013-2 Trenches

The Seyvan trench area was located 500 m. SW of Seyvan village (UTM coordinates: 35 0525151 E – 4419713 N), SW of Çakır fault section (see figure 12). The Çakır section extending W-E from south of Yenice enters a left restraining bend south of Seyvan and continues to Ortaoba with N67°E strike. In this section the fault gains reverse component due to the effect of the restraining bend (Figure 15).

6.1.1. Site Selection

The clearest data belonging to the surface rupture developing during the 1953 YGE are observed in the Çakır section of the YGF. In this area the 1953 surface rupture is characterised by linear fault scarps. In the Seyvan trench area, a probably Holocene or Late Pleistocene dry stream was cut by the YGF and offset 34±2 m laterally to the right (see figure 13). Ketin and Roesly (1953) measured 4,3 m right lateral displacement on the surface rupture of the 1953 earthquake in Seyvan trench area and surroundings. In this study, right lateral displacements varying from 2,50 m to 3,20 m were measured in Seyvan and close surroundings (see figure 12). From this viewpoint, the total displacement of 34±2 m observed on microtopographic maps is predicted to belong to at least 8 earthquakes. The trench site was chosen with this point of view.

In the Seyvan Trench site, two parallel trenches were excavated perpendicular to the fault and these trenches were named Seyvan 2013-1 trench and Seyvan 2013-2 Trench (Figure 16). Seyvan 2013-1 Trench was 10 m long, mean 3 m deep and 5 metres wide, while Seyvan 2013-2 Trench was 8 m long, 3 m deep and 2 m wide.

6.1.2. Stratigraphy and Structural Patterns

Eleven different microstratigraphic levels were defined in the Seyvan trenches. In both trenches the basement was altered volcanics (volcanic and pyroclastic rocks) from the Late Oligocene-Early Miocene Hallaçlar formation. These units were

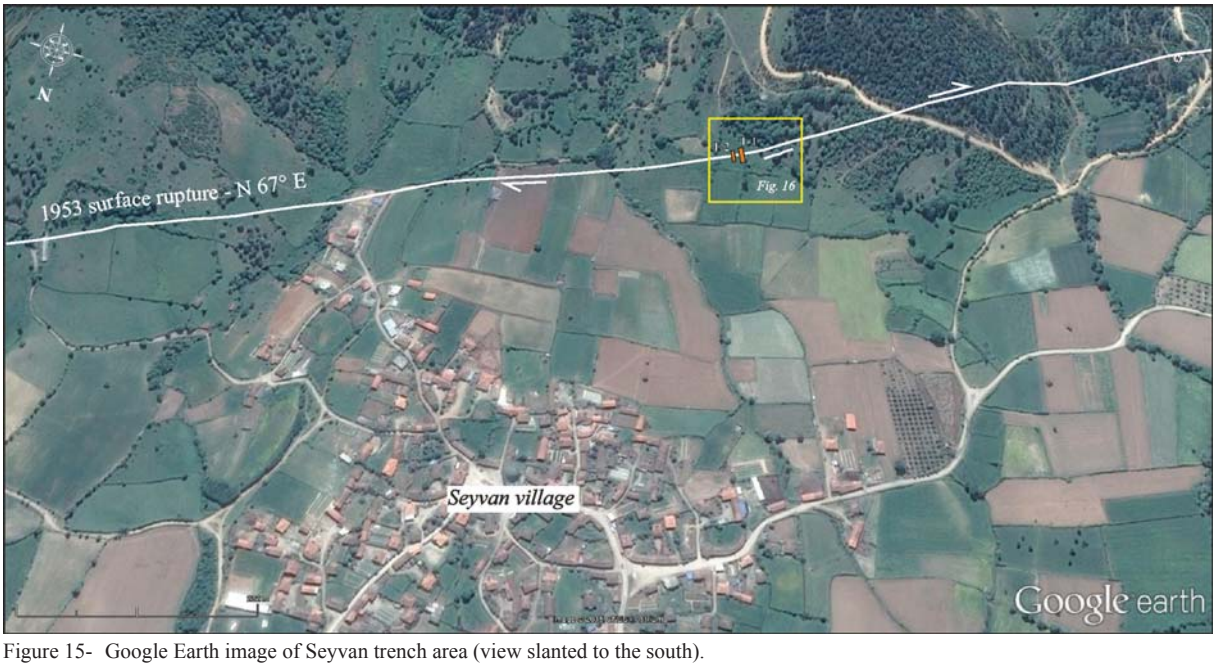

Figure 15- Google Earth image of Seyvan trench area (view slanted to the south).

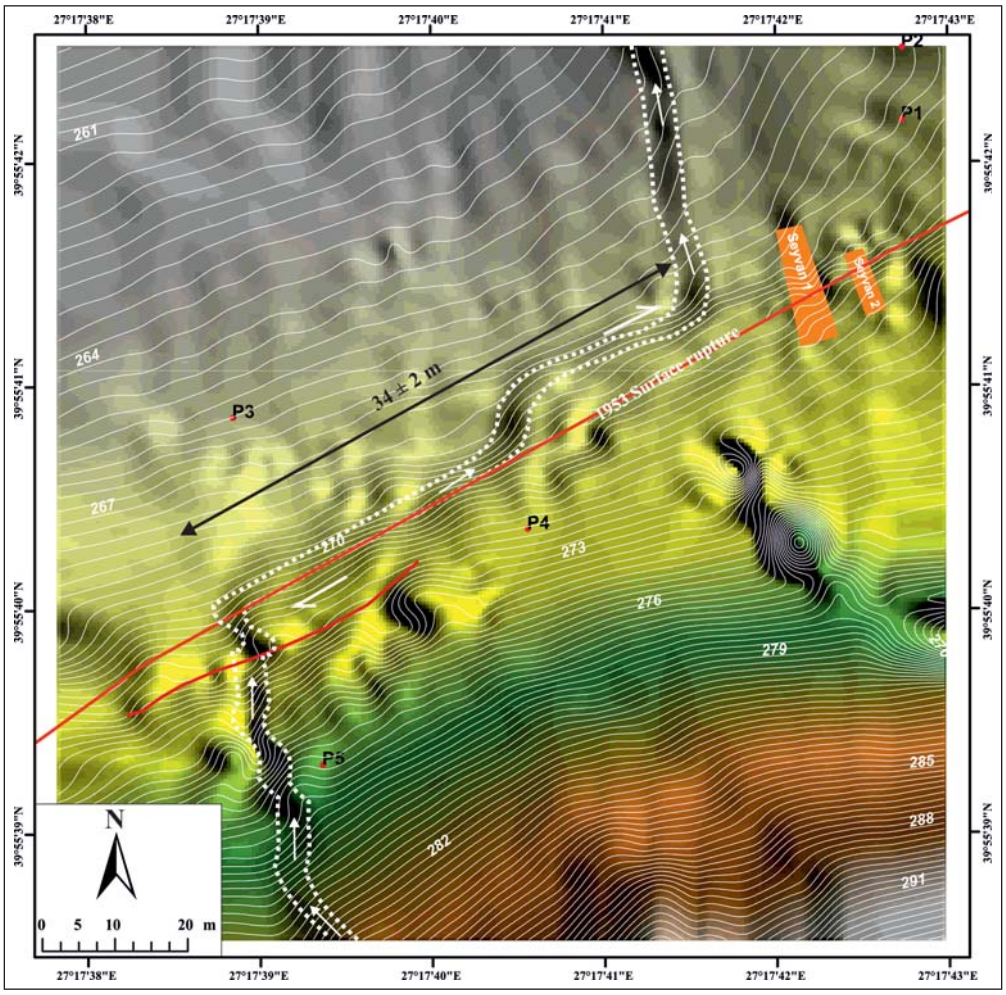

Figure 16- Microtopography map of the Seyvan trench site. Contour interval 20 cm (Kürçer et al., 2016).

unconformably overlain by fan sediments and fault colluvial sediments (Figure 17 and figure 18). In the Seyvan trenches, units numbered 6 and 7 are fault colluvial sediments defining the north of the main fault zone. The structural deformation in the walls of the trenches indicates a transpressive regime. This situation may be explained by the local fault geometry in the trench area.

Considering palaeoseismologic criteria like the tectonostratigraphic relationships between the units, fault colluvial wedge geometry and upward termination of the fault strands, 6 earthquakes resulting in surface ruptures were defined and dated in the Seyvan trenches in the last 6200 years, including the 1953 earthquake. Data belonging to Earthquakes 1, 3, 5 and 6 are present in Seyvan 2013-1 trench, while data for earthquakes 1, 2, 4, 5 and 6 were obtained from Seyvan 2013-2 trench (Figure 17 and Figure 18).

6.1.3. Dating

With the aim of dating the earthquakes identified in the trenches, 20 coal and organic sediment samples were collected and sent to the Beta Analytic Laboratory in the USA for analysis (Table 5). Additionally, 6 sample were collected from levels without carbon-rich material for optically stimulated luminescence dating method (OSL) and these samples were analysed at Ankara University Department of Physical Engineering (Table 6).

6.1.4. Paleoseismologic Interpretation

Earthquake 6: Earthquake 6, which could be determined in both trenches, had an event horizon determined at the base of unit number 5. In Seyvan 2013-1 and 2 trenches, faults north of the main fault zone (between 4th and 5th metres) cut units 1, 2, 3 and 4 and are covered by the gravel in unit number 5.

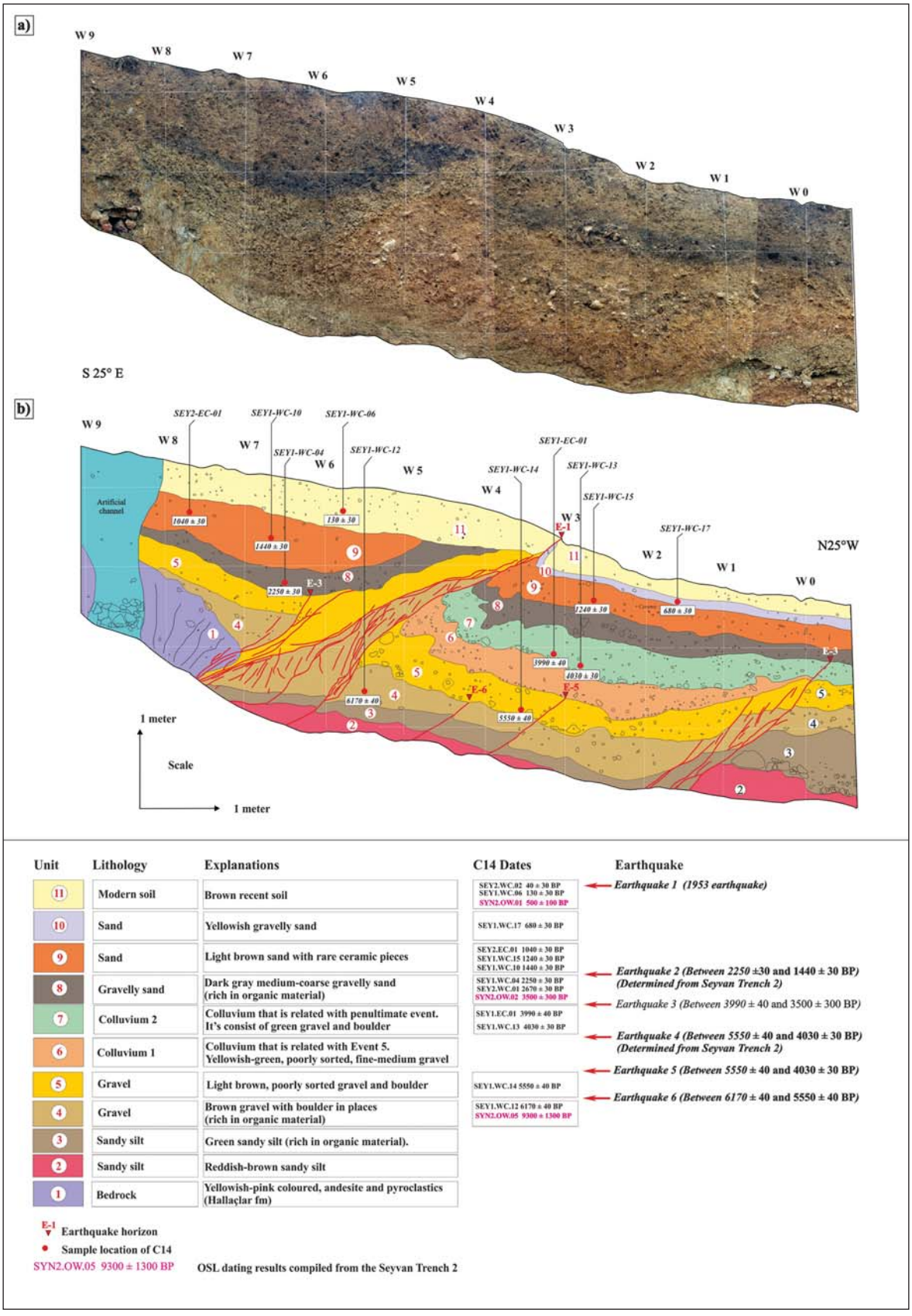

Figure 17- a) Uninterpreted photomosaic of the west wall of Seyvan 2013-1 trench b) Trench log of the west wall of Seyvan 2013-1 trench (adapted from Kürçer et al., 2016).

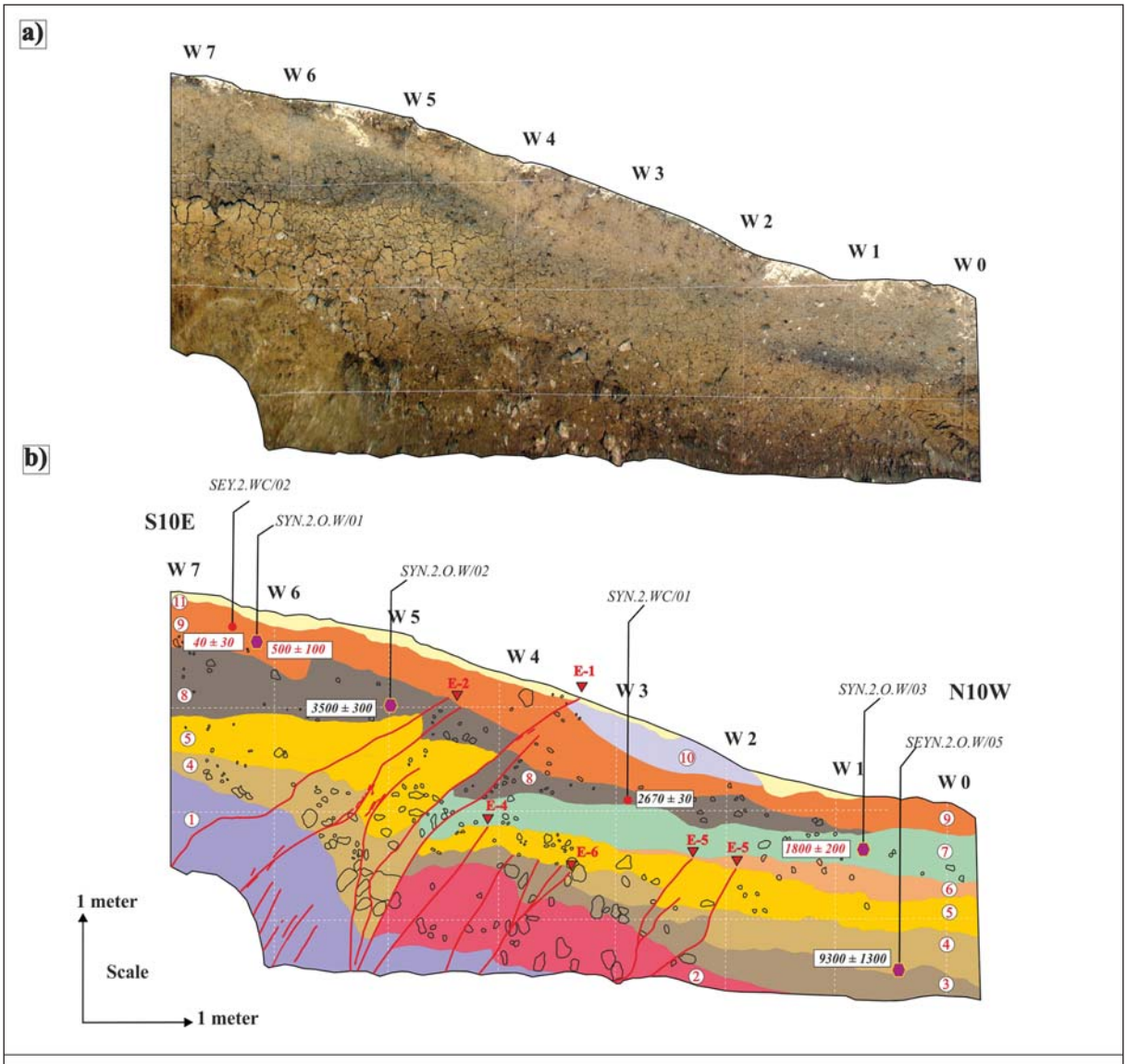

Unit	Lithology	Explanations	14C Dates	Earthquake
11	Modern Soil	Brown recent soil	SEY1.WC.06 130 ± 30 BP	Earthquake 1 (1953 Earthquake)
10	Sand	Yellowish, rare gravelly sand	SEY1.WC.17 680 ± 30 BP	
9	Sand	Light brown, sand with rare ceramic pieces	SEY2.WC.02 40 ± 30 BP SYN2.OW.01 500 ± 100 BP SEY2.EC.01 1040 ± 30 BP SEY1.WC.15 1240 ± 30 BP SEY1.WC.10 1440 ± 30 BP	Earthquake 2 (Between 2250 ± 30 and 1440 ± 30 BP)
8	Gravelly Sand	Dark gray medium-coarse gravelly sand (rich in organic material)	SEY1.WC.04 2250 ± 30 BP SEY2.WC.01 2670 ± 30 BP SYN2.OW.02 3500 ± 300 BP	Earthquake 3 (Between 3990 ± 40 and 3500 ± 300 BP) (Determined from Seyvan Trench 1)
7	Colluvium 2	Colluvium that is releated with penultimate event. It's consists of green gravel and boulder.	SEY1.EC.01 3990 ± 40 BP SEY1.WC.13 4030 ± 30 BP	Earthquake 4 (Between 5550 ± 40 and 4030 ± 30 BP)
6	Colluvium 1	Colluvium that is releated with Event 5 Yellowish green, poorly sorted fine-medium gravel		Earthquake 5 (Between 5550 ± 40 and 4030 ± 30 BP)
5	Gravel	Light brown, poorly sorted gravel and bloulder	SEY1.WC.14 5550 ± 40 BP	
4	Gravel	Brown, rich in organic matter, coarse-grained gravel in places.	SEY1.WC.12 6170 ± 40 BP SYN2.OW.05 9300 ± 1300 BP	Earthquake 6 (Between 6170 ± 40 and 5550 ± 40 BP)
3	Sandy Silt	Green sandy silt (rich in organic material)		
2	Sandy Silt	Reddish brown sandy silt.		
1	Bedrock	Yellowish-pink, andesite and pyroclastic rock (Hallaçlar Formation)		

E-1 Earthquake Horizon
C14 sample location
OSL sample location

Figure 18- a) Uninterpreted photomosaic of the west wall of Seyvan 2013-2 trench b) Trench log of the west wall of Seyvan 2013-2 trench.

Table 5- Radiocarbon dating results of samples from Seyvan 2013-1, Seyvan 2013-2 and Çakır 2013 trenches.

Trench Wall	Sample No	Laboratory No (BETA)	Stratigraphic unit	Material	Measured radiocarbon age (BP)	^{13}C / ^{12}C (‰)	Traditional radiocarbon age (BP)	Calibrated age interval (2σ)
Çakır 2013- West	CKR-A.W-01	366225	3	Organic sediment	5140±40	-24,0	5160±40	BC 4040 - 4010 BC 4000 - 3940 BC 3860 - 3840 BC 3840 - 3820
Çakır 2013- West	CKR-A.W-02	366226	1	Organic sediment	7050±40	-25,0	7050±40	BC 5980 BC 5940 BC 5920
Çakır 2013- West	CKR-A.W-03	366227	8	Organic sediment	1770±30	-23,9	1790±30	AD 130 - 260 AD 280 - 330
Çakır 2013- West	CKR-A.W-04	366228	4	Organic sediment	3980±30	-24,2	3990±30	BC 2570 - 2460
Çakır 2013- West	CKR-A.W-05	366229	9	Organic sediment	60±30	-25,0	60±30	AD 1690 - 1730 AD 1810 - 1840 AD 1840 - 1850 AD 1860 - 1860 AD 1870 - 1920 AD Post 1950
Çakır 2013- West	CKR-C.W-01	366230	5	Organic sediment	3150±30	-25,0	3150±30	BC 1490 - 1470 BC 1460 - 1390
Çakır 2013-West	CKR-C.W-02	366231	5	Organic sediment	2960±30	-25,0	2970±30	BC 1300 - 1120
Çakır 2013- West	CKR-C.W-04	366232	5	Organic sediment	3260±30	-25,5	3250±30	BC 1610 - 1450
Seyvan 2013-1 - East	SEY.1-EC-01	366233	7	Coalified material	3970±40	-24,0	3990±40	BC 2580 - 2460
Seyvan 2013-1 - West	SEY.1-WC-04	366238	8	Coalified material	2290±30	-27,2	2250±30	BC 390 to 350 BC 320 to 210
Seyvan 2013-1 - West	SEY.1-WC-06	366239	11	Coalified material	160±30	-26,6	130±30	AD 1670 to 1780 AD 1800 to 1900 AD 1900 to 1940 AD 1950 to post 1950
Seyvan 2013-1 - West	SEY.1-WC-10	366241	9	Organic sediment	1420±30	-23,7	1440±30	AD 570 to 650
Seyvan 2013-1 - West	SEY.1-WC-12	366242	4	Organic sediment	6160±40	-24,1	6170±40	BC 5220 to 5000
Seyvan 2013-1 - West	SEY.1-WC-13	366243	7	Organic sediment	4000±30	-23,0	4030±30	BC 2620 to 2470
Seyvan 2013-1 - West	SEY.1-WC-14	366244	5	Organic sediment	5520±40	-23,1	5550±40	BC 4460 to 4340
Seyvan 2013-1 - West	SEY.1-WC-15	366245	9	Organic sediment	1220±30	-23,6	1240±30	AD 680 to 880
Seyvan 2013-1 - West	SEY.1-WC-17	366246	10	Organic sediment	660±30	-23,9	680±30	AD 1270 to 1310 AD 1360 to 1390
Seyvan 2013-2-Doğu	SEY.2-EC-01	366248	9	Organic sediment	1010±30	-23,1	1040±30	AD 900 to 910 AD 970 to 1030
Seyvan 2013-2-West	SEY.2-WC-01	366249	8	Coalified material	2700±30	-26,8	2670±30	BC 890 to 880 BC 850 to 800
Sey Seyvan 2013-2- West	SEY.2-WC-02	366250	11	Coalified material	70±30	-26,8	40±30	AD 1710 to 1720 AD 1830 to 1830 AD 1890 to 1910 AD Post 1950

Table 6- Optically stimulated luminescence (OSL) dating results for samples from Seyvan 2013-1, Seyvan 2013-2 and Çakır 2013 trenches.

Trench Wall	Sample No	Stratigraphic unit	Material	Equal dose (Gy)	Measured OSL age (BP)
Seyvan 2013-2- West	SYN2-OW-01	9	Rough sand	2,1±0,2	500±100
Seyvan 2013-2- West	SYN2-OW-02	8	Pebbly sand	15,5±1,1	3500±300
Seyvan 2013-2- West	SYN2-OW-05	4	Sand	42,7±5,5	9300±1300
Çakır 2013 - West	CKR-OW-03	1	Silty clay	45,4±3,9	7700±800
Çakır 2013 - West	CKR-OW-04	6	Mud	22,5±1,6	3700±300
Çakır 2013 - West	CKR-OW-05	3	Sandy gravel	34,6±4,9	6100±900

The youngest unit cut by faults related to Earthquake 6 is unit number 4 with age dates obtained as 6170±40 years BP. The youngest age obtained above the event horizon (between unit number 4 and 5) is 5550±40 years BP. According to this stratigraphy and age data, the predicted earthquake date for Earthquake 6 is determined to be between 6170±60 BP and 5550±40 BP.

Earthquake 5: Data belonging to Earthquake 5 were found in both trenches. The event horizon for this earthquake was determined to be based in unit number 6. Faults north of the main fault zone between the 2nd and 4th metres in Seyvan 2013-1 and 2 trenches cut all units up to unit number 5 and are covered by colluvial sediments of unit number 6. The youngest age obtained from unit number 5 is 5550±40 years BP. Though age dates could not be obtained from colluvial sediments in unit number 6 covering Earthquake 5, an age of 4030±30 years BP was obtained from the base level of unit number 7 above this. In this situation, the estimated earthquake date for Earthquake 5 is between 5550±40 years and 4030±30 years BP.

Earthquake 4: Evidence of this event was present between the 4th and 5th meters of Seyvan 2013-2 Trench. The event horizon for Earthquake 4 was determined at the base of unit number 7. The youngest unit cut by a fault belonging to this earthquake was unit number 6 and no age dates could be obtained. As a result, the lower age for the earthquake can be given as 5550±40 BP obtained from unit number 5. The youngest age obtained from unit 7 covering unit 6 is 4030±30 years BP. According to this age data, the estimated earthquake date for Earthquake 4 can be given as between 5550±40 years and 4030±30 years BP, similar to Earthquake 5.

Earthquake 3: Earthquake 3 can be clearly distinguished in Seyvan 2013-1 trench. The dark grey coloured pebbly-sand (unit number 8) observed as a marker level in the trench walls forms the event horizon for this earthquake. Two fault branches north and south of the main fault zone end at the base of unit number 8. With the aim of dating the earthquake, the date of 3990±40 years BP was obtained from unit number 7, the youngest unit cut by the fault. Both OSL and C-14 dates were obtained from unit number 8 covering the event horizon. The OSL age obtained from a level close to the base of this unit was 3500±300 years. According to this stratigraphy and age data, Earthquake 3 must have occurred between 3990±40 and 3500±300 years BP.

Earthquake 2: According to Seyvan 2013-2 trench, the event horizon for Earthquake 2 was determined as the base of unit number 9. In Seyvan 2013-2 trench, two faults south of the main fault zone (between 4th and 5th metres) cut unit number 8 and are covered by unit number 9. The youngest age obtained from unit number 8 is 2250±30 years BP. The base of unit 9 covering the event horizon is 1440±30 years BP. According to this data, Earthquake 2 must have occurred between 2250±30 and 1440±30 years BP.

Earthquake 1 (1953 Earthquake): The surface rupture of the 1953 earthquake is clearly observed in both trenches. In the first trench the 1953 earthquake is represented by a narrow deformation zone, while in the second trench there are two fault branches visible. The age obtained from the youngest unit cut by the 1953 earthquake surface rupture is 130±30 years BP.

6.2. Çakır 2013 Trench

The Çakır trench site is located in the central part of the Çakır fault section (see figure 12). The Çakır fault section extends trending N67°E after a restraining bend to the left south of Seyvan and continues within flood plain sediments of the Yenice Stream from south of Çakır to Güzeloba village (see figure 3). In this section the fault is characterised by unique topography of right-lateral strike-slip faulting. Displacements in this section related to the 1953

Figure 19- Google Earth image of Çakır trench site (Oblique view toward the south).

earthquake and total displacements of the Holocene drainage system were measured (see figure 14). The Çakır trench site is located 1250 m ESE of Çakır village (UTM coordinates: 35 05299973 E – 4422153 N; figure 19).

6.2.1. Site Selection

In this area, field boundaries are systematically displaced by the 1953 earthquake surface rupture. The Çakır trench site and surroundings had 300±30 cm to 320±30 cm right lateral displacements measured during the 1953 YGE (see figure 13). Additionally, east and west of the Çakır trench site, right lateral total displacements of 18±2 m and 24±2 m were measured in the Holocene drainage system (see figure 12). The Çakır trench site, where systematic field boundary offsets are clearly observed, is located on flood plain sediments of Yenice Stream. With the aim of determining microtopographic properties of the Çakır trench area, total station equipment was used to produce microtopographic maps (Figure 20). In the Çakır trench site and surroundings, field boundaries systematically offset during the 1953 earthquake are present. These offsets can be clearly observed on microtopographic maps with 20 cm contour intervals produced using the total station (Figure 20).

In the Çakır trench site, one trench was excavated with 10 m length, mean 2,5 m depth and 5 m width perpendicular to the fault.

6.2.2. Stratigraphy and Structural Patterns

The 9 different microstratigraphic levels, were defined in Çakır 2013 trench. Most of these units consists of flood plain sediments of Yenice Stream and partly fault colluvial sediments (Figure 21). The style of structural deformation in the Çakır Trench indicates strike-slip deformation. The faults have transpressive character linked to the local fault geometry in the trench site (Figure 21).

6.2.3. Dating

With the aim of dating the earthquakes identified in the Çakır trench, 8 radiocarbon and 3 OSL samples were reviewed and analysed. For the analysis results, please see table 5 and table 6.

6.2.4. Paleoseismologic Interpretation

Based on the paleoseismological criteria, 5 paleo earthquakes, resulting in surface rupture, were identified and dated within the last 7000 years in Çakır Trench site (Figure 21).

Earthquake 5: At the 6th metre of the Çakır 2013 trench, the event horizon for Earthquake 5, with typical colluvial wedge geometry, was determined at the base of colluvial unit number 2. A date of 7050±40 years BP was obtained from unit number 1, the youngest unit cut by the fault associated with this

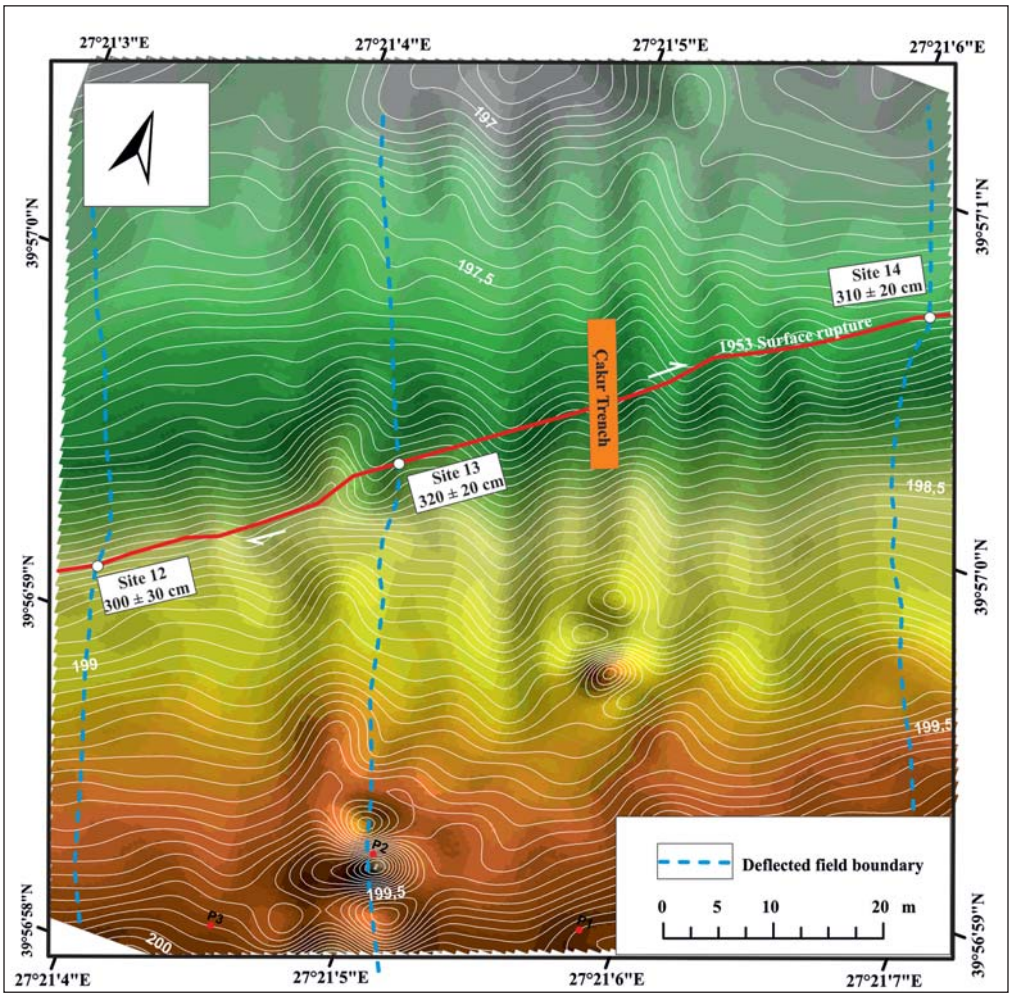

Figure 20- Microtopography map of the Çakır trench site. Contour interval is 20 cm.

event. Though age dates could not be obtained from unit 2 covering this event horizon, an age of 6100±900 years BP was obtained for unit number 3 just above this unit. According to this age data, the recommended age interval for Earthquake 5 is between 7050±40 and 6100±900 years BP.

Earthquake 4: Data belonging to this event are observed between the 7th and 8th metres of this trench. In this section the fault clearly cuts unit number 3 and is covered by unit number 5. As unit number 4 was not observed in the south block of the main fault zone, the event horizon for Earthquake 4 was determined as the base of unit number 5. An age of 3990±30 years BP was obtained from unit number 4. An age of 3250±30 years BP was obtained from the base of unit 5 covering the event horizon. According to this data, the age of Earthquake 4 was determined between 3990±30 and 3250±30 years BP.

Earthquake 3: The event horizon for Earthquake 3 identified in Çakır 2013 trench is at the base of unit number 7. Data belonging to this event are clearly observed between the 4th and 5th metres in the trench. An age of 3700±300 years BP was obtained from unit number 6 under the event horizon. There was no dateable material found in unit number 7 above the event horizon. For this reason, the 1790±30 year BP age date obtained from unit number 8 above this unit was used. Accordingly, the date for Earthquake 3 is proposed to be between 3700±300 and 1790±30 years BP.

Earthquake 2: Clearly observed between the 4th and 5th metres in the trench, the event horizon for Earthquake 2 was determined as the base of unit number 8. As no age data could be obtained for unit number 7, the recommended dates for Earthquake 3 of 3700±300 to 1790±30 years BP were adopted for Earthquake 2.

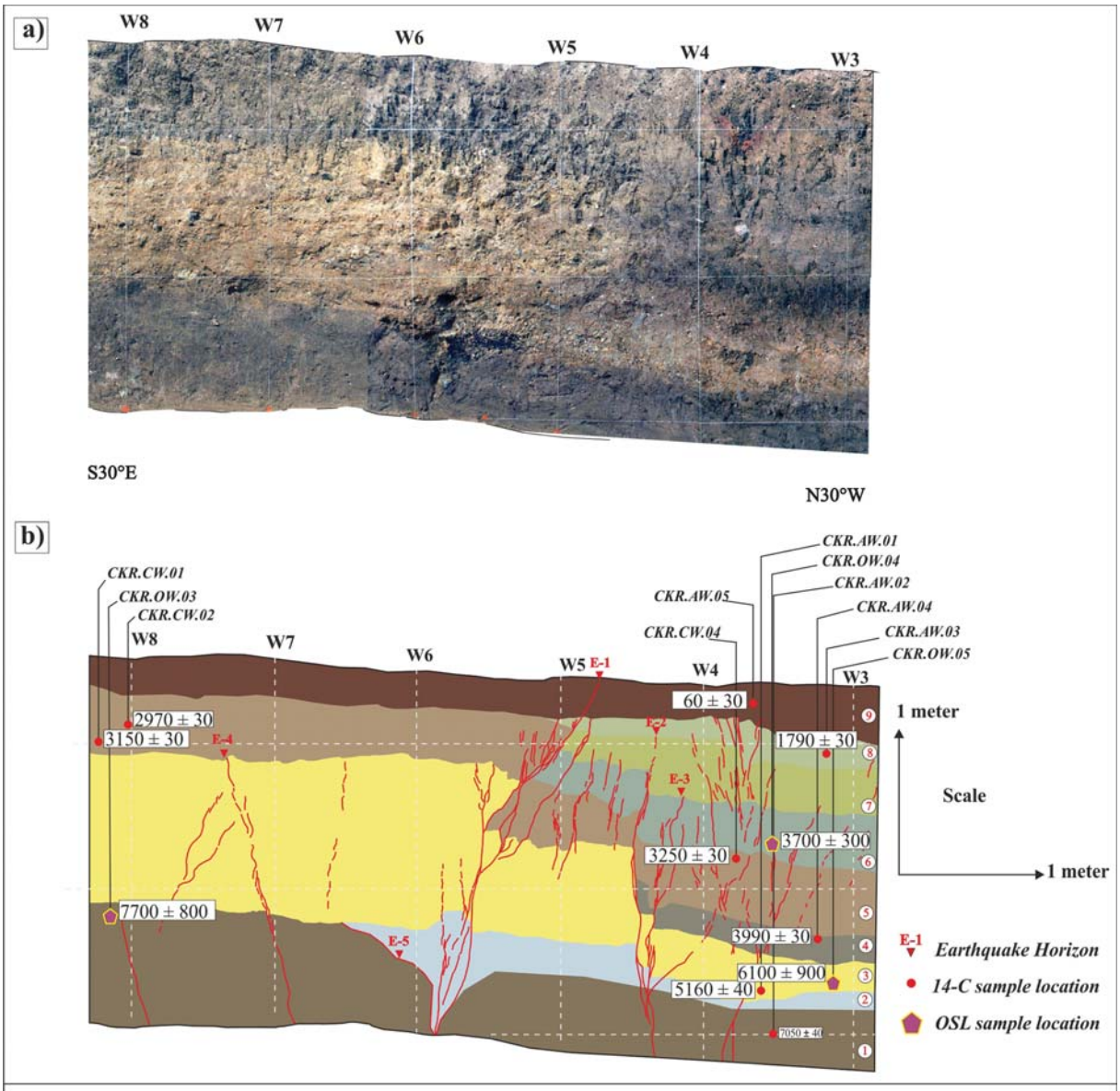

Unit	Lithology	Explanations	14C Dates	Earthquake
9	Modern Soil	Brown recent soil	CKR.AW.05 60 ± 30 BP	Earthquake 1 (1953 Earthquake)
8	Clayey silt	Greenish gray clayey silt	CKR.AW.03 1790 ± 30 BP	Earthquake 2 (Between 3700 ± 300 and 1790 ± 30 BP)
7	Silt	Greenish gray silt		
6	Silty clay	Gray, silty clay-mud with rare gravel	CKR.OW.04 3700 ± 300 BP	Earthquake 3 (Between 3700 ± 300 and 1790 ± 30 BP)
5	Mud	Gray, brown, rare fine gravel, mud with coal	CKR.CW.02 2970 ± 30 BP CKR.CW.01 3150 ± 30 BP CKR.CW.04 3250 ± 30 BP	Earthquake 4 (Between 3990 ± 30 and 3250 ± 30 BP)
4	Mud	Dark gray mud with rare fine gravel	CKR.AW.04 3990 ± 30 BP	
3	Gravel	Yellow, sandy gravel with mud lens in places	CKR.AW.01 5160 ± 40 BP CKR.OW.05 6100 ± 900 BP	
2	Colluvium	Colluvium		
1	Clay	Dark gray - brown silty clay.	CKR.AW.02 7050 ± 40 BP CKR.OW.03 7700 ± 800 BP	Earthquake 5 (Between 7050 ± 40 and 6100 ± 900 BP)

Figure 21- a) Uninterpreted photomosaic of the west wall of Çakır, 2013 trench, b) Trench log for the west wall of Çakır, 2013 trench.

Earthquake 1 (1953 Earthquake): The surface rupture of the 1953 YGE can be clearly observed in Çakır 2013 trench. The main fault branch extends upwards and cuts very young current soil levels dated to 60±30 years BP.

6.3. Comparison of Seyvan and Çakır Trenches

As a result of evaluating the identified and dated earthquakes from the Seyvan (2013-1 and 2013-2) and Çakır 2013 trenches together, a total of 6 earthquakes that resulted in surface rupture were identified and dated on the YGF in the last 6200 years, including the 1953 earthquake (Figure 22). The evaluation of these earthquakes is presented in the Discussion and Conclusion section.

7. Evaluation of Total Offset, Annual Slip Rate (Late Quaternary-Present) and Age of the Yenice-Gönen Fault

For the first time in this study, the total offset and annual slip rate of the YGF was calculated for the last 300.000 years (Late Quaternary) to the present day. The data indicating the total offset of the YGF in the Late Quaternary comes from Gönen River. West of Gönen, Gönen River is cut by the YGF and offset 800±50 m right-laterally (Figure 23). Kazancı et al. (2014) stated the excavation times for large valleys in the South Marmara Region could not go back further than 300,000 years to erosion and deposition rates. This study accepted the incision time for Gönen River

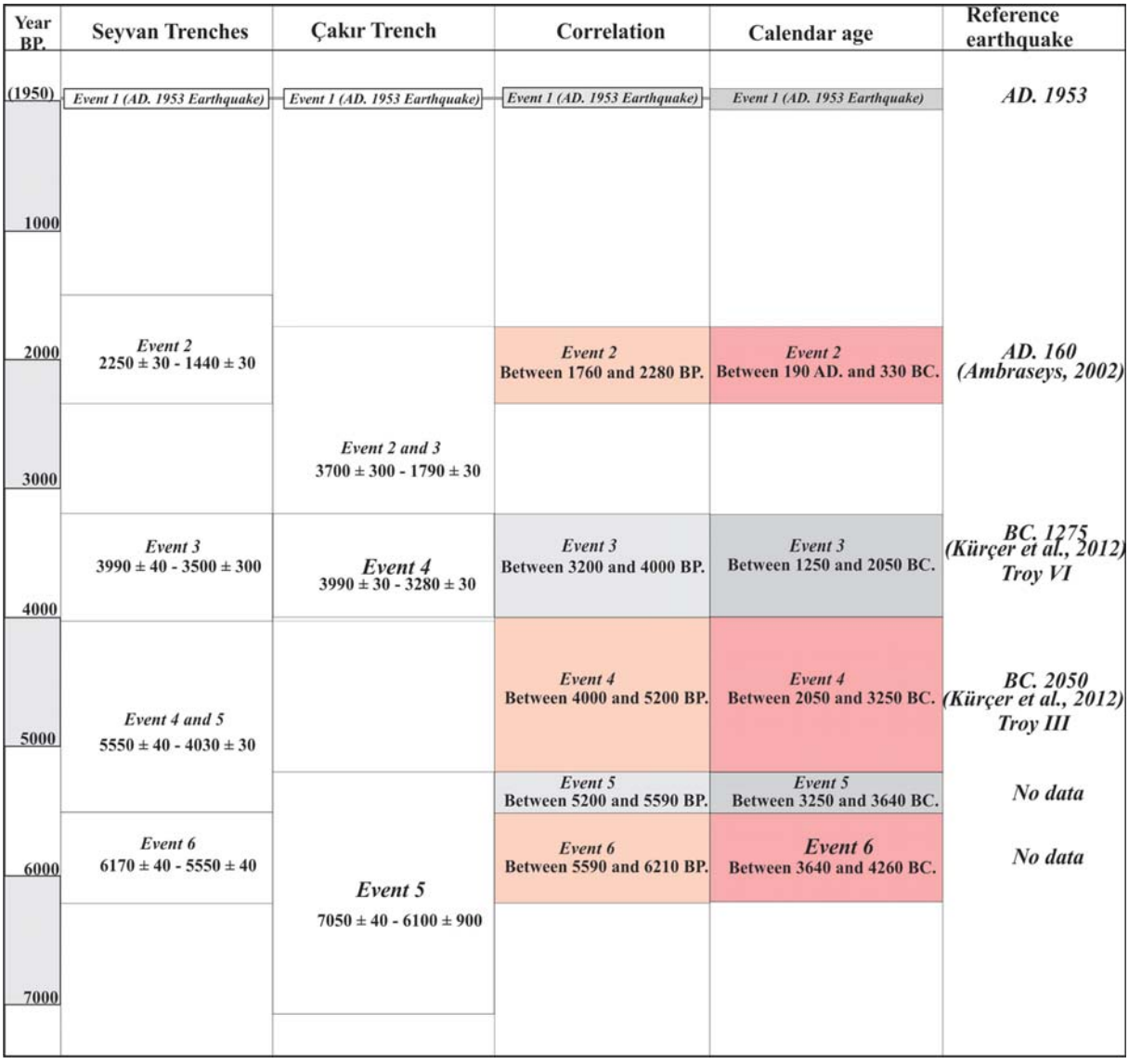

Figure 22- Comparison of earthquakes identified and dated in the Seyvan and Çakır trenches.

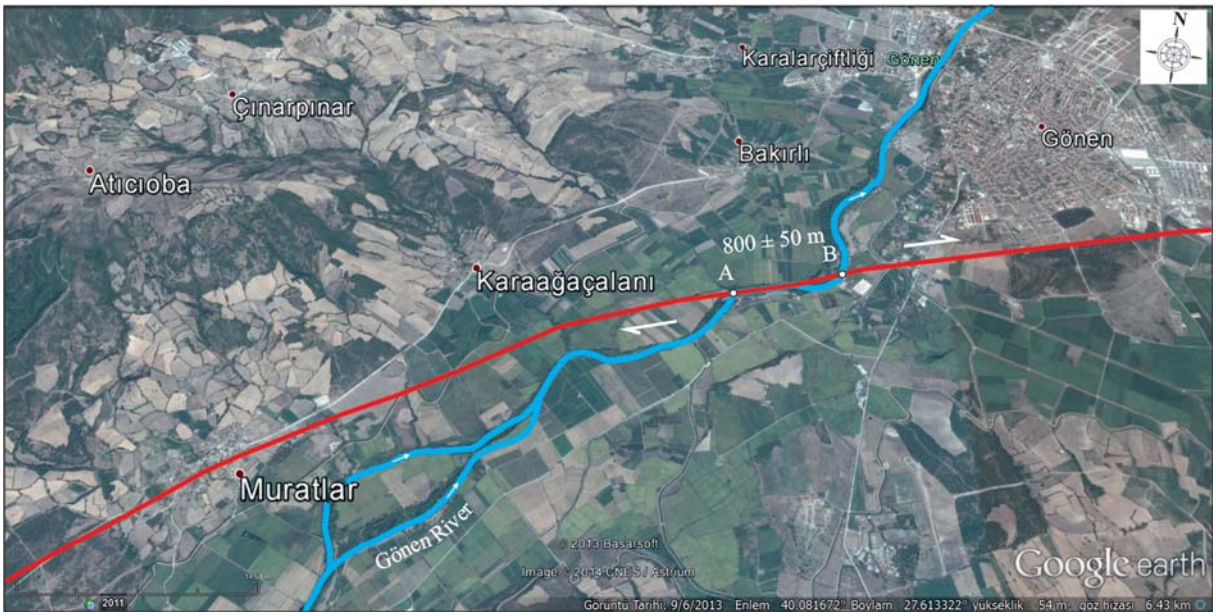

Figure 23- Google Earth image of total displacement on the Gönen River.

as 300,000 years. Calculations using the incision time for Gönen River (300.000 years) and total displacement amount (800±50) found the annual slip rate on the YGF as 2,65±0,15 mm/year. This value complies with previous studies and regional GPS studies. Current GPS studies show the total annual right-lateral slip rate on active faults with NE-SW trending in the Southern Marmara Region is 6-8 mm (Meade et al., 2002; Kreemer et al., 2004). Emre et al. (2012) proposed the annual slip rate on the YGF was 2-3 mm based on the fact that this value has to be shared between the Yenice-Gönen, Sarıköy and Çan-Biga fault zones.

Gürer et al. (2003) in a study of the neotectonic development of the southeast Marmara region described the region as a transition zone between the NAF zone and the Western Anatolia Extensional system. Selim et al. (2013) reported the southern branch of the NAF was effective on the morphotectonic development of the South Marmara region. Selim and Tüysüz (2013) assessed the Bursa-Gönen depression as a complex basin and stated the basin began opening as a small pull-apart basin in the Late Pliocene and later evolved into a large basin. The geomorphology of the Biga Peninsula where the study area is located began to be shaped by the effect of the Western Anatolia Extensional System from the beginning of the Miocene. In this period, small lacustrine basins like Bayramiç, Çan, Yenice, Kalkım, and Gönen developed under the control of normal or strike-slip normal faults. In these basins, the Çan and Soma Formations, occasionally containing coal, developed from the lacustrine facies in the Middle Miocene, while the Bayramiç formation developed from terrestrial, occasionally fluvial, facies in the Pliocene. The Yenice Basin is initially assessed as forming a half graben in the Upper Miocene-Pliocene with the effect of the Western Anatolia Extensional System. The structural evidence for this tectonic phase is present south of Yenice. Slip data measured on fault planes in Oligo-Miocene aged granites (Tg) south of Yenice document that the Yenice Basin initially developed under the control of oblique-slip normal faults (Figure 24). Later in the process, the right-lateral strike-slip YGF cut the basin sediments.

Additionally, new data was reached about the geological offset of the YGF. In the Yenice area, the Late Oligocene-Early Miocene Hallaçlar formation is cut by the YGF with 4,7±0,3 km right-lateral offset (Figure 25). However, as this offset amount could only be measured linked to a single contact, it is open to debate.

When the annual slip rate (2,65±0,15 mm) calculated for the YGF in this study and the 4,7±0,3 km geological offset are assessed together, the formation age of the YGF is expected to be nearly 1,9 million years. However, as can be clearly seen on Figure 24, the Yenice Basin had a half graben form shaped by strike-slip normal faults initially.

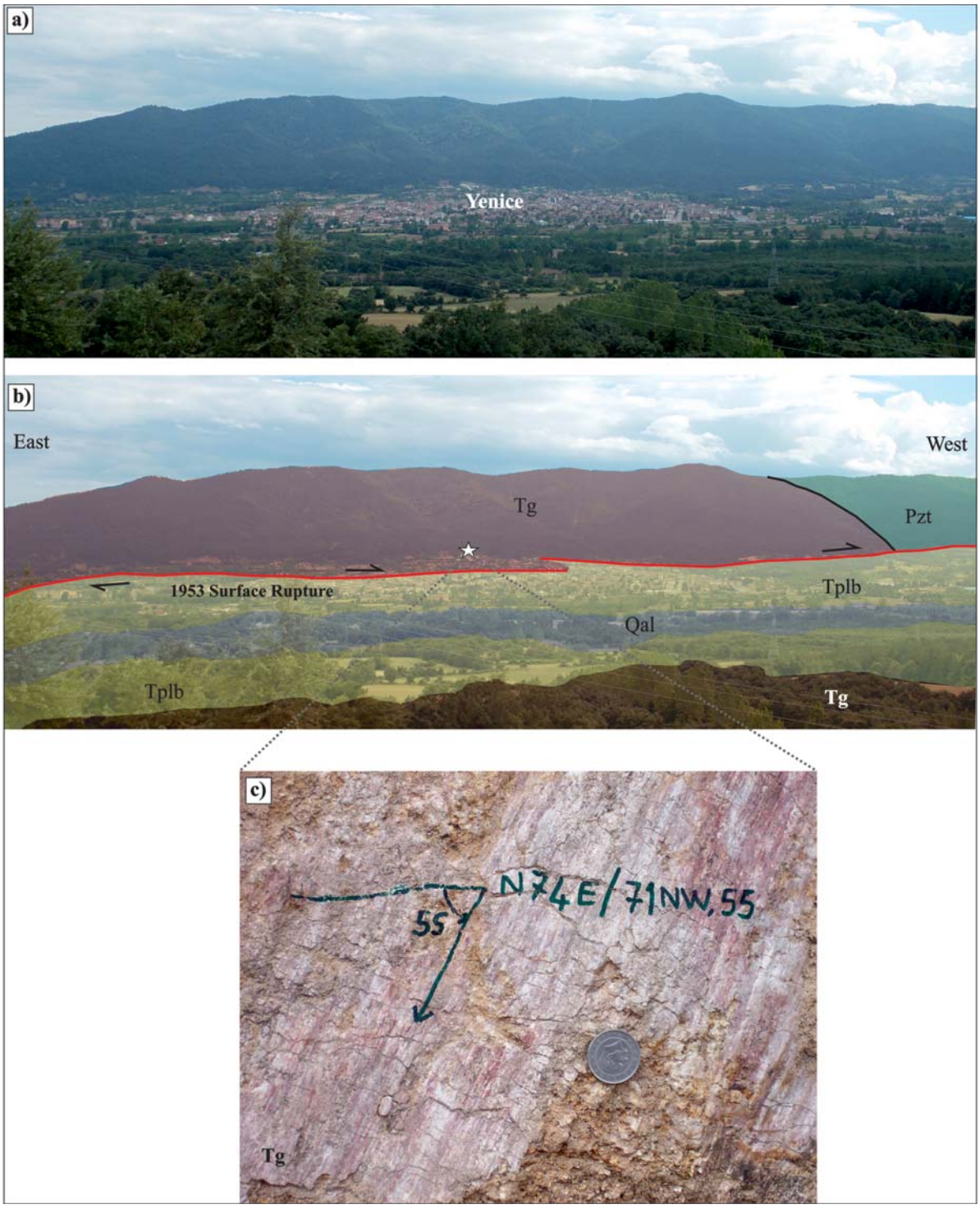

Figure 24- a) Panoramic view of the Yenice Basin, b) Field photograph showing rock units outcropping in the south of the Yenice Basin. For explanations of rock units see figure 3. Star: shows fault plane observation point. c) Oblique slip normal fault plane at the basin edge measured in Tertiary-aged granitoids (Taken from Kürçer, 2006) (view to the south).

As a result, a significant amount of the 4,7±0,3 km geological offset measured in the Late Oligocene-Early Miocene Hallaçlar formation south of Yenice must be associated with the strike-slip normal faulting during basin development. In this situation, the age of the YGF may be assessed as being much younger than 1,9 million years.

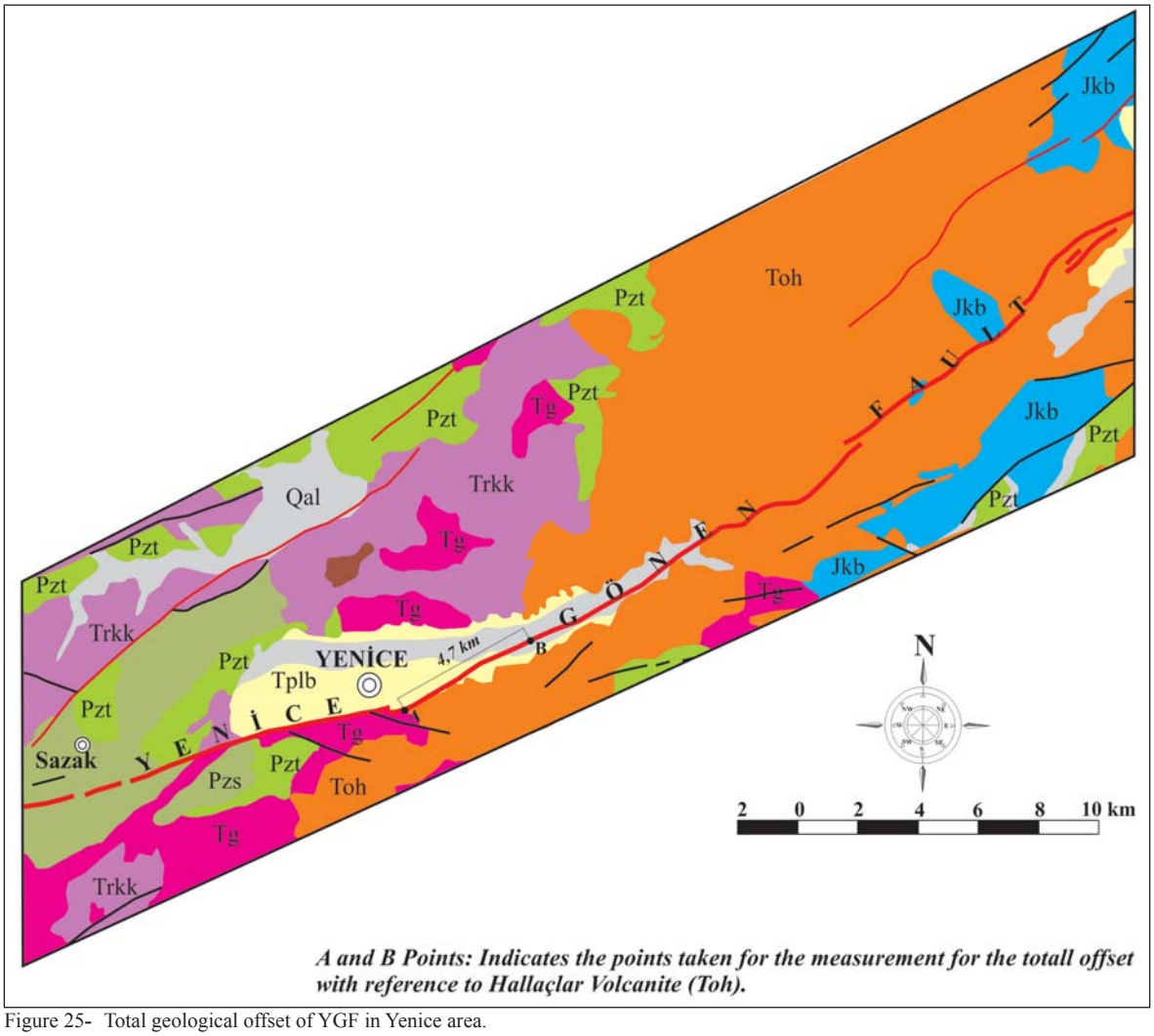

Figure 25- Total geological offset of YGF in Yenice area.

8. Discussion and Conclusions

In this paper, the properties of the 18 March 1953 YGE surface rupture, active tectonics and palaeoseismologic characteristics of the YGF were assessed holistically.

The YGF is an earthquake segment with total length of 70 km comprising 6 fault sections with lengths varying from 5,5 to 19 km separated by releasing or restraining steps or bends (Figure 3 and 4).

Right-lateral displacements varying between 1,70±0,1 m and 3,2±0,2 m were measured on the YGE surface rupture, with the largest displacement of 3,2±0,2 m measured southeast of Çakır village (Figure 12). The displacement amounts show relative reductions in the NE and SW directions, showing the rupture during the 1953 earthquake began NE of Yenice (between Çakır and Karaköy) and generally progressed in both directions toward the NE and partly toward the SW. Total displacement of between 18±2 m and 24±2 m measured in the Holocene drainage system is morphotectonic evidence that the YGF produced earthquakes resulting in surface rupture at least six times during the Holocene.

According to paleoseismology studies on the Çakır fault section of the YGE segment, 6 earthquakes resulting in surface rupture were identified on the YGF in the last 6200 years including the 1953 earthquake. These earthquakes were dated with radiometric methods (^{14}C and OSL) (Figure 22).

As a result of assessing the trenches together, the earthquake (Earthquake 2) before the 1953 earthquake was determined to have occurred between 330 BC and 190 AD and was correlated with the 160 AD

earthquake. In historical earthquake catalogues, there is no historical earthquake data that can be compared with some of the earthquakes (Earthquakes 3, 4, 5 and 6) identified and dated in this study. Additionally, there is archaeological evidence that ancient Troy, located west of the study area and dated to 3000 BC to 400 AD, was destroyed or damaged by ancient earthquakes (Rose, 1994 and 1996). Kürçer et al. (2012) found traces of ancient earthquakes in the remains from layers 3 and 6 in Troy. On an izoseist map for the 1953 YGE (Kalafat et al., 2007), it appears the area around Troy was affected by MSK=VIII (see figure 23 in Kürçer et al., 2012). Earthquakes 3 and 4 identified in this study may be assessed as the earthquakes destroying Troy layers 3 and 6 in Troy. Earthquake 3 is proposed to date to 1275 BC, the final date for Troy layer 6 (1800-1275 BC), and Earthquake 4 is proposed to date to 2050 BC, the final date for Troy layer 3. There is no historical earthquake or archaeological information found for comparison with Earthquakes 5 and 6. The predicted date for Earthquake 5 is between 3250 and 3650 BC. For Earthquake 6, the period from 3640 to 4260 BC is proposed.

According to palaeoseismology studies in Kürçer (2006) and Kürçer et al. (2008) with data obtained from three earthquakes including the 1953 earthquake, the averagely earthquake recurrence interval for the YGF is proposed as 660±160 years. According to the earthquake dates obtained in this study, the YGF has a variable and irregular earthquake recurrence interval from 505 years to 1793 years. Accordingly, the averagely earthquake recurrence interval for the YGF is proposed as 1180 years.

The temporal and spatial proximity of some earthquakes identified in this study (Earthquake 1 and 2) with earthquakes occurring in the instrumental and historical periods in the region is noteworthy (see figure 2). This data point out that historical and instrumental earthquakes occurring on active faults in the region may be caused stress transfer to neighbouring fault segments.

In this paper, the total offset and annual slip rate for the YGF was calculated for the last 300,000 years (Late Quaternary-present). Data illustrating the total offset of the YGF since the Late Quaternary comes from Gönen River. According to erosion and deposition rates, Kazancı et al. (2014) stated the incision times for large valleys in the Southern Marmara region did not extend beyond 300,000 years. Selim et al. (2013) proposed the Gönen River was cut by the YGF and offset by a total of 5,5 km. However, the fault location stated for the YGF in this study (see figure 5 in Selim et al., 2013) is very different to the location known in the literature and adopted in this study. Considering the excavation times for large rivers in the Southern Marmara region do not extend beyond 300.000 years (Kazancı et al., 2014), for the YGF to cause a total of 5,5 km offset on the Gönen River, the annual slip rate on the fault must be 18 mm which does not comply with regional geology, and active fault and geodesy studies. In this study the total displacement amount on Gönen River west of Gönen was measured as 800±50 m (Figure 23). Calculations using the incision time of Gönen River (300.000 years) and total displacement amount (800 ±50 m) found the annual slip rate on the YGF was 2,65±0,15 mm/year. This value complies with previous studies and regional GPS studies. Current GPS studies show the total annual right-lateral slip rate on NE-SW striking active faults located in the Southern Marmara region is 6-8 mm (Meade et al., 2002; Kreemer et al., 2004). Emre et al. (2012) stated that this value must be shared between the Yenice-Gönen, Sarıköy and Çan-Biga fault zones. In this situation, after the YGF, the remaining amount of the 6-8 mm/year slip rate calculated from GPS studies is considered to be shared by other active right-lateral strike-slip faults within the Biga Peninsula led by the Sarıköy and Çan-Biga fault zones.

The geological offset of the YGF was determined as 4,7±0,3 km in the Late Oligocene-Early Miocene Hallaçlar formation near Yenice (Figure 25). When the annual slip rate (2,65±0,15 mm) and 4,7 km geological offset are assessed together, the formation age of the YGF is predicted as 1,9 million years. However, the Yenice Basin began as a half-graben shaped by an oblique-slip normal fault. As a result, a significant portion of the 4,7 km geological offset measured in the Late Oligocene-Early Miocene Hallaçlar formation may be associated with oblique-slip normal faulting during basin development. In this situation, the age of the YGF may be assessed as much younger than 1,9 million years.

Acknowledgements

This study was completed within the scope of the Turkish National Paleoseismology Research Project (TURKPAP). Project no: 2013-30-14-07. We would like to thank sincerely to Prof. Dr. Okan Tüysüz (İstanbul Technical University), Prof. Dr. Hasan Sözbilir (Dokuz Eylül University), Prof. Dr.

Alexandros Chatzipetros (Aristotle University of Thessaloniki) and anonymous referee whose valuable comments and useful criticisms have greatly improved the manuscript.

References

Allmendinger, R. W., Cardozo, N., Fisher, D. 2012. Structural geology algorithms: Vectors and tensors in structural geology. Cambridge University Press, 302 p.

Altunkaynak, Ş., Dilek, Y., Genç, C. Ş., Sunal, G., Gertisser, R., Furnes, H., Yang, J. 2012. Spatial, temporal and geochemical evolution of Oligo–Miocene granitoid magmatism in western Anatolia, Turkey. Gondwana Research, 21 (4), 961-986.

Ambraseys, N.N. 2002. The seismic activity of the Marmara Sea region over the last 2000 years. Bulletin of the Seismological Society of America, 92 (1), 1-18.

Ambraseys, N.N., Finkel, C.F. 1991. Long-term seismicity of İstanbul and of the Marmara Sea region. Terra Nova 3, 527–39

Ambraseys, N., Jackson, J. 2000. Seismicity of the Sea of Marmara (Turkey) since 1500, Geophys. J. Int., 141**,** F1–F6.

Armijo, R., Meyer, B., Hubert-Ferrari, A., Barka, A. 1999. Westward propagation of North Anatolian Fault into the Northern Aegean: timing and kinematics. Geology, 27, 267–70

Ayhan, E. E., Alsan, N., Sancaklı, S.B., Üçer, B. 1981. Türkiye ve Dolayları Deprem Kataloğu (1881-1990). Boğaziçi Üniversitesi Yayınları, 126 s.

Aysal, N. 2015. Mineral chemistry, crystallization conditions and geodynamic implications of the Oligo–Miocene granitoids in the Biga Peninsula, Northwest Turkey. Journal of Asian Earth Sciences, 105, 68-84.

Aysal, N., Ustaömer, T., Öngen, S., Keskin, M., Köksal, S., Peytcheva, I., Fanning, M. 2012*a*. Origin of the Early-Middle Devonian magmatism in the Sakarya Zone, NW Turkey: geochronology, geochemistry and isotope systematics. Journal of Asian Earth Sciences, 45, 201-222.

Aysal, N., Öngen, S., Peytcheva, I., Keskin, M. 2012*b*. Origin and evolution of the Havran Unit, Western Sakarya basement (NW Turkey): new LA-ICP-MS U-Pb dating of the metasedimentary-metagranitic rocks and possible affiliation to Avalonian microcontinent. Geodinamica Acta, 25 (3-4), 226-247.

Barka, A.A., Kadinsky-Cade, K. 1988. Strike-slip fault geometry in Turkey and its influence on earthquake activity. Tectonics, 7 (3), 663–684.

Barka, A., Gülen, L. 1988. New constrains on age and total offset on the North Anatolian Fault Zone: Implications for tectonics of the Estern Mediterranean Region. METU Journal of Pure and Applied Sciences, 21, 39–63.

Barka, A., Akyüz., S., Altunel, E., Sunal., G., Çakır, Z., Dikbaş, A., Yerli, B., Armijo, R., Meyer, B., de Chabalier, J. B., Rockwell, T., Dolan, J.R., Hartleb, R., Dawson, T., Christofferson, S., Tucker, A., Furnal, T., Langridge, R., Stenner, H., Lettis, Bachhuber, J., ve Page, W. 2002. The Surface Rupture and Slip Distribution of the 17 August 1999 İzmit Earthquake (M 7.4), North Anatolian Fault. Bull. Seism. Soc. Amer. 92 (1): 43-60.

Bozkurt, E. 2001. Neotectonics of Turkey – A synthesis. Geodinamica Acta, 14, 3–30.

Canıtez N, Üçer S.B. 1967. A Catalogue of Focal Mechanism Diagrams for Turkey and Adjoining Areas. İTÜ Maden Fak., Arz Fiziği Enst. Yayın No. 25. 111 pp.

Dirik, K., Belindir, F., Özsayın, E., Kutluay, A. 2008. Neotectonic features and paleoseismology of Yenice- Gönen Fault Zone. Final report of TUBİTAK. Report no: TUJJB-UDP04-02, Ankara.

dePolo, C. M., Clark, D. G., Slemmons, D. B., Aymand, W. H. 1989. Historical Basin and Range Province surface faulting and fault segmentation. In Fault Segmentation and Controls of Rupture Initiation and Termination (D. P. Schwartz, and R. H. Sibson, Eds.), U.S. Geol. Surv. Open File Rep. 89–315, pp. 131–162.

dePolo, C. M., Clark, D. G., Slemmons, D. B., Ramelli, A. R. 1991. Historical surface faulting in the Basin and Range Province, western North America—Implications for fault segmentation. J. Struct. Geol. 13, 123–136.

Duru, M., Pehlivan, Ş., Okay, A.İ., Şentürk, Y., Kar, H. 2012. Biga Yarımadası'nın Tersiyer Öncesi Jeolojisi. Yüzer, E. ve Tunay, G. (Ed.), Biga Yarımadası'nın Genel ve Ekonomik Jeolojisi (7-74). Ankara: ISBN: 978-605-5310-18-9. Maden Tetkik ve Arama Genel Müdürlüğü Özel Yayın Serisi 28, 7-74.

Emre, Ö., Doğan, A., Yıldırım, C. 2012. Biga Yarımadasının diri fayları ve deprem potansiyeli. In: Yüzer, E. ve Tünay, G. (Eds.), Biga Yarımadası'nın Genel ve Ekonomik Jeolojisi, Maden Tetkik ve Arama Genel Müdürlüğü Özel Yayın Serisi 28, 163-198, Ankara-Türkiye.

Emre, Ö., Duman, T. Y., Özalp, S., Elmacı, H., Olgun, Ş., Şaroğlu, Ş. 2013. Açıklamalı Türkiye Diri Fay Haritası, Maden Tetkik ve Arama Özel Yayın Serisi 30.

GCMT Catalogue. The Harvard Centroid Moment Tensor Ctaloque. The Global Centroid-Moment Tensor (CMT) Project, 1976-2012, http://globalcmt.org7

Gürer, Ö.F., Kaymakçı, N., Çakır, Ş., Özburan, M. 2003. Neotectonics of the southeast Marmara region, NW Anatolia, Turkey. Journal of Asian Earth Sciences 21, 1041–1051.

Harvard Univ. 1998. Dep. Earth Planet. Sci., Cambridge, MA. http://www.seismology.harvard.edu

Herece, E. 1990. 1953 Yenice–Gönen deprem kırığı ve Kuzey Anadolu fay sisteminin Biga Yarımadası'ndaki uzantıları, Maden Tetkik ve Arama Dergisi, 111, pp. 47–59.

Jackson, J., McKenzie, D.P. 1984. Active tectonics of the Alpine–Himalayan Belt between western Turkey and Pakistan. Geophys. J. R. Astron. Soc., 77, 185–246.

Karacık, Z., Yılmaz, Y., Pearce, J. A., Ece, Ö. I. 2008. Petrochemistry of the south Marmara granitoids, northwest Anatolia, Turkey. International Journal of Earth Sciences, 97 (6), 1181-1200.

Karakaisis, G. F., Papazachos, C. F., Scordilis, E. M. 2010. Seismic sources and main seismic faults in the aegean and surrounding area, Bulletin of the Geological Society of Greece. Proceedings of the 12th International Congress (pp. 2016–2042). Patras.

Kazancı, N., Emre, Ö., Erturaç, K., Leroy, S.A.G., Öncel, S., İleri, Ö., Toprak, Ö. 2014. Possible incision time of the large valleys in southern Marmara region, NW Turkey. Maden Tetkik ve Arama Dergisi 148, pp. 1–17.

Ketin, I., Roesly, F. 1953. Makroseismische Untersuchungen über das nordwestanatolische Beben vom 18. Marz 1953. Eclogae Geol. Helv. 46, 187–208.

Kocaefe, S., Ataman, G. 1976. Anadolu'da sismotektonik olaylar: Antalya-Fethiye-Denizli üçgeni içinde yer alan bölgenin incelenmesi. Hacettepe Univ. Yerbilim. Derg. 2, 55–70

Kreemer, C., Chamot-Roke, N., Le Pichon, X. 2004. Constraints on the evolution and vertical coherency of deformation in the North Aegean from a comparison of geodetic, geologic and seismologic data. Earth Planet. Sci. Lett. 225, 329–346.

Kürçer, A. 2006. Yenice Gönen Civarının Neotektonik Özellikleri ve 18 Mart 1953 Yenice Gönen Deprem (Mw=7.2) Fayı'nın Paleosismolojisi, KB Türkiye. Yüksek Lisans Tezi, Tez No: 185774, Çanakkale Onsekiz Mart Üniversitesi, Fen Bilimleri Enstitüsü, 190 sayfa (unpublished).

Kürçer, A. 2008. Yenice Gönen Fayı ve sismotektonik anlamı, KB Anadolu, Türkiye. Ulusal Jeomorfoloji Sempozyumu, Bildiriler, 213-214. Çanakkale, 2008.

Kürçer, A. 2012. Tuz Gölü Fay Zonu'nun Neotektonik Özellikleri ve Paleosismolojisi, Orta Anadolu, Türkiye, Doktora Tezi, Tez No: 318203, Ankara Üniversitesi, Fen Bilimleri Enstitüsü, 318 sayfa (unpublished).

Kürçer, A., Chatzipetros, A., Tutkun, S. Z., Pavlides, S., Ateş, Ö., Valkaniotis, S. 2008. The Yenice–Gönen active fault (NW Turkey): Active tectonics and palaeoseismology. Tectonophysics, 453, 263–275.

Kürçer, A., Chatzipetros, A., Tutkun, S. Z., Pavlides, S., Özden, S., Syrides, G., Vouvalides, K., Ekinci, Y. L. 2012. An assessment of the earthquakes of ancient Troy, NW Anatolia, Turkey (pp. 171–200). In E. Sharkov (Ed.), Tectonics – Recent advances (chapter 7, pp. 171–200). Ankara: InTech. ISBN: 978-953-51-0675-3.

Kürçer, A., Yalçın, H., Gülen, L., Kalafat, D. 2015. 8 January 2013 Mw = 5.7 North Aegean Sea earthquake and its seismotectonic significance, Geodinamica Acta, 27, 2-3, 175-188, DOI:10.1080/09853111.2014.957503

Kürçer, A., Özalp, S., Özdemir, E., Uygun Güldoğan, Ç., Duman, T.Y. 2016. Yüzey Kırığı Oluşturmuş Faylar üzerinde aktif tektonik ve paleosismolojik araştırmalar hakkında örnek çalışma: Yenice Gönen Fayı, KB Türkiye. Maden Tetkik ve Arama Genel Müdürlüğü, Doğal Kay. ve Eko. Bült. 21, 1-18.

Kürçer, A., Özaksoy, V., Özalp, S., Uygun Güldoğan, Ç., Özdemir, E., Duman, T.Y. 2017. The Manyas Fault Zone (southern Marmara Region, NW Turkey): active tectonics and paleoseismology. Geodinamica Acta, 29, 1, 42-61, DOI: 10.1080/09853111.2017.1294013.

Le Pichon, X Chamot-Rooke, N., Lallemant,S., Noomen, R., Veis, G. 1995. Geodetic determination of the kinematics of central Greece with respect to Europe implications for eastern Mediterranean tectonics, J. Geophys. Res. 100, 12675-12690.

McKenzie, D.P. 1972. Active tectonics of the Mediterranean region. Geophys. J. R. Astron. Soc. 30 (2), 109–185.

McKenzie, D.P. 1978. Active tectonics of the Alpine Himalayan Belt The Aegean Sea and surrounding regions, Geophys. J. R. Astron. Soc. 55, 217-254.

Meade, B., Hager, B., Reilinger, R. 2002. Estimates of seismic potential in the Marmara region from block models of secular deformation constrained by GPS measurements. Bull. Seismol. Soc. Am. 92 (1), 208–215.

Okay, A. İ. Göncüoğlu, M.C. 2004. The Karakaya Complex: a review of data and concepts. Turkish Journal of Earth Sciences 13, 2, 75-95.

Okay, A. İ., Kaşlılar-Özcan, A., İmren, C., Boztepe-Güney, A., Demirbağ, E., Kuşçu, İ. 2000. Active faults and evolving strike-slip basins in the Marmara Sea, northwest Turkey: A multichannel seismic reflection study. Tectonophysics, 321, 189–218.

Örgülü, G., Aktar, M. 2001. Regional moment tensor inversion for strong aftershocks of the August 17, 1999 İzmit earthquake (Mw= 7.4). Geophys. Res. Lett. 28, 371–74

Özalaybey, S., Ergin, M., Aktar, M., Tapırdamaz, C., Biçmen, F., Yörük, A. 2002. The 1999 ˙Izmit earthquake sequence in Turkey: seismological and tectonic aspects. Bull. Seismol. Soc. Am. 92, 376–86.

Özden, S., Bekler, T., Tutkun, S. Z., Kürçer, A., Ateş, Ö., Bekler, F., Kalafat, D., Gündoğdu, E., Bircan, F., Çınar, S., Çağlayan, Ö., Gürgen, M., İşler, H., Yalçınöz, A. 2008. Biga Yarımadası ve Güney Marmara bölgesinin sismotektoniği. Aktif Tektonik Araştırma Grubu 12. Toplantısı, Bildiri Özleri Kitabı, s. 48-49, Akçakoca, Maden Tetkik ve Arama Genel Müdürlüğü, Türkiye.

Papadopoulos, G.A., Kondopoulou, D.P., Leventakis, G.A., Pavlides, S.B. 1986. Seismotectonics of the Aegean region. Tectonophysics 124, 67–84

Pınar, N. 1953. Preliminary Note on the Earthquake of Yenice Gönen, Turkey, March 18, 1953. Bull. Seismol. Soc. Am., vol. 43, pp. 307–310.

Reilinger, R.E., McClusky, S.C., Oral, M.B., King, R.W., Toksöz, M.N., Barka, A.A., Kinik, I., Lenk, O., Sanli, I. 1997. Global positioning system measurements of present day crustal movements in the Arabian–African–Eurasian plate collision zone. J. Geophys. Res. 102, 9983–9999.

Reilinger, R., McClusky, S., Vernant, P., Lawrence, S., Ergintav, S., Çakmak, R., Özener, H., Kadrov, F., Guliev, I., Stepanyan, R., Nadariya, M., Hahubia, G., Mahmoud, S., Sakr, K., ArRajeh, A., Paradissis, D., Al-Aydrus, A., Prilepin, M., Guseva, T., Evren, E., Dmitrotsa, A., Filikov, S.V., Gomez, F., Al-Ghazzi, R., Karam, G. 2006. GPS constraints on continental deformation in the Africa-Arabia-Eurasia continental collision zone and implications for the dynamics of plate interactions. Journal of Geophysical Research 111, B05411.

Rose, C.B. 1994. The 1993 post-Bronze Age excavations at Troia. Studia Troica 4: 75–104

Rose, C.B. 1996. The 1995 post-Bronze Age research and excavations at Troia. Studia Troica 6, 97–101

Selim, H., Tüysüz, O. 2013. The Bursa–Gönen Depression, NW Turkey: a complex basin developed on the North Anatolian Fault. Geol. Mag. 150 (5), 2013, pp. 801–821.

Selim, H., Tüysüz, O., Karabaş, A., Taş, K.Ö. 2013. Morphotectonic evidence from the southern branch of the North Anatolian Fault (NAF) and basins of the south Marmara sub-region, NW Turkey. Quaternary International, 292, 176-192.

Straub, C.S. 1996. Recent crustal deformation and strain accumulation in the Marmara Sea region, N.W. Anatolia, inferred from GPS measurements. unpub. Ph.D. dissertation, Swiss Federal Institute of Technology at Zurich, p.122, plus appendices.

Straub, C., Kahle, H. 1997. Active crustal deformation in the Marmara Sea region, NW Anatolia, inferred from GPS measurements. Geophys. Res. Lett. 22 (18), 2533–2536.

Şengör, A. M. C. 1979. The North Anatolian transform fault: Its age, offset and tectonic significance. Journal of the Geological Society, 136, 269–282.

Şengör, A.M.C. 1980. Türkiye'nin Neotektoniği'nin Esasları, Türkiye Jeoloji Kurumu Konferans Serisi 2.

Şengör, A. M. C., Barka, A. A. 1992. Evolution of escape-related strike-slip systems: Implications for distribution of collisional orogens. 29th International Geological Congress, Kyoto, Japan, Abstracts, 1, 232.

Şengör, A. M. C., Görür, N., Şaroğlu, F. 1985. Strike-slip faulting and related basin formation in zones of tectonic escape: Turkey as a case study. K. T. Biddle, K.T.,Christie-Blick, N. (Eds.), Strike-slip Deformation, Basin Formation and Sedimentation. SEMP Special Publication 37, 227–264.

Şengör, A. M. C., Tüysüz, O., İmren, C., Sakınç, M., Eyidoğan, H., Görür, N., Rangin, C. 2004. The North Anatolian fault: A new look. Annual Review of Earth and Planetary Sciences, 33, 1–77. doi:10.1146/annure.earth.32.101802.120415

Taymaz, T., Jackson, J., McKenzie, D. P. 1991. Active tectonics of the north and central Aegean Sea. Geophysical Journal International, 106, 433–490.

Bulletin of the Mineral Research and Exploration

http://bulletin.mta.gov.tr

Paleoseismological catalog of Pre-2012 trench studies on the active faults in Turkey

Şule GÜRBOĞA[a*] and Oktay GÖKÇE[b]

[a]*General Directorate of Mineral Research and Exploration, Department of Marine Research, Ankara, Turkey. orcid.org/0000-0002-5225-5895*
[b]*Prime Ministry Disaster and Emergency Management Presidency, Ankara, Turkey. orcid.org/0000-0003-0553-3511*

Review Article

Keywords:
Earthquakes, Paleoseismological catalogue, Trenches, Active faults, Turkey.

ABSTRACT

Instrumental and historical earthquake catalogues have to be examined and evaluated to understand the long-term seismic behaviour of active faults. Although the instrumental records have been determined from the national and international observatories, the historical seismic catalogues are very limited in Turkey. For the reason, we aimed to compile paleoseismological trench studies carried out before 2012 in the areas of onshore and offshore sections of Turkey. In terms of a Turkey Paleoseismological Project (TURKPAP) posted by General Directorate of Mineral Research and Exploration (MTA) in the 2012 year, a number of paleoseismological investigations have been initiated and documented for archiving at a standardized data layout. In this study, we compiled all paleoseismological trench surveys with the definite dates of past strong seismic events occurred in Turkey before that date. By using this compilation, not only the historical earthquakes but also many paleoseismologic parameters of the studies have been listed clearly.

Received Date: 14.10.2017
Accepted Date: 06.05.2019

1. Introduction

The areas, experienced strong seismic events, have been the target for paleoseismological studies. In this manner, historical earthquakes could be determined. It could allow us to obtain detailed data about spatial and temporal attitudes of active faults, and assessment of paleo-earthquake records. The catalogues of destructive earthquakes in the European Archive of Historical Earthquake Data (AHEAD) system are updated continuously. But this system is not going to solve the problem of lack of proper historical catalogue in Turkey. For this reason, Turkey needs a historical earthquake archive. Without information about the past seismic events sourced from active faults, it is impossible to achieve assessment and planning the hazard and risk studies. In this paper, all paleoseismological trench surveys compiled in Turkey to be the foundation for future studies. All studies completed up to 2012 years were examined regarding the national boundary of Turkey that has paleoseismological data on land, sea and lake studies including definite dating results about the past seismological events. After 2012, a systematic catalogue started to organize in the content of paleoseismology project (TURKPAP) prepared by General Directorate of Mineral Research and Exploration.Because of that, the investigations in the content of TURKPAP and the other papers have not been included in this catalogue.

In this paper, we exploited and compiled all paleoseismological trench studies that discovered and confirmed the presence of historical and pre-historical earthquakes. Only the definite trench locations were issued in this catalogue. Geographically unknown locations could not be included. All used data have been collected, selected, listed and inserted into

Citation Info: Gürboğa, Ş., Gökçe, O. 2019. Paleoseismological catalog of Pre-2012 trench studies on the active faults in Turkey. Bulletin of Mineral Research and Exploration, 159, 63-87. *http: //dx.doi.org/10.19111/bulletinofmre.561925*

** Corresponding author: Şule GÜRBOĞA, sule.gurboga@mta.gov.tr*

a new paleoseismological catalogue of Turkey. Another focus of our work is the development of long earthquake records that are critical for determining the distribution of earthquake recurrence intervals along the active faults. Electronic supplementary material in this paper gives a chance to readers for comparing the recurrence interval and source of devastating earthquakes.

2. Active Faults in Turkey

Turkey has very complex tectonic features because of the Arabian, African and Eurasian plate motions. This situation creates a number of single active faults and fault systems. They generated devastating earthquakes in the past, and are capable to produce many of them in the future. Taking their various characteristics and locations into account, we grouped them to represent their paleoseismological outcomes. They are handled in the given order; 1) North Anatolian Fault System; 2) East Anatolian Fault System; 3) Horst-graben system in western Anatolia, 4) Central Anatolia, and 5) A part of Dead Sea Fault System inside the border of Turkey.

North Anatolian Fault System (NAFS) is the subject of several studies to understand the long-term behaviour of its different segments. In fact, it is one of the most active strike-slip structures in the world comprising the plate boundary between Eurasia and Anatolia. The NAFS is a 1500 km long right-lateral strike-slip fault system running convex to the Black Sea coast. It is located between Karlıova in the east and the Aegean Sea in the west (Figure 1). Most of the paleoseismologic studies were performed along the NAFS in Turkey. Some of the events occurred in adjacent segments could be correlated with each other. Because different recurrence intervals for the same segments have been suggested owing to suspicious dating results. It is not surprising outcomes regarding the various characteristics of each segment. This catalogue provides the comparison of previous earthquakes dated by paleoseismological researches.

Another important megastructure in Turkey is the East Anatolian Fault System (EAFS). It is the 580 km long and NE-SW-trending sinistral zone of deformation located between Karlıova in the NE and Antakya in the southwest (Arpat and Şaroğlu, 1972; Lovelock, 1984; Şaroğlu et al., 1992; Şengör et al., 1985) (Figure 1). The last known devastating earthquakes sourced from the EAFS are the 1874 Lake Hazar and the 1971 Bingöl earthquakes that created surface ruptures (Jackson and McKenzie, 1984; Ambraseys and Jackson, 1998). Thus, all the geological studies in literature evidently indicate the

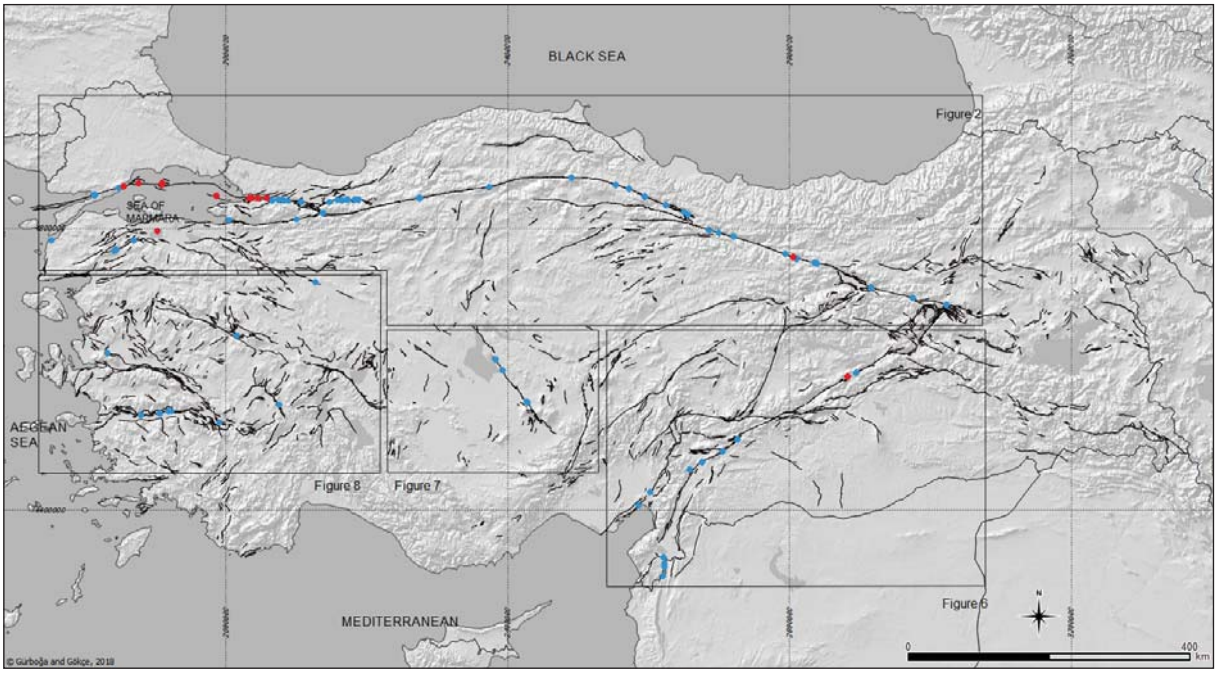

Figure 1- Active fault map of Turkey. Different coloured circles represent the locations of paleoseismological trench surveys on land (blue) and core surveys on lake-marine (red). Active faults are compiled from Emre et al., 2013 and 2018.

activeness of EAFS. Even if the historical seismicity and field observation indicate the high activeness of the EAFS, its seismicity is relatively lower than the NAFS. For this quiescence, the EAFS may be locked and accumulating the energy (Dewey et al., 1986; Yönlü et al., 2017). Therewithal, paleoseismological trench surveys are very limited along the EAFS (Yönlü et al., 2017). We added the paleoseismological studies along both the DSFS and the EAFS in this paper.

Horst-graben system in western Anatolia is very famous active continental extensional province in the world. Margin-boundary active faults have created moderate to large earthquakes recently (Tan et al., 2008). In terms of paleoseismological studies carried out along these active normal faults, reliable conclusions were obtained.

All the NAFS, EAFS, and the western and central Anatolian graben-horst systems were taken into account to classify the trench studies along the active faults. In each research, different active fault maps and references have been used to define fault segments, thus, more than one names came up for the same fault and segment. To produce uniformity, active fault map prepared by Emre et al. (2013 and 2018) are used as a base map in this paper (Figure 1). The term segment preferred by authors of this manuscript means that it is a section of a single fault separated from the adjacent fault parts by the intervening variations such as bending, bifurcation, and jumping. Moreover, main attributes of this catalogue are seen in table 1.

2.1. Paleoseismological Studies Along The North Anatolian Fault System

The total length of the NAFS was examined under three parts (Figure 2). These are the eastern_NAFS (Figure 3 and table 2), the central NAFS (Figure 4 and table 3), and the western_NAFS (Figure 5 and table 4). The locations of the paleoseismological trenches are illustrated from the east towards the west regarding the segments in the relevant tables.

Paleoseismology studies the core samples to provide reliable dating results. The water-saturated core sediments make materials suitable for radiocarbon dating. Both the marine and lacustrine core samples were taken from Sea of Marmara and small lakes along the NAFS and they produced a well correlated data. As the attributes are listed in table 5, their results are given in the red circles in figures 1, 2.

2.2. Paleoseismological Studies Along the East Anatolian Fault System

There is no common agreement on the segmentation of the EAFS as is those on the NAFS. The number of segments varies between 2 and 14 according to different authors (Barka and Kadinsky-Cade, 1988; Perinçek and Çemen, 1990; Şaroğlu et al., 1992; Hempton and Dewey 1981; Muehlberger and Gordon 1987; Westaway, 1994; Duman and Emre, 2013; Yönlü et al., 2017). To be consistent, the segmentation prepared by Emre et al., (2013 and 2018) is on this catalogue. Red and blue circles define the offshore and onshore paleoseismological surveys, respectively (Figure 6 and table 6-7).

2.3. Paleoseismological Studies on the Central Anatolia

Paleoseismological investigations are very limited in Central Anatolia. Only one trenching was performed along the Lake Salt Fault Zone by Kürçer (2012). The locations and results are in figure 7 and table 8.

2.4. Paleoseismological Studies on the Area of Horst-Graben System in Western Anatolia

Western Turkey is one of the most important areas experiencing the intracontinental extension in the world. The extensional regime yields a number of horst-graben structures bounded by the normal faults. The recent earthquake activity indicates the earthquake potential of the area (Tan et al., 2008; Kalafat et al., 2011; Kadirioğlu et al., 2018). Even though paleoseismological researches are more important for such seismically active areas, we have 23 studies with radiometric dating results (Figure 8 and table 9).

Table 1- The sample format of catalogue: F. name of fault system, S. name of segments, Tr. name of trench, T. given name of trenches in here, Lon. Longitude, Lat. Latitude, T. number of total events, Eq date min. oldest dated earthquake, Eq date max. youngest dated earthquake, Corr. correlated event date with historical catalogue, Rptr L. calculated rupture length, Rupture M. calculated rupture magnitude, Slip R. calculated slip rate on the segment, Rec Int. calculated recurrence interval, Last rup. the last event rupture along the segment, and Ref. obtained references.

No	Name_ of_F	Name_ of_S	Name_ of_Tr	Code_T	Lon	Lat	Event_T	Eq_date_ min	Eq_date_ max	Corr	Rptr_L	Rptr_M	Slip_R	Rec_Int	Last_rup	Ref
19										1939	400	7,9	22	200-350		
20										1254	150	-		200-350		
21										1045		-		200-350		
22	NAFS	Refahiye	Yaylabeli	Re2	38,94000383	39,95808632	5	717	844			-		200-350	1939	Kozacı et al., 2011
23								302	724	499		-		200-350		
28								-881	-673		360	7,7-8,4				
29								-1406	-1291		170	7,2-7,8				

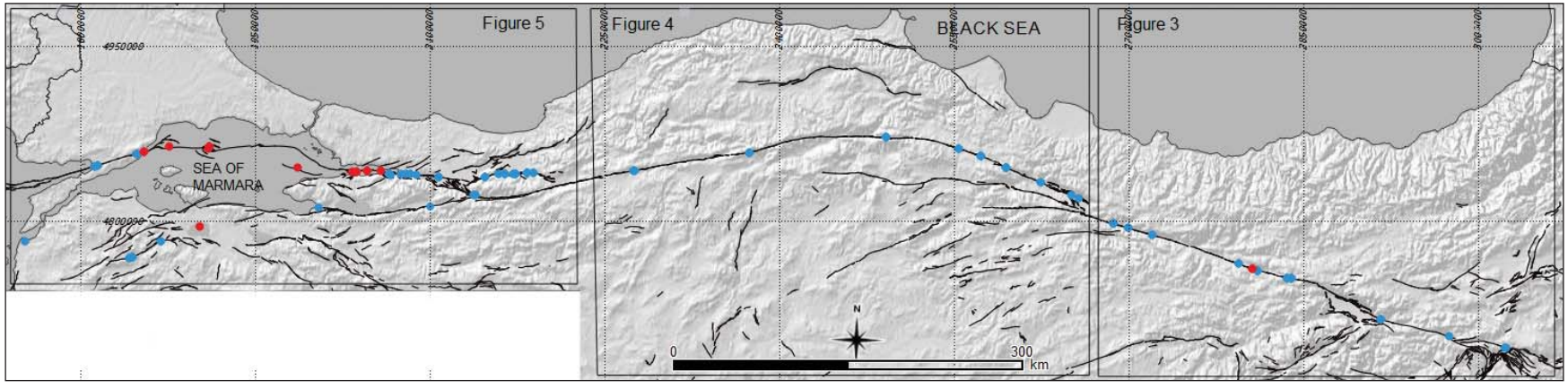

Figure 2- The simplified active fault map of NAFS (Emre et al., 2013 and 2018). The blue circles point out the locations of paleoseismological trench sites on land. Red circles represent the locations of core samples from lake and sea. The locations of figure 3, 4, and 5 were illustrated in the figure.

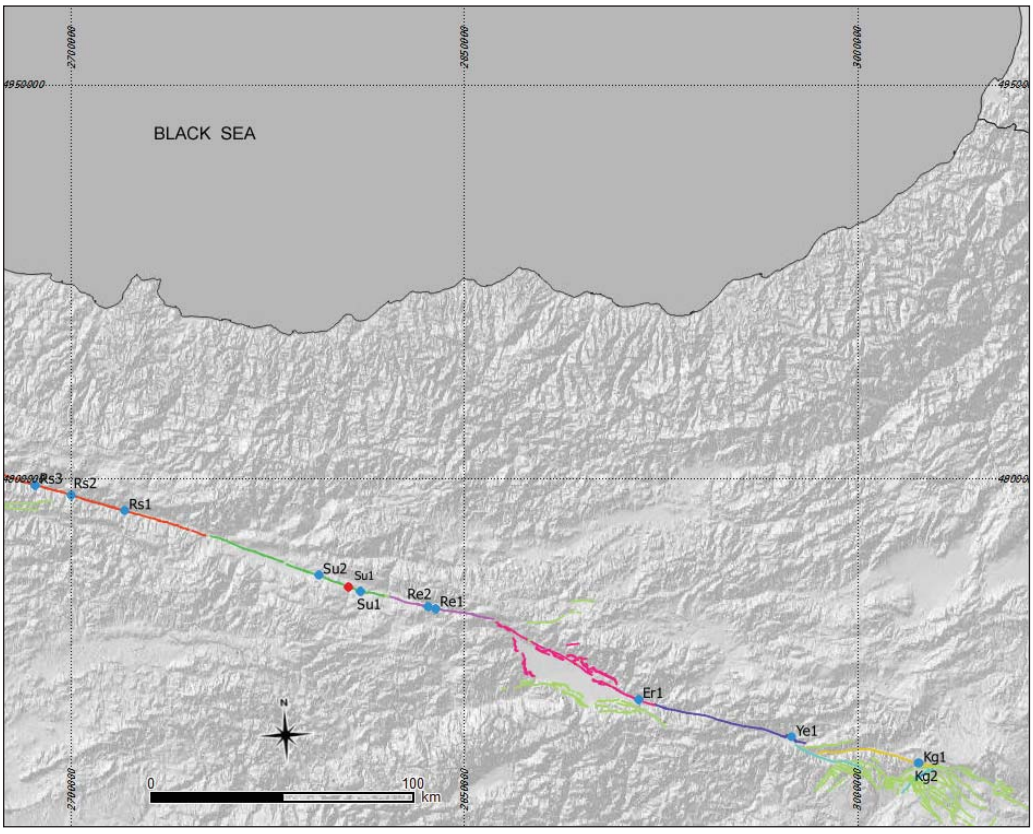

Figure 3- The map shows the east NAFS (Emre et al., 2013 and 2018), and trench locations on the digital elevation model. Their attributes are in table 2. The colouring makes a distinction among fault segmentations.

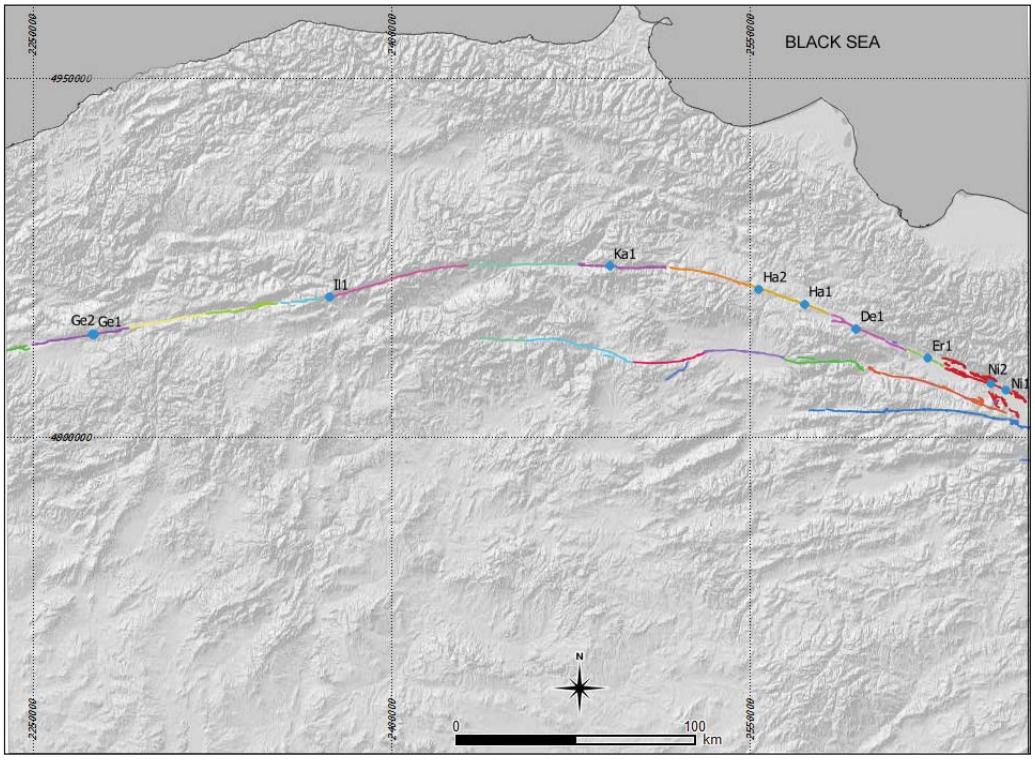

Figure 4- The map shows the central NAFS (Emre et al., 2013 and 2018) and the trench locations on the digital elevation model. The attributes are in table 3. The colouring makes a distinction among fault segmentations.

Table 2- The paleoseismological catalogue of the east_NAFS.

No	Name_of_F	Name_of_S	Name_of_Tr	Code_T	Lon	Lat	Event_T	Eq_date_min	Eq_date_max	Corr	Rptr_L	Rptr_M	Slip_R	Rec_Int	Last_rup	Ref
1	NAFS	Kargapazarı	Yoncalık1	Kg1	41,08346391	39,32817372	2	-8500	-6150			-				Sancar and Akyüz, 2007
2								-5960	-4300			-				
3			Yoncalık2	Kg2	41,07599539	39,32993262	2		-6325			-				
4								-6325	-2105			-				
5		Yedisu	NA	Ye1	40,5272098	39,44612412	2	450				-			1784	
6								50	450			-				
7		Erzincan	NA	Er1	39,8565447	39,60596802	5	1673	1950	1784		-		200-250		Okumura et al., 1994
8								1461	1639			-		200-250		
9								1323	1524			-		200-250		
10								1066	1275			-		200-250		
11								684	935			-		200-250		
12		Refahiye	Çukurçimen	Re1	38,97311	39,95147615	7			1939		-		200-900	1939	Hartleb et al., 2006
13								980	1420	1254		-		200-900		
14								930	1070	1045		-		200-900		
15								360	540	499		-		200-900		
16								-230	50			-		200-900		
17								-1450	-800			-		200-900		
18								-2880	-200			-		200-900		
19			Yaylabeli	Re2	38,94000383	39,95808632	5			1939	400	7,9	22	200-350	1939	Kozacı et al., 2011
20										1254	150	-		200-350		
21										1045		-		200-350		
22								717	844			-		200-350		
23								302	724	499		-		200-350		

Table 2- continued

No	Name_of_F	Name_of_S	Name_of_Tr	Code_T	Lon	Lat	Event_T	Eq_date_min	Eq_date_max	Corr	Rptr_L	Rptr_M	Slip_R	Rec_Int	Last_rup	Ref
24		Suşehri	Günalan	Su1	38,637781	40,021301	6			1939	350	7,7-8,3			1939	Fraser et al., 2012
25										1668	250	7,6-8,3				
26										1254	170	7,2-7,8				
27										499	360	7,7-8,4				
28								-881	-673		360	7,7-8,4				
29								-1406	-1291		170	7,2-7,8				
30			Eskibağ	Su2	38,45680753	40,08078116	4			1939		-			1939	Polat et al., 2012
31												-				
32									580	499		-				
33								-840				-				
34		Reşadiye	Umurca	Rs1	37,596501	40,324874	3			1939		7,8			1939	Zabcı et al., 2011
35										1668		-				
36										1254		-				
37			Reşadiye	Rs2	37,355531	40,384651				1939		-				
38										1254		-				
39										1045		-				
40		Reşadiye	Reşadiye A	Rs3	37,19827468	40,42081951	7			1939		-		1-1375	1939	Fraser, 2009
41								1570	1939	1668		-		1-1375		
42								261	642	499		-		1-1375		
43								-257	260			-		1-1375		
44								-908	-705			-		1-1375		
45								-2019	-1804			-		1-1375		
46								-2280	-2067			-		1-1375		

Table 3- The paleoseismological catalog of the mid_NAFS.

No	Name_of_F	Name_of_S	Name_of_Tr	Code_T	Lon	Lat	Event_T	Eq_date_min	Eq_date_max	Corr	Rptr_L	Rptr_M	Slip_R	Rec_Int	Last_rup	Ref
47	NAFS	Niksar	Direkli	Ni1	36,85324306	40,62788542	2			1942					1942	Akyüz et al., 2009
48								-480	-412							
49			Alanıcı	Ni2	36,77970833	40,65340625	2			1942					1942	
50									500							
51		Erbaa	Çevresu	Er1	36,47409553	40,752534	3			1942	48	7			1942	Kürçer et al., 2009
52										1668						
53								700	1300							
54		Destek	Destek	De1	36,1210966	40,86727874	8			1943				385±166	1943	Fraser et al., 2009
55								1438	1787	1668				385±166		
56								1034	1325					385±166		
57								549	721					385±166		
58								17	585	236				385±166		
59								-351	28					385±166		
60								-705	-392					385±166		
61								-913	-595					385±166		
62		Havza	Alayurt	Ha1	35,86532194	40,96235961	6			1943		7,7			1943	Hartleb et al., 2003
63								800	1200							
64										236						
65								400	1000							
66								-4600	-3550							
67			NA	Ha2	35,6396014	41,01836178	4			1943				600-900	1943	Yoshioka et al., 2000
68								1159	1374					600-900		
69								365	740					600-900		
70								-2330	-1557					600-900		

Table 3- continued

No	Name_of_F	Name_of_S	Name_of_Tr	Code_T	Lon	Lat	Event_T	Eq_date_min	Eq_date_max	Corr	Rptr_L	Rptr_M	Slip_R	Rec_Int	Last_rup	Ref
71	NAFS	Kamil	Elmacık	Ka1	34,89651403	41,10719986	8			1943	280	7,6	25	97-912	1943	Fraser et al., 2010
72								549	651	529			25	97-912		
73								-23	103				25	97-912		
74								-609	-185				25	97-912		
75								-971	-814				25	97-912		
76								-1227	-968	-1200			25	97-912		
77								-2050	-1777				25	97-912		
78								-2556	-2235				25	97-912		
79		Ilgaz	Ilgaz_Aluç	Il1	33,504261	40,9817499	5			1943			12,5	280-620	1943	Sugai et al., 1999
80								1495	1850	1668			12,5	280-620		
81								890	1190	1050			12,5	280-620		
82								640	810					280-620		
83								0	150					280-620		
84		Gerede	Ardıçlı	Ge1	32,34083333	40,82305556	5			1944					1944	Okumura et al., 2002, 2003
85										1668						
86								1171	1668							
87								943	1298	1050						
88								643	918							
89			Demirtepe	Ge2	32,32899671	40,82162075	4			1944			17	330	1944	Kondo et al., 2004 and 2010
90								1640		1668			17	330		
91								1210	1460				17	330		
92								840	960	1035			17	330		

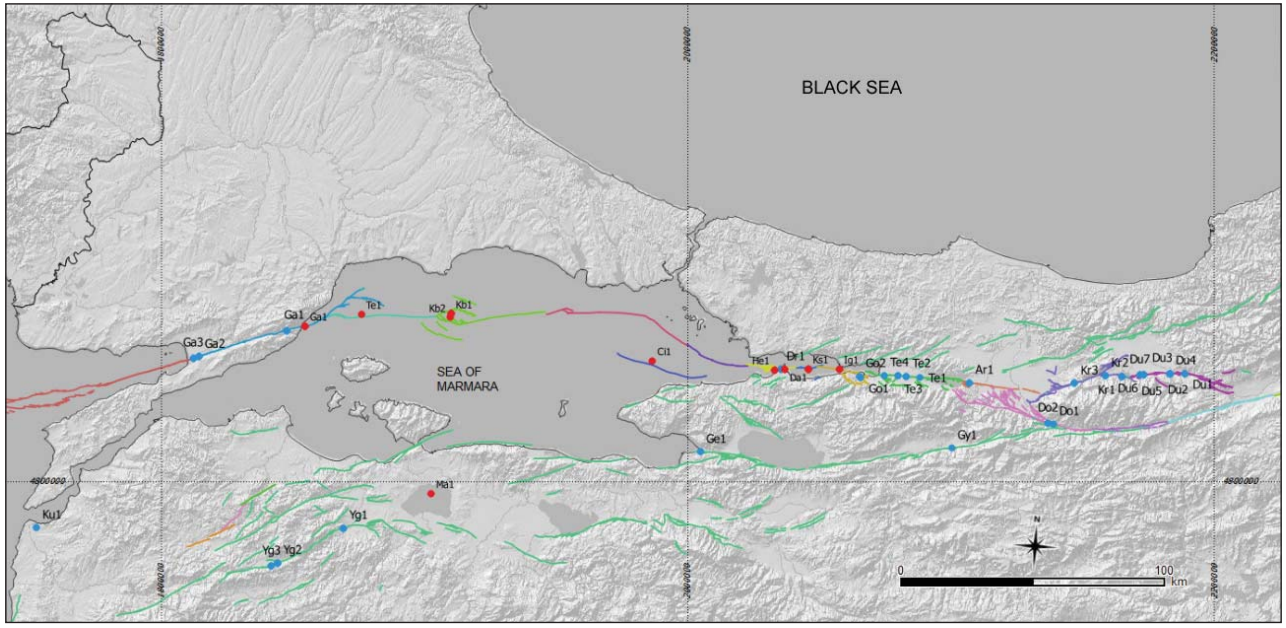

Figure 5-The map shows the western NAFS (Emre et al., 2013 and 2018) and trench locations on the digital elevation model. Related attributes are in table 4 and 5. The colouring makes a distinction among fault segmentations.

Table 4- The paleoseismological catalogue of the west_NAFS.

No	Name_of_F	Name_of_S	Name_of_Tr	Code_T	Lon	Lat	Event_T	Eq_date_min	Eq_date_max	Corr	Rptr_L	Rptr_M	Slip_R	Rec_Int	Last_rup	Ref
93	NAFS	Düzce	Kaynaşlı	Du1	31,31385751	40,77609568	4			1999					1999	Pantosti et al., 2008
94								1475		1878						
95								1035	1640							
96								685	1220	967						
97			Mengencik	Du2	31,24884726	40,774718	3			1999					1999	
98								1685	1900	1878						
99									1685							
100				Du3	31,24635776	40,77466174	3			1999					1999	
101								1700	1900	1878						
102								1445	1900							
103				Du4	31,24604613	40,77466434	2			1999					1999	
104								1495	1900							

Table 4- continued.

No	Name_of_F	Name_of_S	Name_of_Tr	Code_T	Lon	Lat	Event_T	Eq_date_min	Eq_date_max	Corr	Rptr_L	Rptr_M	Slip_R	Rec_Int	Last_rup	Ref
105	NAFS	Düzce	Çakır Hacı Ibrahim	Du5	31,13142313	40,76621592	3			1999					1999	Pantosti et al., 2008
106								1488	1900	1878						
107								1488	1900							
108				Du6	31,13083814	40,76708091	2			1999					1999	Emre et al., 2001
109								1700	1900	1719						
110			Çınarlı	Du7	31,11182353	40,76553579	3			1999					1999	Pantosti et al., 2008
111								1675	1900	1878						
112								1280	1700							
113		Karadere	Eften	Kr1	31,02969988	40,7583738	5			1999				400-500	1999	Sugai et al., 2001
114								1551	1929					400-500		
115								892	1232					400-500		
116								54	353					400-500		
117								-147	120					400-500		
118			Aksu	Kr2	30,95620694	40,75690868	3			1999					1999	Pantosti et al., 2008
119								1670	1900	1878						
120								685	1020							
121			Kazımiye	Kr3	30,82077942	40,72638926	5			1999					1999	Dikbas and Akyüz, 2010
122										1719						
123										1419						
124								420	584	554						
125								231	584	358						
126		Dokurcun	Relief	Do1	30,73289469	40,58398436	2			1967				200-300	1967	Palyvos et al., 2007
127								1693						200-300		
128			Mudurnu_ Beldibi	Do2	30,70939821	40,58649144	2			1967	55	7,1			1967	Ikeda et al., 1991
129								1650		1668						
130		Arifiye	NA	Ar1	30,34772	40,71097	4			1999			22		1999	Dikbas et al., 2009
131										1719			22			
132										1567			22			
133										1000			22			
134		Geyve	Loc5	Gy1	30,28289093	40,48516157	1	-398	-204							Yoshioka and Kuscu, 1994

Table 4- continued.

No	Name_of_F	Name_of_S	Name_of_Tr	Code_T	Lon	Lat	Event_T	Eq_date_min	Eq_date_max	Corr	Rptr_L	Rptr_M	Slip_R	Rec_Int	Last_rup	Ref
135	NAFS	Tepetarla	Acısu	Te1	30,12375089	40,71967278	1	1120	1280	1180					1999	Pavlides et al., 2006
136			Ottoman_ Canal	Te2	30,06301	40,72169	3			1999					1999	Rockwell et al., 2001b
137										1754		7				
138										1719		7,5				
139			Köseköy	Te3	30,02527	40,72359	3			1999					1999	Rockwell et al., 2001b Rockwell et al., 2009
140								1754	1894	1878		7				
141										1719		7,5				
142			Asağıyuvacık	Te4	29,96326	40,72101	2			1999					1999	Pavlides et al., 2006
143								1290	1630	1509						
144		Gölcük	Hisar River	Go1	29,85926418	40,70830343	3			1999		7,4		210-280	1999	Klinger et al., 2003
145								1539	1825	1719		7,4		210-280		
146								1357	1548	1509				210-280		
147			Denizevler	Go2	29,85346	40,71328	4			1999					1999	Pavlides et al., 2006
148								-3131	920	554						
149								-4575	-3616	-4096						
150								-9058	-7530	-8294						
151		Darıca	Hersek MT	Dr1	29,49720	40,72134	4			1894					1999	Özaksoy et al., 2010
152										1754						
153										1719						
154										1509						
155		Gemlik	Terme	Ge1	29,15977	40,42246	2			1857			5	438	1857	Özalp et al., 2013
156								1216	1770	1419	95		5	438	1857	Özalp et al., 2013, 2003
157		Yenice_ Gönen	Muratlar	Yg1	27,59485	40,07472	3			1953					1953	Kürçe et al., 2008
158								1208	1538	1440						
159																
160			Seyvan	Yg2	27,31502	39,93714	6			1953				300-600	1953	Dirik et al., 2008
161								1290	1410					300-600		
162								650	900					300-600		
163								240	530					300-600		
164								-50	140					300-600		
165								-400	-340					300-600		
166				Yg3	27,2901	39,92495	3			1953				660±160	1953	Kürçer et al., 2008 Pavlides et al., 2009
167								620	1270	620				660±160		
168								-2500						660±160		

Table 4- continued.

No	Name_of_F	Name_of_S	Name_of_Tr	Code_T	Lon	Lat	Event_T	Eq_date_min	Eq_date_max	Corr	Rptr_L	Rptr_M	Slip_R	Rec_Int	Last_rup	Ref
169	NAFS	Ganos	Güzelköy	Ga1	27,26931	40,73172	5			1912		7,4	17	323±142	1912	Meghraoui et al., 2012
170								1429	1776	1766						
171								1311	1397	1354						
172								692	1320	1063						
173								-1042	76							
174			Kavaklı	Ga2	26,88568	40,61564	5			1912		7,4	18	275	1912	Rockwell et al., 2001a
175										1766						
176										1354						
177								824	1350	1063						
178								-2000	-2000							
179			Saroz	Ga3	26,86186	40,61019	4	1655		1912				283+113	1912	Rockwell et al., 2001b Rockwell et al., 2009
180								1655		1766				283+113		
181								900		1354				283+113		
182								900		1063				283+113		
183		Kumkale fault	Kumkale	Ku1	26,23313	39,98318	2	130	780							Kürçer et al., 2012
184								1000	1300							

Table 5- The paleoseismological catalogue of onshore core samples along the NAFS.

No	Name_of_F	Name_of_S	Name_of_Tr	Code_T	Lon	Lat	Event_T	Eq_date_min	Eq_date_max	Corr	Rptr_L	Rptr_M	Slip_R	Rec_Int	Last_rup	Ref
w1	NAFS	Darıca	Hersek west	He1	29,46950777	40,71829668	3			1894						McHugh et al., 2006
w2										1766						
w3										1509						
w4		Suşehri	Asağı Tepecik_ Core	Su1	38,58849	40,03884	4			1668					1939	Hubert_ Ferrari et al., 2012
w5										1543					1939	
w6										1254					1939	
w7										1939		7,9			1939	
w8		Manyas	Manyas_ Core	Ma1	27,97317	40,21588	2			460						Leroy et al., 2002
w9										368						
w10		Ganos	Transform basin	Ga1	27,34987	40,75183	5			1965						McHugh et al., 2006
w11										1912						
w12										1859						
w13										1828						
w14								1810	1922							

Table 5- continued.

No	Name_of_F	Name_of_S	Name_of_Tr	Code_T	Lon	Lat	Event_T	Eq_date_min	Eq_date_max	Corr	Rptr_L	Rptr_M	Slip_R	Rec_Int	Last_rup	Ref
w15	NAFS	Kumburgaz	Central_Basin_core	Ku2	27,9994	40,8208	2			1343						McHugh et al., 2006
w16										740						
w17		Tekirdağ	Tekirdağ_Basin_Core	Te1	27,59718	40,80774	2			1912						
w18										1063						
w19		İzmit_Körfez	İzmit	Ig1	29,75936	40,7338	3			1999						
w20									824	740						
w21									182	181						
w22		Çınarcık	Çınarcık	Ci1	28,92013537	40,72271163	2			986						Sarı and Çağatay, 2006
w23										553						
w24		Darıca	Lag	Da1	29,51579	40,72175	4			1719						Bertrand et al., 2011
w25										1509						
w26										987						
w27										740						
w28		Kumburgaz	Central	Kb1	27,99999	40,83338	6			1963						McHugh et al., 2006
w29										1343						
w30										860						
w31										740						
w32										557						
w33										268						
w34		Karamürsel	Karamürsel	Ks1	29,62	40,72836	8			1999						Çağatay et al., 2012
w35										1509		7,2				
w36										1296						
w37										865						
w38										740						
w39										358						
w40										268						
w41										-427						

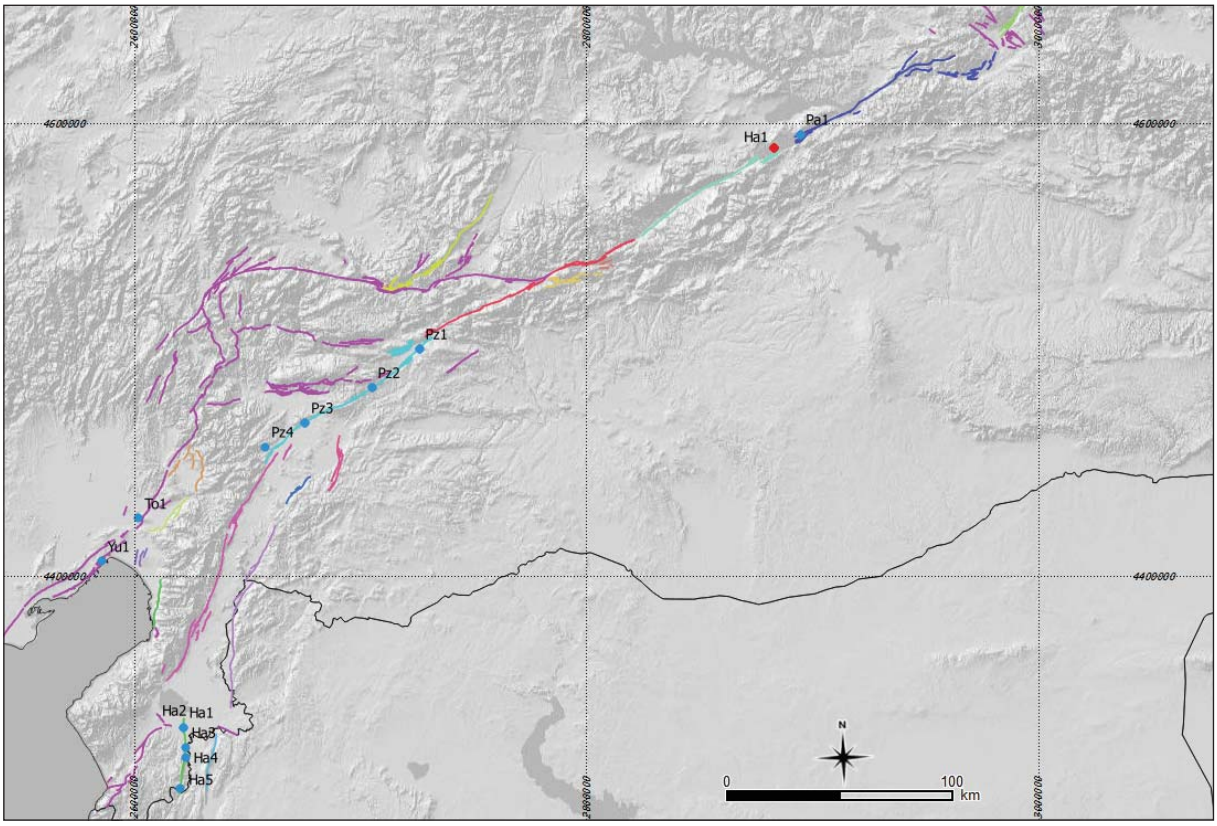

Figure 6- Paleoseismological trench (blue) and an offshore core sample from lake sediments (red) points along the EAFS. Their attributes are in tables 6 and 7. Colouring makes a distinction among fault segmentations.

Table 6- The paleoseismological catalogue of onshore core samples along the EAFS.

No	Name_ of_F	Name_ of_S	Name_ of_Tr	Code_ T	Lon	Lat	Event _T	Eq_ date_ min	Eq_ date_ max	Corr	Rptr _L	Rptr _M	Slip _R	Rec_ Int	Last_ rup	Ref
w42	EAFS	Pötürge-Palu	Hazar lake	Ha1	39,39556	38,48198	8			1874				300		Hubert_ Ferrari et al., 2005
w43										1789						
w44										1513						
w45										1284						
w46										995						
w47										602						
w48								440	1							
w49								-650	-300							

Table 7- The paleoseismological catalogue of the EAFS and DSFS.

No	Name_of_F	Name_of_S	Name_of_Tr	Code_T	Lon	Lat	Event_T	Eq_date_min	Eq_date_max	Corr	Rptr_L	Rptr_M	Slip_R	Rec_Int	Last_rup	Ref
185	EAFS	Palu	Hazar Gölü	Pa1	39,53072	38,53218	5	1680	1940	1874		7,1		100-360		Çetin et al., 2003
186									1420	1513		7,4		100-360		
187									400	450				100-360		
188										150				100-360		
189										-3620				100-360		
190		Pazarcık	Balkar	Pz1	37,56969	37,73666	5	900	1200	1114	60			1000-1200		Karabacak et al., 2012
191								-420	-200		40			1000-1200		
192										-1800				1000-1200		
193								-2800			80			1000-1200		
194										-8500	60			1000-1200		
195			Nacar	Pz2	37,32592	37,58721	3	900	1200	1114	60			1000-1200		
196								300	399					1000-1200		
197									-1000					1000-1200		
198			Tevekkeli	Pz3	36,98811	37,453574	5	1500	1600	1513	40			1200-1300		
199								200	250		70			1200-1300		
200								-4000	-3000		80			1200-1300		
201								-5400	-5000					1200-1300		
202								-8000	-7500		35			1200-1300		
203			Imalı	Pz4	36,78698	37,36097	2		-100							
204																
205		Toprakkale	Toprakkale	To1	36,14924	37,08404	2	425	570	524	40					
206								-1900	400	-1000	60					
207		Yumurtalık	İncirli	Yu1	35,96248	36,9145	2		-544	-1000	60					
208								-7292	-2814							
209	DEAD SEA	Hacıpaşa	Demirköprü	Ha1	36,35586	36,24927	2	1470		1872						Altunel et al., 2009
210									1442	1408						
211				Ha2	36,35588	36,2477	2	1801	1940	1872						
212										1408						
213			Ziyaret	Ha3	36,3653	36,16881	2	1650		1872				464-549		Akyüz et al., 2006
214								1310	1442	1408	20			464-549		
215			Yazlık	Ha4	36,36279	36,12799	2	1310	1426	1408	20			464-549		
216									1390	859				464-549		
217			Harabe	Ha5	36,33669	36,0071	2	1019		1408				464-549		
218									1019					464-549		

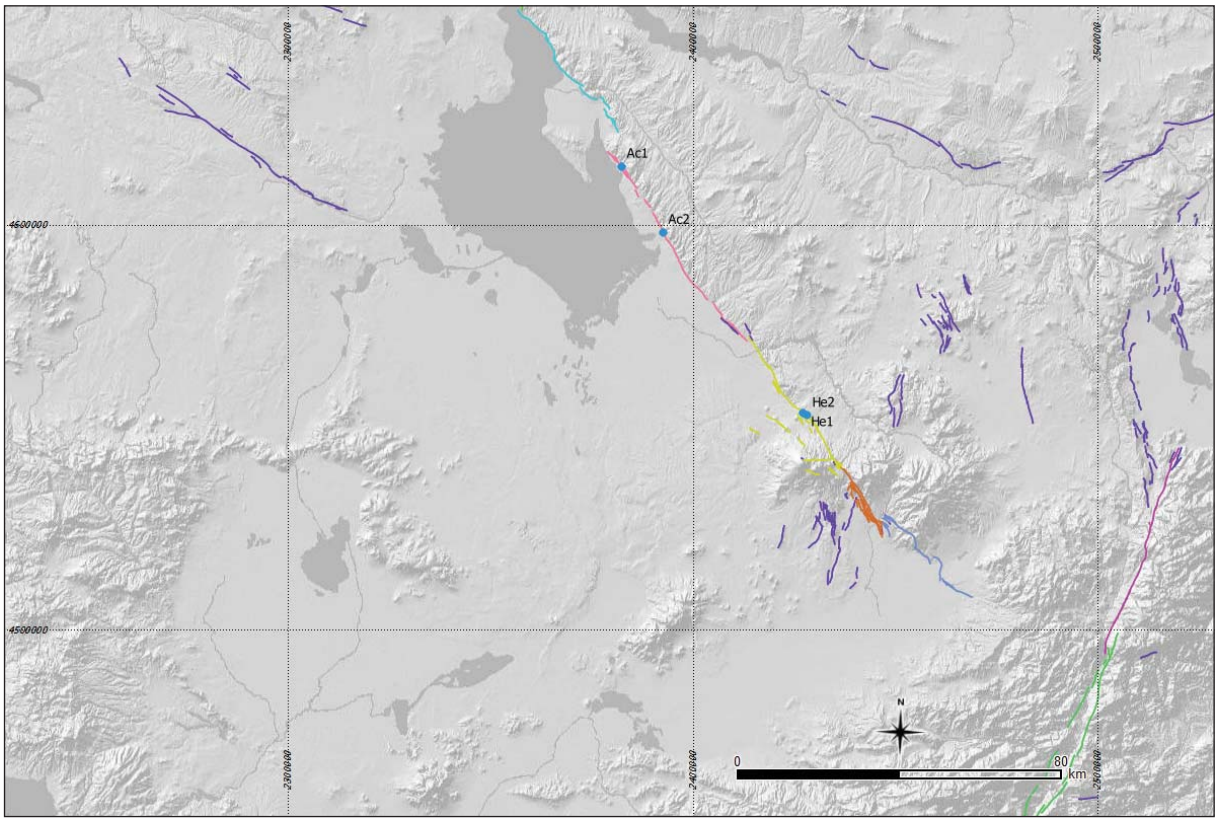

Figure 7- The map shows paleoseismological trench locations along active faults (Emre et al., 2013 and 2018) in central Anatolia. The attributes are in table 8. Colouring is for fault segmentation.

Table 8- The list of attributes for paleoseismological catalogue of the central Turkey.

No	Name_ of_F	Name_ of_S	Name_ of_Tr	Code _T	Lon	Lat	Event _T	Eq_ date_ min	Eq_ date_ max	Corr	Rptr _L	Rptr _M	Slip _R	Rec_ Int	Last_ rup	Ref
219	Tuz Gölü	Acıpınar	Tuzgölü	Ac1	33,64574	38,78449	4	-2130	-1660				0,05			Kürçer et al., 2011
220								-9630	-4940							
221								-21980	-16580							
222								-32590	-25410							
223			Altınkaya	Ac2	33,76614	38,63866	3	-7190	-1990				0,05			
224								-11310	-7190							
225								-24540	-16010							
226		Helvadere	Duru	He1	34,1696	38,23969	3	-1360	1950				0,03	4664		
227								-10550	-3600							
228								-27640	-14710							
229			Bağlar-kayası	He2	34,17942	38,23503	2	-3710	-580				0,03	4664		Kürçer et al., 2011
230								-8460	-7700							

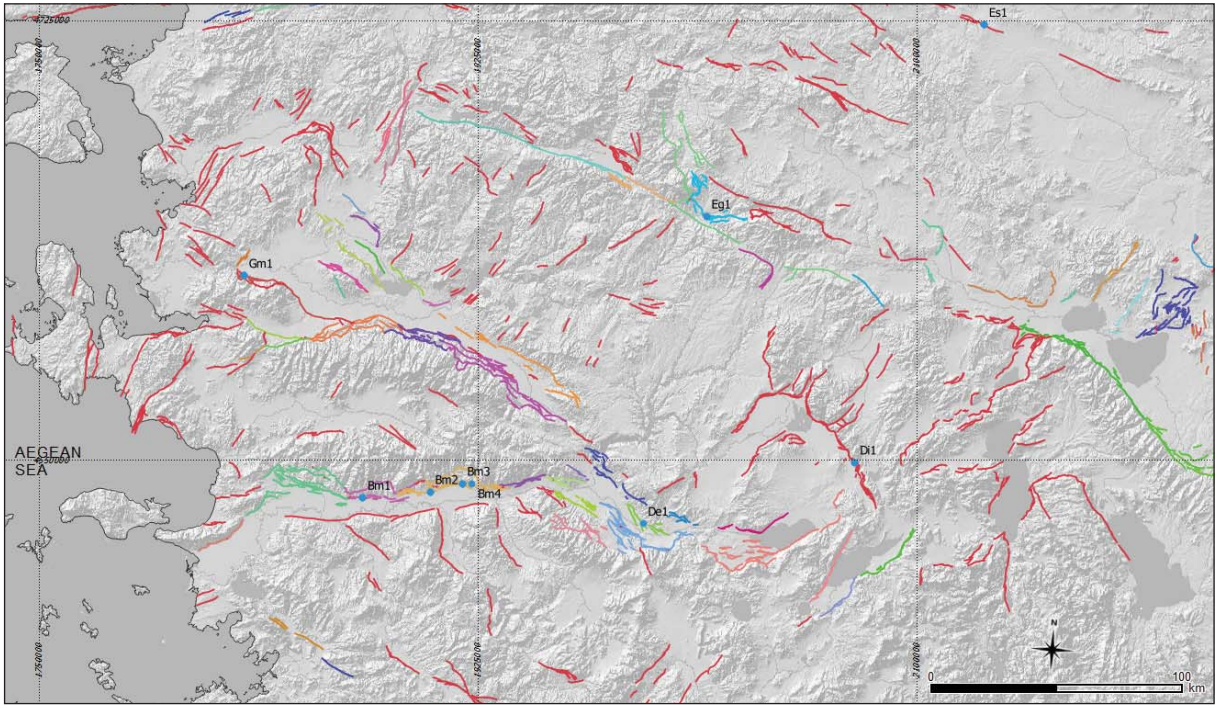

Figure 8- The map shows paleoseismological trench locations along the active faults (Emre et al., 2013 and 2018). Their attributes are in table 9. Fault coloring is for segmentation.

Table 9- The list of attributes for paleoseismological catalog of the western Turkey.

No	Name_ of_F	Name_of_S	Name_of_ Tr	Code_T	Lon	Lat	Event_T	Eq_date_ min	Eq_ date_ max	Corr	Rptr_L	Rptr_M	Slip_R	Rec_Int	Last_ rup	Ref
231	Manisa	Gediz - Manisa	Trench1-2	Gm1	27,3129506	38,6189389	4			926						Özkaymak et al., 2011
232										1595						
233										1664						
234										1845						
235	Büyük Menderes - Umurlu	Büyük Menderes - Umurlu	Umurlu	Bm1	27,93353	37,85839	4	1668		1899						Altunel et al., 2009
236								1488	1668	1653						
237									1441							
238								732	1190							

Table 9- continued.

No	Name_ of_F	Name_of_S	Name_of_ Tr	Code_T	Lon	Lat	Event_T	Eq_date_ min	Eq_ date_ max	Corr	Rptr_L	Rptr_M	Slip_R	Rec_Int	Last_ rup	Ref
239	Büyük Menderes - Atca	Büyük Menderes - Atca	Atca	Bm2	28,23628	37,89711	3	721								Altunel et al., 2009
240								353	721							
241								141	353							
242			Nazilli	Bm3	28,37878	37,93538	4			1653						
243									1017							
244								545	595							
245								17	220							
246				Bm4	28,42102	37,9378	1		597							
247	Denizli	Denizli	Kocadere	De1	29,2092706	37,83614272	1	-584								Meriç et al., 2006
248	Erdoğmuş	Gediz	Erdogmus1	Eg1	29,41141	38,95168	2			1970						Gürboğa, 2011, 2013
249								990	1020							
250	Dinar	Dinar	NA	Di1	30,15391	38,09996	2			80			1	1500	1995	Altunel et al., 1999
251								-1500	53	-1500			1	1500	1995	
252	Eskişehir	Eskişehir	Kanlıpınar	Es1	30,64542	39,69331	3	1280	1320			6,5				Kürçer et al., 2012
253								-390	20			6,5				
254								-810	-770			6,5				

3. Discussion

In agreement with historical and instrumental information, all previous researches confirm that NAFS reactivated during destructive earthquakes in the past centuries (Tan et al., 2008; Kalafat et al., 2011; Kadirioğlu et al., 2018). For this reason, we focused on the NAFS and analyzed its seismic activity segment by segment for the first usage of this catalogue. As is known from literature (Barka and KadinskyCade, 1988; Crone and Hailer, 1991; Knuepfer et al., 1989; Wheeler, 1987; dePolo et al., 1989; Crone and Hailer, 1991), the seismic and geometric segments of faults are still under discussion.

If any geometric segment or some part of it reactivates and creates a noteworthy earthquake, it is called a seismic segment. Such description creates some hesitations about the existence of huge past events on different segments. Similar controversial segmentations are present along the NAFS for destructive earthquakes. For this reason, we use the geometric segmentation suggested by Emre et al. (2013 and 2018) in our paper. Thus, the compilation of earthquakes and their usage in catalogues are very efficient for the scientific applications. Radiocarbon dating results from the palaeoseismological researches may not allow accessing a reliable data about certain strong earthquake all the time. However, most of them could be achieved by systematic trenching along the active faults, and the results enable to reach the certain data in this way. For instance, the 1688 earthquake was a very destructive event. It was identified and dated by the researchers along the NAFS. But the question is that which segments were reactivated. The catalogue evaluation could help us to answer of the question. The Erbaa, Destek, Ilgaz and Gerede segments are the sources of the 1688 earthquake according to previous works. On the other hand, the trenches along the Havza and Kamil segments located between Destek and Ilgaz do not record the 1688 earthquake (Figure 9). In this frame, were there two events happened along the different segments in 1688 or the 1688 event could not be determined along Destek and Ilgaz segments? Obviously, this catalogue will provide important data when it is necessary to make such a discussion and try to solve them in scientific ways.

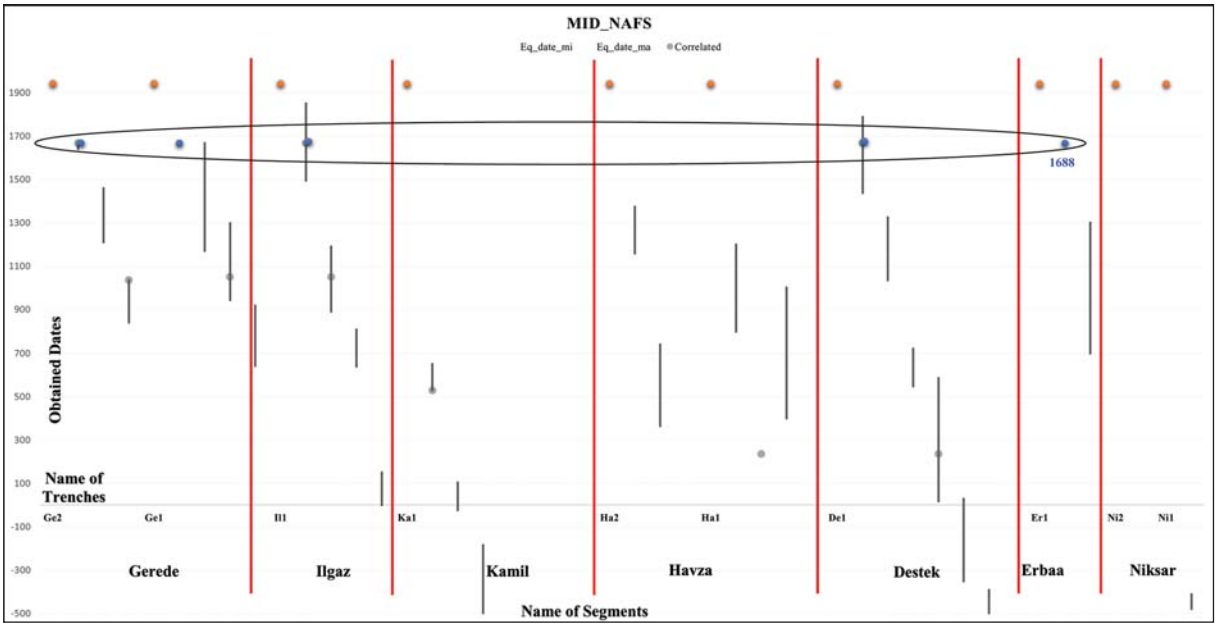

Figure 9- The chart shows comparison of the historical earthquakes from trenches in the central part of the NAFS. Red lines are the boundary of segments. The 1688 earthquake is an example for the problematic situations occurred along the central NAFS.

4. Conclusion

Totally 250 events obtained from the trenches on land, and 49 offshore data sets from core samples evaluated in paleoseismological studies published in both the national and international publications before 2012 were used for this catalogue. Only the studies that have definite locations, dating results and recurrence intervals are in it. The locations of all trenches are in the format of WGS84 system regarding given coordinate information in the source papers.

Excluding some parts of the NAFS, paleoseismological studies are scarce, locations of trenches and recurrence intervals in some researches are not clear along the active faults. Although some missing information is present in this catalogue due to the incomplete data in references, it is the first compiled catalogue including paleoseismological results covering whole Turkey. We believe that this compilation is to be very helpful for the researchers who would like to apply more paleoseismological works or seismic risk analyses.

Comparison results of trench studies along the NAFS, EASF, Western Turkey, and central Anatolia indicate that paleoseismological researches are very limited in central Anatolia (Tan et al., 2008). This is associated to very long recurrence interval of earthquakes in this area. If the trenching surveys are being increased in the future, this evaluation will come closer to the truth. The other comparison between segments and destructive earthquakes is done by using the Electronic Supplementary Material in this paper.

Acknowledgement

This article is a compilation of trench data selected from literature. The authors would like to thank Prof. Dr. Hasan Sözbilir, Dr. Selim Özalp and another anonymous reviewer. Their suggestions and critical reading significantly improved this manuscript. The authors are also grateful for support of handling Editor Assoc. Prof. Dr. Ayhan Ilgar spending much time for this paper.

References

AHEAD, 2018. https://www.emidius.eu/AHEAD/query_event/.

Akyüz, H.S., Altunel, E., Karabacak, V., Yalçıner, C.Ç. 2006. Historical earthquake activity of the northern part of the Dead Sea Fault Zone, southern Turkey. Tectonophysics, 426, 281 – 293.

Akyüz, H.S., Karabacak, V., Zabcı, C., Altunel, E., Gürsoy, H., Tatar, O. 2009. Paleoseismic Trenching on 1939 Erzincan and 1942 Niksar-Erbaa Earthquake Surface Ruptures, the North Anatolian Fault (Turkey). Geophysical Research Abstracts EGU General Assembly 11, EGU2009-12152.

Altunel, E., Barka, A.A., Akyüz, S. 1999. Paleoseismology of Dinar fault, SW Turkey. Terra Nova, 11, 297–302.

Altunel, E., Meghraoui, M., Karabacak, V., Akyüz, H.S., Ferry, M., Yalçıner, C.Ç., Munschy, M. 2009. Archaeological sites (Tell and Road) ofset by the Dead Sea Fault in the Amik Basin, Southern Turkey. Geophy J Int, 179, 1313 – 1329.

Ambraseys, N.N., Jackson, J.A. 1998. Faulting associated with historical and recent earthquakes in the eastern Mediterranean region. Geophysical Journal International, 133, 390–406.

Arpat, E., Şaroğlu, F. 1972. The East Anatolian Fault System; Thoughts on its Development. Bulletin of the Mineral Research and Exploration, 78, 33 – 39.

Barka, A., Kadinsky-Cade, K. 1988. Strike-slip fault geometry in Turkey and its influence on earthquake activity. Tectonics, 7, 663 – 684.

Bertrand, S., Doner, L., Akçer, S., Sancar, Ü., Schudack, U., Mischke, S., Çağatay, M.N., Leroy, S.A. 2011. Sedimentary record of coseismic subsidence in Hersek coastal lagoon (İzmit Bay, Turkey) and the late Holocene activity of the North Anatolian Fault. Geochemistry, Geophyics, Geosystems, 12 (6), 1-17.

Çağatay, M.N., Erel, L., Bellucci, L.G., Polonia, A., Gasperini, L., Eriş, E., Sancar, Ü., Biltekin, D., Uçarkuş, G., Ülgen, U.B., Damcı, E. 2012. Sedimentary earthquake records in the İzmit Gulf, Sea of Marmara, Turkey. Sedimentary Geology, 282, 347-359.

Çetin, H., Güneyli, H., Mayer, L. 2003. Paleoseismology of the Palu-Lake Hazar segment of the East Anatolian Fault Zone, Turkey. Tectonophysics, 374, 163 – 197.

Crone, A. J., Hailer, K. M. 1991. Segmentation and the coseismic behavior of Basin and Range normal faults: examples from eastcentral Idaho and southwestern Montana, U.S.A.J. Struct. Geol. 13, 151-164.

dePolo, C.M., Clark, D.G., Slemmons, D.B., Aymard, W.H. 1989. Historical Basin and Range province surface faulting and fault segmentation. U.S. geol. Surv. Open-file Rep. 89-315, 131-163

Dewey, J.F., Hempton, M.R., Kidd, W.S.F., Şaroğlu, F., Şengör, A.M.C. 1986. Shortening of continental lithosphere: the neotectonics of Eastern Anatolia-a

young collision zone. In: Coward, M.P. and Ries, A.C (Eds.), Collision Tectonics. Geological Society, London, Special Publications, 19, 1-36.

Dikbaş, A., Akyüz, H.S. 2010. KAF Zonu üzerinde İzmit-Sapanca Gölü segmentinin fay morfolojisi ve paleosismolojisi". İTÜ Dergisi, 3, 141 – 152.

Dikbaş, A., Akyüz, H.S., Gutsuz, P., Zabcı, C,. Sancar, T., Karabacak, V. 2009. Palaeoseismology of Karadere Segment (Between Akyazı-Gölyaka) on the Western Part of the North Anatolian Fault. 62nd Geological Assembly of Turkey, 13−17 April 2009, pp. 1017.

Dirik, K., Belindir, F., Özsayın, E., Kutluay, A. 2008. Yenice-Gönen Fay Zonu'nun Neotektonik Özellikleri ve Paleosismolojisi. TUJJB-UDP Project.

Duman, T.Y., Emre, Ö. 2013. The East Anatolian Fault: geometry, segmentation and jog characteristics. Geol. Soc. (London) Spec. Publ., 372, 495-529.

Emre, Ö., Duman, T.Y., Toda, S., Okuno, M., Doğan, A., Özalp, S., Tsutsumi, H., Tokay, F., Haraguchi, T., Kondo, H., Sugito, N., Nakamura, T. 2001. Paleoseismologic findings on the Düzce Fault: North Anatolian Fault Zone, NW Turkey. EOS Transactions. American Geophysical Union 82, 47, S52C-0651.

Emre, Ö., Duman, T.Y., Özalp, S., Elmacı, H., Olgun, Ş., Şaroğlu, F. 2013. Açıklamalı Türkiye Diri Fay Haritası Ölçek 1/1.125.000: Maden Tetkik ve Arama Genel Müdürlüğü Özel Yayın Serisi 30. ISBN: 978-605- 5310-56-1.

Emre, Ö., Duman, T.Y., Özalp, S., Şaroğlu, F., Olgun, Ş., Elmacı, H., Çan, T. 2018. Active fault database of Turkey. Bulletin of Earthquake Engineering, 16 (8), 3229-3275, doi: 10.1007/s10518-016-0041-2.

Fraser, J.G. 2009. Four new paleoseismic investigations on the North Anatolian Fault, Turkey, in the context of existing data, Ph.D. thesis, Univ. Libre de Bruxelles, Belgium, Brussels, pp. 284 pp.

Fraser, J., Pigati J.S., Hubert-Ferrari, A., Vanneste, K., Avşar, U., Altınok, S. 2009. A 3000-year record of groundrupturing earthquakes along the Central North natolian Fault near Lake Ladik, Turkey. Bull. of the Seis. Soc. of America, 99, 2681 – 2703.

Fraser, J.G., Hubert-Ferrari, A., Vanneste, K., Altınok, S., Drab, L. 2010. A Relict Paleoseismic Record of Seven Earthquakes between 600 AD and 2000 BC on the Central North Anatolian F ault at Elmacik, near Osmancik, Turkey. Bull. of the Seis. Soc. of America, 122, 11/12 1830–1845.

Fraser, J.G., Hubert-Ferrari, A., Verbeeck, K., Garcia-Moreno, D., Avşar, U., Maricq, N., Coudijzer, A., Vlamynck, N., Venneste, K. 2012. A 3000-year record of surface-rupturing earthquakes at Günalan: variable fault-rupture lengths along the 1939 Erzincan earthquake-rupture segment of the North Anatolian Fault, Turkey. Ann. Geophys., 55(5), 895–927.

Gürboğa, Ş. 2011. Neo- and Seismo-Tectonic Characteristics of the Yenigediz (Kütahya) Area. Midlle East Technical Unversity, PhD Thesis, 314 p, Ankara.

Gürboğa, Ş. 2013. 28 March 1970 Gediz earthquake fault, western Turkey: palaeoseismology and tectonic significance, International Geology Review, 55,10, 1191-1201, DOI: 10.1080/00206814.2013.771420.

Hartleb, R.D., Dolan, J.F., Akyüz, H.S., Yerli, B. 2003. A 2000-year-long paleoseismologic record of earthquakes along the central North Anatolian Fault, from trenches at Alayurt, Turkey. Bull. of the Seis. Soc. of America, 93, 1935 – 1954.

Hartleb, R.D., Dolan, J.F., Kozacı, Ö., Akyüz, H.S., Seitz, G.G. 2006. A 2500-yr-long paleoseismologic record of large, infrequent earthquakes on the North Anatolian fault at Çukurçimen, Turkey. Bull. of the Seis. Soc. of America, 118, 823 – 840.

Hempton, M.R., Dewey, J.F. 1981. Structure and tectonics of the Lake Hazar pull-apart basin, SE Turkey. EOS Transactions, American Geophysical Union 62, pp. 1033.

Hubert-Ferrari, A., Lamair, L., Hage, S., Avşar, U., El Ouahabi, M., Çağatay, M. 2005. Paleoseismological record of the Hazar Lake along the East Anatolian Fault (Turkey). Geophysical Research Abstracts EGU.

Hubert-Ferrari, A, Avşar, U.,, El Ouahabi, M., Lepoint, G., Martinez, P., Fagel, N. 2012. Paleoseismic record obtained by coring a sag-pond along the North Anatolian Fault (Turkey). Annals of Geophysics, 55, 5.

Ikeda, Y., Suzuki, Y., Herece, E., Şaroğlu, F., Işıkara, A.M., Honkura, Y. 1991. Geological evidence for the last two faulting events on the North Anatolian fault zone in the Mudurnu Valley, western Turkey. Tectonophysics, 193(4), 335–345.

Jackson, J., McKenzie, D.P. 1984. Active tectonics of the Alpine–Himalayan Belt between western Turkey and Pakistan. Geophy. Jour. of Royal Astronomical Soc., 77, 185-264.

Kadirioğlu, F.T., Kartal, R.F., Kılıç, T., Kalafat, D., Duman, T.Y., Eroğlu Azak, T., Özalp, S., Emre, Ö. 2018. An Improved earthquake catalogue (M≥4.0) for Turkey and its near vicinity (1900–2012). Bull. Earthq. Eng., 16, 3317–3338.

Kalafat, D., Güneş, Y., Kekovalı, K., Kara, M., Deniz, P., Yılmazer, M. 2011. Bütünleştirilmiş Homojen Türkiye Deprem Kataloğu (1900-2010; M ≥ 4.0).

Boğaziçi Üniversitesi, Kandilli Rasathanesi ve Deprem Araştırma Enstitüsü, Yayın No: 1049, 640p., Bebek-İstanbul.

Karabacak, V., Akyüz, H.S., Kıyak, N.G., Altunel, E., Meghraoui, M., Yönlü, Ö. 2012. Doğu Anadolu Fay Zonu'nun Gölbaşı (Adıyaman) ile Karataş (Adana) arasındaki kesiminin geç Kuvaterner aktivitesi. Tübitak Project, 109Y043.

Klinger, Y., Sieh, K., Altunel, E., Akoğlu, A., Barka, A.A., Dawson, T.E., Gonzalez, T., Meltzner, A.J., Rockwell, T.K. 2003. Paleoseismic evidence of characteristic slip on the western segment of the North Anatolian Fault, Turkey. Bull. Seismol. Soc. Am., 93(6), 2317–2332.

Knuepfer, P. L. K. 1989. Implications of the characteristics of endpoints of historical surface fault ruptures for the nature of fault segmentation. U.S. geol. Surv. Open-file Rep. 89-315, 193-228.

Kondo, H., Özaksoy, V., Yıldırım, C., Awata, Y., Emre, Ö., Okumura, K. 2004. 3D trenching survey at Demir Tepe site on the 1944 earthquake rupture, North Anatolian fault system, Turkey. Japanese No. 4, p. 231-242.

Kondo, H., Özaksoy, V., Yıldırım, C. 2010. Slip history of the 1944 Bolu-Gerede earthquake rupture along the North Anatolian fault system: implications for recurrence behavior of multisegment earthquakes. J. Geophys. Res., 115(B4),1–16.

Kozacı, Ö., Dolan, J.F., Yönlü, Ö., Hartleb, R.D. 2011. Paleoseismologic evidence for the relatively regular recurrence of infrequent, large-magnitude earthquakes on the eastern North Anatolian fault at Yaylabeli, Turkey. Lithosphere, 3(1), 37–54.

Kürçer, A. 2012. Neotectonic Characteristics and Paleoseismology of Tuz Gölü Fault Zone, Central Anatolia, Turkey. Ankara University, PhD Thesis 289p, Ankara.

Kürçer, A., Chatzipetros, A., Tutkun, S.Z., Pavlides, S., Ateş, O., Valkaniotis, S. 2008. The Yenice-Gönen active fault (NW Turkey): active tectonics and palaeoseismology. Tectonophysics, 453(1–4), 263 – 275.

Kürçer, A., Kondo, H., Özalp, S., Emre, Ö. 2009. Paleoseismological findings on the western portion of the surface rupture associated with 1942 Erbaa-Niksar earthquake, North Anatolian fault system, Turkey. EGU General Assembly – Geophysical Research Abstracts, Vienna.

Kürçer, A., Gökten, Y.E., Yeleser, L. 2011. Tuzgölü Fay Zonu Üzerinde Paleosismolojik Hendek Çalışmaları, Orta Anadolu, Türkiye. Aktif Tektonik Araştırma Grubu 15. Toplantısı (ATAG-15), Bildiri Özleri Kitabı, pp. 13-14. 19-22 Ekim 2011, Çukurova Üniversitesi, Jeoloji Mühendisligi Bölümü, Adana.

Kürçer, A., Chatzipetros, A., Pavlides, S., Syrides, G., Vouvalidis, K., Ateş, Ö., Levent, Y. 2012. An Assessment of the Earthquakes of Ancient Troy, NW Anatolia, Turkey. In: E. Sharkov (Hrsg.), Tectonics - Recent Advances, InTech (2012). Doi: 10.5772/48471.

Leroy, S., Kazancı, N., İleri, Ö., Kibar, M., Emre, Ö., McGee, E., Griffits, H.I. 2002. Abrupt environmental changes within a late Holocene lacustrine sequence south of the Marmara Sea (Lake Manyas, N-WTurkey): possible links with seismic events. Marine Geology, 190, 531-552.

Lovelock, P.E.R. 1984. A review of the tectonics of the northern Middle East region. Geol Mag 121: 577 – 587.

McHugh, C.M.G., Seeber, L., Cormier, M.H., Dutton, J., Çağatay, M.N., Polonia, A., Ryan, W.B.F., Görür, N. 2006. Submarine earthquake geology along the North Anatolia Fault in the Marmara Sea, Turkey: A model for transform basin sedimentation. Earth and Planetary Science Letters, 248,661–684.

Meghraoui, M., Aksoy, M.E., Akyüz, H.S., Ferry, M., Dikbaş, A., Altunel, E. 2012. Paleoseismology of the North Anatolian Fault at Güzelköy (Ganos segment, Turkey): size and recurrence time of earthquake ruptures west of the Sea of Marmara. Geochem Geophys Geosyst 13: Q04005.

Meriç, N., Demirtaş, R., Atlıhan, A., Erkmen, C., Yaman, M., Eravcı, B., Tepeuğur, E., Aktan, T. 2006. Büyük Menderes Paleosismolojisi Kapsamında Bölgedeki Diri Fayların Yaş tayinine ön çalışma olarak, Fay Zonların Alınan Numunelerin OSL Metodu ile Paleodoz Miktarının Tayini. Tübitak Project 105Y006.

Muehlberger, W.R., Gordon, M.B. 1987. Observations on the complexity of the East Anatolian fault, Turkey. J. Struc. Geol., 9 (7), 899 – 903.

Okumura, K., Yoshioka, T., Kuşçu, İ., Nakamura, T., Suzuki, Y. 1994. Recent surface faulting on the North Anatolian Fault East of Erzincan Basin, Turkey – a trenching survey. Summaries of Researches using AMS at Nagoya University (in Japanese with English Abstract).

Okumura, K., Awata, Y., Duman, T.Y., Tokay, F., Kuşçu, İ., Kondo, H. 2002. Rupture History of the 1944 Bolu-Gerede Segment of the North Anatolian Fault: Gerede-Ardıçlı Trench Re-excavated. American Geophysical Union, Fall Meeting 2002, abstract id. S11B-1155.

Okumura, K., Rockwell, T.K., Duman, T.Y., Tokay, F., Kondo, H., Yıldırım, C., Özaksoy, V. 2003. Refined slip history of the North Anatolian Fault

at Gerede on the 1944 rupture. EOS Transactions AGU, San Francisco.

Özaksoy, V., Emre, Ö., Yıldırım, C., Doğan, A., Özalp, S., Tokay, F. 2010. Sedimentary Record of Late Holocene Seismicity and uplift of Hersek restraining-bend along the North Anatolian Fault in the Gulf of İzmit, Tectonophysics 487, 1-4, 33-45.

Özalp, S., Doğan, A., Emre, Ö. 2003. The last two faulting events on the southern strand of the North Anatolian fault zone, NW Turkey. EOS Transactions, AGU.

Özalp, S., Emre, Ö., Doğan, A. 2013. The Segment Structure of Southern Branch of The North Anatolian Fault and Paleoseismological Behaviour of The Gemlik Fault, NW Anatolia. Bulletin of the Mineral Research and Exploration, 147: 1 – 17.

Özkaymak, Ç., Sözbilir, H., Uzel, B., Akyüz, H.S. 2011. Geological and Palaeoseismological Evidence for Late Pleistocene−Holocene Activity on the Manisa Fault Zone, Western Anatolia. Turkish J. Earth Sci., 20, 449 – 474.

Palyvos, N., Pantosti, D., Zabcı, C., D'Addezio, G. 2007. Paleoseismological evidence of recent earthquakes on the 1967 Mudurnu valley earthquake segment of the North Anatolian Fault Zone. Bull. Seismol. Soc. Am., 97(5), 1646 – 1661.

Pantosti, D., Pucci, S., Palyvos, N., Martini, P.M.D., D'Addezio, G., Collins, P.E.F., Zabcı, C. 2008. Paleoearthquakes of the Düzce fault (North Anatolian Fault Zone): insights for large surface faulting earthquake recurrence. J. Geophys. Res., 113, B01309.

Pavlides, S.B., Chatzipetros, A., Tutkun, Z.S., Özaksoy, V., Doğan, B. 2006. Evidence for late Holocene activity along the seismogenic fault of the 1999 İzmit earthquake,NW Turkey. Geol. Soc. Spl. Publ., 260, 635 – 647.

Pavlides, S., Tutkun, S.Z., Chatzipetros, A., Michailidou, A., Sboras, S., Syrides, G., Valkaniotis, S., Vouvalidis, K., Zervopoulou, A., Doğan, B., Özaksoy, V., Kürçer, A., Özden, S., Ateş, Ö., Ulugergerli, E.U., Bekler, T., Ekinci, Y.L., Demirci, A., Şengül, E., Elbek, Ş., Gündoğdu, E., Köse, K. 2009. Hidden Earthquakes in the Gölcük-Kavaklı, Yenice-Gönen and Troy Faults, Palaeoseismological and Archaeoseismological Approach. Aktif Tektonik Araştırma Grubu Atag 13. Çalıştayı 08-11 Ekim 2009, Çanakkale.

Perinçek, D., Çemen, İ. 1990. The structural relationship between the East Anatolian and Dead Sea fault zone in south-eastern Turkey. Tectonophysics, 172, 331 – 340.

Polat, A., Tatar, O., Gürsoy, H., Karabacak, V., Zabcı, C., Sançar, T. 2012. Paleoseismological Findings on the Ortakoy-Suşehri Segment of the 1939 Erzincan Earthquake Surface Rupture, North Anatolian Fault Zone. Geological Bulletin of Turkey, 55.

Rockwell ,T., Barka, A., Dawson, T., Akyüz, S., Thorup, K. 2001*a*. Paleoseismology of the Gazikoy-Saros segment of the North Anatolia fault, northwestern Turkey: comparison of the historical and paleoseismic records, implications of regional seismic hazard, and models of earthquake recurrence. J. Seismol., 5(3), 433 – 448.

Rockwell, T., Seitz, G., Langridge, R., Barka, A., Meltzner, A.J., Klinger, Y., Regona, D., Meghraoui, M., Ferry, M. 2001*b*. Paleoearthquake History of the North Anatolian Fault, Western Turkey: An Investigation into the Nature of Earthquake Recurrences as Revealed by Precise Stratigraphic and Historical Records. Geological Society Technical Report.

Rockwell, T., Regona, D., Seitz, G., Langridge, R., Aksoy, M.E., Uçarkuş, G., Ferry, M., Meltzner, A.J., Meghraoui, M., Satır, D., Barka, A., Akbalık, B. 2009. Palaeoseismology of the North Anatolian Fault near the Marmara Sea: Implications for fault segmentation and seismic hazard, in Palaeoseismology: Historical and Prehistorical Records of Earthquake Ground Effects for Seismic Hazard Assessment, edited by K. Reicherter, A. M. Michetti, and P. G. Silva. Geol. Soc. Spec. Publ., 316(1), 31–54.

Sancar, T., Akyüz, H.S. 2007. Preliminary Investigations on Geomorphological and Paleoseismological Studies on Yedisu Seismic Gap, North Anatolian Fault Zone, Eastern Turkey. Geophysical Research Abstracts EGU 9.

Sarı, E., Çağatay, M.N. 2006. Turbidites and their association with past earthquakes in the deep Çinarcik Basin of the Marmara Sea. Geo-Marine Letters, 26 (2), 69-76.

Sugai, T., Emre, O., Duman, T.Y., Yoshioka, T., Kuşçu, İ. 1999. Geologic evidence for five large earthquakes on the North Anatolian Fault at Ilgaz, during the last 2000 years; a result of GSJ-MTA international cooperative research. Paper presented at the paleoseismology workshop.

Sugai, T., Awata, Y., Toda, S., Emre, Ö., Doğan, A., Özalp, S., Haraguchi, T., Kinoshita, H, Takada, K., Yamaguchi, M. 2001. Paleoseismic Investigation of the 1999 Düzce Earthquake Fault at Lake Eft eni, North Anatolian Fault System, Turkey. Annual Report on Active Fault and Paleoearthquake Researches 1. Active Fault Research Center, Tsukuba, Japan.

Şaroğlu, F., Emre, Ö., Kuşçu, İ. 1992. Active Fault Map of Turkey, 1:2,000,000 Scale. Mineral Research and Exploration Institute of Turkey (MTA) Publications, Ankara.

Şengör, A.M.C., Görür, N., Şaroğlu, F. 1985. Strike-slip faulting and related basin formation in zones of tectonic escape: Turkey as a case study, Strike-slip Deformation, Basin Formation, and Sedimentation. Soc. Econ. Paleont. Min. Spec. Pub. 37 (in honor of J.C. Crowell), 227-264.

Tan, O.M., Tapırdamaz, C., Yörük, A. 2008. The earthquake catalogues for Turkey. Turkish Journal of Earth Sciences, 17, 405–418.

Westaway, R. 1994. Present-day kinematics of the Middle East and eastern Mediterranean. J. of Geophy. Research, 99, 12071–12090.

Wheeler, R.L. 1987. Boundaries between segments of normal faults: Criteria for recognition and interpretation. U.S. geol. Surv. Openfile Rep., 87-673, 385-398.

Yoshioka, T., Kuşçu, İ. 1994. Late Holocene faulting events on the İznik-Mekece fault in the western part of the North Anatolian fault zone, Turkey. Bull. Geol. Soc. Jpn., 45(11), 677 – 685.

Yoshioka, T., Okumura, K., Kuşçu, İ., Emre, Ö. 2000. Recent surface faulting of the North Anatolian Fault along the 1943 Ladik earthquake ruptures. Bull. Geol. Survey. Jpn., 51(1), 29–35.

Yönlü, Ö., Altunel, E., Karabacak, V. 2017. Geological and geomorphological evidence for the southwestern extension of the East Anatolian Fault Zone, Turkey. Earth and Planetary Science Letters, 469, 1-14.

Zabcı, C., Akyüz, H.S., Karabacak, V., Sancar, T., Altunel, E., Gürsoy, H., Tatar, O. 2011. Paleoearthquakes on the Kelkit Valley segment of the North Anatolian Fault, Turkey: implications for the surface rupture of the historical 17 August 1668 Anatolian Earthquake, Turkish J. Earth Sci., 20, 411 – 427.

Bulletin of the Mineral Research and Exploration

http://bulletin.mta.gov.tr

Descriptions, systematics and revisions of the subgenera *Alveolina* (*Glomalveolina*) Hottinger, 1960 and *Alveolina* (*Alveolina*) d'Orbigny, 1826 (Foraminiferida)

Şükrü ACAR[a*]

[a]*General Directorate of Mineral Research and Exploration, Department of Geology, 06800, Ankara, Turkey. orcid.org/0000-0003-0204-152X*

Research Article

Keywords:
Subgenus, *Alveolina* (*Glomalveolina*), *Alveolina* (*Alveolina*), *Systematic paleontology.*

ABSTRACT

In this study, the genus *Alveolina* D' Orbigny, 1826 and its *Alveolina (Alveolina)* D' Orbigny, 1826 and *Alveolina (Glomalveolina)* Hottinger, 1960 subgenera were re-examined and identified. Systematics of the subgenera *Alveolina* (*Alveolina*)=*Alv.* (*Alv.*) and *Alveolina (Glomalveolina)=Alv.*(*Glomalv.*) have also been reviewed and revised. *Alv.* (*Glomalv.*) is considered as a subgenus, not a genus (?). Because, all the generic features of microspheric generations (fB) of these two subgenera are identical. Thus, *Alveolina* D' Orbigny, 1826 and *Glomalveolina* Hottinger, 1960 cannot be used as if they were two different genera (?). Otherwise *Glomalveolina* would be the synonym of *Alveolina* in "Systematic Paleontology" chapter. Therefore, *Alv.* (*Alv.*) and *Alv. (Glomalv.*) are both subgenusses, and the structural difference between these subgenera is observed seen in their megalospheric generations (fA). Besides, description of the genus (?) *Glomalveolina* has never been made in any of the studies in which *Glomalveolina* is referred as genus (?). However, the subgenus *Alv.* (*Glomalv.*) has incorrectly been used by many authors as "genus (?) *Glomalveolina* Hottinger, 1960 or 1962".

Received Date: 16.04.2018
Accepted Date: 02.07.2018

1. Introduction

Reichel (1937, p.80) examined Thanetian aged, small sized, spherical or subspherical shaped alveolinids, and realised that nepionic stage (just after the protoconch) of megalospheric generations (fA) of these alveolinids had triloculine chambers in one or two planes, and these chambers were followed by biloculine chambers. It especially differs, with the presence of triloculine chambers, from nepionic stage of the megalospheric generations (fA) of the genus *Alveolina* D' Orbigny (1826). Because, nepionic stage (just after the protoconch) of megalospheric generation (fA) of the genus *Alveolina* has only biloculine chambers. Therefore, Reichel (1937, p.80) proposed a new subgenus in order to indicate this difference (the presence of triloculine chambers in one or two planes) and named as "s.gen. *Glomalveolina* nom.nov.". However, Reichel (1937) is not the author of the subgenus "s.gen. *Glomalveolina* nom.nov.". Because, Reichel (1937, p.80) in that paper, described a new alveolinid species as "*Alveolina primaeva* n.sp" but not as "s.gen. *Glomalveolina primaeva* n.sp.". Therefore, Reichel (1937, p.80) is the first author who proposed the subgenus *Glomalveolina* or he can be considered as the author who has only the rights of the name of the subgenus *Glomalveolina*. The subgenus *Alveolina* (*Glomalveolina*)=*Glomalveolina* s.str.=*Alv.* (*Glomalv.*) Hottinger, 1960 was first described and its systematics was done by Hottinger (1960, p.26, 52) in his PhD thesis, hence he is the author of the subgenus *Alv.* (*Glomalv.*) and its year of publication is 1960 (Figure 1). Cover page of Hottinger's PhD thesis is given below for settling the controversies on the year of the publication of the subgenus *Alv.*(*Glomalv.*) (Figure 1). The year 1960 is clearly observed on the

Citation Info: Acar, Ş. 2019. Descriptions, systematics and revisions of the subgenera *Alveolina* (*Glomalveolina*) Hottinger, 1960 and *Alveolina* (*Alveolina*) d'Orbigny, 1826 (Foraminiferida). Bulletin of Mineral Research and Exploration, 159, 89-97. *https://dx.doi.org/110.19111/bulletinofmre.501688*

** Corresponding author: Şükrü ACAR, dr.sukru.acar@gmail.com*

original cover page of the PhD (Figure 1). So, the year of publication of the subgenus *Alv.*(*Glomalv.*) is not 1962 (Figure 1). On the other hand, Hottinger has no single author paper in 1962! *Glomalveolina* s.str. (in the strict sense) means the subgenus *Glomalveolina* (Prof. Dr. Kuniteru Matsumaru, personal communication; Acar, 1995, p.11).

Many scientists including Hottinger, used the name "subgenus *Alveolina* (*Glomalveolina*) Hottinger, 1960" as "Hottinger, 1960" by referring Hottinger's PhD thesis (Figure 1) (Loeblich and Tappan, 1964; Sirel, 1972, 1975, 1976, 1986, 1998, 1999; Hottinger, 1974; Sirel and Gündüz, 1976; Sirel et al, 1983, 1986; Drobne, 1977; Rahaghi, 1978, 1983; Sartorio and Venturini, 1988; Acar, 1995).

The subgenus *Alv.*(*Glomalv.*) was widely used as a subgenus between the years 1958-1998 (Hottinger, 1958, p. 447, fig. 6f; 1960, p. 26, 52, Pl. 1, figs. 1-33; Pl. 2, figs. 9, 25; 1974, p. 34, fig. 17; Pl. 31, figs. 1-9; Pl. 32, figs. 1-13; Loeblich and Tappan, 1964, p. C504, fig. 391, C509; Sirel, 1972, p. 278, Pl. I, fig. 3; 1975, p. 181; 1976, p. 90, fig. 2, Pl. I, p. 1-18; 1986, p. 154, figs. 2, 7; 1998, p. 63, Pl. 28, fig. 11; Pl. 29, figs. 1-13; Pl. 30, figs. 1-13; Pl. 31, figs. 6-12; 1999, figs. 2, 5; Sirel and Gündüz, 1976, Pl. XIV, fig. 6); Sirel et al, 1983, p. 151, Pl III, figs. 5-7; Drobne, 1977, p. 13, figs. 1a-e, fig. 2e, figs. 3f-i, figs. 4k-n, figs. 5o,p; Rahaghi, 1978, p. 43, Pl. 6, figs. 1-10; 1983, p. 49, Pl. 21, figs. 1-3,10; Sartorio and Venturini, 1988, p. 158; White 1992, p. 54, Table 1; Acar, 1995, p. 16, Pl. 1, figs. 1-11; Pl. 2, figs. 1-6; Pl. 3, figs. 1-9).

However, the subgenus *Alv.*(*Glomalv.*) has been used as a genus (?) since 1998 by some paleontologists including Hottinger (Loeblich and Tappan, 1987, p. 361, 363, Pl. 372, fig. 2; Pl. 376, figs. 6, 7; Hottinger, 1999, p. 388; 2006, p. 96, fig. 57; 2009, p. 7, 9; Bassi and Broglio, 1999, p. 232; Özcan et al, 2001, p. 339; 2010, p. 34, p. 46, fig. 19, p. 47, fig. 20; Çolakoğlu and Özcan, 2003; Sirel, 2004, p. 27, Pl. 27, figs. 5-12; Pl. 28, figs. 1-13; 2009, p. 420; 2010, p. 8, figs. 7; Özgen-Erdem et al, 2005, p. 403; Özgen-Erdem, 2008, p. 69, fig. 3; Sirel and Acar, 2008, p. 4, Pl. 1, figs. 1-8, Pl. 2, figs. 1-13, Pl. 3, figs. 1-16, Pl. 4, figs. 1-16; Pignatti et al, 2008, Pl. 5, fig. 5, Pl., 7, figs. 8a–b; BougDagher-Fadel, 2008, p. 307; Scheibner and Speijer, 2009, p. 210, figs. 11A-F; İbrahimpasic, 2012, p. 32,33).

Remarks: This critical note is on the systematics of the alveolinids in the book about alveolinids written by Sirel and Acar (2008, p.4). *Glomalveolina* is referred as a genus in the book. This is the viewpoint of first author (Sirel). Second author (Acar) disagrees with this idea. The second author accepts *Alveolina* (*Glomalveolina*) as a subgenus.

There has been a confusion in systematic paleontology about Paleocene and Eocene glomalveolinids for 20 years (1998-2018). This paper is prepared in order to clarify this subject. *Alv.* (*Glomalv.*) is a subgenus, definitely not the genus "*Glomalveolina*". Because anybody has not made the description of the genus (?) "*Glomalveolina*" in any place up until today. Therefore, at first, well-known description of the genus *Alveolina* D' Orbigny (1826) which these two subgenus are linked to, is was made here in made and then the subgenera *Alveolina* (*Alveolina*) = *Alveolina* s.str.=*Alv.*(*Alv.*) D'Orbigny 1826 and *Alv.*(*Glomalv.*) Hottinger, 1960 were redescribed. *Alv.*(*Alv.*) and *Alv.*(*Glomalv.*) are both subgenusses. Because, generic features of microspheric generations (fB) of these two subgenera are all the same. In that case, "*Alveolina* D' Orbigny, 1826" and "*Glomalveolina* Hottinger, 1960/1962" whose microspheric forms (fB) are identical in generic characteristics, can't be two different genera. The genus *Alveolina* D' Orbigny, 1826 has been described earlier. In this case, *Glomalveolina* would be a synonym of *Alveolina*. Because of this reason, *Glomalveolina* can never be used as a separate genus. Therefore, *Alv.*(*Alv.*) and *Alv.*(*Glomalv.*) are both subgenusses. and the structural difference between them can only be observed in their megalospheric forms (fA). This structural difference could only be shown as "subgenus" in systematic paleontology (Figs. 2-4) (Hottinger, 1960, p.26, 52, 63). As it is observed, when determining alveolinid genera or species, axial sections of megalospheric (fA) individuals should be taken into consideration. Because, axial sections of alveolinids are more characteristic. While describing species/subspecies, new species or new subspecies especially from a smaller, spherical, subspherical or ovoid shaped *Alv.*(*Alv.*) or *Alv.*(*Glomalv.*), sections must be axial and magnification must be X40. Besides, microspheric (fB) forms should also be described.

2. Systematics and Generic Features of the Genus *Alveolina* D'Orbigny, 1826

In systematic paleontology (Loeblich and Tappan, 1964 and Acar, 1995) are followed.

Phylum: Protozoa GOLDFUSS, 1817,

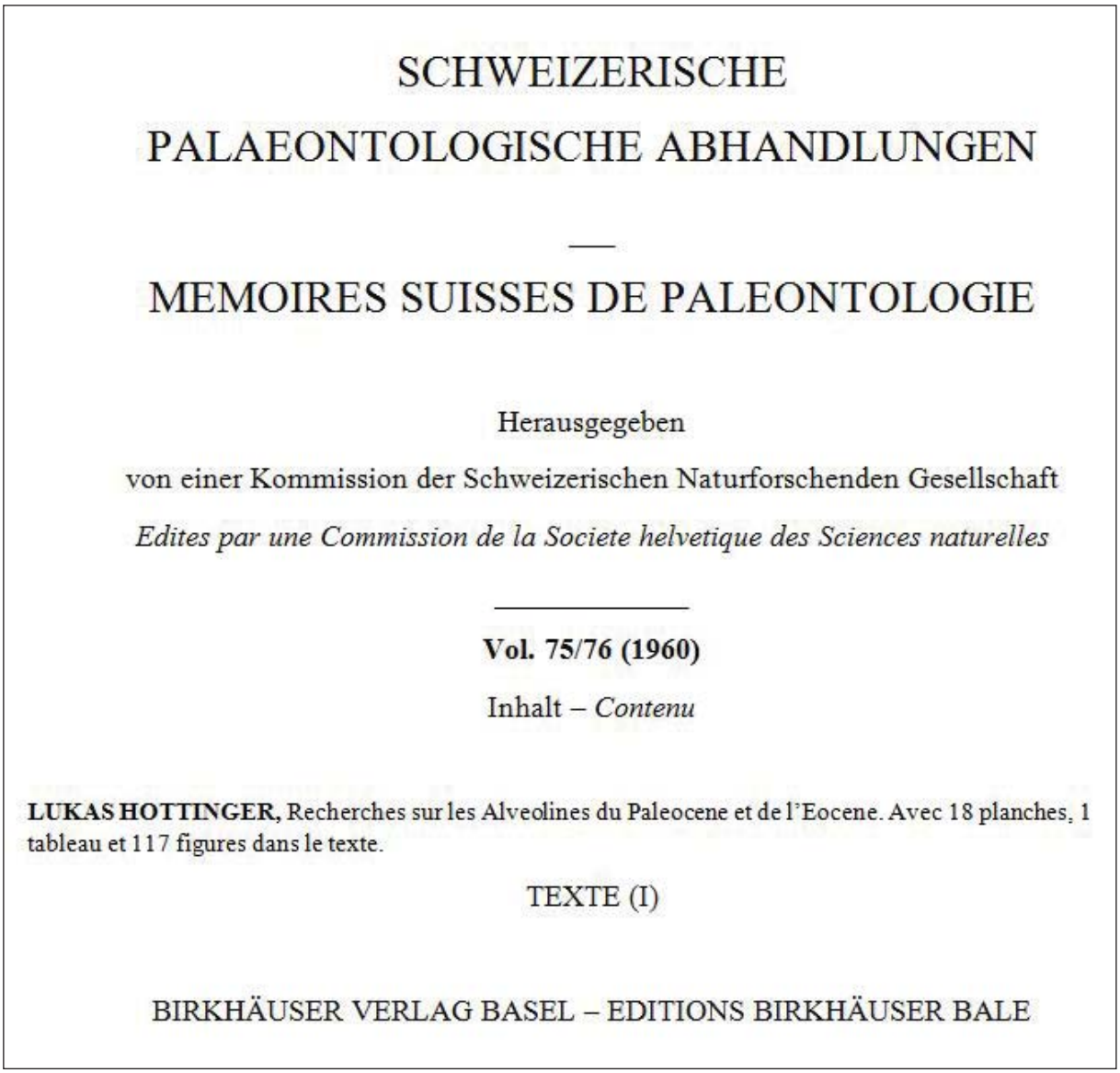
SCHWEIZERISCHE

PALAEONTOLOGISCHE ABHANDLUNGEN

—

MEMOIRES SUISSES DE PALEONTOLOGIE

Herausgegeben

von einer Kommission der Schweizerischen Naturforschenden Gesellschaft

Edites par une Commission de la Societe helvetique des Sciences naturelles

Vol. 75/76 (1960)

Inhalt – *Contenu*

LUKAS HOTTINGER, Recherches sur les Alveolines du Paleocene et de l'Eocene. Avec 18 planches, 1 tableau et 117 figures dans le texte.

TEXTE (I)

BIRKHÄUSER VERLAG BASEL – EDITIONS BIRKHÄUSER BALE

Figure 1- Cover page of Lucas Hottinger's (1960) PhD thesis (original publication).

Subphylum: Sarcodina SCHAMARDA, 1871,

Class: Rhizopodea von SIEBOLD, 1845,

Order: Foraminiferida EICHWALD, 1830,

Suborder: Miliolina DELAGE AND HÉROUARD, 1896,

Super Family: Alveolinacea/Miliolacea EHRENBERG, 1839,

Family: Alveolinidae EHRENBERG, 1839,

Genus: *Alveolina* D'ORBIGNY, 1826,

Type Species: *Oryzaria boscii* DEFRANCE in BRONN, 1825.

1st Subgenus: *Alveolina*(*Alveolina*) D'ORBIGNY, 1826,

1st Type Species: *Oryzaria boscii* DEFRANCE in BRONN, 1825,

2nd Subgenus: *Alveolina* (*Glomalveolina*) HOTTINGER, 1960,

2nd Type Species: *Alveolina dachelensis* SCHWAGER, 1883.

Genus: *Alveolina* D'Orbigny, 1826

Generic features: D'Orbigny (1826) first described the genus *Alveolina* in 1826. Reichel (1931, p.234; figure 1) explained the structural features of the genus

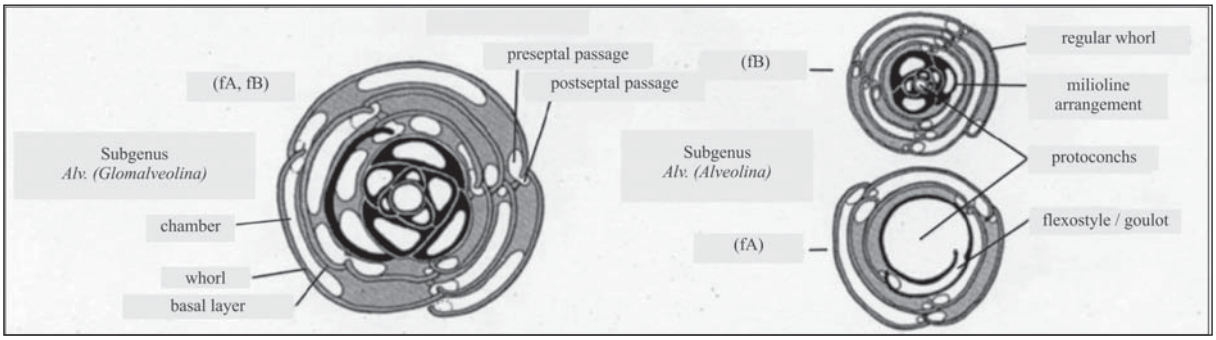

Figure 2- Equatorial sections of megalospheric and microspheric individuals of the subgenera *Alveolina* (*Glomalveolina*) Hottinger, 1960 and *Alveolina* (*Alveolina*) d'Orbigny, 1826, (Modified after Hottinger, 1960, p.26, figure 9).

Sous-genre Alveolina s.str.,

(Hottinger,1960, s. 63)

Figure 3- Systematics of the subgenus *Alveolina* (*Alveolina*) d'Orbigny, 1826 in the original publication (Hottinger, 1960, p.63).

52 L. HOTTINGER, ALVÉOLINES: II. DESCRIPTION SYSTÉMATIQUE

Description systématique

Sous-genre **GLOMALVEOLINA** REICHEL, 1937

Groupe d'*Alveolina* (*Glomalveolina*) *primaeva*

Figure 4- Systematics of the subgenus *Alveolina* (*Glomalveolina*) Hottinger, 1960 in the original publication (Hottinger, 1960, p.52).

Alveolina through figures. Some important studies on the structural elements of the genus *Alveolina* has been conducted later on (Reichel, 1937, p.7, figure 1; Hottinger, 1960, p.26, figure 9; Hottinger, 1974, p.22, figs. 10A-C). Generic features of the genus *Alveolina* are as follows:

1- Preseptal and postseptal canals are present (Figure 2) (Reichel, 1931, p. 294, fig. 1; 1937, p. 7, fig. 1; Hottinger, 1960, p. 26, fig. 9; 1974, p. 22, 34, figs. 10A-C; Loeblich and Tappan, 1964, C 506; Acar, 1995, p. 28, fig. 7, Pl. 38, figs. 1-3).

2- Aperture is consisting of two row of openings which are alternating in position. These apertures include main apertures located between septula and secondary apertures located at the base of septula or on the axis of septula (Reichel, 1931, p. 294, fig. 1; 1937, p. 7, fig. 1; Hottinger, 1960, p. 26, fig. 9; 1974, p. 22, 34, figs. 10A-C; Loeblich and Tappan, 1964, C 506; Acar, 1995, p. 28, fig. 7, Pl. 38, figs. 1-3).

3- Both the septula and the chamberlets are alternating in position (Reichel, 1931, p. 294, fig. 1; 1937, p. 7, fig. 1; Hottinger, 1960, p. 26, fig. 9; 1974, p. 22, 34, figs. 10A-C; Loeblich and Tappan, 1964, C 506; Acar, 1995, p. 28, fig. 7, Pl. 38, figs. 1-3). Dimorphism in the genus *Alveolina* is distinct.

Quinqueloculine, triloculine and biloculine chambers which follow very small spherical protoconch, are present in the axial sections of microspheric (fB) individuals. These biloculine chambers are subdivided into chamberlets by alternating septula (Hottinger, 1960, p. 26, fig. 9; Loeblich and Tappan, 1964, C 506; Acar, 1995, p. 28, fig. 7).

Biloculine chambers which follow the large protoconch, are present in the axial section of megalospheric (fA) individuals and these biloculine chambers are subdivided into chamberlets by alternating septula (Hottinger, 1960, p. 26, fig. 9;

Loeblich and Tappan, 1964, C 506; Acar, 1995, p. 28, fig. 7).

2.1. Systematics and Features of the Subgenus *Alveolina* (*Alveolina*) D'Orbigny, 1826

Family: Alveolinidae EHRENBERG, 1839,

Genus: *Alveolina* D'ORBIGNY, 1826,

Type Species: *Oryzaria boscii* DEFRANCE in BRONN, 1825,

1st Subgenus: *Alveolina*(*Alveolina*) D'ORBIGNY, 1826

1st Type Species: *Oryzaria boscii* DEFRANCE in BRONN, 1825.

1st Subgenus: *Alveolina*(*Alveolina*) D'Orbigny, 1826

Features of the subgenus: Features (canal structures, apertural openings, positions of septula) of the subgenus *Alv.* (*Alv.*) are completely same as in the genus *Alveolina* (Figures 2, 3) (Hottinger, 1960, p. 26, fig. 9, p. 63; Loeblich and Tappan, 1964, C 506; White 1992, p. 63; Acar, 1995, p. 28, fig. 7; 1996, p. 15).

Undivided quinqueloculine and triloculine chambers with biloculine chambers which follow spherical protoconch, are observed in the axial sections of microspheric (fB) specimens. These biloculine chambers are also subdivided into chamberlets by alternating septula (Figure 2) (Hottinger, 1960, p. 26, fig. 9; Loeblich and Tappan, 1964, C 506; Acar, 1995, p. 28, fig. 7; 1996, p. 15).

Divided biloculine chambers are observed just after a large protoconch in the axial sections of megalospheric (fA) specimens. These biloculine chambers are also subdivided into chamberlets by alternating septula (Figure 2) (Hottinger, 1960, p. 26, fig. 9; Loeblich and Tappan, 1964, C 506; Acar, 1995, p. 28, fig. 7; 1996, p. 15).

2.2. Systematics and Features of the Subgenus *Alveolina* (*Glomalveolina*) Hottinger, 1960

Family: Alveolinidae EHRENBERG, 1839,

Genus: *Alveolina* D'ORBIGNY, 1826,

Type Species: *Oryzaria boscii* DEFRANCE in BRONN, 1825,

2nd Subgenus: *Alveolina*(*Glomalveolina*) HOTTINGER, 1960,

2ndType Species: *Alveolina dachelensis* SCHWAGER, 1883.

2nd Subgenus: *Alveolina* (*Glomalveolina*) Hottinger, 1960,

Features of the subgenus: Hottinger (1960, p.52) explained systematics and the features of the subgenus *Alveolina* (*Glomalveolina*) in his PhD (Figures 1, 2). The coiling patterns succeeding protoconch, canal structures, apertural openings and positions of septula in microspheric (fB) forms (which means all the features) of the subgenus *Alv.* (*Glomalv.*) are completely same as in the genus *Alveolina* so in the microspheric (fB) forms of the subgenus *Alv.* (*Alv.*) (Figures 2, 4) (Hottinger, 1960, p. 26, fig. 9, p. 63, Pl.1, figs. 1-33; Loeblich and Tappan, 1964, C 506; Drobne, 1977, p. 14, figs. 1-5; Sirel et al, 1983, Pl. III, figs. 5-7; White 1992, p. 54, Table 1; Acar, 1995, p. 28, fig. 7, Pl. 1, figs. 1-11, Pl. 2, figs. 1-6, Pl. 3, figs. 1-9). There is no structural difference between microspheric (fB) forms of these two subgenera.

Structural features of the megalospheric (fA) specimens are different in each subgenus (Figures 2) (Hottinger, 1960, p. 26, fig. 9; Loeblich and Tappan, 1964, C 506; Drobne, 1977, p. 14, figs. 1a, 1d, figs. 4k, l; Acar, 1995, p. 28, fig. 7). For instance, in the axial sections of megalospheric (fA) specimens of the subgenus *Alv.* (*Glomalv.*), undivided triloculine chambers which come just after the protoconch, are followed by divided biloculine chambers (Hottinger, 1960, Pl. 1, figs. 6, 7, 9, 12, 14, 16, 20, 23, 26, 29; Drobne, 1977, p. 14, figs. 1a, 1d, figs. 4k, l; Sirel et al, 1983, Pl. III, figs. 6, 7; Acar, 1995, p. 16; Pl. 1, figs. 2- 4, 7, Pl. 2, figs. 1, 3, 5, 6, Pl. 3, fig. 3)

In equatorial sections of megalospheric sections (fA) of the subgenus *Alv.* (*Glomalv.*); undivided triloculine chambers come just after the protoconch, these triloculine chambers are followed by septa of planispirally coiled whorls, canals and chambers before and after these septa, are also present (Figure 2) (Hottinger, 1960, p. 26, fig. 9, Pl. 1, figs. 7, 10, 13, 25, 28; Sirel et al, 1983, Pl. III, fig. 5; Acar, 1995, p. 16).

These chambers which are formed by the septa of planispirally coiled whorls in equatorial sections; correspond to the biloculine chambers that are subdivided into chamberlets by septula in axial sections. Especially, the presence of undivided triloculine chambers found in both axial and equatorial sections of megalospheric (fA) specimens of the subgenus *Alv.*

(*Glomalv.*) is the structural difference of the subgenus *Alv.* (*Glomalv.*) (Figure 2) (Hottinger, 1960, p. 26, fig. 9; Loeblich and Tappan, 1964, C 506; Acar, 1995, p. 16) (Figure 5). These triloculine chambers do not exist in the megalospheric (fA) specimens of the subgenus *Alv.* (*Alv.*).

2.3. Structural Difference Between The Subgenera *Alveolina* (*Glomalveolina*) Hottinger, 1960 And *Alveolina* (*Alveolina*) D'Orbigny, 1826

The presence of undivided triloculine chambers found in axial and equatorial (in one or two plans) sections of megalospheric (fA) specimens of the subgenus *Alv.* (*Glomalv.*) is an important structural difference of the subgenus *Alv.* (*Glomalv.*)

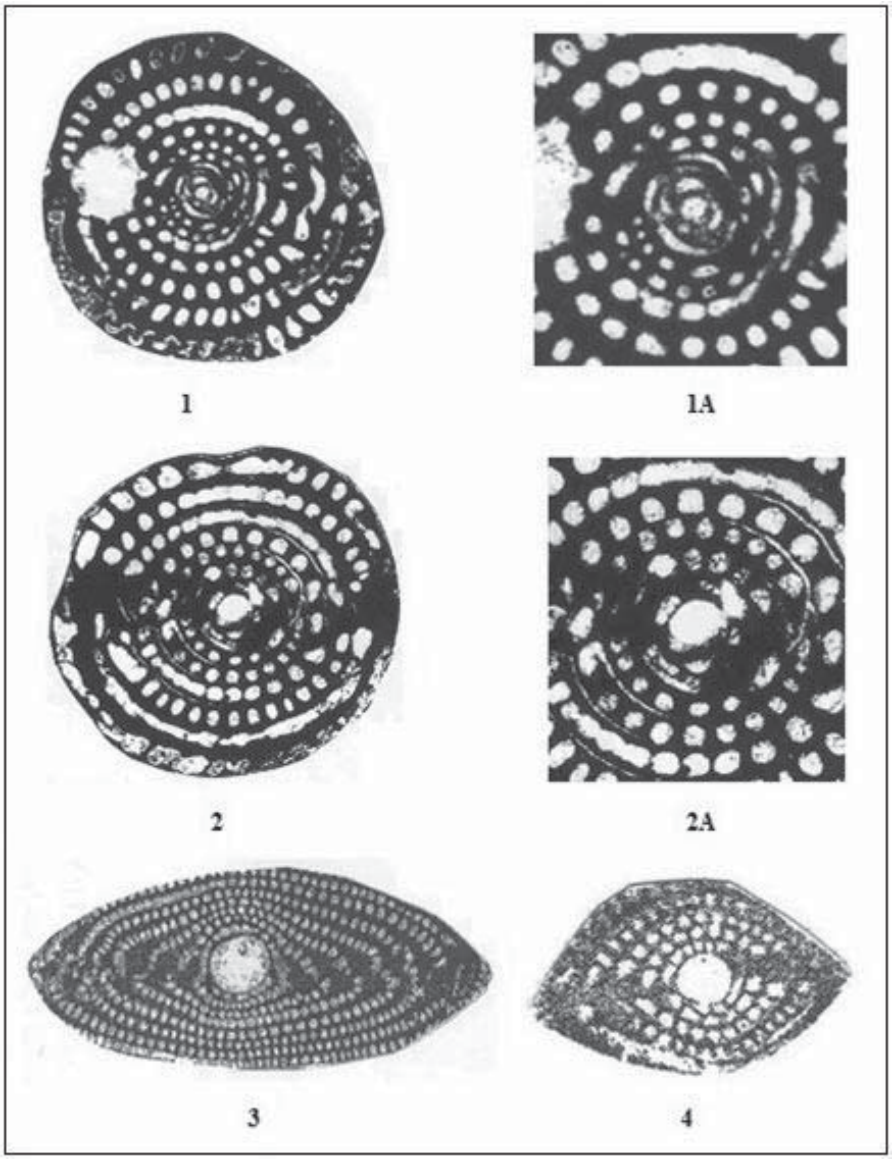

Figure 5- Axial sections of megalospheric (fA) specimens of the subgenera *Alv.*(*Glomalv.*) Hottinger, 1960 and *Alv.*(*Alv.*) d'Orbigny, 1826. 1, 2: *Alv.*(*Glomalv.*) *primaeva* (Reichel, 1937), early Thanetian, X40, (Acar, 1995, Pl. 1, figs. 3, 4). 1A, 2A: Enlarged photo of 1 and 2; protoconch, and the following undivided triloculine chambers and divided biloculine chambers are present in both figures. X75. 3: *Alv.*(*Alv.*) *corbarica* Hottinger, 1960, protoconch and the succeeding divided biloculine chambers are apparent, middle Ilerdian, X20, (Sirel and Acar, 2008, Pl. 38, fig. 6). 4: *Alv.*(*Alv.*) *erki* Acar, 1995, protoconch and the succeeding biloculine chambers which are subdivided into chamberlets are distinct, early Ilerdian, X40, (Acar, 1995, Pl. 3, fig. 10).

(Figure 2) (Hottinger, 1960, p. 26, fig. 9; Loeblich and Tappan, 1964, C 506; Acar, 1995, p. 16) (Figure 5). These triloculine chambers are not present in the megalospheric (fA) specimens of the subgenus *Alv.* (*Alv.*).

3. Conclusions and Suggestions

A- *Glomalveolina* Hottinger (1960) is not a genus. *Alv.*(*Alveolina*) d'Orbigny, 1826 and *Alv.* (*Glomalveolina*) Hottinger, 1960 are both subgenusses since all the generic features of their microspheric (fB) forms are the same (Figure 2) (Hottinger, 1960, p.26, fig. 9). Structural difference between these two subgenera can only be observed in the megalospheric (fA) forms (Figure 2) (Reichel, 1937, p. 80; Hottinger, 1960, p. 26, fig. 9). This structural difference could only be shown as "subgenus" in systematic paleontology (Figures 2-4) (Hottinger, 1960, p. 52,63; Loeblich and Tappan, 1964, C 506). Because of the reason that all the generic features of "*Alveolina*" and "*Glomalveolina*" are the same, these cannot be two different genera, so *Glomalveolina* can never be used as a genus. Since the genus *Alveolina* was first described in 1826, the genus (?) *Glomalveolina* 1960/1962 would be a synonym of the genus *Alveolina*. Consequently, *Alv.*(*Alveolina*) d'Orbigny, 1826 and *Alv.*(*Glomalveolina*) Hottinger, 1960 are both subgenusses, and each has to be used as "subgenus" in the systematic paleontology.

B- The author of the subgenus *Alv.* (*Glomalv.*) is not Reichel but is Hottinger, and the year of publications is not 1962 but is 1960 (Figure 1). Besides, Hottinger has no single author paper in 1962!

C- Axial, equatorial, tangential, and also oblique sections of megalospheric (fA) forms should be used when describing species/subspecies, new species or new subspecies (especially the small sized specimens) of all alveolinids (e.g. *Praebullalveolina* Sirel and Acar, 1982, *Bullalveolina* Reichel, 1937, *Borelis* De Montfort, 1808 and the subgenera *Alv.* (*Alv*) or *Alv.* (*Glomalv.*)). Positions of chambers which follow the protoconch and their internal structures could clearly be observed and examined in axial sections of especially megalospheric (fA) forms. This principle is also current when describing known alveolinid genera or a new genus. In general, standard (magnification) should be used for Late Cretaceous, Paleogene and Neogene alveolinids (Reichel, 1931, 1937; Hottinger, 1960; Drobne, 1977; Acar, 1995; Sirel and Acar, 2008). For instance, in the first description of (new) species *Alveolina* (*Alveolina*) *erki* Acar, 1995, magnification was used as X40, in order to compare with glomalveolinids and to discuss (Acar, 1995, p. 35, Pl. 3, figs. 10–13).

Acknowledgements

The author thanks to Dr. Erdal Herece for computer drawings and, to the reviewers for suggestions and contributions.

References

Acar, Ş. 1995. Türkiye'nin Değişik Bölgelerinin Paleojen'inden Bazı Alveolin Cinslerinin (Alveolina (Alveolina), Alveolina (Glomalveolina), Borelis ve Praebullalveolina) Sistematik Tanımları ve Stratigrafik Dağılımları. Selçuk Üniversitesi Doktora Tezi, 1-166, 38 Levha, Konya-Türkiye.

Acar, Ş. 1996. A New Grouping Method for Subgenus Alveolina(Alveolina) Hottinger, 1960, Species and Subspecies. International workshop Postajna '96: The Role of Impact Processes in the Geological and Biological Evolution of Planet Earth (Poster Presantation), Postajna-Ljubljana, 1996.

Bassi, D., Broglio, C.L. 1999. Alveolinids at the Middle-UpperEocene boundary in Northeastern Italy (Veneto, Colli Berici, Vicenza). Journal of Foraminiferal Research, 29, (3), 222-235.

BouDagher-Fadel, M.K. 2008. Evolution and Geological Significance of Larger Benthic Foraminifera. (Elsevier Science) Development in Paleontology & Stratigraphy, 21, 1-544.

Çolakoğlu, S., Özcan, E. 2003. Orthophragminid Foraminiferal Assemblages From An Ilerdian-Early Cuisian Reference Section (Sakarya Section, Haymana-Polatlı Basin, Central Anatolia-Turkey). Rivista Italiana di Paleontologia e Stratigrafia 109 (3).

D' Orbigny, A.D. 1826. Tableau méthodique de la classe des Cephalopodes. Ann. Sci. Nat. 1, (7), 245-314, pl. 10-17, Paris.

Drobne, K. 1977. Alvéolines paléogenes de la Slovénie et de I'Istrie. Schweizerische Paläontologische Abhandlungen 99, 1-175, 96 figs., 21 pls., Basel.

Hottinger, L. 1958. Geologie du Mont Cayla (Aude, Aquitaine orientale). Eclogae geol. Helv. V.51, no.2, 437-451, Bale.

Hottinger, L. 1960. Recherches sur les Alvéolines du Paléocène et de I' Eocene. Schweizerische Palaeontologische Abhandlungen, 75/76 (1960), Texte (I), 243 s., Atlas (II), 18 Levha, 117 Şekil, 1 Tablo, Bale.

Hottinger, L. 1974. Alveolinids, Cretaceous-Tertiary Larger Foraminifera. Esso Production Research-European Laboratories, (EPR-E-1 SP-74), Basle-Switzerland.

Hottinger, L. 1999. "Odd partnership", a particular size relation between close species of larger foraminifera, with an emendation of an outstandingly odd partner, Glomalveolina delicatissima (SMOUT, 1954), Middle Eocene. Eclogae geologicae Helvetiae, 92,(3),385-393, Basel.

Hottinger, L. 2006. Illustrated glossary of terms used in foraminiferal research. Carnets de Geology. Notebooks on Geology.

Hottinger, L. 2009. The Paleocene and earliest Eocene foraminiferal Family Miscellaneidae: neither nummulitids nor rotaliids. Carnets de Geologie/ Notebooks on Geology Article 2009/06 (CG 2009-A06).

İbrahimpasic, H. 2012. Taxonomy, Palaeoecology and Biostratigraphy of Paleogene Alveolinids from Northwestern and Central part of the Adriatic-Dinaridic Carbonate Platrorm. University of Zagreb Faculty of Science Department of Geology, Doctoral Thesis, p. 1-190; pl.1-54, Zagreb, 2012.

Loeblich, A.R., Tappan, H. 1964. Treatise on invertebrate Paleontology. Part C, Protista 2, 900s., 653 şekil, Lawrence, Kansas (Kansas Univ. Press).

Loeblich, A.R., Tappan, H. 1987. Foraminiferal genera and their classification. 1, 1-970; 2, 212s., 847 Levha, New York (Von Nostrand Reinhold).

Özcan, E., Sirel, E., Altıner, S., Ö., Çolakoğlu, S. 2001. Late Paleocene Orthophragminae (foraminifera) from the Haymana-Polatlı Basin, (central Turkey) and description of a new taxon, Orbitoclypeus haymanaensis. Micropaleontology, 47 (4) 339-357.

Özcan, E., Less, G., Okay, A.I., Baldi-Beke, M., Kollanyi, K., Yılmaz, İ.Ö. 2010. Stratigraphy and Larger Foraminifera of the Eocene Shallow-Marine and Olistostromal Units of the Southern Part of the Trace Basin, NW Turkey. Turkish Journal of Earth Sciences, 19, 27-77.

Özgen-Erdem, N. 2008. Akçataş - Cebeci Yöresinin (KB Tosya - GD Kastamonu) Tanesiyen -Ilerdiyen Bentik Foraminifer Biyostratigrafisi. Maden Tetkik ve Arama Dergisi, 137, 67-77.

Özgen-Erdem, N., İnan, N., Akyazı, M., Tunoğlu, C. 2005. Benthic foraminiferal assemlages and microfacies analysis of Paleocene-Eocene carbonate rocks in the Kastamonu region, Northern Turkey. Journal of Asian Earth Sciences 25, 403-417.

Pignatti, J., Massimo, C., Andrea, B., Cecilia, B., Antonino, B., Manuela, F., Ruggero, M., Gianluca, P., Michela, R. 2008. SBZ 2-6 Larger Foraminiferal Assemblages From The Apulian And Pre-Apulian Domians. Atti Mus. Civ. Stor. Nat. Trieste, Suppl. al 53, 131-146.

Rahaghi, A. 1978. Paleogene biostratigraphy of some parts of Iran. National Iranian Oil Company Geological Lab. Publication No. 7, Tehran.

Rahaghi, A. 1983. Stratigraphy and Faunal assemblage of Paleocene-Lower Eocene in Iran. National Iranian Oil Company Geological Lab. Pub. No.10, 73s.,49 levha., Tehran.

Reichel, M. 1931. Sur la structure des Alvéolines. Eclogae geol. Helv. 24, (2), 289-303, pl. 13-18, Bale.

Reichel, M. 1937. Etude sur les Alveolines. Schweizerische Palaeontologische Abhandlungen; 57/59, (1), 147p., pl. 1-11.

Sartorio, D., Venturini, S. 1988. Southern Tethys Biofacies. Agip, 235p. (pls.14-225) Italya.

Scheibner, C., Speijer, R.P. 2009. Recalibration of the Tethyan shallow-benthic zonation across the Paleocene-Eocene boundary: the Egyptian record. Geologica Acta,.7, (1-2), 195-214.

Sirel, E. 1972. Systematic study of new species of the general Fabularia and Kathina from Paleocene. Bull. of the Geol. Soc. of Turkey, 15, 277-294.

Sirel, E. 1975. Polatlı (GB Ankara) güneyinin stratigrafisi. Türkiye Jeoloji Kurumu Bülteni, 18, 181-192.

Sirel, E. 1976. Polatlı (GB Ankara) güneyinde bulunan Alveolina, Nummulites, Ranikothalia ve Assilina cinslerinin bazı türlerinin sistematik incelemeleri. Türkiye Jeoloji Kurumu Bülteni,.19,(2), 89-102.

Sirel, E. 1986. Lacazina oeztemueri Sirel, 1981, renamed as Pseudolacazina oeztemueri (Sirel) from The Thanetian limestone (Central Turkey). Bulletin of the Mineral Research and Exploration Institute of Turkey, 105/106: 123-126, pl.3.

Sirel, E. 1998. Foraminiferal description and biostratigraphy of the Paleocene-Lower Eocene shallow-water limestones and discussion on the Cretaceous-Tertiary boundary in Turkey. General Directorate of Mineral Research and Exploration. Monography 2, 117p.

Sirel, E. 1999. Four new genera (Haymanella, Kayseriella, Elazıgella and Orduella) new species of Hottingerina from the Paleocene of Turkey. Micropaleontology, 45 (2), 113-137.

Sirel, E. 2004. Türkiye'nin Mesozoyik ve Senozoyik Yeni Bentik Foraminiferleri. TMMOB Jeoloji Mühendisleri Odası (Emeğin Bilimsel Sentezi Özel Sayı 1).

Sirel, E. 2009. Reference sections and key localities of the Paleocene Stages and their very shallow/shallow-water three benthic foraminifera in Turkey. Revue de Paleontologie, 28 (2), 413-435, Geneve.

Sirel, E. 2010. Haymana-Polatlı Basin. Jeoloji Mühendisleri Odası Teknik Geziler Serisi 6, 1-29.

Sirel, E., Gündüz, H. 1976. Haymana (G. Ankara) yöresi Ilerdiyen, Küviziyen ve Lütesiyen'deki Nummulites, Assilina ve Alveolina cinslerinin bazı türlerinin tanımları ve stratigrafik dağılımları. Türkiye Jeoloji Kurumu Bülteni, 19, (1), 31-44.

Sirel, E., Acar, Ş. 2008. Description And Biostratigraphy of The Thanetian-Bartonian Glomalveolinids And Alveolinids Of Turkey. UCTEA Chamber of Geological Engineers Publication 103, Scientific Synthessis of the Lifelong Achievement, Special, 2, 1-108, 78 levha, Ankara.

Sirel, E., Gündüz, H., Acar, Ş. 1983. Sur la presence D'une nouvelle espece D'Orbitokathina Hottinger dans le Thanetien de Van (East de la Turquie). Revue de Paleobiologie, 2, 2, 149-159, Geneve.

Sirel, E., Dağer, Z., Sözeri, B. 1986. Some biostratigraphic and paleogeographic observations on the Cretaceous/Tertiary boundary in the Haymana-Polatlı region (Central Turkey). Lecture Notes in Earth Sciences, 8, 385-396 (Global Bio-Events), Springer-Verlag Berlin Heidelberg.

White, M.R. 1992. On Species Identification in the Foraminiferal Genus Alveolina (Late Paleocene-Middle Eocene). Journal of Foraminiferal Research, 22, (1), 52-70, London.

Bull. Min. Res. Exp. (2019) 159: 99-116

Bulletin of the Mineral Research and Exploration

http://bulletin.mta.gov.tr

Geochemistry and tectonic significance of the ophiolitic rocks of the Yarpuz-Kaypak (Amanoslar, Osmaniye) area

Tamer RIZAOĞLU[a*], Utku BAĞCI[b] and Osman PARLAK[c]

[a]*Kahramanmaraş Sütçü İmam University, Department of Geological Engineering, Kahramanmaraş.orcig.org. 0000-0002-4883-0842*
[b]*Mersin University, Department of Geological Engineering, Mersin. orcid.org. 0000-0002-9295-2898*
[c]*Çukurova University, Department of Geological Engineering, Adana. orcid.org. 0000-0002-4652-3902*

Research Article

Keywords:
Ophiolite, Petrography, Geochemistry, Supra-subduction zone, Neotethys, Turkey

ABSTRACT

Yarpuz-Kaypak (Osmaniye) region, located in Amanos Mountains, contains harzburgitic tectonites and mafic cumulates. The tectonites are represented by serpantinized harzburgites, whereas the cumulates are characterized by gabbronorite and gabbro compositions. The crystallization order within the cumulates is clinopyroxene, orthopyroxene plagioclase and amphibole. The major element compositions of the tectonites and cumulate rocks are consistent with formation in an arc-related tectonic setting. Trace element concentrations of these rocks exhibit large ion litophile element enrichments. Both geochemical and petrographic evidence suggest that the tectonite and cumulate rocks from the Yarpuz-Kaypak (Osmaniye) region represent the remnants of an oceanic lithosphere that formed in a supra-subduction zone tectonic setting during the closure of the Southern Neotethyan ocean and emplaced onto the northern margin of the Arabian platform in Late Cretaceous.

Received Date: 28.02.2018
Accepted Date: 18.07.2018

1. Introduction

The Tethyan evolution of Turkey covers two tectonic periods, the Paleotethys and Neotethys, which show continuity with each other in terms of time. The Paleotethys period took place between Carboniferous and Lias, having an effect particularly in Northern and Central Anatolia (Robertson and Ustaömer, 2009; Göncüoğlu et al., 2000, 2007; Okay, 2000). Whereas the Neotethys period affected the entire Anatolia between the Triassic and Miocene period, and continued its effect up to present time (Şengör and Yılmaz, 1981; Robertson and Dixon, 1984). The Anatolian Plate is an important part of the Alpine-Himalayan orogenic belt which covers the remnants of E-W trending Neotethyan oceanic basins located between metamorphic massifs and/or platform carbonate sequences. The Neotethyan remnants from top to bottom are represented by ophiolites, metamorphic soles and ophiolitic mélanges (Şengör and Yılmaz, 1981; Dilek and Moores, 1990; Dilek et al., 1999; Floyd et al., 2000; Robertson, 2002). The Neotethys is composed of two oceanic basins, namely a northern branch and a southern branch (Şengör and Yılmaz, 1981). The northern branch covers the İzmir-Ankara-Erzincan ocean, Intra-Tauride ocean and Intra-Pontide ocean, whereas the southern branch covers the Berit and South Neotethyan oceans (Şengör and Yılmaz, 1981; Görür et al., 1984; Robertson and Dixon, 1984; Robertson et al., 2012, 2013*a*; Figure 1). As the Neotethys ocean started to close during the Late Cretaceous, ophiolites of both northern and southern branches emplaced over the passive continent margin to the south (Şengör and Yılmaz, 1981; Robertson and Dixon, 1984; Yılmaz et al., 1993; Robertson, 2002; Robertson et al., 2006). The ophiolites, which have a significant place within the Neotethys evolution of Turkey, are of the supra-subduction zone (SSZ) type (Yalınız et al., 1996; Parlak et al., 1996, 2000, 2002,

Citation Info: Rızaoğlu, T., Bağcı, U., Parlak O. 2019. Geochemistry and tectonic significance of the ophiolitic rocks of the Yarpuz-Kaypak (Amanoslar, Osmaniye) area. Bulletin of Mineral Research and Exploration, 159, 99-116.
http://dx.doi.org/10.19111/bulletinofmre.501393

* *Corresponding author: Tamer RIZAOĞLU, tamer@ksu.edu.tr*

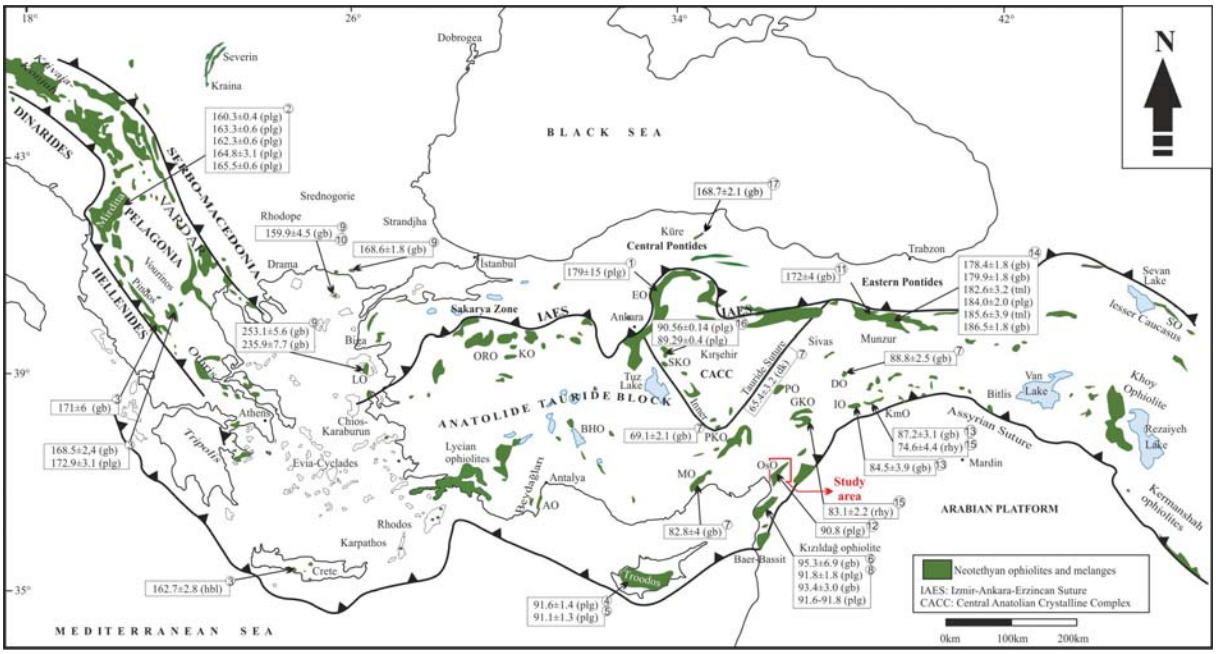

Figure 1- Tectonic map of the East Mediterranean Region showing the distribution of Neothetyan ophiolites and their relative U-Pb ages (after Dilek and Flower, 2003; Çelik et al., 2011). 1) Dilek and Thy 2006, (2) Dilek et al., 2008, (3) Liati et al., 2004, (4) Mukasa and Ludden 1987, (5) Konstantinou et al., 2007, (6) Dilek and Thy 2009, (7) Parlak et al., 2013, (8) Karaoğlan et al., 2013a, (9) Koglin, 2008, (10) Koglin et al., 2009, (11) Topuz et al., 2013, (12) Sarıfakıoğlu et al., 2012, (13) Karaoğlan et al., 2012, (14) Robertson et al., 2013b, (15) Karaoğlan et al., 2013b, (16) van Hinsbergen et al., 2016, (17) Alparslan and Dilek 2018. Abbreviations: LO: Lesvos Ophiolite, AO: Antalya Ophiolite, BHO: Beyşehir-Hoyran Ophiolite, ORO: Orhaneli Ophiolite, KO: Kınık Ophiolite, EO: Eldivan Ophiolite, MO: Mersin Ophiolite, PKO: Pozantı-Karsantı Ophiolite; OsO: Osmaniye Ophiolite, GKO: Göksun (Kahramanmaraş) Ophiolite, PO: Pınarbaşı Ophiolite, IO: Ispendere Ophiolite, DO: Divriği Ophiolite, KmO: Kömürhan Ophiolite, SO: Sevan Ophiolite, SKO: Sarıkaraman Ophiolite; plg: plagiogranite, gb: gabbro, dk: dike, tnl: tonalite, rhy: rhyolite.

2009; Robertson, 2002; Çelik and Delaloye 2003, 2006; Vergili and Parlak, 2005; Bağcı et al., 2005, 2006, Rızaoğlu et al., 2006; Bağcı et al., 2008; Bağcı and Parlak, 2009; Sarıfakıoğlu et al., 2009; Dilek and Thy 2009), and their formation and emplacement, respectively, reflect the sequence of events that they shared since the Late Cretaceous.

Amanos mountains are characterized by having wide-spread ophiolitic rocks (Yılmaz et al., 1984). The ophiolitic nappes in the Amanos mountains are seen in the form of separated nappes and clips which cover an area of about 13.000 km^2 (Tekeli and Erendil, 1986). Many detailed petrological, geochemical and geochronological studies have been carried out particularly in the Kızıldağ (Hatay) ophiolite and in ophiolitic rocks of the Amanos mountains which constitute the northwest margin of the Arabian platform (Dubertret, 1955; Çoğulu, 1975; Parrot, 1973; Delaloye et al., 1980; Tinkler et al., 1981; Tekeli and Erendil, 1984; Selçuk, 1985; Pişkin et al., 1990; Dilek and Thy, 2009; Bağcı et al., 2005; 2008; Bağcı, 2013; Boulton et al., 2006; Parlak et al., 2013; Karaoğlan et al., 2013*a*; Tanırlı and Rızaoğlu, 2016).

The study area covers an area of about 40 km^2 in the vicinity of the Yarpuz-Kaypak district in the Osmaniye province. Studies on ophiolites cropping out in this region are limited, and Yılmaz et al. (1984) designated the ophiolites in the Central Amanos and around Osmaniye as Zorkun and Tozaklı ophiolites. Yapıcı (1990) has conducted a study on the geology and petrographic features of the ophiolitic rocks in the region. However, no studies on the geochemistry of ophiolitic sequence in the region, located in the north-northeast of the Amanos mountains, have been carried out so far. In the frame of this study, petrographical and geochemical features of the ophiolitic rocks cropping out in the Yarpuz-Kaypak (Osmaniye) region will be investigated in order to evaluate its tectonic setting and compare to similar units in the region, as well as to better understand processes for the oceanic crust formation in the southern branch of Neotethys.

2. Regional Geology

The Amanos-high in southern Turkey constitutes the northwestern margin of the Arabian platform and

consists of allochthonous and autochthonous units formed between Precambrian and Quaternary. The South Anatolia Orogenic Belt formed as a result of collision of the Tauride and Arabian Platforms, and it is divided into three E-W trending main tectonic zones. From south to north, these are the Arabian Platform, the zone of imbrication and the nappe zone (Yılmaz, 1993). These three structural units are composed as follows: metamorphic massifs (Malatya, Bitlis and Pötürge metamorphic sequences), ophiolitic complexes and thick sedimentary sequence of the Arabian platform. The Arabian platform, which is represented by autochthonous sedimentary rock formations deposited from Early Paleozoic with small interruptions, includes the ophiolite nappes emplaced during Late Cretaceous and cover sediments formed between Late Cretaceous and Miocene. It is divided into three units, namely the lower autochthonous, the upper autochthonous and the allochthonous (ophiolite and mélange) units (Yılmaz, 1993; Yılmaz et al., 1993). Paleozoic clastic sediments of the autochthonous Arabian platform in Yarpuz-Kaypak (Osmaniye) form the basement of the study area in Amanos Mountains, trending SW-NE direction between Antakya and Kahramanmaraş (Figure 2). A carbonatic sequence consisting of Upper Jurassic and Lower Cretaceous dolomite and dolomitic limestones unconformably overlies this basement rocks (Dubertret, 1955; Atan, 1969; Yılmaz et al., 1984; Tekeli and Erendil, 1986). This unit is tectonically overlain by Upper Cretaceous ophiolitic units (Yılmaz et al., 1984; Yapıcı and İşler, 1991; Yılmaz et al., 1993). The sediments covering the ophiolitic nappes in the region are represented by Miocene clastic and carbonate-rich rocks (Gül, 1987; Terlemez et al; 1992). Pliocene rocks consisting of continental clastics and lagoon units and Quaternary basaltic volcanic rocks, alluviums and alluvium fans are the youngest units (Rojay et al. 2001).

The ophiolites observed in the study area are mainly composed of mantle tectonites and cumulate rocks. The tectonites, which cover wide areas in the region, are highly fractured and weathered with red to reddish colored coating, while fresh fracture surfaces

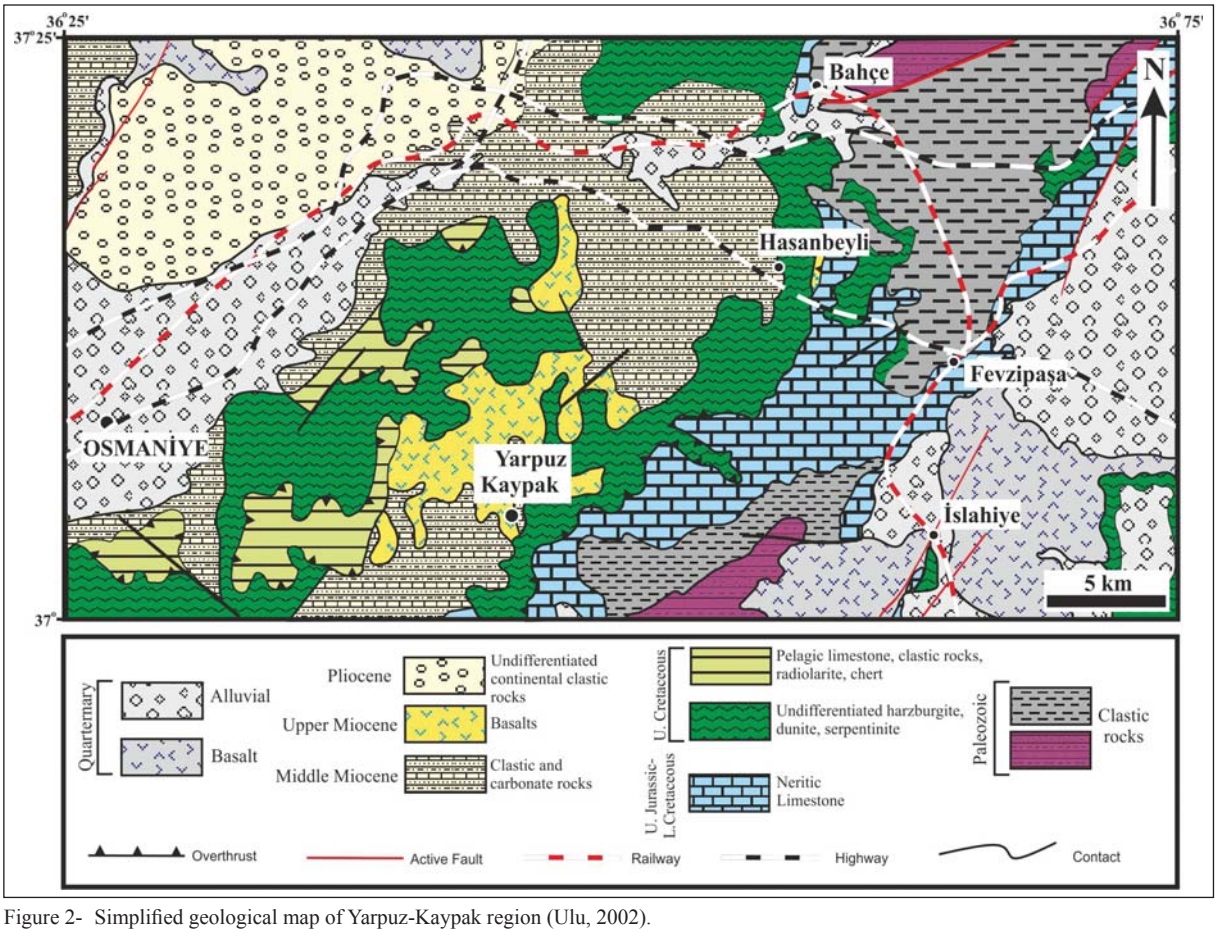

Figure 2- Simplified geological map of Yarpuz-Kaypak region (Ulu, 2002).

are dark green to greenish. The tectonites display structural features such as foliation and lineation, reflecting plastic deformation related to mantle flow. When highly serpentinized, they present greenish to dark black colors and oily brightness. Cumulates show fine to medium grain-size, hard-solid sharp-edged and exhibit cumulate structures such as magmatic banding-lamination.

3. Analytic Method

Thirty-five samples were collected from the study area for petrographic and geochemical analyses. The thin sections were prepared for petrographic observations in the Thin Section Laboratory of the Geological Engineering Department of Çukurova University. The major-trace element analysis of 29 samples were carried out in the Geochemistry Laboratory of the Mineralogy Department of Geneva University, Switzerland. Major elements were measured by means of X-Ray Florescence (XRF) within the glass pellets which were prepared by adding 1/5 of sample and lithium tetraborate ($Li_2B_4O_7$) into platin-gold crucible at 1150 °C. Loss of ignition (LOI) values were calculated by taking the weight difference after heating the samples at 1000 °C. The trace elements were analyzed by means of pellets pressed by the same method.

4. Petrography

The samples were defined as mantle rocks (tectonites) and mafic cumulates as a result of the detailed petrographic determinations on thin sections prepared from the ophiolitic rock samples taken from the Yarpuz-Kaypak (Osmaniye) region.

The tectonites are represented by serpentinized harzburgites and display porphyroclastic (Figure 3a) and sieve textures. Olivine (70–75 vol%) is the most abundant mineral, where the sieve texture is observed, remained partially fresh. When completely serpentinized, tectonites show the typical sieve texture indicative of static replacement of olivine by serpentine (Figure 3b). Orthopyroxene (20-25 vol%) commonly highly replaced by bastite (Figure 3a-b). Furthermore, significant amount of disseminated and elongated chromite crystals observed in tile red color is seen within the rock.

Cumulate rocks are defined as gabbronorite and gabbro (Figure 3c-h). Plagioclase, clinopyroxene, orthopyroxene are observed as cumulus and intercumulus minerals in the cumulate rocks which represent adcumulate, mesocumulate and poikilitic textures. Plagioclase, which is the most abundant mineral of the gabbronorite, represent high degree of sericitization. Plagioclase, occurring as prismatic crystals with ambiguous polysynthetic twins and make ca. 45-50 vol% of the rock. According to the polysynthetic twin measures carried out in fresh mineral, the fact that the angle of extinction was determined as 30 °-35° shows that the plagioclases have a composition ranging from labrador to bytownite. Orthopyroxene, clinopyroxene and amphibole constitute the dark colored minerals of the rock. Orthopyroxenes are polarized in grey tones and include clinopyroxenes in the form of exsolution lamellas. In some clinopyroxenes, $h^1(100)$ twin is observed. Amphibole commonly constitutes the 8-10 vol% of the rock and it occurs as anhedral intercumulus phase.

Gabbro is commonly medium to coarse-grain sized and shows adcumulate texture. Polysynthetic twins are locally distinct in plagioclase which is the dominant mineral phase of the rock. Abundant ferromagnesian mineral is clinopyroxene, and orthopyroxene is locally encountered (gabbronorite). Some of the pyroxene crystals show alteration by uralitization.

Aforementioned textural and mineralogic features show that the crystallization order of mineral phases in the cumulate rocks are as follows: clinopyroxene → orthopyroxene → plagioclase → amphibole.

5. Whole Rock Geochemistry

Whole rock analysis results of the tectonites and the mafic cumulates from the Yarpuz-Kaypak (Osmaniye) region are given in table 1. LOI values are quite high (11,9-14,4 wt%) in tectonites, while they vary between 0,8-2,8 wt% in mafic cumulates. The variation in LOI values indicates that the studied rocks were affected by variable extent of alterations (e.g., serpentinization, uralitization, and sericitization) reflecting the contribution of secondary hydrated and carbonate phases (Rollinson, 1993). For petrologic interpretations, it is suggested to utilize the rare earth elements (REE) and the high-field-strength (HFS) elements generally considered relatively stable (immobile) during rock alteration (Pearce and Cann, 1973; Smith and Smith, 1976; Floyd and Winchester, 1978), in contrast to the mobility of major elements

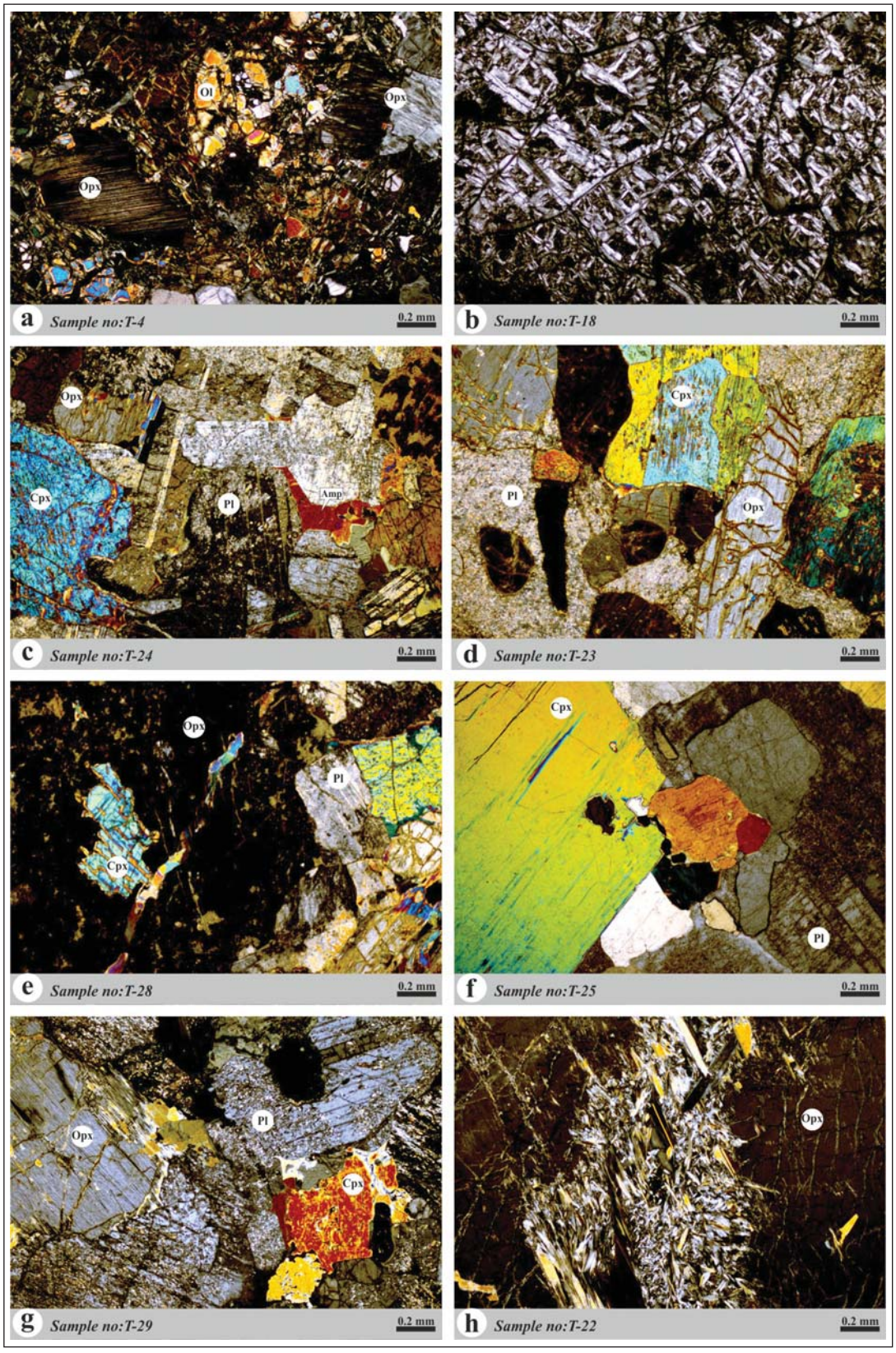

Figure 3- Thin section images of Yarpuz-Kaypakophiolites. (a) harzburgite showing porphyroclastic texture, (b) sieve texture, (c) gabbronorite showing adcumulate texture, (d-e) gabbronorite showing poikilitic texture, (f) adcumulate gabbro, (g) sericitization seen in plagioclases, (h) uralitization seen in pyroxenes, (Mineral abbreviations are taken from Whitney and Evans, 2010).

Table 1- Major (%) and trace (ppm) element contents of mantle tectonites and mafic cumulate rocks of Yarpuz-Kaypak region.

	Harzburgite																					Gabbronorite							Gabbro
Sample	**T 4**	**T 5**	**T 6**	**T 13**	**T 14**	**T 15**	**T 18**	**T 19**	**T 26**	**T 27**	**T 31**	**T 32**	**T 33**	**T 34**	**T 35**	**T 36**	**T 37**	**T 39**	**T 40**	**T 49**	**T 50**	**T 20**	**T 21**	**T 22**	**T 23**	**T 24**	**T 28**	**T 29**	**T 30**
SiO_2	39.17	38.90	39.92	39.94	40.20	39.05	38.48	39.69	40.23	39.50	38.10	39.04	39.85	39.21	39.47	39.40	39.06	39.37	38.60	39.30	39.34	51.85	48.96	48.39	49.21	47.96	47.63	48.53	45.88
TiO_2	0.01	0.01	0.02	0.04	0.01	0.03	0.03	0.02	0.02	0.01	0.03	0.01	0.02	0.01	0.01	0.01	0.01	0.01	0.02	0.05	0.08	0.06	0.04	0.13	0.09	0.11	0.10	0.10	0.18
Al_2O_3	0.78	0.68	0.97	0.85	0.89	0.81	2.87	0.88	1.18	0.89	3.23	1.26	0.70	0.83	0.90	0.77	0.66	0.81	0.91	1.55	1.83	7.82	13.53	6.73	14.42	18.69	17.59	18.89	9.79
tFe_2O_3	8.25	8.17	8.01	8.29	8.34	8.11	7.37	7.52	7.41	7.98	8.78	8.14	8.02	8.30	9.49	7.95	8.53	7.82	8.40	7.80	7.71	7.96	6.32	8.73	8.10	7.22	8.33	7.19	9.56
MnO	0.11	0.12	0.12	0.12	0.13	0.12	0.16	0.10	0.12	0.10	0.11	0.15	0.12	0.16	0.10	0.13	0.13	0.12	0.10	0.14	0.15	0.17	0.13	0.17	0.18	0.13	0.16	0.13	0.17
MgO	38.47	37.78	37.39	36.76	36.77	38.19	37.23	38.49	37.43	38.19	32.49	36.61	36.62	36.79	36.58	37.49	37.20	37.24	36.92	35.27	34.79	22.21	17.13	18.28	14.01	9.71	10.07	9.43	16.09
CaO	0.71	0.08	0.65	0.49	0.04	0.11	0.16	0.06	0.15	0.07	4.47	0.24	0.66	0.08	0.04	0.05	0.04	0.11	0.06	0.37	0.44	8.41	10.54	14.09	7.73	10.79	9.58	11.12	14.19
Na_2O	0.00	0.00	0.00	0.00	0.00	0.00	0.00	0.00	0.00	0.00	0.00	0.00	0.00	0.00	0.00	0.00	0.00	0.00	0.06	0.00	0.03	0.00	0.11	0.09	0.46	1.16	1.35	1.25	0.17
K_2O	0.00	0.00	0.00	0.01	0.00	0.01	0.00	0.00	0.00	0.01	0.00	0.02	0.00	0.01	0.00	0.00	0.00	0.00	0.02	0.02	0.03	0.79	0.74	0.02	2.71	1.41	1.71	1.08	0.03
Cr_2O_3	0.40	0.36	0.54	0.47	0.58	0.45	0.43	0.37	0.52	0.40	0.43	0.54	0.45	0.54	0.40	0.46	0.42	0.40	0.46	0.42	0.45	0.26	0.19	0.27	0.16	0.02	0.03	0.02	0.23
NiO	0.33	0.35	0.32	0.36	0.36	0.35	0.32	0.37	0.32	0.34	0.28	0.30	0.35	0.35	0.31	0.35	0.34	0.34	0.35	0.36	0.33	0.07	0.06	0.05	0.04	0.02	0.03	0.02	0.05
P_2O_5	0.01	0.01	0.01	0.02	0.01	0.01	0.01	0.01	0.01	0.01	0.01	0.01	0.01	0.01	0.01	0.01	0.01	0.01	0.02	0.02	0.02	0.01	0.01	0.01	0.01	0.01	0.01	0.01	0.02
LOI	12.00	13.38	12.23	13.16	13.23	13.38	13.03	12.99	12.91	12.82	11.86	13.09	13.02	13.49	12.50	13.00	13.68	13.81	13.68	14.30	14.40	0.77	1.03	2.79	2.22	1.93	2.37	2.23	2.65
Total	100.11	99.71	100.05	100.40	100.45	100.50	99.96	100.36	100.20	100.18	99.69	99.34	99.72	99.70	99.72	99.50	99.98	99.97	99.61	99.53	99.58	100.36	98.79	99.74	99.33	99.14	98.94	99.99	98.99
Ba	74	80	82	104	114	94	89	90	96	85	77	81	80	108	92	89	85	94	91	93	98	163	124	26	35	33	24	42	<9<
Rb	3	3	4	4	4	4	4	3	4	5	5	3	4	4	4	3	4	3	4	4	4	20	19	5	69	39	45	30	4
Sr	9	1	4	4	2	6	2	2	2	3	3	<1<	3	2	2	1	1	1	1	2	4	141	206	14	311	301	388	303	24
Y	2	2	3	2	3	3	3	3	3	2	3	2	3	3	2	3	3	2	3	3	3	4	4	9	6	7	6	5	8
Zr	14	16	16	16	16	16	17	17	17	17	15	17	16	16	16	16	16	16	16	16	15	6	4	12	3	5	5	5	10
Nb	10	10	10	11	11	11	10	10	10	10	9	10	11	11	11	10	11	10	11	10	10	4	<1<	5	<1<	<1<	<1<	<1<	3
Th	2	3	3	3	3	3	3	3	3	3	3	3	3	3	3	3	3	3	3	3	3	<2<	3	3	2	<2<	2	<2<	3
Pb	18	18	19	20	22	20	19	21	21	22	23	21	22	20	23	20	22	20	21	19	19	14	10	19	9	7	9	8	16
Ga	3	2	2	3	2	3	4	3	3	4	4	3	3	3	2	3	2	2	2	4	4	5	7	7	10	13	11	12	9
Zn	43	48	45	42	57	56	49	40	44	39	39	45	49	63	37	51	47	44	43	48	57	43	37	54	47	42	49	41	62
Ni	1366	1445	1273	1419	1408	1375	1240	1350	1203	1272	1320	1233	1357	1440	1332	1341	1394	1310	1431	1478	1376	373	302	260	239	122	149	122	304
V	45	37	59	38	87	44	76	41	64	48	87	52	42	64	51	59	56	53	51	59	82	165	125	202	170	181	199	168	222
Cr	2929	2543	3766	2709	3667	3225	2635	2219	3602	2511	2951	3334	3010	3984	2684	3112	2543	2850	3451	3058	3564	1921	1189	1604	876	116	169	215	1517
Hf	<1<	<1<	<1<	<1<	<1<	<1<	<1<	<1<	<1<	<1<	<1<	<1<	<1<	<1<	<1<	<1<	<1<	<1<	<1<	<1<	<1<	<1<	<1<	<1<	<1<	<1<	<1<	<1<	<1<
Sc	31	33	45	42	66	35	72	32	64	46	62	57	30	55	25	65	27	41	43	31	43	76	47	65	42	35	32	34	52
Co	120	133	121	133	130	133	131	135	123	128	119	126	136	142	114	134	135	127	141	132	127	60	49	59	48	40	49	40	63
U	<2<	<2<	<2<	<2<	<2<	2	<2<	<2<	2	2	2	<2<	<2<	<2<	<2<	<2<	2	<2<	<2<	<2<	2	<2<	2	3	<2<	<2<	2	<2<	2
La	<4<	4	7	<4<	<4<	<4<	<4<	<4<	11	7	9	10	9	<4<	<4<	5	6	<4<	11	5	8	<4<	13	5	<4<	5	7	9	<4<
Ce	<3<	<3<	<3<	<3<	<3<	10	<3<	<3<	<3<	<3<	<3<	12	<3<	<3<	6	20	<3<	3	23	16	<3<	9	10	9	4	13	9	11	5
Nd	<4<	<4<	<4<	<4<	<4<	<4<	<4<	<4<	<4<	<4<	<4<	<4<	<4<	7	<4<	6	<4<	9	<4<	5	<4<	9	<4<	6	<4<	7	4	<4<	<4<

tFe_2O_3: total iron; LOI: loss on ignition

and large-ion lithophile elements (LIL) commonly attributed to alteration (Hart et al., 1974; Humphris and Thompson, 1978; Thompson, 1991). Therefore, the high field strength elements are utilized in order to define the petrologic features of the rocks.

Tectonites are the most depleted rocks and have composition characterized by low SiO_2 (38,1-40,2 wt%), Al_2O_3 (0,7-3,2 wt%), Fe_2O_3 (7,4-9,5 wt%), CaO (0-4,5 wt%), Sr (1-6 ppm), Ga (2-4 ppm), V (38-87 ppm), and high Ni (1203-1478 ppm) and Cr (2219-3984 ppm). Whereas the mafic cumulates is represented by high SiO_2 (45,9-51,8 wt%), Al_2O_3 (6,7-18,9 wt%), Fe_2O_3 (6,3-9,6 wt%), CaO (7,7-14,2 wt%), Sr (14-388 ppm), Ga (5-13 pmm), V (125-222 ppm), low Ni (122-373 ppm) and Cr (116-1921 ppm).

When we analyze the variations in major oxide values of the tectonites and mafic cumulates of the ophiolite sequence with respect to the MgO content (Figure 4a-d); SiO_2, Al_2O_3, CaO have a negative trend from tectonites to the mafic cumulates. The selected

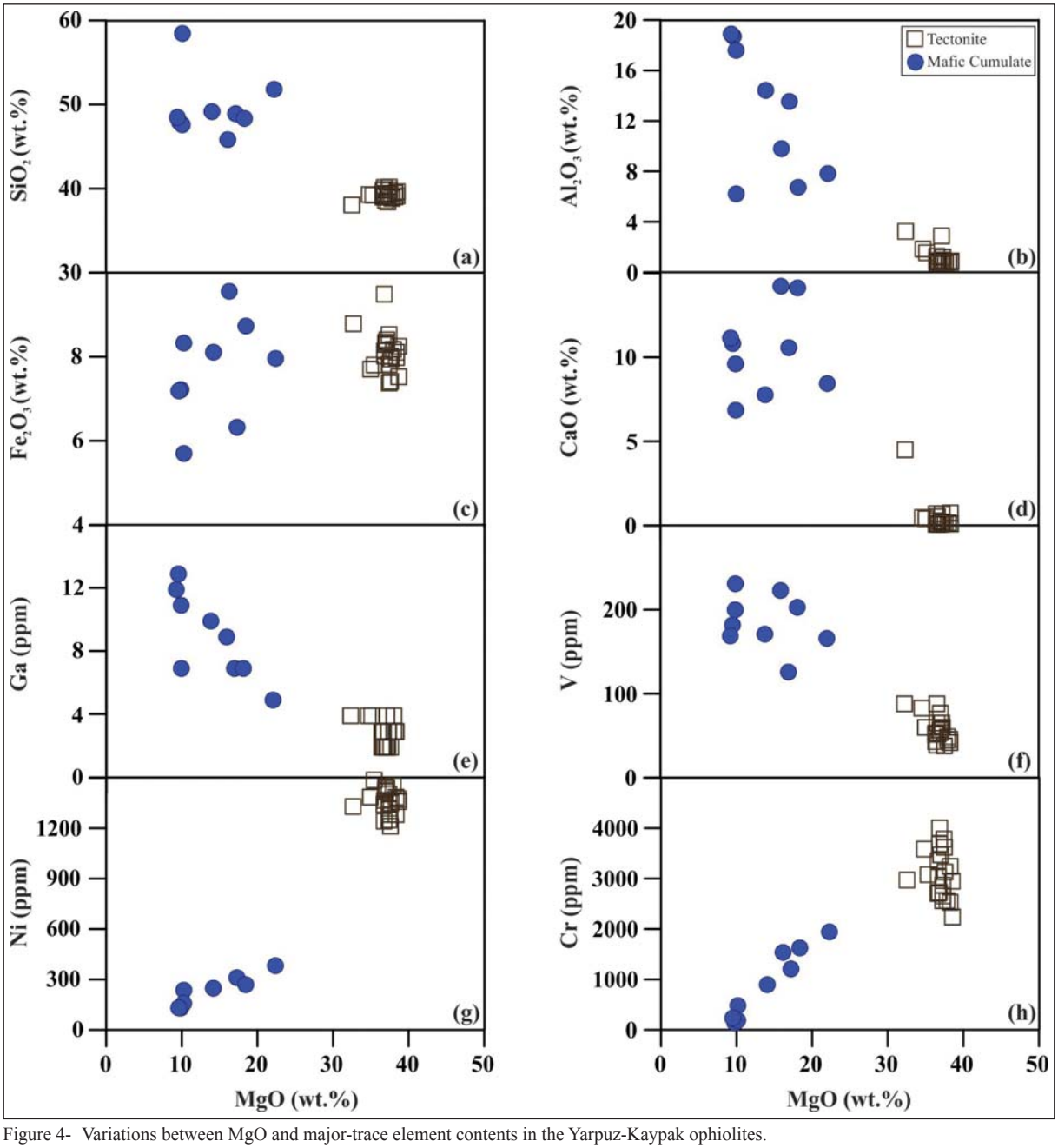

Figure 4- Variations between MgO and major-trace element contents in the Yarpuz-Kaypak ophiolites.

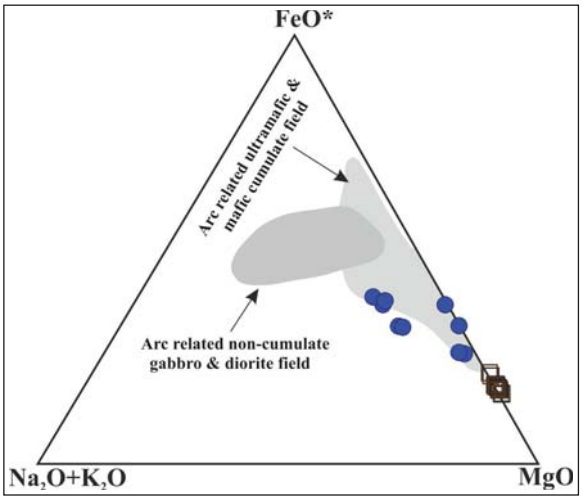

Figure 5- AFM diagram of mafic cumulates of Yarpuz-Kaypak ophiolites. Fields of cumulate and non-cumulate rocks are from Beard (1986). Symbols are as in figure 4.

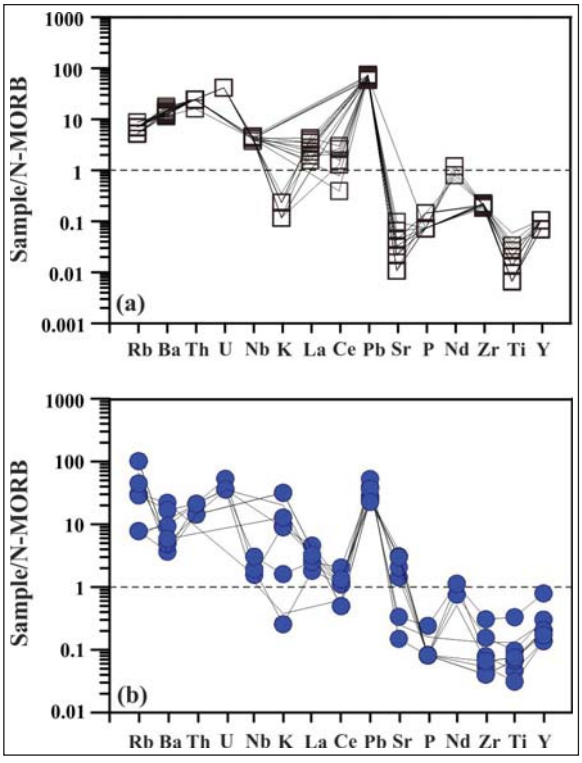

Figure 6- N-MORB normalized spider diagrams for the tectonites and mafic cumulates of Yarpuz-Kaypak ophiolites. Normalized values from Sun and McDonough, 1989. Symbols are as in figure 4.

trace elements such as Ga and V display a negative trend, whereas Ni and Cr display a positive trend with increasing MgO (Figure 4e-h). In AFM diagram (Beard, 1986), from mafic cumulates, there is an enrichment from MgO to FeO (Figure 5). N-MORB normalized spider diagrams for the tectonite and mafic cumulate rocks (Figure 6a-b) indicate that there is an enrichment in large ion lithophile (LIL) elements (Rb, Ba, Th) and depletion in high field strength (HFS) elements.

6. Discussion

6.1. Petrogenesis

The petrography and geochemistry of crustal rocks belonging to the ophiolite sequence observed in Yarpuz-Kaypak (Osmaniye) region indicate evidence of fractional crystallization. The increase in SiO_2, Al_2O_3 and CaO in mafic cumulate rocks (Figure 4a, b, d) shows that olivine and pyroxene minerals decrease while plagioclase mineral increases, due to magma differentiation. The Ga element shows a negative relationship with MgO (Figure 4e) since the Ga is incompatible in olivine. Existence of V in clinopyroxene (Ross et al., 1954; Borisenko, 1967; Ballantyne, 1992) is consistent with the higher amounts of V in mafic cumulates with respect to tectonites (Figure 4f); the Sr increasing in mafic cumulates (Table 1) suggests higher amount of plagioclase crystallization (Grove and Baker, 1984; Beard, 1986). The high content of compatible trace elements such as Ni, Cr within tectonites (Figure 4g-h) with respect to the lower content in mafic cumulates indicate that olivine, spinel and clinopyroxene fractionated in the studied rocks. All the cumulates with low content of HFS elements such as Zr, Y, Nb (Table 1), indicate high proportion of cumulus minerals and a small amount of intercumulus liquid, as supported by textural evidence. Furthermore the spider diagram of cumulate rocks suggests that the LIL elements (Rb, Ba, and Sr) have been enriched by hydrous solutions derived from a subducting oceanic slab (Pearce, 1982; Arculus and Powel, 1986; Yogodzinski et al., 1993; Wallin and Metcalf, 1998).

The geochemical features of the cumulate rocks belonging to the studied ophiolitic sequence (Figure 4, 5, 6) exhibit similarities with those of the Kızıldağ (Hatay) ophiolite cumulate gabbro formed in the supra-subduction zone fore-arc environment (Bağcı et al., 2005; Dilek and Thy, 2009), the ultramafic-mafic cumulates from the ophiolitic rocks of the south of Kahramanmaraş province (Bağcı, 2013; Tanırlı and Rızaoğlu, 2016), and the mafic cumulates of Kuluncak (Malatya) ophiolite (Camuzcuoğlu, et al., 2017). Moreover, the geochemical features of the mantle

tectonites exhibit close similarity to depleted residual mantle peridotites from suprasubduction zone (SSZ) settings (Uysal et al., 2012; Saka et al., 2014).

Ophiolites are commonly classified as mid-ocean ridge ophiolites (MORB) and supra-subduction zone (SSZ) ophiolites depending on their internal structures and composition, geochemical and tectonic features, (Pearce et al., 1984; Shervais, 2001; Robertson, 2002; Saccani and Photiades 2004; Arai et al., 2006; Pearce, 2008). Dilek and Furnes (2011) made a new classification of the ophiolites as subduction-related and non-subduction-related ophiolites; these authors classified the subduction-related ophiolites as subduction zone (SZ) and volcanic arc (VA) ophiolites, whereas classified the non-subduction-related ophiolites as continental margin (CM), mid-ocean ridge (MOR) and mantle plume (P) ophiolites. They also classified the supra-subduction zone ophiolites (SSZ) as back-arc (BA), fore-arc (FA), oceanic back-arc (OBA) and continental back-arc (CBA) ophiolites.

Supra-subduction zone ophiolites in general are formed in the first stages of the intra-ocean subduction. The crustal rocks of the supra-subduction zone ophiolites have the geochemical characteristics of island arcs. The distinct features are as follows: mantle series are highly depleted, there are more common presence of podiform chromite deposits, clinopyroxene crystallizes before plagioclase, wehrlite is relatively dominant compared to troctolite in the cumulate series. Most of the best preserved ophiolites in the orogenic belts are of the SSZ-type (Pearce et al., 1984). In SSZ-type ophiolites, clinopyroxene typically crystallizes before plagioclase (Pearce et al., 1984; Hébert and Laurent 1990; Parlak et al., 1996, 2000, 2002; Bağcı et al., 2005, 2006; Bağcı, 2013). The crystallization order of the minerals within the cumulate rocks in the Yarpuz-Kaypak (Osmaniye) region is clinopyroxene + orthopyroxene + plagioclase + amphibole, and exhibits the similarities with cumulate rocks formed in the supra-subduction zone environments.

In terms of their ages and geodynamic environment of formation, the ophiolites observed along the Alpine-Himalayan orogenic belt are divided into two groups, namely the Western and the Eastern Mediterranean ophiolites. In the Western Mediterranean, there are ophiolites remaining in the west of Albania, Hellenides and Dinarides. These ophiolites are of Jurassic age and formed in mid-ocean ridge settings (MORB) (Koller and Höck, 1990). In the Eastern Mediterranean belt, there are Pindos, Vourinos (Greece), Troodos (Cyprus) ophiolites, all ophiolites in Turkey, Baer-Bassit (Syria) and Oman ophiolites further towards southeast. The ophiolites in Turkey have a crystallization age of Late Cretaceous in general. However, it has been stated that there are ophiolites and metamorphic soles with Early-Middle Jurassic age in the central and eastern section of İzmir-Ankara-Erzincan Suture Zone (Çelik et al., 2011; Topuz et al., 2013; Robertson et al., 2013*a*). All of the Turkish ophiolites formed in a variety of tectonic settings within a SSZ environment, including back-arc, arc and fore-arc. There does not exist any MORB-type ophiolite body in the Turkish part of the eastern Mediterranean region. Most MORB-type oceanic crust was subducted, or preserved only as dismembered thrust sheets or blocks in ophiolitic mélange (Robertson, 2002). Recent studies performed on mantle rocks of ophiolites in southwest Turkey have shown that compositions of mantle rocks from different tectonic environments are the results of different styles of depletion and refertilization events and varying degrees of partial melting (Aldanmaz et al., 2009; Aldanmaz, 2012; Uysal et al., 2012).

Except for one rock (T-31), the fact that the mantle tectonites in the study area have quite low CaO and Al_2O_3 values indicates the relationship with Ca depletion during serpentinization process (Coleman, 1963; Puga et al., 1999; Li et al., 2004; Palandri and Reed 2004; Shervais et al., 2005). On this diagram (Figure 7a) the studied rocks are very depleted in Al_2O_3 and CaO and similar to fore-arc peridotites (Ishii et al., 1992; Pearce et al., 1992). Abyssal peridotites formed by the extraction of relatively low melt fractions (3-15%) under dry melting conditions (Dick and Bullen, 1984; Johnson et al., 1990; Niu, 1997, 2004; Jean et al., 2010) while peridotites from the mantle wedge above subduction zones are depleted, and formed by the extraction of relatively large melt fractions (> 20%) in hydrous melting conditions (Ishii et al., 1992; Parkinson et al., 1992; Arai, 1994; Parkinson and Pearce, 1998; Pearce et al., 2000; Uysal et al., 2012). The partial melting trend (Niu, 1997) and the Al_2O_3 and MgO contents of tectonites are shown in figure 7b. It has been observed that most of the samples are the remnants of 15-25% partial melting compared to the primary mantle. The low MgO content of the tectonites is related to the MgO depletion by the alteration caused by the sea water (Niu, 2004). Low CaO and Al_2O_3 values (Table 1) of the tectonites of the Yarpuz-Kaypak (Osmaniye) region show that

tectonite samples are partially the remnants of high-grade partial melting, and resemble to the subduction-related fore-arc peridotites (Parkinson and Pearce, 1998). With these features, mantle peridotites of the study area represent similarities with mantle rocks of Pozantı-Karsantı ophiolite in the South Turkey (Saka et al., 2014).

According to the AFM diagram (Beard, 1986), the mafic cumulate rocks display enrichment from MgO to FeO and plot within the field of arc-related ultramafic-mafic cumulate rocks, suggesting their subduction related origin (Figure 5).

Existence of plagioclases with high An content in the mafic cumulates indicates high water vapor pressure (P-H_2O) (Arculus and Wills, 1980; Sisson and Grove, 1993; Panjasawatwong et al., 1995) and large Ca/(Ca+Na) ratio in the magma during crystallization (Jaques, 1981; Sisson and Grove, 1993). The formation of amphibole mineral in the hydrous magmas conditions of the arc regions is a likely process (Jakes and White, 1972; Arculus and Wills, 1980; Foden, 1983; Hébert and Laurent, 1990). The presence of amphibole and An-rich plagioclase in the mafic cumulates of Yarpuz-Kaypak (Osmaniye) region indicate hydrous environment during the oceanic crust development, and represent similarities to supra-subduction zone ophiolites of Eastern Mediterranean (Hébert and Laurent, 1990; Parlak et al., 1996, 2000; Bağcı et al., 2005, 2006; Rızaoğlu et al., 2006; Sarıfakıoğlu et al., 2009; Bağcı, 2013; Tanırlı and Rızaoğlu, 2016; Camuzcuoğlu et al., 2017) and gabbroic rocks of island arcs (Arculus and Wills 1980; Dupuy et al., 1982; Beard, 1986; Debari and Coleman, 1989; Fujimaki, 1986; DeBari et al., 1987).

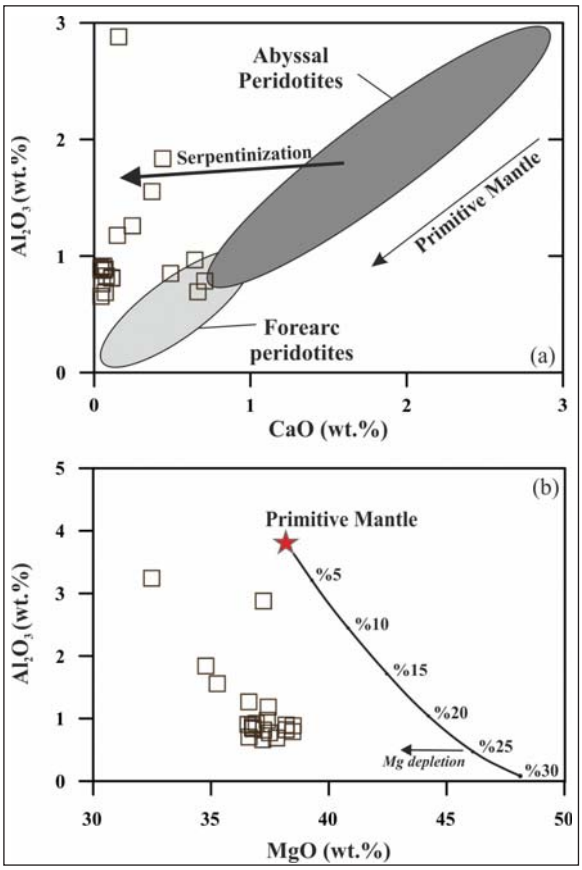

Figure 7- (a) Variations of whole rock Al_2O_3 contents with respect to CaO contents in all tectonites of Yarpuz-Kaypak ophiolitic sequence; the fields of abyssal and fore-arc peridotites and mantle depletion trend have been taken from Ishii et al. (1992) and Pearce et al. (1992). (b) Variations of whole rock Al_2O_3 contents with respect to CaO contents; the depletion trend of the primitive mantle and partial melting have been taken from Niu (1997). Symbols are as in figure 4.

6.2. Geodynamic Environment

Depending on the spreading of South Atlantic Ocean at the end of Early Cretaceous, the regime in the Neotethys oceanic basin situated between Eurasian and African plates shifted from divergent to convergent regime (Livermoore and Smith, 1984; Savostin et al., 1986). As a result of this convergent regime, a northward subduction started in the southern branch of the Neotethys. Cold and dense Triassic-Cretaceous aged oceanic lithosphere segment subducted northward into asthenosphere and enabled the formation of SSZ-type ophiolites within the intra-ocean subduction zone. Two ophiolite belts, namely the southern and northern belts, trending about NE-SW are presently observed in the Southeast Anatolia. The south belt includes Troodos (South Cyprus), Baer-Bassit (Syria), Tekirova (Antalya), Kızıldağ (Hatay), Amanos (Osmaniye), Koçali (Adıyaman) ophiolites. These ophiolites were formed at Southern Neotethys between Bitlis-Pütürge metamorphic and Arabian platform (Figure 8). The northern belt includes Göksun (Kahramanmaraş), İspendere (Malatya), Kömürhan and Guleman (Elazığ) ophiolites. These ophiolites were formed in the Berit Ocean which was developed between Bitlis-Pütürge and Tauride platform (Figure 8) (Robertson et al., 2012, 2013*a*; Karaoğlan et al., 2013*b*). Although the ophiolites of both belts were formed at intra-ocean subduction zones, they represent differences in terms of tectonic relationship, ophiolite stratigraphy, petrography and petrologic features (Parlak et al., 2009). The northern belt ophiolites are tectonically overlain by the Tauride (Malatya-Keban)

platform at the top and in turn overthrust Middle Eocene Maden Complex at the bottom contact. Moreover, the northern belt ophiolites and theTauride platform were cut by Late Cretaceous-Eocene I-type calk-alkaline arc granitoids (Parlak, 2006; Rızaoğlu et al., 2009; Karaoğlan et al., 2016; Nurlu et al., 2016). The Kızıldağ (Hatay), Koçali (Adıyaman) and Baer-Bassit (Syria) ophiolites of the southern belt are directly emplaced over the Arabian Platform and no granitoid intrusion is seen (Selçuk, 1981; Robertson, 1986). The Bitlis metamorphic massif, which shows widespread outcrops in the southern of northern belt ophiolites, carries the traces of high pressure-low temperature (HP/LT) metamorphism.The Kesandere (Bitlis) eclogitic rocks underwent HP peak metamorphism in Late Cretaceous (84.4±0.9 – 82.4±0.9 My) under the conditions of 19-24 kbar and 480-540°C (Oberhansli, 2013). Furthermore, glaucophane-rich blueschist rocks have undergone (HP/LT) metamorphism in Late Cretaceous (Ar-Ar: 79-74 My) under 10-11 kbar and 350-400°C (Oberhanslı et al., 2012). This data indicates that the Bitlis metamorphics had undergone subduction and HP/LT metamorphism in Late Cretaceous age. Therefore, some researchers have suggested that there might be development of two different oceanic basins (the Berit ocean and the

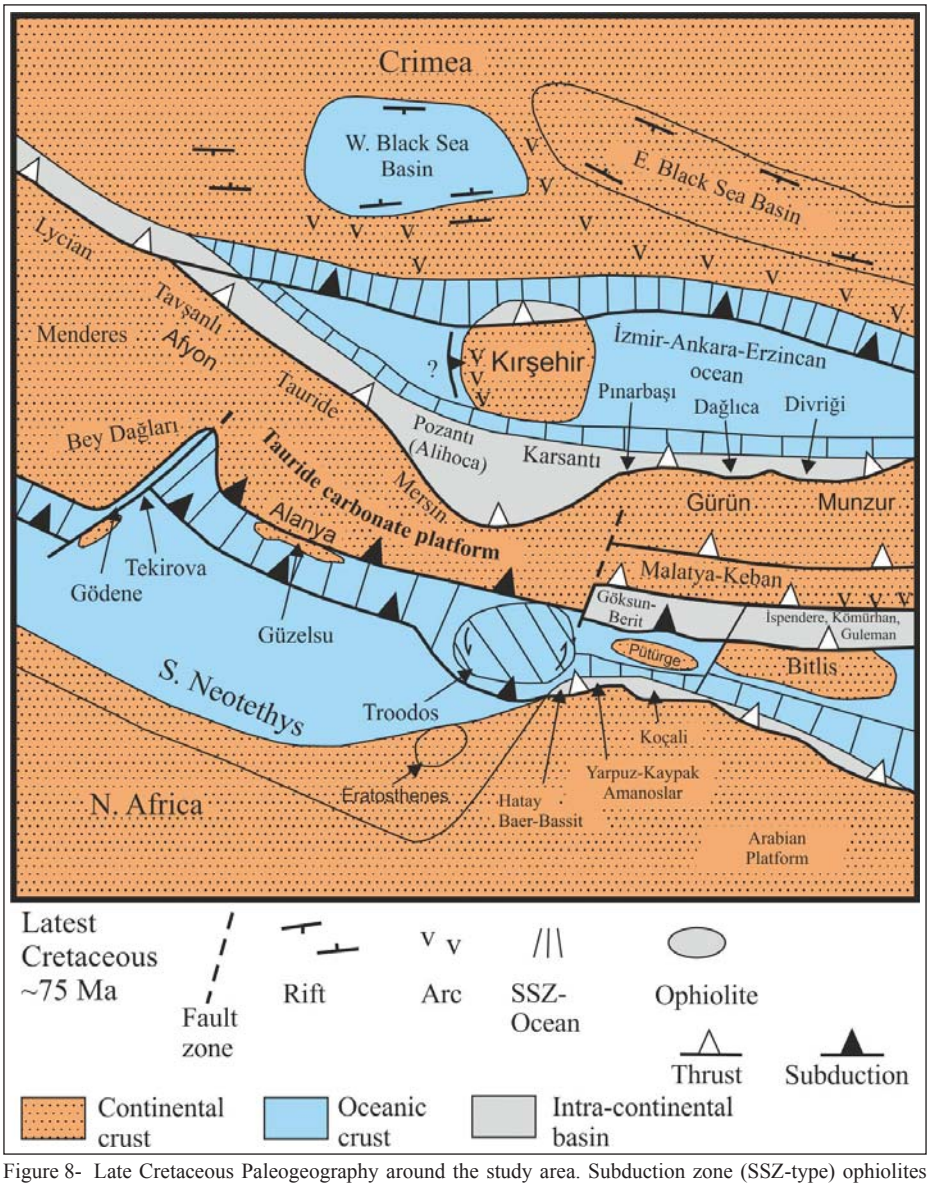

Figure 8- Late Cretaceous Paleogeography around the study area. Subduction zone (SSZ-type) ophiolites emplaced on the passive continental margin to the south (Arabian platform and microcontinents). On the other hand, arc volcanism accompanying the subduction is seen in Pontides, Southeast Turkey and North Cyprus (Robertson et al., 2012).

Southern Neotethys ocean) to the northbetween Bitlis/Pütürge continent and the Tauride platform and to the south between Bitlis/Pütürge continent and the Arabian platform (Robertson et al., 2012, 2013*a*).

Our results, in addition to general models for the life cycle of ophiolites (Shervais, 2001; Pearce, 2003) and a number of tectonic models related to the southeast Anatolian orogen (Yazgan and Chessex, 1991; Yılmaz et al., 1993; Beyarslan and Bingöl, 2000; Robertson et al., 2007) point that Yarpuz-Kaypak (Osmaniye) ophiolites in Amanos Mountains were formed in a supra-subduction zone environment and emplaced onto the passive continental margin of Arabian plate from the southern branch of Neotethys during Late Cretaceous.

7. Conclusions

(a) Yarpuz-Kaypak (Osmaniye) ophiolites are represented by harzburgitic mantle tectonites and mafic cumulate rocks.

(b) Mafic cumulates are composed of gabbronorite and gabbro; displaying adcumulate, mesocumulate and poikilitic textures.

(c) Major and trace element geochemistry of the harzburgitic tectonites and mafic cumulates indicate an intra-oceanic subduction-related setting.

(d) The petrographic and geochemical data obtained from this study suggest that Yarpuz-Kaypak (Osmaniye) ophiolites were formed in an intra-ocean subduction zone during closure of southern branch of Neotethys during Late Cretaceous and emplaced onto the northern margin of Arabian platform.

Acknowledgement

We thank to Fabio Capponi (Geneva University) who conducted the geochemical analysis. We also thank to Prof. Dr. Mehmet Arslan, Dr. Paola Tartarotti (Universita Degli Studi Di Milano) and other anonymous referee due to their valuable contributions. We also thank editor Prof. Dr. Taner Ünlü for handling the manuscript.

References

Aldanmaz, E. 2012. Trace element geochemistry of primary mantle minerals in spinel-peridotites from polygenetic MOR–SSZ suites of SW Turkey: constraints from an LA-ICP-MS study and implications for mantle metasomatism. Geological Journal, 47, 59–76.

Aldanmaz, E., Schmidt, M.W., Gourgaud, A., Meisel, T. 2009. Mid-ocean ridge and suprasubduction geochemical signatures in spinel–peridotites from the Neotethyan ophiolites in SW Turkey: implications for upper mantle melting processes. Lithos, 113, 691–708.

Alparslan, G., Dilek, Y. 2018. Seafloor spreading structure, geochronology and tectonic evolution of the Küre ophiolite, Turkey: A Jurassic continental backarc basin oceanic lithosphere in southern Eurasia. Lithosphere, 10, 14–34.

Arai, S. 1994. Characterization of spinel peridotites by olivine-spinel compositional relationships, review and interpretation. Chemical Geology 113, 191–204.

Arai, S., Kadoshima, K., Morishita, T. 2006. Widespread arc-related melting in the mantle section of the northern Oman ophiolite as inferred from detrital chromian spinels. Journal of the Geological Society of London, 163, 1–11.

Arculus R.J., Powell R. 1986. Source component mixing in the regions of arc magma generation. The Journal of Geophysical Research, 91: 5913–5926.

Arculus, R.J., Wills, K.J.A. 1980. The petrology of plutonic blocks and inclusions from Lesser Antilles island arc. Journal of Petrology, 21: 743–799.

Atan, R. O. 1969. Eğribucak-Karacaören (Hassa)-Ceyhanlı-Dazevleri (Kırıkhan) arasındaki Amanos dağlarının jeolojisi: Maden Tetkik ve Arama Genel Müdürlüğü Yayını No: 139, 85 s.

Bağcı U. 2013. The geochemistry and petrology of the ophiolitic rocks from the Kahramanmaraş region, southern Turkey. Turkish Journal Earth Sciences, 22: 536–562.

Bağcı, U., Parlak, O. 2009. Petrology of the Tekirova (Antalya) ophiolite (Southern Turkey): Evidence for diverse magma generations and their tectonic implications during Neotethyan-subduction. International Journal of Earth Sciences, 98: 387–405.

Bağcı, U., Parlak, O., Höck, V. 2005. Whole rock and mineral chemistry of cumulates from the Kızıldağ (Hatay) ophiolite (Turkey): clues for multiple magma generation during crustal accretion in the sourhern Neotethyan ocean. Mineralogical Magazine, 69: 39–62.

Bağcı, U., Parlak, O., Höck, V. 2006. Geochemical character and tectonic environment of ultramafic to mafic cumulates from the Tekirova (Antalya) ophiolite (southern Turkey). Geological Journal, 41: 193-219.

Bağcı, U., Parlak, O., Höck, V. 2008. Geochemistry and tectonic environment of diverse magma generations forming the crustal units of the

Kızıldağ (Hatay) ophiolite southern Turkey. Turkish Journal of Earth Sciences, 17: 43–71.

Ballantyne, P. 1992. Petrology and geochemistry of the plutonic rocks of the Halmahera ophiolite, eastern Indonesia, an analogue of modern oceanic forearcs. *In:* Parson Lm, Murton Bj., Browning P (eds), Ophiolites and Their Modern Oceanic Analogues. Geological Society, London, Special Publication, 60, 179–202.

Beard, J.S. 1986. Characteristic mineralogy of arc-related cumulate gabbros: implications for the tectonic setting of gabbroic plutons and for andesite genesis. Geology, 14: 848-851.

Beyarslan, M., Bingöl, A.F. 2000. Petrology of a supra-subduction zone ophiolite (Elazığ, Turkey). Canadian Journal of Earth Sciences, 37: 1411–1424.

Borisenko, L.F. 1967. Trace elements in pyroxenes and amphiboles from ultramafic rocks of the Urals. Mineralogical Magazine, 36, 403–410.

Boulton, S.J., Robertson, A. H. F., Ünlügenç, U.C. 2006. Tectonic and sedimentary evolution of the Cenozoic Hatay Graben, Southern Turkey: a two-phase model for graben formation, foreland basin then transtensional basin model. In: Robertson, A.H.F., Mountrakis, D. (Eds.), Tectonic Evolution of the Eastern Mediterranean. Geological Society, London, Special Publications, 260, 613-634.

Camuzcuoğlu, M., Bağcı, U., Koepke, J.Wolff, P. 2017. Tectonic significance of the cumulate gabbros within Kuluncak ophiolitic suite (Malatya, SE Turkey) inferred from geochemical data. Ofioliti, 42, 81-103.

Coleman, R.G. 1963. Serpentinites, Rodingites, and Tectonic Inclusions in Alpine-type Mountain Chains, Geological Society of America, Special Papers, vol. 73.

Çelik, Ö.F., Delaloye, M.F. 2003. Origin of metamorphic soles and their post-kinematic mafic dyke swarms in the Antalya and Lycian ophiolites, SW Turkey. Geological Journal, 38, 235–256.

Çelik, Ö.F., Delaloye, M.F. 2006. Characteristics of ophiolite-related metamorphic rocks in the Beyşehir ophiolitic mélange (Central Taurides, Turkey), deduced from whole rock and mineral chemistry. Journal of Asian Earth Sciences, 26, 461–476.

Çelik, O.F., Marzoli, A., Marschik, R., Chiaradia, M. 2011. Early-Middle Jurassic intra-oceanic subduction in the İzmir-Ankara-Erzincan ocean, northern Turkey. Tectonophysics, 509, 120-134.

Çoğulu, H.E. 1975. Hatay Ultramafitlerinin Jeolojisi ve Petrolojisi. Proje TBAG-62 (Tübitak), Turkey, 90 p.

DeBari, S.M., Coleman, R.G. 1989. Examination of the deep levels of an island arc: evidence from the Tonsina ultramafic-mafic assemblage, Tonsina, Alaska. Journal of Geophysical Research, 94: 4373–4391.

DeBari, S.M., Kay, S.M., Kay, R.W. 1987. Ultramafic xenoliths from Adagdak volcano, Adak, Aleutian Islands, Alaska: deformed igneous cumulates from the Moho of an island arc. Journal of Geology, 95: 329–341.

Delaloye, M., Pişkin, Ö., Selçuk, H., Vuagnat, M., Wagner, J.J. 1980. Geological Section Through the Hatay Ophiolite along the Mediterranean Coast, Southern Turkey. Ofioliti, 5 (2/3), 205-216.

Dick, H.J.B., Bullen, T. 1984. Chromium spinel as a petrogenetic indicator in abyssal and Alpine-type peridotites and spatially associated lavas. Contributions to Mineralogy and Petrology 86, 54–76.

Dilek, Y., Moores, E.M. 1990. Regional tectonics of the eastern Mediterranean ophiolites. In: Malpas. J., Moores, E., Panayiotou, A. & Xenophontos, C. (eds), Proceeding of Troodos Ophiolite Symposium. Cyprus Geological Survey Department 295–309.

Dilek, Y., Flower, M.F.J. 2003. Arc-trench rollback and forearc accretion: 2. A model template for ophiolites in Albania, Cyprus, and Oman. In: Ophiolites in Earth History, Dilek, Y., Robinson, P.T. (eds). Geological Society, London, Special Publications, 218: 43–68.

Dilek, Y., Thy, P. 2006. Age and petrogenesis of plagiogranite intrusions in the Ankara mélange central Turkey. Island Arc, 15, 44-57.

Dilek, Y., Thy, P. 2009. Island arc tholeiite to boninitic melt evolution of the Cretaceous Kızıldağ (Turkey) ophiolite: Model for multi-stage early arc–forearc magmatism in Tethyan subduction factories. Lithos, 113: 68–87.

Dilek, Y., Furnes, H. 2011. Ophiolite genesis and global tectonics: Geochemical and tectonic fingerprinting of ancient oceanic lithosphere. Geological Society of America Bulletin, 123, 387–411.

Dilek, Y., Thy, P., Hacker, B., Grundvig, S. 1999. Structure and petrology of Tauride ophiolites and mafic dyke intrusions (Turkey): implications for the Neotethyan ocean. Geological Society of America Bulletin, 111: 1192-1216.

Dilek, Y., Furnes, H., Shallo, M. 2008. Geochemistry of the Jurassic Mirdita ophiolite (Albania) and the MORB to SSZ evolution of a marginal basin oceanic crust. Lithos, 100, 174-209.

Dubertret, L. 1955. Géologie des roches vertes du nord-ouest de la Syrie et du Hatay (Turquie). Notes Mémoires Moyen-Orient, 6, 227.

Dupuy, C., Dostal, J., Marcelot, G., Bougault, H., Joron, J.L., Treuil, M. 1982. Geochemistry of basalt from central and southern New Hebrides arc: Implications for their source rock composition. Earth Planet Science. Letter., 60: 207-225.

Floyd, P.A., Winchester, J.A. 1978. Identification and discrimination of altered and metamorphosed volcanic rocks using immobile elements. Chemical Geology, 21: 291-306.

Floyd, P.A., Göncüoğlu, M.C., Winchester, J.A., Yalınız, M.K. 2000. Geochemical character and tectonic environment of Neotethyan ophiolitic fragments and metabasites in the Central Anatolian Crystalline Complex, Turkey. Pp. In Tectonics and Magmatism in Turkey and the Surroundings Area, Bozkurt, E., Winchester, J.A., Piper, J.D.A. (eds). Geological Society, London, Special Publications, 173: 183-202

Foden, J.D. 1983. The petrology of calcalkaline lavas of Rindjani volcano, East Sunda Arc: Model for island arcs. Journal of Petrology, 24:98-130.

Fujimaki, H. 1986. Fractional crystallization of the basaltic suite of Usu volcano, southwest Hokkaido, Japan, and its relationships with the associated felsic suite. Lithos, 19: 129–140.

Göncüoğlu, M., Turhan, N., Şentürk, K., Özcan, A., Uysal, S. 2000. A geotraverse across NW Turkey: tectonic units of the Central Sakarya region and their tectonic evolution. In: Bozkurt, E., Winchester, J.A., Piper, J.D. (Eds.), Tectonics and Magmatism in Turkey and the Surrounding Area. Geological Society, London Special Publication, 173, 139–162.

Göncüoğlu, M.C., Çapkınoğlu, Ş., Gürsu, S., Noble, P., Turhan, N., Tekin, U.K., Okuyucu, C.,Göncüoğlu, Y. 2007. The Mississippian in the Central and Eastern Taurides (Turkey): constraints on the tectonic setting of the Tauride–Anatolide Platform. Geologica Carpathica, 58, 427–442.

Görür, N., Oktay, F.Y., Seymen, I., Şengör, A.M.C. 1984. Paleotectonic evolution of Tuz Gölü Basin complex, central Turkey. In: Dixon, J.E., Robertson, A.H.F. (eds.), The Geological Evolution of the Eastern Mediterranean. Geological Society, London, Special Publications, 17, 81–96.

Grove, T.L., Baker M.B. 1984. Phase equilibrium controls on the tholeiitic versus calc-alkaline differentiation trends. Journal of Geophysical Research, 89, 3253–3274.

Gül, M. 1987. Kahramanmaraş bölgesinin jeolojisi ve petrol olanakları. TPAO Report No. 2359, Ankara.

Hart, S.R., Erlank, A.J., Kable, E.J.D. 1974. Sea floor basalt alteration: some chemical and Sr isotopic effects. Contributions to Mineralogy and Petrology, 44: 219-230.

Hébert, R., Laurent, R. 1990. Mineral chemistry of the plutonic section of the Troodos ophiolite: New constraints for genesis of arc-related ophiolites. In Proceedins of Troodos Ophiolite Symposium, Malpas, J., Moores, E., Panayiotou, A., Xenophontos, C. (eds). Cyprus Geological Survey Department: 149–163.

Humphris, S.E., Thompson, G. 1978. Trace element mobility during hydrothermal alteration of oceanic basalts. Geochimica et Cosmochimica Acta, 42, 127–136.

Ishii, T., Robinson, P.T., Maekawa, H., Fiske, R. 1992. Petrological studies of peridotites from diapiric serpentinite seamounts in the Izu-Ogasawara-Mariana Forearc, Leg 125. In: Fryer, P., Pearce, J.A., Stokking, L.B., (eds.), Proceedings of the Ocean Drilling Program, Scientific Results, College Station, TX (Ocean Drilling Program), 125, 445-485.

Jakes, P., White, A.J.R. 1972. Hornblendes from calcalkaline volcanic rocks of island arcs and continental margins. American Mineralogist, 57, 887–902.

Jaques, A.L. 1981. Petrology and petrogenesis of cumulate peridotite and gabbro from the Marum ophiolite complex, northern Papau-New Guinea. Journal of Petrology, 22: 1-40.

Jean, M.M., Shervais, J.W., Choi, S.H., Mukasa, S.B. 2010. Melt extraction and melt refertilization in mantle peridotite of the Coast Range ophiolite: an LA–ICP–MS study. Contributions to Mineralogy and Petrology 159, 113–136.

Johnson, K.T.M., Dick, H.J.B., Shimizu, N. 1990. Melting in the oceanic upper mantle: an ion microprobe study of diopsides in abyssal peridotites. Journal of Geophysical Research 95, 2661–2678.

Karaoğlan, F., Parlak, O., Klötzli, U., Thöni, M., Koller, F. 2012. U-Pb and Sm-Nd geochronology of the ophiolites from the SE Turkey: Implications for the Neotethyan evolution. Geodinamica Acta, 25, 146-161.

Karaoğlan, F., Parlak, O., Klötzli, U., Thöni, M., Koller, F. 2013*a*. U-Pb and Sm-Nd geochronology of the Kızıldag (Hatay, Turkey) ophiolite: implications for the timing and duration of suprasubduction zone type oceanic crust formation in southern Neotethys. Geological Magazine, 283–299.

Karaoğlan, F., Parlak, O., Klötzli, U., Koller, F., Rızaoğlu, T. 2013*b*. Age and duration of intra-oceanic arc volcanism built on a suprasubduction zone type oceanic crust in southern Neotethys, SE Anatolia. Geoscience Frontiers, 4, 399-408.

Karaoğlan, F., Parlak, O., Hejl, E., Neubaver, F., Kloetzli, U. 2016. The temporal evolution of the active margin along the Southeast Anatolian Orogenic Belt (SE Turkey): Evidence from U-Pb, Ar-Ar and fission track chronology. Gondwana Research, 33, 190-208.

Koglin, N. 2008. Geochemistry, petrogenesis and tectonic setting of ophiolites and mafic-ultramafic complexes in the Northeastern Aegean region: New trace-element, isotopic and age constraints. PhD thesis, University of Mainz, Germany.

Koglin, N., Kostopoulos, D., Reichmann, T. 2009. Reichmann, Geochemistry, petrogenesis and tectonic setting of the Samothraki mafic suite, NE Greece: Trace-element, isotopic and zircon age constraints. Tectonophysics, 473, 53-68.

Koller, F., Höck, V. 1990. Mesozoic Ophiolites in the Eastern Alps. In: Malpas, J., Moores, E., Panayiotou, A. and Xenophontos, C. (eds.) Ophiolites-Oceanic Crustal Analogues. Proceedings of Troodos Ophiolite Symposium-1987, 253-263.

Konstantinou, A., Wirth, K.R., Vervoort, J. 2007. U-Pb isotopic dating of Troodos plagiogranite, Cyprus by LA-ICP-MS. Geological Society of America, Annual Meeting, Denver, CO, 28, p31.

Li, X-P., Rahn, M., Bucher, K. 2004. Metamorphic processes in rodingites of the Zermatt–Saas ophiolites, International Geology Review, 2004, 46, 28-51.

Liati, A., Gebauer, D., Fanning, M. 2004. The age of ophiolitic rocks of the Hellenides (Vourinos, Pindos, Crete): First U-Pb ion microprobe (SHRIMP) zircon ages. Chemical Geology, 207, 171-188.

Livermore, R.A., Smith, A.G. 1984. Some boundary conditions for the evolution of the Mediterrannean Region. In Geological Evolution of the Mediterranean Basin, Stanley, D.J., Wezel, F.C. (eds). Springer-Verlag: Berlin; 83–100.

Mukasa, S.B., Ludden, J.N. 1987. Uranium-lead ages of plagiogranites from the Troodos ophiolite, Cyprus, and their tectonic significance. Geology, 5, 825-828.

Niu, Y. 1997. Mantle melting and melt extraction processes beneath ocean ridges: Evidence from abyssal peridotites. Journal of Petrology, 38, 1047–1074.

Niu, Y. 2004. Bulk–rock major and trace element composition of abyssal peridotites, implications for mantle melting, melt extraction and post–melting processes beneath Mid–ocean Ridges. Journal of Petrology, 45, 2423–2458.

Nurlu, N., Parlak, O., Robertson, A.H.F., Quadt, A.V. 2016. Implications of Late cretaceous U-Pb zircon ages of granitic intrusions cutting ophiolitic and volcanogenic rocks for the assembly of the Tauride allochthon in SE Anatolia (Helete area, Kahramanmaraş Region, SE Turkey). International. Journal Earth Sciences (Geol. Rundsch), 105:283-314.

Oberhansli, R. 2013. High-pressure-low-temperature evolution in the Indus-Tsangpa suture along the Kohistan are (Kaghan Valley, NF. Pakistan). Episodes, 36(2), 87-93.

Oberhansli, R., Bousquet, R., Candan, O., Okay, A.I. 2012. Dating subduction event in East Anatolia. Turkish Journal Earth Sciences, 21:1-17.

Okay, A.I. 2000. Was the Late Triassic orogeny in Turkey caused by the collision of an oceanic plateau? In: Bozkurt, E., Winchester, J.A., Piper, J.D.A. (eds.), Tectonics and Magmatism in Turkey and Surrounding Area. Geological Society, London, Special Publications, 173, 25–41.

Palandri, J.L., Reed, M.H. 2004 Geochemical models of metasomatism in ultramafic systems: Serpentinization, rodingitization, and sea floor carbonate chimney precipitation, Geochimica et Cosmochimica Acta, 2004, 68, 1115-1133.

Panjasawatwong, Y., Danyushevsky, L.V., Crawford, A.J., Haris, K.L. 1995. An experimental study of the effects of melt composition on plagioclase-melt equilibria at 5 and 10 kbars: implications for the origin of magmatic high-An plagioclase. Contributions to Mineralogy and Petrology, 11: 420–432.

Parkinson, I.J., Pearce, J.A. 1998. Peridotites from the Izu-Bonin-Mariana forearc (ODP Leg 125), evidence for mantle melting and melt–mantle interaction in a suprasubduction zone setting. Journal of Petrology, 39, 1577–1618.

Parkinson, I.J., Pearce, J.A., Thirlwall,M.F., Johnson, K.T.M., Ingram, G. 1992. Trace element geochemistry of peridotites from the Izu–Bonin–Mariana forearc, Leg 125. In: Fryer, P., Pearce, J.A., Stokking, L.B., et al. (Eds.), Proceedings of the Ocean Drilling Program Scientific Results, 125. Ocean Drilling Program, College Station, TX, pp. 487–506.

Parlak, O. 2006. Geodynamic significance of granitoid magmatism in southeast Anatolia: geochemical and geochronogical evidence from Göksun-Afşin (Kahramanmaraş, Turkey) region. International Journal Earth Sciences (Geol. Rundsch), 95:609-627.

Parlak, O., Delaloye, M., Bingöl, E. 1996. Mineral chemistry of ultramafic and mafic cumulates as an indicator

of the arc-related origin of the Mersin ophiolite (Southern Turkey). Geologische Rundschau, 85: 647–661.

Parlak, O., Höck, V, Delaloye, M. 2000. Suprasubduction zone origin of the Pozantı-Karsantı ophiolite (southern Turkey) deduced from whole-rock and mineral chemistry of the gabbroic cumulates. In Tectonics and Magmatism in Turkey and the Surroundings Area, Bozkurt, E., Winchester, J.A., Piper, J.D.A. (eds). Geological Society, London, Special Publications, 173: 219–234.

Parlak, O., Höck, V., Delaloye, M. 2002. The suprasubduction zone Pozantı-Karsantı ophiolite, southern Turkey: evidence for high-pressure crystal fractionation of ultramafic cumulates. Lithos, 65: 205–224.

Parlak, O., Rızaoğlu, T., Bağcı, U., Karaoğlan, F., Höck, V. 2009. Tectonic significance of the geochemistry and petrology of ophiolites in southeast Anatolia, Turkey. Tectonophysics, 473: 173–187.

Parlak, O., Karaoğlan F., Rızaoğlu, T., Klötzli, U., Koller, F., Billor, Z. 2013. U-Pb And Ar-40-Ar-39 Geochronology of the ophiolites and granitoids from the Tauride Belt: Implications for the evolution of the Inner Tauride Suture, Journal Of Geodynamics, vol.65, pp. 22-37.

Parrot, J.F. 1973. Petrologie de la Coupe du Djebel Moussa Massif Basique-Ultrabasique du Kızıldağ (Hatay-Turquie). Sci. De la Tere, t XVIII, 2, 143-172.

Pearce, J.A., 1982. Trace element characteristics of lavas from destructive plate boundaries. In: R.S. Thorpe (Editor), Andesites. New York. John Wiley & Sons., 525–48.

Pearce, J.A. 2003. Supra-subduction zone ophiolites: The search for modern analogues. In Ophiolite concept and the evolution of geological thought. In: Dilek, Y., Newcomb, S. (eds). Geological Society of America Special Paper, 373: 269–293.

Pearce, J.A. 2008. Geochemical fingerprinting of oceanic basalts with applications to ophiolite classification and the search for Archean oceanic crust. Lithos, 100, 14–48.

Pearce, J.A., Cann, J.R. 1973. Tectonic setting of basaltic volcanic rocks determined using trace element analysis. Earth Planet Science Letters, 19: 290–300.

Pearce, J.A., Lippard, S.J., Roberts, S. 1984. Characteristics and tectonic significance of supra-subduction zone ophiolites. In Marginal Basin Geology, Kokelaar, B.P., Howells, M.F. (eds). Geological Society, London, Special Publications, 16: 77–89.

Pearce, J.A., van der Laan, S.R., Arculus, R. J., Murton, B. J., Ishii, T., Peate, D.W., Parkinson, I.J. 1992. Boninite and harzburgite from LEG125 (Bonin–Mariana Forearc): a case study of magma genesis during the initial stages of subduction. In: Fryer P, Pearce JA, Stokking LB (eds) Proceedings of the Ocean Drilling Program, Scientific Results, Ocean Drilling Program, College Station, 125, 623–657.

Pearce, J.A., Barker, P.F., Edwards, S.J., Parkinson, I.J., Leat, P.T. 2000. Geochemistry and tectonic significance of peridotites from the South Sandwich Arc-basin Systems, South Atlantic. Contributions to Mineralogy and Petrology 139, 36–53.

Pişkin, Ö., Delaloye, M., Moritz, R., Wagner, J.J. 1990. Geochemistry and geothermometry of the Hatay complex Turkey: implication for genesis of the ophiolite sequence. In Proceeding of Troodos Ophiolite Symposium, Malpas, J., Moores, E., Panayiotou, A., Xenophontos, C. (eds). Cyprus Geological Survey Department: 329–337.

Puga. E., Nieto, J.M., Diaz de Federico, A., Bodinier, J.L, Morten, L. 1999. Petrology and metamorphic evolution of ultramafic rocks and dolerite dykes of the Betic ophiolitic association (Mulhacen Complex, SE Spain): evidence of eo-Alpine subduction following an ocean-floor metasomatic process, Lithos, 1999, vol. 49, 23-56.

Rızaoğlu, T., Parlak, O., Höck, V., İşler, F. 2006. Nature and significance of Late Cretaceous ophiolitic rocks and its relation to the Baskil granitoid in Elazığ region, SE Turkey. In Tectonic Development of the Eastern Mediterranean, Robertson, A.H.F., Mountrakis, D. (eds). Geological Society, London, Special Publication, 260: 327–350.

Rızaoğlu, T., Parlak, O., Höck, V., Koller, F., Hames, W.E. Billor, Z. 2009. Andean-type active margin formation in the eastern Taurides: Geochemical and geochronogical evidence from the Baskil granitoid (Elazığ, SE Turkey). Tectonophysics, 473, 188-207.

Robertson, A.H.F. 1986*a*. Geochemistry and tectonic implications of metalliferous and volcaniclastic sedimentary rocks associated with late ophiolitic extrusives in the Hatay area, southern Turkey. Ofioliti, 11, 121-40.

Robertson, A.H.F. 2002. Overwiev of the genesis and emplacement of Mesozoic ophiolites in the Eastern Mediterranean Tethyan region. Lithos, 65: 1–67.

Robertson, A.H.F., Dixon, J.E. 1984. Introduction: aspects of the geological evolution ofthe Eastern Mediterranean. In: Dixon, J.E., Robertson, A.H.F. (Eds.), The GeologicalEvolution of the Eastern Mediterranean. Geological Society, London Special Publication, vol. 17, pp. 1–74.

Robertson, A.H.F., Ustaömer, T. 2009. Formation of the Late Palaeozoic Konya Complex and comparable units in southernTurkey by subduction–accretion processes: Implications for the tectonicdevelopment of Tethys in the Eastern Mediterranean region. Tectonophysics, 473, 113-148.

Robertson, A.H., Ustaömer, T., Parlak, O., Ünlügenç, U.C., Taslı, K., İnan, N. 2006. The Berit transect of the Tauride thrust belt, S. Turkey: Late Cretaceous–Early Cenozoic accretionary/collisional processes related to closure of the southern Neotethys. Journal of Asian Earth Sciences, 27: 108–145.

Robertson, A.H.F., Parlak, O., Rızaoğlu, T., Ünlügenç, U.C., İnan, N., Taslı, K., Ustaömer, T. 2007. Tectonic Evolution of the South Tethyan Ocean: Evidence from the Eastern Taurus Mountains (Elazığ region, SE Turkey). *In:* Ries, A.C., Butler, R.W.H. & Graham, R.H. (eds), Deformation of the Continental Crust. The Legacy of Mike Coward, Geological Society, London, Special Publication, 272, 231–270.

Robertson, A.H.F., Parlak, O., Ustaömer, T. 2012. Overview of the Palaeozoic-Neogene evolution of Neotethys in the Eastern Mediterranean region (S Turkey, Cyprus, Syria). Petroleum Geoscience, Vol. 18, 381-404.

Robertson, A.H.F., Parlak, O., Metin, Y., Vergili, Ö., Taslı, K., İnan, N., Soycan, H. 2013*a*. Late Palaeozoic-Cenozoic tectonic development of carbonate platform, margin and oceanic units in the Eastern Taurides, Turkey. In A.H.F. Robertson, O. Parlak and U.C. Ünlügenç (Eds.), Geological Development of Anatolia and the Easternmost Mediterranean Region. Geological Society, London, Special Publication, 372: 167–218.

Robertson, A. H. F., Parlak, O., Ustaömer, T., Taslı, K., İnan, N., Dumitrica, P., Karaoğlan, F. 2013*b*. Subduction, ophiolite genesis and collision history of Tethys adjacent to the Eurasian continental margin: new evidence from the Eastern Pontides, Turkey. Geodinamica Acta, 26 (3-4), 230-293.

Rojay, B., Heimann, A., Toprak, V. 2001. Neotectonic and volcanic characteristics of the Karasu fault zone (Anatolia, Turkey): the transition zone between the Dead Sea transform and the East Anatolian fault zone. Geodinamica Acta, 14, 197–212.

Rollinson, H. 1993. Using Geochemical Data: Evaluation, presentation, interpretation. Longman Scientific and Technical, Harlow.

Ross, C.S., Foster, M.D., Myers, A.T. 1954. Origin of dunites and olivine rich inclusions in basaltic Rocks. American Mineralogist, 39, 693-737.

Saccani, E., Photiades, A. 2004. Mid-ocean ridge and supra-subduction affinities in the Pindos Massif ophiolites (Greece): implications for magma genesis in a proto-forearc setting. Lithos, 73, 229–53.

Saka, S., Uysal, İ., Akmaz, R.M., Kaliwoda, M., Hochleitner, R. 2014. The effects of partial melting, melt-mantle interaction and fractionation on ophiolite generation: constraints from the Late Cretaceous Pozanti-Karsanti Ophiolite, Southern Turkey". Lithos, 202, 300-316.

Sarıfakıoğlu, E., Özen, H., Winchester, J.A. 2009. Whole rock and mineral chemistry of ultramafic-mafic cumulates from the Orhaneli (Bursa) ophiolite, NW Anatolia. Turkish Journal of Earth Sciences, 18: 55–83.

Sarıfakıoğlu, E., Dilek, Y., Uysal, I. 2012. The Petrogenesis and geodynamic significance of Bahçe (Osmaniye) ophiolite. 5th Geochemistry Symposium, Abstracts, 112-113.

Savostin, L.A., Sibuet, J.C., Zonenshain, L.P., Le Pichon, X., Rolet, J. 1986. Kinematic evolution of the Tethys belt, from the Atlantic to the Pamirs since the Triassic. Tectonophysics, 123: 1–35.

Selçuk, H. 1981. Etude geologique de la partie meridonale du Hatay (Turquie), PhD. Thesis, Univ. De Geneve, 116p.

Selçuk, H. 1985. Kızıldağ-Keldağ-Hatay dolayının jeolojisi ve jeodinamik evrimi. Maden Tetkik ve Arama Genel Müdürlüğü Jeoloji Etütler Dairesi Başkanlığı, Report No, 1787. Ankara (unpublished).

Shervais, J.W. 2001. Birth, death and resurrection: The life cycle of suprasubduction zone ophiolites. Geochemistry Geophysics Geosystems, 2: 45.

Shervais, J.W., Kolesar, P., Andreasen, K. 2005. A field and chemical study of serpentinization—Stonyford, California: chemical flux and mass balance, International Geology Review, 2005, 47, 1-28.

Sisson, T.W., Grove, T.L. 1993. Experimental investigations of the role of H_2O in calc-alkaline differentiation and subduction zone magmatism. Contributions to Mineralogy and Petrology, 113: 143–166.

Smith, R.E., Smith, S.E. 1976. Comments on the use of Ti, Zr, Y, Sr, K, P and Nb in classification of basaltic magmas. Earth and Planetary Science Letters, 32, 114–120.

Sun, S.S., Mcdonough, W.F. 1989. Chemical and isotopic systematics of ocean basalts: Implications for mantle composition and processes. In Magmatism in the Ocean Basins, Saunders, A.D., Norry, M.J. (eds). Geological Society, London, Special Publication, 42: 313–46.

Şengör, A.M.C., Yılmaz, Y. 1981. Tethyan evolution of Turkey: a plate tectonic approach. Tectonophysics, 75, 181-241.

Tanırlı, M., Rızaoğlu, T. 2016. Whole-rock and mineral chemistry of mafic cumulates from the low-Ti ophiolite in the southern part of Kahramanmaraş, Turkey. Russian Geology and Geophysics, 57(10): 1398–1418.

Tekeli, O., Erendil, M. 1984. Kızıldağ ofiyolitinin (Hatay) jeolojisi ve petrolojisi. Maden Tetkik ve Arama Genel Müdürlüğü (Temel Araştırmalar Dairesi), Report No, 7778. Ankara (unpublished).

Tekeli, O.. Erendil, M. 1986. Geology and petrology of the Kızıldağ ophiolite (Hatay). Bulletin of Mineral Research and Exploration, No: 107, 21-37.

Terlemez, H.Ç.İ., Şentürk, K., Ateş, Ş., Sümengen, M., Oral, A. 1992. Gaziantep dolayının ve Pazarcık-Sakçagöz-Kilis-Elbeyli-Oğuzeli arasının jeolojisi Maden Tetkik ve Arama Genel Müdürlüğü Report No: 9526, Ankara (unpublished).

Thompson, G. 1991. Metamorphic and hydrothermal processes: basalt seawater interactions. In: FLOYD, P.A. (ed), Oceanic Basalts. Blackie, 148–173.

Tinkler, C., Wagner, J.J., Delaloye, M., Selçuk, H. 1981. Tectonic history of the Hatay ophiolites (south Turkey) and their interpretation with the Dead Sea rift. Tectonophysics, 72, 23–41.

Topuz, G., Göçmengil, G., Rolland, Y., Çelik, F, Zack, T., Schmitt, A.K. 2013. Jurassic accretionary complex and ophiolite from northeast Turkey: No evidence for the Cimmerian continental ribbon. Geology, 41, 255-258.

Ulu, Ü. 2002. Maden Tetkik ve Arama Genel Müdürlüğü 1/500.000 ölçekli Türkiye Jeoloji Haritaları Serisi, Hatay Paftası. Ankara.

Uysal, İ., Ersoy, E.Y., Karslı, O., Dilek Y., Sadıklar, M.B., Ottley, C.J., Tieplo, M., Meisel, T. 2012. Coexistence of abyssal and ultra-depleted SSZ type mantle peridotites in a Neo-Tethyan Ophiolite in SW Turkey: Constraints from mineral composition, whole-rock geochemistry (major–trace–REE–PGE), and Re–Os isotope systematics. Lithos 132–133, 50–69.

van Hinsbergen, D.J., Maffione, M., Plunder, A., Kaymakci, N., Ganerød, M., Hendriks, B.W.H., Corfu, F., Gürer, D., de Gelder, G.I.N.O., Peters, K., McPhee, P.J., Brouwer, F.M., Advokaat, E.L., Vissers, R.L.M. 2016. Tectonic evolution and paleogeography of the Kırşehir Block and the Central Anatolian Ophiolites, Turkey. Tectonics, 35, 983-1014.

Vergili, Ö., Parlak, O. 2005. Geochemistry and tectonic setting of metamorphic sole rocks and mafic dikes from the Pınarbaşı (Kayseri) ophiolite, Central Anatolia. Ofioliti, 30: 37-52.

Wallin, E.T., Metcalfe, R.V. 1998. Supra-subduction zone ophiolite formed in an extensional forearc: Trinity Terrane, Klamath Mountains, California. Journal of Geology, 106: 591-608.

Whitney, D.L., Evans, B.W. 2010. Abbreviations for names of rock-forming minerals. American Mineralogist, 95: 185–187.

Yalınız, K.M., Floyd, P., Göncüoğlu, M.C. 1996. Supra-subduction zone ophiolites of Central Anatolia: geochemical evidence from the Sarikaraman ophiolite, Aksaray, Turkey. Mineralogical Magazine, 60: 697-710.

Yapıcı, N. 1990. Yarpuz-Kaypak (Adana) yöresi jeolojisi mineralojisi ve petrografisi. Çukurova Üniversitesi Fen Bilimleri Enstitüsü, Jeoloji Mühendisliği Anabilim Dalı, 81s.

Yapıcı, N., İşler, F. 1991. Yarpuz-Kaypak (Osmaniye) yöresinin jeolojisi ve petrografik incelenmesi Ahmet ACAR Jeoloji Sempozyumu, Adana, Bildiri özleri kitabı, 269-275.

Yazgan, E., Chessex, R. 1991. Geology and tectonic evolution of the southeastern Taurides in the region of Malatya. Turkish Association of Petroleum Geologist, 3, 1–42.

Yılmaz, Y. 1993. New evidence and model on the evolution of the Southeast Anatolian orogen. Bulletin of Geological Society of America, 105: 251-71.

Yılmaz, Y., Demirkol, C., Yalçın, N., Yiğitbaş, E., Gürpınar, O., Yetiş, C., Günay, Y., Sarıtaş, B. 1984. Amanos Dağlarının Jeolojisi, II Ofiyolit. İstanbul Teknik Üniversitesi Mühendislik Fakültesi Yayını 351.

Yılmaz, Y., Yiğitbaş, E., Genç, Ş.C. 1993. Ophiolitic and metamorphic assemblages of southeast Anatolia and their significance in the geological evolution of the orogenic Belt. Tectonics, 12: 1280-1297.

Yogodzinski, G.M., Rubenstone, J.L., Kay, S.M., Kay, R.W. 1993. Magmatic and tectonic development of the western Aleutians: An oceanic arc in a strike-slip setting. Journal of Geophysical Research, 98: 11807–11834.

Bulletin of the Mineral Research and Exploration

http://bulletin.mta.gov.tr

Typomorphic features of the quartz of various mineral paragenesis from the gold mineralization in Karakshatau Mountains (West Uzbekistan)

Svetlana KOLOSKOVA[a] and Jakhongir MOVLANOV[a*]

[a]*Institute of Mineral Resources State Enterprise of the State Committee of the Republic of Uzbekistan on Geology and Mineral Resources, Tashkent*

Research Article

Keywords:
Gold, Mineralogical mapping, Typomorphism, Quartz, Karakchatau, Uzbekistan, Genetic type.

ABSTRACT

As a result of complex studies - geological-structural, morphostructural analytical, mineralogical mapping of quartz formations, detailed geochemical work and analysis of geochemical fields – forecasting prospecting features of gold ore taxon's: ore zone; ore field; deposit and ore body. They are characterized by groups of criteria: morphostructural, stratigraphic-lithological, structural-tectonic, magmatic, geophysical, metasomatic, mineralogical, geochemical factors and attributes, and a geological-genetic model of the gold-bearing ore-forming system in the collapse zone. Favorable geological and structural conditions for the localization of gold mineralization in the mountains of Karakchatau are associated with the areas of long-term tectonic-magmatic activation in metalliferous sediments of Є-O contrast lithological composition. The coincidence of manifestations of gold mineralization to the blocks formed by transverse faults at the sites where they intersected the Karakchatau crush zone was noted. To the channel-localizing parts inside are blocky and unextended interblock tectonic structures with positions in favorable "structural traps" in their azimuthal curvatures of executed productive types of hydrothermal, sulfidizing quartz. The results of mineralogical mapping of quartz formations along the Karakchatau crush zone (Western Uzbekistan) are considered. Five genetic types of quartz are distinguished. The most productive of them is hydrothermal quartz of types 3 and 4 associated with pyrite,arsenopyrite and gold, which forms vein fields in areas of kinks and expansion of the zone of crushing. Identification of any goods and services that can be used for commercial purposes, including in the geological structure, other regions of Western Uzbekistan.

Received Date: 03.04.2018
Accepted Date: 02.06.2018

1. Introduction

The Karakchatau mountains are taken place among the areas with the potential of covered ore-grade gold in Nurata region. The purpose of this study is to expand and reveal the mineral resource base of the Republic of Uzbekistan for gold, covered, inaccessible depths, mineralization in areas with operating mining enterprises.

With modern definition, typomorphism is a phenomenon in which a number of minerals and their paragenesis are formed in strictly defined, relatively narrow in the range, thermodynamic conditions, clearly recording the nature of these conditions. Theory of the typomorphism of minerals mainly include - general geological, crystal and morphological, chemical, structural, isotopic and thermal and barometric characteristics. A mineralogical study of the rock samples from vein quartz formations of various genetic types of the Karakchatau shear zone focused on the features of the external appearance of

Citation Info: Koloskova, S., Movlanov, J. 2019. Typomorphic features of the quartz of various mineral paragenesis from the gold mineralization in Karakshatau Mountains (West Uzbekistan). Bulletin of Mineral Research and Exploration, 159, 117-127. *http://dx.doi.org/10.19111/bulletinofmre.432046*

** Corresponding author: Jakhongir MOVLANOV, jahongir79@mail.ru*

quartz, the mineral composition of paragenesis, and the interrelationships of minerals and the morphology of quartz (Babaev, 1951; 1985).

2. Regional Geology

The Karakchatau mountains are located in the Zarafshan-Turkestan structural-formation zone, where the prevailing part of the industrial gold potential of Western Uzbekistan is associated with (Figure 1). The regional ore controlling structures of the first order are the branches of the South Nurata Fault - the North and South, the component link of the last Karakchatau and Karatau fault zones (Koloskova, 2007). During collisional stage, the shear zones are important structures for ore-bearing hydrothermal systems and ore-controlling structures and also variety of mineralization is so common in these zones. Shear zones are outcropped in Pre-Mesozoic basement rocks along 90 to 180 km, respectively, the width of them from 1-2 to 5-6 km. On the bearing of these zones, local shear zones are revealed, representing individual branches of the general structure.

The features of the geological structure and ore content, that developed in intensively deformed Pre-Mesozoic basement rocks are represented with two main rock types: sedimentary - terrigenous, siliceous and carbonate rocks; and intrusive – dikes. The sediment covered-folded structure of the mountains of Karakchataus, as well as of the South Nuratau region as a whole, was formed because of prolonged processes of sedimentation (Koloskova, 2007; 2008; Yanovsky, 1990).

3. Material and Method

Study of the typomorphism of quartz minerals is based on visually observed signs, polished thin sections investigation, scanning electron microscope (SEM), and spectral data analysis. Mineralogical mapping study was completed by using 2000 points of random distributed quartz minerals which are located in outcropped part of pre-Mesozoic basement rocks. Quantitative indicators identify anomalous areas identified within the individual segments of the zone.

4. Distribution of the Quartz Bodies

The index of “silicification”, represents average length and thickness of quartz bodies in higher values, indicates the level of ore bearing quartzolite in the

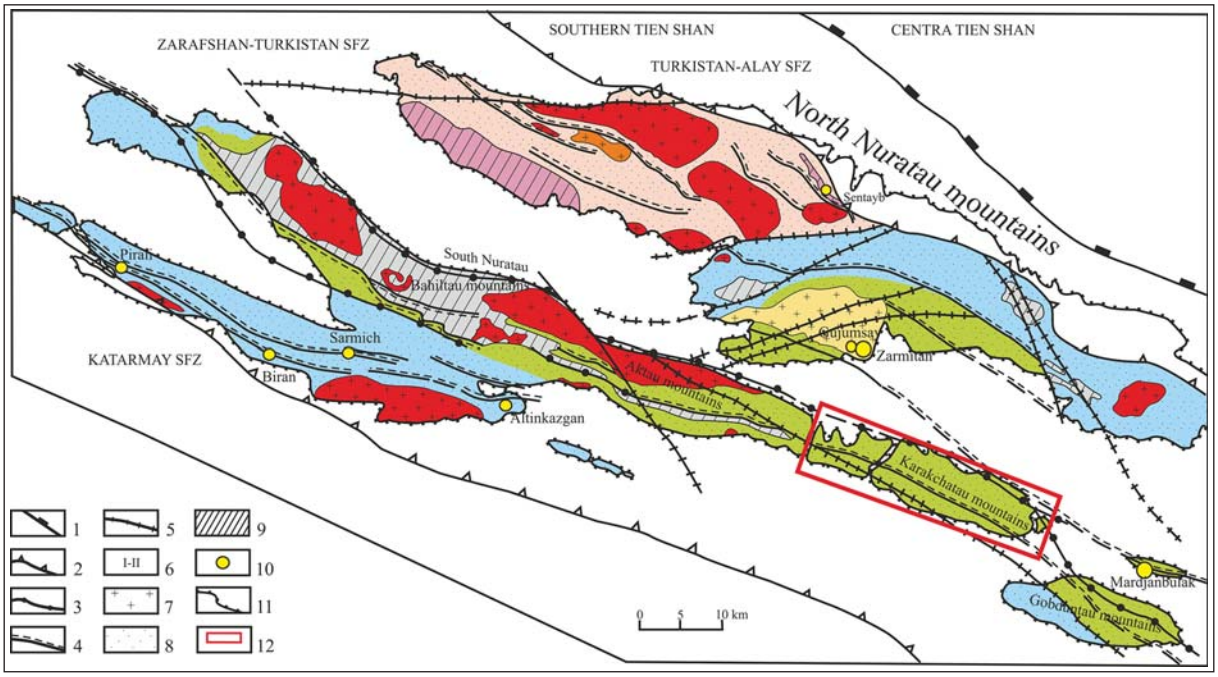

Figure 1- Geological map of study area. Structures: 1 - boundary of folded systems of the Middle and Southern Tien Shan; 2 -4 boundary of structural and formation zones; mainly intra-block, with functions of ore-bearing and ore-distributing; 5-block forming faults with functions of ore-destroying, 6 – shear zones: I-South-Nurata (1-southern branch, 2-northern branch), II-Karatau; 7 - 9 - rock complexes of the Zarafshan-Turkestan, SFZ: 7 - intrusive, 8 - terrigenous, 9 - carbonate; 10 - gold ore deposits; 11 - the boundaries of the outcrops of pre-mesozoic formations; 12 - the boundary of the research area.

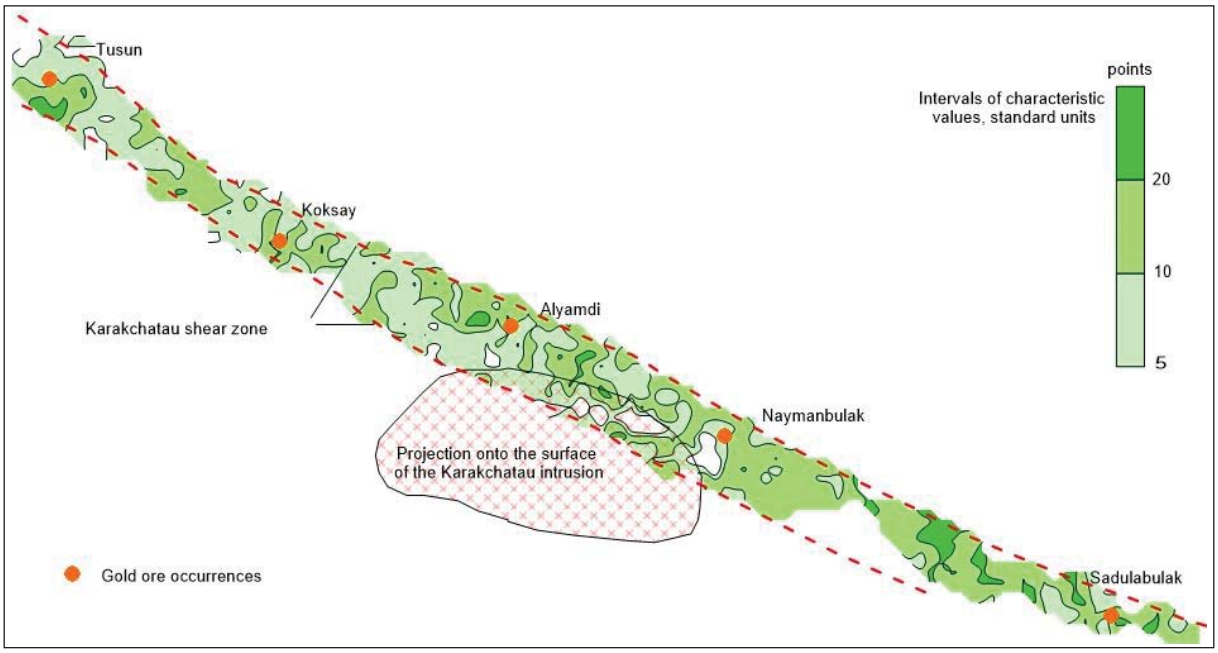

Figure 2- (Extension) Distribution of vein silicification at observation points. Extensity is the prevalence of quartz mineralization from the observation point (10x10 m area): 1 - within the observation point; 2 - beyond the boundaries of the point (up to 25 m); 3 - can be traced at a considerable distance (up to 50-75 m).

above- and near-intrusive position of the non-eroded granitoid body and disparate anomalies in other parts of the zone (Figure 2). The morphology of quartzolite bodies depends on the intensity and nature of the ductile and brittle -deformation, and the mechanical properties of the rocks: veins intensity, both individual and accompanied , which follow the distribution are linear veins, quartz nests, and differently oriented interlacing veins are negligible. Quartz crystal or quarzolite has the ability to respond to stress by changing the internal structure, under the ductile or brittle deformation. In some areas, changes predominate without disrupting the continuity of the crystal bending deformations; in others, deformation is expressed in the mosaic disintegration of crystals into inhomogeneous areas (Koloskova, 2007; Yurgenson, 1984).

Extensive development of quartz mineralization, correlated in the observation point and at a distance from it to 50-75 m, fixes the high saturation of the Karakchatau shear zone of crumpling by quartz veins (Figure 2).

5. Deformation Degrees of the Quartz Crystals

With bending deformation, gradual and unidirectional turns of (frame) structure predominate. The degree of deformation is determined by the magnitude of the maximum deviation in the orientation of extinction of different parts of the same grain, referred to the diameter of this grain, which characterizes, as it was, the "curvature of the bend" of the lattice. Intensive deformation is seen only in crystals of primary quartz - about 6-8° per 0.1 mm. In secondary ones, it is about 2-3° per 0.1 mm. Among the deformation of bend, stages of deformation; simple deformation (in the form of extinction by one wave), complex-striped (several parallel waves), spotted (areas of heterogeneous orientation) are distinguished. This is the first degree of deformation.

With mosaic texture, the large grain of quartz does not get a general bend, but as if broken into parts. The degree of deformation is expressed by the angle of the relative rotation of the mosaic blocks, (fixed in a polarized light) defined under polarized microscopy by their non-simultaneous extinction. This is the secondary degree of deformation.

Brittle deformation is defined in the appearance of microcracks along the boundaries of crystals and mosaic blocks. The extreme degree of deformation is represented by the breccia texture of quartz grains. In the early stages, recrystallization is closely intertwined with granulation. Fine-grained sugary crystals, consisting of pure and distorted crystals, are products of recrystallization with a partial reprecipitation of deformed veined-filling quartz.

There is an increase in the intensity of brittle-ductile deformations of quartz, as well as other minerals as they approach large deformation zones (Petrovskaya, 1956). The peak degree of bending deformation in quartz are observed along the contacts of the veins and environments close to inclusions in the veins.

6. Mineralogy

Five genetic types of quartz crystals are distinguished according to the features. Metamorphogenic quartz (Q-1): Macroscopically it is white or grayish in color, glassy, often translucent and folded with the surrounding rocks.. Under the microscope, this type of quartz is characterized by heterogeneity with the predominance of coarse crystals measuring 0,1-2,0 mm and larger. The mineral boundaries are irregular and broken. Ductile and brittle deformation are characterized by the microgranulation, and recrystallization along the crystals boundaries and microcracks along the feldspars, chlorite, muscovite, sericite, biotite, rare cubic pyrite mineral boundaries. The extinction of the crystals is predominantly undulatory simple or mosaic- undulatory, in addition, there are a band-gap undulatory and undulatory extinction converging toward the center. The angle of propagation of the undulatory extinction (APEW) is about 2-30 by 0,1 mm. Brittle deformation occurred in the form of cracks, is heterogeneous. In fine veins, it is noted that small-medium-grained hypidiomorphic quartz crystals are poorly ductily deformed which is defined under microscope by the determination undulatory, irregular or wrinkled extinction of individual grains of quartz.

Feldspar minerals, especially orthoclase, in white and cream coloured samples, are formed up to 1-2 mm in size and rarely more, the form is usually isometric or slightly elongated. In thin sections, dust like appearance is interpreted as pelitization, weak kaolinisation. Microcline is rarely observed. Late-ordered, fine-grained albite-quartz minerals are hexagonal shaped and overlap the below ones.

Pyrite is observed in the form of disseminated impregnation of small cubic crystals or pseudomorphs of iron hydroxides in pyrite. It is possible to observe brownish, reddish, and dark yellow-colored iron hydroxides along microcracks.

The gold content of metamorphogenic quartz is usually lower than the sensitivity of gold-spectral analysis, sometimes it increases up to 0,1-0,2 g/t, but usually, in quartz the Au content does not exceed 0.0n g/t.

Metamorphogenic-hydrothermal quartz with inclusions of feldspar (Q-2): Feldspar-quartz formations of this type often form cutting veins, sub-coarse small lenticular veins, nests of metamorphogenic quartz and metamorphosed sandy-schist rocks. A characteristic feature of this type is an increased amount of cream and pinkish colored feldspars, reaching up to 50-60% of the volume of mineral content. During the vein formation and development process, pseudo-breccia texture may form and the granular matrix of pink feldspar contains relatively isomorphic crystals of quartz.

Quartz minerals are seen in white to grayish, translucent, sugar-like and vitreous. Under cross-polarized microscope, undulatory extinction and the initial stages of the mosaic texture are observed but more often the crystals are almost undeformed. The texture is hypidiomorphic, grained, with grain sizes in the range 0,02-2,0 mm. Length of creamy and pinkish-colored feldspar is up to 2-3 cm in size and granular feldspar crystals are in between quartz minerals. Feldspar is usually replaced by sericite and kaolinite, which is from single scales to 20-25% of the volume of feldspar outcrops.

The main typomorphic feature of this type is a large amount of feldspar, saturated with clay-like particles. The crystals of feldspar (albite and orthoclase, predominate albite) have good-developed cleavage and are distinguished by irregular shape of faces. Among them, sections of large crystals up to 1-1,5 mm and zones of fine-grained crystals up to 0,1 mm in length are allocated. Among the crystals of quartz, large differences up to 2 mm or more are of primary importance. However, along with them, a large volume of the section is occupied by medium- and fine-grained albite crystals of the metasomatic appearance, which forms intergrowths with quartz. On the surface of quartz, there dust-like inclusions, and possibly kaolinite, are found much lesser amount than on the surface of feldspar. Forms of crystals are very diverse - from angular elongated to irregular and slightly rounded.

In general, the gold grade is measured as 0,0015 g/t one of the locations, it increases up to 0,8 g/t with an increased content of iron hydroxides in quartz.

Pneumatolytic-hydrothermal quartz (Q-3): Macroscopically quartz from white and light gray

to dark gray, coarse-grained, from translucent to transparent in shallow cracks. This type of quartz minerals are characterized by matte luster. There are veins with a patchy uneven random distribution of color from almost transparent to dark gray, rarely reddish. The external appearance in the field, quartz minerals are observed as sugar to vitreous is both opaque and translucent. The texture of vein filling is medium- and coarse-grained, cryptocrystalline. In the large quartz veins, a rhythmic banding was observed, caused by alternating of 1-2 mm of translucent and opaque quartz. The veins contain small isometric and elongated inclusions of muscovite, transparent, slightly greenish and brown iron, white and cream-colored feldspar up to several mm in size. Individual crystals of pyrite, iron hydroxides and manganese are observed along cracks up to 0,5-1 cm.

Under microscope, medium-coarse-grained crystals idiomorphic or hypidiomorphic texture. In some cases, grain boundaries are irregular and sinuous. Quartz crystals are characterized by the absence of dust-like inclusions, which distinguishes it from other types of quartz. The outflow has normal characteristics of undeformed quartz or weak cloudy and undulatory. It is possible to observe fine-grained, recrystallized quartz crystals and related chlorite and carbonate. Single rutile crystals of isometric and elongated sections up to 0,01-0,01 mm in size, apatite of irregular shape up to 0,2 mm in size are observed (Ivankin and Nazarova, 2001)

Some of the veins that filled by white and grayish pneumatolytic-hydrothermal quartz, also contain broken and supergene sulfide mineralization, represented by pyrite and iron hydroxides. Under the microscope, broken and allotriomorphic-grained quartz minerals, with optical signs of bending deformation, are overlapped by sulfide minerals are observed. The fine-granied and granular texture of quartz develop intensively along microcracks and grain boundaries. This quartz is characterized by intensive fracturing both unsystematic and oriented lamellar. The nonmetallic minerals, fine-grained ferrous carbonate, sericite, kaolinite, hydromica, chlorite are developed along the fissures. Often these minerals are associated with the occurrences of ore mineralization. There are crystals of feldspar up to 2-3 mm in size.

Ore minerals are observed as disseminated, lens, nests in quartz veins are intensively replaced by secondary minerals of the oxidation zone. Iron hydroxides are disseminated, nests and widespread in quartz veins and cracks.

Hydrothermal gold mineralization in Alyamdi region is, developed along the veins and related pneumatolytic-hydrothermal quartz. In the samples selected of gold-bearing quartz veins, are dark yellow-colored, brittle, branched and 5-6 cm in size, colloform-texture, consist of limonite, inclusions of reddish-brown goethite, veins of jarosite with a thickness of up to 2-3 mm, rare primitive scorodite (Figure 3-4).

Hypidiomorphic medium and coarse-grained quartz minerals are intergrowths with albite. Quartz has a weak cloudy-undulatory extinction and albite is represented by colorless tabular crystals with polysynthetic twinning (Sample 1017, Figure 3c, d). Cracks develop fine-grained idiomorphic-grained quartz, apatite grains are up to 0,2 mm, short-prismatic rutile crystals up to 0,02 mm in size. The distribution of ore mineralization is controlled by cracks in the albite-quartz crystals and is also associated with later cutting quartz-carbonate (ankerite, calcite) veins. Post-ore veins are filled by calcite (Mikhailov et al., 2004).

In the heavy fraction of the sample of Alyamdi, rare pyrite, malachite, cerussite and native gold are observed (Figure 3b). The color of gold varies from light yellow to reddish-yellow. Gold grains are mostly less than 0,1 mm and represent a thin dust-like form. The texture of gold is granular, rounded, elongated and irregular. Gold is interlocked with quartz. Larger golds have nodular surface (Figure 4).

Probably the presence of bismuthinite, scheelite, molybdenite within quartz, as indicated by the increased contents of Bi, W, and Mo in the samples, as is the case for As, Ag, and Cu in some other samples are increased in some samples.

Hydrothermal quartz associated with pyrite, arsenopyrite and gold (Q-4): Hydrothermal gold-bearing quartz is macroscopically white, grayish and light gray, in some parts, is randomly spotted and a bluish-colored, represented by cryptocrystalline opaque crystals of porcelain or sugar-like texture (Figure 5a). Q-4-grouped quartz minerals contain inclusions of creamy-pink feldspar from 0,1-0,2 mm to 2-2,5 mm, veins and micro-allocation of carbonate, chlorite, sericite, kaolinite. Under the microscope, quartz is characterized by large-crystal with abundant

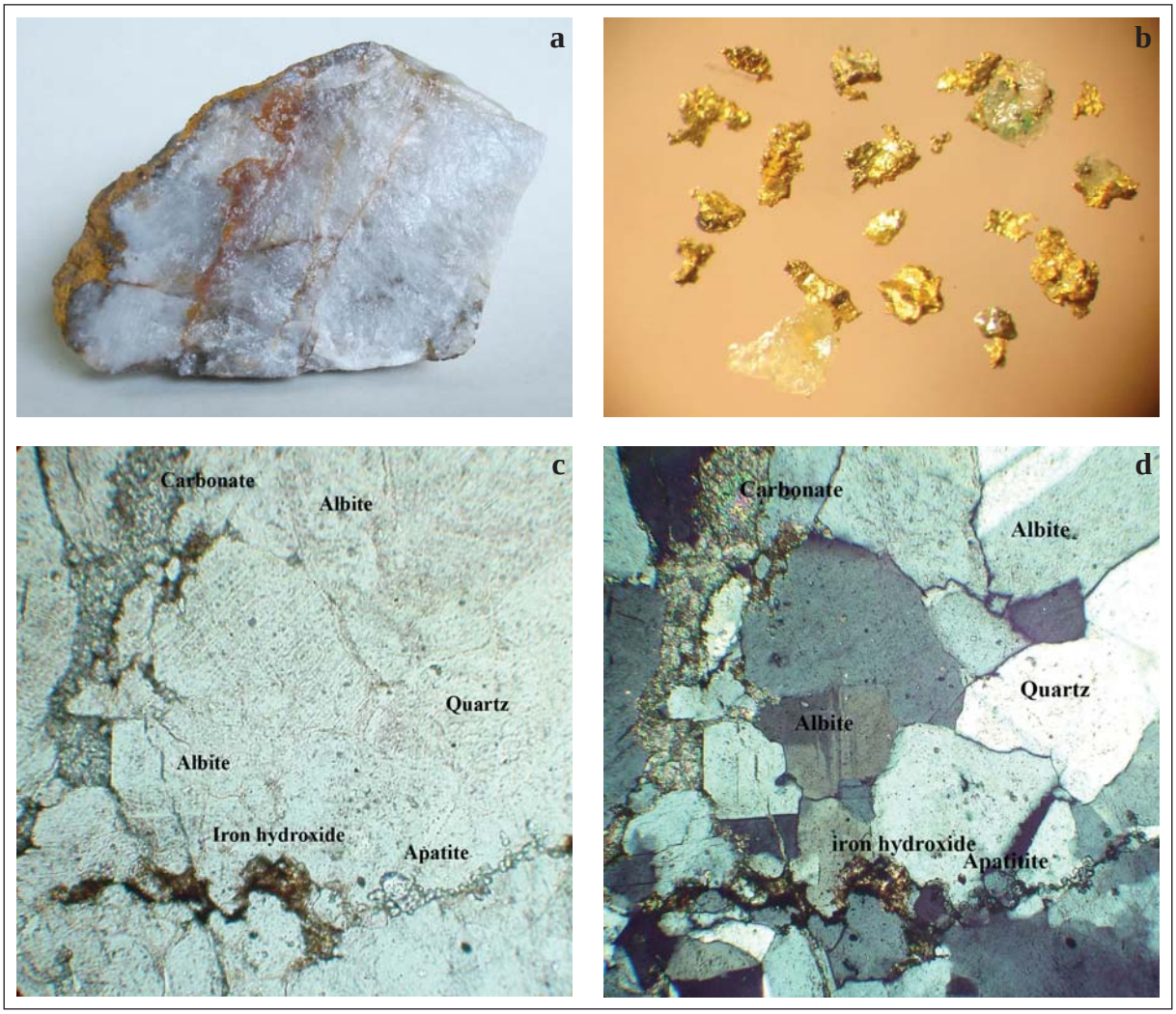

Figure 3- a) View of gold-bearing quartz from the Alyamdi Gold Deposits:b) View of gold, c, d) view of mineral compound under the microscope.

pulverous inclusions forming “wrinkles” apperance. Hydrothermal quartz is characterized by intense brittle-ductile deformation, characterized by irregular cloudy-undulatory extinction, the mosaic texture of crystals, formation of granular quartz along cracks and grain boundaries (Figure 5b), transparent, without inclusions. A fine-grained-quartz crystals with carbonates, sericite, kaolinite, chlorite, pseudomorphs of iron hydroxides through pyrite, jarosite, and native gold develop along the fissures (Figure 5c). Rare nests and impregnations of pyrite are observed in some sections of quartz veins up to a few mm in size; accumulation of iron hydroxides are widespread in the veins, and cracks.

In the concentrates of the crushed sample from the limonitized quartz veins, the Tusun mineralization contains native gold, pyrite, chalcopyrite, arsenopyrite, galena, malachite, scorodite minerals. Native gold in the heavy fraction of crushed sample 1209 are characterized by free gold of light-yellow color and in intergrowths with quartz, and by dusty inclusions in quartz. The size of the gold is from 0,01 to 0,75 mm. The texture of gold is: cloudy, lamellar, complex interstitial, elongated and isometric (Figure 5d). The surface of the native gold is smooth, as well as tuberculate, and turbinate, as occurred more often. In polished sections of the same quartz vein, the individual elongated, vein-like and isometric lumpy and dusty gold are confined to microcracks in quartz (Figure 5c). Accumulations of gold from 0,005 to 0.1 mm in size are associated with microcracks that contain quartz-sericite-hydromica-kaolinite and gold inclusions are also observed in iron hydroxides.

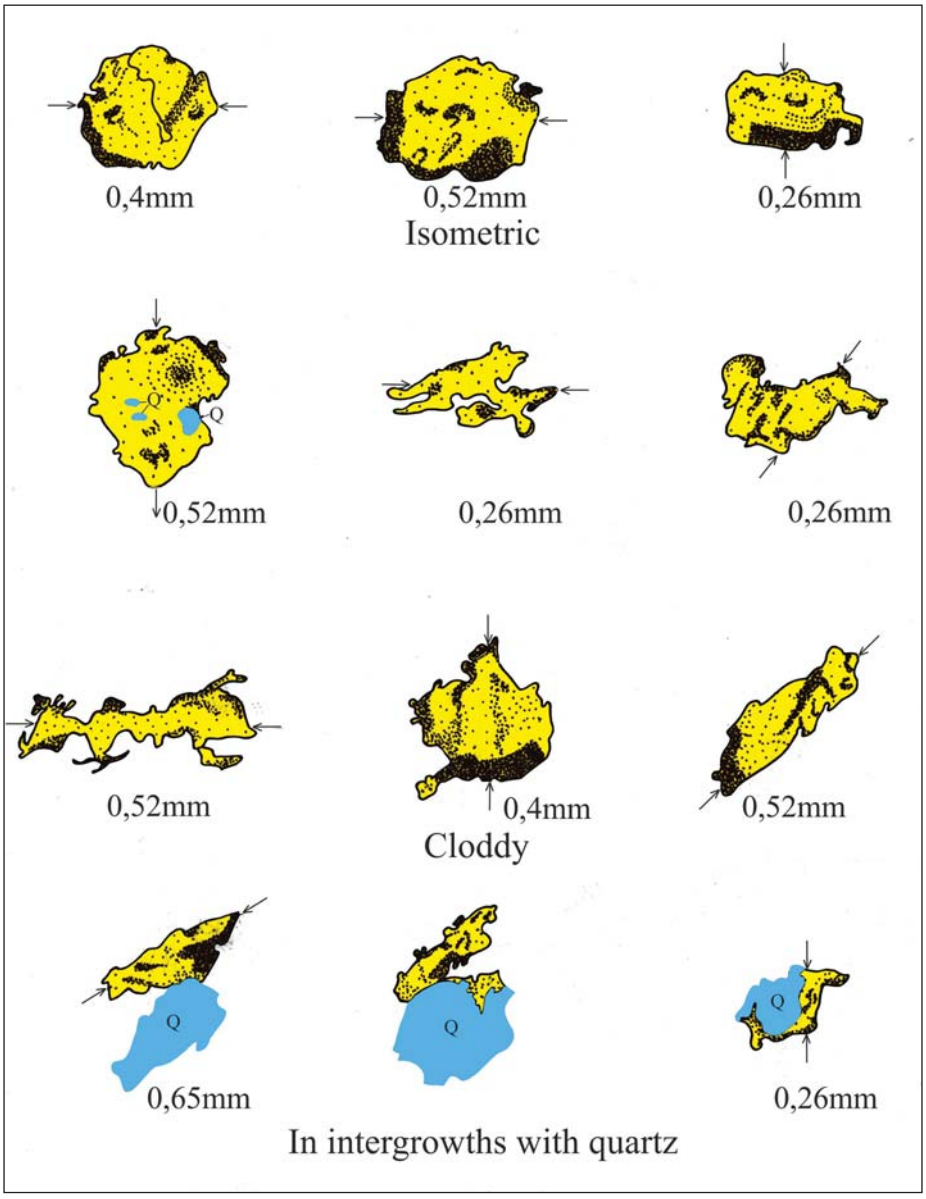

Figure 4- View of gold minerals in hydrothermal feldspar-quartz veins from Alyamdi Gold Deposits.

According to the results of the semi-quantitative spectral analysis, the lead content in this same vein is increased by 0,48%, arsenic 0,1%, copper 0,1%, silver 415 g/t, gold 26,25 g/t. High Pb contents suggest the presence of galena.

In Naymanbulak and Tusun area, veins are filled by porcelain quartz (Q-4), and in Ingichkasay, west of Naymanbulak area, quatz veins with gold content of 0,1-0,8 g/t are covered by loose material. In Tusun region, some parts of porcelain quartz veins contain dark yellow colored iron hydroxides up to 10-12 cm in thickness, have high gold concentration. Post-ore, hydrothermal low-temperature quartz (Q-5): It forms in veins which developed in tectonic zones and the breccia texture is observed in quartz minerals. Macroscopically it is white and grayish in color, sugar-like, sometimes finely-grained and metasomatic in appearance.

The fine-grained quartz breccia contains intensely silicified rock fragments as observed point 836. Intensely silicified rocks are between 1-2 mm and 3-5 cm in size, usually acute-angled, contain from 5-10 to 40-50% of quartz. Under the microscope, amorphous quartz crystals are hypidiomorphic (a combination of xenomorphic crystals and crystalline forms) and 0,05-0,1 to 0,5-0,6 mm in size, and weakly deformed. In

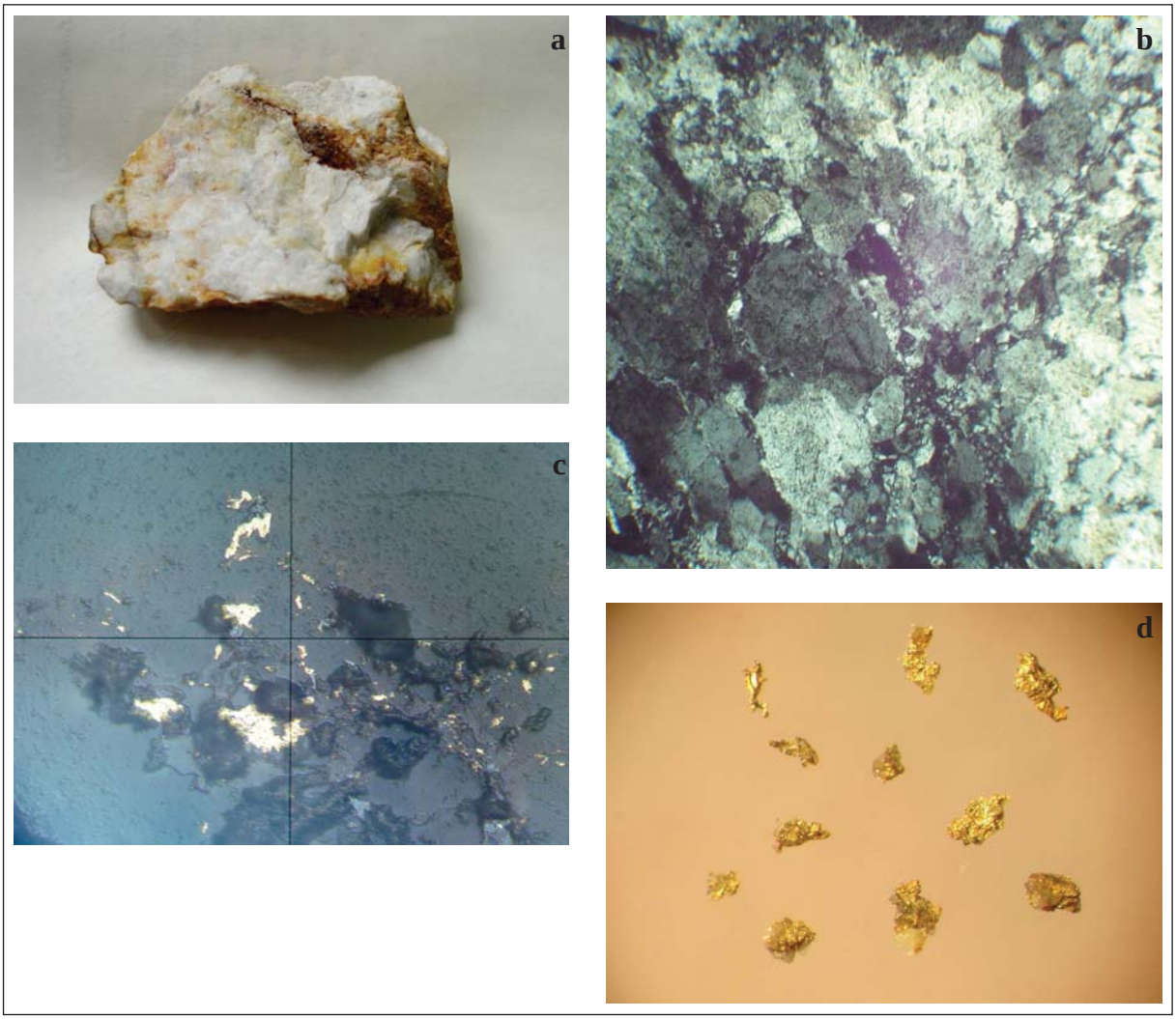

Figure 5- Gold-bearing veins in Tusun region; a) a sample of white porcelain quartz (Q-4) from the core (sample 1209, 0.9g/t concentrated gold); b) compressional deformation and the mosaic texture of quartz crystals and micrograins in cracks (sample 1209, cross-polarized light, X56); c) native gold (light-colored) in quartz-kaolinite-carbonate microfractures (dark) (sample 1209, X60); d) 0.15-0.55 mm in size gold in quartz vein (sample 1209, X36).

association with post-ore quartz formation, formation of chlorite, sericite, albite, calcite, kaolinite flake, gypsum are also observed.

The results of mineralogical mapping of quartz vein along the Karakchatau Shear Zone show that quartz veins are most intensively developed in the central part of the zone. They form linear zones and fields, concentrated in local geological blocks; vein fields develop in the areas of expansion of the Karakchatau shear zone, and in the areas of its clamping the intensity of quartz mineralization decreases; the location of the fields and their morphology depend on the nature of the block deformation of the shear zone.

The typomorphic mineralogical-geochemical features of quartz veins from different genesis, defined as a result of research, are comparable with the available data from other shear zones with the same geological features, which allows them to determine target area for gold prospecting projects.

6.1. SEM (Scanning Electron Microscope) Study Results

Under the SEM, vitreous metamorphogenic quartz (Q-1) (sample 1140) of a cryptocrystalline structure with a grain size range from about 0,1 to 0,2 microns and a banded, lace-like texture contains scattered impregnation of ore minerals up to several microns

in size. As a result of replacement processes, quartz minerals are recrystallized and get sugar-like texture that contains small gaseous-liquid inclusions of 1 to1.5 microns in size. A comb texture of quartz is observed at the background of a thin-globular surface with precipitates of a presumably carbonaceous substance which has an isometric and elongated shape ranging from 0,1 to 2 microns in nodes. Some crystals have radial-radiant structure.

Q-3 type quartz show idiomorphic crystals under SEM (Figure 6a). (Figure 6a). Random distribution of irregular-shaped gaseous-liquid inclusions are located on the edges of crystals, are probable indicated as secondary origin (Figure 6b).

Under the SEM, presence of isometric and 15-20 microns in size gaseous-liquid inclusions are observed in the cleavages, developed in fine-grained porcelain hydrothermal quartz (Q-4). In coarse-grained quartz crystals there are disseminated ore minerals, there are hexagonal quartz crystals and largely elongated gaseous-liquid inclusions over quartz growth zones. The "wrinkle texture" of quartz is observed in crystal growth zones by pulverized gaseous-liquid inclusions and fracutures along the microinclusions of ore minerals which are (Figures 7a,b).

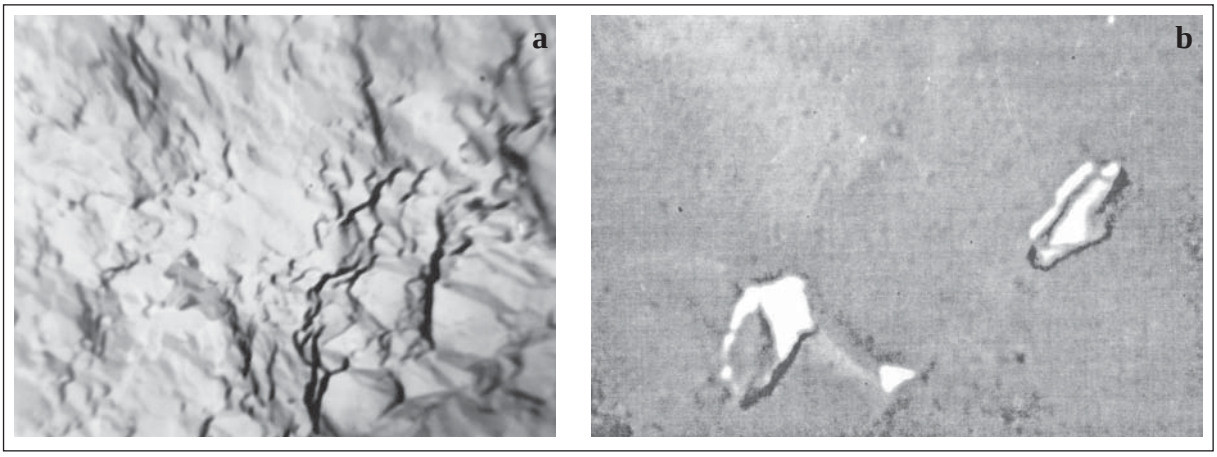

Figure 6- a) View of high-temperature quartz (Q-3) fom sample 1187; b) View of 2 micron-sized gaseous-liquid inclusions in high-temperature quartz (Q-3) minerals from Sample 1017.-

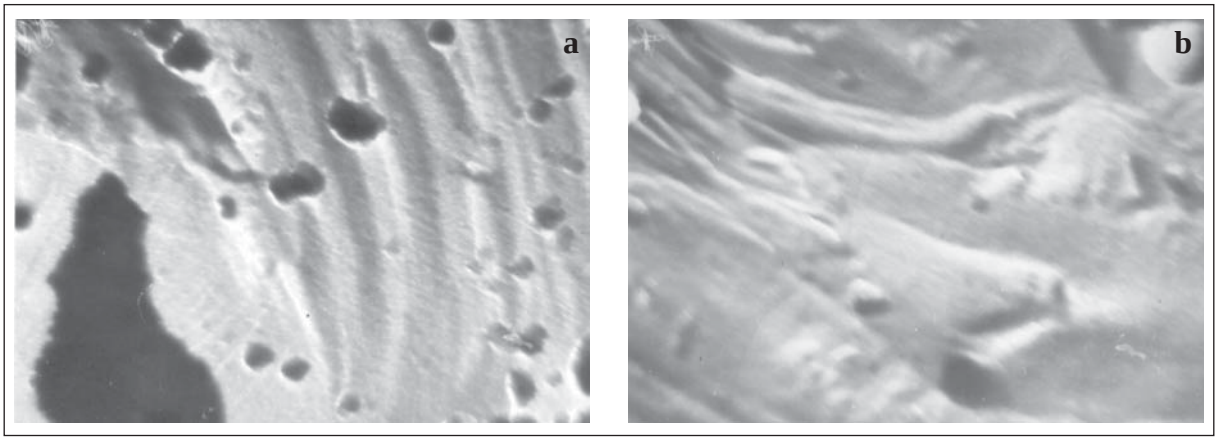

Figure 7- SEM images of the sample 371. Zonal structure of hydrothermal quartz crystals (Q-4); a) sulfide impregnated "Wrinkled" quartz crystals. (X6000); b) the same with gaseous-liquid inclusions by growth zones (X6000).

7. Discussion

The evolution of ore-forming processes in the gold-bearing quartz veins of crushing in terrigenous sequences of the cover-folded regions of Western Uzbekistan is controlled by geological, metasomatic, mineralogical and geochemical features. In this research, the typomorphic features of quartz minerals in the Karakchatau shear zone are studied, since quartz varies by properties and properties of mineral-forming processes (Yurgenson, 1984, Babaev, 1985). The obtained data makes it possible to clarify geological evolution of ore forming conditions in the studied area.

Gold mineralization is formed as a result hydrothermal fluid circulation in fractures and faults in the early stage of development of the shear zone, pneumatolytic-hydrothermal processes associated with granitoids, and telethermal processes with late stage of deep structures (Koloskova, 2007). Late Silurian processes of movement of lithospheric plates provided suitable environment for the migration of ascending fluid flows from the subduction zone. Pre-Devonian regional metamorphism is considered by most researchers as one of the earliest processes of concentrating gold in sedimentary strata. In the early-collision stage, during the middle Carboniferous, complications of early over thrust along the borders of the covers occur and large plates, which in the late- and post-collision period took the form of shear zones conformal cover-fold structure. At first, the period of collision, when the granite-gneiss layer was not yet formed, the deformation zones were the structures of migration of mantle fluids, which contributed to the formation of metamorphogenic-metasomatic rocks with a high background metal content, including gold content (Ivankin and Nazarova, 2001): 1) carbonate-sulphide-carbon metasomatites; 2) albite-quartz metasomatites and vein-veinlet formations of a similar composition. The formation of polygenic collision granitoids of the S-type need to be explained was accompanied by a large-scale migration of gold and a number of ore-bearing elements in the geothermal gradient field of intrusions with a concentration in favorable positions. Dislocations of this period control the placement of dyke and vein type quartz mineralization. With periods of post-collisional tectonic activation of the associated formation of quartz breccias, gold-bearing quartz.

8. Conclusions

In this article, we considered the practical application of one of the geological phenomena defined by the term “typomorphism of minerals”. Field mineralogical mapping of quartz formations was performed along the ore-saturated Karakchatau fault zone with potential of hidden gold mineralization.

Mineralogical study of rock samples from different genetic type quartz veins of the Karakchatau Shear Zone paid attention to the peculiarities of the external appearance of quartz, the mineral composition of paragenesis, and the interrelationships of minerals and the morphology of quartz crystals.

Five genetic types of quartz formations are distinguished by a complex of characters that include metamorphogenic quartz (Q-1); metamorphogenic-hydrothermal (Q-2); pneumatolytic-hydrothermal quartz (Q-3); hydrothermal quartz with sulfides and gold (Q-4); hydrothermal low-temperature quartz, post-ore (Q-5). Mineralogical mapping was carried out in that mapping: in the Karakchatau Shear Zone, quartz veins are most intensively developed in its central part.

Result of typomorphic mineralogical-geochemical features of different genetic type quartz veins are provided and allows to compare with other shear zones from similar geological backgorund, that may help to determine new target areas for gold mineralization.

Acknowledgement

This study was conducted within the framework of the state budget topic “Analysis of geological and structural conditions for the location of gold ore occurrences of the Karakchatau Mountains and an assessment of their prospects”. We express our gratitude to the Vladimir Tsoy for critical discussion of the article.

We would like to thank Cahit Dönmez for his support for us to contribute an article to this journal. We also would like Prof. Dr. Emin Çiftçi and an anonymous reviewers for their insightful comments on the paper, as these comments led us to an improvement of the work.

References

Babaev, K.L. 1951. Genetic characteristics of quartz formations of the Nuratau range. Tr. Institute of Geology 6, Tashkent, ANUSSR,

Babaev, K.L. 1985. Genetic types of quartz // Zap.Uzb.otd. WMO. Issue. 38. Tashkent: Fan, 5-10.

Ivankin, P.F., Nazarova N.I. 2001. Deep fluidization of the earth's crust and its role in petro-labor, salt and oil formation. Moscow, TsNIGRI, 206 p.

Koloskova, S.M. 2007. Geological and genetic model of the development of the gold-bearing ore-forming system in the Southnuratau zone of collapse. Geology and Mineral Resources 2, 44-49.

Koloskova, S.M. 2008. Ore-forming processes in the gold-bearing zones of the crushing of the cover-fold regions of Western Uzbekistan: the genesis and typomorphism of quartz formations // Problems of geology of ore deposits, mineralogy, petrology and geochemistry. Conference proceedings. - Moscow: IGEM RAS, 2008. p. 92-94

Mikhailova, Yu.V., Mansurov, M.M. 2004. Polyformativity of gold ore deposits of the Kyzylkum-Nuratau region in connection with its geodynamic development. Problems of geology of the Phanerozoic Tien Shan. Conference proceedings. Issue 2, Tashkent, 95-102.

Petrovskaya, N.V. 1956. Some features of intrathoric metamorphism of gold-quartz formations on the example of deposits of the Yenisei Ridge. Tr. Institute "Nigrisoloto" *21,* Moscow, 3-44.

Yurgenson, G.A. 1984. Typomorphism and ore-bearing property of veined quartz. Moscow, Nedra, 149 p.

Yanovsky, V.M. 1990. Ore-controlling structures of terrigenous miogeosyncline. Moscow, Nedra,– 246 p.

Bulletin of the Mineral Research and Exploration

http://bulletin.mta.gov.tr

Rare earth element (REE) resources of Turkey: An overview of their characteristics and origin

Hüseyin ÖZTÜRK[a*], Nurullah HANİLÇİ[b], Sinan ALTUNCU[c] and Cem KASAPÇI[d]

[a]*İstanbul University- Cerrahpaşa, Department of Geological Engineering, Avcılar Campus, Avcılar- İstanbul, Turkey. orcid.org.0000-0001-7290-1279.*
[b]*İstanbul University- Cerrahpaşa, Department of Geological Engineering, Avcılar Campus, Avcılar- İstanbul, Turkey. orcid.org/0000-0002-7720-1551*
[c]*Niğde Ömer Halisdemir University, Department of Geological Engineering, Niğde, Turkey. orcid.org/ 0000-0002-0863-4169*
[d]*İstanbul University- Cerrahpaşa, Department of Geological Engineering, Avcılar Campus, Avcılar- İstanbul, Turkey. orcid.org/ 0000-0003-2763-5930*

Research Article

Keywords:
Rare earth element geochemistry, Carbonatite, Shale, Bauxide, Turkey

ABSTRACT

The Rare Earth Elements (REE) deposits and mineralization of Turkey can be divided into four types based on their geological setting and origin. First are deposits associated with carbonatite-alkaline magmatic rocks, rich in Light Rare Earth Elements (LREE). The best known examples are the Kızılcaören (Eskişehir) and Kuluncak (Malatya) deposits with TREE grades of 2.9% and 0.7% respectively, and typical enrichment of La-Ce. Lower grade REE mineralization at Keban (0.05% TREE) and Divriği (0.13% TREE) is associated with abundant fluorite and all four occurrences show similar ranges for homogenization temperatures and salinities for fluid inclusions in fluorite and REE profiles. The second type are Triassic shales and the bauxites formed from them in the Bolkardağı region. Enrichment of Heavy REE (HREE) is typical and TREE grades are about 0.15% in bauxites and its protolith. These occurrences are geochemically similar to "ion adsorption type" deposits associated with lateritic clay on the weathered granitic rocks of China. Third is the placer type, represented by the Çanaklı (Burdur) deposit which is enriched in U, Th and HREE and heavy minerals such as; magnetite, zircon and rutile and has an average grade of about 0.08% TREE. The fourth potential source of REE is phosphorites. These rocks host the world's largest resources elsewhere, however the Cretaceous Mazidag deposits in Turkey are very low grade (40ppm TREE) and clearly uneconomic. Consideration of the environmental and health issues associated with exploitation and processing of REE has identified the more favorable outcomes associated with exploitation of the ion adsorption type of deposits and justification for further evaluation of the resources and processing technologies that would enable exploitation of REE-enriched bauxites in the Bolkardağı region.

Received Date: 26.02.2018
Accepted Date: 03.05.2018

1. Introduction

The Rare Earth Elements (REE) consist of a total of 17 elements, including 14 natural and 1 artificial element known as the Lanthanides (La) starting from the mass number of 57 up to Lutetium (Lu) with mass number of 71, plus Y and Sc, due to their similar geochemical properties. In this REE group where the ion charge is usually +3 valence; La, Ce, Pr, Nd and Sm elements are called as the LREE, and Gd, Tb, Dy, Ho, Er, Tm, Yb, Lu and Y elements are called as the HREE. Because of its geochemical characteristics, the REE group is widely used for the analysis of geotectonic-petrogenetic environment, the interpretation of physicochemical conditions and for many other geological problems. However, more

Citation Info: Öztürk, H., Hanilçi, N., Altuncu, S., Kasapçı, C. 2019. Rare earth element (REE) resources of Turkey: An overview of their characteristics and origin. Bulletin of Mineral Research and Exploration, 159, 129-143.
http://dx.doi.org/10.19111/bulletinofmre.471205

** Corresponding author: Hüseyin ÖZTÜRK, ozturkh@istanbul.edu.tr*

importantly, the REE mining has gained extraordinary importance in the world over the last fifty years due to demand from the electronics and defense industries.

Some raw materials are regarded as strategic and critical according to their supply risk and economic importance (http://ec.europa.eu/growth/sectors/raw-materials/specific-interest/critical_en) and the REEs are at the top of these critical raw materials (Figure 1). Eighty-five percent of the total REE of 140 thousand tons produced per year in the world is realized by China. China supplies 65% of its production from bastnasite, the main mineral of hydrothermal deposits associated with carbonatites, and the remaining from clays formed by supergene processes.

The reason why China is the main leader in the worlds REE production is not only the rarity of deposits elsewhere in the world, but also the usual presence of high levels of radioactive elements, such as Th and U, which in turn limits the production. Exposure to radiation during production, processing, and storage of waste containing U and Th, can result inserious health threat both to workers and for all post-production environmental damage.

The world's major REE resources include (i) bastnasites (REE, $Ce(CO_3)F$) in carbonatites (eg, Mt Pass Deposit USA) Hewett (1954), Bayan Obo Deposit China, Xu et al. (2012) (ii) monazites located in the ocean shore placers ($REEPO_4$) (eg, Indian and Australian shores) Paleparthi et al. (2017), (iii) xenotime (Y, $REEPO_4$), a byproduct of Ti, Zr, Sn deposits, (iv) sedimentary phosphate deposits (Emsbo et al., 2015), (v) bauxites (Deady et al., 2016*b*), and (vi) ion adsorption clays - type deposits result from deep tropical weathering of granites (Voßenkaul et al., 2015), where the combination of high precipitation and temperature decomposes the REE-bearing minerals (Sanematsu and Watanabe, 2016). Following their exploitation in China, similar deposits were discovered in Madagascar and Brazil (Rocha et al., 2013).

Except for REE resources associated with monazite and xenotime, the geological environments

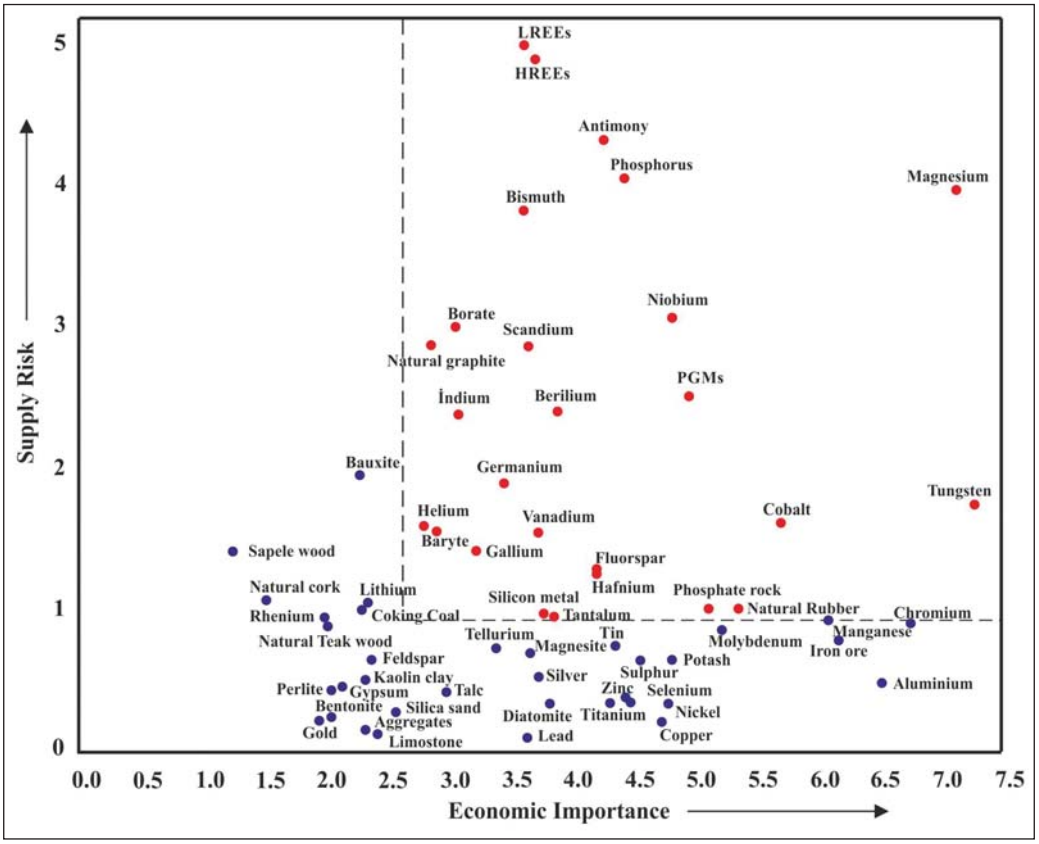

Figure 1- Position of the raw materials critical to the EU Commission for the year 2017 according to the threshold of supply risk and economic importance (see upper right-hand region, http://ec.europa.eu/growth/sectors/raw-materials/specific-interest/critical_ en).

and formations for the other types of REE deposits are observed in Turkey (Figure 2). The geological setting, mineralogy, trace element and REE geochemistry and fluid inclusion properties of these deposits and occurrences will be discussed in this article.

2. Method

In this study, a total of 44 ore samples were taken from the deposits and mineralization with REE potential from different geological environments in Turkey (sample numbers of deposits and mineralization are seen in Tables 1 and 2). Their mineralogical, petrographical, geochemical (REE, major oxide and trace element geochemistry) and fluid inclusion properties were studied, with geochemical analyses carried out in Canada at the ACME Laboratories using ICP-AES for main oxides and the loss on ignition, and ICP-MS for the other elements. Boynton (1984) values were used in the chondrite normalization. Fluid inclusion analyzes were carried out on the Linkham THMG-600 instrument at the Geological Engineering Department of Istanbul University- Cerrahpaşa. In this study, the fluid inclusion data are given as a summary and results relating to the REE geochemistry are discussed. As REE is transported in the form of fluorine complexes in hydrothermal systems (Migdisov et al., 2009), the REE geochemistry and fluid inclusion properties of all fluorite deposits in Turkey were examined. However, only the mineralizations that show REE enrichment were introduced among fluorite deposits of Turkey.

3. REE Sources Associated with Carbonatite and Alkaline Magmatic Rocks

REE enrichment associated with carbonatites occur at Kızılcaören (Eskişehir) and Kuluncak-Başören (Malatya). Alkaline magmatic rocks-related REE-bearing fluorite deposits occur at Keban (Elazığ) and Divriği (Sivas). All these deposits are always associated with fluorite. This is due to the fact that REE is transported by the fluorine forming complex ions (Migdisov et al., 2009). The most important example of carbonatite-hosted deposit in Turkey is Kızılcaören (Eskişehir) (Kaplan, 1977*a*; Stumpel and Kırıkoğlu, 1985; Nikiforov et al., 2014). This deposit also contains Th which has strategic significance. Apart from Kızılcaören, the Kuluncak Fluorite-REE mineralization in the vicinity of the Başören village (Kuluncak-Malatya) has been studied by MTA with a similar interest in terms of Th (Özgenç and Kibici, 1994). The MTA has also conducted a research on the Cu-F mineralization of Divriği (Sivas) for uranium, and the high REE content of the mineralization will be presented in this study for the first time.

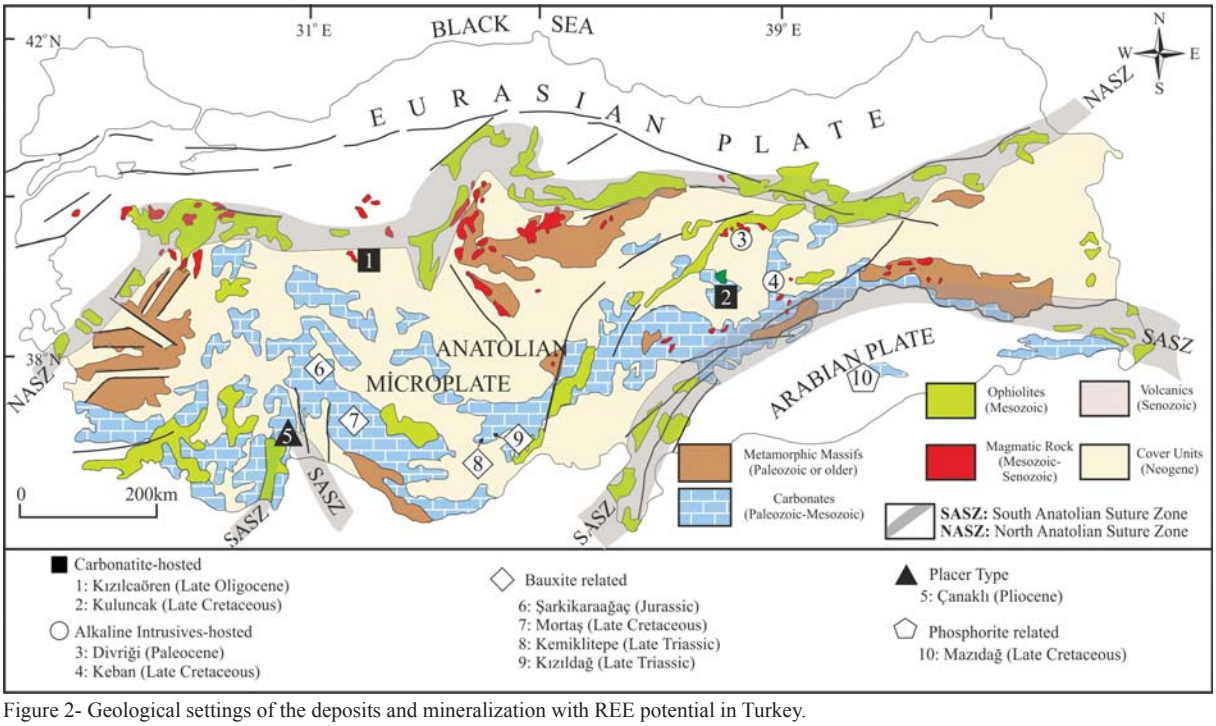

Figure 2- Geological settings of the deposits and mineralization with REE potential in Turkey.

Table 1- The REE+Y, Th, U contents of REE deposits and the rocks that have potential for REE of Turkey. Kızıldağ shale (protolith of bauxites), Kemikli Tepe and Mortaş bauxite data are from Hanilçi (2013), the red mud data is from Deady et al. (2016*b*), the Canaklı placer data is from Cox et al. (2013), the ion absorption clay deposit data of China is from Voßenkaul et al. (2015) and the Seydişehir phyllite data is from Karadağ et al. (2009). The other data are produced in this study (n.d: no data; Please see table 2 for sample locations).

NTE Resource	La	Ce	Pr	Nd	Sm	Eu	Gd	Tb	Dy	Ho	Er	Tm	Yb	Lu	ΣNTE	Y	U	Th
Kızılcaören Carbonatite (n=10)	9380	15070	1234	3584	289	57	224	15	66	9,4	25	3,9	23	2,9	29982	331,7	123	1072
Kuluncak Carbonatite (n=6)	2919	3317,1	248,8	598,4	48,8	8,7	43,1	5,4	29	5,8	16	2,2	11	1	7254,7	214,6	14,4	297,5
Divriği Alkali Magmatite (n=6)	299,7	507,6	62,4	237,8	58,8	7,3	61,2	9,4	53	9,9	27	3,8	22	2,6	1362,9	698,5	116	2,8
Keban Alkali Magmatite (n=10)	219,2	247,2	19,3	42,4	3,5	0,8	3,2	0,4	2,2	0,4	1	0,1	0,8	0,1	540,5	13,2	46	8,8
Çanaklı (Placer)	191	325	34	120	16	4,1	11,1	1,4	6,7	1,1	3,3	0,5	3,2	0,5	717,2	37	10,4	49
Kemiklitepe Bauxite (n=2)	337,1	635,7	91,8	376,1	71,9	15	65,2	8	42	7,2	19	2,9	18	2,7	1693,1	126,2	15,6	47,7
Kızıldağ Shale (n=3)	398,9	467,7	96,5	361,1	65,8	13	58,7	8	39	6,7	16	2,3	14	2,1	1548,5	125,2	10,2	26,4
Mortaş Bauxite (n=1)	39,5	191,6	10,5	38	8,6	1,8	7,8	1,5	11	2,1	6,9	1,1	8	1,2	329,2	49,7	6	47,8
Red mud (Bauxite waste, Seydişehir)	356,2	728,5	102,7	346,7	67,9	14	8,2	52	43	8,2	22	3,3	22	3,3	1777,4	180,2	vy	vy
Seydişehir (Phyllite)	58,1	124,6	13,7	54	10,1	2,0	8,5	1,4	7,8	1,5	4,5	0,7	4,3	0,7	292,0	vy	vy	vy
Şarkikaraağaç Bauxite (n=2)	44,6	110	13,6	63,4	16,3	5,5	14,5	2	10	2	4,9	0,8	4,4	0,6	293	42,4	1,3	4,5
Şarkikaraağaç (Bauxite-protolith is basalt)	17,2	33,4	4,21	18,0	4,11	1,32	4,45	0,71	4,18	0,72	1,9	0,3	1,67	0,24	92,41	18,6	0,5	2,3
Mazıdağı phosphorite (n=4)	15,1	5	1,51	6,2	1,12	0,3	1,67	0,2	2,3	0,7	2,2	0,2	2	0,4	39	45,3	71,8	< 0,2
Ganzhou (China clay deposit)	287	311	65	278	44	8	36	5	26	5	14	2	11	2	1094	157	vy	vy

3.1. Kızılcaören REE Deposit

The Kızılcaören deposit is the biggest REE deposit in Turkey and also the largest occurrence of F-Ba-Th. It consists of sub-horizontal banded ore and sub-vertical vein-type mineralization within steeply dipping Permo-Triassic conglomerates, sandstones and schists (Figure 3). The sub-horizontal mineralization shows variation between the bands and individual bands can be rich in either fluorite, manganese oxide, barite or fine-grained silica. These banded ores are coarse grained but have a soft and earthy features. The sub-vertical veins lack banding and this harder mineralization is finer grained and includes locally flow structures. Alkali metasomatism is indicated by widespread fenite veins of K-feldspar and alkali amphiboles that sometimes form small outcrops and feldspathic bands within the deposit.

Table 2- Major oxide and trace element contents of the REE deposits and probable REE sources of Turkey. Data of Bayan Obo deposit from Yang et al. (2003) (**KO:** Kızılcaören deposit; **KUL:** Kuluncak mineralization; **DIV:** Divriği mineralization, **KB:** Keban mineralization; **KM:** Kemikli tepe bauxite deposits, **KD:** Kızıldağ protholith, **MR:** Mortaş bauxite deposit, **SK:** Şarkikaraağaç iron-rich bauxite deposit, **MD:** Mazıdağı phosphorites).

	Deposits	**KO**	**KUL**	**DIV**	**KB**	**KM**	**KD**	**MR**	**SK**	**MD**	**Bayan Obo**
	Sheet and Coordinate	İ26c4 Y: 60195 X: 85070	K39a2 Y: 83370 X: 12620	J40a2 Y: 31124 X: 66040	K41a3 Y: 96750 X: 76300	N32c2 Y: 88220 X: 09990	N32c1 Y: 13247 X: 11735	N27b3 Y: 01005 X: 27500	M26b2 Y: 65030 X: 06563	N44b1 Y: 15840 X: 50023	
Major Oxides (%)		*(n=10)*	*(n=6)*	*(n=6)*	*(n=10)*	*(n=2)*	*(n=3)*	*(n=1)*	*(n=2)*	(n=4)	*Yang vd.,2003*
	SiO_2	2,22	6,12	11,11	7,08	3,50	9,60	8,91	11,265	0,37	1,64
	Al_2O_3	0,95	1,38	0,39	2,07	57,90	49,70	56,89	12,9	0,02	0,29
	Fe_2O_3	4,23	1,65	16,16	2,58	22,90	26,50	17,31	55,735	0,07	11,78
	MgO	0,15	0,27	0,05	1,52	0,10	0,40	0,15	0,97	0,18	9,23
	CaO	37,63	56,97	45,23	53,18	0,10	0,10	0,13	0,305	55,72	23,92
	Na_2O	0,06	0,09	0,01	0,07	0,10	0,10	0,03	0,03	0,67	0,02
	K_2O	0,08	1,21	0,09	1,31	0,00	0,20	0,22	0,19	-	0,09
	TiO_2	0,05	0,33	0,01	0,06	2,90	2,60	2,52	0,53	-	0,30
	MnO	0,44	0,17	0,07	0,15	0,10	0,10	-	12,485	-	1,58
	P_2O_5	0,49	0,53	0,01	0,08	0,00	0,10	-	0,03	30,60	0,26
	LOI	4,46	8,55	5,55	13,84	11,70	8,10	13,60	5,3	12,10	
	Total	**50,76**	**77,27**	**78,68**	**81,94**	**99,40**	**97,60**	**99,76**	**99,74**	**99,71**	
Trace Elements (ppm)	Ba	>50000,00	226,80	9,20	1505,90	24,00	55,00	36,00	313	103,50	1089,00
	Rb	3,00	61,30	4,20	73,00	1,10	7,90	11,80	4,55	-	5,00
	Sr	3290,00	1474,70	39,70	880,40	56,20	40,30	13,40	104,95	1424,35	1621,00
	Th	1071,60	297,50	2,80	8,80	47,70	45,60	47,80	8,9	-	
	U	123,20	14,40	116,30	46,00	15,60	20,60	6,00	4,25	65,88	
	V	334,10	16,80	8,70	22,10	501,00	579,00	241,00	77	97,50	44,00
	Zr	21,30	360,40	12,50	15,30	612,10	619,60	464,10	114,6	12,25	1,00
	Y	331,70	214,60	698,50	13,20	191,50	87,40	49,70	30,2	41,95	132,00
	Nb	56,00	312,90	21,30	7,90	71,00	74,60	43,20	10,35	0,10	340,00
	Ga	3,30	11,10	2,90	4,60	71,10	61,80	50,90	28	-	
	Hf	0,60	2,80	0,60	0,50	16,90	17,50	13,60	3,05	0,10	
	Ta	0,96	2,66	0,76	0,18	5,00	5,00	3,50	0,75	-	
	Mo	56,00	3,80	11,90	1594,10	0,90	1,10	7,70	3,2	1,03	
	Cu	3,40	8,50	9160,50	291,80	13,10	18,20	3,30	35,25	27,05	13,00
	Pb	520,00	457,50	177,70	6661,60	61,30	17,20	57,50	197,7	6,15	
	Zn	244,50	219,00	484,80	1832,90	97,00	50,30	7,00	328,5	509,00	81,00
	Ni	21,10	108,00	385,30	177,20	83,90	73,60	66,20	78,85	12,38	5,00

K/Ar radiometric dating of the phonolites and alkali vein rocks in the deposit indicates that the mineralization is Upper Oligocene (23 Ma, Nikiforov et al., 2014).

Exploratory drilling by MTA at Kızılcaören indicates reserves of 0,38 million tons of ore with a grade of 0,212 % ThO_2 and 4,78 million tons ore with an average grade of 2,78% NTE (Ce + La + Nd + Y) (Kaplan 1977*a*, *b*). MTA also identifies the potential

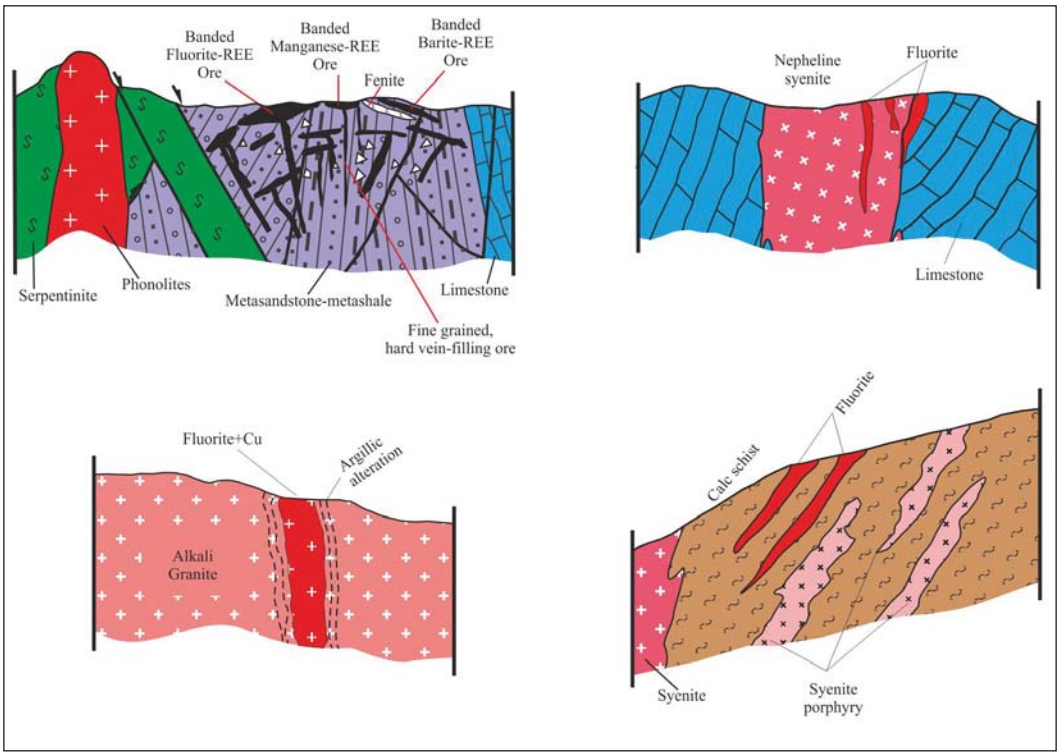

Figure 3- Sections showing the wall rock relationships of the carbonatite-hosted Kızılcaören REE-F-Ba-Th deposit and the carbonatite-nepheline syenite-hosted Kuluncak REE-bearing fluorite and the Keban and Divriği Fluorite-REE mineralization associated with alkaline intrusives (not to scale).

for ten million tons of fluoride and barite (Kaplan, 1997*b*). The current license holder, Eti Mining, carried out a detailed study between 2015-2017 related to resources and technological studies on the recovery of barite, fluorite and thorium.

The main REE mineral is bastnasite (Kaplan 1977*a*, Özgenç, 1993) and microprobe data indicates that it also contains thorium (Nikiforov et al., 2014). Studies indicate that fluorite, barite, pyrite and Mn-carbonate minerals are paragenetically linked to bastnasite with oxidation of carbonates and pyrite leading to Fe and Mn oxides. Enrichment of La and Ce enrichment is typical, and the chondrite normalized REE pattern shows a strong decrease from LREE towards HREE (Figure 4).

Fluid inclusion studies indicate multiple phases of mineralization. For example, purple and green fluorites contain both two phase and three phase inclusions with homogenization temperatures of between 150-394°C. Salinities are about 11% for two-phase inclusions and 32% (NaCl weight equivalent) for three-phase inclusions (Altuncu, 2009) and the results from fluid inclusion studies at Kızılcaören resemble those for the Kuluncak, Divriği and Keban mineralization.

Fluoride minerals expand during fluid inclusion measurements, which cause higher homogenization values to be measured than the actual homogenization temperature. For this reason, it should be taken into consideration that the homogenization temperatures obtained from fluoride minerals may be higher than actual temperatures.

3.2. Kuluncak REE-bearing Fluorite Mineralization

The Kuluncak REE - bearing Fluorite mineralization is located near the Başaören village of Kuluncak district in Malatya within a license held by MTA which is undertaking intensive exploration. The mineralization is observed in the Upper Cretaceous-Paleocene (Leo et al., 1974) nepheline syenite and in narrow zones at the contacts with Cretaceous limestone within an ophiolitic mélange setting. Purple fluorites are the main ore mineral and compared to other formations except the REE high Nb and Ta are observed in the chemical analyzes carried out in the mineralization. The TREE value in the fluorite ore is 7254,7 ppm. A typical decrease in the chondrite normalized pattern is observed from LREE towards HREE. The Ce and Th-rich mineral, britholite was

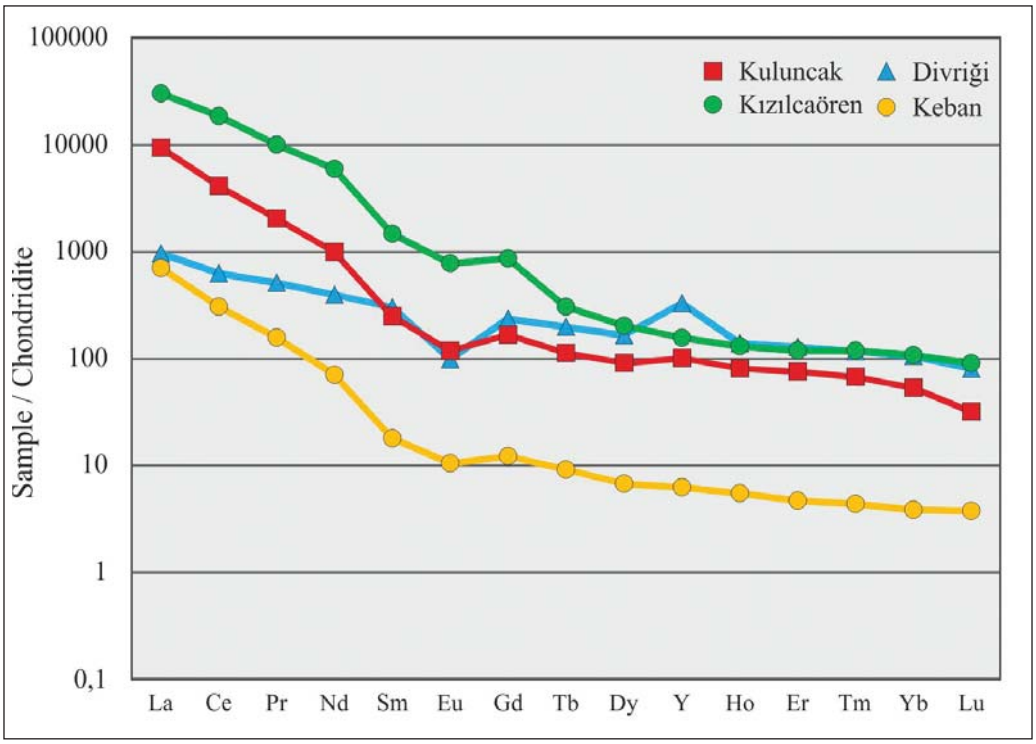

Figure 4- Chondrite normalized REE patterns of Kızılcaören, Kuluncak, Keban and Divriği Fluorite-REE mineralization. A decrease from LREE to HREE is clearly seen in the chondrite normalized patterns of the four deposits.

detected by Özgenç and Kibici (1994). Fluid inclusion data for the Kuluncak fluorites give homogenization temperatures ranging from 145-600°C with salinities between 4-64 % NaCl equivalent, broadly similar to results for the Kızılcaören deposit (Altuncu, 2009).

3.3. Divriği Fluorite-REE-Cu Mineralization

The mineralization in Divriği district of Sivas province is located within the Efendi River at elevations of 1600 m in Paleocene-Eocene (Boztuğ et al., 2007) alkali granites (Figure 3). The mineralised zone has a thickness ranging from 0,6 to 1 m at the surface and a length of approximately 300 m. It was discovered in 1958 by MTA during uranium exploration where investigations, including drilling, revealed 50m long galleries and an estimated 35,000 tons of Cu-fluorite mineralization. The center of the ore vein is green fluorite and the wall zones are rich in chalcopyrite, galena and sphalerite. The ore also includes arsenopyrite, pyrite, bismutinite, covellite, chalcocite calcite, quartz, clay (possibly kaolinite) and limonites after pyrite.

The average TREE value of 6 fluorite-rich samples is 1363 ppm (Table 1), and the REE pattern dominated by LREE is typical. The ore samples contain very high levels of Y with an average of 698,5 ppm (Table 1). Fluid inclusion studies on fluorite indicate hydrothermal solutions at temperatures ranging from 190-455 °C and salinity ranges between 10-32% (NaCl weight equivalent) (Altuncu, 2009).

3.4. Keban Fluorite-REE Mineralization

Keban Fluorite-REE mineralization occurs as veins within Permo-Triassic calcareous schists. The schists are cut by the Upper Cretaceous Keban syenites (Kuşcu et al., 2013) and numerous syenite porphyry dykes and Fluorite-REE mineralizations are common in the region. Fluorite mineralizations consist of stockwork veins reaching one meter in thickness and contain 540 ppm TREE in average (Table 1). The amount of Pb and Zn is higher among the trace elements (Table 2). Fluorite specimens contain fluid inclusions with two and three phases and homogenization temperatures range from 125-600°C with salinities from 7-61% (NaCl equivalent) (Altuncu, 2009). The three-phase fluid inclusions show resemblance with Kızılcaören, Kuluncak and Divriği ores. The REE pattern of the Keban mineralization is enriched in LREE, similar to three deposits described above (Figure 4).

4. Bauxite Deposits and REE Contents of Source Rocks

All bauxite deposits in Turkey are located in the Taurus belt except for the Kokaksu (Zonguldak) deposit (Figure 1). Some of these bauxite deposits and their source rocks (protoliths) contain significant REE and therefore may be a potential source, given Chinese production of REE from clays in the ion adsorbtion deposits. Therefore, we have investigated the chemistry of the bauxite deposits and their source rocks in the Taurus belt to enable comparison with both bauxite and protolith compositions for the REE deposits in China (Tables 1 and 2). Some data were taken from Karadağ et al. (2006) and Hanilçi (2013).

REE contents and chemical composition of bauxite deposits in Turkey are recorded in tables 1 and 2. This data includes: bauxite and phyllitic source rocks in the Seydişehir region by Karadağ et al. (2009); red mud waste from the Seydişehir bauxite deposits, by Karadağ et al. (2006) and Deady et al. (2016*b*); the Kemiklitepe and Kızıldağ bauxites and the slate protoliths of Kızıldağ bauxites in the Bolkardağı region by Hanilçi (2013); and the Yalvaç-Şarkikaraağaç bauxites and basaltic protolith in the Isparta region (this study). REE analyses indicate wide variation with highest REE values in the bauxites and protolith of the Bolkardağı region, comparable to the values for the REE deposits of the Ganzhou region in China (Table 1). The REE contents of bauxite and protolites of Bolkardağı region are largely similar to REE elements in Ganzhou region clays in China (Figure 5).

4.1. Mortaş and Doğankuzu Bauxites

The Mortaş-Doğankuz bauxite deposits are located in the discordance line Cenomanian-Turonian of the Upper Cretaceous limestones (Karadağ, 1987; Öztürk et al., 2002, Figure 6a). The provide ore is for the Seydişehir alumina smelter. At the bottom and top of the bauxites, and also along internal fracture lines, are greenish-colored zones rich in fine grained pyrite and marcasite. The TREE values of the Mortaş bauxites range between 282-986 ppm (Karadağ et al., 2006). The red mud waste from alumina production contains approximately 80 ppm Y and 1777 ppm TREE (Deady et al., 2016*b*) (Table 1). However, analysis by Karadağ et al. (2006), gave 1966 ppm TREE, including both Y and Sc.

4.2. Yalvaç-Şarkikaraağaç Bauxites

The Yalvaç-Şarkikaraağaç bauxites are observed in three main zones within Upper Jurassic units in the Isparta region that extend for tens of kilometers (Ayhan and Karadağ, 1985). Each zone developed from weathering of Jurassic basalt with the transition from basalt to bauxite clearly evident, as shown in figure 6b. These bauxites are the only deposits identified on basalt protolith within the Taurus belt and their iron-rich character has prevented production, despite large reserves. The low TREE value of 293 ppm and uranium content of 1 ppm,10 times less than other bauxites, reflects the low values within the basalt protolith (Table 1).

4.3. REE Content of the Bolkardağı Bauxites and Source Rocks

The geology and geochemistry of the bauxites in the Bolkardağı region and protoliths were detailed by Hanilçi (2013). These bauxites developed on Lower and Upper Triassic shales (Figures 2 and 7) and show enrichment in REE. Among bauxites in the region, especially the shales, which are the source rock (protolith) of the Kızıldağ bauxites, and the Kemiklitepe bauxites show enrichment in terms of HREE and their average TREE values are 1545 and 1693 ppm, respectively (Table 1). The REE composition of the Kemiklitepe bauxite deposit and the Lower Triassic shales which are the source rocks of the Kızıldağ bauxite mineralization, show one to one resemblance with REE values of the Guangzhou clays in China (Table 1). The low U and Th contents of the clays, bauxites and bauxite protoliths when the compared to hydrothermal and placer type REE mineralization (Table 1) provides a significant advantage in processing due to minimal radioactive waste.

The Lower Triassic shales forming the protolith of bauxites in the Bolkardağı region were probably derived from the Ordovician Seydişehir schists because of the similarity of REE patterns and absence of granite or aluminosilicatic metamorphic rocks in the region. The bauxites developed in the Upper Triassic-Aalenian (Middle Jurassic) period (Hanilçi, 2013), when the pre-Aalenian Tauride Anatolide continent should have been located in tropical latitudes suitable for lateritic soil development. As a result, it is likely that significant REE resources would have been stored in the Upper Triassic clays of the Tauride-Anatolide

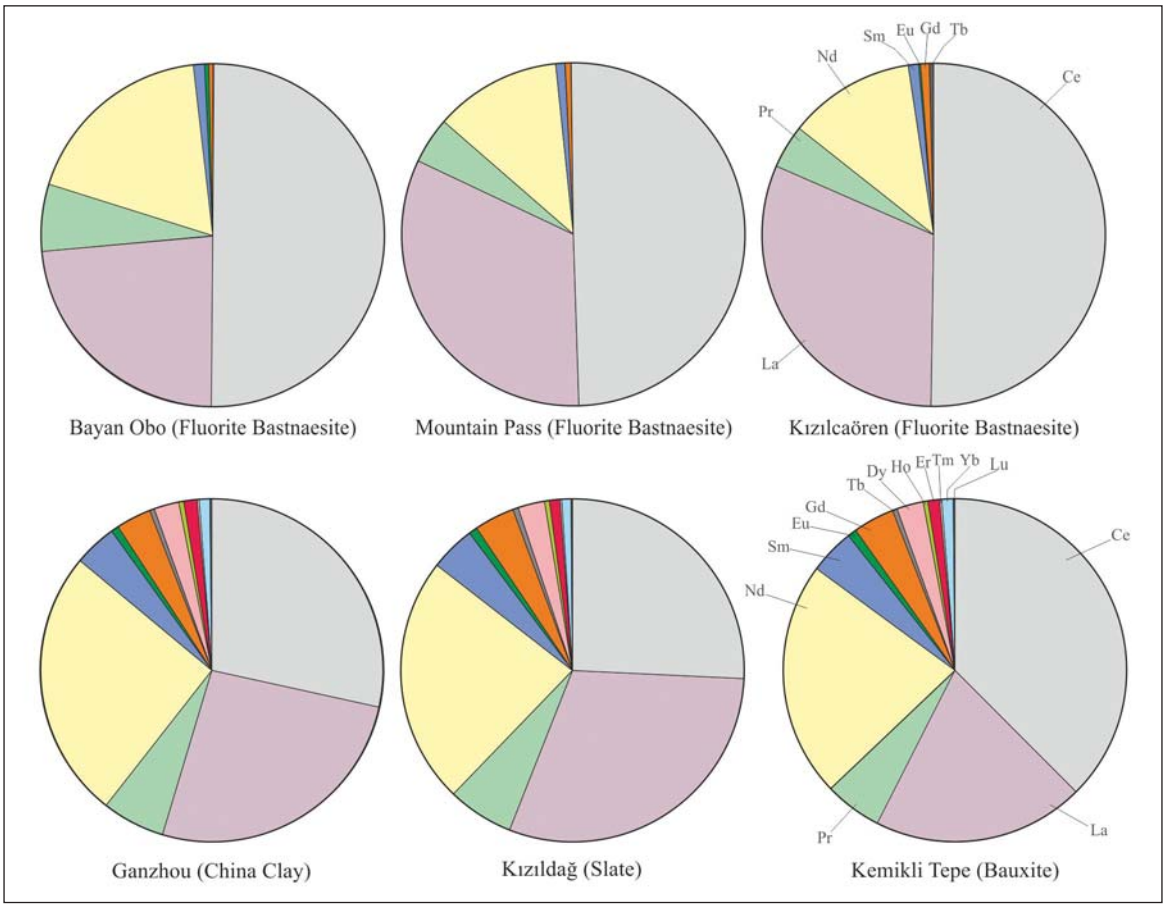

Figure 5- Comparison of REE abundance in the Bayan Obo (China), Mt. Pass (USA) and Kızılcaören REE deposits associated with carbonatite-alkaline magmatic rocks (top row), and the clay based Ganzhou region deposits with the Lower Triassic slate protoliths of the Kızıldağ bauxites and Kemiklitepe bauxites (bottom row). Data for Bayan Obo and Mt. Pass deposits from Haque et al. (2014); for Kızıldağ and Kemikli Tepe from Hanilçi (2013). The REE composition, the Kızılcaören deposit resembles the well-known carbonatite deposits (Mt Pass, USA and Bayan Obo, China), while the REE profile and abundances for bauxite and Triassic slate protoliths from the Bolkardağı region resemble deposits of the Ganzhou province in China.

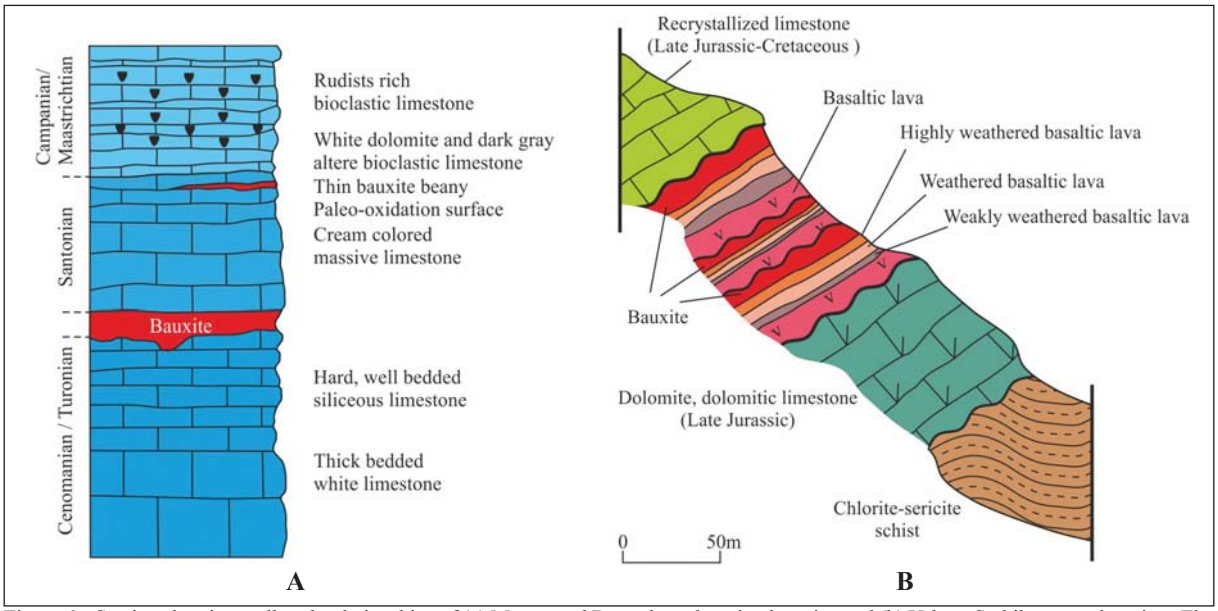

Figure 6- Section showing wall rock relationships of (a) Mortaş and Doğankuzu bauxite deposits, and (b) Yalvaç-Şarkikaraağaç bauxites. The different REE contents of both bauxite deposits (see table 1) clearly indicates their different source rocks.

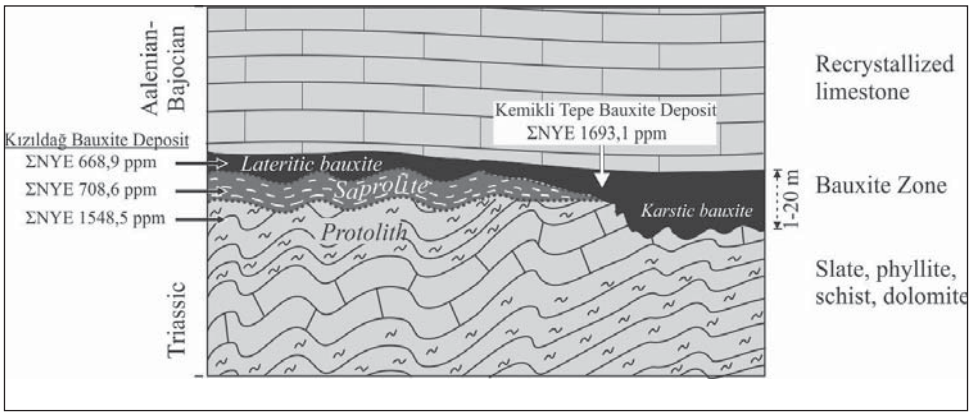

Figure 7- Relationship of the Triassic shales which are source rocks (protolith) of bauxite and the bauxites in Bolkardağı province (Hanilçi, 2013).

belt. Clay grains formed during lateritic weathering will balance any electrostatic charge deficit at their outer margins with ions of Ca^{+2}, Na^{+1}, NTE^{-3} etc. leading to enrichment by adsorption on to their outer surface. This process can lead to REE enrichment in clays and their subsequent incorporation into bauxites.

5. REE and Heavy Mineral - Bearing Placer Formations

The Çanaklı REE and heavy mineral-bearing mineralization in the Burdur region (Figure 2) is a unique placer formation that is relatively HREE -rich. The mineralization is a terrestrial accumulation of the Plio-quaternary limestones. Drillings has defined reserve of 80 million tons in the Canaklı-1 area with approximately 808 ppm TREE, and grades of 0.72% TiO_2 and 490 ppm ZrO_2, and 414 million tons of reserve with 627 ppm TREE, and grades of 0.7% TiO_2 and 404 ppm ZrO_2 in the Çanaklı-2 region (Cox et al., 2013; Deady et al., 2016*a*). The major minerals containing REE are allanite, cehvkinite, titanite and apatite, and the minerals containing thorium and uranium are torite, uranotorite and betafite. It was reported that this mineralization was the result of terrestrial decomposition of a Pliocene alkaline volcanic eruption (Cox et al., 2013)

6. Sedimentary Phosphorites

Marine sedimentary phosphorite deposits are regarded as the world's most abundant and clean REE mineral deposits (Emsbo et al., 2015). TREE values of the phosphorites in different age ranges ranging from Paleozoic to recent in different regions of the world reached 1200 ppm (0.12%). REE substitutes for Ca in flour-apatite ($Ca_5(PO_4)_3F$) as does Sr and U. Within Paleozoic phosphate deposits in the USA, there are varying amounts of TREE (900-1200 ppm) and HREE (400-600 ppm). According to Emsbo et al. (2015), these HREE values are higher than in deposits currently operated by China (50-200 ppm). The phosphorites are likened to REE of the deep sea muds (Kato et al., 2011) both because of their negative Ce pattern and high values (Emsbo et al., 2015).

Phosphate deposits are located in cherty levels of the Upper Cretaceous limestones around Mazıdağ (Mardin) in Turkey. This deposit is made up of three main mineralized zones called Taşıt at the bottom, Kasrik in the middle and Şemikan at the top. Etibank identified total reserves of 330 million tons (Apaydın and Erseçen, 1981) with 270 million tons at a grade of 10-12% P_2O_5, 30 million tons with a grade of 22% P_2O_5, and 30 million tons of calcareous ore requiring calcination with a grade of 14% P_2O_5.

The Eti Bakır Company has initiated work to build a modern plant for phosphate production and carried out additional drilling studies in the deposit since 2013. The most important mineralization is the upper Şemikan phosphate zone (Imamoğlu et al., 2009) and REE analyses were carried out on four specimens taken from this zone. It consists of 1,5-2 m thick, massive phosphate ore with shark teeth fossils, overlain by two or three thin phosphate levels (10-20 cm) among thin chert bands and white massive chert (Figure 8). TREE values are extremely low at 40 ppm (excluding Y), similar to the lateral equivalent of the Jordan deposit (Al-Shereideh et al., 2010), with a typical negative Ce anomaly. Uranium values are relatively high at 71 ppm (Table 1).

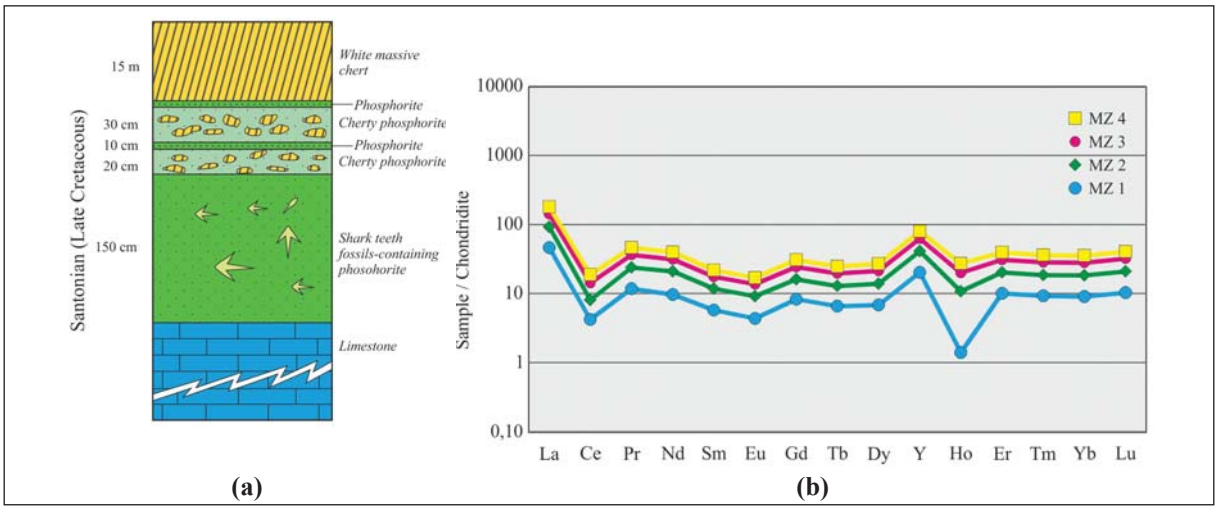

Figure 8- (a) Stratigraphic position and (b) the chondrite normalized REE pattern of the Mazıdağ phosphorites. The horizontal REE pattern indicates that HREE and LREE did not differentiate. Mazıdağ phosphorites with their strong negative Ce and Ho and positive Y anomaly and low REE pattern resemble the Jordanian phosphorites.

7. Discussion and Results

REE deposits associated with carbonatite-alkaline magmatism in Turkey are in the form of vein type hydrothermal-pegmatitic fillings and rich in LREE like La and Ce. They exhibit mineralogic and geochemical similarities to USA's Mt. Pass and China's Bayan Obo deposits. At the same time, the Kızılcaören REE-Ba-F-Th deposit is also contains significant levels of Th with 10 samples averaging 1072 ppm Th. Due to radioactive elements such as Th and U in these deposits they can often be detected with relative ease, however their exploitation and processing can result in environmental and public health problems occurs during the REE production. Similar problems are to be expected from exploitation of placer deposits linked to alkaline magmatism, such as Canakli.

In contrast, the clay-based HREE deposits contain minimal radioactivity and can be exploited with blasting and rock breaking, resulting in lower mining costs. In this context, it is necessary to seriously consider the recovery of REE from the HREE-rich shales and clayey schists of the Bolkardağı region. For example, mining operations at more than 200 deposits located at 24° northern latitudes in Jiangxi province, southern China, REEs are stripped from the exterior of clays by ion exchange. The recovery rate of TREEs from these deposits ranges from 40% to 85% with an average of about 70%. TREEs of the deposits (including Y) range between 300-6500 ppm (Roskill, 2011) and their average is around 1500 ppm. In ore recovery, the application of $(NH_4)_2SO_4$ leads to NH_4^{+1} entering the clay with REE being adsorbed to form $REE_2(SO_4)_3$ (Wu et al., 1990, Chi and Tian, 2008). Addition of oxalic acid forms REE oxalate ($REE_2(C_2O_4)_3$) precipitate that is heated to 900°C to leave a REE oxide residue (Papangelakis and Moldoveanu, 2014). These REE oxides are then subject to individual REE element separation. According to Papangelakis and Moldoveanu (2014), the recovery of REE from clays occurs in the following reactions:

$$2\text{Clay-REE}+3M_2SO_4 = 2\ \text{Clay}M_3+REE_2(SO_4)_3$$

$$REE_2(SO4)_3+3\ H_2C_2O_4+10\ H_2O = REE_2(C_2O_4)_3\cdot 10H_2O+H_2SO_4$$

$$REE_2(C_2O_4)_3\cdot 10H_2O = REE_2O_3+3CO+3CO_2+10H_2O$$

REE recovery can proceed by tank leach or heap leach, with NaCl used in previous times because of its ability to ion exchange, instead of ammonium sulfate. The production from clay based REE deposits in China constituted 26% of China's total REE production between 1988 and 2007, and has increased to 36% after 2009 (Yang et al., 2013). Recovery of the HREEs is lower due to their stronger bond with clays. The very low level of U and Th eliminates any problems linked to radiation and REE acquisition from clays is increasingly preferred.

In Turkey, shales rich in REE occur on the Tauride-Anatolide platform and include the Ordovician Seydişehir schists (Monod, 1967) with TREE of 300 ppm (Karadağ et al., 2009) and the Lower Triassic shale-slates in the Bolkardağı region contain much

higher TREE (Table 1, and Hanilçi, 2013). Figure 9 shows the similarity between chondrite-normalized patterns of the Triassic shale-slates and Seydişehir phyllites. Under tropical weathering conditions during the Triassic, it is likely that clays developed on the Seydişehir phyllites contained TREE of between 500-1800 ppm, based on REE enrichment in China. If these REE-enriched clays were eroded into a sedimentary basin during the Triassic, it could explain the similarity between the chondrite-normalised REE patterns of the Ordovician Phyllites and Triassic shales-slates. Subsequent exposure and tropical weathering of these Triassic sediments would then give rise to the bauxites in the Bolkardağı region with relatively high REE content. The Triassic bauxite and shales were subsequently covered by marine carbonates in the Jurassic and metamorphosed to lower greenschist facies during Cretaceous-Eocene orogenesis (Hanilçi, 2013).

Our study indicates that the occurrence of REE-enriched Triassic shales and slates, and potentially economic REE deposits in the some Triassic-Jurassic bauxites of the Bolkardağı region can be explained by the REE content of the Ordovician Seydişehir phyllites and their exposure to tropical weathering during the Triassic. Interestingly, the chondrite-normalized REE patterns in the deposits of the Ganzhou region in China are similar to the REE patterns of bauxite and its source rocks in the Bolkardağı region (Figure 9). In addition, the clay-based REE deposits in China are enriched by a factor of six compared with the REE content of the Mesozoic peraluminous granites (average 350 ppm TREE) which form the protolith. This REE enrichment factor is comparable to the difference between the REE content of the Seydişehir phyllites and Triassic shales-slates (Table 1). These comparisons indicate that the Triassic shales-slates of the Tauride belt warrant further investigation for bauxite-associated REE deposits.

Operating deposits in the Ganzhou region of China have TREE grades (including Y) > 500 ppm. Deposits with reserves >0.5 million tons are classified as large, and between 0.5-0.05 million tons are medium-size (Sanematsu and Watanabe, 2016). Ore zones are usually 6-10 meters thick, locally 30 m, and rarely reaching 60 m (Yang et al., 1981; Chen, 2011). The protolith is mainly ilmenite type granite, and very rarely on phyllites (Zhang, 1990). The estimated reserve of REE deposits in China (excluding potential resources) is around 15 million tons (Sanematsu and Watanabe, 2016). Factors such as degree of weathering and the specific REE-bearing mineralogy (bastnasite,

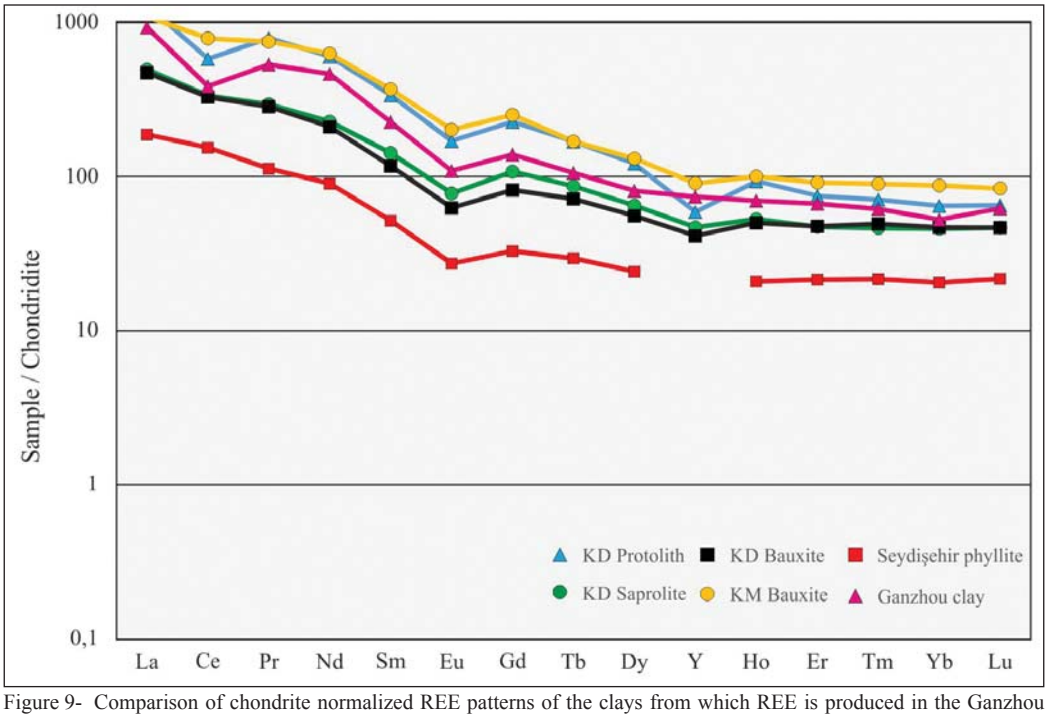

Figure 9- Comparison of chondrite normalized REE patterns of the clays from which REE is produced in the Ganzhou region of China and bauxite in the Taurus belt and its possible source rocks (KD: Kızıldağ, KD Pro: Kızıldağ protolith, KD Sap: Kızıldağ saprolite, KM: Kemiklitepe).

fluorite, apatite, allanite, xenotime etc.) determine the activation and fractionation of REE (Yusoff et al., 2013). For example, in the uppermost soil zone there is a positive Ce anomaly, due to oxidation of Ce from +3 to +4 and accumulation in the form of CeO_2, with a corresponding Ce depletion in the REE accumulation zone beneath it (Berger et al., 2014). Whilst there are similarities between the Triassic shales and bauxites of Turkey and the chondrite normalized patterns and REE contents of the "Ion Adsorption Type" ore in China, there are significant differences to be considered in evaluating the potential of the Bolkardağı region bauxites. For example, with granitic protolith REE can be transported at surface conditions by bonding with carbonates and bicarbonates ($REECOO_3^+$, $REEHCO_3^{2+}$; see Liu and Byrae, 1998), and also fluorides and organic complexes (Chen et al., 2001) when HREE bond more strongly with organic complexes. In addition, the host mineralogy can be more important than the chemical complex. Whereas REE are adsorbed on the outside of clays in China and can yield high recoveries in processing, in Turkey the bauxites have experienced low grade metamorphism and REE are more likely to be hosted within the crystal lattice and yield lower recoveries. Therefore, any new evaluation of the bauxite-related REE potential in the Bolkardağı region and Tauride belt will need to understand these differences and their potential impact on the size of the resource base required for viable operations.

In contrast the Cretaceous phosphorite occurrences in Turkey contain only one twentieth of the REE content of the REE-rich phosphorite deposits elsewhere in the world and are clearly uneconomic as a source of REE. Nevertheless, investigation of the REE potential of phosphatic sediments in the Lower Paleozoic belt in Turkey should not be ignored.

Acknowledgements

The authors are grateful to the General Directorate of Eti Maden for permitting field study in the Kızılcaören Deposit and to the İstanbul University-Cerrahpaşa Scientific Research Projects Unit (Project no: 54348) for their financial contributions.

References

Al-Shereideh, S.A., Khaled Tarawneh, K., Nawafleh, H., El-Radaideh, N., Moumani, K. 2010. Geology and Mineralogy of Jabal Kabid Phosphorite Deposits, Southeastern Jordan. Jordan Journal of Earth and Environmental Sciences 3, 99-110

Altuncu, S. 2009. Türkiye Fluorit Yataklarının Karşılaştırmalı İncelenmesi. Doktora Tezi, İstanbul Üniversitesi, Fen Bilimleri Enstitüsü, 147 s. (unpublished).

Apaydın, N., Erseçen, N.1981. Known ore and mineral resources of Turkey: Ankara, Mineral Research and Exploration Institute of Turkey, 67 p.

Ayhan, A., Karadağ, M., M. 1985. Şarkikaraağaç (Isparta) güneyinde bulunan boksitli demir ve demirli boksit yataklarının jeolojisi ve oluşumu. Türkiye Jeoloji Kurumu Bülteni 28, 137-146.

Berger, A., Janots, E., Gnos, E., Frei, R., Bernier, F. 2014. Rare earth element mineralogy and geochemistry in a laterite profile from Madagascar. Applied Geochemistry 41, 218–228.

Boynton, W.V. 1984. Geochemistry of the rare earth elements: meteorite studies. In: Rare earth element geochemistry, P.Henderson (ed.), Elsevier, 63-114.

Boztuğ, D., Harlavan, Y., Arehart, G.B., Satır, M., Avcı, N. 2007. K-Ar age, whole-rock and isotope geochemistry of A-type granitoids in the Divriği-Sivas region, eastern-central Anatolia, Turkey. Lithos 97, 193-218.

Chen, Z. 2011. Global Rare Earth Resources and Scenarios for Future Rare Earth Industry, Journal of Rare Earths 29, 1-6

Chen, B.H., Wu, F.H., Liu, F. F. 2001. Experimental study on the effects of organic acids on the dissolution of REE in the weathering crust of granite. Chinese Journal of Geochemistry 20, 144–151.

Chi, R., A. Tian, J. 2008. Weathered crust elution-deposited rare earth ores: New York, Nova Science Publishers, 288 p.

Cox J.J. Fayram, T. 2013. NI 43-101 Technical Report on the Aksu Diamas Rare Earth Element Project, Isparta district, Turkey. AMK Mineral Inc. Toronto, Canada, 29 p.

Deady, E., Goodenough K., Lacinska A., Hardy L., Shaw R. 2016*a*. Rare earth element placer deposits and alkaline volcanics: a case study from Aksu Diamas, Çanaklı, Turkey. Applied Earth Science 125, 79-80.

Deady, E.A., Muchos, E., Goodenough, K., Williamson, B. J., Wall, F. 2016*b*. A review of the potential for rare earth element resources from European red muds: examples from Seydişehir, Turkey and Parnassus-Giona, Greece Mineralogical Magazine 80, 43-61.

Emsbo, P., McLaughlin P.I., George N., Breit, G.N., Edward A. du Bray., Koenig, A.E. 2015. Rare earth elements in sedimentary phosphate deposits: Solution to the global REE crisis? Gondwana Research 27, 2, 776-785

Hanilçi, N. 2013. Geological and geochemical evolution of the Bolkardağı bauxite deposits, Karaman, Turkey: Transformation from shale to bauxite. Journal of Geochemical Exploration 133, 118-137.

Haque, N., Hughes, A., Lim, S., Vernon, C. 2014. Rare earth elements: Overview of mining mineralogy uses sustainability and environmental impact. Resources 3, 614–635.

Hewett, D.F. 1954. History of discovery at Mountain Pass, California. In Rare-earth mineral deposits of the Mountain Pass District, San Bernardino, County, California. USGS Prof. 261 p.

İmamoğlu, M.Ş., Nathan, Y., Coban H., Soudry D., Glenn C. 2009. Geochemical, mineralogical and isotopic signatures of the Semikan, West Kasrık Turkish phosphorites from the Derik–Mazıdağı–Mardin area, SE Anatolia. International Journal of Earth Sciences (Geol Rundsch) 98,1679–1690

Kaplan, H. 1977*a*. Eskişehir-Sivrihisar-Kızılcaören köyü yakın güneyi bastnaesit-barit -flourit kompleks cevher yatağı nihai etüd raporu, Maden Tetkik ve Arama Genel Müdürlüğü Rad. Min. Servisi, Rapor. No 482.

Kaplan, H. 1977*b*. Eskişehir-Sivrihisar-Kızılcaören köyü yakın güneyi Nadir Toprak Elementleri ve toryum kompleks cevher yatağı: Jeoloji Mühendisliği Dergisi 2, 29-34.

Karadağ, M. 1987. Seydişehir bölgesi boksitlerinin jeolojik petrografik ve jenetik incelenmesi: Doktora Tezi, Selçuk Üniv., Fen Bil. Ens., (yayımlanmamış), 265 s.

Karadağ, M. M., Arık, F., Ayhan, A., Döyen., A., Küpeli, Ş., Zedef, V. 2006. Mortaş (Seydişehir-Konya) boksit yatağının Nadir Toprak element (NTE) potansiyeli. 59. Türkiye Jeoloji Kurultayı, Bildiri Özleri Kitabı, 154-156.

Karadağ, M.M., Küpeli, Ş., Arık, F., Ayhan, A., Zedef, V., Döyen, A. 2009. Rare earth element (REE) geochemistry and genetic implications of the Mortaş-bauxite deposit (Seydişehir/Konya-Southern Turkey). Chem. Erde Geochem. 69, 143-159.

Kato, Y., Fujinaga, K., Nakamura, K., Takaya, Y., Kitamura, K., Ohta, J., Toda, R., Nakashima, T., Iwamori, H. 2011. Deep-sea mud in the Pacific Ocean as a potential resource for rare-earth elements. Nature Geoscience 4, 535-539.

Kuşcu, İ, Tosdal, RM., Gençalioğlu-Kuşcu, G., Friedman, R. 2013. Late Cretaceous to middle Eocene magmatism and metallogeny of a portion of the Southeastern Anatolian Orogenic Belt, east central Turkey, Economic Geology 108, 641-666

Leo, G. W., Marvin, R. F., Mehnert, H. H. 1974. Geologic framework of the Kuluncak-Sofular area, east-central Turkey, and K-Ar ages of igneous rocks: Geological Society of America Bulletin 85, 1785-1788.

Liu, X.W., Byrne, R.H. 1998. Comprehensive investigation of yttrium and rare earth element complexation by carbonate ions using ICP-Mass Spectrometry: Journal of Solution Chemistry 27, 803-815.

Migdisov, A. A., Williams-Jones A. E., Wagner, T. 2009. An experimental study of the solubility and speciation of the Rare Earth Elements (III) in fluoride-and chloride-bearing aqueous solutions at temperatures up to 300 C. Geochimica et Cosmochimica Acta, 7087-7109.

Monod, O. 1967. Batı Toros Kalkerlerinin temelindeki Seydişelıir şistlerinde bulunan Ordovisyen bir fauna. Maden Tetkik ve Arama Dergisi 69, 76-86.

Nikiforov A.V., Öztürk, H., Altuncu, S., Lebedev, V.A. 2014. Kızılcaören Ore-bearing Complex with Carbonatites (Northwestern Anatolia, Turkey): Formation Time and Mineralogy of Rocks. Geology of Ore Deposits 56, 35-60.

Özgenç, İ. 1993. Kızılcaören (Sivrihisar-Eskişehir) karbotermal bastneazit-fluorit-barit yatağının jeolojisi ve NTE jeokimyası: Türkiye Jeoloji Bülteni 36, 75-80.

Özgenç, İ. Kibici, Y. 1994. The geology and chemical-mineralogical properties of Britholite veins of Başören village (Kuluncak-Malatya), Turkey. Geological Bulletin of Turkey 37, 77-85.

Öztürk, H., Hein, J., Hanilçi, N. 2002. Genesis of the Doğankuzu and Mortaş bauxite deposits, Taurides, Turkey: Separation of Al, Fe, and Mn and implications for passive margin metallogeny. Economic Geology 97, 1063-1077.

Paleparthi, J., Chakrabarti, R., Banerjee, D., Guin, R., Ghosal, S., Agrahari, S., Sengupta, D. 2017. Economically viable rare earth element deposits along beach

placers of Andhra Pradesh, eastern coast of India. Arabian Journal of Geosciences,2-8.

Papangelakis, V.G., Moldoveanu, G.A. 2014. Recovery of rare earth elements from clay minerals. In: Proceedings of the 1st Rare Earth Resources Conference, Milos, 191-202.

Rocha, A., Schissel, D., Sprecher, A., de Tarso, P., Goode, J. 2013. Process Development for the Serra Verde Weathered Crust Elution-deposited Rare Earth Deposit in Brazil, in Rare Earth Elements-Proceedings of the 52nd Conference of Metallurgists (COM 2013), London, I., Goode, J., Moldoveanu, G., and Rayat, M. eds., Metallurgical Society of the Canadian Institute of Mining, Metallurgy and Petroleum (MetSoc-CIM), Montreal, Canada, 277-288.

Roskill, 2011. Rare Earths Yttrium: Market Outlook to 2015, 14th edition, 2011: Roskill Information Services, Ltd., London, 492 p.

Sanematsu, K., Watanabe, Y. 2016. Characteristics and Genesis of Ion Adsorption-Type Rare Earth Element Deposits. Society of Economic Geologists, Inc. Reviews in Economic Geology 18, 55-79.

Stumpel, E.F., Kırıkoğlu, M.S. 1985. Fluorite-Barite-Rare Earths Deposits at Kızılcaören, Turkey. Mitt. Österr. Geol. Ges. 78, 193-200.

Voßenkaul, D., Stoltz, N.B., Meyer, F.M., Friedrich, B. 2015. Extraction of Rare Earth Elements from Ion Adsorption Clays, European Metallurgical Conference. Proceedings of EMC, Germany, 1-11.

Wu, C.Y., Huang, D.H., Guo, Z.G. 1990. REE geochemistry in the weathered crust of granites, Longnan area, Jiangxi Province. Acta W Geologica Sinica 3, 193-210.

Xu, C., Taylor, R.N., Li, W., Kynicky, J., Chakhmouradian, A.R., Song, W. 2012. Comparison of fluorite geochemistry from REE deposits in the Panxi region and Bayan Obo, China. Journal Asian Earth Sciences 57, 76-89.

Yang, X.J., Lin, A.J., Li, X.L., Wu, Y.D., Zhou, W.B., Chen, Z.H. 2013. China's ion-adsorption rare earth resources, mining consequences and preservation. Environmental Development, 8, 131-136.

Yang, X.M., Yang, X.Y., Zheng, Y.F., Le Bas, M.J. 2003. A rare earth element-rich carbonatite dyke at Bayan Obo, Inner Mongolia, North China Mineralogy and Petrology, 78 , pp. 93-110.

Yang, Y.Q., Hu, Z.S., Luo, Z.M. 1981. Geological characteristics of mineralization of rare earth deposits of the ion-adsorption type and their prospecting direction. Bulletin of Institute of Mineral Deposit, Chinese Academy of Geological Sciences 2, 102-118 (in Chinese with English abstract).

Yusoff, Z.M., Ngwenya, B.T., Parsons, I. 2013. Mobility and fractionation of REEs during deep weathering of geochemically contrasting granites in a tropical setting, Malaysia. Chemical Geology 349, 71-86.

Zhang, Z.H. 1990. A study on weathering crust ion adsorption type REE deposit, South China: Contributions to Geology and Mineral Resources Research 5, 57-, 71 (in Chinese with English abstract).

Bulletin of the Mineral Research and Exploration

http://bulletin.mta.gov.tr

Relationship between petroleum and iodine in Southeastern Anatolia Basin

Adil ÖZDEMİR[a*]

[a]*Adil Özdemir Consulting, Ankara, Türkey. orcid.org/0000-0002-3975-2846*

Research Article

Keywords:
Southeastern Anatolia basin, Iodine, Petroleum hydrogeology, Oil and gas exploration, Oilfield waters, Formation waters.

ABSTRACT

This study was made for investigating the relationship between iodine and hydrocarbon accumulations and to determine iodine contents of formation waters in the Southeastern Anatolia basin oilfields where have been produced almost all of the Turkey oils (more than 95%). Formation water samples have taken from 234 production wells in 49 oilfields which have different geological structures where oil and gas production has performed by the Turkish Petroleum Company (TPAO). Also, the drilling mud samples from EBY-17 oilwell in Elbeyli (Adıyaman) field has collected, and their iodine analyses were carried out. Although the fields in the Southeastern Anatolia basin are old and some fields the secondary production methods are used, the high relationship between the oil and gas deposits and iodine were proved. As well as in other oil and gas fields in the world, not all reservoir waters in the Southeastern Anatolia basin are saline. However, all of them are rich in iodine. Therefore, the iodine-rich waters are a direct indicator for oil and gas producible reservoirs (containing mature hydrocarbon). Reservoir-targeted iodine geology and hydrogeology methods have simple sampling process, and laboratory analyses can result at a short time. The results are low cost, reliable and consistent. In the case when these data are utilized with other geological and geophysical methods, it is determined will be a practical and useful tool to reduce the hydrocarbon exploration risk to a minimum and to discover new deposits suitable for commercial production.

Received Date: 12.04.2018
Accepted Date: 12.06.2018

1. Introduction

Russians suggested the iodine as a hydrogeochemical indicator for oil and gas. Kartsev et al. (1959) stated that a vast amount of iodine in waters is originating from petroleum, and, iodine is a direct hydrogeochemical indicator for petroleum. Kovda and Salvin (1951) determined in their studies that the iodine content in soil usually is 10-4 %. However, iodine content of soils covering oil and gas fields increase up to 10^3% or 10^2%. Iodine has been used to discover an oil and gasfield in the many studies (e.g. Ginis, 1966; Kudel'sky, 1977; Gallagher, 1984; Allexan et al., 1986; Singh et al., 1987; Tedesco et al., 1987; Gordon and Ikramuddin, 1988; Tedesco and Goudge, 1989; Leaver and Thomasson, 2002; Goudge, 2007, 2009; Mani et al., 2011; Hummel, 2011). Collins and Egleson (1967), Collins (1969, 1975), Bojarsky (1970), Schoeneich (1971), Kudel'sky (1977) and Levinson (1980), in these studies, have proved the relationship between petroleum and iodine-rich waters in hydrocarbon production basins. Current studies are showing that supporting geological and geophysical survey with iodine geochemistry increases the efficiency of hydrocarbon exploration. Use of iodine for the discovery of hydrocarbon fields has the advantage of both having reliable and consistent results and being simple and cost-effective. Besides, as anomaly results are controllable and repeatable, risks and costs of exploration are mitigated to a great extent (Leaver and Thomasson, 2002).

Citation Info: Özdemir, A. 2019. Relationship between petroleum and iodine in Southeastern Anatolia Basin**.** Bulletin of Mineral Research and Exploration, 159, 145-183. *https://doi.org/10.19111/bulletinofmre.501519*

** Corresponding author: Adil ÖZDEMİR, adilozdemir2000@yahoo.com*

This study was made for investigating the relationship between iodine and hydrocarbon accumulations and to determine iodine contents of formation waters in the Southeastern Anatolia basin oilfields where have been produced almost all of the Turkey oils (more than 95%). Formation water samples have taken from 234 production wells in 49 oilfields which have different geological structures where oil and gas production has performed by the Turkish Petroleum Company (TPAO). Also, the drilling mud samples from EBY-17 oilwell in Elbeyli (Adıyaman) field has collected, and their iodine analyses were carried out. The samples were selected considering different formations in which the production is carried out in each oilfield, the well that has different oil (bbl) / water (bbl) and water % (bbl) ratios and oilfield dimensions. Total oil production in the Southeastern Anatolia basin is 34917 bbl/day, and the total oil production of oilfields in which the iodine analysis was carried out is 32692 bbl/day. The share of the oilfields in which the iodine analysis is carried out in the total oil production of the basin is 93.6% (production data of September 2017).

2. Material and Method

All formation water samples, except for Mardin and Şırnak oilfields, were taken from the wellhead of the production well shown as figure 2. The samples from wells in Mardin (Çamurlu, İkiztepe, and Eastern Sınırtepe) and Şırnak (Güney Dinçer and Batı Kozluca) oilfields were taken from the separator due to finding gas together with the oil in wells. The samples taken from separator and wellhead have been performed tests in samples of oilfields belonging to the Adıyaman Regional Directorate of TPAO for detecting whether or not any difference between iodine values. According to the result of this study, it was seen that iodine values taken from separator were lower than the values taken from the wellhead. On formation water samples were carried out Iodine analyses using the titration technique based on the Hach (1992) method

Figure 1- Location map of oil and gas production fields in the Southeastern Anatolia basin of Turkish Petroleum Company (TPAO) in which the iodine analysis is carried out in the formation waters.

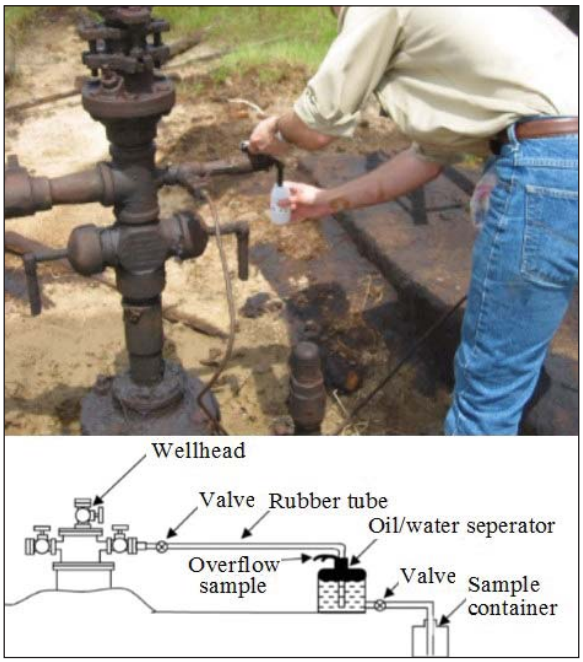

Figure 2- Schematical view of sample collection method from the oilwell formation water for iodine analysis.

and UV spectrophotometry device in TPAO Batman and Adıyaman Regional Directorates (Figure 3). The total iodine concentrations (mg/L) of the samples were detected by these analyses, and these concentrations were used directly in assessments.

3. Relationship between Iodine and Petroleum

Iodine, which was discovered by Courtois in 1811 by extracting from seaweed ash, is scarcely found on Earth's crust. 99,6 % of Earth's crust is composed of 32 main elements. Remaining 0.4% shared among 64 trace elements. Ranking 61 among these 64 elements concerning abundance, iodine is one of scarcest non-metal elements within the composition of Earth's crust (Hora, 2016). It is a halogen with Symbol I, atomic number 53, atomic mass 126,92, density 4,93 gr/cm^3 and valency -1, +1, +3, +5, +7. In seawater, there is 0,05 ppm iodide ion concentration. The behaviors of iodine significantly differ from that of chlorine, since it has the most biophilic features among the halogens. The most significant reservoir of chlorine in the world is seawater (2,66x10^{16} tonnes, 72,2% of total chlorine), whereas the source of iodine is marine sediments (5,90x10^{12} tonnes, 68.2% of total iodine) (Muramatsu and Wedepohl, 1998). Thus, iodine enrichment is more related to the accumulation of iodine by marine phytoplankton, algae and organic matter deposition on the marine sediments rather

Figure 3- An UV spectrophotometer device.

than seawater (Tsunogai, 1971; Price and Calvert, 1977; Elderfield and Truesdale, 1980; Harvey, 1980; Lloyd et al. 1982; Tomaru et al., 2009a, b). Iodine distribution in seawaters and oceanic waters shows that sediments closer to the shore include more iodine than the deep sea sediments (Figure 4) (Shishkina and Pavlova, 1965).

Huang (1984) stated that most available geologically places for iodine accumulation of large and well covered, less deformed structures in areas where young and thick marine sediments are found (external neritic/bathyal reduction environment). Also, he defined the porous and permeable sandstones as the iodine reservoirs, the thick organic-rich shales as the source of iodine and the algae-rich organic matters as the accumulation regions of iodine. A vast amount of iodine (excluding potassium nitrate-caliche deposits in the Chile and seaweeds) find in the formation waters in oil and gas fields. Alvarez et al. (2015 and 2016) have determined that the source of the iodine in the Atacama (Chile), the most significant iodine deposit in the world, is the Jurassic, old organic-rich sedimentary basement. Some marine organism types like some seaweeds, planktonic algae, and corals take the iodine from the seawater and accumulate it in their bodies (Huang, 1984). Iodine accumulation mechanism in the mud of seafloor is as follows; 1) Accumulation in seaweeds, plankton diatoms, algae, and other marine organisms, 2) Accumulation of dead organisms on the seafloor. Iodine finds on the surface of organic sediments absorbed by colloid surfaces or bound to carbon components, and it is mostly immobile (Fuge, 1974). Marine organisms accumulate the iodine on external neritic seafloor together with inorganic

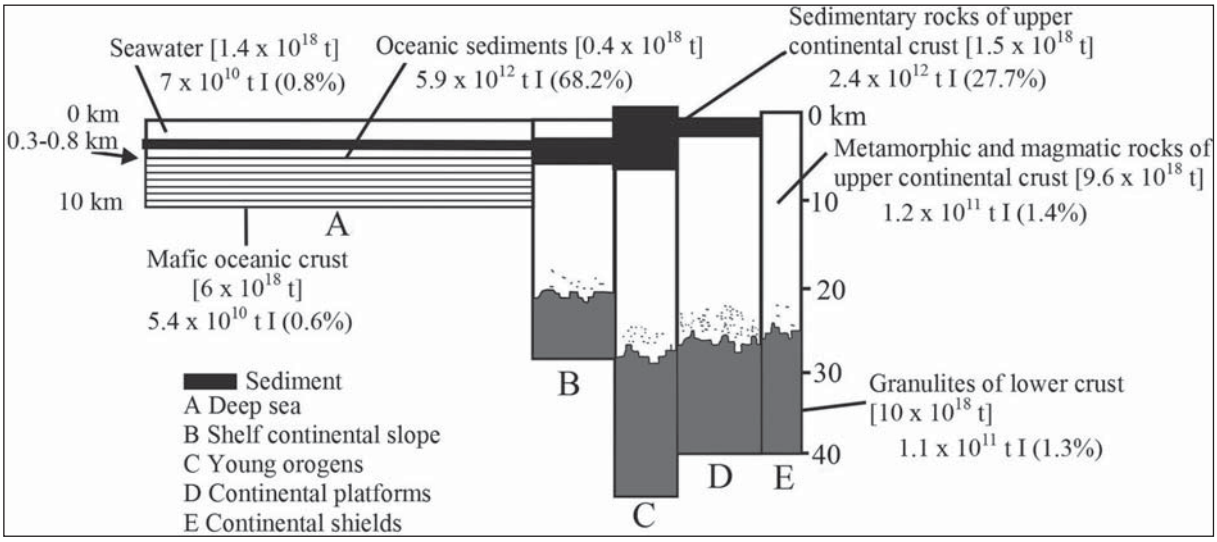

Figure 4- The distribution of iodine in the earth crust (Muramatsu and Wedepohl, 1998).

matters and in bathyal reduction environment, and also in clayed sediments which are primary sources of iodine in oil and gas reservoir waters. Iodine-rich waters have classified in two groups; (1) gaseous or petroliferous iodine-rich waters in oil and gas fields, (2) iodine-rich waters with the dry gas (dissolved natural gas) (Figure 5) (Huang, 1984).

The main reservoir of iodine in actual marine environments is organic matters. Organicrich sediments or their volatile derivatives (hydrocarbons) are primary sources of iodine in many sedimentary basins. Iodine enrichment in waters increases with proximity to petroleum reservoirs and depth of burial. Iodine increase in porewaters is faster than bromine (Warren, 2006; Martin et al., 1993). Salt lakes either contain a little iodine or no iodine at all (Warren, 2006).

The Organic-rich marine sediments and halite are primary sources for iodine in the terrestrial environment (Figure 6). These sources can be differentiated with I/Br ratios (Elderfield and Truesdale, 1980; Moran et al., 1995; Muramatsu and Wedepohl, 1998). Buried marine organic matter produces microbial/thermal methane and releases iodine. Meanwhile, iodine and

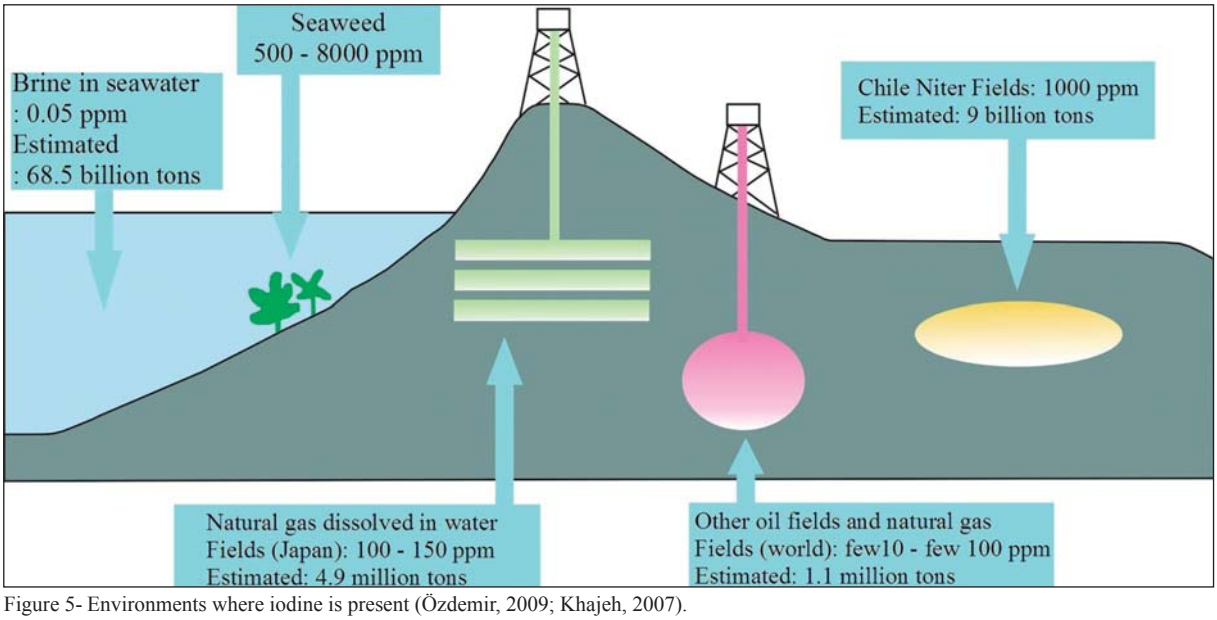

Figure 5- Environments where iodine is present (Özdemir, 2009; Khajeh, 2007).

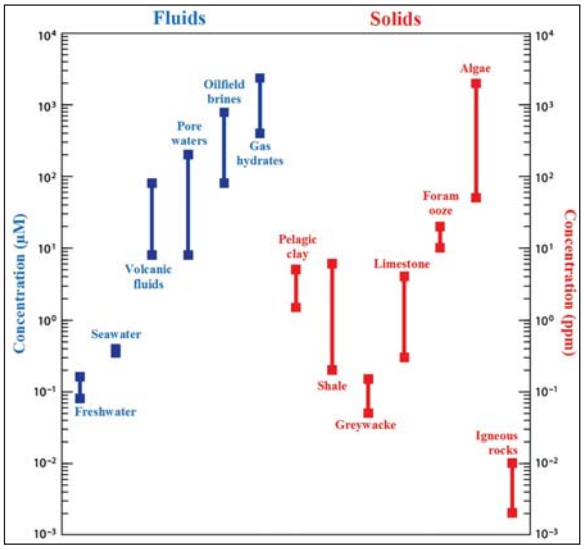

Figure 6- Iodine contents of different fluids and solid materials (Fehn, 2012).

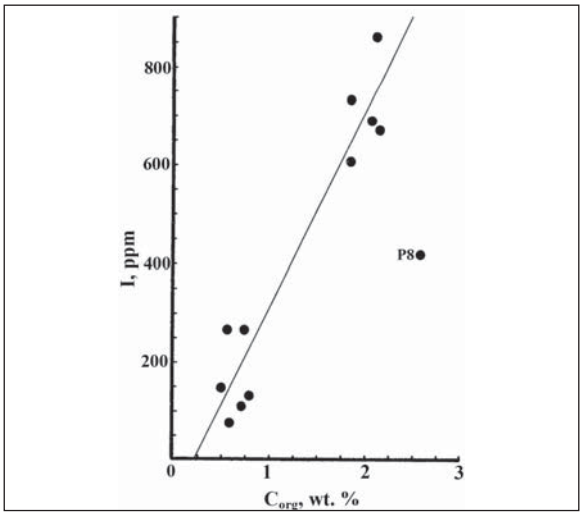

Figure 7- The relationship between salt-free iodine and organic carbon in Panama basin surface sediments. Sample P8 was omitted from the regression calculations since it deviates strongly from linearity. This deviation may be due to the presence of reworked, relatively refractory carbon in the core (Peterson, 1979).

methane (CH_4) which leave sediments accumulate in pore waters. These fluids which are rich in methane and iodine achieve to surface with leakages or trapped in sedimentary rocks in terrestrial environments. There is a vast amount of iodine in oil and gas field waters (Moran et al., 1995). The amount of decomposed organic matter during generating of hydrocarbon in the marine environment affects the amount of released iodine (Fuge and Johnson, 1986).

High concentration of iodine accumulation in near-coastal and continent margin sediments has reported in various studies (Vinogradov, 1939; Shishkina and Pavlova, 1965; Price et al., 1970; Pavlova and Shishkina, 1973; Price and Calvert, 1973). In sediments in the early stages of diagenesis are seen that the iodine and bromine contents generally decrease with the increasing burial depth (Shishkina and Pavlova, 1965; Pavlova and Shishkina, 1973; Price and Calvert, 1977). The loss of iodine in sediments is accompanied by the gradual decrease in organic carbon content and by iodine increase in pore waters (Pavlova and Shishkina, 1973). A similar increase can be expected in the content of bromine in pore waters. It is found that iodine increase in surface sediments is in direct proportion with organic carbon content (Figure 7; Peterson, 1979).

Iodine enrichment is a precise indicator of iodine-rich organic buried matter and is related to the rate of sedimentation (Figure 8). In zones with rapid sedimentation, iodine-rich organic matter buried rapidly, and most of the iodine trapped in pore waters. In slow sedimentation zones most of the iodine is also released into seawater (Martin et al., 1993).

The biological connection between iodine and carbon systems have well established. There is a strong relation between organic carbon and iodine concentrations in marine sediments. Iodine is found in low concentration in sedimentary rocks (for instance in carbonates <1 ppm, in marine evaporites <0.1 ppm). Shales generally contain high iodine concentrations like 1-20 ppm. The iodine amount found in sedimentary rocks cannot be found in any rock-forming mineral and cannot be absorbed in clay. It is more related to preserved organic carbon (Cosgrove, 1970; Collins et al., 1971). High amounts of iodine concentrations have measured in shales containing kerogen, the primary organic matter (Cosgrove, 1970). Wilke-Dörfurt (1927) and Cosgrove (1970) studies are shown close link between oil contents of shale ($r^2 = 0.98$) and organic carbon content ($r^2 = 0.76$), and iodine content of Lias (Posidonia) shales and Kimmeridge shales, the source rocks of North Sea (England) oil and gas fields. As iodine content is increasing in shales, oil and organic carbon contents are seen that increased (Figures 11 and 12). Greenhalgh (2016) stated that TOC (Total Organic Carbon) value of Kimmeridge shales is >10%, Hilger (2003) stated that carbon content of Lias shales is 9% and oil yield as 40-45 liter/tonnes.

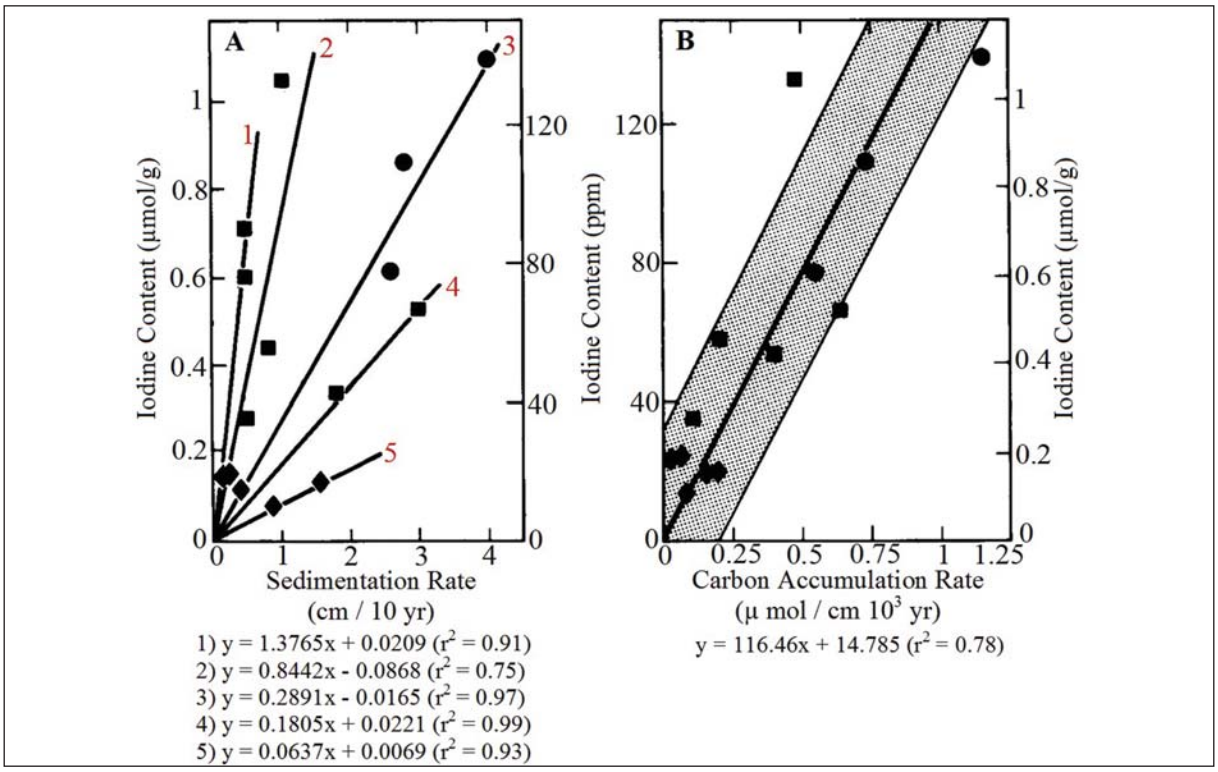

Figure 8- The relationship between iodine content, sedimentation rate, and carbon accumulation rate. The equations were determined from graphics by the author (from Kennedy and Elderfiel, 1987).

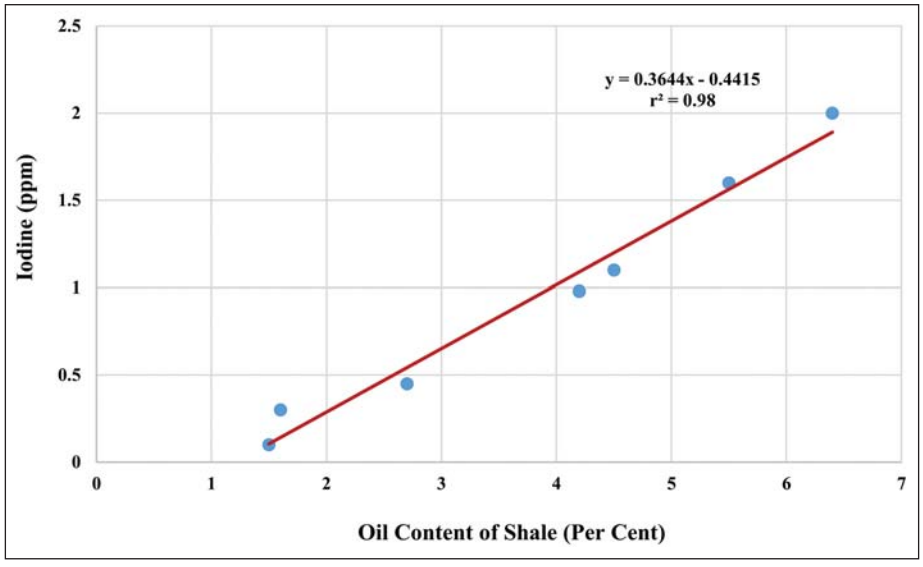

Figure 9- The relationship between oil and iodine contents of Lias shales (Data: Wilke-Dörfurt, 1927).

Compaction in deeply buried marine sediments pushes iodine-rich porewaters towards sands which are more conductive from clays and muds. Decomposition of organic matter releases iodine to porewaters, though slowly conditions of such process. Diagenesis of marine muds to shales causes a decline approximately 40% to 10% in the porosity from less and from 50 to 8 ppm in iodine content (solid phase). This process is a function of the pace of release, the age of sediment, depth and mineralogy, formation

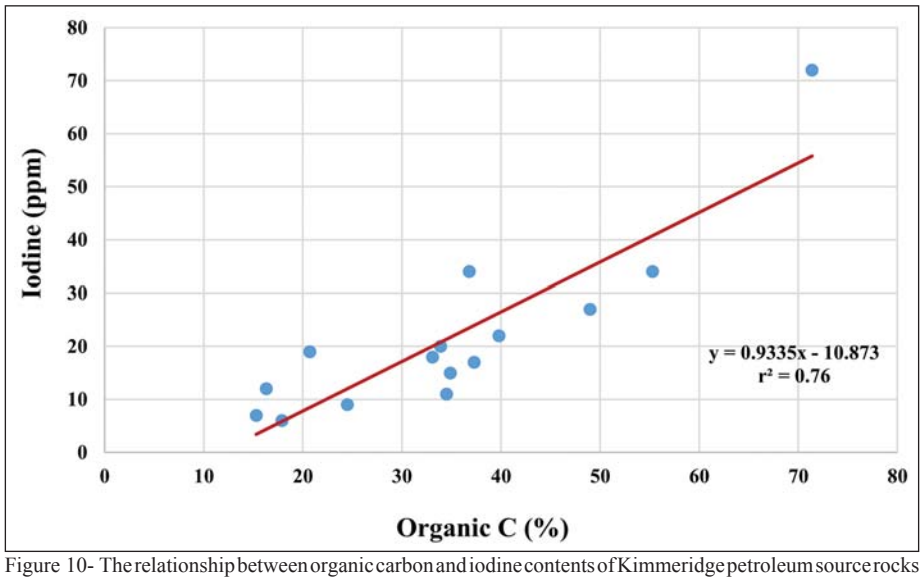

Figure 10- The relationship between organic carbon and iodine contents of Kimmeridge petroleum source rocks (Data: Cosgrove, 1970).

temperature and nature of bound iodine (Figures 11 and 12) (Fabryka-Martin, 1984). While organic matter turns into petroleum, most of the iodine is released to related waters (Fehn et al., 1990).

In halogen systematics of marine porewaters are seen that gas hydrates and most of the organic bromine are merged whereas maturing hydrocarbons, H_2S, CH_4, and iodine together are migrated from the basin

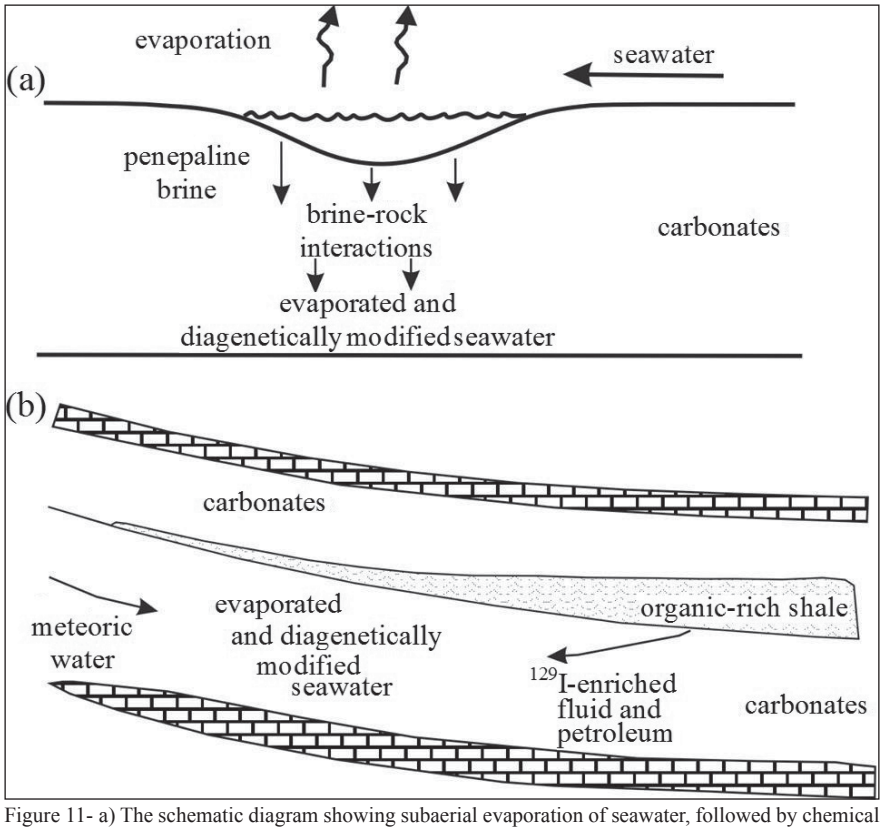

Figure 11- a) The schematic diagram showing subaerial evaporation of seawater, followed by chemical modification of penesaline brine in the subsurface. (b) Schematic diagram showing subsequent mixing of remnant brine with an I-enriched fluid from shales and with meteoric water from recharge areas (modified from Stueber and Walter, 1991).

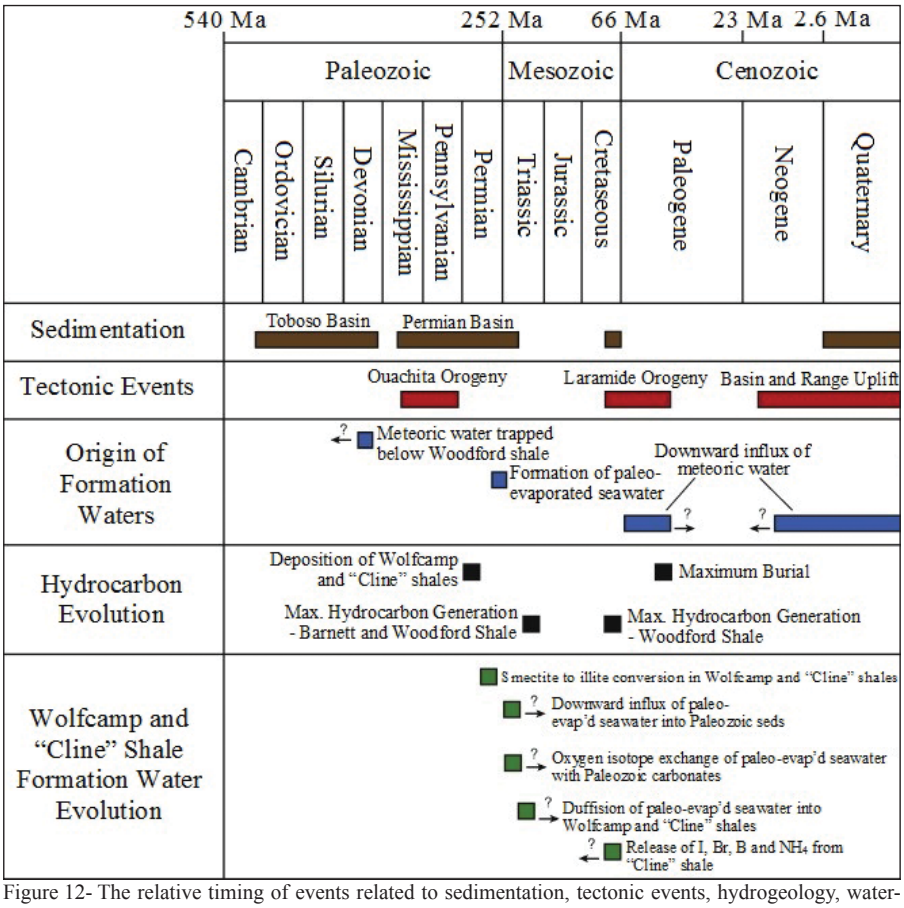

Figure 12- The relative timing of events related to sedimentation, tectonic events, hydrogeology, water-rock interaction, and hydrocarbon evolution in Permian Basin (Engle et al., 2016).

(Figure 13) (Kendrick et al., 2011; Fehn et al., 2003; Gieskes and Mahn, 2007; Muramatsu et al., 2007). Therefore, the potential of hydrocarbons to influence iodine and bromine contents of formation waters is high. High saline formation waters ensure organic Br contribution. Combined noble gas and halogen analyses provide an intriguing new method for investigating hydrocarbon-groundwater interactions because hydrocarbons have elevated Br and I contents and noble gases and halogens are both fractionated between hydrocarbons and groundwater (Kendrick et al., 2011).

Buried organic matter, which turn into petroleum after maturing and which cause to increase of iodine concentration in surrounding waters and which is the source of iodine in waters of sedimentary basins having vast amounts of hydrocarbon accumulation have dominant control over total iodine concentration. Chen et al. (2016) have stated that these iodine-rich waters mediate the hydrocarbon migration. Therefore, iodine concentrations of basin fluids can be used as a first approach to tracer the interaction between fluids and organic-rich sediments (Osborn et al., 2012).

Land (1991) and Stueber et al. (1993) studies have proved that to be a flow mechanism from depths towards Earth's surface of fluids in sedimentary basins. Harrison and Summa (1991) has calculated vertical velocities of fluids in sedimentary basins and suggested iodine releasing model from thermal alteration of organic matter in solution (Mani et al., 2011). Synder and Fabryka-Martin (2007) stated that formation water has same 129I/I age with on the environment it derives and organic matter it interacts. Moran et al. (1995) submitted long distance vertical migration model for hydrocarbons and waters related with iodine, in the study made on fluid movements in sedimentary basins and age of source. Problems in these models are whether or not the iodine is bound to organic molecules for millions of years. It is an important subject. Because, iodine concentration of crude oil is very low (<1 ppm) (Fehn et al., 1990; Tullai et al., 1987). Therefore, iodine has preserved

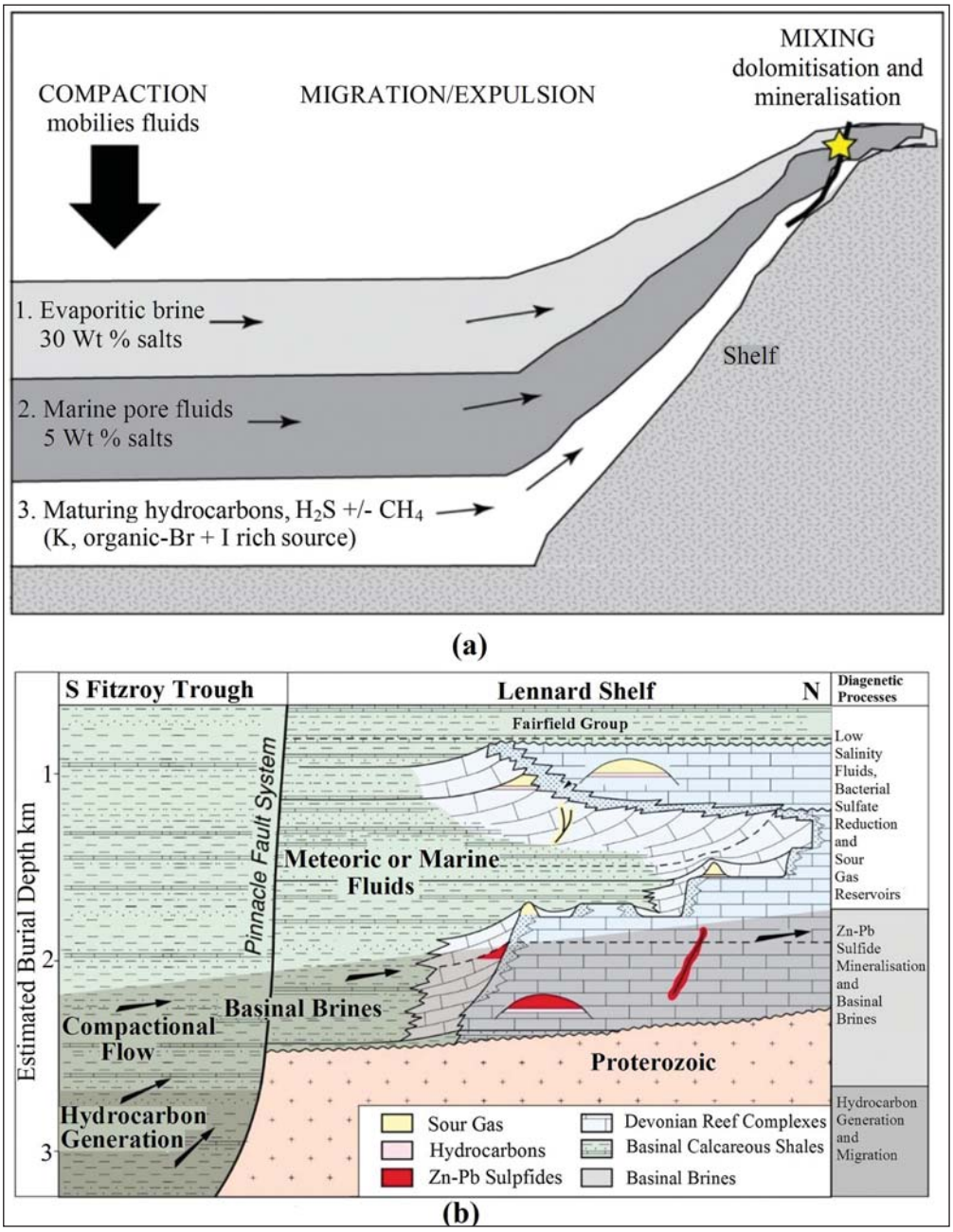

Figure 13- In the Lernard shelve of maturing hydrocarbons and iodine, (a) migration (from Kendrick et al., 2011), (b) trapping (Wallace et al., 2002) models.

its relation with organic C throughout decomposition of organic matter and sedimentation process and has released in water during thermal maturing. As iodine protects its close relation with organic C systems, the age of iodine will be the age of the organic matter with which iodine is in relation (Moran et al., 1998).

4. Discussion

Based on results of iodine analysis of water samples taken from oilwells of Southeastern Anatolia basin were evaluated iodine content of the formation waters in the wells and source of iodine in the basin. Also, the relationship between basin depth, oil (bbl)/ water (bbl) ratios in wells, water % in wells, reserves of oilfields with the iodine contents of formation waters were studied.

4.1. Source of Iodine in Waters and Iodine Contents of Waters Associated with Hydrocarbon Accumulations

Iodine contents in the formation waters of the Southeastern Anatolia basin are consistent with the studies of Bojarski (1970) and Collins (1975). Iodine source in iodine-rich reservoir waters (iodine content >1 mg/L) of the Southeastern Anatolia basin, which is an oil and gas basin, is the organic-rich Silurian and Jurassic-Cretaceous petroleum source rocks. The results of iodine analysis of oilwells are given in figures 14-18 and Appendix-1.

In preliminary studies have been observed that formation waters of all oil and gas production basins in the world (including Southeastern Anatolia basin and Thrace basin) are contained >1 mg/L iodine (USGS Produced Water Database; Engle et al., 2016; Oppo et al., 2014; Oppo and Capozzi, 2015; Sudo, 1967; Kaiho, 2015; Kharaka et al., 1987; Dia et al., 1999; Dresel and Rose, 2010, Rowan et al., 2015; Mirnejad et al., 2011; Xun et al., 1997; Fisher and Kreitler, 1987; Dickey et al., 1972; Land, 1995; Birkle et al., 2002; Birkle et al., 2009; Franks and Uchytil, 2016; Hitchton et al., 1971; Machperson, 1992; Kokh and Novikov, 2014; Novikov, 2013*a, b*; Novikov, 2012; Novikov and Shvartsev, 2009, Demir and Seyler, 1999, Kurchikov and Plavnik, 2009, Fu and Zhan, 2009, Kireeva, 2010, Bagheri et al., 2014). However, there are also production wells with formation waters containing iodine <1 mg/L in Southeastern Anatolia and Thrace basins (Appendix-1), Dörtyol (Hatay) gasfield, Cambay basin/India (Rebary et al., 2014) and in basins of other global oil and gas fields. Looking at the iodine contents of formation water samples of Southeastern Anatolia and Thrace basins, 60 of them >1 mg/L, 59 of them between 0,5-1 mg/L, 108 of them between 0,1-0,5 mg/L and 16 of them range between 0,01-0,08 mg/L (Figure 19). Formation waters with iodine content <1 mg/L in production wells, the oilfield waters are iodine content decreased waters as results of mixing with other water types (meteoric and reinjection waters) in the basin of oilfield waters with iodine content >1 mg/L. Çelik and Sarı (2002) detected meteoric water effect in the water sample produced from a well in the Karababa C formation which was one of the reservoir rocks of the Adıyaman oilfields. In another study (Çelik et al., 1998), has determined that formation waters in Adıyaman region could be trapped in marine units and they have been mixed with the meteoric water.

4.2. The Relationship between Depth and Iodine Content

Özdemir (2009) study carried out for iodine production from formation waters in the Gorgan (Iran) region it is seen that the iodine content increases in parallel with the increase in the depth. In this study, change of iodine content with depth was studied, and usability condition as an indicator of whether there is oil or gas in well during oilwell drilling of change of iodine content was evaluated. For this aim, iodine analyses have carried out by means of titration and UV spectrophotometer based on Hach (1992) method in laboratories of Adıyaman Regional Directorate of TPAO in drilling mud samples (well inlet and outlet) taken as parallel to penetration during drilling of EBY-17 oilwell drilled Elbeyli (Adıyaman) field and total iodine concentrations (mg/L) were detected.

According to the results of the analysis, the iodine content in the well increased in parallel with the increase in depth up to the oil zone. In the well which started with drilling mud containing 0,20 mg/L iodine at 100 m depth, when the well has reached 700 m depth, the content of iodine of drilling mud increased to over 1 mg/L. It was seen that the relation between the increase in iodine content of drilling mud up to 1900 m and depth increase was linear (iodine content at 1900 m is 4,07 mg/L). At a depth of 2000 m, the content of iodine of drilling mud suddenly increased to 10,72 mg/L. This zone was defined as water zone (containing gas + condensate?) above the oil zone. In oil zone, the content of iodine of drilling significantly decreased (average 0,55 mg/L), because, the content of iodine of crude oil is less than 1 mg/L (Fehn et al., 1987). At a depth of 2330 m, the lower water zone was entered leaving the oil zone (Figures 20 and 21). In this zone, the iodine content of drilling mud again increased (>1 mg/L). Oilwell was terminated at a depth of 2337 m. Production perforate zones of the wells in Elbeyli oilfield are at depths of 2050 - 2392 m. Reservoir units are Sayındere, Karaboğaz and Karababa C formations. As a result of the interpretation of geophysical log data obtained in EBY-17 oilwell was decided to perforate ranges between 2013 - 2115 m, 2138 - 2146 m, 2159 - 2168 m, 2177 - 2186 m, 2195 - 2203 m and 2234 - 2257 m of Sayındere formation; range between 2287 - 2294 m of Karaboğaz formation and range between 2308 - 2324 m of Karababa C formation. Zones to be perforated determined through geophysical logs and oil zones are compatible with oil zones determined by drilling mud iodine analysis.

No.	Oilfield	Average Depth (m)	API Gravity	Oil production percentage in southeast Anatolian basin (%)*	Maximum Iodine Content (mg/L)
1	Batı Raman	1300	13	22.30	2.81
2	Raman	1350	18	19.44	6.45
3	Beykan	1900	33.2	6.10	1.81
4	Karakuş	2700	30.1	4.66	6.58
5	Kurkan	1600	31.4	3.27	0.52
6	Beşikli	2100	25.6	3.06	3.65
7	Silivanka	2350	23.5	2.29	1.18
8	Garzan	1450	24	2.05	1.36
9	Cendere	2700	29	2.05	7.94
10	Elbeyi	2300	26.1	2.00	29.80
		Total (%)		**67.25**	**Average iodine content: 6.21 mg/L**

* Total oil production in the Southeastern Anatolia basin: 34917 bbl/day (September 2017 production data)

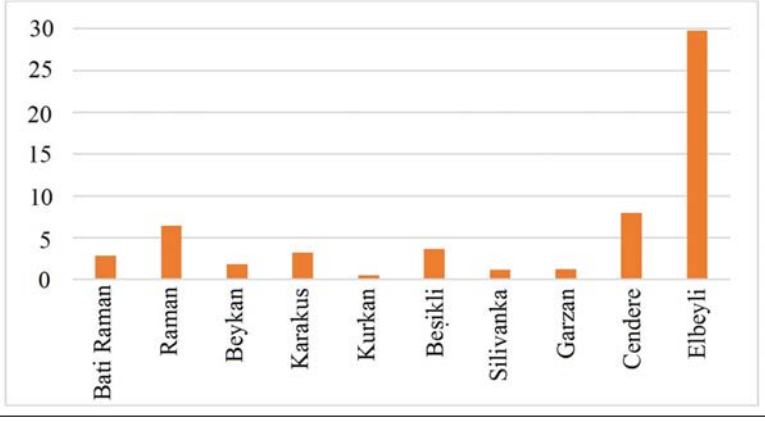

Figure 14- The highest iodine contents of formation waters in most productive 10 fields of the Southeastern Anatolia basin (blue polygons show the production fields).

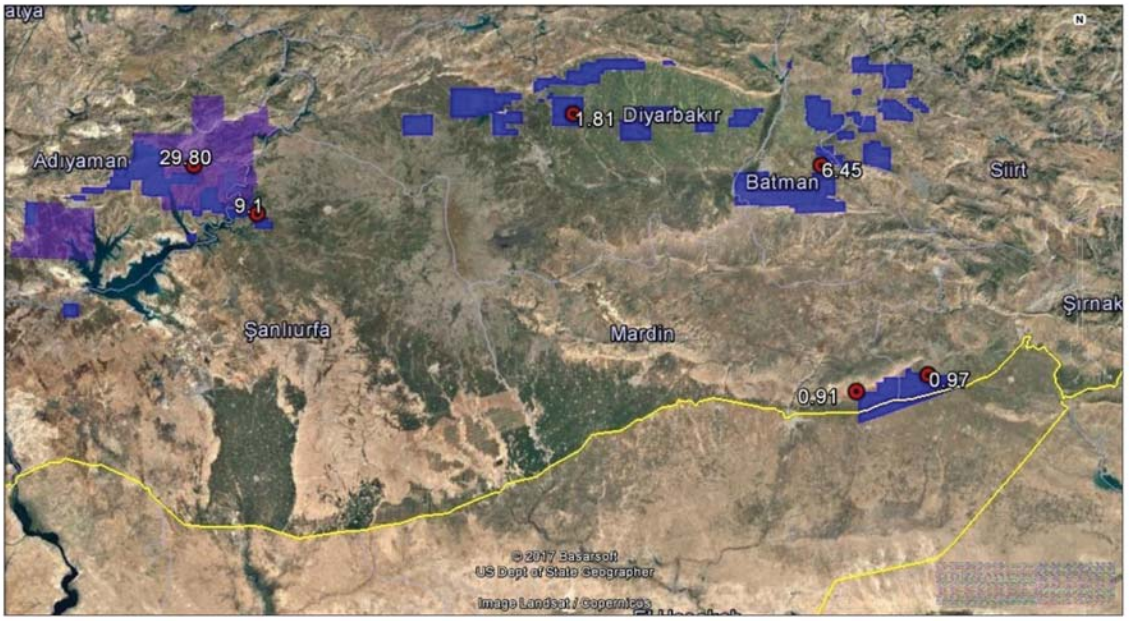

City	Analyzed oilfield number	Analyzed well number	Oil production percentage in the Southeastern Anatolia basin (%)	Maximum Iodine Content (mg/L)
Batman	4	42	49.40	6.45
Diyarbakır	13	74	19.55	1.81
Mardin	4	17	2.14	0.91*
Şırnak	2	21	1.84	0.97*
Adıyaman	22	74	25.05	29.80
Şanlıurfa	4	6	2.01	9.10
Toplam	49	234	99.99	**Average iodine content: 8.17 mg/L**

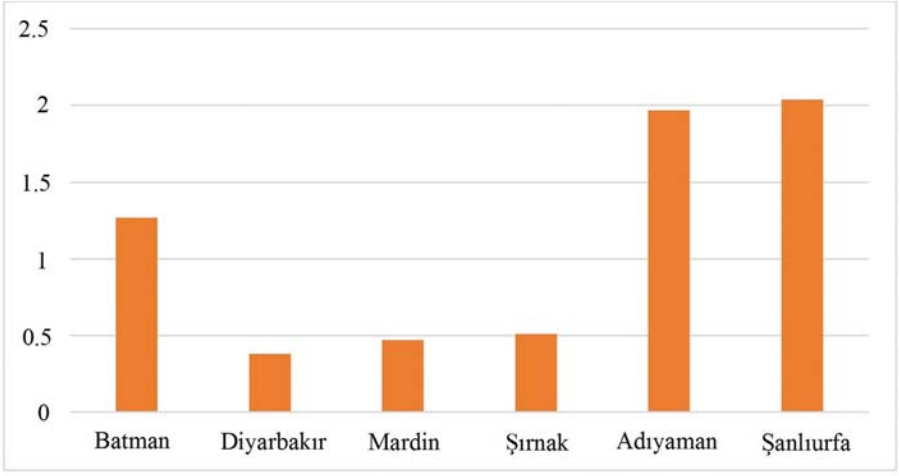

Figure 15- The highest iodine contents of formation waters in cities where oil and gas production in the Southeastern Anatolia region are made (blue polygons show production fields, *= water samples were taken from separator).

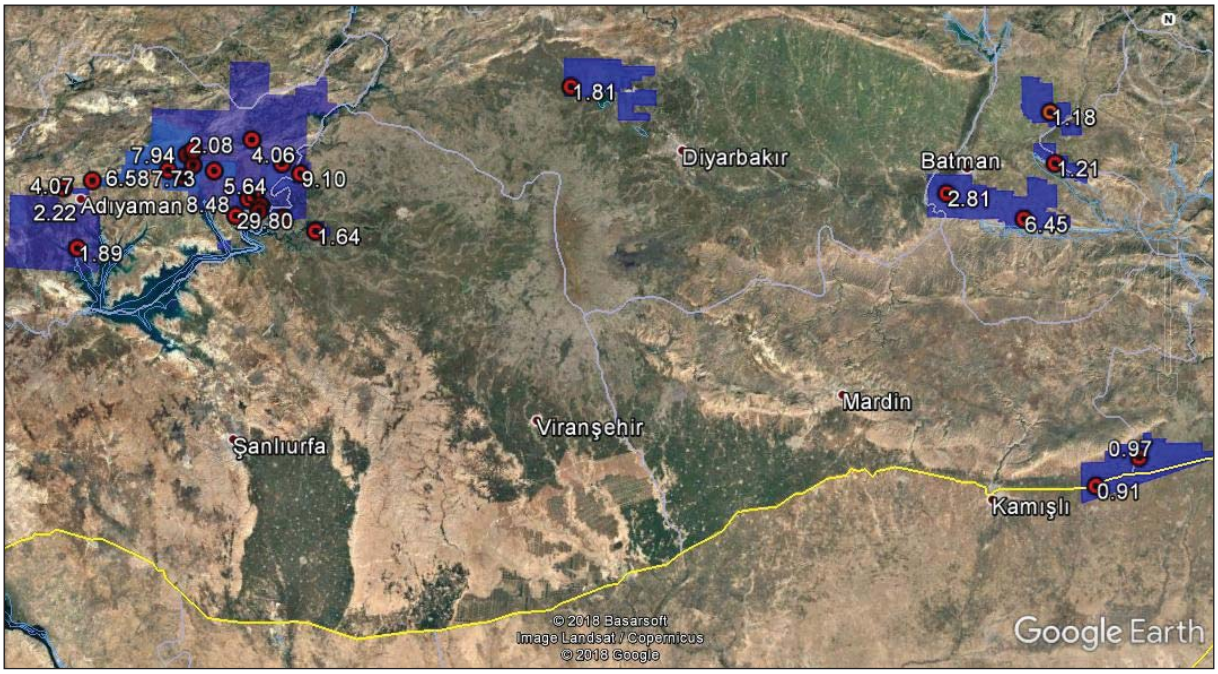

Figure 16- The highest iodine contents of formation waters in production wells of oil and gas fields in the Southeastern Anatolia basin (blue polygons show production fields and values are in mg/L. Mardin, and Şırnak water samples were taken from separator).

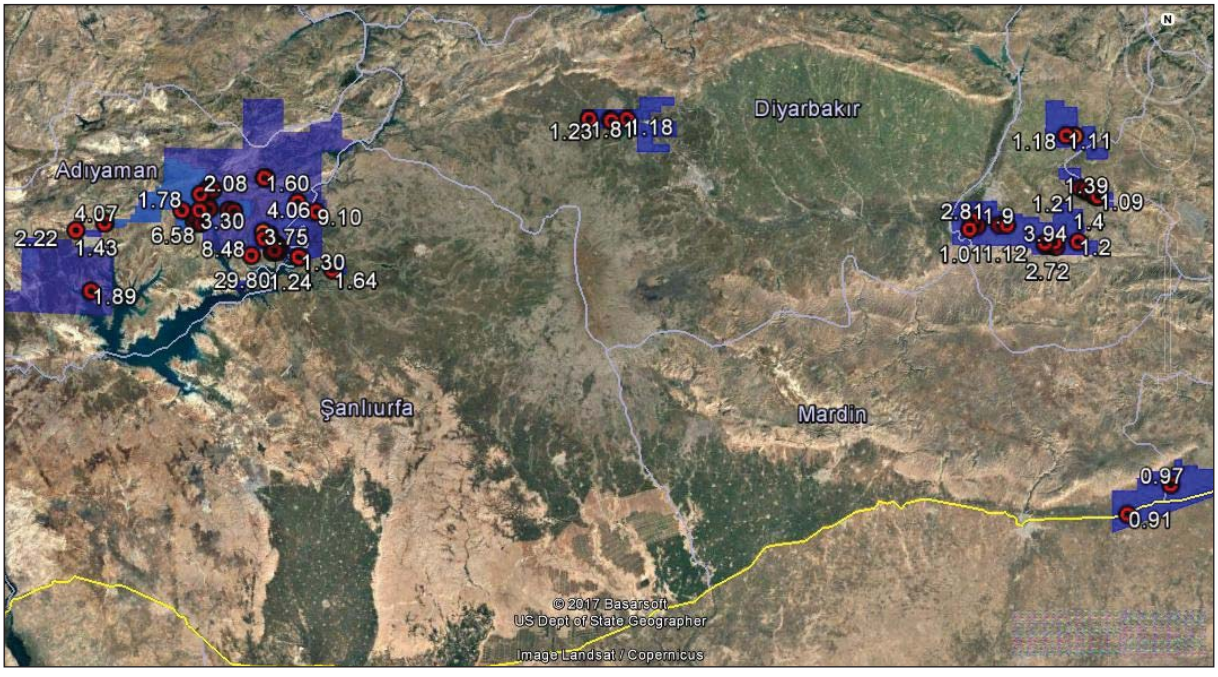

Figure 17- Distribution of oilwells with iodine content >1 mg/L in oil and gas production fields of the Southeastern Anatolia basin (blue polygons show production fields and values are in mg/L. Mardin and Şırnak water samples were taken from separator).

Net 512 barrels of oil is produced as daily from non-water EBY-17 oilwell. EBY-17 oilwell is highest net oil producing well of Southeastern Anatolia basin with this production. EBY-17 oilwell is highest net oil producing well of Southeastern Anatolia basin with this production. Water sample of the well as there was only oil in this well could not be taken so iodine analysis could not be performed. However, with a simple approach, it is thought that of iodine content of the well may be minimum two-fold of the iodine

City	Analyzed oilfield number	Analyzed well number	Oil production percentage in the Southeastern Anatolia basin (%)	Maximum Iodine Content (mg/L)	Average Iodine Content (mg/L)
Batman	4	42	49.40	6.45	1.27
Diyarbakır	13	74	19.55	1.81	0.39
Mardin	4	17	2.14	0.91*	0.47*
Şırnak	2	21	1.84	0.97*	0.51*
Adıyaman	22	74	25.05	29.8	1.97
Şanlıurfa	4	6	2.01	9.1	2.04
Total	49	234	99.99	**Maximum iodine content of oilfields in the Southeastern Anatolia basin : 29.80 mg/L**	**Average iodine content of oilfields in the Southeastern Anatolia basin : 1.11 mg/lt**

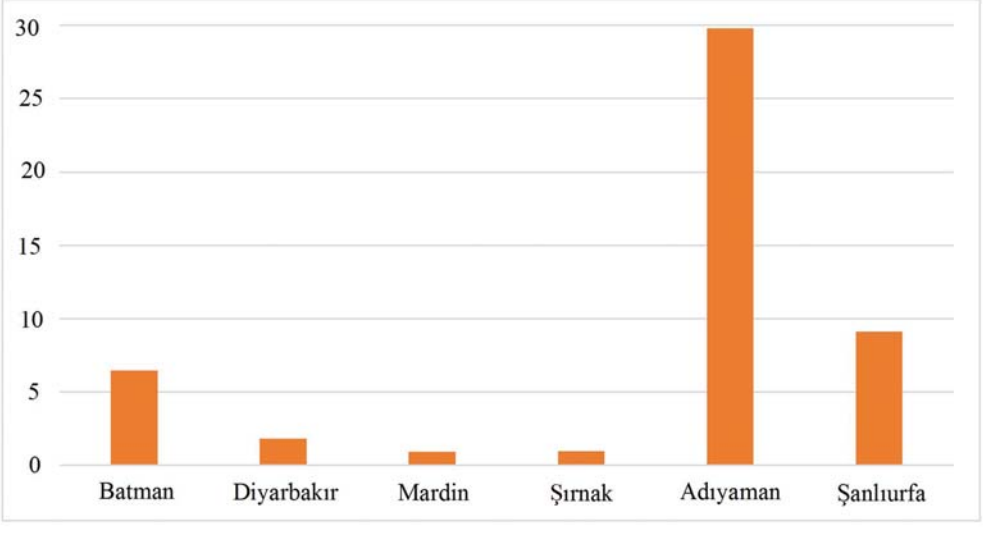

Figure 18- Average iodine contents of formation waters in cities where oil and gas production in the Southeastern Anatolia basin are made (blue areas show production fields, *= samples were taken from separator).

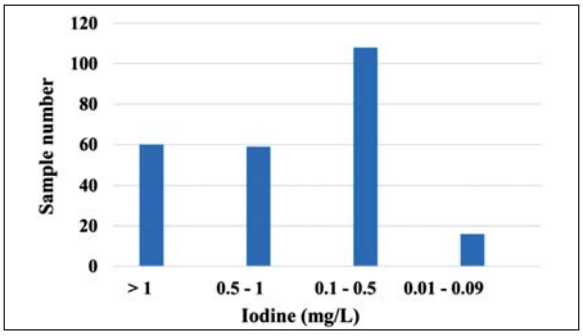

Figure 19- Iodine contents of formation waters in the Southeastern Anatolia and Thrace basins.

content of drilling mud. However, with a simple approach, it is thought that of iodine content of the well may be minimum two-fold of the iodine content of drilling mud. The highest iodine content in drilling mud was measured as 10,72 mg/L. This content is second highest iodine content measured in iodine analysis of oilwells (approximately 250 wells) in Southeastern Anatolia basin. In Southeastern Anatolia basin, the highest content of iodine is 29,80 mg/L in EBY-7 well in Elbeyli oilfield. From this well, 350 barrels of net oil is still produced daily.

According to Özdemir (2009) and results of this study, with iodine analysis to be performed on mud samples during drilling, are seen that it is possible that the prediction of oil volume to be produced from well and the detection whether there is oil or gas in the well (from increases/peaks in iodine contents of drilling mud both in entrance and exit of oil zone). Besides, these data from the EBY-17 oilwell is showed that iodine could be used as an excellent hydrocarbon accumulation indicator during both the exploration and drilling.

4.3. The Relationships between Oil (Bbl)/Water (Bbl) Ratios, Water% (Bbl) Ratios, and Iodine Contents of Formation Waters

Oil and gas reservoirs produced by primary methods have a natural water layer. These iodine-rich water constitute the most significant part of the volume of fluid produced during oil and gas production processes. Produced water amounts are different in oil and gas production fields. The amount of produced water depends on oil extraction technology and reservoir characteristics. Generally, gas wells contain less water than oil wells (Campos et al., 2002; Qiao et al., 2008). The average water/oil ratio in the world is 2/1 - 3/1, the 7/1 in the US. According to the produced

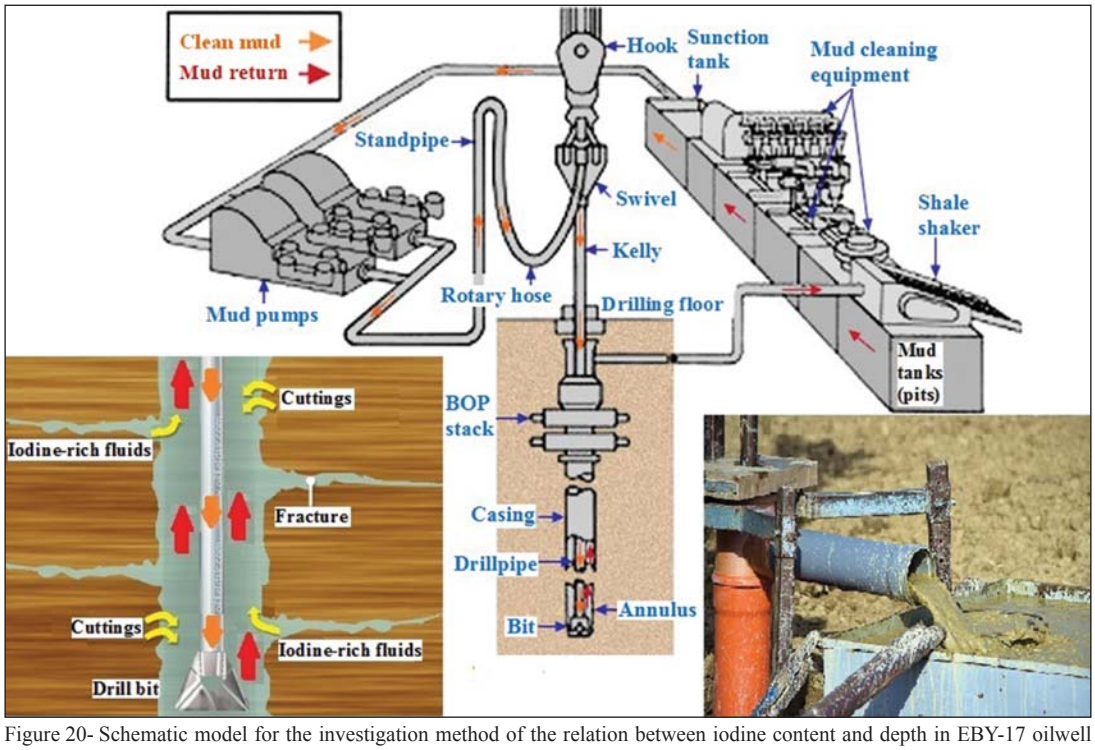

Figure 20- Schematic model for the investigation method of the relation between iodine content and depth in EBY-17 oilwell drilling mud.

Depth (m)	Sample location	Measured iodine (mg/L)	Iodine content (mg/L)
-100	Mud return	0.22	0.02
	Clear mud	0.20	
-200	Mud return	0.28	0.25
	Clear mud	0.03	
-300	Mud return	0.74	0.49
	Clear mud	0.25	
-400	Mud return	0.74	0.62
	Clear mud	0.12	
-500	Mud return	0.90	0.78
	Clear mud	0.12	
-600	Mud return	1.18	0.41
	Clear mud	0.77	
-700	Mud return	1.24	1.14
	Clear mud	0.10	
-800	Mud return	1.43	1.43
	Clear mud	0.00	
-900	Mud return	1.35	1.15
	Clear mud	0.20	
-1000	Mud return	1.22	1.13
	Clear mud	0.09	
-1150	Mud return	1.68	1.52
	Clear mud	0.16	
-1200	Mud return	0.59	1.46
	Clear mud	0.04	
-1300	Mud return	1.63	1.46
	Clear mud	0.17	
-1400	Mud return	3.19	3.19
	Clear mud	0.00	
-1500	Mud return	2.37	2.25
	Clear mud	0.12	
-1600	Mud return	2.73	2.73
	Clear mud	0.00	
-1700	Mud return	3.22	3.09
	Clear mud	0.13	
-1800	Mud return	3.31	3.26
	Clear mud	0.05	
-1900	Mud return	4.07	4.07
	Clear mud	0.00	
-2000	Mud return	10.72	10.65
	Clear mud	0.07	
-2100	Mud return	0.81	0.71
	Clear mud	0.10	
-2150	Mud return	0.77	0.67
	Clear mud	0.10	
-2200	Mud return	0.69	0.37
	Clear mud	0.32	
-2250	Mud return	0.74	0.69
	Clear mud	0.05	
-2300	Mud return	0.49	0.29
	Clear mud	0.20	
-2330	Mud return	1.08	1. 07
	Clear mud	0.01	
-2335	Mud return	1.82	1.74
	Clear mud	0.08	
-2340	Mud return	1.10	1.05
	Clear mud	0.05	

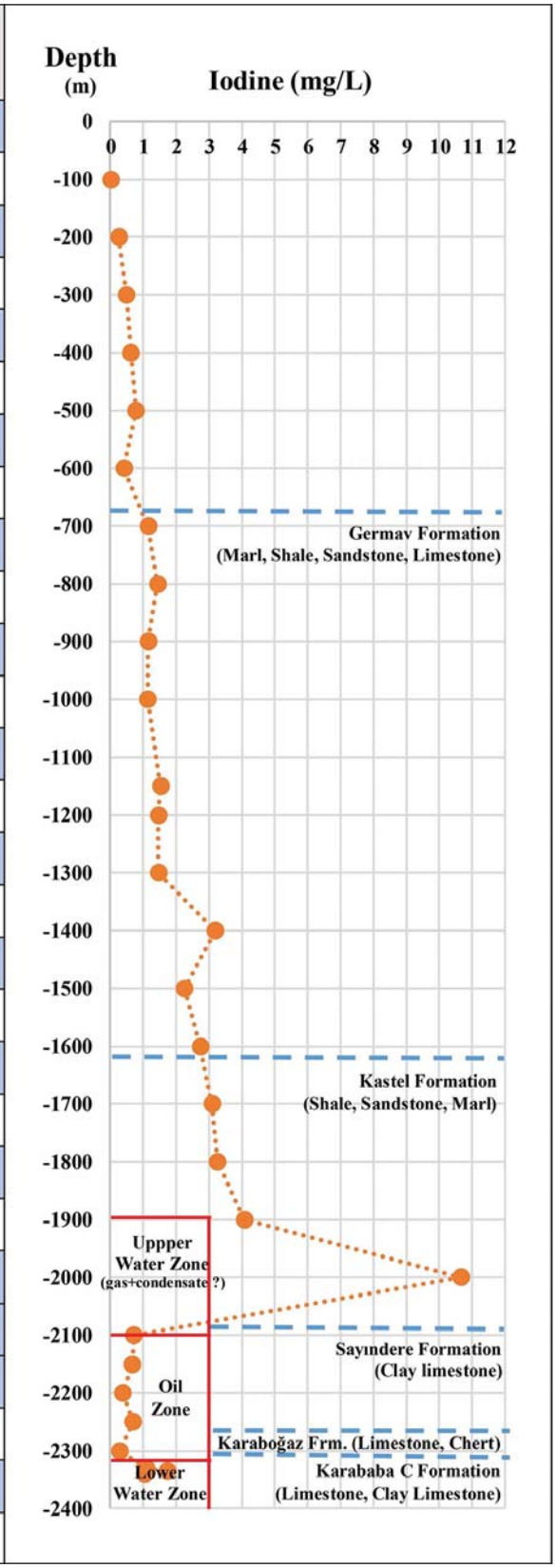

Figure 21- The graphics of depth and iodine content in EBY-17 oilwell.

water researches of the API (The American Petroleum Institute), the amount of produced water increase as a result of the age of oil production wells. In old wells in the US, this value is increased up to > 50/1 (Veil, 2006). In studies of API, the oil/water ratio has calculated as approximately 7,5 barrels of water per oil barrel. In oil wells which have reached the end of production life, the amount of water can be 10-20 barrels per of oil barrel. When water management cost starts to be very high, oilwell starts to none economic benefit (Lee et al., 2002; Veil, 2006).

Water chemistry data in western Siberia (Russia) is used to estimate the amount and phase composition of hydrocarbons in reservoirs. Water chemistry data are useful indicators for migration processes as well as the formation of hydrocarbon accumulations and phase stages. Amount of total dissolved solids and content of salt ions (Na, Ca, Mg, Cl, HCO_3 and others), trace elements (I, B, Br) and dissolved gases have essential effects on the reservoir potential (Kurchikov and Plavnik, 2009; Plavnik et al., 2007; Pogodaeva et al., 2007; Borodkin et al., 2005; Shvartsev and Novikov, 2004; Surkov et al., 1999).

Results of iodine analysis in Southeastern Anatolia basin oil and gas fields and relations between oil (bbl)/water (bbl) ratios and water% (bbl) ratios were examined. A significant relationship was found between measured iodine contents and Cumulative Oil (bbl)/Water (bbl) ratios (r^2=0,89). As the iodine content increased, oil (bbl)/water (bbl) ratio also increased (Figure 22). There was also found a significant relationship between iodine contents and water% (bbl) ratio (r^2=0,82). As iodine content increased, water% (bbl) ratio decreased (Figure 23).

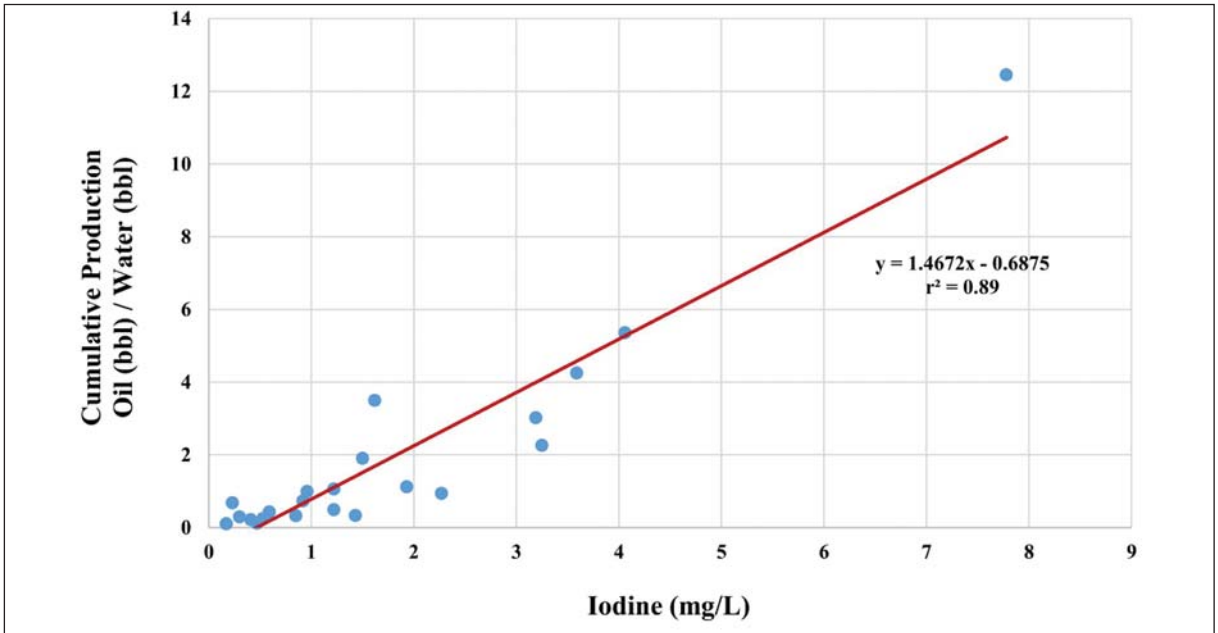

Oilfield	Cumulative Production Oil (bbl)/Water (bbl)	Average Iodine Content (mg/L)	Oilfield	Cumulative Production Oil (bbl)/Water (bbl)	Average Iodine Content (mg/L)
Adıyaman	0.53	0.25	Akgün	1.22	1.06
Çemberlitaş	1.22	0.49	Batı Raman	1.62	3.5
Karakuş	1.5	1.9	Raman	1.43	0.33
Kuzey Karakuş	0.47	0.12	Garzan	0.92	0.73
Cendere	2.27	0.94	Barbes	0.17	0.1
Beşikli	1.93	1.12	Beykan	0.85	0.32
Doğu Beşikli	0.96	0.99	Güney Kırtepe	0.59	0.43
Tokaris	3.25	2.26	Güney Sarıcak	0.23	0.68
İkizce	4.06	5.36	Güney Sahaban	0.11	0.3
Batı Gökce	3.19	3.02	Karacan	0.17	0.1
Gölgeli	3.59	4.25	Kurkan	0.3	0.29
Elbeyi	7.78	12.45	Yeniköy	0.41	0.22

Figure 22- The relationship between iodine content of formation waters and cumulative production Oil (bbl)/Water (bbl) ratios in oilfields of Southeastern Anatolia basin (Cumulative Production Oil/Water ratios of oilfields data are 2017 production data).

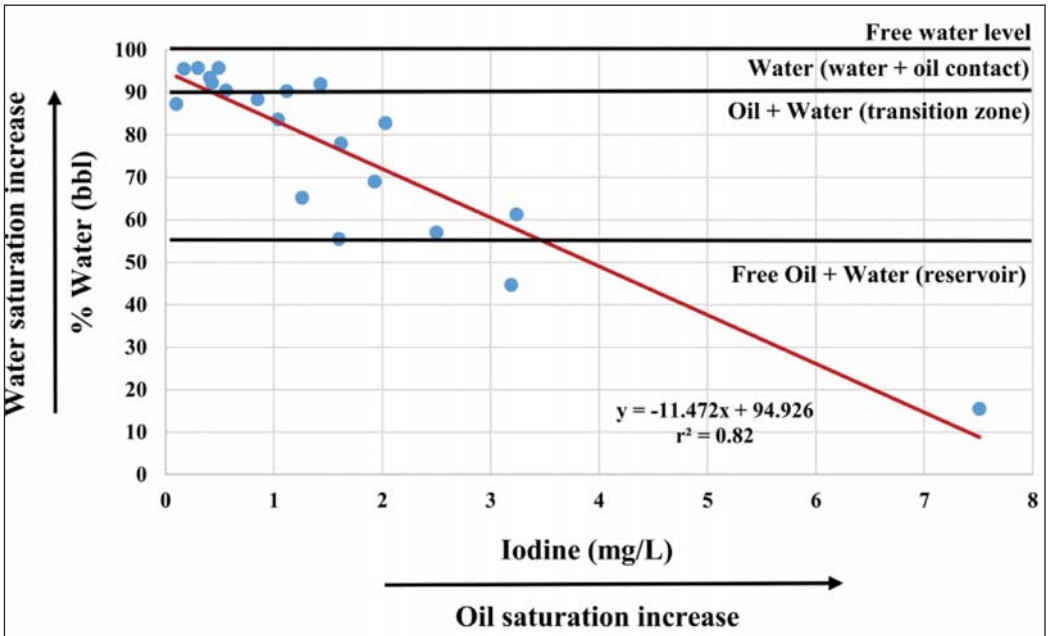

Field	Iodine Content (mg/L)	Water% (bbl)	Field	Iodine Content (mg/L)	Water% (bbl)
Adıyaman	0.49	95.75	Batı Raman	1.62	78
Batı Gökçe	3.19	44.67	Raman	1.43	92
Beşikli	1.93	69	Garzan	1.12	90.33
Cendere	2.03	82.81	Barbeş	0.17	95.56
Çemberlitaş	1.04	83.67	Beykan	0.85	88.38
Elbeyi	7.51	15.5	G. Kırtepe	0.43	92.25
Karakuş	1.24	66.2	G. Sarıcak	0.56	90.44
K. Karakuş	1.26	65.2	G. Şahaban	0.30	95.75
G. Karakuş	2.50	57	Karacan	0.10	87.33
Tokaris	3.24	61.3	Yeniköy	0.41	93.5

Figure 23- The relationship between iodine contents of formation waters and %water (bbl) ratios in oilfields of Southeastern Anatolia basin (Water% ratio data of oilfields are 2017 production data).

It is known that a vast amount of water is produced together with oil in Cambay basin (India) oilfields found formation waters with low iodine content (0,08-1,89 mg/L, the average value: 0,83 mg/L). Iodine contents of Ahmedabad oilfield formation waters: lowest 0,25 mg/L, highest 1,89 mg/L, average 1,06 mg/L; Ankleshwar oilfield: lowest 0,08 mg/L, highest 1,10 mg/L, average 0,48 mg/L and Mehsana oilfield: lowest 0,19 mg/L, highest 1,79 mg/L, average 0,96 mg/L (Rebary et al., 2014). The Ahmedabad oilfield, including 25 subfields, has discovered in 60's year and has been producing oil for more than 50 years. These are the fact that it has problems such as; multi-layer, heterogeneous, low permeable, low productive per well, and contains tight reservoirs. These difficulties bring various exploration and production challenges (water injection to the reservoir, etc.) to produce oil and gas from this area (Gupta et al., 2016). Similarly, iodine contents are low, and a vast amount of water is produced with oil in Southeastern Anatolia basin. Besides, there are also difficulties of exploration and production similar to Cambay basin.

The relationship between iodine and organic matter/organic carbon is linear (Figures 7, 8 and 10). Therefore, iodine contents of reservoir waters (petroleum saturation, oil/water ratio) are high in petroliferous basins found of source rocks containing high organic matter (kerogen). In the case, water saturation (water% ratio) of production wells will decrease because the abundance of iodine in formation waters is due to the release of most of the

iodine in organic matter into related water during the transformation from organic matter to petroleum. This opinion is supported, the fact that these wells are highest net oil producing and least containing water wells (with highest iodine content) in Adıyaman region, EBY-17 well (512 barrels of net oil production, iodine content of drilling mud: 10,72 mg/L), EBY-7 well (350 barrels of net oil production, iodine content of formation water: 29,80 mg/L) and PYK-3 well (210 barrels of net oil production, iodine content of formation water: 9,1 mg/L).

4.4. The Relationship between Reserve and Iodine Content of the Formation Water

The relationship between the average iodine contents in formation waters and highest reserve oilfields in Southeastern Anatolia basin is given in figure 24. In the graph, it is seen that the reserves of oilfields are increase as the iodine content of formation waters increase (r^2=0,81). The reserves of Southeastern Anatolia basin fields with an average of 1,1 mg/L iodine content are similar to the fields in Cambay (India) basin with an average of 0,83 mg/L iodine content and total basin reserve of 170 million bbls (Figure 25).

The relationship between some basins containing giant oil and gas fields of USA and reserves of the oilfields in Southeastern Anatolia and Cambay (India) basins, and average iodine contents of formation waters are given in figure 25 (giant oilfield >500 million bbls of oil or oil equivalent gas reserve oilfield). The reserves of fields are increase as iodine contents of reservoir waters increase (r^2=0,89). It is seen that iodine contents of formation waters of basins containing giant oilfields are 8 mg/L or more. Besides, iodine contents of formation waters in giant oil and gas

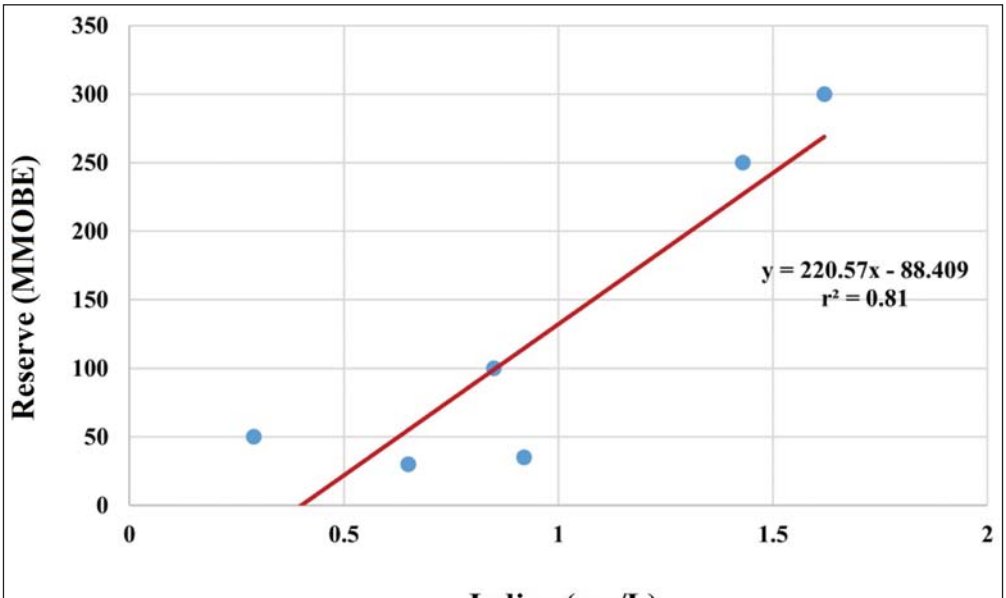

Oilfield	Oil production percentage in the Southeastern Anatolia basin (%)		Iodine content (mg/L)		Reserve (MMOBE)
			Max.	Min.	
Batı Raman	22.30		2.81	1.62	300
Raman	19.44		6.45	1.43	250
Beykan	6.10		1.81	0.85	100
Kurkan	3.27		0.52	0.29	50
Garzan	2.05		1.43	0.92	35
Kuzey Karakuş	2.00		1.74	0.65	30
Total	55.16	**Average**	2.46	0.96	127.5

Figure 24- The relationship between oil reserves and iodine contents of formation waters in oilfields of Southeastern Anatolia basin. Iodine content data of formation waters in the oilfields: this study, reserve data of the oilfields: Özgür (2016) and 2017 production data of Turkish Petroleum Company (TPAO).

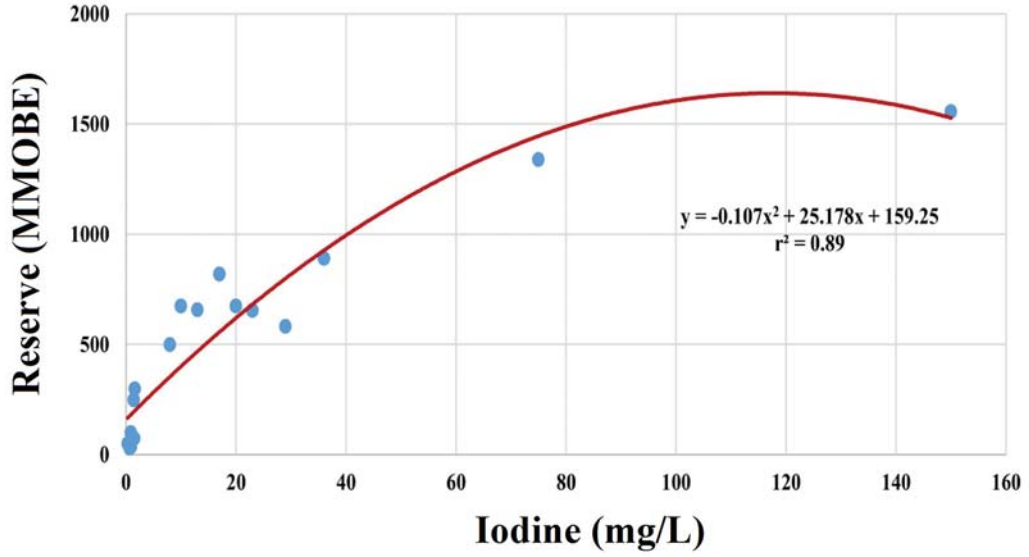

Basins Containing Giant Oil- and Gasfield				Major Oilfields			
Basin	Iodine Content (mg/L)		Reserve (MMOBE)	Field/Basin	Iodine Content (mg/L)		Reserve (MMOBE)
	Max.	Average			Max.	Average	
Anadarko	1480	150	1558	Batı Raman	2.8	1.6	300
Los Angelas	190	75	1340	Raman	6.5	1.4	250
Mississippi-Louisiana	106	36	892	Garzan	1.4	0.9	35
Sacramento	74	29	583	Beykan	1.8	0.9	100
Western Gulf	86	23	656	Cambay	1.9	0.8	60
Cherokee Platformu	188	20	623	Kuzey Karakuş	1.7	0.7	35
Powder River	54	20	676	Kurkan	0.5	0.3	50
Permian	320	17	820				
Appalachian	105	13	658				
Illinois	210	10	675				
Big Horn	23	8	500				

Figure 25- The relationship between reserves and iodine contents of formation waters of basins containing giant oil and gas fields of US, and main oilfields of Southeastern Anatolia (Turkey) and Cambay (India). (Iodine content data of US giant fields: USGS Produced Water Database, iodine content data in Southeastern Anatolian basin: this study, average iodine content data of Cambay basin: Rebar et al., 2014, Average reserve data of giant fields in US: Mann et al., (2003), reserve data of oilfields in Southeastern Anatolian basin: Özgür (2016) and 2017 production data of Turkish Petroleum Company (TPAO), reserve data of Cambay basin: www.selanoil.com

fields of US are quite higher than Southeastern Anatolia and Cambay basins (India). Therefore, reserves of fields will also be high in basins where found the high iodine contents waters because iodine enrichment is a sensitive indicator for the history of the buried iodine-rich organic matter. Thus, iodine contents of waters will be high due to fast sedimentation and high carbon deposition rate in basins where giant oil and gas fields are located. In basins where low reserve oil and gas fields, iodine contents of waters will be low due to slow sedimentation and low carbon deposition rate and release of iodine into the sea (Figure 8). The fact that there is not discovered any giant field in 1,1 mg/L iodine-containing Southeastern Anatolia basin which exploration and production have been made since 1930 and in 0,83 mg/L iodine-containing Cambay (India) basin which exploration and production have been made since 1950 is supported this result. Moran (1996) proved that the source of both very high iodine content of waters and hydrocarbons observed in Anadarko basin oil and gas fields are Woodford shales quite rich in organic matter using geochemical and hydrogeochemical methods.

4.5. The Relation between Salinity of Formation Water and Iodine

The Oilfield waters are fossil marine waters. Therefore, salinity ratios are expected close or higher than seawater. However, in addition to oil and gas fields containing saline water, there are containing brackish waters (Total dissolved solids, TDS: 1000 - 10000 mg/L) and freshwaters (Total dissolved solids, TDS: 1000 mg/L) many oilfields around worldwide (Table 1). The salinity of most oilfield waters in Southeastern Anatolia basin is also lower than seawater salinity (Table 2). However, distinguishing property among all oilfield waters and other water types (seawater, freshwater and saline waters derived from evaporates, etc.) is because the amount of iodine in oilfield waters is higher than other water resources. The ratio of I/Cl is a more remarkable distinctive (Figures 26 and 27) (Lemay and Konhauser, 2006; Whittemore et al., 1981; Lloyd et al., 1982). Iodine-rich waters are direct indicators for reservoirs in which the oil and gas can be produced (containing mature hydrocarbons). For this reason, it is more appropriate to use iodine-rich or iodized water definition instead of saline water for oilfield reservoir waters (Figure 28).

5. Conclusion and Suggestions

Pirson (1942) has defined success rates for different search methods as; random drilling 5,8%; geology + drilling 8,2%; geophysics + drilling 14,9% and geology + geochemistry + geophysics + drilling 57,8%. In the active tectonic (dynamically "excited" - "unbalanced") and geologically complex basins of the Alpine mobile belts, the implementation of the standard exploration strategy and techniques rooted in the half-century-old exploration empirics within relatively simple, tectonically "quiescent" platform regions with the dominating old foursome of "source

Table 1- Salinity and I/IC ratios of low saline formation waters in some oil and gas production fields. Formation water data: Yang (2017), Fu and Zhan (2009), Kurchikov and Plavnik (2009), Novikov (2013*a, b*), Novikov (2012), Kokh and Novikov (2014); USGS Produced Water database, Seawater data: Oppo and Capozzi (2015). Giant field: > 500 million bbl oil or oil equivalent gas reserve field. Total salinity values of regions are average salinity values of oilwells in the region.

Oilfield field / region	Total Salinity (mg/L)	I (mg/L)	Cl (mg/L)	I/Cl (x 10^{-5})
Renqie (China, giant field)	178	-	43	-
Gudao, Shengli (China, giant field)	3228	-	1036	-
Shengli (China, giant oilfield)	17960	-	10402	-
Daqang (China, giant oilfield)	16316	-	7896	-
Furrial-Musipan (Venezuela, giant oilfield)	5643	-	1780	-
Prudhoe Bay (ABD, giant oilfield)	18863	16.5	9270	177.9
Yarudei region (Russian)	18400	7.20	10767	66.8
Severnyı Arch region (Russian)	21779	7.35	12325	59.6
Western Khatanga region (Russian)	8230	8.24	3877	212.5
Yamal Peninsula region (Russian)	15788	24.26	8345	290.7
Yenise-Khatanga region (Russian)	8936	8.47	4233	200.1
Seawater	35148	0.05	19500	0.26

Table 2- Salinity and I/Cl ratios of formation waters of some oil production wells in Adıyaman and Thrace oilfields. Chemical data: Çelik and Sarı (2002); Hoşhan et al. (2008), Okandan et al. (1994). Iodine data of formation waters: this study, seawater data: Oppo and Capozzi (2015).

Well	Total Salinity (mg/L)	I (mg/L)	Cl (mg/L)	I/Cl (x 10^{-5})
Adıyaman-7	13595	0.79	8250	9.5
Adıyaman-44	879	0.12	480	25
Batı Fırat 2	25104	4.06	15234	26.6
Beşikli 10	18161	0.11	9713	1.1
Çemberlitaş-44	9526	0.20	5024	4
Güney Karakuş-11	25112	3.20	13692	23.4
Vakıflar	10150	0.56	3601	15.55
Kuzey Osmancık	21695	0.37	12980	2.85
Seawater	35148	0.05	19500	0.26

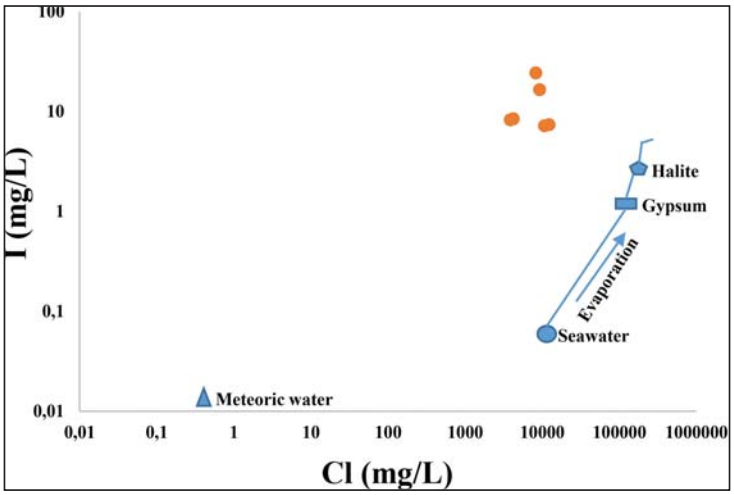

Figure 26- I/Cl ratios of low saline formation waters in some oil and gas production fields (data: Table 1). Seawater evaporation line was created using data of Chen et al. (2016), GERM (2004), Zherebtsova and Volkova (1966).

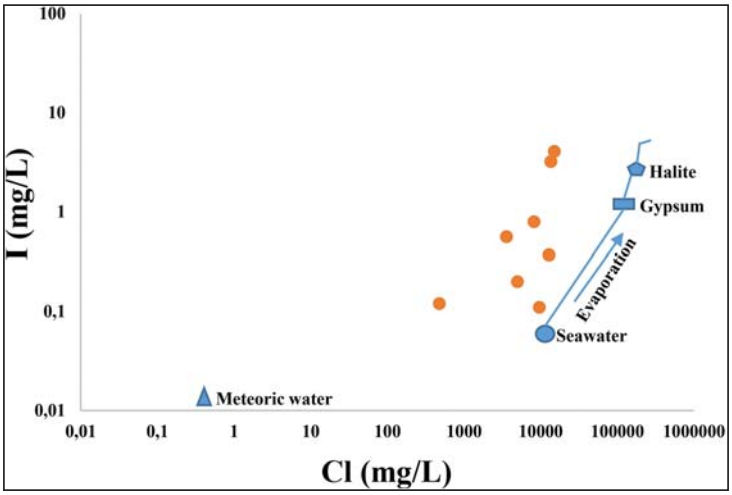

Figure 27- I/Cl ratios of formations waters of some oil production wells in Adıyaman and Thrace oilfields. Chemical data: Çelik and Sarı (2002); Hoşhan et al. (2008), Okandan et al. (1994). Iodine data: this study. Seawater evaporation line was created using data of Chen et al. (2016), GERM (2004), Zherebtsova and Volkova (1966).

rocks/traps/reservoir rocks/seals" turns out to be costly and often unsuccessful. A most telling example is the South-Caspian Basin (SCB). There, the largest western transnational companies and consortia, working under the PSA arrangements from 1995 through 2008, drilled 28 exploratory wells, up to 7301 m depth (almost 24,000 feet). The wells were spudded on the structures deemed highly potential and preliminarily subjected to high-resolution 3D seismic surveys. The effort cost about $1 billion and did not result in a single commercial discovery (Rachinsky and Kerimov, 2015).

Today, hydrogeochemical research is carried out primarily in regions where many water resources (cold and hot springs and wells) found and the petroleum potential not known in detail. This hydrogeochemical data are highly valuable the regions where the geology and the chemical composition of waters are well-known. Because hydrogeochemical research mainly based on the interpretation of existing water analysis and if necessary results of the new analyses. Since the reservoir characteristics of rocks do not take into consideration, it is not possible to estimate the commercial value of the areas, which have high

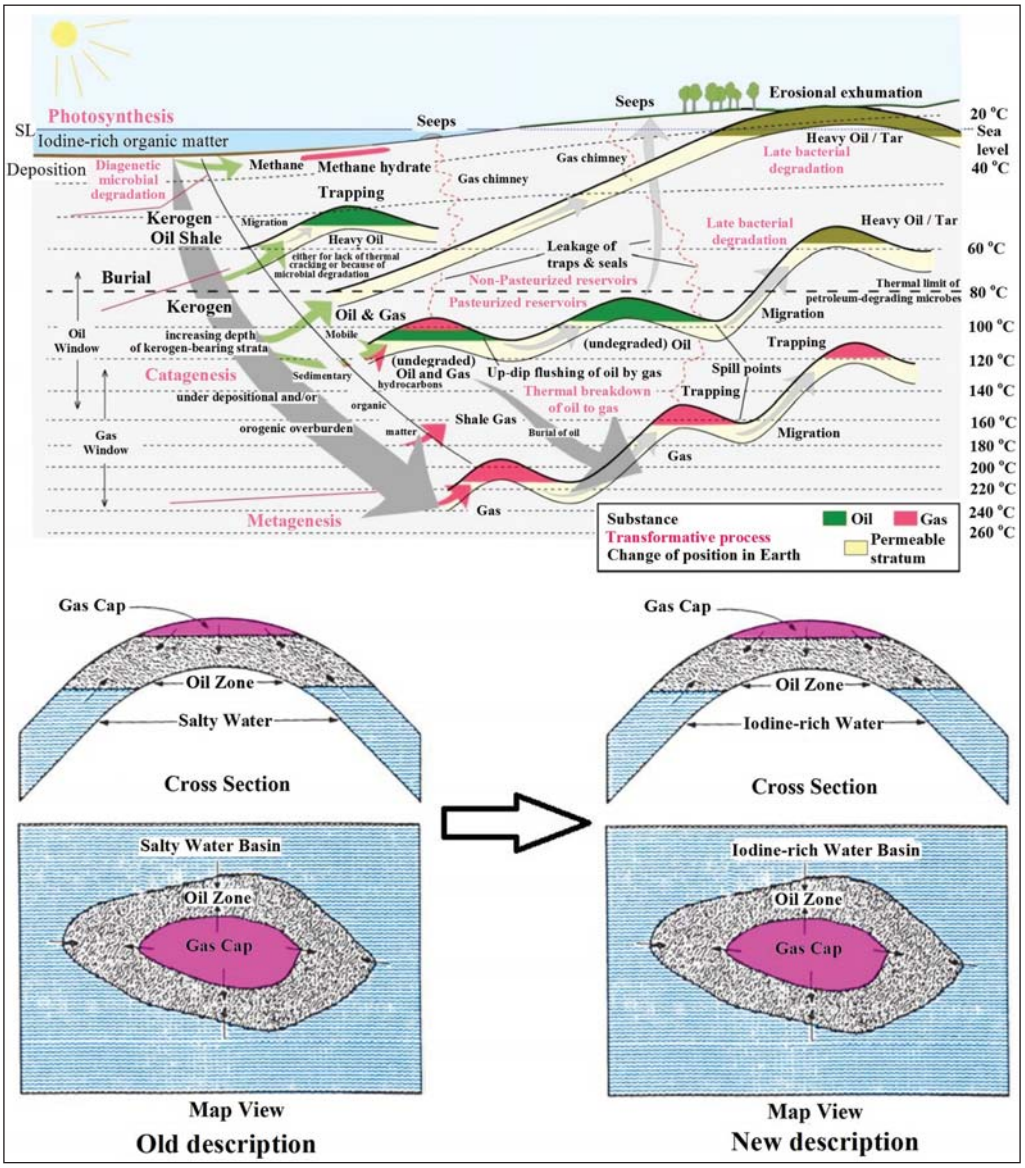

Figure 28- Transformation of iodine-rich organic matter to hydrocarbon and evolutionary process of occurrence of iodine-rich waters in Southeastern Anatolian basin.

oil and gas potential, based on the hydrogeochemical data. However, Sukharev (1948) has shown that in some cases hydrogeochemical data predict petroleum presence and commercial value in a given region, as well as even the estimation of the structure of deposits. While it is not entirely possible to estimate the cost of a groundwater based petroleum exploration model, this research method could reduce the cost of exploration on onshore by up to 50% (Tooth, 1987).

The hydrogeochemical and isotopic analysis as to make in all production wells of oilfields in the basin are critical to describe the unknown petroleum systems in the basin for future exploration and production activities in Southeastern Anatolia basin. Detailed chemical (TPHTotal Petroleum Hydrocarbons, TOC-Total Organic Carbon, CPI-Carbon Preference Index, BTEX-Benzene, toluene, ethylbenzene and xylene), isotopic (^{129}I and ^{127}I) analyses and mapping studies should be carried out in order to understand dominant factors controlling types and amounts of iodine in waters and soils of the Southeastern Anatolia basin. Iodine is a stable biophilic element and finds in highly enriched amounts in fluids associated with hydrocarbons such as oilfield waters. Due to this feature, iodine isotope (^{129}I) is used in recent years to determine hydrocarbon sources in various structures and the age of formation water associated with these

hydrocarbon sources (since the age of the iodine in the formation waters is also the age of hydrocarbons in the basin) and migration processes (some studies: Fehn et al., 1987, 1990; Martin et al., 1993; Moran et al., 1995; Liu et al., 1997; Birkle, 2006; Fehn et al., 2007; Muramatsu et al., 2007; Lu et al., 2008; Tomaru et al., 2009*a, b*; Togo et al., 2014; Alvarez et al., 2015, 2016; Santschi et al., 2016; Chen et al., 2016). The occurrence of hydrocarbons, time of maturation and the starting of migration are critical questions in understanding the processes of formation of oil reservoirs. Liu et al. (1997) have used the 129I isotope system to find answers to these questions (Figure 29).

Chen et al. (2016) study, is seen that 129I isotope system can provide useful information in reducing the costs of petroleum exploration activities and increasing efficiency (Figure 30). This data can be beneficial for petroleum exploration because hydrocarbon migration is related to water movement.

Worden (1996) approach based on I/Br ratio of iodine-rich waters settled to the reservoir and migrated together with maturing hydrocarbons derived from source rock can be used to determine kerogen type generating the hydrocarbons (Figure 31).

Specifically, the determination of iodine type (iodate, iodide or organic iodine) and their proportion in production oilwells may explain why different quality oils produced in the basin is of different quality. General Directorate of Mineral Research and Exploration of Turkey has been preparing soil and rock geochemistry maps of all elements (except iodine) throughout the country for the mineral exploration. It should prepare anomaly maps with this data and should determine the isotopic properties (^{129}I,^{127}I) and iodine types (iodate, iodide or organic iodine) found in oil and gas well waters (case study; Voutchkova et al., 2014), and in the soils (case studies: Tedesco et al., 1987, 1995; Allexan et al., 1986; Xuejing and Binzhong,

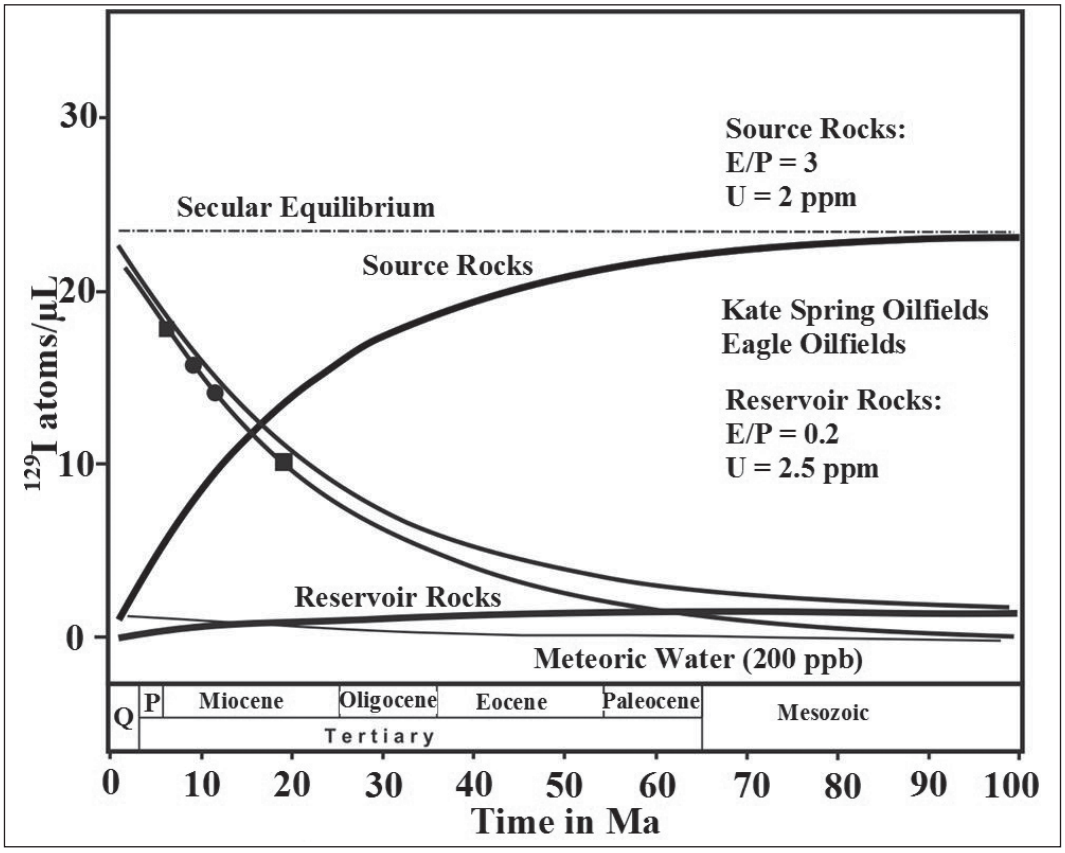

Figure 29- The evolution of ^{129}I concentrations in source rocks and reservoir rocks (heavy lines) and the decrease of ^{129}I concentrations after the separation from the source rocks (thin lines). The numerical time scale refers to residence times associated with the decay curves (thin lines), the geological times cale to the age of formations and the buildup curves (heavy lines). Data points are plotted on the uncorrected decay curve, the line above it indicates the decay corrected for the contribution from the production in the reservoir rock. Potential contribution from pre-anthropogenic meteoric water is also shown in the diagram (Liu et al., 1997).

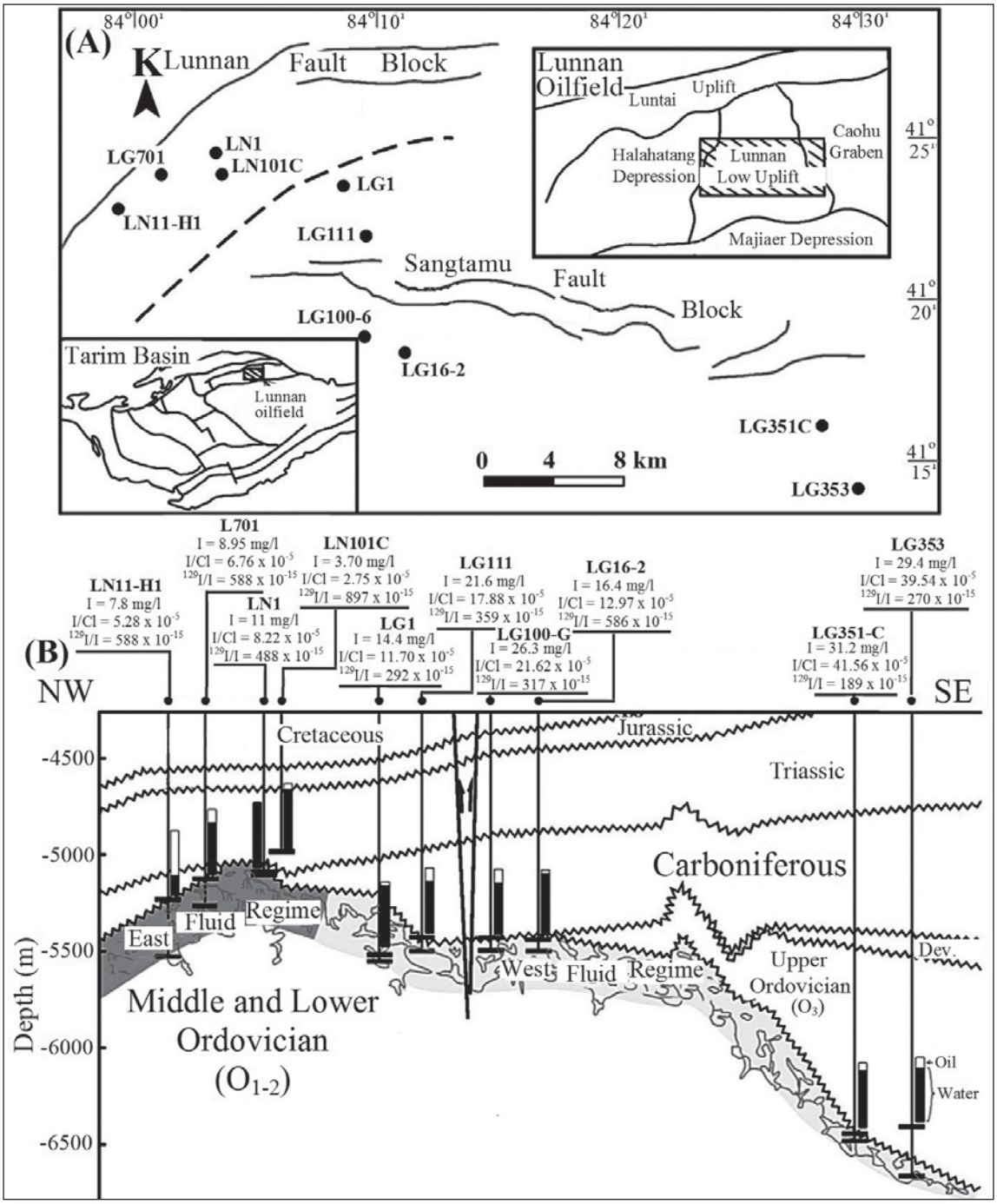

Figure 30- (A) The structural map of Tarim basin and the Lunnan oilfield (China). (B) the iodine contents of formation waters, and the water ratios, I/Cl and $^{129}I/I$ ratios of the oilwells (modified from Chen et al., 2016).

1989; Leaver and Thomasson, 2002; Mani et al., 2011) in the Southeastern Anatolia basin. Besides, the identification of oil and gas potential of the basin in detail and the determination of new exploration areas and the selection of new well locations will be drilled in existing licenses of these analyses are expected to provide significant contributions.

Iodine source in iodine-rich reservoir waters (iodine content >1 mg/L) of the Southeastern Anatolia basin, which is an oil and gas basin, is the organic-rich Silurian and JurassicCretaceous petroleum source rocks. It was seen that iodine contents of formation waters of oil and gas production fields in Southeastern Anatolia basin are >1 mg/L. However, there are also

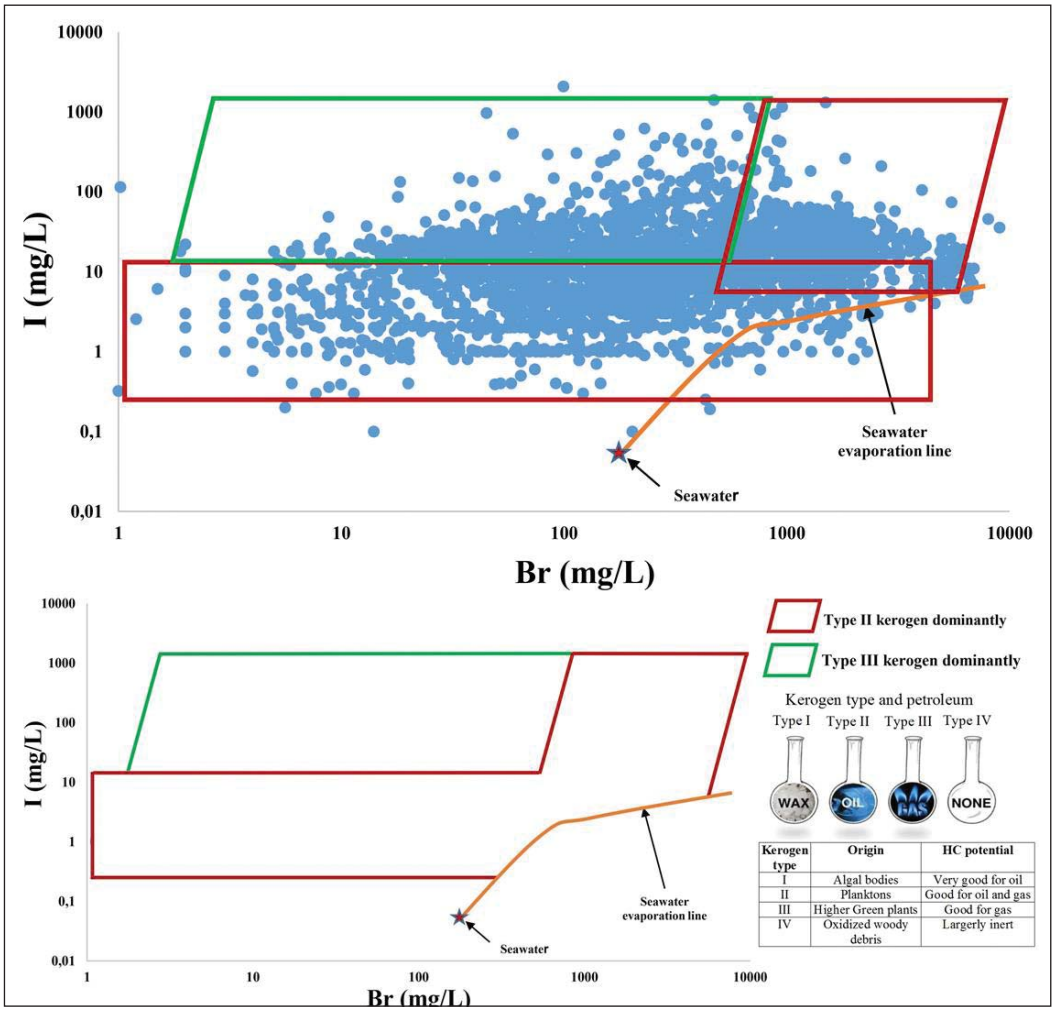

Figure 31- The relationship between kerogen type and I/Br ratios of formation waters. Worden (1996) model was taken as the basis in preparing the graph. The iodine data of formasyon waters of oil and gas fields: USGS Produced Water Database; Engle et al., 2016; Chen et al., 2016; Oppo et al., 2014; Oppo and Capozzi, 2015; Sudo, 1967; Kaiho, 2015; Kharaka et al., 1987; Dia et al., 1999; Dresel and Rose, 2010, Rowan et al., 2015; Mirnejad et al., 2011; Xun et al., 1997; Fisher and Kreitler, 1987; Dickey et al., 1972; Land, 1995; Birkle et al., 2002; Birkle et al., 2009; Franks and Uchytil, 2016; Hitchton et al., 1971; Machperson, 1992; Kokh and Novikov, 2014; Novikov, 2013*a, b*; Novikov, 2012; Novikov and Shvartsev, 2009; Demir and Seyler, 1999; Kurchikov and Plavnik, 2009; Fu and Zhan, 2009; Kireeva, 2010; Bagheri et al., 2014; this study, sample numbers: 3673).

production wells with formation waters containing iodine <1 mg/L. Total of 60 formation waters consist of 1 mg/L, 59 of them range between 0,5-1 mg/L, 108 of them range between 0,1-0,5 mg/L and 16 of them range between 0,01-0,08 mg/L iodine in the Southeastern Anatolian basin. Formation waters with iodine content <1 mg/L in production wells, the oilfield waters are iodine content decreased waters as results of mixing with other water types (meteoric and reinjection waters) in the basin of oilfield waters with iodine content >1 mg/L.

As result of this study, with iodine analysis to be performed on mud samples during drilling, are seen that it is possible that the prediction of oil volume to be produced from well and the detection whether there is oil or gas in the well (from increases/peaks in iodine contents of drilling mud both in entrance and exit of oil zone). Besides, these data from the EBY-17 oilwell is showed that iodine could be used as an excellent hydrocarbon accumulation indicator during both the exploration and drilling.

In the Southeastern Anatolia basin, the iodine ratios are considerably lower than that of basins containing giant oil and gas fields, and a large amount of water is produced with oil. The relationship between iodine and organic matter/organic carbon

is linear. Therefore, iodine contents of reservoir waters (petroleum saturation, oil/water ratio) are high in petroliferous basins found of source rocks containing high organic matter (kerogen). In the case, water saturation (water% ratio) of production wells will decrease because the abundance of iodine in formation waters is due to the release of most of the iodine in organic matter into related water during the transformation from organic matter to petroleum. This opinion is supported, the fact that these wells are highest net oil producing and least containing-water wells (with highest iodine content) in Adıyaman region, EBY-17 well (512 barrels of net oil production, iodine content of drilling mud: 10,72 mg/L), EBY-7 well (350 barrels of net oil production, iodine content of formation water: 29,80 mg/L) and PYK-3 well (210 barrels of net oil production, iodine content of formation water: 9,1 mg/L). Therefore, reserves of fields will also be high in basins where found the high iodine contents waters because iodine enrichment is a sensitive indicator for the history of the buried iodine-rich organic matter. Thus, iodine contents of waters will be high due to fast sedimentation and high carbon deposition rate in basins where giant oil and gas fields are located. In basins where low reserve oil and gas fields, iodine contents of waters will be low due to slow sedimentation and low carbon deposition rate and release of iodine into the sea.

As well as in other oil and gas fields in the world, not all reservoir waters in the Southeastern Anatolia basin are saline. However, all of them are rich in iodine. Therefore, iodine-rich waters are a direct indicator for oil and gas producible reservoirs (containing mature hydrocarbons). For this reason, it is more appropriate to use iodine rich or iodized water definition instead of saline water for oilfield reservoir waters. Iodine-rich waters are direct indicators for reservoirs in which the oil and gas can be produced (containing mature hydrocarbons) in the Southeastern Anatolia basin.

Although the fields in the Southeastern Anatolia basin are old and some fields the secondary production methods are used, the high relationship between the oil and gas deposits and iodine were proved. This study also gives an idea about how iodine geology and hydrogeology data (formation water iodine content and I/Cl - Cl ratio) will affect the success of oil and gas exploration projects in the basin or field scale. The explorations in oil and gas industry are carried out as structure-targeted (trap) with seismic survey and source rock-targeted with the organic geochemical survey. The success ratio of commercial oil discovery is 10-20% with the data obtained through these methods. Reservoir-targeted iodine geology and hydrogeology methods have simple sampling process, and laboratory analyses can result at a short time. The results are low cost, reliable and consistent. In the case when these data are utilized with other geological and geophysical methods, it is determined will be a practical and useful tool to reduce the hydrocarbon exploration risk to a minimum and to discover new deposits suitable for commercial production. Due to the results can be controlled and easily repeated are thought that the method will reduce the exploratory risk and costs. It is also foreseen that iodine analyses (chemical and isotopic) that will be carried out in drilled wells in oilfields at the production stage will provide significant contributions in selecting new well locations and accordingly determining the direction of field development.

Acknowledgements

The author special thanks to Melih Han Bilgin, General Manager of Turkish Petroleum Company (TPAO), who encouraged and supported the provision of iodine data for oilfield waters and carrying out this study. Furthermore; thanks to Abdurrahman Tiryaki, Head of Production Department, Abdullah Öner, Vice President of Research Center and Oğuz Şahin, Production Manager of Adıyaman Regional Directorate, who contributed a lot in providing formation waters of TPAO production fields and logistics, to laboratory chiefs Ender Taptık (Batman Regional Directorate) and Zekeriya Kılıçkara (Adıyaman Regional Directorate) who performed iodine analyses rigorously, Asst. Prof. Alperen Şahinoğlu (İstanbul Rumeli University) for his invaluable supports, Prof. Reyhan Kara Gülbay (Karadeniz Technical University) and to the other reviewer who contributed a lot in criticizing this article during the development of this study.

References

Allexan, S., Fausnaugh, J., Goudge, C., Tedesco, S. 1986. The use of iodine in geochemical exploration for hydrocarbons. Assoc. of Petroleum Geochemical Explorationist, II, 1, 12/86, pp.71-93.

Alvarez, A.A. Reich, M., Pe´rez-Fodich, A., Snyder, G., Muramatsu, Y., Vargas, G., Fehn, U., 2015. Sources, sinks and long-term cycling of iodine in the hyperarid Atacama continental margin. Geochimica et Cosmochimica Acta, 161, pp.50-70.

Alvarez, F., Reich, M., Snyder, G., Perez-Fodich, A., Muramatsu, Y., Daniele, L., Fehn, U. 2016. Iodine budget in surface waters from Atacama: Natural and anthropogenic iodine sources revealed by halogen geochemistry and iodine-129 isotopes. Applied Geochemistry, 68, pp.53-63.

Bagheri, R., Nadri, A., Raeisi, E., Shariati, A., Mirbagheri, M., Bahadori, F. 2014. Chemical evolution of a gas-capped deep aquifer, southwest of Iran. Environmental Earth Sciences, 71, 7, pp.3171-3180.

Birkle, P. 2006. Application of $^{129}I/^{127}I$ to define the source of hydrocarbons of the Pol-Chuc, Abkatún and Taratunich-Batab oil reservoirs, Bay of Campeche, southern Mexico. Journal of Geochemical Exploration, 89, pp.15-18.

Birkle, P., Aragon, J.J.P., Portugal, E., Aguilar, J.L.F. 2002. Evolution and origin of deep reservoir water at the Activo Luna oil field, Gulf of Mexico, Mexico. AAPG Bulletin, 86(3), pp.457-484.

Birkle, P., García, B.M., Padrón, C.M.M. 2009. Origin and evolution of formation water at the Jujo-Tecominoacán oil reservoir, Gulf of Mexico. Part 1: Chemical evolution and water-rock interaction, Applied Geochemistry, 24, pp.543-554.

Bojarski, L. 1970. Die Anwendung der hydrochemischen klassifikation bei Sucharbeiten auf Erdol. 2. Angew. Geol., 16:123-125 (in Collins, A.G. 1975. Geochemistry of Oilfield Waters. Developments in Petroleum Science, 1, Elsevier Scientific Publishing Company, Amsterdam, 496p.).

Borodkin, V.N., Khorobrykh, D.L., Lyubimov, S.A. 2005. The Achimovka clinoform reservoir in northern West Siberia: groundwater chemistry data. Gornye Vedomosti, 8, pp.52-56.

Campos J.C., Borges R.M.H., Filho A.M.O., Nobrega R., and Sant'Anna Jr. G.L. 2002. Oilfield wastewater treatment by combined microfiltration and biological processes. Water Research, 36, pp.95-104.

Chen, J., Liu, D., Peng, P., Ning, C., Xiaolin, H., Baoshou, Z. 2016. Iodine-129 chronological study of brines from an Ordovician paleokarst reservoir in the Lunnan oilfield, Tarim Basin. Applied Geochemistry, 65, pp.14-21.

Collins, A.G. 1969. Chemistry of some Anadarko Basin brines containing high concentration of iodine: Chemical Geology, 4, pp.169-187.

Collins, A.G. 1975. Geochemistry of Oilfield Waters. Developments in Petroleum Science-1, Elsevier, 496p.

Collins, A.G., Egleeson, G.C. 1967. Iodine abundance in oilfield brines in Oklahoma. Science, 156, pp.934-935.

Collins, A. G., Bennett, J. H., Manuel, O. H. 1971. Iodine and algae in sedimentary rocks associated with iodine rich brines. Geol. Soc. Am. Bull., 82, pp.2607-2610.

Cosgrove, M.E. 1970. Iodine in bituminous Kimmeridge shale of the Dorset coast in England: Geochim. Cosmochim. Acta, 34, pp.830-836.

Çelik, M., Sarı, A. 2002. Geochemistry of formation waters from upper cretaceous calcareous rocks of Southeast Turkey. Journal Geological Society of India. 59, pp.419-430.

Çelik, M., Sarı, A., Bahtiyar, I., Afşin, M. 1998. Origin of formation waters in Adıyaman oil fields. 12th International Petroleum Congress and Exhibition of Turkey, pp.149-159.

Demir, I., Seyler, B. 1999. Chemical composition and geologic history of saline waters in Aux Vases and Cypress Formations, Illinois Basin. Aquatic Geochemistry, 5, pp.281-311.

Dia, A.N., Castrec-Rouelle, M., Boulegue, J., Comeau, P. 1999. Trinidad mud volcanoes: Where do the expelled fluids come from ? . Geochimica et Cosmochimica Acta, 63(7/8), pp.1023-1038.

Dickey, P.A., Collins, A.G., Fajardo M.I. 1972. Chemical composition of deep formation waters in Southwestern Louisiana. AAPG Bulletin, 56(8), pp.1530-1570.

DPT (Devlet Planlama Teşkilatı), 2001. Petrol-Doğalgaz Çalışma Grubu Raporu, 130p.

Dresel, P. E., Rose, A.W. 2010. Chemistry and origin of oil and gas well brines in western Pennsylvania: Pennsylvania Geological Survey, 4th ser., Open-File Report OFOG 10-01.0, 48p.

Elderfield, H., Truesdale, V.W. 1980. On the biophilic nature of iodine in sea water. Earth Planet. Sci. Lett. 50, pp.105-111.

Engle, M.A., Reyes, F.R., Varonka, M.S., Orem, W.H., Ma, L., Ianno, A.J., Schell, T.M., Xu, P., Carroll, K.C. 2016. Geochemistry of formation waters from the Wolfcamp and "Cline" shales: Insights into brine origin, reservoir connectivity, and fluid flow in the Permian Basin, USA. Chemical Geology, 425, pp.76-92

Fabryka-Martin, J.T. 1984. Natural iodine-129 as environmental tracer. University of Arizona. MSc. Thesis, 149p.

Fehn, U. 2012. Tracing crustal fluids: Applications of natural ^{129}I and ^{36}Cl. Annu. Rev. Earth Planet. Sci, 40, pp.45-67.

Fehn, U., Tullai, S., Teng, R.T.D., Elmore, D., Kubik, P.W. 1987. Determination of ^{129}I in heavy residues of two crude oils: Nucl. Instrum. Methods Phys. Res., B52, pp.446-450.

Fehn, U., Tullai-Fitzpatrick, S., Teng, R.T.D., Gove, H.E., Kubik, P.W., Sharma, P., Elmore, D. 1990. Dating of oil field brines using ^{129}I. Nuclear Instruments and Methods in Physics Research B52, pp.446-450.

Fehn, U., Snyder, G.T., Matsumoto, R., Muramatsu, Y., Tomaru, H. 2003. Iodine dating of pore waters associated with gas hydrates in the Nankai area, Japan. Geology, 31, pp.521-524.

Fehn, U., Snyder, G.T., Muramatsu, Y. 2007. Iodine as a tracer of organic material: ^{129}I results from gas hydrate systems and fore arc fluids. Journal of Geochemical Exploration. 95(1-3), pp.66-80.

Fisher, R.S., Kreitler, C.W. 1987. Geochemistry and hydrodynamics of deep-basin brines, Palo Duro Basin, Texas, U.S.A. Applied Geochemistry, 2, pp.459-76.

Franks, S.G., Uchytil, S.J. 2016. Geochemistry of formation waters from the subsalt Tubular Bells Field, offshore Gulf of Mexico: Implications for fluid movement and reservoir continuity, AAPG Bulletin, 100(6), pp.943-967.

Fu, Y., Zhan, H. 2009. On the origin of oil-field water in the Biyang Depression of China. Environmental Geology, 58, pp.1191-1196.

Fuge, R. 1974. Iodine, Chapter 53 in: Handbook of Geochemistry, Vol. II, Pt. 4, (K. H. Wedepohl, ed.), Springer-Verlag NY.

Fuge, R., Johnson, C.C. 1986. The geochemistry of iodine - a review. Environ. Geochem. Health. 8(2), pp.31-54.

Gallagher, A.V. 1984. Iodine: A pathfinder for petroleum deposits, in Unconventional Methods in Exploration Ill**,** Southern Methodist University, Dallas, TX, pp.148-159.

GERM, 2004. Geochemical Reference Model. http://earthref.Org/GERM/.

Ginis, Y.V. 1966. Hydrogeological conditions and hydrochemistry of iodine-bromine waters in the Kura lowlands and prospects of exploration for new fields. Dissertation. Baku.

Gieskes, J.M., Mahn, C. 2007. Halide systematics in interstitial waters of ocean drilling sediment cores. Appl. Geochem., 22, pp.515-533.

Gordon, T.L., Ikramuddin, M. 1988. The use of iodine and selected trace metals in petroleum and gas exploration. Geologic Society of America Abstracts with Programs, 20(7), 228p.

Goudge, C.K. 2007. Geochemical Exploration, Sample Collection and Survey Design in Society of Independent Professional Earth Scientists Quarterly, v. XXXXIIII, no. 1.

Goudge, C.K. 2009. Graystone Exploration Labs Inc, Golden, Colorado. Retrieved from www.graystonelab.com.

Greenhalgh, E. 2016. The Jurassic shales of the Wessex Area: geology and shale oil and shale gas resource estimation. British Geological Survey for the Oil and Gas Authority, 72p.

Gupta, A., Gupta, P., Saxena, E. 2016. First application of Multistage Fracturing Technology in onshore field of ONGC - A new breakthrough. PETROTECH-2016, 12th International Oil & Gas Conference and Exhibition. New Delhi, İndia, Technical Paper. http://petrotech.in/uploadfiles/434id_Abstract%20for%20Multistage%20Fracturing.pdf.

Hach Chemical Co. 1992. DPD method for iodine (adapted Palin, A.T., 1967. Method for the determination, in water, of free and combined available chlorine, chlorine dioxide and chlorite, bromine, iodine, and ozone, using diethyl-p-phenylene diamine -DPD. J. Inst. Water Eng. 21, pp.537-547).

Harrison, W.J., Summa, L.L. 1991. Paleohydrology of the Gulf Coast of Mexico Basin. Am. J. Sci., 291, pp.109-176.

Harvey, G.R. 1980. A study of the chemistry of iodine and bromine in marine sediments. Marine Chemistry 8, pp.327-332.

Hilger, J. 2003. Combined utilization of oil shale energy and oil shale minerals within the production of cement and other hydraulic binders. Oil Shale, 20(3), pp.347-355.

Hitchon, B., Billings, G.K., Klovan, J.E. 1971. Geochemistry and origin of formation waters in the western Canada sedimentary basin-III. Factors

controlling chemical composition. Geochimica et Cosmochimica Acta. 35, pp.567-598.

Hora, K. 2016. Iodine production and industrial applications. IDD Newsletter, http://www.ign.org/newsletter/idd_aug16_iodine_production.pdf .

Hoşhan, P., Çelik, S., Çanga, B. 2008. Inspection and control of corrosion problems for production oil wells tubing and rod in Adıyaman oil fields. International Corrosion Symposium, Izmir, Turkey, pp.13-20.

Huang, L. 1984. Iodine contents in formation waters from wildcats, southern Taiwan. Petroleum Geology of Taiwan, 20, pp.231-235.

Hummel, S. 2011. The Use of Iodine to Characterize Formation Waters in Oil and Gas Fields. Syracuse University. MSc. Thesis, 66p.

Kaiho, T. (Ed.) 2015. Iodine Chemistry and Applications. John Wiley & Sons, Inc., 635p.

Kartsev, A.A., Tabasaranskii, S.A., Subbota, M.I., Mogilevsky, G.A. 1954. Geochemical methods of prospecting and exploration for petroleum and natural gas (P. A. Witherspoon and W. D, Romey, eds., English translation) : Berkeley, Univ. Calif. Press, 1959, 238p.

Kendrick, M.A., Phillips, D., Wallace, M., Miller, J.McL. 2011. Halogens and noble gases in sedimentary formation waters and Zn-Pb deposits: A case study from the Lennard Shelf, Australia. Applied Geochemistry, 26, pp.2089-2100.

Kennedy, H.A., Elderfiel, H. 1987. Iodine diagenesis in pelagic deep-sea sediments. Geochimica et Cosmochimica Acta, 51, pp.2489-2504.

Khajeh, M. 2007. Gorgan Bölgesi (İran) iyot üretimi çalışmaları sunumu (unpublished).

Kharaka, Y.K., Maest, A.S., Carothers, W.W., Law, L.M., Lamothe, P.J., Fries, T.L. 1987. Geochemistry of metal-rich brines from central Mississippi Salt Dome basin, U.S.A., Applied Geochemistry, 2, pp.543-561.

Kireeva, T.A. 2010. Genesis of the underground water from the White Tiger Deposit, south Vietnam Shelf, in relation to its petroleum resource potential. Moscow University Geology Bulletin, 65(4), pp.244-249.

Kokh, A.A., Novikov, D.A. 2014. Hydrodynamic conditions and vertical hydrogeochemical zonality of groundwater in the western Khatanga artesian basin. Water Resources, 41(4), pp.396-405.

Kovda, V. A., Salvin, P. S. 1951. Soil-geochemical indicators of deep oil bearing rocks: Akad. Nauk. SSSR (Kartsev, A.A., Tabasaranskii, S.A., Subbota, M.I., Mogilevsky, G.A., 1954. Geochemical methods of prospecting and exploration for petroleum and natural gas (in P. A. Witherspoon and W. D, Romey, eds., English translation : Berkeley, Univ. Calif. Press, 1959, 238p.).

Kurchikov, A.R., Plavnik, A.G. 2009. Clustering of groundwater chemistry data with implications for reservoir appraisal in West Siberia. Russian Geology and Geophysics 50, pp.943-949.

Kudel'sky, A.V. 1977. Prediction of oil and gas properties on a basis of iodine content of subsurface waters. Geologiya Nefti i Gaza, 4, pp.45-49.

Land, L.S. 1991. Evidence for vertical movement of fluids, Gulf Coast Sedimentary Basin: Geophys. Res. Lett., 18(5), pp.919-922.

Land, L.S. 1995. Na-Ca-Cl saline formation waters, Frio Formation (Oligocene), south Texas, USA: Products of diagenesis. Geochimica et Cosmochimica Acta, 59, 11, pp.2163-2174.

Leaver, J.S., Thomasson, M.R. 2002. Case studies relating soil-iodine geochemistry to subsequent drilling results. in Schumacher, D., and LeSchack, L. D., eds., Surface Exploration Case Histories: Application of Geochemistry, Magnetics and Remote Sensing, AAPG Studies in Geology no. 48, and SEG Geophysical References Series no. 11, pp.41-57.

Lee, R., Seright, R., Hightower, M., Sattler, A., Cather, M., McPherson, B., Wrotenbery, L., Martin, D., Whitworth, M. 2002. Strategies for Produced Water Handling in New Mexico. Groundwater Protection Council Produced Water Conference, http://www.gwpc.org/meetings/special/PW%202002/Papers/ Robert_Lee_PWC2002.pdf.

Lemay, T.G., Konhauser, K.O. 2006. Water Chemistry of Coalbed Methane Reservoirs. Alberta Geological Survey. Special Report 081. 354p.

Levinson, A.A. 1980. Introduction to Exploration Geochemistry. Applied Publishing, IL, 924p.

Liu, X., Fehn, U., Teng, R.T.D. 1997. Oil formation and fluid convection in Railroad Valley, NV: a study using cosmogenic isotopes to determine the onset of hydrocarbon migration. Nuclear Instruments and Methods in Physics Research B 123 (1997), pp.356-360.

Lloyd, J.W., Howard, K.W.F., Pacey, N.R., Tellam, J.H. 1982. The value of iodide as a parameter in the chemical characterization of groundwaters, Journal of Hydrology, 57, pp.247-265.

Lu, Z., Hensen, C., Fehn, U., Wallmann, K. 2008. Halogen and ^{129}I systematics in gas hydrate fields at the

northern Cascadia margin (IODP Expedition 311): Insights from numerical modeling. Geochem. Geophys. Geosyst., 9, Q10006, doi:10.1029/2008GC002156.

Macpherson, G.L. 1992. Regional variations in formation water chemistry: major and minor elements, Frio formation fluids, Texas. AAPG Bulletin, 76(5), pp.740-757.

Mani, D., Kumar, T.S., Rasheed, M.A., Patil, D.J., Dayal, A.M., Rao, T.G., Balaram, V. 2011. Soil iodine determination in Deccan Syneclise, India: Implications for near surface geochemical hydrocarbon prospecting. Natural Resources Research, 20(1), pp.75-88.

Mann, P., Gahagan, L., Gordon, M.B. 2003. Tectonic setting of the world's giant oil and gas fields, in M. T. Halbouty, ed., Giant oil and gas fields of the decade 1990-1999, AAPG Memoir 78, pp.15-105.

Martin, J.B., Gieskes, J.M., Torres, M., Kastner, M. 1993. Bromine and iodine in Peru margin sediments and pore fluids: Implications for fluid origins. Geochimico et Cosmochlmica Acta, 51, pp.4377-4389.

Mirnejad, H., Sisakht, V., Mohammadzadeh, H., Amini, A.H., Rostron, B.R., G. Haghparast, G. 2011. Major, minor element chemistry and oxygen and hydrogen isotopic compositions of Marun oil-field brines, SW Iran: Source history and economic potential. Geological Journal, 46, pp.1-9.

Moran, J. E. 1996. Origin of iodine in the Anadarko Basin, Oklahoma: an ^{129}I study. Am. Assoc. Petrol. Geol. Bull., 80(5), pp.685-694.

Moran, J.E., Fehn, U., Hanor, J.S. 1995. Determination of source ages and migration of brines from the U.S. Gulf Coast basin using 129 I. Geochim. Cosmochim. Acta 59, pp.5055-5069.

Moran, J.E., Fehn, U., Ray, T.D. 1998. Variations in $^{129}I/^{127}I$ in recent marine sediments: evidence for a fossil organic component. Chemical Geology, 152, pp.193-203.

Muramatsu, Y., Wedepohl, K.H. 1998. The distribution of iodine in the earth's crust. Chemical Geology, 147, pp.201-216.

Muramatsu, Y., Doi, T., Tomaru, H., Fehn, U., Takeuchi, R., Matsumoto, R. 2007. Halogen concentrations in pore waters and sediments of the Nankai Trough, Japan: implications for the origin of gas hydrates. Appl. Geochem., 22, pp.534-556.

Novikov, D.A. 2012. Hydrogeology of oil-and-gas bearing deposits of the Severnyi arch (Northern areas of the West Siberian Megabasin (WSMB). Oil and Gas Business, 4, pp.521-535.

Novikov, D.A. 2013*a*. Hydrogeochemical features of petroleum-bearing deposits of the Yamal Peninsula. Oil and Gas Business, 1, pp.114-143.

Novikov, D.A. 2013*b*. Hydrogeology of the western part of the Yenisei-Khatanga regional trough. Neftegazovaya Geologiya, Teoriya I Praktika, 8(1), www.ngtp.ru/rub/4/2_2013.eng.pdf.

Novikov, D.A., Shvartsev, S.L. 2009. Hydrogeological conditions of the Pre-Yenisei petroleum subprovince. Russian Geology and Geophysics, 50, pp.873-883.

Okandan, E., Mehmetoğlu, T., Doyuran, V., Demiral, B., Parlaktuna, M., Gümrah, F., Kuru, E., Behlülgil, K., Karacan, Ö. ve Karaaslan, U. 1994. Petrol Arama ve Üretim Faaliyetlerinin Çevre Üzerindeki Etkisi, Proje No.YBAG-0057, 92p. (unpublished).

Oppo, D., Capozzi, R. 2015. Spatial association of mud volcano and sandstone intrusions, Boyadag anticline, western Turkmenistan. Basin Research, 1-13, doi: 10.1111/bre.12136.

Oppo, D., Capozzi, R., Nigarov, A., Esenov, P. 2014. Mud volcanism and fluid geochemistry in the Cheleken Peninsula, western Turkmenistan, Marine and Petroleum Geology, 57, pp.122-134.

Osborn, S.G., Mcintosh, J.C., Hanor, J.S., Biddulph, D. 2012. Iodine-129, $^{87}Sr/^{86}Sr$, and trace elemental geochemistry of northern Appalachian basin brines: evidence for basinal-scale fluid migration and clay mineral diagenesis. American Journal of Science, 312, pp.263-287.

Özdemir, A. 2009. İyot üretimi amaçlı yapılan sondaj çalışmaları. Madencilik Türkiye Dergisi, 1, 26-28 .

Pavlova, G.A., Shisekina O.V. 1973. Accumulation of iodine in interstitial water during metamorphism in relation to the iodine distribution in Pacific sediments. Geochem. Int. 10, pp.804-813.

Peterson, T.F. 1979. The geochemistry of sediments of the Panama Basin, Eastern Equatorial Pacific Ocean. PhD. Thesis, University of Edinburgh, 235 p.

Plavnik, A.G., Plavnik, G.I., Itskovich, M.V., Oleinik, E.V. 2007. Water chemistry of clinoform reservoirs BV4-5, BV6–7, and BV8–9, in: Karasev, V.I., Shpilman, A.V., Volkov, V.A. (Eds.), Development of the Petroleum Potential of the Khanty-Mansi Autonomous Area [in Russian]. Izdatnaukaservis, Khanty-Mansiisk, Book 1 (1), pp.205-212.

PİGM (Petrol İşleri Genel Müdürlüğü), 2008. 2005-2006-2007 Türkiye Petrol Faaliyetleri, 288p.

Pirson, S.J. 1942. Theoretical and economic significance of geodynamic prospecting. World Petrol., 13, pp.38-42.

Pogodaeva, T.V., Zemskaya, T.I., Golobokova, L.P., Khlystov, O.M., Minami, H., Sakagami, H. 2007. Chemical composition of pore waters of bottom sediments in different Baikal basins. Russian Geology and Geophysics (Geologiya i Geofizika) 48 (11), pp.886-900 (1144-1160).

Price, N. B., Calvert, S.E. 1973. The geochemistry of iodine in oxidized and reduced recent marine sediments: Geochim. Cosmochim. Acta, 37, pp.2149-2158.

Price, N.B., Calvert, S.E. 1977. The contrasting geochemical behaviors of iodine and bromine in recent sediments from the Namibian shelf. Geochimica et Cosmochimica Acta 41, pp.1769-1775.

Price, N.B., Calvert, S.E., Jones P.G.W. 1970. The distribution of iodine and bromine in the sediments of the South Western Barents Sea. J. Mar. Res. 28, pp.22-34.

Qiao, X., Zhang, Z., Yu, J., Ye, X. 2008. Performance characteristics of a hybrid membrane pilot-scale plant for oilfield-produced wastewater. Desalination, 225(1-3), pp.113-122.

Rachinsky, M.Z., Kerimov, V.Y. 2015. Fluid Dynamics of Oil and Gas Reservoirs. Scrivener Publishing LLC - John Wiley and Sons, Inc., 613p.

Rebary, B., Raichura, M., Mangukia, S.R., Patidar, R. 2014. Mapping of iodine, lithium and strontium in oilfield water of Cambay basin, Gujarat. Journal Geological Society of India. 83, pp.669-675.

Rowan, E.L., Engle, M.A., Kraemer, T.F., Schroeder, K.T., Hammack, R.W., Doughten, M.W. 2015. Geochemical and isotopic evolution of water produced from Middle Devonian Marcellus shale gas wells, Appalachian basin, Pennsylvania. AAPG Bulletin, 99(2), pp.181-206.

Santschi, P.H., Xu, C., Zhang, S., Schwehr, K.A., Grandbois, R., Kaplan, D.I., Yeager, C. 2016. Iodine and plutonium association with natural organic matter: A review of recent advances. Applied Geochemistry (2016), doi: 10.1016/j.apgeochem.2016.11.009.

Schoeneich, K. 1971. Indices of oil bearing deposits as based on the formation waters of Poland. Nafta (Pol.), 27, 154-157 (in Coustau, H. 1977. Formation waters and hydrodynamics. Journal of Geochemical Exploration, 7, pp.213-241).

Shishkina, O.V., Pavlova, G.A. 1965. Iodine distribution in marine and oceanicbottom muds and in their pore fluids. Geochemical Internatioal, 2, pp.559-565.

Shvartsev, C.L., Novikov, D.A. 2004. The nature of vertical hydrogeochemical zoning of petroleum deposits (exemplified by the Nadym-Taz interfluve, West Siberia). Geologiya i Geofizika (Russian Geology and Geophysics) 45 (8), pp.1008-1020 (960-972).

Singh, R.R. Saxena, J.G. Sahota, S.K., Chandra, K. 1987. On the use of iodine as an indicator of petroleum in Indian basins. 1st India Oil and Natural Gas Comm. Petroleum Geochemistry and Exploration in the Afro-Asian Region International Conference Proceedings, pp. 105-107.

Snyder, G.T., Fabryka-Martin, J.T. 2007. ^{129}I and ^{36}Cl in dilute hydrocarbon waters: Marine-cosmogenic, in situ, and anthropogenic sources. In: G.T. Snyder and J.E. Moran (Eds.), special issue: The halogens and their isotopes in marine and terrestrial aqueous systems, Applied Geochemistry, 22, pp.692-704.

Stueber, A.M., Walter, L.M. 1991. Origin and chemical evolution of formation waters from Silurian-Devonian strata in the Illinois basin, USA. Geochimica et Cosmochimica Acta, 55, pp.309-325.

Stueber, A.M., Walter, L.M., Huston, T.J., Pushkar, P. 1993. Formation waters from Mississippian-Pennsylvanian reservoirs, Illinois basin, USA: Chemical and isotopic constraints on evolution and migration. Geochimica et Cosmochimica Acta, 57, pp.163-784.

Sudo, Y. 1967. Geochemical study of brine from oil and gas fields in Japan. Journal of The Japanese Association of Petroleum Technologists. 32, 5, pp.286-296 .

Sukharev, G.M. 1948. Hydrogeological conditions of formation of oil and gas deposits in Tersk-Dagestan oil province. Groz. obi. izd-vo (in Kartsev, A. A., Tabasaranskii, S. A., Subbota, M. I., Mogilevsky, G. A., 1954. Geochemical methods of prospecting and exploration for petroleum and natural gas. P. A. Witherspoon and W. D, Romey, eds., English translation, Berkeley, Univ. Calif. Press, 1959, 238p.).

Surkov, V.S., Kazakov, A.M., Devyatov, V.P., Smirnov, L.V., Shiganova, O.V., Ekhanin, A.E., Zaitsev, S.P., Serebrennikova, O.V., Gulaya, E.V. 1999. Lower-Middle Jurassic strata of the southern West Siberia (geochemistry, groundwater geology, and petroleum potential). Geologiya Nefti i Gaza, 3-4, pp.3-11.

Tedesco, S.A. 1995. Surface Geochemistry in Petroleum Exploration. Springer-Science+Business Media, BV., 206p.

Tedesco, S., Goudge, C. 1989. Application of iodine surface geochemistry in the Denver-Julesburg Basin, Association of Petroleum Geochemical Explorationists Bulletin, **5**(I), pp.49-72.

Tedesco, S.A., Goudge, C., Fausnaugh, J., Alexon, S. 1987. Iodine-an exploration tool for oil and gas: Oil & Gas Journal, 85(26), pp.74-77.

Togo, Y.S., Kazahaya, K., Tosaki, Y., Morikawa, N., Matsuzaki, H., Takahashi, M., Sato, T. 2014. Groundwater, possibly originated from subducted sediments, in Joban and Hamadori areas, southern Tohoku, Japan. Earth, Planets and Space, 66, 131p.

Tomaru, H., Lu, Z., Fehn, U., Muramatsu, Y. 2009*a*. Origin of hydrocarbons in the Green Tuff region of Japan: ^{129}I results from oil field brines and hot springs in the Akita and Niigata Basins. Chemical Geology, 264, pp.221-231.

Tomaru, H., Fehn, U., Lu, Z., Takeuchi, R., Inagaki, F., Imachi, H., Kotani, R., Matsumoto, R., Aoike, K. 2009*b*. Dating of dissolved iodine in pore waters from the gas hydrate occurrence offshore Shimokita Peninsula, Japan: ^{129}I results from the D/V Chikyu Shakedown Cruise. Resource Geology, 59(4), pp.359-373

Tooth, J. 1987. Petroleum hydrogeology: a potential application of groundwater science. Journal of Geological Survey of India, 29(1), pp.172-179.

Tsunogai, S. 1971. Iodine in the deep water of the ocean. Deep Sea Research and Oceanographic Abstracts 18, pp.913-919.

Tullai, S., Tubbs, L. E., Fehn, U. 1987. Iodine extraction from petroleum for analysis of ^{129}I/I ratios by AMS: Nucl. Instrum. Methods Phys. Res. B, 29, pp.383-386.

U.S. Geological Survey National Produced Waters Geochemical Database v2.2.

Veil, J.A. 2006. Comparison of two international approaches to controlling risk from *produced water* discharges. Paper presented at the 70th PERF meeting, Paris, France.

Vinogradov A.P. 1939. Iodine in marine muds. To the problem of the origin of iodine-bromine waters in petroliferous regions (In Russian). Tr. Biogeokhim. Lab. Akad. Nauk SSSR 5, 19-32 (English pp.33-46).

Voutchkova, D.D., Ernstsen, V., Hansen, B., Sørensen, B.L., Zhang, C., Kristiansen, S.M. 2014. Assessment of spatial variation in drinking water iodine and its implications for dietary intake: A new conceptual model for Denmark. Science of the Total Environment, 493, pp.432-444.

Wallace, M.M., Middleton, H., Basil, J., Marshallsea, S. 2002. Hydrocarbons and Mississippi Valley type sulfides in the Devonian reef complexes of the eastern Lennard Shelf, Canning Basin, Western Australia. In: Keep, M., Moss, S.J. Eds. The Sedimentary Basins of Western Australia III: Procedings of the West Australasian Basins Symposium (WABS) III.; pp.795-816.

Warren, J.K. 2006. Evaporites: Sediments, Resources and Hydrocarbons. Springer-Verlag Berlin Heidelberg. 1035p.

Whittemore, D.O., Basel, C.L., Galle, O.K., Waugh, T.C. 1981. Geochemical Identification of Saltwater Sources in the Smoky Hill River Valley, McPherson, Saline, and Dickson Countries, Kansas, Kansas Geological Survey, Open-file Report 81-6, 78p.

Wilke-Dörfurt, E. 1927. Über den Jodgehalt einiger Gesteine und seine Beziehungen zum chemischen Teil des Kropfproblems. Ann. Chem., 453, 288 (in Correns, C.W. 1956. The geochemistry of the halogens. Physics and Chemistry of the Earth, 1, pp.181-233).

Worden, R.H. 1996. Controls on halogen concentrations in sedimentary formation waters. Mineralogical Magazine, 60, pp.259-274.

Xuejing, X., Binzhong, Y. 1989. Application of multiparametric geochemical methods in the search for oil in the Qinggang region near Daqing Oil Field: J. Geochem. Explor., 33, pp.203-213.

Xun, Z., Cijun, L., Xiumin, J., Qiang, D., Lihomg, T. 1997. Origin of subsurface brines in the Sichuan basin, Groundwater, 35(1), pp.53-58.

Yang, S. 2017. Fundamentals of Petrophysics. Springer-Verlag GmbH, 502p.

Zherebtsova, I.K., Volkova, N.N. 1966. Experimental study of behavior of trace elements in the process of natural solar evaporation of Black Sea water and Sasyk-Sivash brine. Geochemical International, 3, pp.656-670.

APPENDIX: Results of Iodine Analysis of Oilfield Waters in Southeast Anatolian Basin

Results of Iodine Analysis of Oilfield Waters in Batman Region (Data: DPT, 2001 and this study)

Province	Field	Discovery year	Well number in oilfield	Producing formation	Average depth (m)	Oil production percentage in southeast Anatolian basin (%)	Average iodine (mg/L)	Max. iodine (mg/L)	Min. iodine (mg/L)	Water sampling method
Batman	Batı Raman	1961	327	Garzan	1300	22.30	**1.62**	**6.45**	0.08	wellhead
	Raman	1945	221	Garzan + Mardin	1360	19.44	**1.51**	**2.81**	0.2	wellhead
	Garzan	1951	42	Garzan	1435 - 1450	2.05	**0.92**	**1.36**	0.23	wellhead
	Silivanka	1962	21	Garzan + Beloka	2250 - 2500	2.29	**0.65**	**1.18**	0.12	wellhead
Sırnak	Güney Dinçer	1981	24	Beloka	1626	0.29	**0.4**	**0.97**	0.1	seperator
	Batı Kozluca	1984	29	Sinan	1515	1.43	**0.61**	**0.81**	0.44	seperator
Mardin	Çamurlu	1976	40	Sinan	1450	1.37	**0.45**	**0.71**	0.03	seperator
	İkiztepe	1976	15	Sinan	1490	0.23	**0.58**	**0.85**	0.39	seperator
	Doğu Sınırtepe		5			0.40	**0.5**	**0.91**	0.29	seperator
Diyarbakır	Beykan	1964	42	Mardin Group	1889	6.10	**0.85**	**1.81**	0.36	wellhead
	Güney Sarıcak	1973	21	Derdere	1600	1.30	**0.62**	**0.86**	0.03	wellhead
	Yeniköy	1973	20	Derdere + Sabunsuyu	1940 - 2100	1.21	**0.41**	**0.79**	0.12	wellhead
	Barbes	1972	14	Mardin Group	2272	1.83	**0.19**	**0.42**	0.03	wellhead
	Malatepe	1970	9	Mardin Group	1685	1.36	**0.055**	**0.11**	0.01	wellhead
	Güney Şahaban	1978	6	Derdere	1660	0.14	**0.3**	**0.41**	0.22	wellhead
	Kurkan	1963	37	Mardin Group	1621	3.27	**0.29**	**0.52**	0.12	wellhead
	Karacan		7			1.00	**0.1**	**0.12**	0.08	wellhead
	Güney Kırtepe		14			0.67	**0.43**	**0.6**	0.14	wellhead
	Mehmetdere	1982	5	Derdere	2000	0.14	**0.14**	**0.14**	0.14	wellhead
	Katin	1971	5	Mardin Group	2611	0.13	**0.09**	**0.12**	0.06	wellhead
	Doğu Yatır	1974	6	Mardin Group	1563	0.68	**0.075**	**0.09**	0.06	wellhead
	Güney Kayaköy	1976	6	Derdere	2620	0.43	**0.125**	**0.13**	0.12	wellhead

* Total oil production in the Southeastern Anatolia basin: 34917 bbl/day (September 2017 production data)

Results of Iodine Analysis of Oilfield Waters in Adıyaman Region (Data: DPT, 2001 and this study)

Province	Field	Discovery year	Well number in oilfield	Producing formation	Average depth (m)	Oil production percentage in southeast Anatolian basin (%)	Average iodine (mg/L)	Max. iodine (mg/L)	Min. iodine (mg/L)	Water sampling method
	Karakuş									
Adıyaman	Karakus Beşikli	1988	27	Karabogaz + Karababa + Derdere + S.suyu	2700	4.66	1.51	6.58	0.13	wellhead
	Besikli	1990	28	Karabogaz + Karababa	1900	3.06	1.93	3.65	0.11	wellhead
	Cendere	1989	18	Karabogaz + Karababa + Derdere	2700	2.05	2.27	7.94	0.10	wellhead
	Elbeyli		13			2.00	14.97	29.8	0.13	wellhead
	Kuzey Karakuş	1990	18	Karababa + Derdere	2590	2.00	0.65	1.74	0.10	wellhead
	Güney Karakuş	1989	21	Karababa + Derdere	2370	1.40	2.10	4.05	0.60	wellhead
	Adıyaman	1971	23	Karababa	1750	1.20	0.49	2.22	0.12	wellhead
	Ikizce	1991	14	Karabogaz + Karababa	2285	1.00	3.39	5.64	0.78	wellhead
	Bozhüyük		5			0.89	1.89	1.89	1.89	Other
	Çemberlitaş	1983	11	Karababa + Derdere	3200	0.70	1.04	4.07	0.13	wellhead
	Tokaris	1991	10	Karabogaz + Karababa + Derdere	2410	0.69	4.58	8.48	0.67	wellhead
	Doğu Karakuş		6			0.42	3.19	3.65	2.72	wellhead
	Batı Gökçe		13			0.49	3.19	7.73	0.29	wellhead
	Batı Fırat	1985		Karababa + Derdere	2570	0.06	2.33	4.06	0.60	wellhead
	Yalankoz		1			0.19	0.72	0.72	0.72	wellhead
	Akgün	1998	4	Karababa	2130	0.32	1.73	3.36	0.10	wellhead
	Ozan Sungurlu	1991	2	Sayindere + Karabogaz + Karababa + Derdere	2800	0.07	1.84	2.08	1.60	wellhead
	B.Altıntop		1			0.15	0.17	0.17	0.17	wellhead
	Çaylarbaşı		8			0.31	0.99	1.64	0.34	wellhead
	Şambayat		12			0.77	0.19	0.37	0.11	wellhead
	Doğu Şambayat		2			0.27	0.14	0.16	0.12	wellhead
Şanlıurfa	Piyanko		1			0.43	9.10	9.10	9.10	wellhead
	Doğu Beşikli	1991	6	Karababa + Derdere	1860	0.82	0.96	1.30	0.34	wellhead
	Bozova		6			0.46	0.125	0.13	0.12	wellhead

* Total oil production in Southeastern Anatolia basin: 34917 bbl/day (September 2017 production data)

Results of Iodine Analysis of Oilfield Waters in Batman City

No.	Well	Iodine (mg/L)	No.	Well	Iodine (mg/L)
1	Batı Raman-71	0.84	22	Raman-268	0.75
2	Batı Raman-183	0.77	23	Raman-169	1
3	Batı Raman-210	0.2	24	Raman-188	1.12
4	Batı Raman-286	2.65	25	Raman-230	0.45
5	Batı Raman-336	1.9	26	Raman-289	1.2
6	Batı Raman-364	2.81	27	Garzan-8	0.23
7	Batı Raman-403	2.78	28	Garzan-9	1.4
8	Batı Raman-470	1.01	29	Garzan-20	1.14
9	Raman-22	6.45	30	Garzan-36	2.21
10	Raman-211	2.72	31	Garzan-58	1.05
11	Raman-232	4.33	32	Garzan-63	0.35
12	Raman-284	3.94	33	Garzan-69	1.21
13	Raman-88	0.22	34	Garzan-76	1.36
14	Raman-105	0.29	35	Garzan-79	1.09
15	Raman-144	0.23	36	Silivanka-32	0.46
16	Raman-174	0.8	37	Silivanka-33	1.18
17	Raman-180	0.08	38	Silivanka-34	1.11
18	Raman-187	0.32	39	Silivanka-41	0.54
19	Raman-235	0.33	40	Silivanka-19	0.12
20	Raman-245	0.94	41	Silivanka-25	0.41
21	Raman-264	0.57	42	Silivanka-28	0.74

Results of Iodine Analysis of Oilfield Waters in Adiyaman City

No.	Well	Iodine (mg/L)	No.	Well	Iodine (mg/L)
1	Adıyaman-4	2.22	38	Çemberlitaş-52	4.07
2	Adıyaman-7	0.79	39	Çemberlitaş-53	1.43
3	Adıyaman-8	0.14	40	Doğu Karakuş-2	3.65
4	Adıyaman-14	0.22	41	Doğu Karakuş-9	2.72
5	Adıyaman -24	0.12	42	Doğu Sambayat-1	0.12
6	Adıyaman-39	0.85	43	Doğu Sambayat-6	0.16
7	Adıyaman-44	0.12	44	Elbeyi-7	29.8
8	Adıyaman-48	0.13	45	Elbeyi-14	0.13
9	Adıyaman-56	0.15	46	Güney Karakuş-8	0.6
10	Akgün-2	0.1	47	Güney Karakuş-10	1.15
11	Akgün-3	3.36	48	Güney Karakuş-11	3.2
12	Batı Altıntop-1	0.17	49	Güney Karakuş-22	4.05
13	Batı Fırat-2	4.06	50	Güney Karakuş-29	1.5
14	Batı Fırat-13	0.6	51	İkizce-5	5.64
15	Batı Gökçe-1	7.73	52	İkizce-7	3.75
16	Batı Gökçe-4	1.55	53	İkizce-C1	0.78
17	Batı Gökçe-9	0.29	54	Karakuş-3	0.13
18	Beşikli-2	1.85	55	Karakuş-7	0.15
19	Beşikli-10	0.11	56	Karakuş-11	0.15
20	Beşikli-14	2.29	57	Karakuş-13	0.14
21	Beşikli-31	2.35	58	Karakuş-24	3.30
22	Beşikli-26	1.31	59	Karakuş-29	0.15
23	Beşikli-34	3.65	60	Karakuş-38	6.58
24	Bozhöyük (Avg.)	1.89	61	Kuzey Karakuş-5	0.11
25	Cendere-1	7.94	62	Kuzey Karakuş-21	0.1
26	Cendere-3	0.37	63	Kuzey Karakuş-24	1.74
27	Cendere-7	0.11	64	Ozan Sungurlu-1	2.08
28	Cendere-9	0.10	65	Ozan Sungurlu-4	1.6
29	Cendere-10	6.83	66	Paşaoğlu-2	0.58
30	Cendere-13	0.42	67	Sambayat-1	0.14
31	Cendere-23	0.14	68	Sambayat-7	0.37
32	Çaybaşı-1	1.64	69	Sambayat-17	0.11
33	Çaybaşı-5	0.34	70	Sambayat-20	0.13
34	Doğu Çemberlitaş-3	0.13	71	Tokaris-3	0.67
35	Çemberlitaş-5	0.24	72	Tokaris-12	8.48
36	Çemberlitaş-27	0.17	73	Tokaris-14	0.57
37	Çemberlitaş-44	0.20	74	Yalankoz-2	0.72

Results of Iodine Analysis of Oilfield Waters in Diyarbakir City

No.	Well	Iodine (mg/L)	No.	Well	Iodine (mg/L)
1	Barbes-5	0.11	38	Güney Sarıcak-25	0.60
2	Barbes-6	0.14	39	Güney Sarıcak-30	0.72
3	Barbes-12	0.12	40	Güney Sahaban-2	0.22
4	Barbes-13	0.08	41	Güney Sahaban-7	0.24
5	Barbes-14	0.14	42	Güney Sahaban-10	0.32
6	Barbes-16	0.23	43	Güney Sahaban-15	0.41
7	Barbes-19	0.25	44	Karacan-3	0.12
8	Barbes-20	0.08	45	Karacan-5	0.10
9	Barbes-23	0.42	46	Karacan-7	0.08
10	Beykan-1	1.12	47	Katin-2	0.12
11	Beykan-9	0.97	48	Katin-7	0.06
12	Beykan-14	1.18	49	Kurkan-5	0.18
13	Beykan-17	0.83	50	Kurkan-11	0.29
14	Beykan-22	0.58	51	Kurkan-12	0.12
15	Beykan-23	1.81	52	Kurkan-15	0.25
16	Beykan-27	0.65	53	Kurkan-23	0.30
17	Beykan-30	0.60	54	Kurkan-30	0.42
18	Beykan-33	0.46	55	Kurkan-39	0.52
19	Beykan-36	0.59	56	Kurkan-44	0.13
20	Beykan-37	1.23	57	Kurkan-52	0.37
21	Beykan-38	0.36	58	Malatepe-2	0.06
22	Beykan-58	0.61	59	Malatepe-6	0.01
23	Doğu Yatır-3	0.06	60	Malatepe-8	0.01
24	Doğu Yatır-4	0.09	61	Malatepe-13	0.05
25	Güney Kayaköy-7	0.12	62	Malatepe-30	0.11
26	Güney Kayaköy-8	0.13	63	Malatepe-32	0.09
27	Güney Kırtepe-2	0.60	64	Mehmetdere-9	0.14
28	Güney Kırtepe-3	0.14	65	Yenikoy-14	0.79
29	Güney Kırtepe-7	0.51	66	Yenikoy-18	0.41
30	Güney Kırtepe-11	0.47	67	Yenikoy-20	0.22
31	Güney Sarıcak-2	0.57	68	Yenikoy-26	0.51
32	Güney Sarıcak-5	0.35	69	Yenikoy-30	0.61
33	Güney Sarıcak-6	0.03	70	Yenikoy-33	0.27
34	Güney Sarıcak-7	0.72	71	Yenikoy-35	0.46
35	Güney Sarıcak-15	0.71	72	Yenikoy-36	0.56
36	Güney Sarıcak-18	0.86	73	Yenikoy-39	0.15
37	Güney Sarıcak-19	0.44	74	Yenikoy-40	0.12

Results of Iodine Analysis of Oilfield Waters in Mardin City

No.	Well	Iodine (mg/L)
1	Çamurlu-2	0.51
2	Çamurlu-10	0.59
3	Çamurlu-26	0.03
4	Çamurlu-28	0.03
5	Çamurlu-30	0.41
6	Çamurlu-31	0.62
7	Çamurlu-35	0.71
8	Çamurlu-39	0.53
9	Çamurlu-51	0.29
10	Doğu Sınırtepe-1	0.91
11	Doğu Sınırtepe-2	0.29
12	Doğu Sınırtepe-5	0.43
13	Doğu Sınırtepe-7	0.38
14	İkiztepe-1	0.39
15	İkiztepe-6	0.85
16	İkiztepe-CP2	0.44
17	İkiztepe-CP4	0.64

Results of Iodine Analysis of Oilfield Waters in Sirnak City

No.	Well	Iodine (mg/L)
1	Batı Kozluca-1	0.54
2	Batı Kozluca-5	0.49
3	Batı Kozluca-6	0.72
4	Batı Kozluca-9	0.68
5	Batı Kozluca-19	0.74
6	Batı Kozluca-22	0.6
7	Batı Kozluca-28	0.44
8	Batı Kozluca-29	0.51
9	Batı Kozluca-30	0.49
10	Batı Kozluca-31	0.81
11	Batı Kozluca-34	0.64
12	Güney Dinçer B1	0.21
13	Güney Dinçer 1	0.41
14	Güney Dinçer 6	0.46
15	Güney Dinçer 8	0.56
16	Güney Dinçer 13	0.37
17	Güney Dinçer 14	0.22
18	Güney Dinçer 15	0.32
19	Güney Dinçer 16	0.39
20	Güney Dinçer 23	0.97
21	Güney Dinçer 29	0.10

Results of Iodine Analysis of Oilfield Waters in Sanliurfa City Basin

No.	Well	Iodine (mg/L)
1	Doğu Beşikli-5	1.30
2	Doğu Beşikli -7	0.34
3	Doğu Beşikli -11	1.24
4	Bozova-1	0.13
5	Bozova-8	0.11
6	Piyanko-3	9.10

Results of Iodine Analysis of Oilfield Waters in Thrace

No.	Well	Iodine (mg/L)
1	Vakıflar-1	0.26
2	Vakıflar-4	0.21
3	Vakıflar-5	0.29
4	Vakıflar-7	0.80
5	Vakıflar-14	1.24
6	Kuzey Osmancık-2	0.08
7	Kuzey Osmancık-8	0.66
8	Deveçatağı-2	0.74
9	Deveçatağı-9	0.56

Bulletin of the Mineral Research and Exploration

http://bulletin.mta.gov.tr

Multivariate analysis of log-ratio transformed data and its priority in mining science: Porphyry and polymetallic vein deposits case studies

Farshad DARABİ-GOLESTAN[a*] and Ardeshir HEZARKHANI[b]

[a] *Department of Mining and Metallurgical Engineering, Amirkabir University of Technology, 424 Hafez Ave, Tehran, Iran. Orcid.org 0000-0002-4648-152X*

[b] *Department of Mining and Metallurgical Engineering, Amirkabir University of Technology, 424 Hafez Ave, Tehran, Iran orcid.org/0000-0002-1149-3440*

Research Article

Keywords:
Isometric log-ratio transformation, Subcompositional coherence, Correspondence analysis, Principal component analysis, Geochemical compositional data, Polymetallic and porphyry deposits.

ABSTRACT

Each mineralization style is characterized by typical signature associations between elements due to elemental interactions, therefore the coherence and closure effects problem must be overcome in geochemical processing. The coherence indicates the ratios between two components (rows or columns) remains the same whether they are considered in a subcomposition or in the full composition. The log-ratio transformation (LRT) has recognized as a standard procedure to support subcompositional coherence. The log-transformed data is applicable for geochemical data to unveil such associations, prior to applying the multivariate analysis like correspondence analysis (CA) and principal component analysis (PCA). At the present study, subcompositional coherence is overcome by inverse iso-metric log-ratio transformation for geochemical compositional data at two polymetallic and porphyry deposits. Based on Ilr-transformed data, Ag, Au, As, Pb, Te, Mo and rather S, W, Cu are enriched as polymetallic elements at Glojeh, while Au-Cu-(Mo) compositions indicate a porphyry deposit occurred in Dalli deposit. The ability to handle zero values in the data matrix and determining an elemental eccentricity from the center of each axis based on Euclidean distances are the advantages of CA method, with compression to LRT. Whereas, loading factors which spread in every direction and providing subcompositional coherence are the competitive advantages of PCA based on LRT, for both case studies. Results with these techniques show significant ability to draw an inference in such geochemical data, and in improving the performance of multivariate techniques using LRT.

Received Date: 20.11.2017
Accepted Date: 01.07.2018

1. Introduction

Applied geochemical data such as most mining data are often defined as compositional (Reimann et al., 2011). The compositional data are indicated as parts per million (ppm), percentages, proportions, and other quantities which is concerned with relative and sums up to a constant value like 100 percent or 1 (Aitchison and Greenacre, 2002). Hence, the individual or compositional variables are not independent and variables can not be freed to vary from the others. Accordingly, the problem of data closure effects needs to be considered in geochemical data evaluation (Reimann et al., 2012; Reimann et al., 2011; Zuo et al., 2013). Aitchison (1982, 1983, 1986) proposed that the log-ratio transformation (LRT) is an appropriate method to evaluate the total variability of the compositional data. The subcompositional coherence means that the correlation coefficient or the distance between two components in a subcomposition (subset) is the same as that for the same two components in the full composition (Greenacre, 2011). Using LRT

Citation Info: Darabi-Golestan, F., Hezarkhani, A. 2019. Multivariate analysis of log-ratio transformed data and its priority in mining science, porphyry and polymetallic vein deposits case studies. Bulletin of Mineral Research and Exploration, 159, 185-200. *http://dx.doi.org/10.19111/bulletinofmre.456958*

* *Corresponding author: F. DARABİ GOLESTAN, pooyan@aut.ac.ir*

this problem is posed and consistent results were obtained because the values of a selected element represent its proportions in the complete sample, whether one works with the subcomposition or in the full composition (Filzmoser et al., 2009*c*; Pawlowsky-Glahn and Egozcue, 2006). The closure effect problem of elements and samples is commonly apparent in the simply log-transformed scores of a geochemical compositional data. In order to overcome this problem, this data can be transformed by using the LRT, e.g. centered log-ratio (clr), the iso-metric log-ratio (ilr), and the additive log-ratio (alr), prior to using any of the multivariate methods (Carranza, 2011; Filzmoser and Hron, 2008; Filzmoser et al., 2009*a*; Silverman et al., 2016; Templ et al., 2008).

Correspondence analysis (CA) is a comprehensive and exploratory method which can widely be applied to recognize various genetic associations and elemental distribution in geochemical exploration. This technique is conducted according to the two main R-mode (factor scores related to elements) and Q-mode (factor scores related to samples) methods (David et al., 1974; Março and Scarminio, 2007). These methods are used to reduce high-dimensional data into low-dimensional subspaces that explain the main variances and qualitative and/or quantitative variation among the whole data (Akbarpour et al., 2013; Carranza, 2009). Principal component analysis (PCA) is another method that is mainly used to compress large data matrices and extract the common factors (De Winter and Dodou, 2016; Pommer et al., 2004). PCA method is a data-driven multivariate technique that can reveal similarities based on the correlation or covariance matrix (Croux and Haesbroeck, 2000; Olofsson et al., 2009). In addition, the PCA based upon LRT of the geochemical compositional data is applied to reveal underlying patterns in the data, in a more vivid manner. In the geochemical exploration and to have full rank with spreading in a full circle distribution, Ilr transformation is better than Clr transformed data (Carranza, 2011; Filzmoser et al., 2009*a,* 2010). It was indicated using inverse Ilr transformed data that each variable of the biplot is related to one of the components. Greenacre (2010) pointed out that in compositional data using that PCA of Clr-transformed data (or totally LRT) and CA through the Box–Cox power transformation the same results were obtained. He indicates as long as the weighted form of LRT is used, so in this respect the sub-compositionally coherent is much better. Totally, LRT is considered as a limited case of CA (Greenacre, 2010). The obvious benefit of CA is the ability to deal with zero values in the data which can be analyzed for nonzero power parameter of the Box-Cox transformation while it is a problem in LRT (Greenacre, 2010; Martín-Fernández et al., 2003).

The objective of this paper is to apply various CA and PCA opened by log-transformed and LRT data for two different types of Au mineralization, the Glojeh polymetallic and Dalli porphyry deposit. Our case studies demonstrate that the closure effect is an inherent problem for geochemical and environmental compositional data which cannot be overcome by simply log-transformation. The present study aims to investigate: (1) A better insight to sense and explore the essential information on mineralization, and relationship between elements and samples; (2) a comparison between the log-transformed and Ilr-transformed data form two genetic types of polymetallic vein and porphyry Au deposits; and (3) a comparison between CA and PCA of compositional geochemical data.

2. Material and Method

2.1. Case studies

Two different types of polymetallic vein and porphyry mineralization were investigated to evaluate the relationship, interaction, and closure effect between elements. These specifications could ease the interpretation of geochemical dispersion pattern of elements. The first case study is the Glojeh polymetallic vein deposit. It is located in NW Iran, central part of the Tarom- Hashtjin Metallogenic Province (THMP). It is recognized as the main metallogenic province in the western Alborz magmatic arc (Darabi-Golestan and Hezarkhani, 2016; figure 1). There are two main polymetallic Au-Ag-Cu-Pb-Zn veins and several veinlets that were displaced by east-west striking in Glojeh. The offset veins (and parallel in some places) have a length of about 1,5 km and a width range from 0,1 to 4 m (averages 2,5 m). The veins were intersected by BH2N1 (borehole) at 26,2-33,9 m and 79,68-81,51 m, respectively. Different exploration works have been carried out in the area (eleven boreholes and twelve trenches), but just 153 samples (consist of duplicate and replicate samples) of BH2N1 have been analyzed by inductively coupled plasma mass spectrometry (ICP-MS) for 44 elements at Earth Sciences Development Company Lab of Iran (Darabi-Golestan and Hezarkhani, 2016). The second

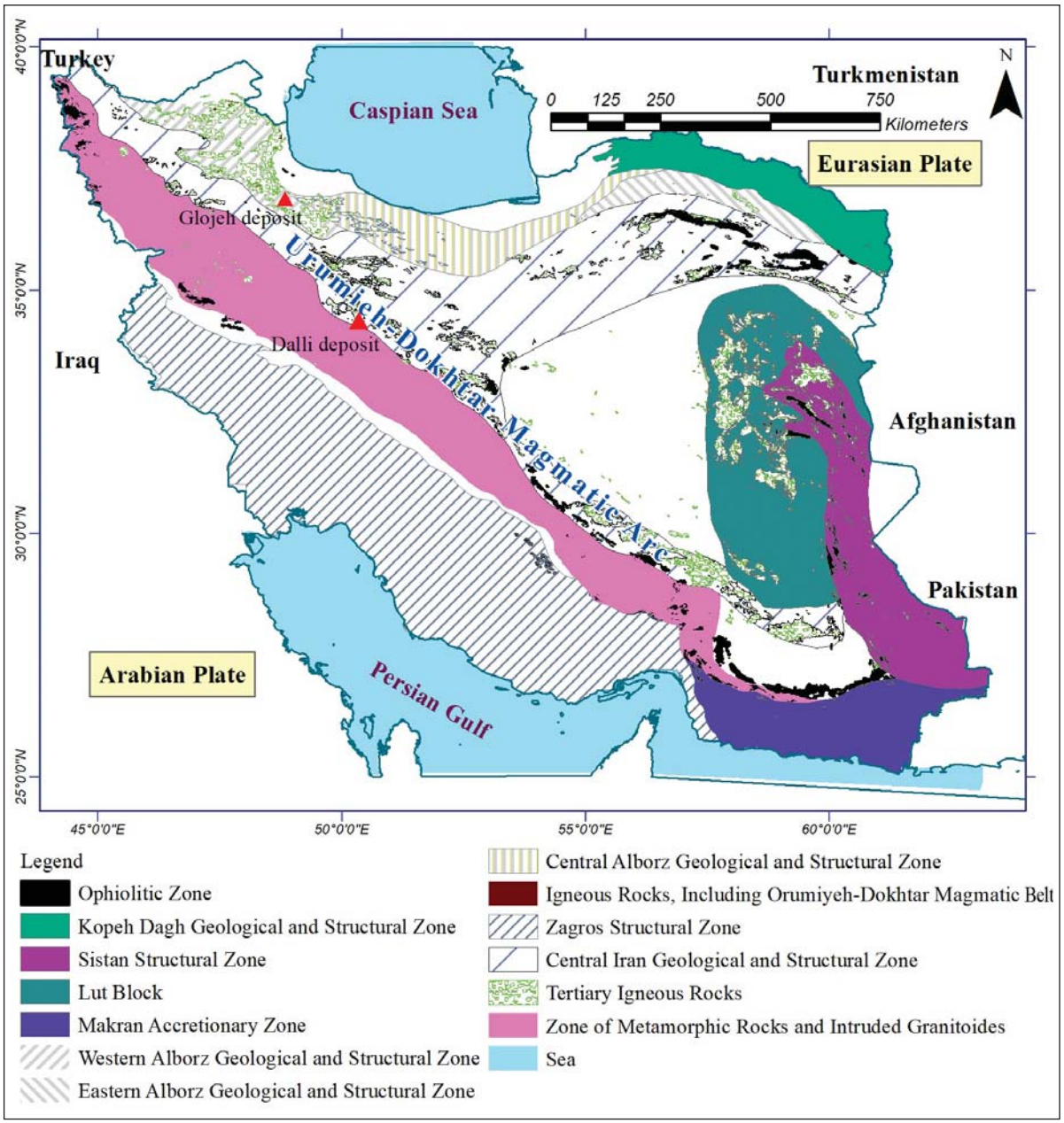

Figure 1- The location map of the deposits, major Iran's structural zones and geological units, including western Alborz zone that consist of Glojeh deposit and Urumieh-Dokhtar Magmatic Arc including Dalli deposit. The western, central, and eastern Alborz, and Sanandaj-Sirjan zone of metamorphic rocks and intruded granitoids parallel to Urumieh-Dokhtar Magmatic Arc ranges are highlighted.

case study is Northern Dalli porphyry deposit which located in the central province of Iran, 70 Km away from Arak (Darabi-Golestan et al., 2013*a*; figure 1). In total, 149 (plus 16 replicate sample) soil samples were taken from the area, with a grid net of 50 m×50 m. They were analyzed for 45 elements by using ICP-MS method in the ANDL Lab Australia (Darabi-Golestan et al., 2013*b*). Both these data sets have compositional specification.

2.2. Quality Control

The total number of 20 duplicate and 20 replicate samples were collected from original samples of Glojeh deposit. They were prepared and analyzed by ICP-MS for 44 elements, individually. The quality of analytical data were evaluated using the Thompson-Howarth graphical method (Stanley, 2006; Thompson and Howarth, 1976). The duplicate (or/and replicate)

samples were applied to assessment of precision or accuracy (geochemical QA/QC) in analysis (Darabi-Golestan and Hezarkhani, 2018). The mean of the main-duplicate (or replicate) pairs are plotted along the X-axis, while the absolute difference of values is shown along the Y-axis for Au analysis at Glojeh. The two default lines corresponding to the $d_{99\%}$ and $d_{50\%}$ (or 1% and 50% error, relative standard deviation) were used onto the Thompson and Howarth (1976) scatterplot (Stanley, 2006). The lines $d_{99\%}$ and $d_{50\%}$ the 99th and 50th percentiles of the absolute difference between duplicate and replicate samples, which is represented as a function of concentration are respectively. Also, if all the samples are located under the $d_{99\%}$, it will be assumed that there is a normal distribution of error. Repeatability of measurements in the Glojeh deposit was assessed by the Thompson-Howarth error model. It indicates that the repeatability precision is under the control line of 1:1 (or y=x) for duplicate and replicate samples. The highest accuracy and lowest precision are related to the D10 and R10 samples which is located near the control line 99% for Au analyses, compared to the main sample (Figure 2).

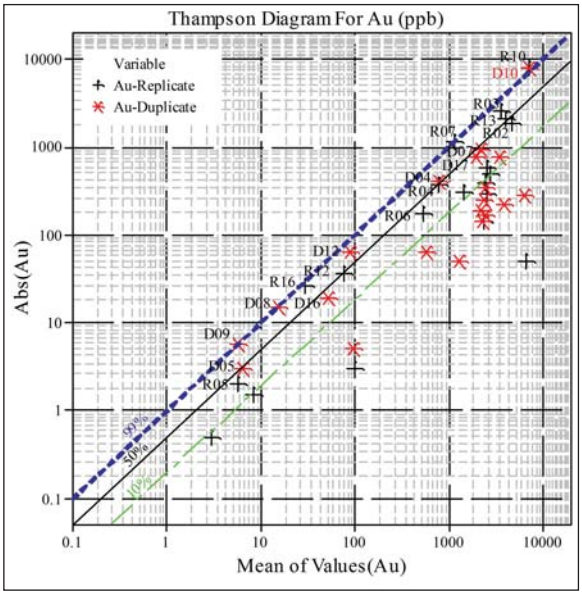

Figure 2- Estimation of precision of the Au analyses using diagram of Thompson and Howarth (1978). The mean of the replicate pairs is plotted along the X-axis, the absolute difference of the two results along the Y-axis.

In addition, just three replicate samples were taken for the porphyry deposit case study. These samples were analyzed for 44 elements that was determined by ICP-MS. Due to the small number of duplicate measurements, the accuracy of these samples were evaluated for all the elements. Quality control of main vs. replicate pair samples at Dalli deposit were given at figure 3, where all the main vs. replicate samples overlay on y=x line.

2.3. Log-ratio Transformation

The LRT has become a frequently used standard procedure to support subcompositional coherence within data (Aitchison, 1990; Greenacre, 2011). The ratios between the two components remain same, whether they are considered in a subcomposition or in the full composition (Greenacre, 2007). A family of log-ratio transformation consist of the clr, ilr, and alr space (Aitchison, 1986; Carranza, 2017; Egozcue et al., 2003; Thió-Henestrosa and Martín-Fernández, 2005). LRT may be done weighted (not for samples, but compositional elements can be weighted by the average level of each component) or unweighted (Greenacre, 2011). The frequently used unweighted version is applied for this paper based on the method that show sincoherence in the present data set using the Euclidean distance. The unweighted LRT has been proposed in detail by Kazmierczak (1985), afterward Aitchison and Greenacre (2002) suggests a biplot to a better representation of results.

In this study, the Ilr-transformed values were used for PCA analysis, while they were obtained by the CoDaPack software v 2.01 (available at http://www.compositionaldata.com/). The clr transformation (Aitchison, 1986) could be applied on composition of the data set (X), so can be written as:

$$\mathbf{Y} = clr(\mathbf{X}) = \left\{y_i\right\}_{i=1,\ldots,n} = \left\{\log \frac{x_i}{g(x)}\right\}_{i=1,\ldots,n} \qquad \text{Eqs. (1)}$$

where all components have been divided by the $g(X)$. The $g(X)$ is the geometric mean of X_i components from the X symmetrically (Egozcue et al., 2003; Filzmoser et al., 2009*a*). It is calculated as follows:

$$g(\mathbf{X}) = \sqrt[n]{x_1.x_2\ldots x_n} = \left(\prod_{i=1}^{n} x_i\right)^{\frac{1}{n}} \qquad \text{Eqs. (2)}$$

The resulted data (Y) based on this transformation show collinear relationship as $\sum_{i=1}^{n} y_i = 0$, i.e. the sum of each clr transformed data for a variable is zero (Aitchison, 1986), which rely on full rank data matrices, like standard robust covariance estimators

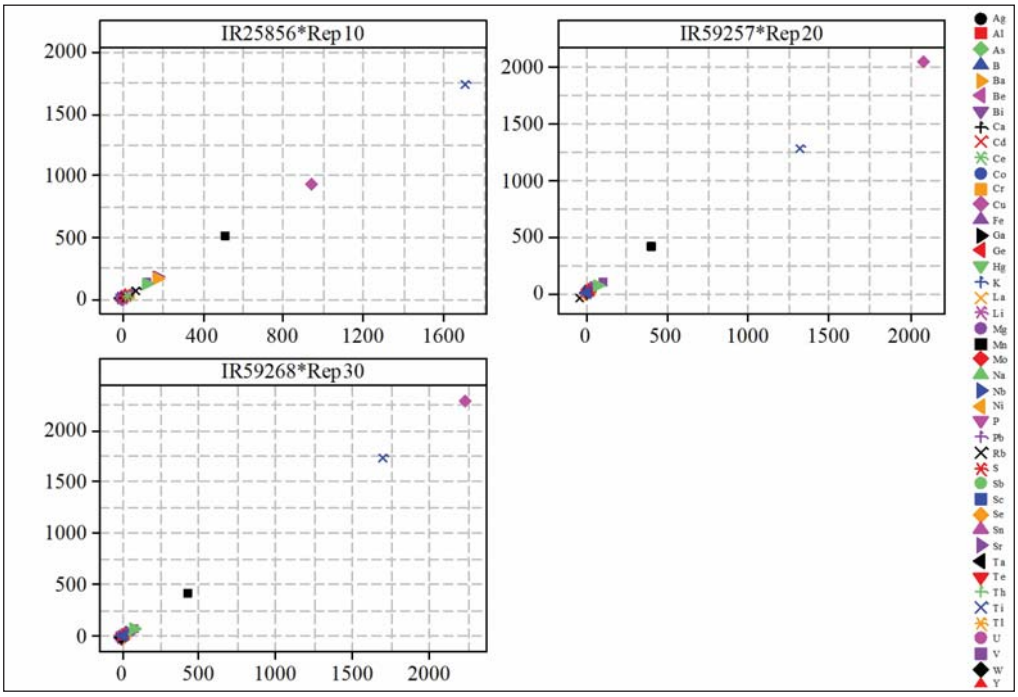

Figure 3- Quality control of main vs. replicated samples for ICP-MS analyzed data at Dalli deposit. All the main vs. replicated samples overlay on y=x line.

(Maronna et al., 2006). The ilr transformation could preserve all the advantages of clr transformation. In addition it can overcome on the disadvantageous treatment of data colinearity or the singularity of clr in Euclidean space (Egozcue et al., 2003; Pawlowsky-Glahn and Buccianti, 2011). For a composition X, the ilr transformation can be expressed as follows:

$$\mathbf{Y} = ilr(\mathbf{X}) = \{y_i\}_{i=1,\ldots,n-1} = (y_1, y_2, \ldots, y_{n-1}) \quad \text{Eqs. (3)}$$

$$y_i = \frac{1}{\sqrt{i(i+1)}} \ln\left(\frac{\prod_{j=1}^{i} x_j}{(x_{i+1})^i}\right) \quad i = 1,\ldots,n-1 \quad \text{Eqs. (4)}$$

It is clear based on the fundamental of Ilr transformation, only n-1 variables can be obtained for n components data (Thió-Henestrosa and Martín-Fernández, 2005). Therefore, the interpretation of new ilr transformed variables is not straightforward and there is no direct connection to the original variables (Filzmoser et al., 2009*b*). Whatever, the Ilr transformation does not show any clear simplest or canonical basis, but it has significant conceptual advantages (Pawlowsky-Glahn and Buccianti, 2011). The results obtained from ilr variables can be back-transformed to clr coefficients aided by an orthonormal basis (Egozcue et al., 2003; Liu et al., 2016). By using LRT, the subcompositional coherence is aided since the ratio between two data values (elements or samples) remains the same whether or not rows or columns are excluded from the table (Greenacre, 2007).

2.4. Correspondence Analysis (CA)

With application CA on the indicator matrix will provide two sets of factor scores for the rows (samples) and columns (elements). These factor scores are scaled such that their variance is equal to their corresponding eigenvalues (Abdi and Valentin, 2007; Greenacre and Blasius, 2006). At the CA method, it is possible to calculate the squared (χ^2) distance (Euclidean distances) between the observations or variables to look for the quantitative or qualitative objects of a given point or a set of points (Tekaia, 2016). It is supposed thatthe data matrix is X, and it has I ×J table of compositional data array. Each of these vectors was calculated from the following equations:

$$r_i = x_{i1} + x_{i2} + \ldots + x_{im} \quad \text{Eqs. (5)}$$

$$c_j = x_{j1} + x_{j2} + \ldots + x_{jn} \quad \text{Eqs. (6)}$$

Two diagonal matrices of $R_{n\times n}$ and $C_{m\times m}$ are defined as (Diday and Noirhomme-Fraiture, 2008; Greenacre, 1984; Ji et al., 2007; Ji et al., 1995):

$$R = \mathrm{diag}(r_1, r_2, \ldots, r_n) \quad \text{Eqs. (7)}$$

$$C = \mathrm{diag}(c_1, c_2, \ldots, c_m) \quad \text{Eqs. (8)}$$

The W and H matrices are defined as [(Eqs. (9) and (10)]:

$$W = R^{-1/2} X C^{-1/2} \quad \text{Eqs. (9)}$$

$$H = W^{T} W \quad \text{Eqs. (10)}$$

The H matrix eigenvalues and eigenvectors will be calculated. The information resulted in p (where $p \leq m-1$) dimension. Thus, the number of P eigenvalues were obtained as $0<\lambda p \leq ... \leq \lambda_2 \leq \lambda_1 < 1$ (Diday and Noirhomme-Fraiture, 2008; Gu et al., 2015). Afterward, eigenvectors [a_p] corresponding to each eigenvalue (λ_p) were calculated. Then the two matrices of Λ and A were generated based on eigenvalues and eigenvectors:

$$\Lambda_{(p\times p)} = \mathrm{diag}(\lambda_1, \lambda_2, ..., \lambda_p) \quad \text{Eqs. (11)}$$

$$A_{(m\times p)} = (a_1, a_2, ..., a_p) \quad \text{Eqs. (12)}$$

$U_{m\times p}$ and $V_{n\times p}$ matrices could introduce the relationship between variables and samples, respectively (Golestan et al., 2013; Ji et al., 2007). They were calculated as follows:

$$U = C^{-1/2} A \Lambda^{1/2} \quad \text{Eqs. (13)}$$

$$V = R^{-1/2} W A \quad \text{Eqs. (14)}$$

$$F = \begin{bmatrix} \mathbf{V} \\ \mathbf{U} \end{bmatrix} \quad \text{Eqs. (15)}$$

The $F_{(m+n)\times p}$ matrix (Eqs. 15) is a combination of the two important results of the CA, namely the U-matrix (R-mode; represented as a column-to-column or element-to-element criterion) and the V-matrix (Q-mode; represented as a row-to-row or sample-to-sample criterion) as a two important results of the CA (Darabi-Golestan and Hezarkhani, 2018; Ji et al., 2007). Therefore, the CA calculates the association or similarity between each variable (R-mode) and samples (Q-mode) within factor scores.

In another definition of CA, X is divided by its grand total x_{++} to obtain the so-called correspondence matrix $P=(1/x_{++})X$ (Greenacre, 2010). Let r and c vectors be the row and column of P, respectively. Therefore, the Eqs. (9) can be rewritten as Eqs. (16):

$$W = R^{-1/2} (P - rc^{T}) C^{-1/2} \quad \text{Eqs. (16)}$$

By performing a power (Box–Cox) transformation of the X matrix as $x_{ij}(\alpha) = x_{ij}^{\alpha}$, the CA is performed on the new correspondence matrix as X(α). The convergence and similar results of CA with LRT is a direct result of the Box-Cox transformation represented as $f(x) = (1/a)(X^{\alpha} - 1)$, $\alpha>0$ or $f(x) = g(x)$ when $\alpha=0$ which f(x) tends to log(x) as tends to 0 (Greenacre, 2010, 2011).

2.5. Principal Component Analysis (PCA)

The PCA is a multivariate technique that applies frequently to illustrate the multidimensional data into lower dimensional factors without losing important information in the data (Collins and Ovalles, 1988; Fávaro et al., 2007). It could be done with both normalized and non-normalized data (Pawlowsky-Glahn et al., 2007). In this method, original data are transformed into a new set of data which led to a better results to explore the essential information (García-Izquierdo and Ríos-Rísquez, 2012; Ramasamy et al., 2013). The data matrix **X** consists of n samples (objects) which is analyzed for p elements (variables), in environmental, mining and geosciences studies. PCA decomposes the initial matrix **X** into two main produced matrices, introduced as a score matrix (**T**) and loading matrix (**P**). It can be expressed as following equation:

$$\mathbf{X} = \mathbf{T}_{n\times q} \mathbf{P}^{T}_{q\times p} + \mathbf{E}_{n\times p} \quad \text{Eqs. (17)}$$

where E is a matrix of residuals and $\mathbf{P}^{T}$ is the transpose of **P** (Março and Scarminio, 2007). Therefore, the major patterns of the data variance and correlations among measurements (according to their similarities) were showed in q vectors that were known as the principal components (PC; Bitner-Mathé and Klaczko, 1999; Darabi-Golestan et al., 2017; Karamanis et al., 2009; Março and Scarminio, 2007). These reduced factors indicate the largest amount of variability and associations between variables (Abdi et al., 2013; Golestan et al., 2013; Tokatli et al., 2014). Applying the visualization technique to show the factor scores and loading factors make this method comprehensible and could improve the prediction performance by visualizing large amounts of data (Hayton et al., 2004; Jeong et al., 2009). Reducing dimensionality of data at the PCA has a similar process to that of CA (Greenacre, 2007).

3. Results

3.1. Correspondence Analysis (CA)

The R-mode and Q-mode on the first and second dimension of U and V-matrices are represented in the biplot for the Glojeh (Figure 4) and Dalli (Figure 5)

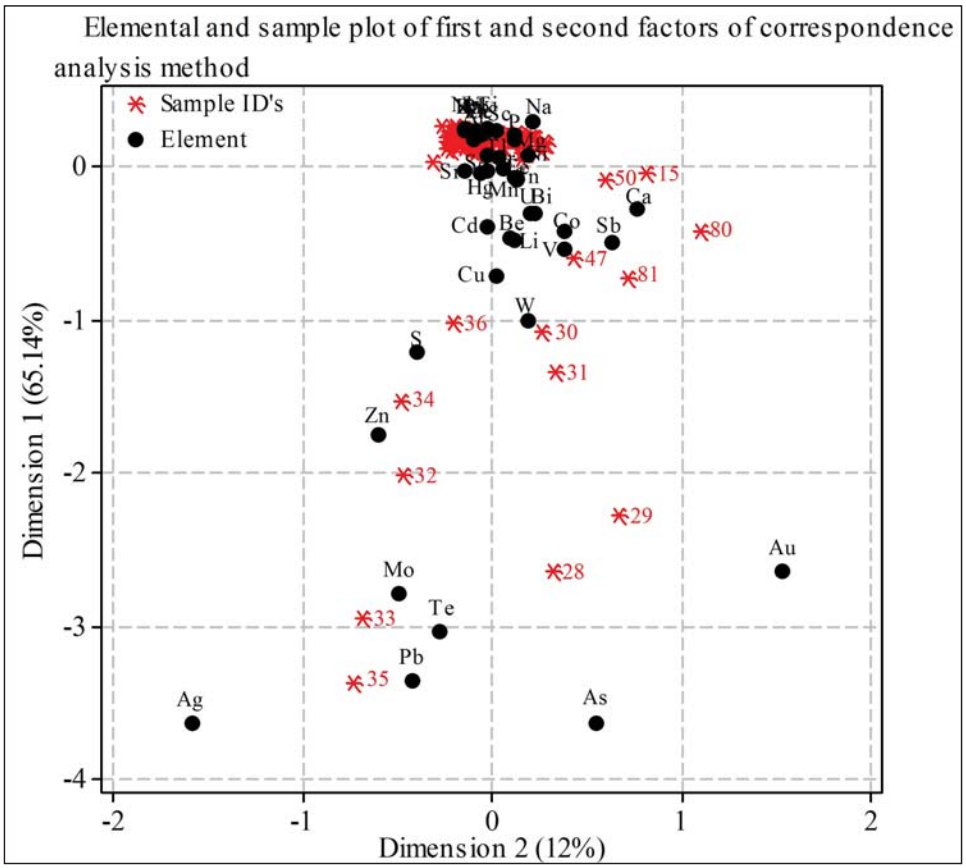

Figure 4- The two-dimensional visual representation of the two main factors; first and second factor explained 77.1% of the total variance at Glojeh using correspondence analysis. Both the row and column were displayed as principal coordinates in simultaneous plot.

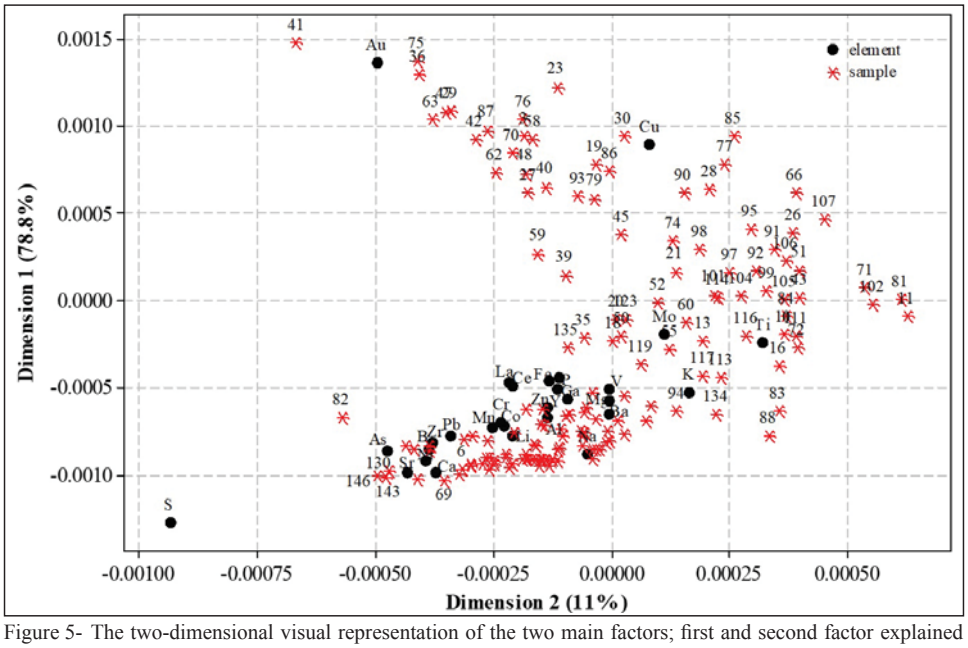

Figure 5- The two-dimensional visual representation of the two main factors; first and second factor explained 89.8% of the total variance at Dalli using correspondence analysis. Both the row and column were displayed as principal coordinates in symmetric plot.

deposits simultaneously. The Dimension 1 versus Dimension 2 (D1 versus D2) of Q-mode and R-mode combination analysis showed that two factors explained 77,14% of the total variance in Glojeh deposit. This percentage is sufficiently high to indicate a visual representation of the relationship between elements and samples. The first dimension indicates the strongest phase of mineralization that explains 65,14% of the total inertia and variance (Figure 4). On the other hand, the second dimension of variations (D2) indicates that Au and Ag show two different trends. The positive Au mineralization accompanied by Ca, As, and Sb association, while negative trend of Ag occurred with Zn, Mo, Pb, S, and Te elements.

The Dalli deposit is the second case study, which has been evaluated by 149 soil samples. The first dimension of CA indicates a strong mineralization of Cu-Au accompanied by high anomalous data for Mo, Ti, K, V and Fe, due to the related distances from other elements on this axis (Figure 5). On the other hand, the second phase of variations (Dimension 2) indicates that S, As, Au, and Sr show anomalous trends. The sample ID's of 36, 41, 75, 82, 130 and 146 show enrichment for them. The two-dimensional visual representation of indicated first and second dimension of CA explains 89.8% of the total variance, while the first dimension explains 78.8% of the total variance in district (Figure 5). The intuitive graphical figure 5 represents that D1 and D2 combination can display Cu-Au (Mo) mineralization, based on the highest distance and stretching outward from the center cluster, at D1 axis. As we discussed the first dimension was about seven times stronger than the second dimension.

3.2. Principal Component Analysis (PCA)

The geochemical compositional data were opened within the CoDaPack software v 2.01 and were transformed using the Isometric log-ratio (Ilr) transformations, prior to using any of the multivariate methods. The PCA for Ilr transformed data can be used to enhance the results of the CA for simultaneous study of elements in polymetallic and porphyry deposits when the data are compositional and suffering from closure problem.

Polymetallic vein deposit: At first, the PCA was done by log-transformation of geochemical data at Glojeh polymetallic vein deposit. The scree plot of eigenvalues indicates that the first (PC1) and second (PC2) significant factors of PCA explaining 56.3% of the total variance (Figure 6a). The PC1 explains the largest variance equal to 34.9% of the total variance. The PC1 indicates that the red group consists of Cu, Ag, Mo, Pb, Zn, Te, As, Au, Be, W, Se, and Cd elements are gained, while the blue group which is composed of Nb, K, La, Zr, Ba, Ce, Rb, Al, and Y elements is depleted at the Glojeh deposit. The factor loadings for these components are shown in figure 6a, while they are occurring between the –1 to +1 values and imply how the factors characterize the variables. Therefore, the association of Au, Ag, Cu, Pb, and Zn are more considerable for mineralization with As, Be, W, Te, and Mo in the Glojeh deposit.

On the other hand, based on the compositional properties of the data, all the data were transformed to Ilr space. The PCA method was applied to all above (43 elements) described elements within Ilr space. The first and second PC loadings of Ilr-transformed geochemical data explains 51,9% of the total variance in district (Figure 7a). The PC1 which includes the mineralization process explains 40,2% of total variation at the area (Figure 7a). Accordingly, it is comparable with the results of log-transformed data, by the higher value of variance (40,2% vs. 34,9%) and spread loading vectors and scores (Figure 7b).

Porphyry deposit: As a comparative case study, the Northern Dalli deposit has been investigated by log-transformed and LRT, based on 149 soil samples. The PC1 indicates 27,8% of total variation according to strong loading of Au and Cu against Li, Al, Mn, Ni, B, Co, Sr, and Cr elements. The PC2 shows 19% of total variance, indicated by V, Fe, To, Ga, Mg, K versus lower intense value of B, As and certainly La and Ce in this axis (Figure 8a). It is confirmed by score of samples such as 74 and 114 which are the strongest mineralized and depleted samples for Au and Cu respectively (Figure 8b). On the other hand, sample ID's of 11, 42 and 106 are the mineralized ones for V, Fe and Ti and 53, 142, and 131 are the loosest sample for them.

The biplot of the corresponding PC1 (29,5% of total variance) and PC2 (19,6% of total variance) of the Ilr transformed data, shows a clear separation between loadings and score of samples (Figure 9b). Therefore, the closure problem is overcome by Ilr-transformation, and curved shape of scores at figure 8b is depicted according to Ilr-transformation at figure 9b become spread apart and according to the spatial distribution of the observations become further apart.

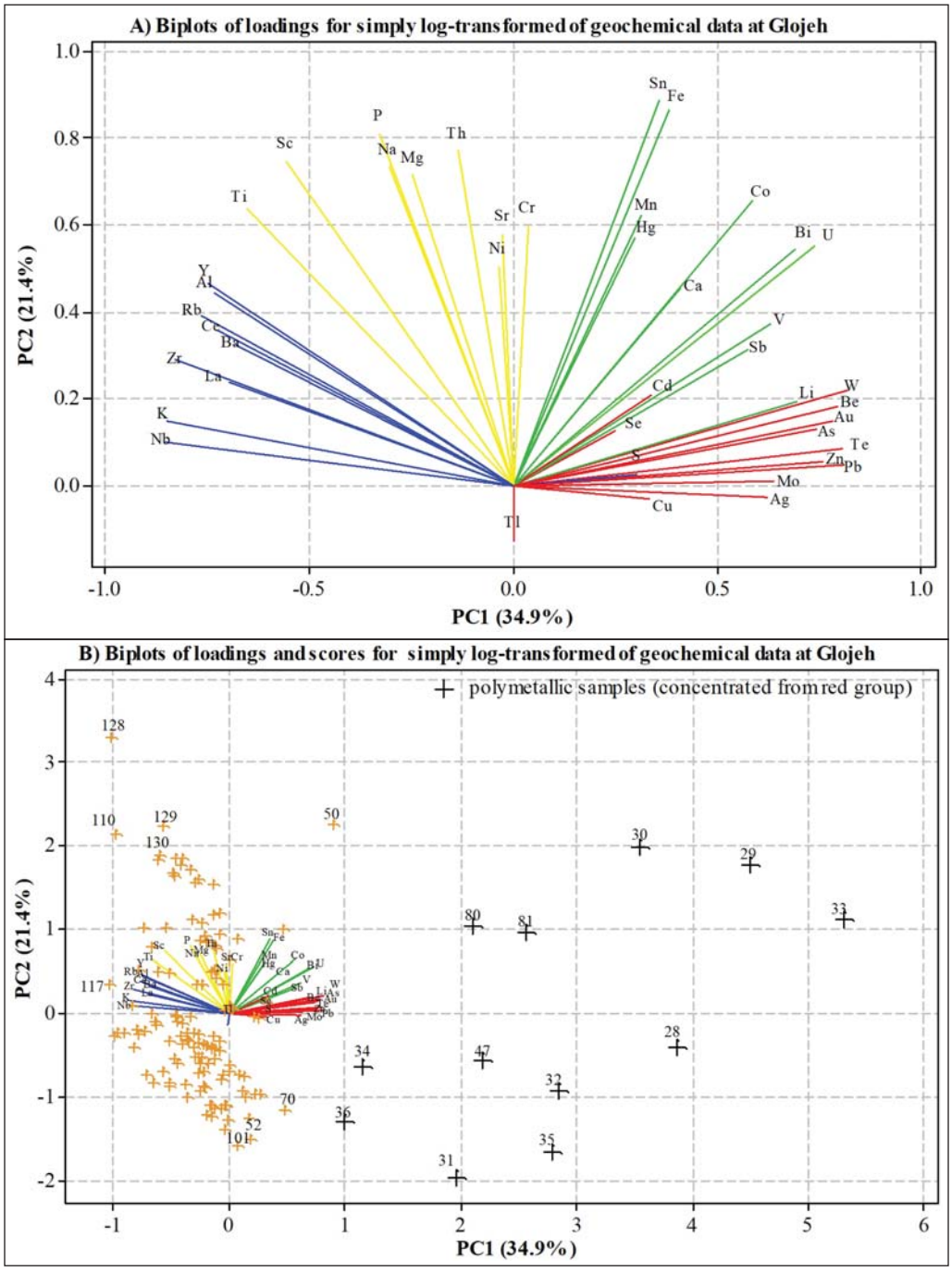

Figure 6- The loading plot (A), and symetric scores and loadings plot (B) on the PC1 versus PC2 of log-transformed data at Glojeh polymetallic deposit.

4. Discussion

4.1. CA

Polymetallic deposit: Zhu et al. (2011) proposed that the associations of Au-As or Au-Sb is common in different gold deposit, certainly in polymetallic veins that is consistent with the D2 here. The D1– D2 biplot (Figure 4) demonstrates the multi-element associations of Au-As-Ag-Pb-Te-Mo-Zn accompanied by S-Cu-W and Sb describing a polymetallic mineralization at Glojeh deposits directly. They have very high eccentricity from the center of the axis (0, 0) and sample ID's of 28, 29, 30, 31, 32, 33, 34, 35, 36 and 81 confirming this mineralization as indicator samples. The results show the potential for polymetallic

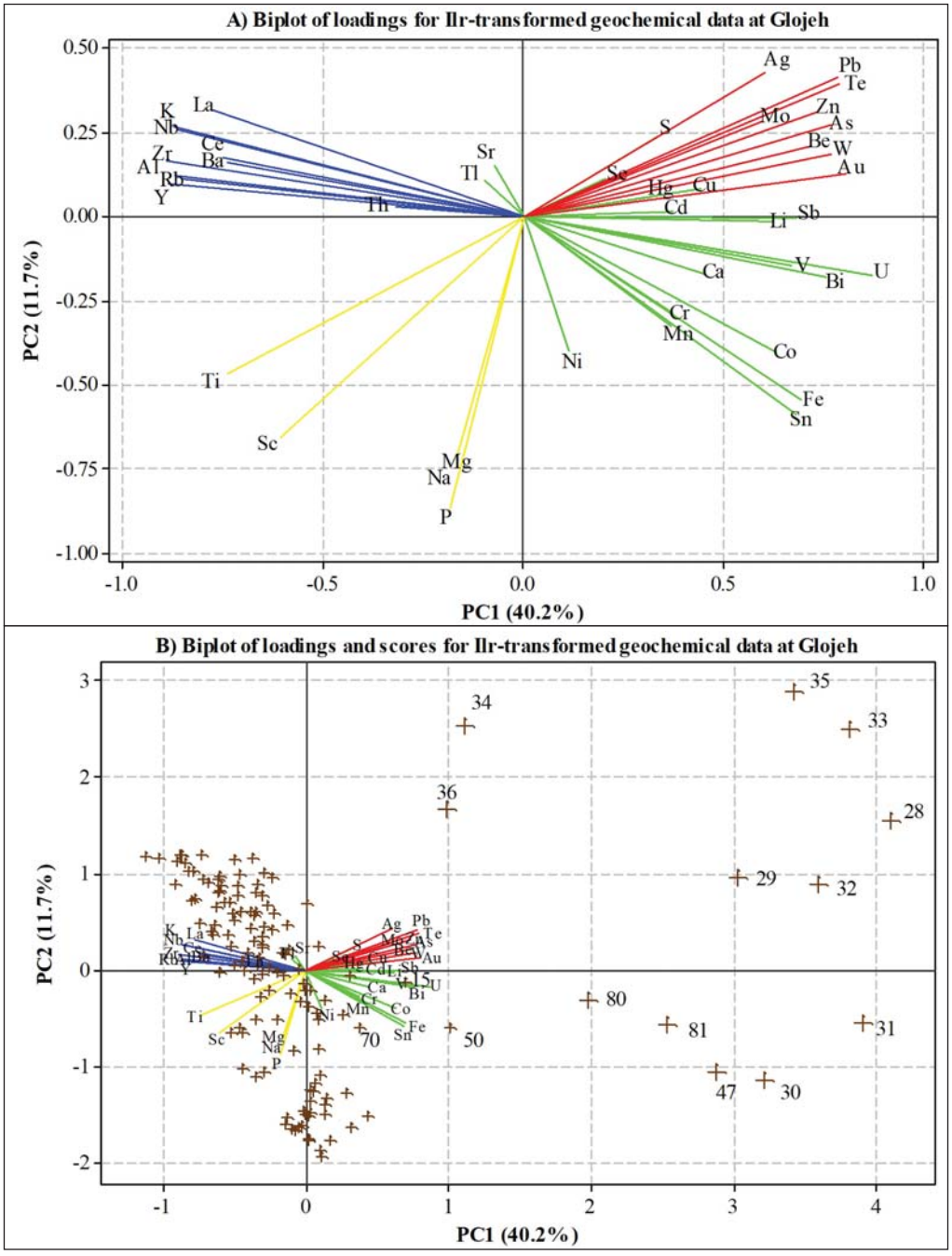

Figure 7- The loading plot (A), and symetric scores and loadings plot (B) on the PC1 versus PC2 of log-ratio transformed (Ilr space) data at Glojeh polymetallic deposit.

(highly anomalous elements are Ag, As, Pb and Au) veins mineralization. Cu and S association may be indicated that the polymetallic Au, Ag, Cu, Pb and Zn mineralization in the Glojeh deposit can be linked to a porphyry deposit in depth. Therefore, As, Te, Mo and minor S, W are more considerable for mineralization with Au, Ag, Cu, Pb and Zn in the Glojeh deposit (Darabi-Golestan and Hezarkhani, 2017).

Porphyry deposit: On the other hand, a porphyry mineralization at the Dalli deposit is verified by sample ID's of 23, 29, 35, 41, 42, 47, 63, 75, 76, 87 and too many samples. Figure 5 emphasizes on the S, As, Sr anomalous data according to the sample ID's of 82, 130 and 146. The Q-mode (score of samples) analysis approved the R-mode (score of elements) results, elemental associations, and mineralization in

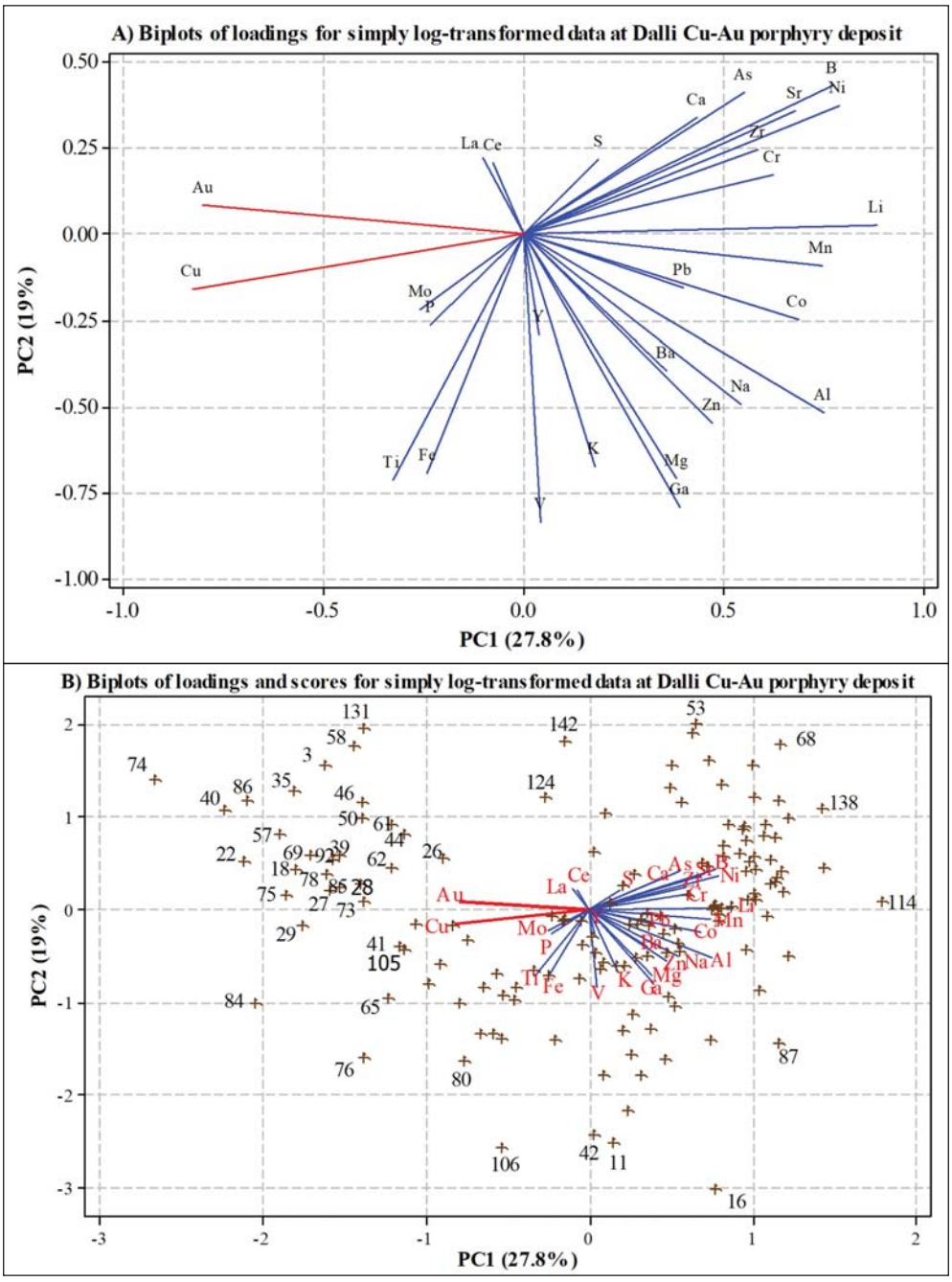

Figure 8- The loading plot (A), and symmetric scores and loadings plot (B) on the PC1 versus PC2 of log-transformed data at Dalli porphyry deposit.

order to avoid the creation of false anomalies due to different dimensions between or among the different elements. , the curved-shape configuration of the sample and element scores is a typical distribution for data closure problems in this coordinate.

4.2. PCA for log and Ilr Transformed Data

Polymetallic deposit: The biplot of the first two PC loadings for log-transformed data in a polymetallic deposit shows clearly the closure problem between

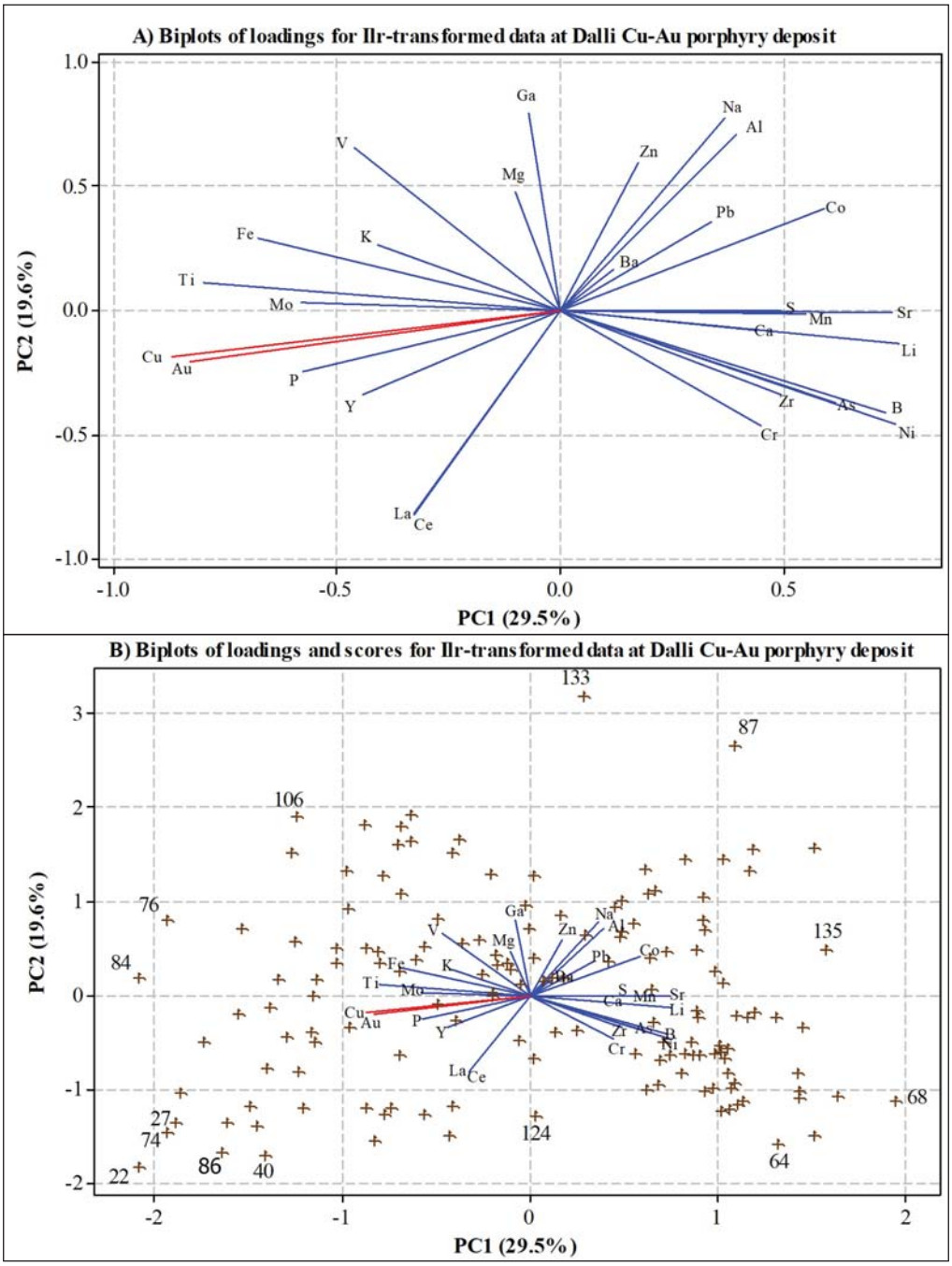

Figure 9- The loading plot (A), and symetric scores and loadings plot (B) on the PC1 versus PC2 of log-ratio transformed data at Dalli porphyry deposit.

loadings, as they are constrained in a semicircle (Figure 6a). The biplot of loadings and scores for log-transformed data (Figure 6b) shows that the red group is concentrated in sample ID's of 28, 29, 30, 31, 32, 33, 34, 35, 36, 47, 50 and 81. These samples indicate vein, veinlet and brecciated zones, while they are depleted from blue group. By the way, it is resulted that the samples 128, 110,129 and 130 are concentrated for the yellow group. The yellow and green groups are more relevant by the PC2. On the other hand, the visualized plot of multi-elemental association from PC1 vs. PC2 indicates that the closure problem in compositional data is posed and the loadings are spread in a circular, using Ilr-transformed data. The combination of loadings and scores at figure 7b indicates a better relationship and interaction between elemental loadings and sample scores, whereas the closure effect problem is minimized. Figure 7b could

ease the interpretation of geochemical dispersion pattern of elements and samples.

Both the PCA opened using log-transformed and Ilr-transformed geochemical data indicate sample ID's of 28, 29, 30, 31, 32, 33, 34, 35, 36, 47, 80 and 81 as anomalous samples that taken from polymetallic (Au, Ag, Cu, Pb, and Zn) veins. But Ilr-transformed data show better inherent in compositional and overcome on the closure effect of loadings and scores.

Porphyry deposit: The loadings (Figure 8a) and scores (Figure 8b) of the two first PC's (from log-transformed data) show the closure problem, give that all the loadings except Au, Cu, La, and Ce are restricted to a semicircle (180°) and score of samples distributed closely. Because of data closure effect problem there is compositional data at Dalli deposit, the score of samples shows a strong curve shape as shown in figure 8b.

Using appropriate Ilr transformations prior to PCA analysis, the loadings of compositional data plot along all directions on the biplot (Figure 9a), while the loadings of the log-transformed data are mostly constrained in a semi-circle (Figure 8a). Figure 9a suggests that Mo-Ti-Fe-K-V and Y-La-Ce associations that represented in PC1 vs. PC2 biplot of Ilr space, show more realistic signature in Cu-Au porphyry deposit, compared to their associations represented in simply log-transformed biplot at figure 8a. This interpretation is supported by the different spatial distribution of scores at figure 8b and 9b. Figure 8b demonstrates that the known Cu-Au-(Mo) deposit in the study area has stronger positive correlation with the Mo-Ti-Fe-K-V and Y-La-Ce associations, which is concordant with Cu-Au-(Mo) porphyry deposit. With a comparison to log-transformed, loadings of the ilr-transformed show a strong Cu-Au mineralization followed by lower Mo concentrations, that are supported by too many scores of samples. Previous studies at this deposit, revealed a clear trend of sequential enrichment of Mo→Cu→Au from depth to surface (Darabi-Golestan et al., 2013*a*), that is covered by the results of ilr-transformed data from soil samples at this study. The intensely mineralized Au-Cu-(Mo) occur at sample ID's of 22, 28, 35, 40, 46, 74, 84, 86 and many others, and these are in connection with Cu-Au porphyry mineralization at the deposit (Figure 8b and 9b). According to lithological soil samples using CA (Figure 5), PCA analysis of log-transformed (Figure 8) and Ilr-transformed data (Figure 9), this trend is confirmed by higher intensity of (Au, Cu)>Mo. Darabi-Golestan et al. (2013*a*) proposed that the higher concentrations of Au and Cu are associated with mineralized zone within quartz diorite porphyry rocks that were enriched partly from Fe and Ti that were dominantly covered by potassic (K) alterations, which are more consistent with the CA and PCA of LRT data of graphical plot at the present study.

5. Conclusion

Most of mineralization has occurred because of the elemental interaction effect and physico-chemical exchanges within or/and between fluids and host rock. Therefore, the closure effects problem needs to be considered to understand the geochemical dispersion pattern of elements. Subcompositional coherence is overcome by LRT (certainly, Ilr transformation) for two genetic types of polymetallic vein and porphyry Au deposits at this study, while simply used log-transformed values are not good enough. Accordingly, by application Ilr-transformed data compared to log-transformed data the PC1 are improved from 34,9% to 40,2% at Glojeh and 27,8% to 29,5% at Dalli deposit. The ability to handle zero values in the data matrix and determining an elemental eccentricity from the center of axis based on Euclidean distances are the advantages of CA method. On the other hand, a clear picture of loading factors which spread in a full circle providing subcompositional coherence are the competitive advantages of PCA based on Log-Ratio transformation. Accordingly, Ag, Au, As, Pb, Te, Mo and rather S, W, Cu are enriched as polymetallic elements at Glojeh, while Au-Cu (Mo) indicates a porphyry deposit occurred in Dalli. Both anomalies are accompanied by a lot of samples that show enrichment for them. However, the closure problem between samples and elements is solved by LRT and these techniques show significant ability to draw an inference in such deposits.

Acknowledgements

The authors are grateful to the Iranian Mines and Mining Industries Development and Renovation Organization (IMIDRO) for their permission to have access to Glojeh deposit dataset. The authors are also thankful to Mr. Fattahi and Mr. Hemmati for their encouragement and valuable help hugely.

References

Abdi, H., Valentin, D. 2007. Multiple correspondence analysis. Encyclopedia of measurement and statistics, 651-657.

Abdi, H., Williams, L. J., Valentin, D. 2013. Multiple factor analysis: Principal component analysis for multi-table and multi-block data sets. Computational Statistics 5, 149-179.

Aitchison, J. 1982. The statistical analysis of compositional data. Journal of the Royal Statistical Society. Series B (Methodological), 139-177.

Aitchison, J. 1983. Principal component analysis of compositional data. Biometrika, 57-65.

Aitchison, J. 1986. The statistical analysis of compositional data. Monographs on Statistics and Applied Probability, 416 p.

Aitchison, J. 1990. Relative variation diagrams for describing patterns of compositional variability. Mathematical Geology 22, 487-511.

Aitchison, J., Greenacre, M. 2002. Biplots of compositional data. Journal of the Royal Statistical Society: Series C (Applied Statistics) 51, 375-392.

Akbarpour, A., Gholami, N., Azizi, H., Torab, F. M. 2013. Cluster and R-mode factor analyses on soil geochemical data of Masjed-Daghi exploration area, northwestern Iran. Arabian Journal of Geosciences 6, 3397-3408.

Bitner-Mathé, B. C., Klaczko, L. B. 1999. Heritability, phenotypic and genetic correlations of size and shape of Drosophila mediopunctata wings. Heredity 83, 688-696.

Carranza, E. J. M. 2009. Controls on mineral deposit occurrence inferred from analysis of their spatial pattern and spatial association with geological features. Ore Geology Reviews 35, 383-400.

Carranza, E. J. M. 2011. Analysis and mapping of geochemical anomalies using logratio-transformed stream sediment data with censored values. Journal of Geochemical Exploration 110, 167-185.

Carranza, E. J. M. 2017. Geochemical Mineral Exploration: Should We Use Enrichment Factors or Log-Ratios? Natural Resources Research 26, 411-428.

Collins, M., Ovalles, F. 1988. Variability of northwest Florida soils by principal component analysis. Soil Science Society of America Journal 52, 1430-1435.

Croux, C., Haesbroeck, G. 2000. Principal component analysis based on robust estimators of the covariance or correlation matrix: influence functions and efficiencies. Biometrika 87, 603-618.

Darabi-Golestan, F., Ghavami-Riabi, R., Asadi-Harooni, H. 2013*a*. Alteration, zoning model, and mineralogical structure considering lithogeochemical investigation in Northern Dalli Cu–Au porphyry. Arabian Journal of Geosciences 6, 4821-4831.

Darabi-Golestan, F., Ghavami-Riabi, R., Khalokakaie, R., Asadi-Haroni, H., Seyedrahimi-Nyaragh, M. 2013*b*. Interpretation of lithogeochemical and geophysical data to identify the buried mineralized area in Cu-Au porphyry of Dalli-Northern Hill. Arabian Journal of Geosciences 6, 4499-4509.

Darabi-Golestan, F., Hezarkhani, A. 2016. High precision analysis modeling by backward elimination with attitude on interaction effects on Au (Ag)-polymetallic mineralization of Glojeh, Iran. Journal of African Earth Sciences 124, 505-516.

Darabi-Golestan, F., Hezarkhani, A. 2017. R- and Q-mode multivariate analysis to sense spatial mineralization rather than uni-elemental fractal modeling in polymetallic vein deposits. Geosystem Engineering, 1-10.

Darabi-Golestan, F., Hezarkhani, A. 2018. Evaluation of elemental mineralization rank using fractal and multivariate techniques and improving the performance by log-ratio transformation. Journal of Geochemical Exploration 189, 11-24.

Darabi-Golestan, F., Hezarkhani, A., Zare, M. 2017. Assessment of 226 Ra, 238 U, 232 Th, 137 Cs and 40 K activities from the northern coastline of Oman Sea (water and sediments). Marine Pollution Bulletin 118, 197-205.

David, M., Campiglio, C., Darling, R. 1974. Progresses in R-and Q-mode analysis: correspondence analysis and its application to the study of geological processes. Canadian Journal of Earth Sciences 11, 131-146.

Diday, E., Noirhomme-Fraiture, M. 2008. Symbolic data analysis and the SODAS software, Wiley Online Library, Namur, Belgium.

Egozcue, J. J., Pawlowsky-Glahn, V., Mateu-Figueras, G., Barcelo-Vidal, C. 2003. Isometric logratio transformations for compositional data analysis. Mathematical Geology 35, 279-300.

Fávaro, D., Damatto, S., Moreira, E., Mazzilli, B., Campagnoli, F. 2007. Chemical characterization and recent sedimentation rates in sediment cores from Rio Grande reservoir, SP, Brazil. Journal of Radioanalytical and Nuclear Chemistry 273, 451-463.

Filzmoser, P., Hron, K. 2008. Outlier detection for compositional data using robust methods. Mathematical Geosciences 40, 233-248.

Filzmoser, P., Hron, K., Reimann, C. 2009*a*. Principal component analysis for compositional data with outliers. Environmetrics 20, 621-632.

Filzmoser, P., Hron, K., Reimann, C. 2009*b*. Univariate statistical analysis of environmental (compositional) data: problems and possibilities. Science of the Total Environment 407, 6100-6108.

Filzmoser, P., Hron, K., Reimann, C., Garrett, R. 2009*c*. Robust factor analysis for compositional data. Computers ve Geosciences 35, 1854-1861.

Filzmoser, P., Hron, K., Reimann, C. 2010. The bivariate statistical analysis of environmental (compositional) data. Science of the Total Environment 408, 4230-4238.

García-Izquierdo, M., Ríos-Rísquez, M. I. 2012. The relationship between psychosocial job stress and burnout in emergency departments: an exploratory study. Nursing outlook 60, 322-329.

Golestan, F. D., Hezarkhani, A., Zare, M. 2013. Interpretation of the Sources of Radioactive Elements and Relationship between them by Using Multivariate Analyses in Anzali Wetland Area. Geoinformatics & Geostatistics: An Overview 1, 1-10.

Greenacre, M. 2007. "Correspondence analysis in practice," CRC press.

Greenacre, M. 2010. Log-ratio analysis is a limiting case of correspondence analysis. Mathematical Geosciences 42, 129-134.

Greenacre, M. 2011. Measuring subcompositional incoherence. Mathematical Geosciences 43, 681-693.

Greenacre, M., Blasius, J. 2006. "Multiple correspondence analysis and related methods," CRC press.

Greenacre, M. J. 1984. "Theory and applications of correspondence analysis."

Gu, X., Liu, C., Wang, S., Zhao, C. 2015. Feature extraction using adaptive slow feature discriminant analysis. Neurocomputing 154, 139-148.

Hayton, J. C., Allen, D. G., Scarpello, V. 2004. Factor retention decisions in exploratory factor analysis: A tutorial on parallel analysis. Organizational research methods 7, 191-205.

Jeong, D. H., Ziemkiewicz, C., Fisher, B., Ribarsky, W., Chang, R. 2009. iPCA: An Interactive System for PCA-based Visual Analytics. In "Computer Graphics Forum", Vol. 28, pp. 767-774. Wiley Online Library.

Ji, H., Zhu, Y., Wu, X. 1995. Correspondence cluster analysis and its application in exploration geochemistry. Journal of geochemical Exploration 55, 137-144.

Ji, H., Zeng, D., Shi, Y., Wu, Y., Wu, X. 2007. Semi-hierarchical correspondence cluster analysis and regional geochemical pattern recognition. Journal of Geochemical Exploration 93, 109-119.

Karamanis, D., Ioannides, K., Stamoulis, K. 2009. Environmental assessment of natural radionuclides and heavy metals in waters discharged from a lignite-fired power plant. Fuel 88, 2046-2052.

Kazmierczak, J. 1985. Analyse logarithmique: deux exemples d'application. Revue de statistique appliquée 33, 13-24.

Liu, Y., Cheng, Q., Zhou, K., Xia, Q., Wang, X. 2016. Multivariate analysis for geochemical process identification using stream sediment geochemical data: A perspective from compositional data. Geochemical Journal 50, 293-314.

Março, P. H., Scarminio, I. S. 2007. Q-mode curve resolution of UV–vis spectra for structural transformation studies of anthocyanins in acidic solutions. Analytica chimica acta 583, 138-146.

Maronna, R., Martin, R. D., Yohai, V. 2006. "Robust statistics: Theory and Methods," John Wiley & Sons, Chichester. ISBN.

Martín-Fernández, J. A., Barceló-Vidal, C., Pawlowsky-Glahn, V. 2003. Dealing with zeros and missing values in compositional data sets using nonparametric imputation. Mathematical Geology 35, 253-278.

Olofsson, T., Andersson, S., Sjögren, J.-U. 2009. Building energy parameter investigations based on multivariate analysis. Energy and Buildings 41, 71-80.

Pawlowsky-Glahn, V., Egozcue, J. J. 2006. Compositional data and their analysis: an introduction. Geological Society, London, Special Publications 264, 1-10.

Pawlowsky-Glahn, V., Buccianti, A. 2011. "Compositional data analysis: Theory and applications," John Wiley & Sons.

Pawlowsky-Glahn, V., Egozcue, J. J., Tolosana Delgado, R. 2007. Lecture notes on compositional data analysis.

Pommer, L., Fick, J., Sundell, J., Nilsson, C., Sjöström, M., Stenberg, B., Andersson, B. 2004. Class separation of buildings with high and low prevalence of SBS by principal component analysis. Indoor Air 14, 16-23.

Ramasamy, V., Sundarrajan, M., Paramasivam, K., Meenakshisundaram, V., Suresh, G. 2013. Assessment of spatial distribution and radiological hazardous nature of radionuclides in high

background radiation area, Kerala, India. Applied Radiation and Isotopes 73, 21-31.

Reimann, C., Filzmoser, P., Garrett, R., Dutter, R. 2011. "Statistical data analysis explained: applied environmental statistics with R," John Wiley & Sons.

Reimann, C., Filzmoser, P., Fabian, K., Hron, K., Birke, M., Demetriades, A., Dinelli, E., Ladenberger, A., Team, T. G. P. 2012. The concept of compositional data analysis in practice—total major element concentrations in agricultural and grazing land soils of Europe. Science of the total environment 426, 196-210.

Silverman, J. D., Washburne, A., Mukherjee, S., David, L. A. 2016. A phylogenetic transform enhances analysis of compositional microbiota data. bioRxiv, 072413.

Stanley, C. R. 2006. On the special application of Thompson–Howarth error analysis to geochemical variables exhibiting a nugget effect. Geochemistry: Exploration, Environment, Analysis 6, 357-368.

Templ, M., Filzmoser, P., Reimann, C. 2008. Cluster analysis applied to regional geochemical data: problems and possibilities. Applied Geochemistry 23, 2198-2213.

Thió-Henestrosa, S., Martín-Fernández, J. 2005. Dealing with compositional data: the freeware CoDaPack. Mathematical Geology 37, 773-793.

Thompson, M., Howarth, R. J. 1976. Duplicate analysis in geochemical practice. Part I. Theoretical approach and estimation of analytical reproducibility. Analyst 101, 690-698.

Tokatlı, C., Köse, E., Çiçek, A. 2014. Assessment of the effects of large borate deposits on surface water quality by multi statistical approaches: A case study of Seydisuyu Stream (Turkey). Polish Journal of Environmental Studies 23, 1741-1751.

Zhu, Y., An, F., Tan, J. 2011. Geochemistry of hydrothermal gold deposits: a review. Geoscience Frontiers 2, 367-374.

Zuo, R., Xia, Q., Wang, H. 2013. Compositional data analysis in the study of integrated geochemical anomalies associated with mineralization. Applied geochemistry 28, 202-211.

Bulletin of the Mineral Research and Exploration

http://bulletin.mta.gov.tr

Statistical assessment of radiation exposure risks of farmers in Odo Oba, Southwestern Nigeria

Theophilus Aanuoluwa ADAGUNODO[a,*], Lukman Ayobami SUNMONU[b], Moruffdeen Adedapo ADABANIJA[c], Maxwell OMEJE[a], Oluwole Akinwumi ODETUNMİBİ[e] and Victor IJEH[f]

[a] *Department of Physics, Covenant University, Ota, Ogun State, Nigeria orcid.org/0000-0001-7810-3323*
[b] *Department of Pure and Applied Physics, Ladoke Akintola University of Technology, Ogbomoso, Oyo State, Nigeria. orcid.org/0000-0002-4305-8363*
[c] *Department of Earth Sciences, Ladoke Akintola University of Technology, Ogbomoso, Oyo State, Nigeria. orcid.org/0000-0002-3737-0350*
[d] *Department of Physics, Covenant University, Ota, Ogun State, Nigeria. orcid.org/0000-0001-9124-1093.*
[e] *Department of Mathematics, Covenant University, Ota, Ogun State, Nigeria. orcid.org/0000-0003-1395-579X.*
[f] *Department of Pure and Applied Physics, Ladoke Akintola University of Technology, Ogbomoso, Oyo State, Nigeria. orcid.org/0000-0002-1649-6915*

Research Article

Keywords:
Radiation exposure, Farmers' exposure risks, Inductively coupled plasma mass spectrometry, Radiological risks, Statistical assessment.

ABSTRACT

The toxicity risks of being over exposed to ionizing radiation in the environments are of great concern to environmental and health scientists. The distribution of radioactivity concentrations of thorium, uranium and potassium were studied in randomly selected soil samples from ten (10) farm locations in Odo Oba, southwestern Nigeria in order to determine the radiological risks of farmers' exposure to radionuclides. The mean estimation of thorium and potassium are greater than the global average by factors of 1,5 and 2,7, while that of uranium fall below the global average. The estimation of radioactivity ratios showed a depletion of uranium and enrichment of thorium in the study area. Further analysis on the radioelements (that is, thorium, uranium and potassium) showed that 83% of the estimated radiological risks are above the global average. The multivariate analyses involving Pearson's correlation, Factor Analysis, Hierarchical Cluster Analysis were also used to explain the correlations among the data sets. It was affirmed from the multivariate analysis that the radiological hazards occur as a result of contributions from the three naturally occurring radionuclides. The values obtained in this study revealed that the sampled locations are contaminated zones for farmers.

Received Date: 26.02.2018
Accepted Date: 09.07.2018

1. Introduction

All soils are radioactive as a result of primordial and/or cosmogenic radionuclides being present naturally. Radionuclides reach the soil through soil-borne photosynthesis and water absorption, as well as natural radioactive elements of potassium (^{40}K), uranium, thorium and their daughters. The former process occurs when the radioactive carbon (carbon-14) and radioactive hydrogen (tritium) are formed by the action of cosmic rays in the atmosphere which later fall to the surface of the earth. The later are present in the geological formations of many soils. Staying more than the required time in a natural radioactive contaminated area could be dangerous to human as the radionuclides inhaled can be greater than the allowable limit (ATSDR, 1990). Humans can be exposed to radioactive chemicals in the environment (breathing air, drinking, eating, or smoking substances with radioactive constituents), through the physical contact (such as skin), or coming too close to locations with high concentrations of radioactive chemicals, such as when there are industrial accidents or hazardous waste sites. Some of the factors that determine the

Citation Info: Adagunodo, T. A., Sunmonu, L. A., Adabanija, M. A., Omeje, M., Odetunmibi, O. A., Ijeh, V.. 2019. Statistical assessment of radiation exposure risks of farmers in Odo Oba, Southwestern Nigeria. Bulletin of Mineral Research and Exploration, 159, 201-217. *http://dx.doi.org/10.19111/bulletinofmre.495321*

* *Corresponding author: Theophilus Aanuoluwa ADAGUNODO, theophilus.adagunodo@covenantuniversity.edu.ng*

toxicity exposure to hazardous chemicals include: dose, pathway to the exposure, number of chemicals exposed to, and the individual features (for example, eating habits, sex, age, health status, family trait and life style) (ATSDR, 1990).

Nigerian farmers are often referred to as hand-hoe (peasant) farmers. This is due to the fact that mechanization rate in Nigeria is 0.27 hp/hectare, a lower standard to the recommended rate of 1.5 hp/hectare by FAO (2013). Apart from the method becoming obsolete globally, it could serve as a channel for being exposed to natural radioactive materials on a contaminated farm land ignorantly. Exposure to radionuclides in a naturally occurring radioactive contaminated zone needs to be avoided or access the land with protective wears. Long-term exposure to radium and uranium through inhalation has several effects as chronic lung diseases, anemia, acute leucopoenia, necrotizing periodontal disease, tumours in the bones, nasal and cranial nerves. Overexposure to thorium causes cancers of different kinds in human systems such as in lung, bone, pancreas, kidney, and liver. It can also cause hepatic and leukaemia (Ramasamy et al., 2011). Therefore, radionuclide's activity concentrations and the risks associated with farmer's exposure to these radioactive elements should be monitored.

Exposure to natural radioactivity is a function of the natural radioactive elements present in that area (UNSCEAR, 2000). Radioactivity of an area can be used to estimate the dose rates and the risks associated with over exposure to the natural radionuclides in a radioactive contaminated region (Alzubaidi et al., 2016).Thorium -232 and Uranium -238 decay series as well as potassium -40 are the natural radionuclides that are used for estimating the abundance of thorium, uranium and potassium in the subsurface. These natural elements contribute greatly to the dose received by humans. Radionuclides can be transferred to food chain through soil, rocks, and water bodies since they contain appreciable quantities of radioactive elements (Alzubaidi et al., 2016).

Knowledge of natural radioactivity present on farm land will guide in the assessment of possible risks associated with external exposure to radiation through inhalation. Hence, this study is aimed at evaluating the radiation exposure risks to farmers in Odo Oba, Southwestern Nigeria.This study was borne out of the increasing economic activities mostly agriculture (farming and fishing) and cottage industries prompted by population growth. Odo Oba is the source of food crops to Ogbomoso and its environs. Agricultural practices are most eminence in the study area possibly due to the availability of water that Oba River provides. Among the researchers that have investigated on the radioactivity concentration emanating from subsurface and its risks include: Odunaike et al. (2008), Gbadebo and Amos (2010), Akinloye et al. (2012), Avwiri et al. (2012), Chandrasakaran et al. (2014), Qureshi et al. (2014), Rafique et al. (2014), Usikalu et al. (2014), (2017), Ademola et al. (2015), Ravisankar et al. (2015), Alzubaidi et al. (2016), Adagunodo et al. (2017*b*), Adagunodo et al. (2018*a*) and (2018*b*).

2. The Study Area and Its Geology

Odo Oba is located between the latitude 8° 2′ 46.7″ to 8° 2′ 58.5″ N and longitude 4° 8′ 00″ to 4° 9′ 15″ E (Figure 1a). It is a settlement that is situated at the southwest of Ogbomoso, southwestern Nigeria. The average elevation of the study area is about 267 m. Materials being carried from several tributaries over the years are deposited around Oba river, a major river for irrigation in the study area (Figure 1b), due to the planar surface of the study area. This has enhances the deposition of the Quaternary sediments in Odo Oba. The drainage pattern of Odo Oba is dendrite in nature. The climate of the study area is distinguished by averagely high temperature. Moderate-to-heavy rainfall is experienced in the study area between March and July annually, an average annual rainfall of 1,247mm. The Relative Humidity (RH) is at its peak at the early hours of the day, which decrease towards the post meridiem. The minimal and maximal RH is experienced from December – February and July – September annually. The continental air mass blows dry air (with little or no moisture) across the region during the dry season. In turn, the tropical air mass takes charge in the rainy season (Adagunodo et al., 2017*b*).

In Nigeria, four hydrogeological provinces have been reported in literature, these include: Volcanic-, Precambrian basement-, consolidated and unconsolidated sedimentary rocks. Odo Oba lies perfectly on the Precambrian basement domain of SW Nigeria (Figure 2), which composed of metamorphic and crystalline rocks of > 550 My (Sunmonu et al., 2012). This geological domain is constituted by gneiss, meta-sedimentary, and older granites (Jones and Hockey, 1964; Adagunodo and Sunmonu,

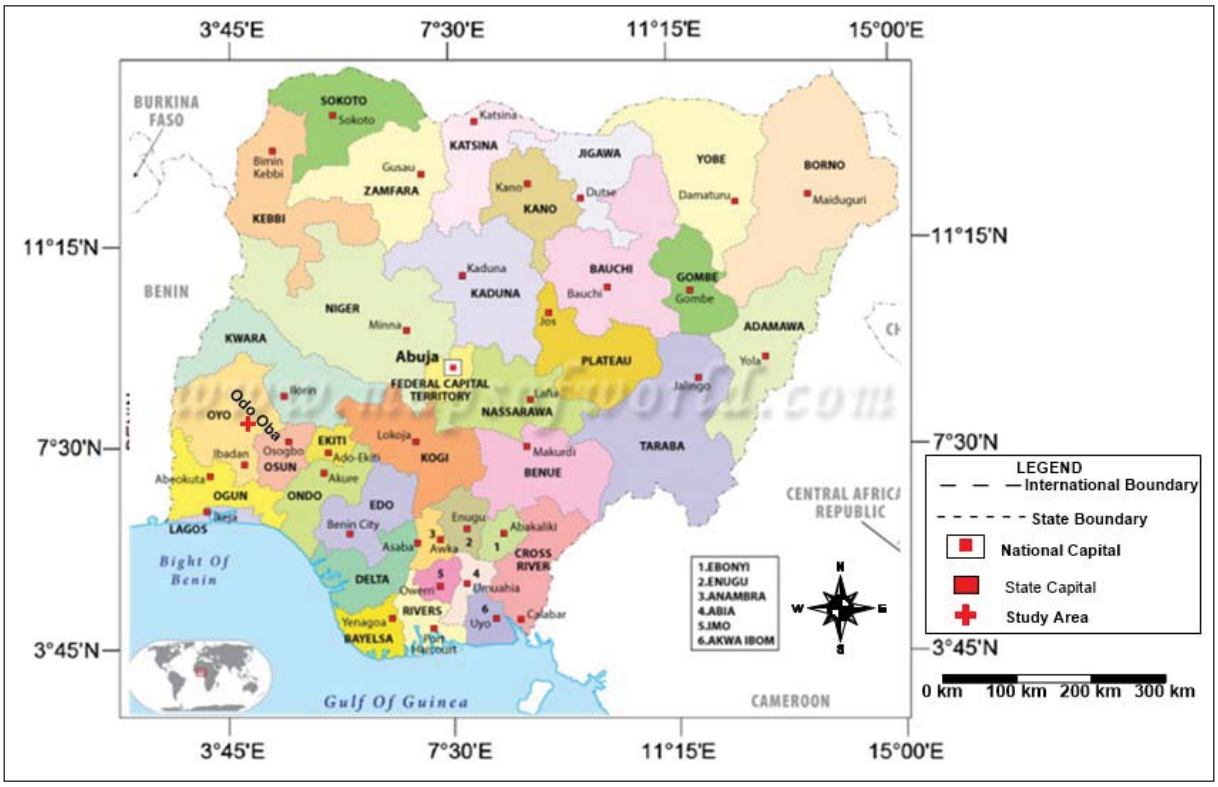

Figure 1a- States and Capitals in Nigeria showing Odo Oba in Oyo state, Nigeria

Figure 1b- Rivers in south-west Nigeria showing Odo Oba (adapted from Rivers of Yorubaland, 2017).

2012; Olafisoye et al., 2012; Sunmonu et al., 2012; Adagunodo et al., 2013*a*; 2013*b*; 2013*c*; Oladejo et al., 2013; Olafisoye et al,. 2013; Adagunodo et al., 2017*a*; 2017*b*). The banded and granite gneisses are the dominant rock units in Odo Oba. The other rock units in the study area are quartzite, and sparsely distributed pegmatite (Adagunodo et al., 2017*b*; 2018*c*) (Figure 2).

3. Materials and Methods

Topsoil samples (up to a depth of 25 cm) from ten (10) farm locations (S1 to S10) were randomly taken for the analysis (Figure 3). This was carried out in order to investigate the toxicity risks of farmers' exposure to natural radioactivity in Odo Oba farm land. The results obtained are expected to reveal the radionuclide dispersions in the area and be used for further hazards' evaluation. In respect of this, the samples collected were dried under ambient temperature for number of weeks, and sieved by a 2 mm mesh to remove larger objects. Each sample was packed into a plastic sock and transported to Canada for Analysis. The analysis was carried out in ACME laboratories, Canada. AcmeLabs is one of the

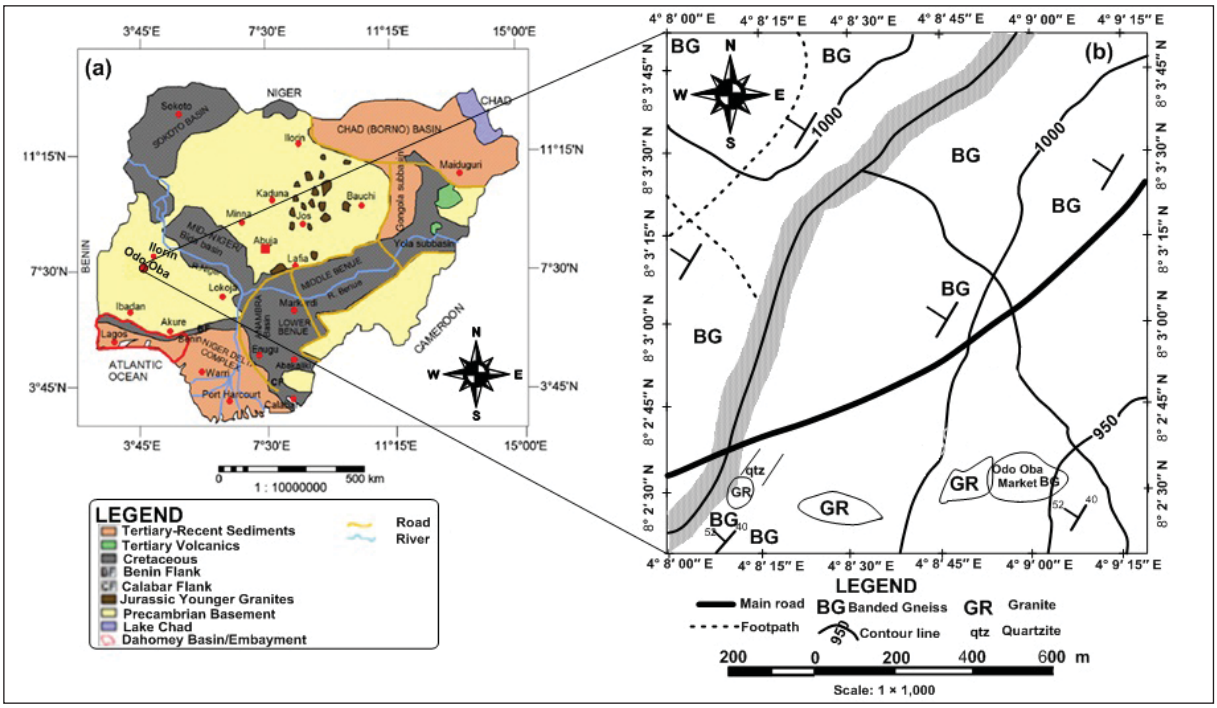

Figure 2- Geological domains in Nigeria revealing Odo-Oba geology (modified from Obaje (2015) and Adagunodo et al. (2017*b*; 2018*c*).

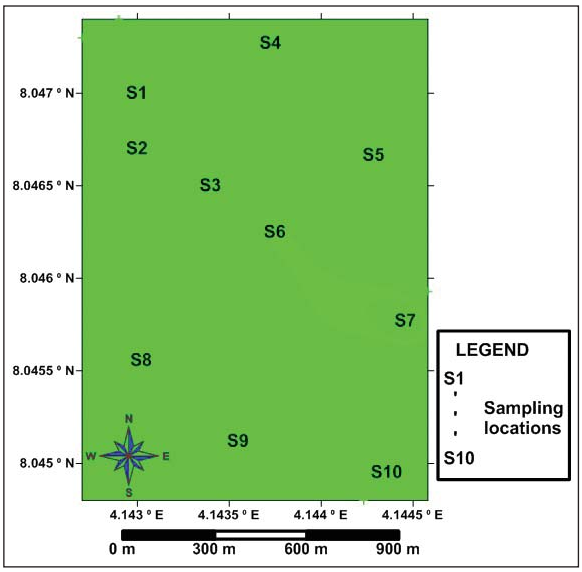

Figure 3- Sampling locations in the study area.

world-class geochemical and assaying laboratories to geoscientists. Inductively Coupled Plasma Mass Spectrometry (ICP-MS) was used to determine the concentrations of radionuclides (^{238}U and ^{232}Th) and potassium (^{40}K) in the samples. ICP-MS is one of the techniques used for radionuclide and elemental analysis either solid or liquid samples. The detection limit of ICP-MS for ^{238}U, ^{232}Th and ^{40}K are 0,05 ppm, 0,1 ppm and 0,01% respectively. The samples were dried at 110°C in the oven to constant weight and further grounded to a powder. After grinding of each sample, high pressure compressor air with nozzle was used to blow the remnant from the grinder in order to avoid cross-contamination. The samples were digested and were transferred to Teflon beakers for evaporation using a hot plate. The residues were dissolved in 10% HNO_3 for fifteen minutes to ensure complete digestion, which was finally dissolved in 100 ml of HNO_3. The certified soil reference material (calibration standard) was digested with the same proportion of HNO_3 for quality control analysis. Prior to the ICP-MS analyses, standard solutions were prepared from SPEX Multi-element Plasma Standard in order to obtain the calibration curves for the analyses. Each sample was analyzed thrice to monitor the reproducibility of each result, which is in line with the standard procedures highlighted by Sahoo et al. (2001) and Bank et al. (2016). The concentrations of potassium, uranium and thorium in each soil sample were given in percent (%) and parts per million (ppm) respectively. Eqs. (1) to (3) were further used to covert respective concentration to Becquerel per kilogram (Bq kg^{-1}) in accordance with IAEA (1989) and Omeje et al. (2013) models. The activity concentrations' results from AcmeLabs (in % and ppm) and the converted results (in Bq kg^{-1}) are revealed in table 1.

Table 1- Concentrations of natural radioactivity in soil samples of Odo Oba.

Samples	Uranium (ppm)	Thorium (ppm)	Potassium (%)	Uranium (Bq kg^{-1})	Thorium (Bq kg^{-1})	Potassium (Bq kg^{-1})
S1	2,60± 0,19	12,80 ± 3,00	2,69 ± 0,35	32,11 ± 2,35	51,97± 12,18	841,97± 109,55
S2	1,00 ± 0,43	2,80 ± 1,00	3,43 ± 0,92	12,35 ± 5,31	11,37± 4,06	1073,59± 287,96
S3	2,20 ± 0,11	9,90 ± 3,00	2,85 ± 0,13	27,17 ± 1,36	40,19± 12,18	892,05± 40,69
S4	1,50 ± 0,92	6,20 ± 2,00	2,52 ± 0,54	18,53± 11,36	25,17± 8,12	788,76± 169,02
S5	2,50 ± 0,21	9,00 ± 2,00	3,29 ± 0,73	30,88± 2,59	36,54± 8,12	1029,77± 228,49
S6	1,10 ± 0,09	3,70 ± 2,00	2,94 ± 0,21	13,59± 1,11	15,02± 8,12	920,22± 65,73
S7	2,10 ± 0,25	10,90 ± 3,00	5,41 ± 0,17	25,94± 3,09	44,25± 12,18	1693,33± 53,21
S8	3,70 ± 0,21	13,70 ± 1,00	3,70 ± 0,37	45,70± 2,59	55,62± 4,06	1158,10± 115,81
S9	4,10 ± 0,56	25,10± 1,00	3,67 ± 0,80	50,64± 6,92	101,91± 4,06	1148,71± 250,40
S10	3,00 ± 0,17	14,90 ± 1,00	4,71 ± 0,29	37,05± 2,10	60,49± 4,06	1174,23± 90,77

N.B: For S1, 2.60 is the mean of the uranium results for sample 1, while ± 0.19 is the standard deviation value.

1% of $^{40}K = 313$ Bq kg^{-1} (1)

1 ppm of $^{238}U = 12,35$ Bq kg^{-1} (2)

1 ppm of $^{232}Th = 4,06$ Bq kg^{-1} (3)

N.B: For S1, 2.60 is the mean of the uranium results for sample 1, while ±0,19 is the standard deviation value.

4. Results and Discussion

4.1.Activities of ^{238}U, ^{232}Th and ^{40}K

The distributions of the activities of ^{238}U, ^{232}Th and ^{40}K in the ten (10) analyzed topsoil samples are presented in form of bar charts, as revealed in figures 4a to 4c. The activities range from 12,35± 5,31 (S2) to 50,64± 6,92 (S9) Bq kg^{-1} for ^{238}U with an average of 29,40 Bq kg^{-1}, 11,37± 4,06 (S2) to 101,91± 4,06 (S9) Bq kg^{-1} for ^{232}Th with an average of 44,25 Bq kg^{-1}, and 788,76± 169,02 (S4) to 1693,3± 53,21 (S7) Bq kg^{-1} for ^{40}K with an average of 1072,07 Bq kg^{-1} respectively. The obtained results of S8, S9 and S10 for ^{238}U are greater than the global average value of 35 Bq kg^{-1}(Sartandel et al., 2009; Chandrasekaran et al., 2014). Apart from S2, S4 and S6 that showed lower values than the global recommended value of 30 Bq kg^{-1} (Chandrasekaran et al., 2014), other samples possessed higher results than the global average for ^{232}Th. However, the results obtained for ^{40}K have higher values than the recommended limit of 400 Bq kg^{-1} as reported by Chandrasekaran et al. (2014). The activities of ^{238}U, ^{232}Th and ^{40}K are in the order ^{238}U $<^{232}Th$ $<^{40}K$ with only ^{238}U showed an average value below the world average value for radionuclides in soil samples of Odo Oba farm.

Thorium is a naturally occurring radioactive metal. This substance is almost present everywhere, at least in small amount. It is found in rocks, soil, surface water, groundwater, animals and plants. Most of the naturally occurring thorium exists as ^{232}Th (isotope). Apart from this natural isotope, there are more than ten (10) isotopes of thorium that can be produced artificially. Thorium does not easily dissolve in water or evaporate from soil or water into the air. The high values recorded for ^{232}Th might be attributed to the topographical settings of Odo Oba (Oba River Basin). From the literature (Adagunodo et al., 2017*b*), the transported materials by the river channels over the years are mixed with the soil structures of Odo Oba, because the study area possess a planar surface. Since the soil containing thorium can be washed into rivers and be transported to another plane (such as Odo Oba), this has justified the average value recorded for thorium which is greater than the global average by a factor of 1,5. Farmers working on this area can be exposed to thorium by inhaling contaminated dust. In addition, people eating food grown on this soil can be contaminated with thorium through transfer factor (ATSDR, 1990). Effects of being exposed to thorium through inhalation include cancers of different forms such as pancreas, lung and bone. It can even result into damage of the body systems or result into death. Other effects through ingestion include: liver diseases, and diseases in the blood stream (ATSDR, 2014). The presence of thorium in an environment can lead to further exposure to hazardous radioactive decay of thorium such as thoron and radium – isotopes of radon. It should be noted that exposure to thorium has not been linked with birth defects or sexual incapability from previous studies (ATSDR, 1990; 2014; Xing-an et al., 2014).

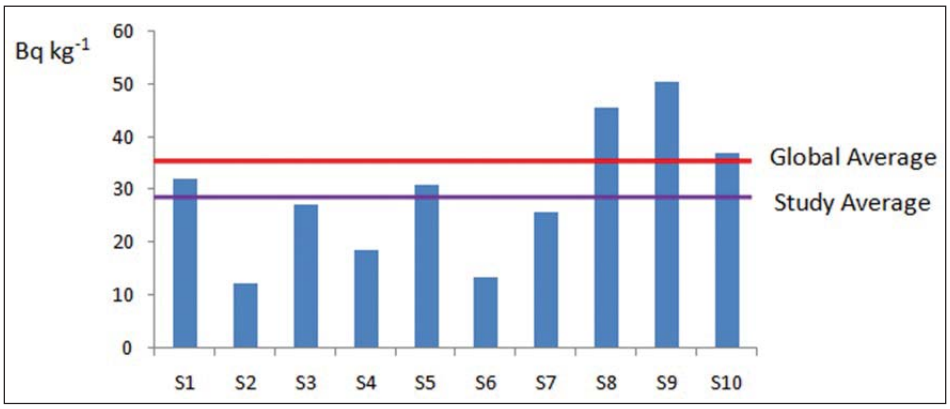

Figure 4a- Activity concentration of ^{238}U.

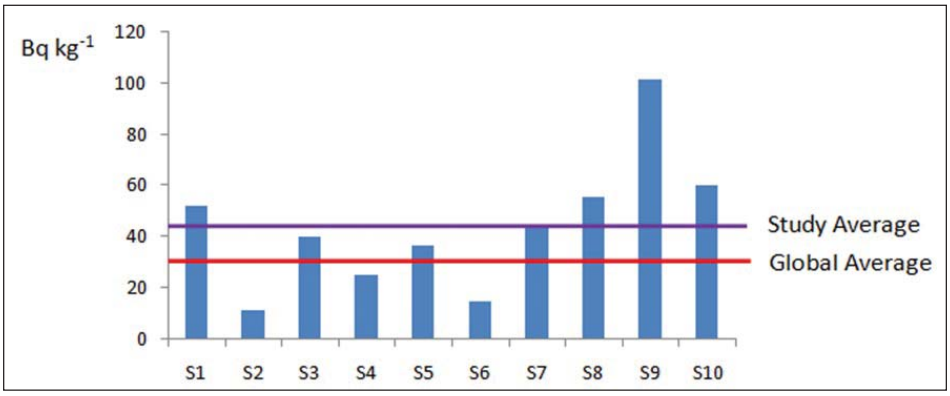

Figure 4b- Activity concentration of ^{232}Th.

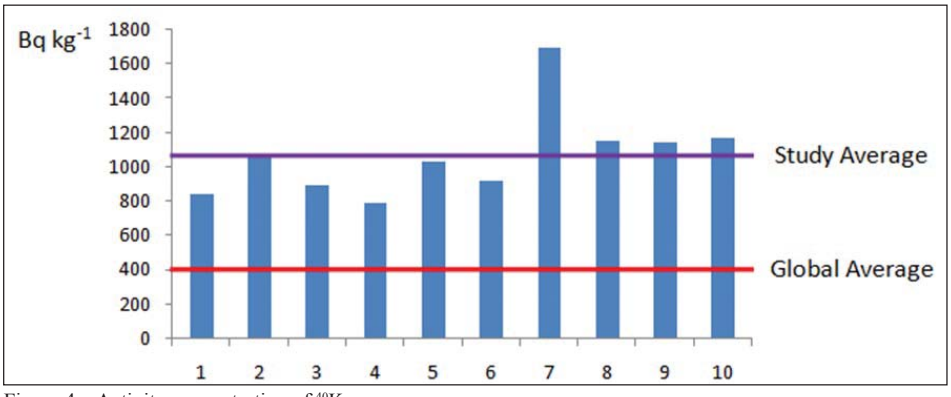

Figure 4c- Activity concentration of ^{40}K.

Potassium is essential in the body but exposure to potassium is worse than its inadequacy. The function of the kidney is to regulate the level of potassium in the body, but for many reasons, the potassium level can exceed the required limit. High concentration of potassium in the body is referred to as hyperkalemia. Effects of high concentration of potassium in the body systems include: nausea, stomach upset, diarrhea, weakness or tiredness, vomiting, tingling, intestinal gas, trouble in breathing, chest pain, listlessness, paralysis, mental confusion, dizziness, irregular heart rhythm or palpitation, low blood pressure, and possibly death (Beckerman, 2016; Wint and Cherney, 2017). The average value recorded for ^{40}K in Odo Oba is greater than the global average by the factor of 2.7.

The ratios of the radioactivity concentrations were estimated and presented in table 2. The ratios of ^{238}U to ^{40}K ranged from 0,012 (S2) to 0,044 (S9), the ratios of ^{232}Th to ^{40}K ranged from 0,011 (S2) to

Table 2- Radioactivity ratios in Odo Oba.

Samples	$^{238}U/^{40}K$	$^{232}Th/^{40}K$	$^{238}U/^{232}Th$	$^{232}Th/^{238}U$
1	0,038	0,062	0,618	1,618
2	0,012	0,011	1,086	0,921
3	0,030	0,045	0,676	1,479
4	0,023	0,032	0,736	1,358
5	0,030	0,035	0,845	1,183
6	0,015	0,016	0,905	1,105
7	0,015	0,026	0,586	1,706
8	0,039	0,048	0,822	1,217
9	0,044	0,089	0,497	2,012
10	0,032	0,052	0,612	1,633
Average	0,028	0,042	0,738	1,423
World Average	0,067[+]	0,067[+]	0,260[+]	3,500[+]

[+] represents UNSCEAR (1988).

0,089 (S9), the ratios of ^{238}U to ^{232}Th ranged from 0,497 (S9) to 1,086 (S2), while that of ^{232}Th to ^{238}U ranged from 0,921 (S2) to 2,012 (S9). The mean of each of the ratio as presented in Table 2 is compared with global average as reported by UNSCEAR (1988) and Qureshi et al. (2014). From the mean of all the estimated activities' ratios, only $^{238}U/^{232}Th$ is greater than the global average by the factor of 2,8, others fall below the global average limit. From table 2, it was revealed that the radioactive level of thorium is greater than that of uranium, hence 90% of $^{238}U/^{232}Th$ results are less than 1 while $^{232}Th/^{238}U$ results are greater than 1. The ratios of thorium to potassium and uranium to potassium are less than 1, because concentrations of potassium are higher than thorium, and uranium concentrations are far less when compared with potassium concentrations. Based on the ratios, there is depletion in uranium and enrichment in thorium concentration in Odo Oba farm (Tzortzis and Tsertos, 2004).

4.2. Dose Rates (DR) and Annual Effective Doses (AED)

The absorbed Dose Rates (DR) ascribed to gamma radiation emanating from subsurface (that is, dose rates from outdoor contributions) as a result of activity concentration of ^{238}U, ^{232}Th and ^{40}K at one meter above the topsoil were estimated in accordance with UNSCEAR (1993) guidelines, assuming that other naturally-occurring radionuclides' (^{87}Rb, ^{147}Sm, ^{235}U, ^{90}Sr, ^{138}La, ^{137}Cs, ^{87}Rb and ^{178}Lu) contributions to the doses from the environmental background are frivolous (Qureshi et al., 2014; Ravisankar et al., 2016). The conversion factors used to estimate the absorbed dose rates in the dry weight of each sample corresponds to 0,436, 0,599 and 0.0417 (nGy h^{-1} Bq^{-1} kg^{-1}) for ^{238}U, ^{232}Th and ^{40}K respectively (Qureshi et al., 2014). However, the absorbed dose rates are estimated using Eq. (4) as given by UNSCEAR (2000).

$$DR = 0,436\ C_U + 0,599\ C_{Th} + 0,0417\ C_K \quad (4)$$

where C_U, C_{Th} and C_K are the activities of ^{238}U, ^{232}Th and ^{40}K respectively. The estimated dose rates in Odo Oba farm range from 53.3 (S6) to 131,0 (S9) nGy hr^{-1} (Figure 5a). The average outdoor dose rate in Odo Oba is higher than the global average of 59 nGy hr^{-1} (UNSCEAR, 2000) by the factor of 1.4

The outdoor Annual Effective Dose (AED) is estimated based on Eq. (5) as given by UNSCEAR (2000) and Qureshi et al. (2014).

$$AED = 8760\ hr\ y^{-1} \times 0,7\ Sv\ Gy^{-1} \times 10^{-6} \times 0,2 \quad (5)$$

From Eq. (5), the outdoor occupancy factor is given as 20% (with an assumption that farmers spend 20% of a day on the field) of hours in 365 days that makes a year. However, the conversion factor that converts external absorbed doses to outdoor annual effective doses is given as 0,7 Sv Gy^{-1}.

In this study, the outdoor annual effective doses range from 0.06 (S2, S4 and S6) to 0,16 (S9) mSv $year^{-1}$ with an average 0.1 mSv $year^{-1}$ (Figure 5b). This value is higher than the global average of 0.07 mSv $year^{-1}$ (UNSCEAR, 2000; Qureshi et al., 2014) by factor of 1,4.

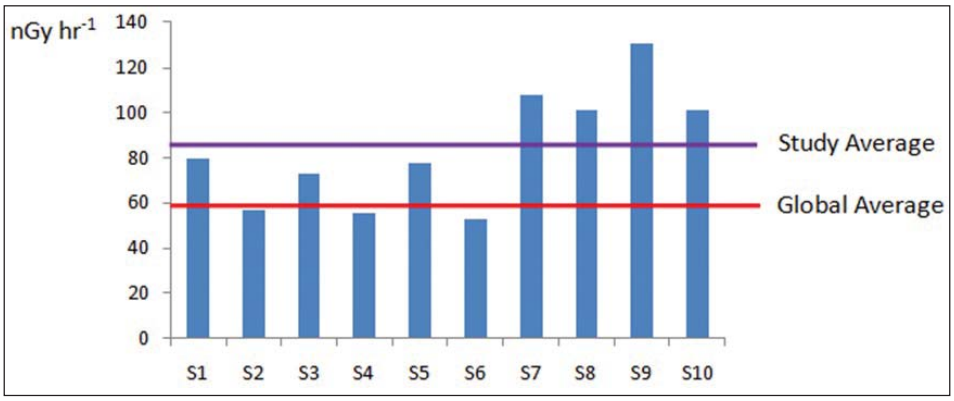

Figure 5a- The absorbed dose roses distributions on Odo Oba farm.

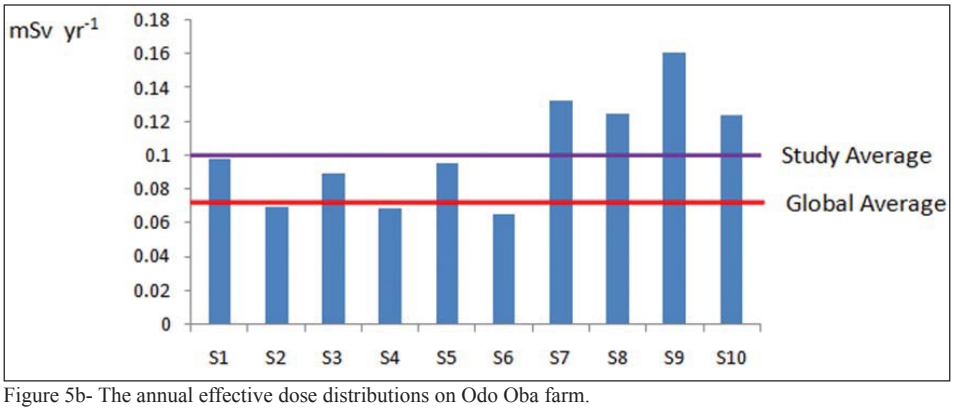

Figure 5b- The annual effective dose distributions on Odo Oba farm.

4.3. Annual Gonadal Equivalent Dose (AGED)

The gonad, bone marrow and the bone surface cells are essential in terms of assessment of level of exposure of human organs to natural occurring radionuclides (UNSCEAR, 1988). It is crucial to include AGED as parts of our assessment to farmers' exposure to natural radionuclides on Odo Oba farm, because farm activities require longer time to execute. As a result of this, AGED emanating from the farm land needs to be estimated. Therefore, the AGED due to activity concentrations of ^{238}U, ^{232}Th and ^{40}K was estimated based on Eq. (6) as given by Mamont-Ciesla et al. (1982).

$$AGED\ (\mu Sv\ y^{-1}) = 3{,}09\ C_U + 4{,}18\ C_{Th} + 0{,}314\ C_K \quad (6)$$

This parameter (that is, AGED) has been used by some authors as part of the radioactivity risk assessment in an environment (Avwiri et al., 2012; Chandrasekara et al., 2014; Ravisankar et al., 2016). The AGED of Odo Oba is presented in figure 6. The values range from 393,7 (S6) to 943,2 (S9) µSv y^{-1}. As it is revealed from figure 6, the mean value in

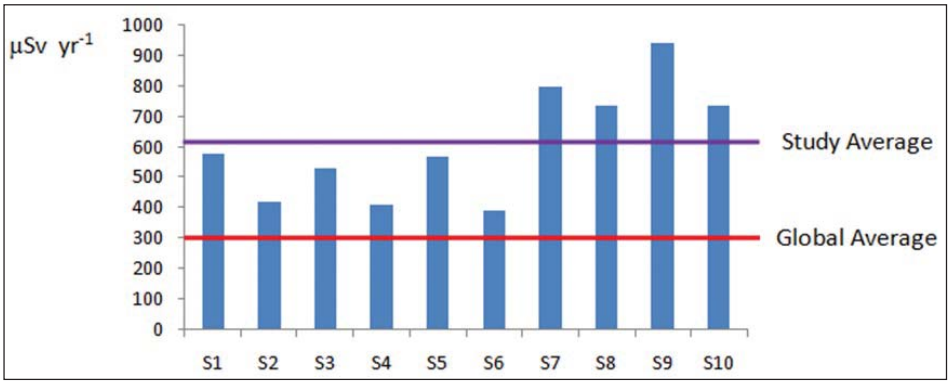

Figure 6- Distributions of annual gonadal equivalent doses on Odo Oba farm.

this present study (612,4 μSv y^{-1}) exceed the global average of 300 μSv y^{-1} by the factor of 2. This result is considered to be hazardous to the farmers in Odo Oba.

4.4. External and Gamma Radiation Hazard Indices

The two indices employed in this present assessment for farmers' exposure to gamma radiation are external radiation hazard index (H_{Ext}) and gamma radiation hazard index ($I_{\gamma r}$). The external radiation hazard index (H_{Ext}) in Odo Oba is estimated based on the model from Krieger (1981), Ibrahiem, (1999), UNSCEAR (2000), and Ravisankar et al. (2016). This equation is presented in Eq. (7).

$$H_{Ext} = \frac{C_U}{370} + \frac{C_{Th}}{259} + \frac{C_K}{4810} \leq 1 \quad (7)$$

The conversion factor of each of the three concentrations (^{238}U, ^{232}Th and ^{40}K) is based on the assumption that 370, 259 and 4810 (Bq kg^{-1}) of ^{238}U, ^{232}Th and ^{40}K produce the same gamma radiation dose rate (OECD, 1979; Akinloye et al. 2012; Qureshi et al. 2014; Ravisankar et al. 2016).The estimated external radiation hazard index in Odo Oba varies from 0,3 (S2, S4 and S6) to 0,9 (S9). The estimated average value of H_{Ext}in Odo Oba is 0,6 (Figure 7). This clearly showed that contributions from H_{Ext} are insignificant and pose no threat or radiological risks to the farmers since it is less than unity.

Gamma radiation hazard index ($I_{\gamma r}$) is one of the indices used to measure the safety of humans when they are exposed to γ-radiation emanating from subsurface (EC, 1999; UNSCEAR, 2000). The $I_{\gamma r}$used in this study is presented in Eq. (8) as given by OECD (1979), Alam et al. (1999) and Uosif et al. (2014).

$$I_{\gamma r} = 0{,}0067\ C_U + 0{,}01\ C_{Th} + 0{,}00067\ C_K \leq 1 \quad (8)$$

where C_U, C_{Th} and C_K have the same definitions as in Eq. (4), (6) and (7) respectively.

The estimated $I_{\gamma r}$ fluctuate from 0.8 (S6) to 2.1 (S9). The average $I_{\gamma r}$ in Odo Oba is 1.4. This is greater than the global average as presented in Eq. (8). From the ten samples analyzed, 30% fluctuate below unity while 70% vividly exceed the acceptable limit (Figure 7). The implication of $I_{\gamma r}$ results is that the radiation emitted from the study area is toxic to man's health as reported by Palomo et al. (2010) and Uosif et al. (2014).

4.5. Excess Lifetime Cancer Risk

Excess Lifetime Cancer Risk (ELCR) is estimated from Eq. (9) as given by Eq. (9).

$$\text{ELCR} = \text{Annual Effective Dose} \times 70 \times 0{,}05 \quad (9)$$

ELCR depends greatly on the results of annual effective dose and other two constants. The first constant (70) is referred to as duration of life which is given as 70 years while the second constant (0.05) is the risk factor which is given as 0,05 S_v^{-1} (ICRP-60, 1990; Taskin et al., 2009; Chandrasekaran et al., 2014; Qureshi et al., 2014; Ravisankar et al., 2016). For stochastic effect, 0.05 was ascribed to the public (ICRP-60, 1990). ELCR is another risk from radiological hazards. It measures the possibility of

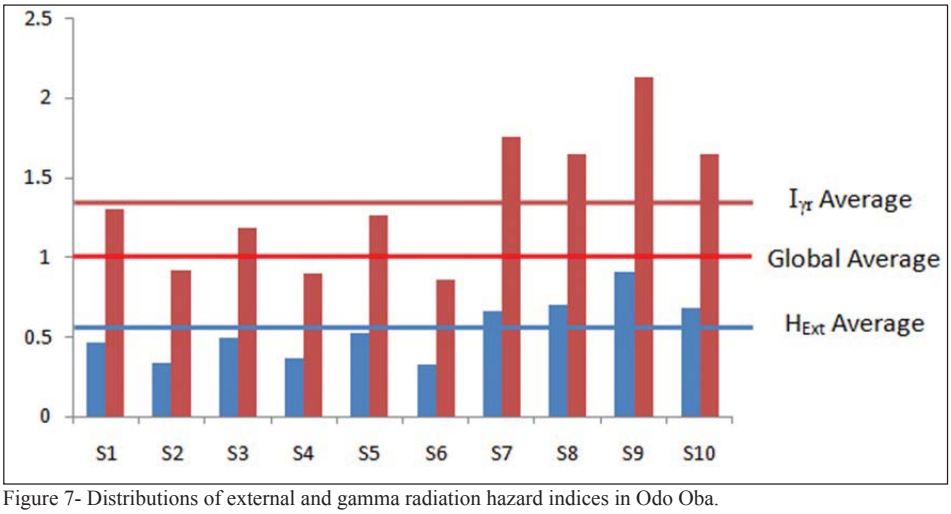

Figure 7- Distributions of external and gamma radiation hazard indices in Odo Oba.

having cancer if someone is overexposed to cancer-causing environment. The estimated range of cancer risk in Odo Oba is 0,23 × 10^{-3} (S6) to 0,56 × 10^{-3} (S9) with a mean of 0,36 × 10^{-3}. This value is higher than the global average of 0,29×10^{-3}(Ravisankar et al. 2007; UNSCEAR, 2000) by the factor of 1.2 (Figure 8).Virtually, only three locations (S2, S4 and S6) (that is, 30% of the total samples) depict lower values than the global average, others depict a higher degree than the recommended limit which varied in factors from 1.1 to 1.9.

4.6. Statistical Analyses of All the Data Sets

The descriptive analysis and multivariate statistics were employed under this section in order to examine the relationship between the variables used in this study. This approach has been found useful from the literature in the recent times (Chandrasekaran et al., 2014; Isinkaye and Emelue, 2015; Raghu et al., 2017). Variations of the mean, standard deviation, skewness, kurtosis, and the global average of all the variables are presented in table 3.

Skewness and kurtosis are parts of data characterization in statistical analysis. The skewness defines the symmetric or asymmetric distributions of data sets. For a normal distribution, skewness is always zero, and nearly equals zero for symmetric data. The skewness with negative value signifies that the data is skewed left and vice versa. The kurtosis measures the 'tailedness' of a normal distribution, whether it is heavy-tailed or light-tailed. Data sets with high kurtosis showed that there are outliers (that is, heavy tails) and vice versa. These two parameters have been used to discuss the variability of data sets by Adagunodo et al. (2017*b*), (2018*a*) and (2018*c*). The skewness and kurtosis were estimated by Eqs. (10) and (11) respectively. Potassium-40 possesses highest values of mean and standard deviation of 1072,07 and 258,28, with the ELCR showing the least mean and standard deviation value of 0,36 × 10^{-3} and 0.11×10^{-3} respectively. Only ^{238}U / ^{40}K showed negative skewness, four (4) variables (^{232}Th, ^{40}K, ^{232}Th / ^{40}K and ^{238}U / ^{232}Th) showed positive kurtosis while 69% of the total variables showed negative kurtosis.

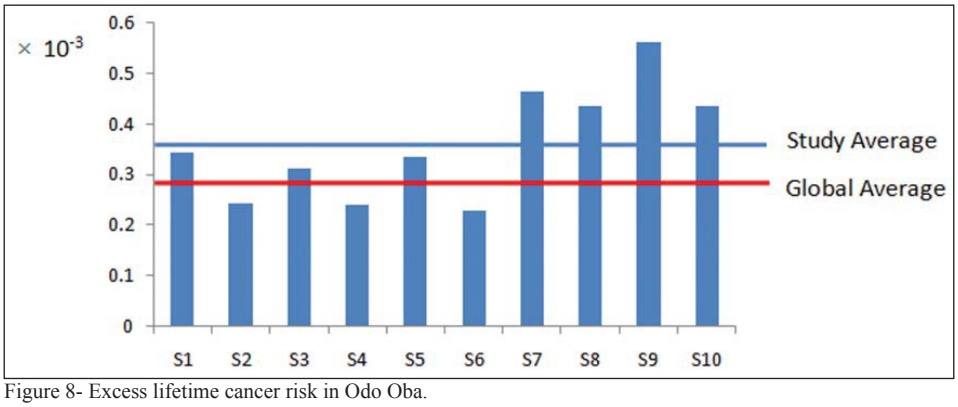

Figure 8- Excess lifetime cancer risk in Odo Oba.

Table 3- Descriptive statistics for the analyzes datasets (N = 10).

Variable	Mean	SD	Skewness	Kurtosis	Global mean as presented in this study
^{238}U	29,40	12,74	0,28	-0,70	35,0 Bq kg^{-1}
^{232}Th	44,25	26,15	1,01	1,81	30,0 Bq kg^{-1}
^{40}K	1072,07	258,23	1,59	3,51	400,0 Bq kg^{-1}
DR	84,03	25,90	0,45	-0,71	59 mGy hr^{-1}
AED	0,10	0,03	0,45	-0,71	0,07 mSv yr^{-1}
AGED	612,44	185,03	0,44	-0,82	300 µSv yr^{-1}
ELCR	0,36 × 10^{-3}	0,11 × 10^{-3}	0,45	-0,71	0,29 × 10^{-3}
^{238}U / ^{40}K	0,03	0,01	-0,17	-1,30	0,067
^{232}Th / ^{40}K	0,04	0,02	0,73	0,77	0,067
^{238}U / ^{232}Th	0,74	0,18	0,67	0,08	0,260
^{232}Th / ^{238}U	1,42	0,33	0,24	-0,41	3,5
H_{Ext}	0,55	0,19	0,44	-0,32	1,0
$I_{\gamma r}$	1,36	0,42	0,46	-0,67	1,0

$$\text{Skewness} = \frac{\sqrt{N(N-1)}}{N-2} \frac{\sum_{i=1}^{N}\left(Y_i - \bar{Y}\right)^3 / N}{s^3} \quad (10)$$

where N is the number of data points or population number, Y is the individual data, $\bar{Y}$ is the mean, s is the standard deviation, and i is the integer.

$$\text{Kurtosis} = \sum_{i=1}^{N} \frac{\left(Y_i - \bar{Y}\right)^4 / N}{s^4} - 3 \quad (11)$$

The multivariate analyses employed are Pearson's correlation, factor analysis, and cluster analysis. The multivariate analysis has been found useful in explanation of correlation among varying data sets without losing much information (Ashley and Lloyd, 1978; Jackson, 1991; Chandrasekaran et al., 2014; Adagunodo et al., 2017*b*). This approach is efficient in data compression without losing its original information, and helpful to draw relationships between or among variables (Chandrasekaran et al., 2014).

A bivariation statistics involving correlation matrix was carried out and presented in table 4, with a view to determining the nature of relationships that exist between the thirteen (13) variables analyzed in ten (10) samples used in this study. A very strong positive correlation exists between ^{232}Th and ^{238}U. This is because the two elements undergo their decay series simultaneously (Tanaskovi et al., 2012). The correlation between ^{40}K and ^{232}Th as well as ^{40}K and ^{238}U are very weak. This might be associated with the different decay series between the two parameters, since ^{40}K has no progeny like ^{238}U and ^{232}The. Generally, very strong positive correlations exist between ^{238}U and the radiological indices as well as radioelements' ratios except ^{238}U / ^{232}Th that showed very strong negative correlation. The correlations between ^{232}Th and the radiological indices, ^{232}Th and radioelements' ratios resemble the type of correlations with uranium-238 and its radiological indices. A very strong positive correlation exist between the radiological indices, while negative correlations exist between ^{40}K and radioelements' ratios except ^{232}Th / ^{238}U that showed very strong positive correlation. The correlation has further confirmed that radiological indices exist due to radionuclides' activities. The approach of correlation analysis has justified that uranium depletion with thorium and potassium enrichments exist in the study area.

The Factor Analysis (FA) was also performed on the variables in order to establish relationship among the parameters (Rodrigues-Barroso et al., 2009; Ramasamy et al., 2011; Chandrasekaran et al., 2014). The FA is carried out on the Pearson's correlation matrix data sets. The extraction method for the factor was achieved through Principal Component Analysis (PCA), which was further rotated by varimax. The communalities of the thirteen (13) variables were presented in table 5. Based on Kaiser's rule with eigen values ≥ 1 (Kaiser, 1960), the initial eigen value of the variables is 1 with the extraction varying from 0,675 (the extraction of ^{238}U / ^{232}Th) to 0,995 (the extraction of DR, AED, AGED, ELCR and $I_{\gamma r}$). Two components were produced from the component matrix based on PCA extraction method (Table 6). Component 1 accounted for 51,30% of the total variance, which constitute high levels of variables such as H_{Ext}, AED, ELCR, DR, AGED, ^{232}Th, ^{238}U, ^{232}Th / ^{40}K, ^{232}Th / ^{238}U, ^{238}U / ^{40}K, ^{238}U / ^{232}Th and ^{40}K with high positive loading varying from 0,741 to 0,991. AED, DR and ^{40}K showed the same loading of 0,977 while AGED and ELCR also showed the loading of 0,972.

Table 4- Pearson's correlation matrix among the analyzed parameters in Odo Oba farm.

Variables	^{238}U	^{232}Th	^{40}K	DR	AED	AGED	ELCR	^{238}U / ^{40}K	^{232}Th / ^{40}K	^{238}U / ^{232}Th	^{232}Th / ^{238}U	H_{Ext}	$I_{\gamma r}$
^{238}U	1,00												
^{232}Th	0,93	1,00											
^{40}K	0,23	0,27	1,00										
DR	0,87	0,91	0,63	1,00									
AED	0,87	0,91	0,63	1,00	1,00								
AGED	0,86	0,91	0,64	1,00	1,00	1,00							
ELCR	0,87	0,91	0,63	1,00	1,00	1,00	1,00						
^{238}U / ^{40}K	0,90	0,82	-0,19	0,61	0,61	0,60	0,61	1,00					
^{232}Th / ^{40}K	0,88	0,94	-0,05	0,73	0,73	0,72	0,73	0,92	1,00				
^{238}U / ^{232}Th	-0,63	-0,79	-0,26	-0,72	-0,72	-0,71	-0,72	-0,59	-0,76	1,00			
^{232}Th / ^{238}U	0,64	0,84	0,32	0,78	0,78	0,78	0,78	0,56	0,80	-0,97	1,00		
H_{Ext}	0,93	0,95	0,51	0,99	0,99	0,99	0,99	0,72	0,81	-0,73	0,78	1,00	
$I_{\gamma r}$	0,87	0,92	0,62	1,00	1,00	1,00	1,00	0,62	0,74	-0,72	0,79	0,99	1,00

Concentration of ^{238}U is the most significant factor to the contributions of component 1. Component 2 accounted for 42,15% of the total variance, which constitute high positive loading of 0,881 for $I_{\gamma r}$. The results of the two components revealed that exposure to radiological hazards in the study area are chiefly from ^{40}K, ^{238}U and ^{232}Th respectively. The plot of eigen value against the component number is presented in figure 9. However, the graphical representation of the two components is presented in figure 10. The plot of the two components revealed that ^{238}U / ^{232}Th and ^{40}K reside in the same community (quadrant 1) with AED, DR, AGED, ^{232}Th / ^{238}U and $I_{\gamma r}$; while H_{Ext}, ELCR, ^{232}Th / ^{40}K, ^{238}U / ^{40}K and ^{238}U / ^{232}Th reside in the fourth quadrant respectively.

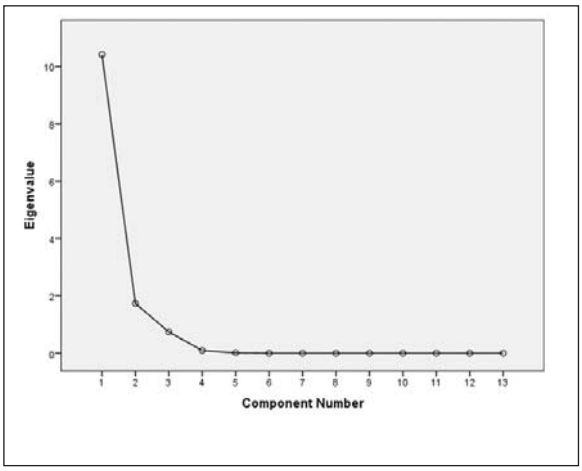

Figure 9- The scree plot of the eigen values against the component number.

Table 5- Communality of the variables.

Variables	Initial	Extraction
^{238}U	1,000	0,895
^{232}Th	1,000	0,982
^{40}K	1,000	0,990
DR	1,000	0,995
AED	1,000	0,995
AGED	1,000	0,995
ELCR	1,000	0,995
^{238}U / ^{40}K	1,000	0,927
^{232}Th / ^{40}K	1,000	0,985
^{238}U / ^{232}Th	1,000	0,675
^{232}Th / ^{238}U	1,000	0,734
H_{Ext}	1,000	0,986
$I_{\gamma r}$	1,000	0,995

Extraction method: PCA

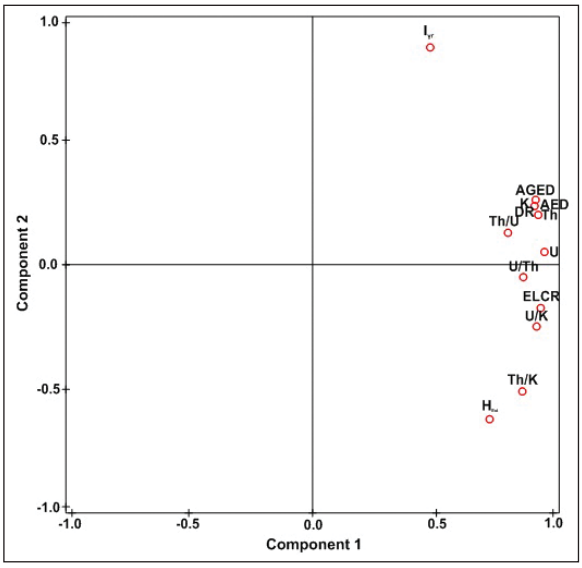

Figure 10- Graphical representation of component 1 and component 2.

Table 6- Component matrix of the variables.

Variables	Component	
	1	2
^{238}U	0,991	0,065
^{232}Th	0,978	0,196
^{40}K	0,977	0,201
DR	0,977	0,201
AED	0,977	0,201
AGED	0,972	0,224
ELCR	0,972	-0,194
^{238}U / ^{40}K	0,919	-0,225
^{232}Th / ^{40}K	0,855	-0,504
^{238}U / ^{232}Th	0,853	-0,083
^{232}Th / ^{238}U	0,809	0,144
H_{Ext}	0,741	-0,615
$I_{\gamma r}$	0,462	0,881
% of variance explained	51,30%	42,15%

Extraction method: PCA

A multivariate statistical technique known as Hierarchical Cluster Analysis (HCA) was adopted to classify the thirteen (13) variables of all the ten (10) occupied stations in this study into categories based on their similarities and to produce dendrogram (Figure 11). A dendrogram is a tree-structured graph that enables one to view the output of calculations from HCA (Fatoba et al., 2017). The output of HCA is usually represented as the distance between the clustered columns or rows based on the description of each measured parameter. The distance or order in dendrogram is estimated based on Eq. (12).

$$\frac{D_{Link}}{D_{Max}} \times 100 \qquad (12)$$

where D_{Link} is the quotient between the linkage distances for certain case, D_{Max} is the maximal linkage distance. The constant in the equation (that is, 100) is used to standardize the linkage distance (Wunderlin et al., 2001; Fatoba et al., 2017). The linkage distance among the variables was estimated using squared Euclidean distance, and the Ward's method was employed for the clustering technique. The most similar variables appear as the first group, while the incongruous variables are far from each other on the dendrogram (Ramasamy et al., 2011; Chandrasekaran et al., 2014). In another words, the distance between any two variables within the clusters are referred to as similarity. Two variables with no distance between them signify 100% similarity, while variables that are disparate are said to possess 0% similarity.

The closest clusters produced are ^{238}U / ^{232}Th – ^{40}K, H_{Ext} – (AED, ELCR, DR), and (AGED, ^{232}Th) – ^{232}Th / ^{40}K, with potassium and thorium being the major natural radionuclide contributors within these clusters. The next clusters produced are ^{238}U / ^{232}Th – ^{238}U / ^{40}K, $I_{\gamma r}$ – ^{238}U, and H_{Ext} – (AGED, ^{40}K), with uranium and thorium being the natural radionuclides in these clusters. From figure 12, five parameters (AED, ELCR, DR, AGED and ^{232}Th) were categorized as two variables. The first category combined three variables which are AED, ELCR and DR, while two variables (AGED and ^{232}Th) were the second set of combined variables. These are as a result of their loading on component matrix (Table 5) which share loadings 0,977 and 0,972 respectively. In the larger clusters, three (3) clusters were present based on the observation from the top. Cluster-I is made up of nine (9) variables. These are ^{238}U / ^{232}Th, ^{40}K, ^{238}U / ^{40}K, $I_{\gamma r}$, ^{238}U, H_{Ext}, (AED, ELCR, DR), (AGED, ^{232}Th) and ^{232}Th / ^{40}K. Cluster-II comprised two variables, which are ^{40}K and ^{238}U. However, only one variable was observed in Cluster-III, which is ^{232}Th / ^{238}U. The dendrogram was able to show from Cluster-I that the radiological hazards occur as a result of contributions from the three naturally occurring radionuclides (that is, thorium, uranium and potassium).

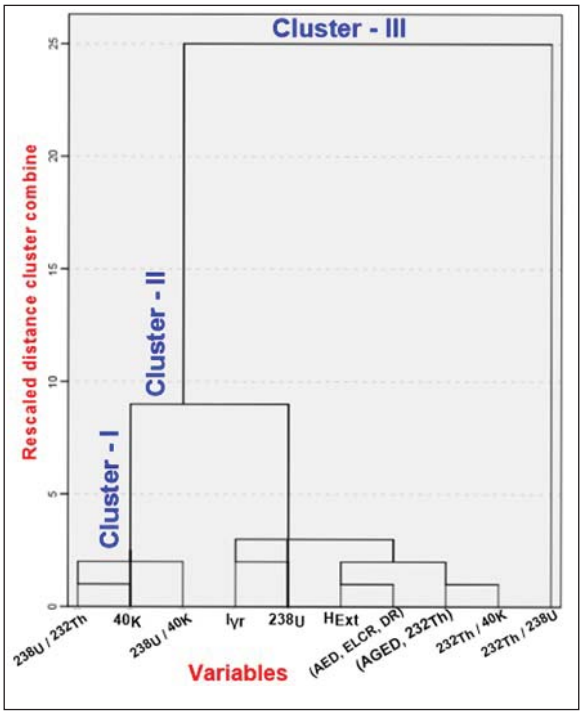

Figure 11- Dendrogram of the HCA of radioactivity concentrations and radiological risks.

5. Conclusion

The concentrations of thorium, uranium and potassium in the ten randomly selected topsoil samples from Odo Oba were determined using ICP-MS from ACME laboratories, Canada. The risks (DR, AED, AGED, ELCR, H_{Ext} and $I_{\gamma r}$) and radioelements' ratios were estimated from the naturally occurring radionuclides in the study area. The mean concentrations of thorium and potassium are greater than the global average of 30 and 400 Bq kg^{-1} while uranium fall below the global average of 35 Bq kg^{-1}. In comparison with the results of other studies from Nigeria and other parts of the world (as presented in table 7), it was revealed that this present study is in agreement with their outcome, except for few cases where the results were below the global average (such as Akinloye et al. (2012), Avwiri et al. (2012) and Isola et al. (2015)). The high concentrations of thorium in the study area are associated with the nature of the terrain, as the thorium enriched materials carried from afar are deposited around Odo Oba over years. Farmers working on Odo Oba can be exposed to thorium by inhaling contaminated dust. The crops grown on the farm land can be contaminated and be transferred to humans by consumption. The estimation of radioactivity ratios showed that depletion of uranium and enrichment of thorium occur in the study area. The estimated radiological risks showed that the mean values of DR, AED, AGED, ELCR and $I_{\gamma r}$ are greater than the global average by the factors of 1,42; 1,43; 2,04; 1,24 and 1,36 respectively. However, the mean of $H_{Ext} < 1$ fall below the global average. The farmers are advised to take safety measures whenever on the farm land in order to prevent themselves from

Table 7- Comparison of the results of radioactivity concentrations in this study with other works.

Authority	^{238}U (Bq kg^{-1})	^{232}Th (Bq kg^{-1})	^{40}K (Bq kg^{-1})	Location
Present study	29,40	44,25	1072,07	SW, Nigeria
Isola et al. (2015)	23,39	19,37	165,14	SW, Nigeria
Akinloye et al. (2012)	25,55	11,60	191,78	SW, Nigeria
Adagunodo et al. (2018*a*)	38,17	65,11	93,90	SW, Nigeria
Adagunodo et al. (2018*b*)	46,67	71,76	108,73	SW, Nigeria
Avwiri et al. (2012) site 1	13,71	10,45	57,17	SE, Nigeria
Avwiri et al. (2012) site 2	11,49	8,83	59,77	SE, Nigeria
Isinkaye and Emelue (2015)	47,89	55,37	1023,00	SE, Nigeria
Chandrasekaran et al. (2014)	19,16	48,56	1146,88	India
Ravisankar et al. (2016)	9,19	45,60	295,11	India
Raghu et al. (2017)	116,10	43,51	300,07	India
Turhan (2009) site 1	39,30	49,60	569,50	Turkey
Turhan (2009) site 2	82,00	94,80	463,60	Turkey

being overexposed to natural radionuclides. However, further studies are recommended in Odo Oba and its environment in order to have a comprehensive report on the radiation level of the environment.

Acknowledgement

The handling Editor of this article and the reviewers are highly appreciated for their contributions.

References

Adagunodo, T.A., Sunmonu, L.A. 2012. Groundmagnetic Survey to Investigate on the Fault Pattern of Industrial Estate Ogbomoso, Southwestern Nigeria. Advances in Applied Science Research 3(5), 3142–3149.

Adagunodo, T.A., Sunmonu, L.A., Ojoawo, A., Oladejo, O.P., Olafisoye, E.R. 2013*a*. The Hydro Geophysical Investigation of Oyo State Industrial Estate Ogbomosho, Southwestern Nigeria Using Vertical Electrical Soundings. Research Journal of Applied Sciences, Engineering and Technology 5(5), 1816–1829.

Adagunodo, T.A., Sunmonu, L.A., Oladejo, O.P., Ojoawo, I.A. 2013*b*. Vertical Electrical Sounding to Determine Fracture Distribution at Adumasun Area, Oniye, Southwestern Nigeria. IOSR Journal of Applied Geology and Geophysics 1(3), 10–22.

Adagunodo, T.A., Sunmonu, L.A., Oladejo, O.P., Olafisoye, E.R. 2013*c*. Groundmagnetic Investigation into the Cause of the Subsidence in the Abandoned Local Government Secretariat, Ogbomoso, Nigeria. ARPN Journal of Earth Sciences 2(3), 101–109.

Adagunodo, T.A., Adeniji, A.A., Erinle, A.V., Akinwumi, S.A., Adewoyin, O.O., Joel, E.S.,Kayode,O.T. 2017*a*. Geophysical Investigation into the Integrity of a Reclaimed Open Dumsite for Civil Engineering Purpose.Interciencia Journal 42(11), 324 – 339.

Adagunodo, T.A., Sunmonu, L.A., Adabanija, M.A., Suleiman, E.A., Odetunmibi, O.A. 2017*b*. Geoexploration of Radioelement's Datasets in a flood plain of Crystalline Bedrock. Data in Brief 15, 809 – 820. https://doi.org/10.1016/j.dib.2017.10.046.

Adagunodo, T.A., George, A.I., Ojoawo, I.A., Ojesanmi, K., Ravisankar, R. 2018*a*. Radioactivity and Radiological Hazards from a Kaolin Mining Field in Ifonyintedo, Nigeria. MethodsX, 5C: 362 – 374. https://doi.org/10.1016/j.mex.2018.04.009.

Adagunodo, T.A., Hammed, O.S., Usikalu, M.R., Ayara, W.A., Ravisankar, R. 2018*b*. Data on the Radiometric Survey over a Kaolinitic Terrain in Dahomey Basin, Nigeria. Data in Brief 18C, 814 – 822. https://doi.org/10.1016/j.dib.2018.03.088.

Adagunodo T.A., Sunmonu L.A., Emetere M.E. 2018*c*. Heavy Metals' Data in Soils for Agricultural Activities. Data in Brief, 18C, 1847 – 1855. https://doi.org/10.1016/j.dib.2018.04.115.

Ademola, A.K., Olaoye, M.A., Abodunrin, P.O. 2015. Radiological Safety Assessment and Determination of Heavy Metals in Soil Samples from some Waste Dumpsites in Lagos and Ogun State, South-western, Nigeria. Journal of Radiation Research and Applied Sciences 8, 148 – 153.

Agency for Toxic Substances and Disease Registry (ATSDR) 1990. Public Health Statement Thorium. Summary Chapter from the Toxicological Profile for Thorium, Series of Public Health Statements about Hazardous Substances and their Health Effects, CAS#, 7440 – 29 – 1.

Agency for Toxic Substances and Disease Registry (ATSDR) 2014. Toxic Substances Portal –Thorium. Atlanta GA: Centers for Disease Control and Prevention. Retrieved on October 18, 2017.

Akinloye, M.K., Isola, G.A., Oladapo, O.O. 2012. Investigation of Natural Gamma Radioactivity levels and Associated Dose Rates from Surface Soils in Ore Metropolis, Ondo State, Nigeria. Environment and Natural Resources Research 2(1), 140 – 145.

Alam, M.N., Chowdhury, M.I., Kamal, M., Ghose, S., Ismal, M.N. 1999. The 226Ra, 232Th and 40K Activities in Beach Sand Minerals and Beach Soils of Cox's Bazar, Bangladesh. Journal of Environmental Radioactivity 46(2), 243 – 250.

Alzubaidi, G., Fauzrah, S.H., Rahman, I.A. 2016. Assessment of Natural Radioactivity Levels and Radiation Hazards in Agricultural and Virgin Soil in the State of Kedah, North of Malaysia. The Scientific World Journal Article ID 6178103, 1 – 9. Dx.doi.org/10.1155/2016/6178103

Ashley, R.P., Lloyd, J.W. 1978. An example of the use of factor analysis and cluster analysis in groundwater chemistry interpretation. J. Hydrol. 39, 335 – 364.

Avwiri, G.O., Osimobi, J.C., Agbalagba, E.O. 2012. Evaluation of Radiation Hazard Indices and Excess Lifetime Cancer Risk due to Natural Radioactivity in Soil Profile of Udi and Ezeagu Local Government areas of Enugu State, Nigeria. Comprehensive Journal of Environmental and Earth Sciences 1(1), 1 – 10.

Bank, T., Roth, E., Tinker, P., Granite, E. 2016. Analysis of Rare Earth Elements in Geologic Samples using Inductively Coupled Plasma Mass Spectrometry. US DOE Topical Report – DOE/NETL – 2016/1794.

Beckerman, J. 2016. Potassium and your Hearth. WebMD Medical Reference, WebMD, LLC. Reviewed on October 6, 2016, Retrieved on October 18, 2017. https://www.webmd.com/heart-disease/potassium-and-your-heart.

Chandrasankaran, A., Ravisankar, R., Senthilkumar, G., Thillaivelavan, K., Dhinakaran, B., Vijayagopal, P., Bramha, S.N., Venkatraman, B. 2014. Spatial Distribution and Lifetime Cancer Risk due to Gamma Radioactivity in Yelagiri Hills, Tamilnadu, India. Egyptian Journal of Basic and Applied Science 1, 38 – 48.

European Commission (EC). 1999. Radiation Protection, 112-Radiological Protection Principles Concerning the Natural Radioactivity of Building Materials. Directorate-General Environment. Nuclear Safety and Civil Protection.

Fatoba, J.O., Sanuade, O.A., Hammed, O.S., Igboama, W.W. 2017. The use of multivariate statistical analysis in the assessment of groundwater hydrochemistry in some parts of southwestern Nigeria. Arab. J. Geosci. 10, 328. https://doi.org/10.1007/s12517-017-3125-7.

Food and Agriculture Organization of the United Nations (FAO). 2013. Agricultural Mechanization in Sub Saharan Africa: Guidelines for preparing a Strategy. Plant Production and Protection Division, Food and Agriculture Organization of the United Nations, Rome. ISBN 978-92-5-107762-7

Gbadebo, A.M., Amos, A.J. 2010. Assessment of Radionuclide Pollutants in Bedrocks and Soils from Ewekoro Cement Factory, Southwest Nigeria. Asian Journal of Applied Sciences 3(2), 135 – 144.

Ibrahiem, N. 1999. Natural Activity of 238U, 232Th and 40K in Building Materials. Journal of Environmental Radioactivity 43(3), 255 – 258.

International Atomic Energy Agency (IEAE). 1989. Construction and Use of Calibration Facilities for Radiometric Field Equipment. Technical Reports Series no. 309, IAEA, Vienna.

International Commission on Radiological Protection (ICRP)-60. 1990. Protection: 1990. Recommendations Methods Part I. Monoenergetic Sources of Natural Radionuclides in the Ground. GSF-B2/90 of ICRP. Pergamon Preis.

Isinkaye M.O., Emelue H.U. 2015. Natural radioactivity measurements and evaluation of radiological hazards in sediment of Oguta Lake, South East Nigeria. Journal of Radiation Research and Applied Sciences, 8, 459 – 469.

Isola G.A., Oni O.M., Akinloye M.K., Awodugba A.O. 2015. Determination of absorbed dose rate and effective dose equivalent due to natural radionuclide present in soil in Oyo and Osun state, South-western Nigeria. Impact: International Journal of Research in Applied, Natural and Social Sciences, 3(3), 27 – 32.

Jackson, J.E. 1991. A user's guide to Principal Components. New York: Wiley.

Jones, H.A., Hockey, R.D. 1964. The geology of the southwestern Nigeria. Geol. Surv. Nig. Bull. 31, pp 101.

Kaiser, H.F. 1960. The application of electronic computers to factor analysis. Educ. Psychol.Meas. 20,141–151.

Krieger, R. 1981. Radioactivity of Construction Materials. Betonw. Fert. Tech. 47, 468 – 473.

Obaje, N.G. 2015. Geology and mineral resources of Nigeria. In: Brooklyn, S.B., Bonn, H.J.N., Gottingen, J.R., Graz, K.S. (Eds.), Lecture notes in Earth Sciences 120. Springer, Pp 221.

Odunaike, R.K., Ozebo, V.C., Alausa, S.K., Alausa, I.M. 2008. Radiation Exposure to Workers and Villagers in and around some Quarry sites in Ogun State of Nigeria. Environmental Research Journal 2(6), 348 – 350.

Oladejo, O.P., Sunmonu, L.A., Ojoawo, A., Adagunodo, T.A., Olafisoye, E.R. 2013. Geophysical investigation for groundwater development at Oyo state housing estate Ogbomosho, southwestern Nigeria. Research Journal of Applied Science, Engineering and Technology 5(5), 1811 – 1815.

Olafisoye, E.R., Sunmonu, L.A., Ojoawo, A., Adagunodo, T.A., Oladejo, O.P. 2012. Application of Very Low Frequency Electromagnetic and Hydro-physicochemical Methods in the Investigation of Groundwater Contamination at Aarada Waste Disposal Site, Ogbomoso, Southwestern Nigeria. Australian Journal of Basic and Applied Sciences 6(8), 401–409.

Olafisoye, E.R., Sunmonu, L.A., Adagunodo, T.A., Oladejo, O.P. 2013. Impact Assessment of Solid Waste on Groundwater: a Case Study of Aarada Dumpsite, Nigeria. ARPN Journal of Earth Sciences 2(2), 45–53.

Omeje, M., Wagiran, H., Ibrahim, N., Lee, S.K., Sabris, S. 2013. Comparison of Activity Concentration of 238U, 232Th and 40K in different Layers of Subsurface Structures in Dei-Dei and Kubwa, Abuja Northcentral Nigeria. Radiation Physics and Chemistry 91, 70 – 80.

Organization for Economic Cooperation and Development (OECD). 1979. Exposure to Radiation from the Natural Radioactivity in Building Materials. Report by a group of Experts, Nuclear Energy Agency, Paris, France.

Palomo, M., Penalver, A., Aguilar, C., Bornull, F. 2010. Presence of Naturally Occurring Radioactive Materials in Sludge Samples from several Spanish Water Treatment Plants. Journal of Hazardous Materials 181(1 – 3), 716 – 720.

Qureshi, A.A., Tariq, S., Din, K.U., Manzoor, S., Calligaris, C., Waheed, A. 2014. Evaluation of Excessive Lifetime Cancer Risk due to Natural Radioactivity in the Rivers Sediments of Northern Pakistan. Journal of Radiation Research and Applied Sources 7, 438 – 447.

Rafique, M., Rahman, S.U., Basharat, M., Aziz, W., Ahmad, I., Lone, K.A., Ahmad, K., Matiullah 2014. Evaluation of Excess Life Time Cancer Risk from Gamma Dose Rates in Jhelum Valley. Journal of Radiation Research and Applied Sciences 7, 29 – 35.

Raghu, Y., Ravisankar, R., Chandrasekaran, A., Vijayagopa, P., Venkatraman, B. 2017. Assessment of natural radioactivity and radiological hazards in building materials used in the Tiruvannamalai District, Tamilnadu, India, using a statistical approach. Journal of Taibah University for Science, 11, 523 – 533.

Ramasamy, V., Suresh, G., Meenakshisundaram, V., Ponnusam, V. 2011. Horizontal and Vertical characterization of radionuclides and minerals in river sediments. Appl. Radiat. Isot. 69, 184 – 195.

Ravisankar, R., Rajalakshmi, A., Eswaran, P., Gajendrian, V., Meenakshisundram, V. 2007. Radioactivity Levels in Soils of Salt Field are Kelambakkam, Tamil Nadu, India. Nucl. Sci. Tech. 18, 372 – 375.

Rodriguez-Barroso, M.R., Garcia-Morales, J.L., Coello-Oviedeo, M.D., Quiroga-Alousa, J.M. 2009. An assessment of heavy metal contamination in surface sediments using statistical analysis. Environmental Monitoring Assessment 163, 489–501.

Ravisankar, R., Chandrasekaran, A., Vijayagopal, P., Venkatraman, B., Senthilkumar, G., Eswaran, P., Rajalakshmi, A. 2012. Natural Radioactivity in Soil Samples of Yelagiri Hills, Tamil Nadu, India and the Associated Radiation Hazards. Radiation Physics and Chemistry 81, 1789 – 1795.

Ravisankar, R., Chandramohan, J., Chandrasekaran, A., Jebakumar, J.P., Vijayalakshmi, I., Vijayagopal, P., Venkatraman, B. 2015. Assessments of Radioactivity Concentration of Natural Radionuclides and Radiological Hazard Indices in Sediment Samples from the East Coast of Tamilnadu, India with Statistical Approach. Marine Pollution Bulletin 97, 419 – 430.

Ravisankar, R., Raghu, Y., Chandrasekaran, A., Gandhi, M.S., Vijayagopal, P., Venkatraman, B. 2016. Determination of Natural Radioactivity and the Associated Radiation Hazards in Building Materials used in Polur, Tiruvannamalai District, Tamilnadu, India using Gamma Ray Spectrometry with Statistical Approach. Journal of Geochemical Exploration 163, 41 – 52.

River of Yorubaland. 2017. Oba River. Categories from Rivers of Nigeria, Osun State, Rivers of Yorubaland, https://en.wikipedia.org/wiki/Oba_River. Retrieved on October 15, 2017.

Sahoo, S.K., Yonehara, H., Kurotaki, K., Shiraishi, K., Ramzaev, V., Barkovski, A. 2001. Determination of Rare Earth Elements, Thorium and Uranium by Inductively Coupled Plasma Mass Spectrometry and Strontium Isotopes by Thermal Ionization Mass Spectrometry in Soil Samples of Bryansk region Contaminated due to Chernobyl Accident. J. Radioanal. Nucl. Chem. 247(2), 341 – 345, doi: 10.1023/A:1006757718985.

Sahoo, S.K., Hosoda, M., Kamagata, S., Sorimachi, A., Ishikawa, T., Tokonami, S., Uchida, S. 2011. Thorium, Uranium and Rare Earth Elements Concentration in Weathered Japanese Soil Samples. Progress in Nuclear Science and Technology 1, 416 – 419.

Sartandel, S.J., Jha, S.K., Bara, S.V., Tripathi, R.M., Puranik, V.D. 2009. Spatial Distribution of Uranium and Thorium in the Surface Soil around Proposed Uranium Mining Site at Lambapur and its Vertical Profile in the Nagarjuna Sagar Dam. J. Environ. Radioact. 100, 831 – 834.

Sunmonu, L.A., Adagunodo, T.A. Olafisoye, E.R., Oladejo, O.P. 2012. The Groundwater Potential Evaluation at Industrial Estate Ogbomoso Southwestern Nigeria. RMZ-Materials and Geoenvironment 59(4), 363–390.

Tanaskovic, I., Golobocanin, D., Milijevic, N. 2012. Multivariate statistical analysis of hydrochemical and radiological data of Serbian spa waters. J. Geochem. Explor. 112, 226 – 234.

Taskin, H., Karavus, M., Ay, P., Topuzoglu, A., Hidiroglu, S., Karahan, G. 2009. Radionuclide Concentrations in Soil and Lifetime Cancer Risk due to the Gamma Radioactivity in Kirklareli, Turkey. J. Environ. Radioact. 1000, 49 – 53.

Tzortzis, M., Tsertos, H. 2004. Determination of Thorium, Uranium and Potassium Elemental Concentrations in surface Soils in Cyprus. Journal of Environmental Radioactivity 77 (3), 325 – 338.

Turhan S. 2009. Radiological impacts of the usability of clay and kaolin as raw material in manufacturing of structural building materials in Turkey. J. Radiol. Prot., 29, 75 – 83.

United Nations Scientific Committee on the Effects of Arsenic Radiation (UNSCEAR). 1988. Sources, Effects and Risks of Ionizing Radiation. New York: United Nations.

United Nations Scientific Committee on the Effects of Arsenic Radiation (UNSCEAR). 1993. Sources and Effects of Ionizing Radiation. UNSCEAR 1993 Report Vol. 1 to the General Assembly, with Scientific Annexes, United Nations Sales Publication, United Nations, New York.

United Nations Scientific Committee on the Effects of Arsenic Radiation (UNSCEAR). 2000. Sources and Effects of Ionizing Radiation. UNSCEAR 2000 Report Vol. 1 to the General Assembly, with Scientific Annexes, United Nations Sales Publication, United Nations, New York.

Uosif, M.A.M., Mostafa, A.M.A., Elsaman, R., Moustafa, E. 2014. Natural Radioactivity Levels and Radiological Hazards Indices of Chemical Fertilizers Commonly used in upper Egypt. Journal of Radiation Research and Applied Sciences 7, 430 – 437.

Usikalu, M.R., Akinyemi, M.L., Achuka, J.A. 2014. Investigation of Radiation Levels in Soil Samples Collected from Selected Locations in Ogun State, Nigeria. IERI Procedia 9, 156 – 161.

Usikalu, M.R., Fuwape, I.A., Jatto, S.S., Awe, O.F., Rabiu, A.B., Achuka, J.A. 2017. Assessment of Radiological Prameters of Soil in Kogi state, Nigeria. Environmental Forensics, 18(1): 1 – 14.

Wint, C., Cherney, K. 2017. High Potassium. Healthline Media. Medically Reviewed by Weatherspoon D on May 22, 2017, Retrieved on October 18, 2017. https://www.healthline.com/health/high-potassium-hyperkalemia#about1

Wunderlin, D.A., Diaz, M.D.P., Ame, M.V., Pesce, S.F., Hued, A.C., Bistoni, M.D. 2001. Pattern recognition techniques for the evaluation of spatial and temporal variations in water quality. A case study: Suquia River Basin (Cordoba-Argentina). Water Res 35(12), 2881–2894. doi: 10.1016/s0043-1354(00)00592-3.

Xing-an, C., Yong-e, C., Huijuan, X., Guodong, F., Yun-hui, D., Zhi-Liang, F., Liang, C., Mao, H.X., Ying-Jie, Y., Huan, D.Z., Rong, Z. 2014. A twenty-year Follow-up study on Health Effects following Long-term Exposure to Thorium Dusts. A project from National Natural Science Foundation of China (Project no. 3860285) and IAEA (Project no. 7715/RB and 11526RBF) https://www.ipen.br/biblioteca/cd/irpa/2004/files/1b9.pdf

Bulletin of the Mineral Research and Exploration

http://bulletin.mta.gov.tr

Evaluation of the alternatives for gold ore grinding circuits by using of laboratory studies results and simulation method; case study: İranian Gold Co.

Hojjat HOSSEINZADEH GHAREHGHESHLAGH[a*], Ayşe Tuğba CEBECİ[b] and Şevket Levent ERGÜN[c]

[a]*Department of Mining Engineering, Urmia University of Technology (UUT), Band road, Urmia, West Azerbaijan, Iran. orcid.org/0000-0002-7763-9596*

[b]*Department of Mining Engineering, Hacettepe University, Beytepe 06532, Ankara, Turkey. orcid.org/0000-0002-7763-9596*

[c]*Department of Mining Engineering, Hacettepe University, Beytepe 06532, Ankara, Turkey. orcid.org/0000-0002-6500-7540*

Research Article

Keywords:
Comminution / Grinding circuit, Modeling and Simulation, JKSimMet, Gold ore, Clayey Minerals.

ABSTRACT

In this study, simulation aided design of grinding circuit for a gold mine in Iran is presented. The main parameters for the design of the grinding circuit are the ore specifications and the considered operating conditions. Ore specifications were characterized by grinding tests, which included the Drop - weigh test (A, b), the abrasion test (t_a) and the Bond Work Index test (W_i). For this study, the operating conditions for the processing plant are the ability to process clayey minerals and the plant throughput and the d_{80} of the hydrocyclone overflow (leaching tank feed), which are 125 tons per hour and 45 µm, respectively. Simulation operations were performed using grinding parameters (A, b, t_a, W_i), operating constraints (plant capacity, d_{80} of the hydrocyclone overflow and ability to work for clayey minerals), existing mathematical models for different types of crushers, mills and separators and JKSimMet software. By completing the simulation process, three different alternatives for the grinding circuit of the considered ore were predicted. These three alternatives have been compared and evaluated with each other in terms of specific energy consumption (kWh/t), sensitivity to operational variables and the ability to process clayey minerals. The optimal circuit must have the capability to process clayey minerals and must have the lowest specific energy consumption and the least sensitivity to operational variables. By considering all these factors, the Alternative 3 is selected and suggested for an efficient grinding circuit.

Received Date: 21.04.2018
Accepted Date: 17.09.2018

1. Introduction

There are different methods for design, optimization and control of a mineral processing system which all of them based on the computer evolutionary programs and simulation software. On the other hand, the foundation of these computer programs and simulation software is the mathematical models defined for the various equipment used in the system. In this case, the more accurate the mathematical models, the results will be so accurate (King et al., 2012).

When designing a processing plant, in summary, two main parameters determine the type of equipment and their capacity. The first parameter is the amount of production or plant capacity (described as tons per hour or tph) with the optimal efficiency (metallurgical and economic). The second parameter is the ability to maneuver against the unpredicted changes occurring in the properties of the ore and operating conditions (Mular et al., 2002).

The capacity of a processing plant depends on many parameters including mine capacity (number

Citation Info: Hosseınzadeh Gharehgheshlagh, H., Cebeci, A. T., Ergün, Ş. L. 2019. Evaluation of the alternatives for gold ore grinding circuits by using of laboratory studies results and simulation method; case study: İranian Gold Co. Bulletin of Mineral Research and Exploration, 159, 219-233. *http://dx.doi.org/10.19111/bulletinofmre.501432*

** Corresponding author: Hojjat HOSSEINZADEH GHAREHGHESHLAGH, h.hoseynzade@uut.ac.ir*

of bench faces or working benches), required capital, type and number of equipment, economic conditions and the price of ore and metals and etc (Mular et al., 2002).

Despite the complexities of defining the optimization criteria and the optimum operating conditions of a processing plant, these parameters have been extensively discussed by Kelly and Spottiswood (1982), Kelly (1991). Generally, the optimum efficiency of a plant depends on the characteristics of the ore and the type and efficiency of the equipments. To achieve optimal efficiency, prior to the design phase, enrichment operations with laboratory devices are performed on the separated size fractions of the ore samples (the type of laboratory equipment should be in line with the type predicted in the industrial process). Each size fraction which has the optimal state for metallurgical and economic efficiency will be considered as an optimal size for industrial concentration plant feed (Depending on the economic conditions, optimal efficiency can be considered as metallurgical efficiency or economic efficiency).

The operational efficiency of the processing plant will be fully affected by the working conditions of the equipment and ore specifications such as grade, texture, physical, chemical and mechanical properties, gang type and clay minerals. Clay minerals are one of the biggest problems in the processing plants, which has a negative effect on the grinding efficiency, enrichment and dewatering systems, and reduces overall plant efficiency (Wills and Napier-Munn, 2011). Due to the nature of mining, these ore properties will fluctuate in different parts of the mine. Therefore, in the absence of prediction of possible changes in the ore properties during the design phase of a plant, the plant will be disrupted and will not achieve to the optimal efficiency in the operational phase and in some cases the plant may come inoperable.

Comminution (crushing and milling) is the most important part of a mineral processing plant whose task is to liberate valuable minerals or metals from the gang (for metallic minerals) or to reach a certain finesse size (for industrial minerals). On the other hand, the optimal design of a comminution system is important in terms of reducing investment and operational costs in the a mineral processing plant, related to the fact that the comminution systems account for about 60% of investment costs, 40 to 50% operating costs and more than 60% of energy costs (Wenzheng, 1991). In some cases, only milling part will account for about 90% of operating costs (Wills and Napier-Munn, 2011).

The aim of this work is to design an optimal crushing circuit for a gold processing plant in Iran that will work with a clayey ore with a specific gravity of 2,70 gr / cm^3. The main parameters for the design of the comminution circuit are the ore specifications and the considered operating conditions. Ore specifications were characterized by grinding tests, which included the Drop -weigh test (A, b), the abrasion test (ta) and the Bond Work Index test (Wi). For this Project, the operating conditions for the processing plant are the plant capacity and the size of the hydrocyclone overflow (the hydrocyclone overflow is fed to the leaching tank, so, the size of the hydrocyclone overflow is equal to the leaching tank feed), which are 125 tons per hour (tph) and 45 microns, respectively. The size of the hydrocyclone overflow (leaching tank feed) is shown using the parameter d_{80} (80% passing size) which has been obtained using previous laboratory studies on the separated size fractions of the ore samples. The results show that the best efficiency of the processing plant will be when the d_{80} of the hydrocyclone overflow (leaching tank feed) is 45 μm.

Furthermore, one of the most important parameters affecting the operation stage is the presence or absence of clay minerals in the ore (Wills and Napier-Munn, 2011). Therefore, in the design phase of the processing plant, the dimensions and type of equipment and their arrangement depend on the properties of the ore, material flowrate, the amount of grinding and the ability to work for clay minerals (Mular et al., 2002). Furthermore, if there are several different systems for the desired purpose, each system that is able to meet the desired criteria with the lowest cost is preferred.

Using the above conditions, simulation operations were performed using grinding parameters (A, b, ta, Wi), operating constraints (plant capacity=125 tph, d_{80}=45μm and ability to work for clayey minerals), JKSimMet software and existing mathematical models for different types of crushers, mills and separators.

By completing the simulation process, three different alternatives for the comminution circuit of the considered ore were predicted. Finally, these three alternatives have been compared with each other and then the appropriate and optimal circuit was chosen.

1.1. Modeling and Simulation in the Mineral Processing

For a complete description of a processing plant or a comminution circuit it is needed to define the models and simulation method of these models.

Simulation is an imitation of a real process or system in a virtual environment (Banks et al.,, 2001), which using it, it is possible to see the response or set of responses of a system or a process to changes made, without doing a real activity on a system or process. By using these observations, it is also possible to decide whether or not to make the necessary changes in reality (Gray and Rumpe, 2016).

To perform a simulation operation, there is a need for mathematical equations describing the behavior of the components and the entire system, which are called the mathematical models (Sokolowski and Banks, 2009). These models represent the principal properties, behaviors and functions of the selected system. In fact, the model symbolized the system itself, while the simulation describes the operation of the system over time (Gray and Rumpe, 2016).

In the mineral processing industry, the tendency to predict the results of changes in the operational and/or design parameters have always been of interest to the researchers. To have a precise and accurate prediction, it is important to know the behavior of that system and the parameters that affect the objective function (Robinson, 1997).

The first mathematical based models in the mineral processing industry were presented in 1933 for modeling the size distribution of materials (Rosin and Rammler, 1933). Epstein (1947; 1948) obtained the breakage and selection functions for mills by using the mass balance model. Then, new models for flotation kinetics (Sutherland, 1948), grindability and Energy – size reduction (Bond, 1952), reduced efficiency curve for cyclone separators (Yoshioka and Hotta, 1955), matrix equations involving breakage, selection and classification functions (Broadbent and Callcott, 1956; Lynch, 1977), kinetic models (Broadbent and Callcott, 1956; Gardner and Austin, 1962; Kelsall and Reid, 1969; Whiten, 1971; Herbst and Fuerstenau, 1980; Austin et al., 1984) and energy balance models (Napier-Munn et al., 1996) were introduced.

Later, by combining simple models and forming complex models, it was possible to study the behavior of various systems such as mills, classifiers, and so on. For example, Whiten (1974) presented a new model called the Perfect Mixing Model by combining the obtained mathematical models (breakage and selection functions, discharge rate and feed and product size distributions of the mill) and the mass balance principle. With the advancement of computer science and the ability to analyze, solve and interpret complex problems with computers, a combination of simple and complex mathematical models in the form of a simulator package was used to predict the desired target functions. Thus, it was possible to use simulations to analyze simple and complex circuits of ore processing systems.

1.2. JKSimMet Software

To simulate a system, one or more models are needed for each of the components of the system and the associated models of these components. The integration of mathematical models of all components forming a comminution system in a simulation package provides the necessary facilities for studying the whole system, the individual components and the interaction of components on each other (such as the effect of the mill efficiency on the hydrocyclone).

In the mineral processing industry, various simulators have been developed to carry out the necessary studies. The JKSimMet software, used in this study, is the most widely used and most reliable simulation software in comminution circuits of the mineral processing plants. This software uses the best math models obtained for various components of the comminution circuit (different types of crushers, mills and separators) and data from hundreds of different processing plants to perform various operations such as mass balance, design, optimization, calibration and comparison of different conditions in a comminution circuit and comparing conditions in different comminution circuits. The initial version of this software was presented in 1980 by Julius Kruttschnitt Mineral Research Centre (JKMRC) and the first commercial edition of JKSimMet was also introduced in 1986, when JKTech, the JKMRC commercial branch, was founded.

As noted, the existence of accurate and validated models and extensive industrial data-base has led to the increasing use of JKSimMet software by various researchers. This software was used in the many comminution plants and joint industry-university

research projects such as Morrell et al. (1996), Hart et al. (2001), Dunne et al. (2001), Nikkhah and Anderson (2001), Ergun et al. (2005), Delboni et al. (2006), Munoz et al. (2008), Pellegrini Rosario (2010), Schwarz and Richardson (2013), Hosseinzadeh Gharehgheshlagh (2014), Shi et al. (2015), Zuo (2015), Maruf Hasan (2016), Tavares and Delboni (2016), Liang et al. (2016), Koch (2017), Palaniandy (2017), Hosseinzadeh Gharehgheshlagh et al. (2017), Wendelin Wikedzi (2018) and etc. Some important models of this software can be summarized as table 1.

Table 1- Important models of the JKSimMet software.

Equipment Models	Researchers
Crushers (Jaw, Gyratory, Cone, Roll and VSI (Vertical Shaft Impact Crusher) Moels	Awachie (1983); Whiten (1984); Andersen (1989)
High Pressure Grinding Rolls (HPGR) Models	Tondo (1996); Morrell et al. (1997); Daniel (2002); Daniel and Morrell (2004)
Ball Mill Model	Whiten (1972; 1976); Lynch (1977); Morrell (1992)
Rod Mill Model	Lynch (1977)
Autogeneous (AG) and Semi-autogeneous (SAG) mills Models	Leung (1987); Leung et al. (1987)
Hydrocyclone Models	Lynch and Rao (1975); Nageswararao (1978)
Breakage Distribution Function (BDF) models	Narayanan and Whiten (1983); Narayanan (1985)
AG and SAG mills and Ball Mill Power Models	Morrell and Morrison (1989); Morrell (1992; 1993; 1996); Morrell et al.(1992)

2. Experimental Studies

Design of grinding circuit for Iranian Gold Co. is carried out in the Mining Engineering department of the Hacettepe University in Turkey. The required feed rate and d_{80} of hydrocyclone overflow were 125 tph and 45 μm, respectively. The JKSimMet software that developed in Julius Kruttschnitt Mineral Research Center (JKMRC) is used for simulations (Napier-Munn et al., 1996).

The experimental studies are divided into two sections; the laboratory works and the simulation process.

2.1. Laboratory Works

In order to use the JKSimMet simulation software, the required parameters for characterizing of Run Of Mine (ROM) ore must be determined via laboratory works. These parameters, for grinding circuit, are the Breakage Distribution Function (BDF) or the Appearance function, the Bond Work Index (BWI) and the Abrasion Index.

2.1.1. Brekage Test

The BDF is one of the important parameters of grinding circuits that is used for design, operation, modeling, simulation and optimization of these circuits. There are different methods to calculate BDF; Batch Grinding test in laboratory mills, Back Calculation methods and Single Particle Breakage under controlled conditions. The Single Particle Breakage under controlled conditions is divided into three methods including Impact test, Slow Compression test and Abrasion test. The Impact methods divide to Single Impact tests and Double Impact tests. Finally, the Double Impact tests divide into four groups including Twin Pendulum tests, Drop Weight tests, Hopkinson Pressure Bar and Ultra-Fast Load Cell tests.

In this study, the Drop Weight Test (DWT) is used for determination of the BDF or impact breakage characteristics of the ore. This method has started since 1938 by Gross (1938). Then, many researches such as Piret (1953), Arbiter (1969), Narayanan and Whiten (1983), Narayanan (1985), Leung (1987), Tavares (1999), Man (2001), Genç et al. (2004), Genç and Benzer (2008), Özer and Whiten (2012) and etc. used this method with different materials, apparatuses and conditions. A new apparatus for the Drop Weight method developed by Narayanan (1985) in the JKMRC is the simplest and most commonly used method for investigation of impact breakage characteristics of materials. A type of this device is used in this study has been given in figure 1.

BDF Determination: There are different approaches to calculate the BDF of materials and represent it mathematically. Leung (1987) gave the following relationship between the specific comminution energy and t_{10} parameter.

$$t_{10} = A \times (1 - e^{(-E_{cs} \times b)}) \quad (1)$$

Where, t_{10} is the impact breakage distribution parameter or breakage index or fineness index which quantifies the amount of material passing 1/10's of the original size, here; geometric mean of the tested size range is known as individual size, is used to

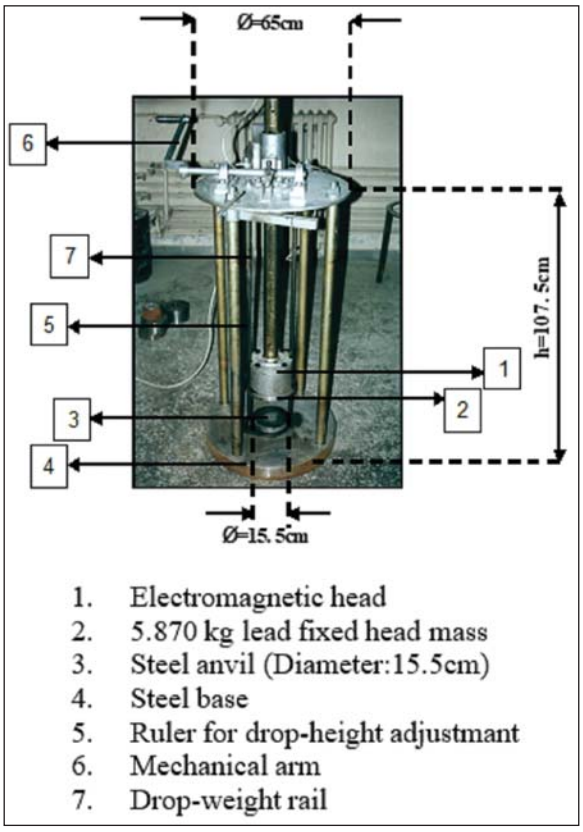

Figure 1- DWT apparatus of Hacettepe University (Genç and Benzer, 2008)

represent the degree of size reduction. E_{cs} is the specific comminution energy (kWh/t) and A and b are impact breakage parameters. The maximum limit of t_{10} is defined as A, and the slope of the straight portion of the t_{10} versus E_{cs} plot gives the value of b. The value of A.b represents the ease of impact breakage in which larger values indicating more breakage occurring for a given energy input (Napier-Munn et al., 1996). Narayanan and Whiten (1983) base the proposed equation of Leung (1987) and calculated normalized breakage distribution function using the approach of t-family curves.

Sample Preparation And Breakage Procedure: To determine BDF, the JKMRC standard is used. In this standard 5 different size fractions with 3 different specific comminution energies for each size fraction are selected, table 2, and with each specific comminution energy 20 particles are breakage. For this purpose, the DWT apparatus of the Hacettepe University (Figure 1) is used.

Table 2- Size intervals and nominal input energy levels (kWh/t) used in JKMRC AG/SAG drop weight test.

	Size interval, mm				
test	-63 +53	-45 +37,5	-31,5 + 26,5	-22,4 + 19	-16 +13,2
1	0,10	0,10	0,25	0,25	0,25
2	0,25	0,25	1,00	1,00	1,00
3	0,50	0,50	2,50	2,50	2,50
	Specific energy, kWh/t				

E_{cs}-t_{10} Model: After the breakage tests, sieve analysis of broken material is obtained for each energy level. Assuming that the geometric mean of each fraction is its initial size, cumulative percent passing of materials is obtained from 1/2, 1/4, 1/10, 1/25, 1/50 and 1/75 of this size that is shown by t_2, t_4, t_{10}, t_{25}, t_{50} and t_{75} respectively (Table 3). Using the equation proposed by Leung and obtained t_{10} values, specific communition

Table 3– E_{cs}-t_{10}-t_n amounts after breakage.

Fraction	Ec	t_i, %					
mm	kWh/t	t_{10}	t_2	t_4	t_{25}	t_{50}	t_{75}
-16+13.2	0,75	46,0	96,5	77,5	29,0	20,0	16,5
	1,00	69,0	100	94,5	50,0	39,0	32,5
	2,50	66,0	100	94,0	45,5	34,0	30,5
-22.4+19	0,25	29,5	93,5	51,0	19,0	14,5	12,5
	1,00	46,0	100	78,0	30,0	22,5	19,0
	2,50	57,0	97,5	86,0	41,5	34,0	30,5
-31.5+26.5	0,25	31,0	79,5	52,0	20,5	15,0	13,0
	1,00	47,5	96,5	74,5	29,0	20,0	16,0
	1,60	54,0	100	88,0	34,0	24,5	21,0
-45+38	0,10	9,5	38,5	19,0	6,5	4,5	4,0
	0,20	24,5	79,5	43,0	14,5	10,5	9,0
	0,40	29,0	88,5	54,5	17,0	12,5	11,0
-63+55	0,10	17,0	55,5	31,5	10,0	7,0	6,0
	0,15	18,5	71,5	37,0	10,0	7,0	5,5
	0,20	31,5	89,0	51,5	19,0	15,0	12,5

energy plotted versus t_{10} (Figure 2). Results show that A and b values for this ore are 59.11 and 2.41 respectively.

t-family Curve: To obtain t-family curve, t_{10} values measured to each specific comminution energy level put as a basis. Then on coordinate axis that X-axis shows t_{10}s and the Y-axis shows corresponding t_ns, a graph will be plotted in which all of the t_2s,t_4s,…t_{75}s will connect to each other with best trend lines. The total set of these lines is called t-family curve (Figure 3).

Calculation of BDF Matrix Arrays from T-Family Curve: To obtain BDF, assuming that the largest mill feed size is 36 mm, a lower triangular square matrix is formed that its largest size is 36 and its under dimensions are the square root of the previous one (the largest size of the matrix corresponds with the biggest size of the mill feed. In this matrix the row number shows the particle sizes, the first row shows the biggest particle and the others show the fine sizes). Firstly, t_{10} value is calculated by using equation 1 and arbitrary specific comminution energy (here, E_{cs} = 1 kWh/t). Secondly, using t-family curves t_n's values (n= 2, 4, 25, 50, 75) are calculated and a unique particle size distribution is formed (to calculate the breakage function for values smaller than Y_{75}, the extrapolation of the last three values is used). Then, using this distribution, the cumulative percent passing values are obtained for all sizes in the matrix. Finally, Using this data, the amount remaining on each size is calculated

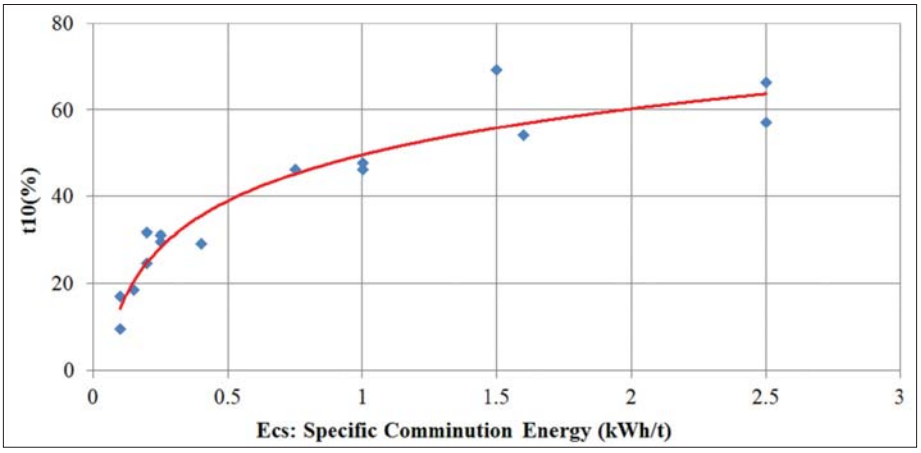

Figure 2- E_{cs}-t_{10} relationship.

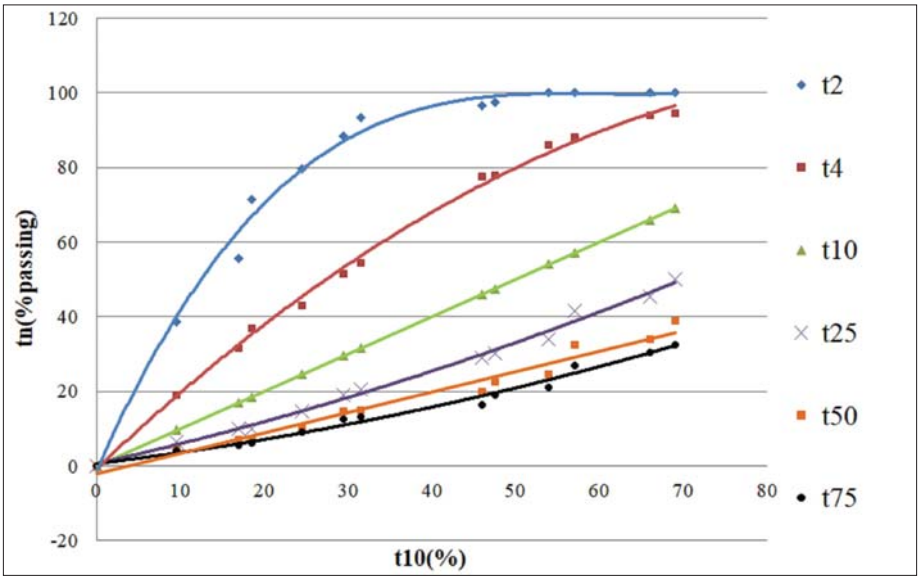

Figure 3- t-family curve.

as a fraction. This data gives the first column of the breakage distribution matrix and called the BDF. The other columns are formed by the downward movement of the previous columns.

2.1.2. Bond Test

The work index is the comminution parameter which expresses the resistance of the material to crushing and grinding; numerically it is the kilowatt hours per ton required to reduce the material from theoretically infinite feed size to 80% passing 100 µm (Bond, 1952). The Bond standard grindability test has been performed in 30.5 - 30.5 cm in diameter and length standard laboratory ball mill that has been described in detail by Deister (1987) and Levin (1989). The Bond equation for calculating W_i value is as below (Bond. 1961):

$$W_i = \frac{48.95}{D^{0.23}\, G_{bp}^{0.82} \left(\frac{10}{\sqrt{P_{80}}} - \frac{10}{\sqrt{F_{80}}}\right)} \quad (2)$$

Where;

W_i: Work Index (kWh/t)

D: Control sieve size (106 µm)

G_{bp}: Grindibility factor (g/rev)

P_{80}: 80% passing size of the final product (µm)

F_{80}: 80% passing size of the mill feed, before grinding, (µm)

Calculation of the work index for this sample was also performed using kinetic grinding test (Gharehgheshlagh, 2016). As a result of the Bond and the kinetic grinding tests performed on Iranian Gold Co. ore Wi value of the ore was determined as 9.20 kWh/t in both methods.

2.1.3. Abrasion Test

For the determination of abrasion parameters a tumbling drum which has 300 mm both in diameter and length is used. There are four 10 mm lifters in the drum. A 3 kg sample of -55+38 mm ore is ground for 10 minutes at 70% critical speed (53 revolution per minute) (Napier-Munn et al., 1996). t_a is the 1/10th of t_{10} value. The t_a value of Iranian Gold Co. ore is 1.70.

2.1.4. Ore Density Test

The density test for Iranian Gold ore sample carried out by using pycnometer and distilled water. The ρs value is obtained as 2,7 gr/cm^3.

2.1.5. Results of Laboratory Studies

Impact breakage characteristics of the ore were measured by the drop weight tester. Abrasion characteristic was determined by tumbling drum test. Ball mill grindability of the ore was determined by standard Bond's test. The specific gravity of the ore was found to be 2,70 gr/cm^3 by using density bottle tests.

The ore specifications determined in experimental studies are given in table 4.

Table 4- Grinding parameters determined for Iranian Gold Co. Ore.

Parameter	Value
A (%)	59,11
B (kWh/t%)	2,41
t_a (%)	1,70
BWI (kWh/t)	9,20
ρs (gr/cm^3)	2,70

By considering A, b, t_a and Wi parameters, the ore hardness can be characterized according to the table 5.

2.2. Simulation Studies

After determination of the ore parameters, the simulation procedure can be performed with the JKSimmet software.

Table 5 – JKTech ore characterization by considering A, b, t_a and W_i parameters (JK Drop Weight Test and JK Bond Ball Mill Index Test).

Property	Very Hard	Hard	Medium	Soft	Very Soft
A*b	< 30	30 - 38	43 - 56	67 - 127	> 127
t_a	< 0.24	0,24 - 0,35	0,41 - 0,54	0,65 - 1,38	> 1,38
W_i (kWh/t)	> 20	14 - 20	9 - 14	7 - 9	< 7

Simulation operations were performed using grinding parameters (A, b, ta, Wi), operating constraints (plant capacity = 125 tph, d_{80} of the hydrocyclone overflow (leaching tank feed) = 45μm and ability to work for clayey minerals), JKSimMet software and existing mathematical models for different types of crushers, mills and separators.

By completing the simulation process, three different alternatives for the comminution circuit of the considered ore were predicted.

These three different alternative circuits were as below:

➢ Alternative 1: SAG Mill/Closed Circuit Ball Mill.

➢ Alternative 2: Open Circuit Coarse Ball Mill and Closed Circuit Fine Grinding Ball Mill.

➢ Alternative 3: Closed Circuit Coarse Ball Mill and Closed Circuit Fine Grinding Ball Mill.

Firstly, these three alternatives compared with each other in terms of specific energy consumption (kW/t), sensitivity to operational variables and the ability to process clayey minerals. Then, the appropriate and optimal circuit was selected. The optimal circuit should have the capability to process clayey minerals and has the lowest energy consumption per unit weight of ore and the least sensitivity to operational variables.

2.2.1. SAG Mill/Closed Circuit Ball Mill

The total energy consumption of this alternative will be 3977 kW. In this alternative ROM ore will be crushed by a jaw crusher. The crushed material will be stockpiled. A SAG mill having 7 m inside diameter and 2.5 m inside length will be used. This SAG mill will work with 31.11% volumetric total load and 1550 kW gross power. The SAG mill discharge will be fed to a vibrating screen having 13 mm aperture. The aim of this screen is to protect the pump from coarse material. Screen oversize will be sent to the SAG mill while undersize will be sent to the cyclone feed sump. 0.8×375 mm cyclones will be used to separate fine material. The cyclone underflow will be fed to a ball mill having 4.5 m inside diameter and 6 m inside length. This mill will work with 35% volumetric total load and 2000 kW mill power. Ball mill discharge will be fed to the cyclone feed sump. The cyclone overflow will be the final product. The simplified flowsheet and mass balance of the Alternative 1 is given in figure 4 and the simulated size distribution of the streams around the circuit is shown in figure 5.

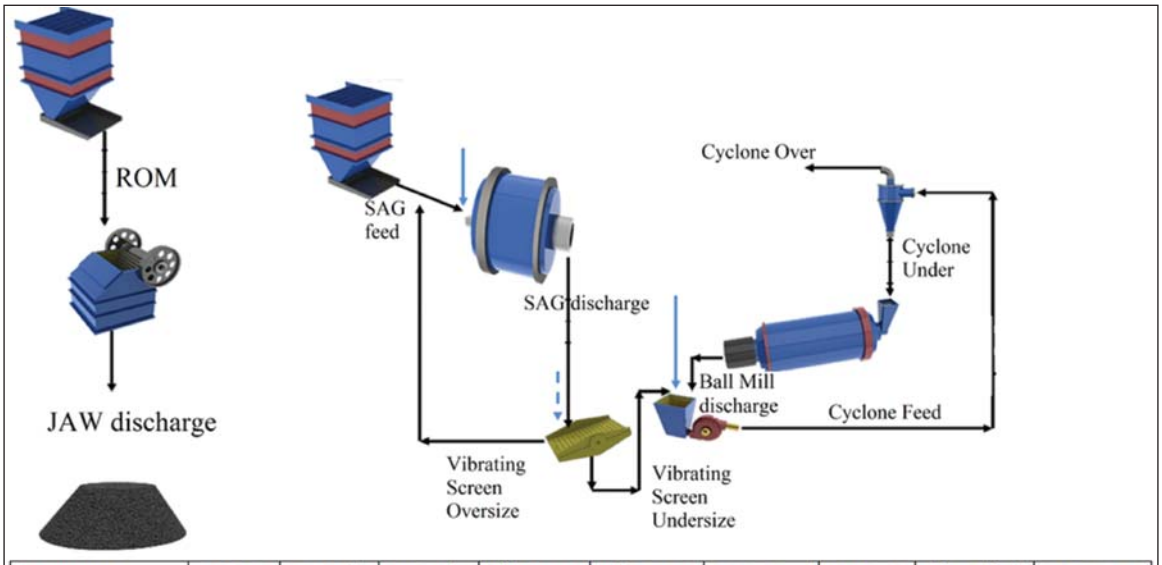

Parameter	ROM	JAW dis.	SAG dis.	Vib Scr. O	Vib Scr. U	CYC. Feed	CYC. U	Ball Mill dis	CYC. Feed
Solids (tph)	350.00	350.00	129.17	4.17	125.00	442.39	317.39	317.39	125.00
Volumetric Flowrate (m3/h)	140.45	140.45	117.39	1.75	115.64	643.11	261.33	261.33	381.78
% Solids by Weig	97.00	97.00	65.00	95.23	64.32	48.00	68.82	68.82	27.15
P80 (mm)	347.690	70.900	0.300	36.740	0.250	0.120	0.150	0.095	0.045

Figure 4- Simplified Flowsheet and Mass Balance of Alternative Circuit 1.

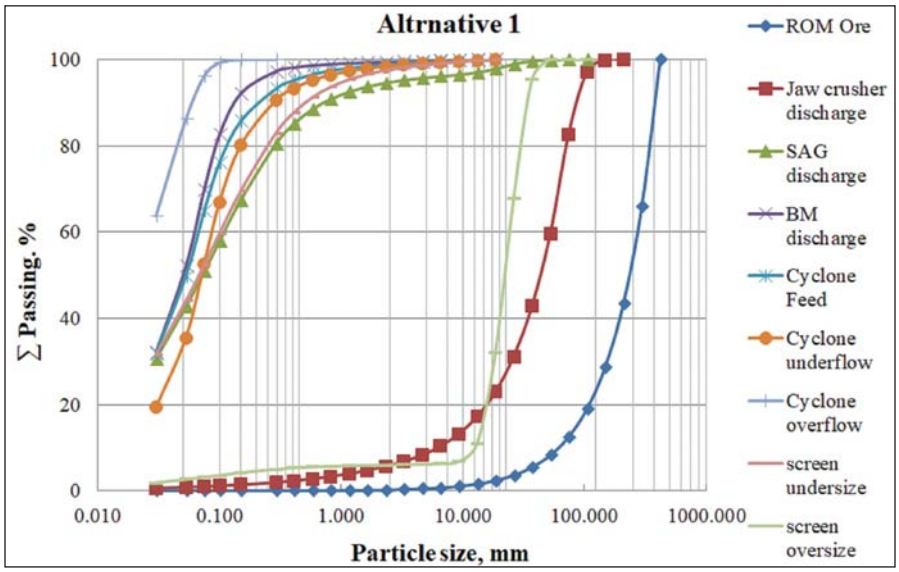

Figure 5- Simulated Size Distributions of the Streams for Alternative Circuit 1.

In this alternative, a jaw crusher which has feed opening of 1300 mm length and 1100 mm width will be used. The motor should be 160 kW. The dimension of the vibrating screen to be used for SAG Mill discharge will be 1×1.5 m which has 13 mm square opening and 54% open area. The diameter of hydrocyclone will be 375 mm. 6 operating and 2 spare cyclones will be used in the cluster. The volume of pump sump will be 25 m^3.

The ball charge distribution in SAG mill will be; 125 mm (30%), 90 mm (30%), 60 mm (30%), 40 mm (5%) and 30 mm (5%) with a total of 36 ton. In the ball mill, too, the largest ball diameter will be 30 mm and combination with weight is 51% (30 mm) and 49% (20 mm).

2.2.2. Open Circuit Coarse Ball Milling and Closed Circuit Fine Grinding Ball Milling

The total energy consumption of this alternative will be 3702 kW. In this alternative ROM ore will be crushed by a jaw crusher. The crushed material will be fed to a vibrating screen having 50 mm square aperture. Screen oversize will be crushed by a toothed roll crusher and crushed material will be fed to the same screen. Screen undersize will be stockpiled. A ball mill having 3,8 m inside diameter and 5 m inside length will be used. This mill will work with 35% volumetric total load and 1300 kW mill power. The ball mill discharge will be fed to the cyclone feed sump. 8×375 mm cyclones will be used to separate fine material. The cyclone underflow will be fed to a secondary ball mill having 4,4 m inside diameter and 6 m inside length. This mill will work with 35% volumetric total load and 1875 kW mill power. Ball mill discharge will be fed to the cyclone feed sump. The cyclone overflow will be the final product. The flowsheet for Alternative 2 is given in figure 6 and the simulated size distribution of the streams around the circuit is shown in figure 7.

A jaw crusher which has feed opening of 1300 mm length and 1100 mm width will be used. The motor should be 160 kW. A toothed roll crusher will used as a secondary crusher. The dimension of the vibrating screen to be used in crushing circuit will be 2,4×6 m which has 50 mm square opening and 71% open area. The diameter of hydrocyclone will be 375 mm. 6 operating and 2 spare cyclones will be used in the cluster. The volume of pump sump is 25 m^3.

2.2.3. Closed Circuit Coarse Ball Milling and Closed Circuit Fine Grinding Ball Milling

The total energy consumption of this alternative will be 3630 kW. This alternative is the same as Alternative 2 in terms of equipment dimensions.

There will be a spiral classifier, with 3 kW power, to operate the primary ball mill as a closed circuit. Primary ball mill discharge will be fed to the spiral classifier. The spiral classifier will has 9 m length and 1.3 m helix diameter. The spiral coarse product will be fed to the primary ball mill while fine product will be sent to the cyclone feed sump. 8×375 mm cyclones

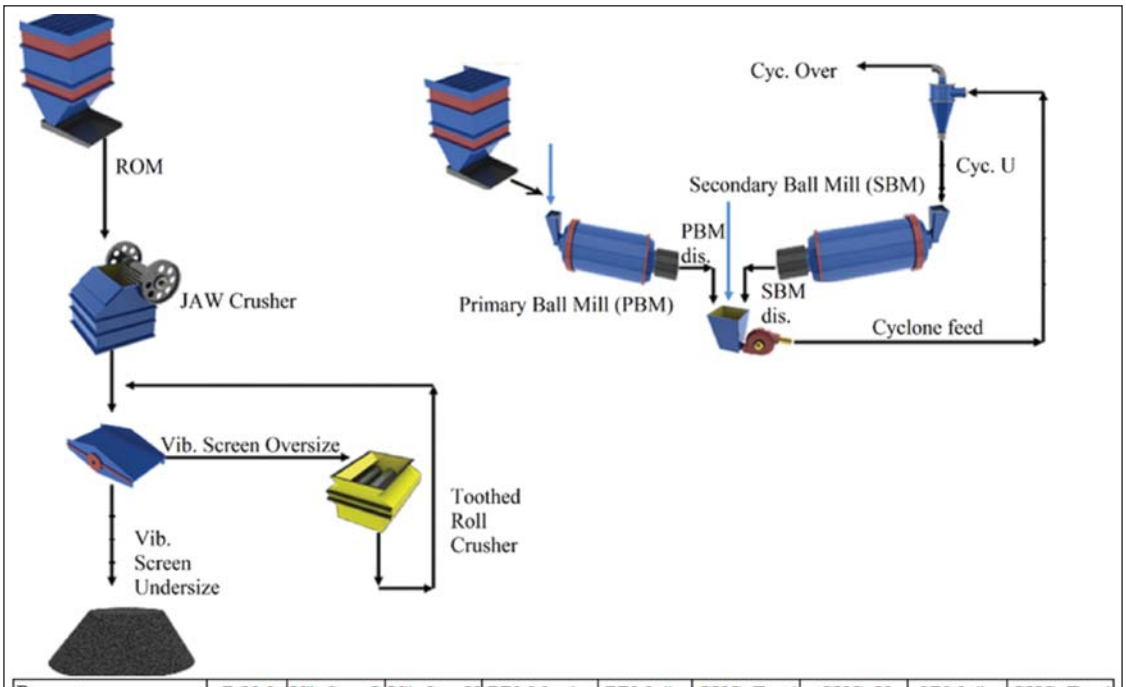

Parameter	ROM	Vib Scr. O	Vib Scr. U	PBM feeder	PBM dis.	CYC. Feed	CYC. U	SBM dis.	CYC. Feed
Solids (tph)	350.00	165.87	350.00	125.00	125	465.07	340.07	340.07	125.00
Volumetric Flowrate (m3/h)	140.45	63.11	140.45	100.32	99.87	676.08	277.10	277.10	398.98
% Solids by Weight	97.00	99.00	97.00	98.00	70	48.00	69.23	69.23	26.17
P80 (mm)	347.690	82.000	35.520	35.520	0.6	0.250	0.400	0.130	0.045

Figure 6- Simplified Flowsheet and Mass Balance of Alternative Circuit 2.

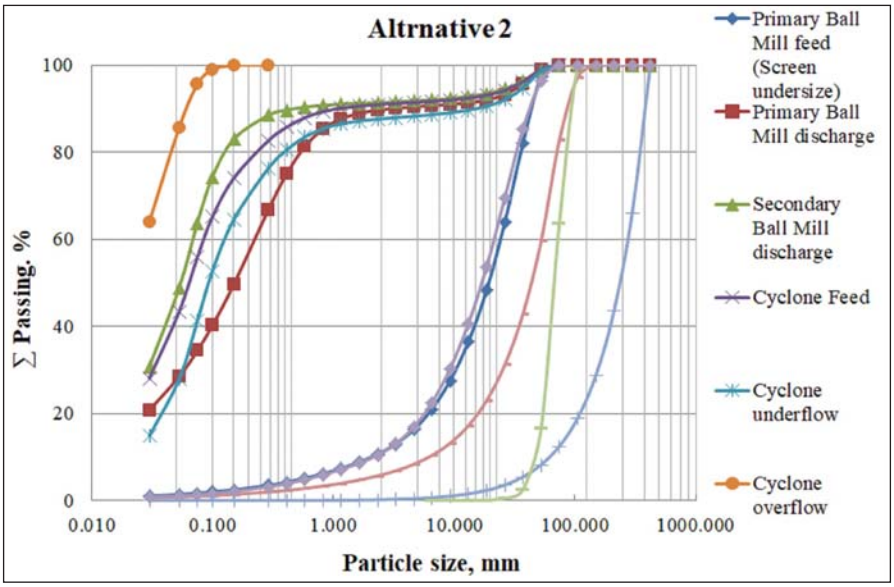

Figure 7- Simulated Size Distributions of the Streams for Alternative Circuit 2.

will be used to separate fine material. The cyclone underflow will be fed to a secondary ball mill having 4.4 m inside diameter and 6 m inside length. Ball mill discharge will be fed to the cyclone feed sump. The cyclone overflow will be the final product.

The flowsheet for Alternative 3 is given in figure 8 and the simulated size distribution of the streams around the circuit is shown in figure 9.

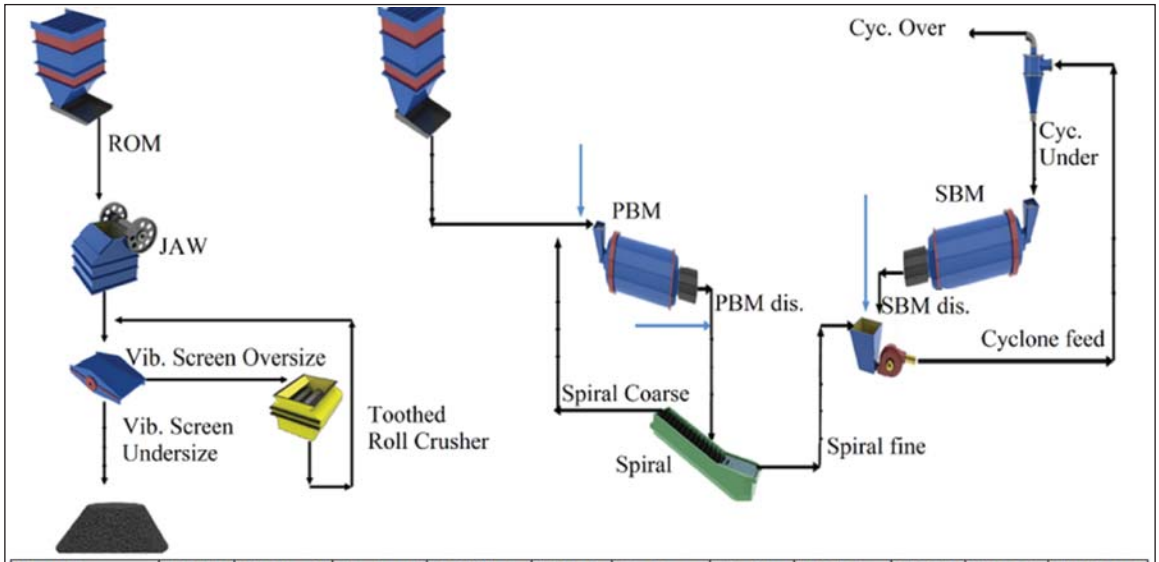

Parameter	ROM	Vib Scr. O	Vib Scr. U	PBM feeder	PBM dis.	Spiral Coarse	Spiral Fine	CYC. Feed	CYC. U	SBM dis.	CYC. Feed
Solids (tph)	350.00	165.87	350.00	125.00	174.79	49.79	125.00	417.31	292.31	292.31	125.00
Volumetric	140.45	63.11	140.45	50.16	139.64	29.88	177.86	452.09	243.89	243.89	362.76
% Solids by Weigh	97.00	99.00	97.00	97.00	70.00	81.31	48.72	48.00	68.31	68.31	28.32
P80 (mm)	347.690	82.000	35.520	35.520	0.800	37.460	0.350	0.150	0.280	0.100	0.045

Figure 8- Simplified Flowsheet and Mass Balance of Alternative Circuit 3.

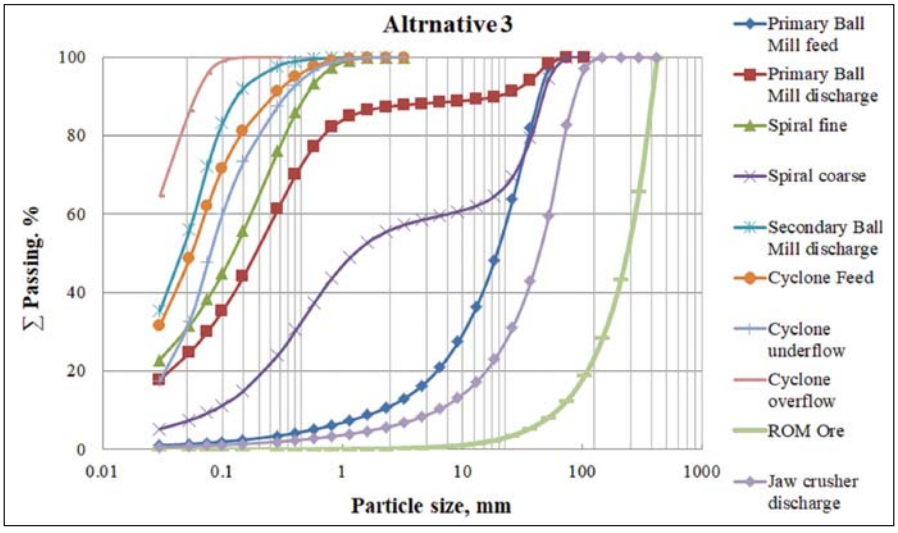

Figure 9- Simulated Size Distributions of the Streams for Alternative Circuit 3.

3. Results and Suggestions

The resulted data from the grinding tests (A, b, t_a, W_i) were used for ore characterization. According to the measured parameters (A = 59,11, b = 2,41, t_a = 1,70, W_i = 9,20 kWh/t) and the table 5 the ore is a relatively soft. For this reason, the use of the SAG mill is impractical and needs further investigation. Furthermore, with this result, it has also been shown that the ball mill can be more useful and can break down the ore to the required size (d_{80} of the hydrocyclone overflow (leaching tank feed) = 45 µm). Therefore, the general structure of the grinding circuit is strongly influenced by the results of the grinding tests, and the selection or rejection of each equipment depends on the measured values of these tests.

By knowing the importance of the grinding parameters on the type of equipment and grinding circuit structure, simulation operations were performed using laboratory data (A, b, ta, Wi), operating constraints (plant capacity = 125 tph, d_{80}=45µm and ability to work for clayey minerals), JKSimMet software and existing mathematical models for different types of crushers, mills and separators. By completing the simulation process, three different alternatives for the grinding circuit of the considered ore were predicted. These grindability and simulation studies showed that:

1) The SAG mill alternative will be very dependent on the size distribution of ROM ore as well as jaw crusher discharge. Large particles have higher rates of abrasion and therefore there may be competency issues during operation. This may reduce the mill capacity and also cause discontinuity in the operation. Alternatively, separate coarse and fine ROM blends can be prepared. However, this complicates operation and the advantage of using a SAG mill would be diminished.

2) AG/SAG mill design usually requires several sets of samples for material characterization to avoid fluctuations, as possible as, in performance throughout the life of the mine.

3) Since the presence of clay is known in the ore, conventional fine crushing by cone crusher is avoided. Therefore, for both Alternative 2 and 3 toothed roll crusher is suggested as a secondary crusher. In this case mill feed will have F_{80}=35.5 mm which is a coarser feed for ball mill.

4) Simulation studies showed that there will be remaining coarse particles in primary ball mill discharge for Alternative 2. This may cause mechanical problems in mill discharge trommel and large particle reporting to pump sump could cause severe wear and mechanical problems in the cyclone feed pump, especially if the grindability of the feed worsens. Those coarse particles will not be broken in the secondary ball mill where finer balls are used and there will be accumulated in the mill and this may cause the mill to be shut down and stopped.

5) The simulation results show that the specific energy consumption of these three alternatives are 31.82, 29.62 and 29.04 kWh/t respectively.

6) It is easier to control of ball mills due to the non sensitivity to the feed hardness and low sensitivity to the changes in mineral properties.

7) These three alternatives have been compared and evaluated with each other in terms of specific energy consumption (kWh/t), sensitivity to operational variables and the ability to process clayey minerals. The optimal circuit must have the capability to process clayey minerals and must have the lowest specific energy consumption and the least sensitivity to operational variables.

By considering all these factors, the Alternative 3 is selected and suggested for an efficient grinding circuit.

Also, in the future, by using of a set of simulation study's results, validated laboratory data, development of more precise models and development of high-throughput computers, it will be possible to simulate complex ore processing circuits and provide high decision-making power to the investors and miners.

Acknowledgements

This study was carried out within the scope of Comminution Circuit Design for Iranian Gold Co. project at Hacettepe University in Turkey. Here, I would like to acknowledge to the Mining Engineering department of Hacettepe University for providing experimental facilities for conducting the research works. The authors also thanks to anonymous reviewers and Editor for their opinions, comments and enlightening discussions due to improve the paper.

Refrences

Andersen, J S. 1989. Development of a Cone Crusher Model. M.Eng.Sc Thesis, University of Queensland.

Arbiter, N., Harris, C.C., Stamboltzis, G.A. 1969. Single fracture of brittle spheres. Trans. Soc. Min. Eng., AIME 244, 118–130.

Austin, L. G., Klimpel, R. R., Luckie, P. T. 1984. Process Engineering of Size Reduction: Ball Milling. Society of Mining Engineers of the American Institute of Mining, Metallurgical and Petroleum Engineers (AIME) Inc, ISBN 0895204215, New York, 556 pp.

Awachie, S.F.A. 1983. Development of crusher models usin g laboratory breakage data, PhD Thesis, University of Queensland.

Banks, J., Carson, J., Nelson, B., Nicol, D. 2001. Discrete-Event System Simulation. Prentice Hall. p. 3. ISBN 0-13-088702-1.

Bond, F.C. 1952. The third theory of comminution. Trans AIME 193, 484–494.

Bond, F.C. 1961. Crushing and grinding calculations, British Chemical Engineering, 6, 6, pp: 378 - 385.

Broadbent, S.R., Callcott, T.G. 1956. A matrix analysis of processes involving particulate assemblies. Phil. Trans Royal Soc. London, Ser. A 249, 99–123.

Daniel, M.J. 2002. HPGR model verification and scale-up. M.Sc Thesis, School of Engineering, University of Queensland, Brisbana, Australia.

Daniel M.J., Morrell S. 2004. HPGR Model Verification and Scale-up. Minerals Engineering, 17, 1149-1161.

Deister, R.J. 1987. How to determine the Bond work index using lab. ball mill grindability tests. Engng. Min. J., 188, 42.

Delboni, H., Marco A., Rosa, N., Maurício, G., Bergerman, Rinaldo P. Nardi. 2006. Optimisation of the Sossego Sag Mill. SAG 2006: SAG Mill Circuit. Int. Conf. on Autogenous and Semi autogenous Grinding Technology, 1: 39-50.

Dunne, R., Morrell, S., Lane, G., Valery, W., Hart, S. 2001. Design of the 40 foot diameter sag mill installed at the Cadia gold copper mine. SAG 2001, mining and mineral process engineering University of British Columbia, Vancouver, Canada.

Epstein, B. 1947. The Material Description of Certain Breakage Mechanisms Leading to the Logorithmic-Normal Distribution, J. Franklin Inst., 244, 471-477.

Epstein, B. 1948. Logarithmico-normal distributions in the breakage of solids. Ind. Eng. Chem., 40, 2289–2291.

Ergün, L., Güulsoy, O., Can, M., Benzer, H. 2005 (June 09-12). Optimization of Çayeli (Çbi) Grinding Circuit by Modelling and Simulation. The 19th International Mining Congress and Fair of Turkey (IMCET2005), İzmir, Turkey.

Gardner, R.P., Austin, L.G. 1962. A Chemical Engineering Treatment of Batch Grinding. Proceedings, First European Symp. Zerkeinern. Edited by H. Rumpf and D. Behrens, Verlag Chemie, Weinheim, 217-247.

Genç, O., Ergün, L., Benzer, H. 2004. Single particle breakage characterization of materials by drop weight testing. XLI Annual Symposium Physicochemical Problems of Mineral Processing and IX International Mineral Processing Meeting, Poland 38, 241–255.

Genç, O., Benzer, H. 2008. Analysis of single particle breakage characteristics of cement clinker and cement additives by drop-weight technique. The Journal of the Chamber of Mining Engineers of Turkey (47) (in Turkish), 13–26.

Gharehgheshlagh, H. H. 2016. Kinetic grinding test approach to estimate the ball mill work index. Physicochemical Problems of Mineral Processing, 52(1), 342-352. https://doi.org/ 10.5277/ ppmp160129.

Gray, J., Rumpe, B. 2016. Models in simulation. Softw Syst Model, 15, 605–607.

Gross, J. 1938. Crushing and grinding. US Bureu of Mines Bulletin 402, 1–148.

Hart, S., Valery, W., Clements, B., Reed, M., Song, M., Dunne, R. 2001. Optimisation of the Cadia Hill Sag mill circuit. SAG 2001. Mining and mineral process engineering university of British Columbia, Vancouver, Canada.

Herbst, J. A., Fuerstenau, D. W. 1980. Scale-Up Procedure for Continuous Grinding Mill Design Using Population Balance Models. International Journal of Mineral Processing, 7, 1-31.

Hosseinzadeh Gharehgheshlagh, H. 2014. An Investigation on Scale - Up of Ball Mills (in Turkish). PHD thesis, Hacettepe University, Mining Engineering Department, 292 pp. Ankara (unpublished), Turkey.

Hosseinzadeh Gharehgheshlagh H., Ergun, L., Chehreghani, S. 2017. Investigation of the laboratory conditions effects on the prediction accuracy of size distribution of industrial ball mill discharge by using of perfect mixing model; case study: Ozdogu copper-molybdenum plant, Physicochemical Problems of Mineral Processing, 53(2), 1175−1187.

JK Bond Ball Mill Index Test, https://jktech.com.au/sites/default/files/brochures/LabServices_BondBallMill.pdf.

JK Drop Weight Test, https://jktech.com.au/sites/default/files/brochures/LabServices_DWTest_Indetail.pdf

Kelly, E.G. 1991. The Evaluation of Separation Efficiency. In Evaluation and Optimisation of Metallurgical Performance. ed. Malhotra, Klimpel, Mular, SME Inc, Littleton, 239-252.

Kelly, E.G., Spottiswood, D.J. 1982. Introduction to mineralprocessing. J. Wiley, Chapters 3 and 25.

Kelsall, D.F., Reid KJ. 1969. Symposium on size reduction, Chemical Engineering Association, Sydney University.

King, R.P., Schneider, C.L., King, E.A. 2012. Modeling and Simulation of Mineral Processing Systems. SME, ISBN-13: 978-0-87335-345-8, Colorado, USA.

Koch, P.H. 2017. Particle Generation for Geometallurgical Process Modeling. Licentiate thesis, Luleå University of Technology, Division of Minerals and Metallurgical Engineering (MiMeR), Department of Civil, Environmental and Natural Resources Engineering, 126 pp. Luleå, Sweden.

Leung, K. 1987. An Energy-based Ore Specific Model for Autogeneous and Semi-autogeneous Grinding. PhD Thesis, JKMRC, University of Queensland.

Leung, K., Morrison, R.D., Whiten, W.J. 1987. An energy based ore specific model for autogenous and semi-autogenous grinding. Copper 87. Chilean Institute of Mining Engineers, Santiago, Chile.

Levin, J. 1989. Observations on the Bond standard grindability test, and a proposal for a standard grindability test for fine materials. J.S. Afr. lnst. Min. Metall, 89, 13.

Liang, G., Wei, D., Xu, X., Xia, X., Li, Y. 2016. Study on the Selection of Comminution Circuits for a Magnetite Ore in Eastern Hebei, China. Minerals, 6(2), 39; https://doi.org/10.3390/min6020039.

Lynch, A. J. 1977. Mineral crushing and grinding circuits: their simulation, optimisation, design, and control. New York: Elsevier Scientific.

Lynch, A. J., Rao, T. C. 1975. Modelling and scale-up of hydrocyclones classifiers. In XI International Mineral Processing Congress, Cagliari, 245-269.

Man, Y.T. 2001. Model-Based Procedure For Scale-up of Wet, Overflow Ball Mills Part-2: Validation and Discussion. Minerals Engineering, Volume 14, No.10, 1259-1265.

Maruf Hasan, Md. 2016. Process Modelling of Gravity Induced Stirred Mills. PHD thesis, University of Queensland, JKMRC, 211 pp. Brisbana, Australia.

Morrell, S. 1992 (January-April). Prediction of Grinding-Mill Power. Transaction of Institute of Mining and Metallurgy, Section C: Mineral Processing and Extractive Metallurgy. 101, 25-32.

Morrell, S. 1993. The prediction of power draw in wet tumbling mills. PhD Thesis, JKMRC, University of Queensland, Brisbane.

Morrell, S. 1996 (January-April). Power Draw of Wet Tumbling Mills and Its Relationship to Charge Dynamics, Part 1: A Continuum Approach to Mathematical Modelling of Mill Power Draw. Transaction of Institute of Mining and Metallurgy, Section C: Mineral Processing and Extractive Metallurgy, 105, 43-53.

Morrell, S. 1996 (January-April). Power Draw of Wet Tumbling Mills and Its Relationship to Charge Dynamics, Part 2: An Empirical Approach to Modelling of Mill Power Draw. Transaction of Institute of Mining and Metallurgy, Section C: Mineral Processing and Extractive Metallurgy, 105, 54-62.

Morrell, S., Morrison, R. 1989. Ore charge, ball load and material flow effects on an energy based SAG mill model. SAG Milling Conference, Murdoch University WA.

Morrell, S., Napier-Munn, T.J., Andersen, J. 1992. The prediction of power draw in comminution machines. Comminution-Theory and Practice, K. Kawatra (ed), SME, Chapter 17, pp. 2 35-247.

Morrell, S., Finch, W.M., Kojovic, T., Delboni Jr., H. 1996. Modelling and simulation of large diameter autogeneous and semi-autogeneous mills. Int. J. Miner. Process, 44-45, 289-300.

Morrell, S., Lim, W., Shi, F., Tondo, L. 1997. Modelling of the HPGR Crusher. Comminution Practices, ed. Kawatra, K.S., Society for Mining, Metallurgy, and Exploration, Inc. (SME), Chapter 17, pp. 117-126.

Mular, A., Halbe, D., Barratt, D. 2002. Mineral Processing Plant Design, Practice, and Control. SME, ISBN 087335-223-8, Colorado, USA.

Munoz, A., Alvarez, L., Colacioppo, J., Valery, W. 2008. Process Integration and Optimisation at Freeport - Mcmoran Candelaria Mine, Copiapó, Chile, Proceedings of the V International Mineral Processing Seminar, PROCEMIN 2008, Santiago, Chile, 303-315.

Nageswararao, K. 1978. Further developments in the modeling and scale-up of industrial hydrocyclones. PHD thesis, JKMRC, University of Queensland, Brisbane, Australia.

Napier-Munn, T.J., Morrell, S., Morrison, R.D., Kolovic, T. 1996. Mineral Comminution Circuits: Their Operation and Optimisation. JKMRC, University of Queensland, Brisbane.

Narayanan, S.S. 1985. Development of a Laboratory Single Particle Breakage Technique and its Application to Ball Mill Modelling and Scale-up. Ph.D. Thesis, University of Queensland.

Narayanan, S.S., Whiten W.J. 1983 (June). Breakage Characteristics for Ores for Ball Mill Modelling. Australias Inst Min Metall, 286, 31-39.

Nikkhah, K., Anderson, C. 2001 (Feb. 26-28). Role of simulation software in design and operation of metallurgical plants: a case study. SME Annual Meeting, Denver, Colorado.

Özer, C., Whiten, W.J. 2012. A multi-component appearance function for the breakage of coal. International Journal of Mineral Processing, 104-105, 37–44.

Palaniandy, S. 2017. Extending the application of JKFBC for gravity induced stirred mills feed ore characterization. Minerals Engineering 101, 1–9.

Pellegrini Rosario, P. 2010. Comminution Circuit Design and Simulation for the Development of a Novel High Pressure Grinding Roll Circuit. PHD thesis, University of British Columbia, Faculty of Mining Engineering, 175 pp. Vancouver, Canada.

Piret, E.L. 1953. Fundamental aspects of grinding. Chemical Engineering Progress, 49, 56–63.

Robinson, S. 1997. Simulation Model Verification and Validation: Increasing The Users' Confidence. Proceedings of the 1997 Winter Simulation Conference, Atlanta, USA.

Rosin, P., Rammler, E. 1933. The laws governing the fineness of powdered coal. J. Inst. Fuel, 7, 29–36.

Schwarz, S., Richardson, J. M. 2013 (Feb. 24 - 27). Modeling and Simulation of Mineral Processing Circuits Using Jksimmet and Jksimfloat. SME annual meeting, Denver Co.

Shi, F., Kojovic, T., Brennan, M. 2015. Modelling of vertical spindle mills. Part 1: Sub-models for comminution and classification. Fuel 143, 595–601.

Sokolowski, J.A., Banks, C.M. 2009. Principles of Modeling and Simulation. Hoboken, NJ: Wiley. p. 6. ISBN 978-0-470-28943-3.

Sutherland, K.L. 1948. Physical chemistry of froth flotation XI Kinetics of the flotation process. J. Phys. Colloid. Chem. 52, 394–425.

Tavares, L.M. 1999. Energy absorbed in breakage of single particles in drop-weight testing. Minerals Engineering, 12 (1), 43–50.

Tavares, L., Delboni, H. 2016. Modelling and Simulation of the Santa Rita Mine Milling Circuit, REM (Revista Escola de Minas), Ouro Preto, 69(2), 207-211.

Tondo L. 1996. Modelling of HPGR crushers. M. Eng Science Thesis, University of Queensland.

Wendelin Wikedzi, A. 2018. Optimization and Performance of Grinding Circuits: The Case of Buzwagi Gold Mine (BGM). PHD thesis, Technische Universität Bergakademie, Faculty of Mechanical, Process and Energy Engineering. 208 pp. Freiberg, Germany.

Wenzheng, L. 1991. Comminution for large concentrator. Transactions of NFsoc, vol. 1, no.1.

Whiten, W.J. 1971. Proceeding, Symposium on Automatic Control Systems Mineral Processing Plants, AusIMM, Southern Queensland branch, 129-148.

Whiten, W. J. 1972. The simulation of crushing plants with models developed using multiple spline regression. In 10th International Symposium on the Application of Computer Methods in the Mineral Industry, Johannesburg, 317-323.

Whiten, W.J. 1974. A matrix theory of comminution machines. Chem. Eng. Sci. No. 29, 585-599.

Whiten, W.J., 1976. Ball mill simulation using small calculators, Proc. Australias. Inst. Min. Me tall., 258, 47 - 53.

Whiten, W.J. 1984. Models and control techniques for crushing plants, Control 84, Minl./ Metall. Process (Am.Inst.Min.Engrs. Annual Meet., Los Angeles, USA, February), 217-225.Queensland branch, 129-148.

Wills, B.A., Napier-Munn, T. 2011. Will's mineral processing technology: An introduction to the practical aspects of ore treatment and mineral recovery. Seventh edition, Elsevier Ltd.

Yoshioka, N., Hotta, Y. 1955. Liquid cyclone as a hydraulic classifier. Chem. Eng. Japan 19, 632–640.

Zuo, W. 2015. A study of the applications and modelling of high voltage pulse comminution for mineral ores. PHD thesis, University of Queensland, JKMRC. 206pp. Brisbana, Australia.

Bulletin of the Mineral Research and Exploration

http://bulletin.mta.gov.tr

A brief note on the effects of floating standard deviation (non- derivative) and horizontal gradient (derivative) filters

Ceyhan Ertan TOKER[a*]

[a]*Department of Marine Researches, General Directorate of Mineral Research and Exploration, Ankara, Turkey. orcid.org.0000.0002.4923.9835*

Short Note

Keywords:
Gravity, Filter, Standard deviation, Long wavelength, Non-derivatives

Received Date: 11.12.2018
Accepted Date: 26.12.2018

ABSTRACT

When processing gravity data, the filters are used in space and frequency environments. The filters allow more selectable parameter estimations than raw data about the structure being examined. Filtering in a broad sense means monitoring the data under the constraints we want. While the filters allow some information to become more noticeable, they allow some information to be lost or become less noticeable from data. In this case, the losses in the data make the interpretation difficult and can cause errors. Derivative and phase filters provide quantitative information about the variation of data in different directions. The display of the change results in a positive or negative manner proportional to derivative sensitivity and phase sharpness, and this may be observed in this data. In the structural boundary analysis, since the sudden changes in the derivative cause oscillations, the boundaries become questionable. Limiting the data neighborhoods with a window by controlling the deviation without using derivative and the filters that allow boundary analysis non-derivative by floating this limitation are used to illuminate the boundary relationships.

1. Introduction

In this paper, the boundary relations in regional scale and plate dimensions will be visualized on gravity data with a filter in which the changes in boundaries of the structure in gravity data are put forward using non-derivative. The computer program, written by the author, has been modified from D'errico 2016. The filter used was introduced in the article in which the Naşa intrusion was clarified (Toker et al., 2018). The floating standard deviation filter of which its sensitivity can be adjusted has been applied here for the first time on a regional scale with long wavelength structures. The data set is a network data generated by the satellite data from a sampling point at each 7 km (http://bgi.omp.obs-mip.fr/links).

2. Purpose

The aim of the study is to form a filter that does not contain derivative elements and that long-wave structures can be interpreted more easily. The network data obtained from the Bouguer gravity data was filtered to ease the interpretation and provide the structural boundary continuity by reconstructing the network with the values obtained from the program after the selection of index for the floating standard deviation window (by taking k=1, in 3x3 size window). It is intended to display the effects of the filter on a large-scale data.

3. Findings

The main tectonic elements are marked as locations in the double-layer figure. The floating standard deviation filter shows similarity when compared with

Citation Info: Toker, C. E. 2019. A brief note on the effects of floating standard deviation (non- derivative) and horizontal gradient (derivative) filters. Bulletin of Mineral Research and Exploration, 159, 235-237. *https://doi.org/10.19111/bulletinofmre.546153*

** Corresponding author: Ceyhan Ertan TOKER, ceyhanertan.toker@mta.gov.tr*

the horizontal gradient (Cordell and Grauch 1985). However, they were obtained without calculating the derivative elements. The horizontal gradient values vary between 0-300 mgal/km, while the floating standard deviation varies from 0-80 mgal. It is possible to say that the standard deviation filter shows less oscillation. In addition to this, it is observed that the stable frequencies with less oscillation are observed in the display of long wavelength structures (Toker et al., 2014). It is possible to produce more clear and interpretable results from the image obtained using the derivative. Figures 1 and 2 show the Bouguer gravity data and the horizontal gradient, respectively. In figure 3, the floating standard deviation is observed. There, it can be observed that the oscillation is less. In figure 4, the main tectonic elements appear to match with the filtered gravity data.

The findings obtained will be examined geologically and geophysically in the continuous studies.

Formulas:

Horizontal gradient amplitude (Cordell and Grauch 1985):

$$HG\ (x,y) = \left[\left(\frac{\delta g}{\delta x}\right)^2 + \left(\frac{\delta g}{\delta y}\right)^2\right]^{1/2} \quad (1)$$

$$HG\ (x,y) = \left[\left(\frac{\delta H}{\delta x}\right)^2 + \left(\frac{\delta H}{\delta y}\right)^2\right]^{1/2} \quad (2)$$

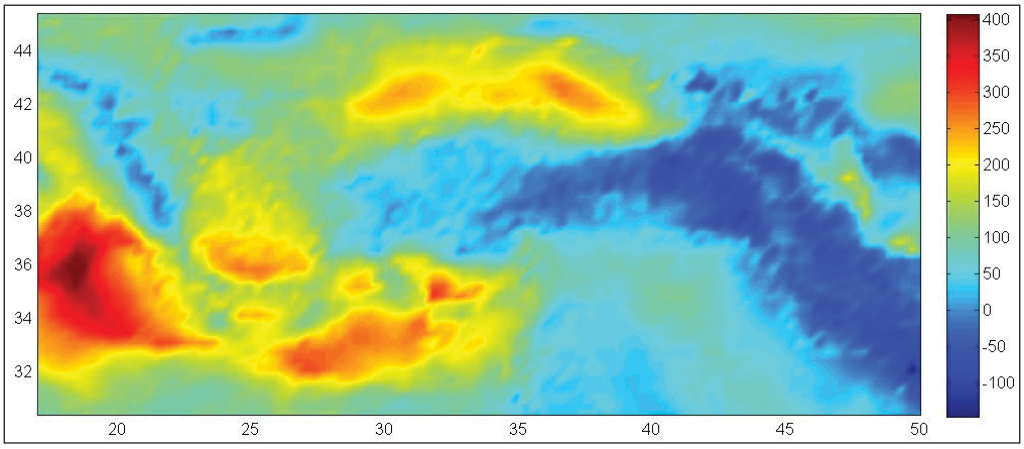

Figure 1- Bouguer gravity data.

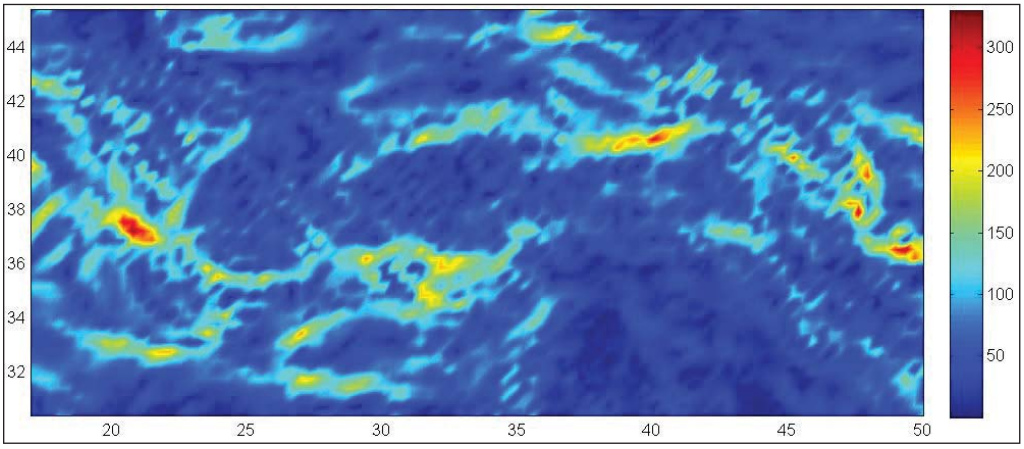

Figure 2- Horizontal gradient.

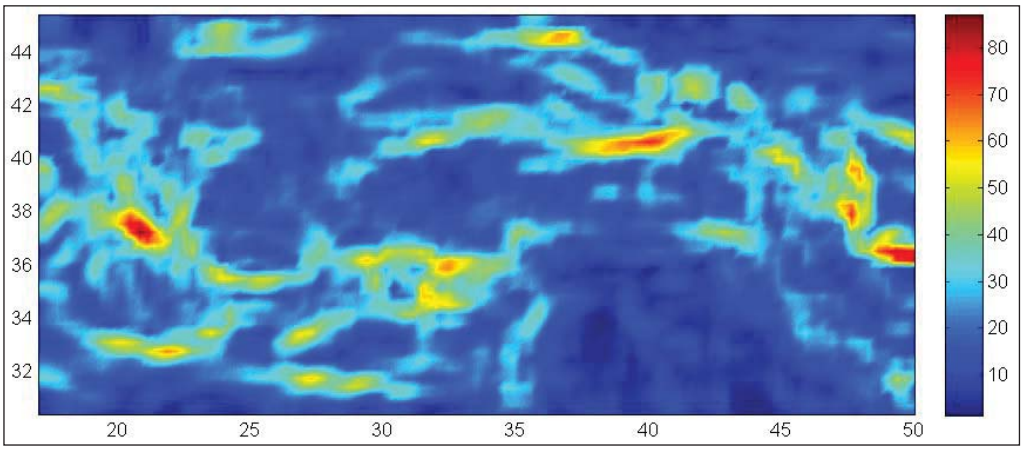

Figure 3- Floating standard deviation.

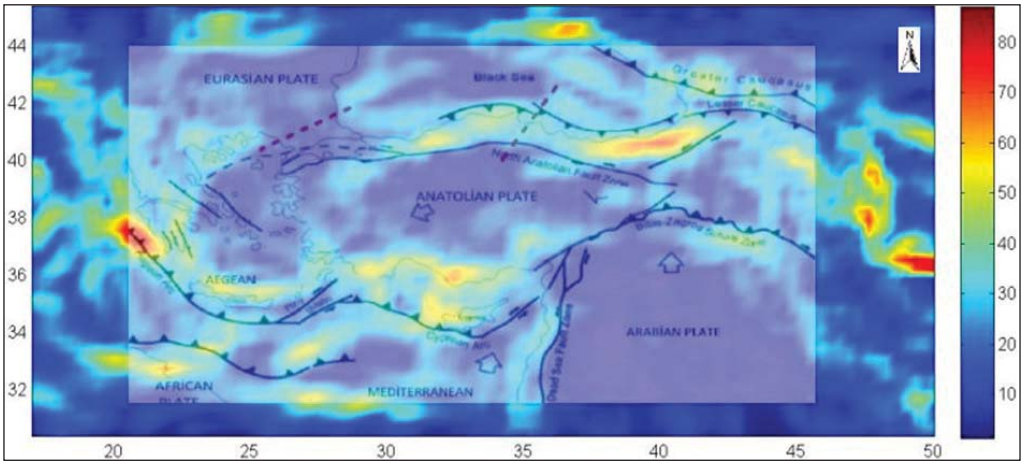

Figure 4- Main tectonic elements.

In formulas (1) and (2); ($\partial g/\partial x$) is the derivative in x direction and ($\partial g/\partial y$) is the derivative in y direction. H is the gravity function.

Standard deviation: $\sigma = ((\sum(X^2) - X^2 n^*)/(n-1))^{1/2}$

References

Cordell, L., Grauch, V.J.S. 1985. Mapping basement magnetization zones from aeromagnetic data in the San Juan Basin, New Mexico, in Hinze, William J. (ed), The utility of regional gravity and magnetic anomaly maps: Society of Exploration Geophysicists, Tulsa, Oklahoma, (1985). Pp:181-197.

D'errico, J. 2016. Personel Web Page https://www.mathworks.com/matlabcentral/.../869215-john

Gravity Data from: Bureau Gravimetrique International (BGI). DOI:10.18168/BGI.

Toker, C. E., Çiftçi, Y., Ayva, A., Kürçer, A. 2014. Two examples for imaging buried geological boundaries: Sinkhole structure and Seyit Hacı fault, Karapınar, Konya. Bulletin of the Mineral Research and Exploration. 149, 189-199, Ankara.

Toker, C. E., Ulugergerli Emin. U., Kılıç, A.R. 2018. Naşa Sokulumu (Batı Anadolu) ve tektonik anlamı: gravite ve deprem verilerinin birlikte analizi. Maden Tetkik ve Arama Dergisi. 156:251-262

PUBLICATION RULES FOR THE BULLETIN OF THE GENERAL DIRECTORATE OF MINERAL RESEARCH AND EXPLORATION

1. Aims of Publication

- To contribute to the providing of scientific communication on geosciences in Turkey and international community.
- To announce and share researches in all fields of geoscientific studies in Turkey with geoscientists worldwide.
- To announce scientific researches and practices on geoscientific surveys carried out by the General Directorate of Mineral Research and Exploration (MTA) to the public.
- To use the journal as an effective media for international publication exchange by keeping the journal in high quality, scope and format.
- To contribute to the development of Turkish language as a scientific language.

2. Scope

At least one of the following qualifications is required for publishing the papers in the *Bulletin of Mineral Research and Exploration*.

2.1. Research Articles and Review Articles

2.1.1. Original Scientific Researches

- These articles cover and contribute to the main subjects of the earth sciences, the original scientific researches and its results related to all aspects of disciplines in geoscience like exploration and evaluation of the underground sources and environmental problems, and
- The studies, which apply new aspects and methods for the solution of problems about the earth sciences and researches, which apply new aspects and methods for the solution of the problems, in the engineering sciences carried out in MTA.

2.1.2. Review articles

- These papers include comphrehensive scholarly review articles that summarize and critically assess previous geoscientific researches with a new perspective and reveal a new approach.

2.2. Discussion/Reply

- This type of article is intended for the discussion of papers that have already been published in the latest issue of the *Bulletin.* The discussion/reply type articles, which criticize all or a part of a recently published article, are published in the following first issue if it is submitted within six months after the publication of the *Bulletin*.
- The discussions are sent to the corresponding author of the original paper to get their reply before publication. The discussions abut the paper with two or more authors are sent only to the corresponding author.
- If the review article is not published within the prescribed preiod then it is published alone. Later sent replies are not published. Re-criticising of the replies is not allowed.
- The authors should obey the rules of scientific ethics and discussions in their discussion/reply papers. The papers in this category should not exceed four printed pages of the journal including figures and tables etc. The format of the papers should be compatible with the "Spelling Rules" of the *Bulletin.*

2.3. Short Notes

- The short notes part of the *Bulletin* covers short, brief and concisely written research reports for papers including the data obtained from ongoing and/or completed scientific researches and practices related to geoscience and new and/or preliminary factual findings from Turkey and worldwide.
- The short notes will follow a streamlined schedule and will normally be published in the following first or second issue shortly after submission of the paper to the *Bulletin*.
- This type of articles should not exceed four printed pages of the journal including figures, tables and an abstract.

3. Submission and Reviewing of Manuscripts

Manuscript to be submitted for publishing in the Journal must be written clearly and concisely in Turkish and/or English and prepared in the *Bulletin of Mineral Research and Exploration* style guidelines. All submissions should be made online at the **http://.dergi.mta.gov.tr** website.

- The manuscript submitted for reviews must not have been published partially or completely previously in another journal.

- The rejected manuscripts are not returned back to author(s) whereas a letter of statement indicating the reason of rejection is sent to the corresponding author.

- Submitted manuscripts must follow the *Bulletin* style and format guidelines. Otherwise, the manuscript which does not follow the journals' style and format guidelines, is given back to corresponding author without any reviewing.

- Every manuscript which passes initial Editorial treatise is reviewed by at least two independent reviewers selected by the Editors. Reviewers' reports are carefully considered by the Editors and associated editors.

- The manuscript that need to be corrected with the advices of reviewer(s) is sent back to corresponding author(s) to assess and make the required corrections suggested by reviewer(s) and editors. The authors should prepare a letter of well-reasoned statement explaining which corrections are considered or not.

- If there are any suggestions given by editors and referees that are not accepted and corrected by the author, then it should be sent to the Editor's Office with corrected copies of the report explaining the reason for not accepting these suggestions and corrections.

- Figures and tabless should be 1/3 of the main text.

- To be published in the *Bulletin of Mineral Research and Exploration,* the printed lenght of the manuscript should not exceed 30 printed pages of the journal including an abstract, figures and tables. The publication of longer manuscripts will be evaluated by Editorial Board if it can be published or not.

- The authors must do the reviewer's corrections and proposals in 60 days and must upload to the system.

- At the printing stage after the last control, the first print of the manuscript are sent to the author/ authors in pdf version and asked from the author/ authors to make the press control.

4. Publication Language and Periods

- *The Bulletin of Mineral Research and Exploration* is published at three times a year and each issue is published both in Turkish and English. Thus, the manuscripts are accepted in Turkish or English. The spelling and punctuation guidelines of Turkish Language Institution are preferred for the Turkish issue. However, the technical terms related to geology are used in accordance with the decision of the Editorial Board.

5. Spelling Draft

- Manuscripts should be written in word format in A4 (29.7 x 21 cm) size and double-spaced with font size Times New Roman 10-point, margins of 25 mm at the sides, top and bottom of each page.

- The formulas requiring the use of special characters and symbols must be submitted by the symbols part of the Microsoft Office Word Program on computer.

- Initial letters of the words in sub-titles must be capital. The first degree titles in the manuscript must be numbered and left-aligned, 10 point bold Times New Roman must be used. The second degree titles must be numbered and left-aligned, they must be written with 10 point normal Times New Roman. The third degree titles must be numbered and left-aligned, they must be written with 10 point italic Times New Roman. The fourth degree titles must be left-aligned without having any number; 10 point italic Times New Roman must be used. The text must continue placing a colon after the title without paragraph returns (See: Sample article: http://bulletin.mta.gov.tr).

- One line spacing must be left after paragraphs within text.

- Paragraphs must begin with 0.5 mm indent.

- The manuscript must include the below sections respectively;

  - Title Page
  - The Name and Surname of the author and * sign (Adress, e-mail adres must be given at the bottom of the page)
  - Abstract
  - Key Words

- o Introduction
- o Body
- o Discussion
- o Conclusion
- o Acknowledgements
- o References

5.1. Title of the Article

- The title must be short, specific and informative and written with small letters font size Times New Roman 10-point bold. The title mustn't contain the subjects insufficiently processed in the article.

5.2. The Name of the Author, Address and E-Mail Adress

- The name and surname of the author/authors must be written without affiliations. Name must be written in small letters, the surname must be written in capital letters.
- At the affiliation (work adres) written after the name and the surname of the author/authors only the name of the company must be written, the author's job mustn't be written.
- Information about the adresses must be given at the next line as 10-point and italic.
- At the articles with two or more than two authors, the numbers must be written above the surnames of the authors, the informations about their adresses must be given at the next line by leaving one space line. Also, at this part the corresponding author must be indicated by the (*) symbol and the telephone, FAX and e-mail address of the corresponding author must be given.
- Abbreviations must not be made while writing the name of the uthor and the affiliation adres. Adresses must be given in Turkish in the Turkish version, in English in the English version.
- At the end of the article the name of the corresponding author and contact informations must be added.

5.3. Abstract

- The abstract must be understandable before having a look at the text.
- The abstract should state briefly the overall purpose of the research, the aim of the article, its contributions to the known theories, new data, principle results and major conclusions.
- Tha abstract must contain short and brief sentences.
- Addressing other sections and illustrations of the text or other writings must be avoided.
- The information, which have not been mentioned in the text, must not be in the abstract.
- The article must be written as one paragraph, preferably. Please provide an abstract which doesn't exceed 200 words.
- The abstract must be written with 10-point, normal Times New Roman in single-spaced lines.
- "Abstract" must not be given for the writings that will be located in "Short Notes" section.
- The English abstract must be under the title of "Abstract".

5.4. Key Words

Immediately after the abstract, please provide up to 5 key words and with each words seperated by comma. These key words will be used for indexing purposes.

5.5. Introduction

- The introduction section should state the objectives of the work, research methods, location of the study area and provide an adequate and brief background by avoiding a detailed literature survey.
- Non-standard or uncommon classifications or abbreviations should be avoided. But if essential, then they must be defined at their first mention and used consistently thereafter. Seperate paragraphs could be organized for each of the subjects at the introduction part. If it is necessary, the subtitle can be given for each of them (for example method, material, terminology etc.).
- When pre-information is needed for facilitating the understanding of the text, this section can also be used (for example, statistical data, bringing out the formulas, experiment or application methods, and others).

5.6. Body

- In this chapter, there must be data, findings and opinions that are intended to convey to the reader about the subject. The body section forms the main part of the article.
- The data used in other sections such as "Abstract", "Discussions", and "Results" are caused by this section.
- While processing the subject, the care must be taken not to go beyond the objective highlighted in the "Introduction" section. The knowledge, which do not contribute to the realization of the purpose of the article or are useless for conclusion, must not be included.
- All data used and the opinions put forward in this section must prove the findings obtained from the studies or they must be based on a reference by citation.
- The guidance and methods to be followed in processing subjects vary according to the characteristics of the subjects mentioned. Various topic titles can be used in this section as many as necessary.

5.7. Discussions

- Discussion of the data and findings that are objectively transferred in the Main Text section of the article should be done in this section. This must be written as a seperate section from the results section.

5.8. Conclusions

- The main conclusion of the study provided by data and findings of the research should be stated concisely and concretely in this section.
- **T**he subjects that are not mentioned sufficiently and/or unprocessed in the body section must not be included in this section.
- The conclusions can be given in the form of substances in order to emphasize the results of the research and to make the expression understandable.

5.9. Acknowledgements

In this section, the significant contributions made in the realization of investigation that form the topic of the paper is specified. While specifying contributions, the attitude diverted the original purpose of this section away is not recommended. Acknowledgements must be made according to the following examples.

- This study was carried out within scope of .....project.
- I/we would like to thank to …… for contributing to the development of this article with his/her critiques.
- Academic and/or authoritorial affiliations are written for the contributions made because of requirement of ordinary task.

For example:

- o "Prof. Dr. İ. Enver Altınlı has led the studies".
- o "The opinions and warnings of Dr. Tandoğan Engin are considered in determining the chemistry of chrome minerals."

- The contributions made out of the requirement of ordinary task:

For example:

o "I would like to thank to Professor Dr. Melih Tokay who gives the opportunity to benefit from unpublished field notes"; "I would like to thank to the preliminary-Plan Chief Engineer Ethem Göğer, State Hydraulic Work, 5th Zone". Academic and / or task-occupational titles are indicated for such contributions.

- The contributions, which are made because of requirement of ordinary task but do not necessitate responsibility of the contributor mustn't be specified.

For example:

o Sentences such as "I would like to thank to our General Manager, Head of Department or Mr. / Mrs. President ……who has provided me the opportunity to research" must not be used.

5.10. References

- All references cited in the text should be given in the reference list.
- The authors must be careful about the accuracy of the references. Publication names must be written in full.

- Reference list must be written in Times New Roman, 9-point type face.
- The reference list must be alphabetized by the last names of the first author of each work.
- If an author's more than one work is mentioned, then ranking must be made with respect to the publication year from old to new.
- In the case that an author's more than one work in the same year is cited, the lower-case alphabet letters must be used right after publication year (for example; Saklar, 2011*a, b*).
- If the same author has a publication with more than one co-author, firstly the ones having single author are ranked in chronological order, then the ones having multiple authors are ranked in chronological order.
- In the following examples, the information related to works cited is regulated in accordance with different document/work types, considering punctuation marks as well.
- If the document is located in a periodical publication (if it is an article), then the information about the document must be given in the following order: surnames of the author/authors, initial letters of author's/authors' first names. Year of publication. Name of the document. Name of the publication where the document is published, volume and/ or the issue number, numbers of the first and last pages of the document.

For example:

- o Pamir, H.N. 1953. Türkiye'de kurulacak bir hidrojeoloji enstitüsü hakkında rapor. Türkiye Jeoloji Bülteni 4, 1, 63-68.
- o Barnes, F., Kaya, O. 1963. İstanbul bölgesinde bulunan Karbonifer'in genel stratigrafisi. Maden Tetkik ve Arama Dergisi 61, 1-9.
- o Robertson, A.H.F. 2002. Overview of the genesis and emplacement of Mesozoic ophiolites in the Eastern Mediterranean Tethyan region. Lithos 65, 1-67.

- If more than one document by the same authors is cited, first the documents having single name must be placed in chronological order, second the documents having two names must be listed in accordance with the chronological order and second author's surname, and finally the docments having multiple names must be listed in accordance with chronological order and third author's surname.
- If the document is a book, then; the surname of the author/authors, initial letters of the author's/ authors' first names. Year of publication. Name of the book (initial letters are capital). Name of the organization, which has published the book, name of the publication where the document is published, volume and/ or the issue number, total pages of the book.

For example

- o Meric, E. 1983. Foraminiferler. Maden Tetkik ve Arama Genel Müdürlüğü Eğitim Serisi 23, 280 s.
- o Einsele, G. 1992. Sedimentary Basins. Springer-Verlag, 628 p.

- If the document is published in a book containing the writings of various authors, the usual sequence is followed for the documents in a periodic publication. Then the editor's surname and initial letters of their name/names are written. "Ed.", which is an abbreviation of the editor word, is written in parentheses. Name of the book containing the document (initial letters are capital). Name of the organization which has published the book. Place of publication, volume number (issue number, if any) of the publication where the document is published, numbers of the first and last page of the document.

For example:

- o Göncüoğlu, M.C., Turhan, N., Şentürk, K., Özcan, A., Uysal, Ş., Yalınız, K. 2000. A geotraverse across northwestern Turkey. Bozkurt, E., Winchester, J.A., Piper, J.D.A. (Ed.). Tectonics and Magmatism in Turkey and the Surrounding Area. Geological Society of London Special Publication 173, 139-162.
- o Anderson, L. 1967. Latest information from seismic observations. Gaskell, T.F. (Ed.). The Earth's Mantle. Academic Press. London, 335-420.

- If the name of a book, where various authors' writings have been collected, is specified, those must be indicated respectively: book's editor/

editors' surname/surnames and initial letters of their name/names. "Ed.", which is an abbreviation of the editor word, must be written in parentheses. Year of Publication. Name of the book (initial letters are capital). Name of the organization which has published the book, total pages of the book.

For example:

- o Gaskel, T.F. (Ed.) 1967. The Earth's Mantle. Academic Press, 520 p.

- If the document is an abstract published in a Proceedings Book of a scientific activity such as conference/symposium/workshop …etc., the information about the document must be given in the following order: surnames of the author/authors, initial letters of author's/authors' first names. Year of publication. Title of the abstract. Name, date and place of the meeting where the Proceedings Book is published, numbers of the first and last pages of the abstract in the Proceedings Book.

For example:

- o Yılmaz, Y. 2001. Some striking features of the Anatolian geology. 4. International Turkish Geology Symposiums 24-28 September 2001, London, 13-14.

- o Öztunalı, Ö., Yeniyol, M. 1980. Yunak (Konya) yöresi kayaçlarının petrojenezi. Türkiye Jeoloji Kurumu 34. Bilim Teknik Kurultayı, 1980, Ankara, 36

- If the document is one of the unpublished documents as a report, lecture notes, and so on, the information about the document must be given by writing the word "unpublished" in parentheses at the end of information about the document after it is specified in accordance with usual order which is implemented for a document included in a periodic publication.

For example:

- o Özdemir, C. Biçen, C. 1971. Erzincan İli, İliç ilçesi ve civarı demir etütleri raporu. General Directorate of Mineral Research and Exploration Report No: 4461, 21 p. Ankara (unpublished).

- o Akyol, E. 1978. Palinoloji ders notları. EÜ Fen Fakültesi Yerbilimleri Bölümü, 45 p., İzmir (unpublished).

- The followings must be specified for the notes of unpublished courses, seminars, and so on: name of the document and course organizer. Place of the meeting, name of the book, corresponding page numbers must be given.

For example:

- o Walker, G. R. Mutti, E. 1973.Turbidite facies and facies associations. Pacific Section Society for Sedimentary Geology Short Course. Annaheim. Turbitides and Deep Water Sedimentation, 119-157.

- If the document is a thesis, the followings are written: surname of the author, initial letter of the author's first name. Year of Publication. Name of the thesis. Thesis type, the university where it is given, the total number of pages, the city and "unpublished" word in parentheses.

For example:

- o Seymen, İ. 1982. Kaman dolayında Kırşehir Masifi'nin jeolojisi. Doçentlik Tezi, İTÜ Maden Fakültesi, 145 s. İstanbul (unpublished).

- Anonymous works must be regulated according to the publishing organization.

For example:

- o MTA. 1964. 1/500.000 ölçekli Türkiye Jeoloji Haritası, İstanbul Paftası. Maden Tetkik ve Arama Genel Müdürlüğü, Ankara.

- The date after the name of the author is not given for on-printing documents; "in press" and / or "on review" words in parenthesis must be written. The name of the article and the source of publication must be specified, volume and page number must not be given.

For example:

- o Ishihara, S. The granitoid and mineralization. Economic Geology 75th Anniversary (in press).

- Organization name, web address, date of access on web address must be indicated for the information downloaded from the internet. Turkish sources must be given directly in Turkish and they must be written in Turkish characters.

For example:

- o ERD (Earthquake Research Department of

Turkey). **http://www.afad.gov.tr**. March 3, 2013.

- While specifying work cited, the original language must be used; translation of the title of the article must not be done.

6. Illustrations

- All drawings, photographs, plates and tables of the article are called as "illustration".
- The illustrations must be used when the use of them is inevitable or when they facilitate the understanding of the subject.
- While selecting and arranging the illustrations' form and dimensions, the page size and layout of the *Bulletin* must be considered. The unnecessary loss of space must be prevented as much as possible.
- The pictures must have high quality, high resolution suitable for printing.
- The number of illustrations must be proportional to the size of the text.
- All illustrations must be sent as in separate files independent from the text.
- While describing illustrations in the text, the abbreviations must be avoided and descriptions must be numbered in the order they are mentioned in the text.
- Photographs and plates must be given as computer files containing EPS, TIFF, or JPEG files in 600 dpi and higher resolutions (1200 dpi is preferable) so that all details can be seen in the stage of examination of writing.

6.1. Figures

- Drawings and photos (except for the plates in the text) will be evaluated together as "Figure" and they must be numbered in the order they are mentioned in the text.
- The figures published in the *Bulletin of Mineral Research and Exploration* must be prepared in computer considering the dimensions of single-column width 7.4 m or double-column width 15.8 cm. Figure area together with the writing at the bottom should not exceed 15.8x21in maximum.
- Unnecessasry details must not be given in figures or care must be taken not to use much space for information transfer.
- Figures must be arranged in such a way to be printed in black/white or colored.
- The figure explanations being justified in two margins must be as follows:

  Figure 1- Sandıklı İlçesinin (Afyon); a) güneybatısının jeolojik haritası, b) İnceleme alanının genel dikme kesiti (Seymen, 1981), c) Türkiye'nin önemli neotektonik yapıları (Koçyiğit, 1994'den değiştirilerek).

  Figure 1- a) Sandıklı ilçesinin güneybatısının jeolojik haritası, b) İnceleme alanının genel dikme kesiti (Seymen, 1981), c) Türkiye'nin önemli neotektonik yapıları (Koçyiğit, 1994'den değiştirilerek).

- Drawings must be made by well-known computer programs painstakingly, neatly and cleanly.
- Using fine lines, which can disappear when figures shrinks, must be avoided. Symbols or letters used in all drawings must be in Times New Roman and not less than 2 mm in size when shrink.
- All standardized icons used in the drawings must be explained preferably in the drawing or with figure caption if they are too long.
- Linear scale must be used for all drawings. Author's name, figure description, figure number must not be included into the drawing.
- Photos must be in quality and quantity that will reflect the objectives of the subject.

6.2. Plates

- Plates must be used when needed a combination of more than one photo and the publication on a special quality paper.
- Plate sizes must be equal to the size of available magazine page space.
- Figure numbers and linear scale must be written under each of the shapes located on the Plate.
- The original plates must be added to the final copy, which will be submitted, if the article is accepted.
- Figures and plates must be independently numbered. Figures must be numbered in Latin numerals and plates with Roman numerals (e.g., Figure1, Plate I).

- There must be no description text on Figures.

6.3. Tables

- All tables must be prepared preferably in word format in Times New Roman fonts.
- Tables together with table top writing must not exceed 15x8 cm in size.
- The table explanations being justified in two margins must be as follows:

Table 1- Hydrogeochemical analysis results of geothermal waters in the study area.

7. Nomenclature and Abbreviations

- Non-standard and uncommon nomenclature abbreviations should be avoided in the text. But if essential, then they must be described as below. In cases where unusual nomenclatures and unstandardized abbreviations are considered to be compulsory, the way followed and method must be described.
- Full stop must not be placed between the initials of words for standardized abbreviations (MER, SHW, etc.).
- Geographical directions must be abbreviated in English language as follows: N, S, E, W, NE …etc.
- The first time used abbreviations in the text are presented in parenthesis, the parenthesis is not used for subsequent uses.
- The metric system must be used as units of measurement.
- Figure, plate and table names in the article must not be abbreviated. For example, "as shown in the generalized stratigraphic cross-section of the region (Figure 1……..."

7.1. Stratigraphic Terminology

Stratigraphic classifications and nomenclatures must be appropriate with the rules of International Commision on Stratigraphy and/or Turkish Stratigraphic Committee. The formation names, which have been accepted by International Commision on Stratigraphy and/or Turkey Stratigraphy Committee, should be used in the manuscript.

7.2. Paleontologic Terminology

Fossil names in phrases must be stated according to the following examples:

o For the use of authentic fossil names;

e.g. Limestone with *Nummulites*

o When the authentic fossil name is not used;

o e.g. nummulitic Limestone

o Other examples of use;

e.g. The type and species of Alveolina/ Alveolina type and species

- Taxonomic ranks must be made according to the following examples:

Super family: Alveolinacea Ehrenberg, 1939	*Not reference, Not stated in the Reference section*
Family: Borelidae Schmarda, 1871	
Type genus: *Borelis* de Montfort, 1808	
Type species: *Borelis melenoides de Montfort, 1808*; *Nautilus melo* Fitchel and Moll, 1789	
Borelis vonderschmitti (Schweighauser, 1951) (Plate, Figure, Figure in Body Text)	*Schweighauser, 1951 not reference*
1951 *Neoalveolina vonderschmitti* Schweighauser, page 468, figure 1-4	*Cited Scweighauser (1951), stated in the Reference section.*
1974 *Borelis vonderschmitti* (Schweighauser), Hottinger, page, 67, plate 98, figure 1.7	*Cited Hottinger (1974), stated in the Reference section.*

- The names of the fossils should be stated according to the rules given below:

  - o For the first use of the fossil names, the type, spieces and the author names must be fully indicated;

    Alveolina aragoensis Hottinger

    Alveolina cf. *aragoensis* Hottinger

    Alveolina aff. *aragoensis Hottinger*

  - o When a species is mentioned for the second time in the text;

    A.aragoensis

    *A.*cf.*aragoensis*

    *A.*aff.*aragoensis*

  - o It is accepted as citiation if stated as *Alveolina aragoensis* Hottinger (1966).

- The statement of plates and figures (especially for the articles of paleontology):

  - o for the statement of species mentioned in the body text;

  Borelis vonderschmitti (Schweighauser, 1951).

  (plate, figure, figure in the body text).

  - o When cited for other articles;

  1951 *Neoalveolina vonderschmitti* Schweighauser, page 468, figure 1-4, figure in body text

  1974 *Borelis vonderschmitti* (Schweighauser), Hottinger, page 67, plate 98, figure 1-7

- For the citation in the text

  (Schweighauser, 1951, page, plate, figure, figure in the body text)

  (Hottinger, 1974, page, plate, figure 67, plate 98, figure 1-7, figure in the body text.)

8. Citations

All citations in the body text must be indicated by the last name of the author(s) and the year of publication, respectively. The citations in the text must be given in following formats:

- For publications written by single author;

  - It is known that fold axes of Devonian and Carboniferious aged units around Istanbul is in NS direction (Ketin, 1953, 1956; Altınlı, 1999).

  - Altınlı (1972, 1976) defined the general characteristics of Bilecik sandstone in detail.

- For publications written by two authors;

  - The upper parts of the unit contain Ilerdian fossils (Sirel and Gündüz, 1976; Keskin and Turhan, 1987, 1989).

- For publications written by three or more authors;

  According to Caner et al. (1975) the Alıcı formation reflects the fluvial conditions.

  The unit disappears by wedging out in the East direction (Tokay et al., 1984).

- If reference is not directly obtained but can be found in another reference, the cross-reference should be given as follows:

  - It is known that Lebling has mentioned the existence of Lias around Çakraz (Lebling, 1932: from Charles, 1933).

9. Reprints

The author(s) will receive (2) two hard copies of the related issues.

10. Copyright and Conditions of Publication

- It is necessary that the work submitted for the publication must be original and has not been previously unpublished in whole or partially.

- It is necessarry that the authors who send their publications to the *Bulletin of Mineral Research and Exploration* hereby accept the conditions of publication of the Bulletin in advance.

- All copyrights of the accepted manuscripts belong to MTA. The author or corresponding author on behalf of all authors (for papers with multiple authors) must sign and give the agreement under the terms indicated by the Regulations of Executive Publication Committee. Upon acceptance of an article, MTA can pay royalty to the authors upon their request according to the terms under the "Regulations of Executive Publication Committe" and the "Regulations of Royalty Payment of Public Office and Institutions"

All the information and forms about the *Bulletin of Mineral Research and Explorations* can be obtained from **http://dergi.mta.gov.tr**